DOI: 10.17238/issn2226-8812.2023.3-4 Июль – Декабрь 3-4 (44-45) 2023

# ПРОСТРАНСТВО, ВРЕМЯ И ФУНДАМЕНТАЛЬНЫЕ ВЗАИМОДЕЙСТВИЯ

научный журнал

**ISSN 2226-8812**



***Издатель***

ООО « ПРОФИЛЬ - 2С »
123007, РОССИЯ, г. Москва,
Хорошевское шоссе, д. 78
тел + 7 (916) 229 03 11
e-mail: profill@profill.ru
сайт: www.profill.ru

***Учредитель***

ООО « ПРОФИЛЬ - 2С »

***Адрес редакции***

123007, РОССИЯ, г. Москва,
Хорошевское шоссе, д. 78
тел + 7 (916) 229 03 11
e-mail: info@stfi.ru
сайт: www.stfi.ru

**Свидетельство о регистрации средства массовой информации**

ПИ № ФС77 - 50013 от 24 мая 2012 года

**Подписной индекс 90995 в Объединенном каталоге «Пресса России»**

---

**Журнал включен в Перечень рецензируемых научных изданий, в которых должны быть опубликованы основные научные результаты на соискание ученой степени кандидата наук, на соискание ученой степени доктора наук.**

Подписано в печать 29.12.2023

# SPACE, TIME AND FUNDAMENTAL INTERACTIONS

scientific journal

**ISSN 2226-8812**



***Publisher***

OOO «PROFILL - 2S»
123007, Moscow, Khoroshevskoe shosse, 78
fone +7 (916) 229 03 11
e-mail: profill@profill.ru
website: www.profill.ru

***Founder***

OOO «PROFILL - 2S»

***Address***

123007, Moscow, Khoroshevskoe shosse, 78
fone +7 (916) 229 03 11
e-mail: info@stfi.ru
website: www.stfi.ru

**The certificate on registration of mass media**
ПИ № ФС77 - 50013 from 24 May 2012

**Subscription index 90995 in the incorporated catalogue «Press of RUSSIA»**

---

**Journal is included in the List of peer-reviewed scientific publications, where must be published basic scientific results on competition of a scientific degree of Candidate of Sciences (Ph.D.) and Doctor of Science**

Signed to print 29.12.2023

# СОДЕРЖАНИЕ CONTENTS

*Гравитация, космология и фундаментальные поля* — *The Gravity, Cosmology and Fundamental Fields*


| | | |
|---|---|---|
| Итоги XXIII Международной научной конференции “Физические интерпретации теории относительности ПИРТ-2023” | Results of the XXIII International Scientific Conference “Physical Interpretations of Relativity Theory PIRT-2023” | **6** |
| Памяти А.А. Старобинского | In memory of A.A. Starobinsky | **8** |
| **Т. К. Адорно, А. И. Бреев, Д. М. Гитман** Квазиклассическое описание электромагнитного излучения ускоренных зарядов | **T. C. Adorno, A. I. Breev, D. M. Gitman** Semiclassical description of the electromagnetic radiation by accelerated charged distributions | **12** |
| **А. М. Баранов, Е. В. Савельев** Модель открытой вселенной с космологической постоянной как задача о движении частицы в силовом поле | **A. M. Baranov, E. V. Saveljev** The open universe model with the cosmological constant as a particle movement task in a force field | **21** |
| **А. В. Белоненко, Ф. С. Гурин, В. Н. Руденко, А. В. Гусев, В. В. Кулагин, С. М. Попов, Г. Д. Манучарян** Фильтрация эффекта гравитационного сдвига частоты для сигналов радиосвязи со спутниками Земли | **A. V. Belonenko, F. S. Gurin, V. N. Rudenko, A. V. Gusev, V. V. Kulagin, S. M. Popov, G. D. Manucharyan** Filtering of the gravitational frequency shift effect for radio communication signals with the Earth satellites | **30** |
| **А. Я. Буринский, Г. Н. Измайлов** Электрон Керра – Ньюмана как адаптивная система | **A. Ya. Burinskii, G. N. Izmailov** Kerr – Newman electron as an adaptive system | **38** |
| **А. А. Черницкий** О лептонах в теории пространственно-временной плёнки | **A. A. Chernitskii** About leptons in space-time film theory | **48** |
| **В. И. Докучаев** Спины сверхмассивных черных дыр | **V. I. Dokuchaev** Spins of supermassive black holes | **54** |
| **П. И. Дядина, Н. А. Авдеев** Свойства аккреционных дисков в гибридной метрической-Палатини f(R)-гравитации | **P. I. Dyadina, N. A. Avdeev** Properties of accretion disks in hybrid metric-palatini f(R) gravity | **63** |
| **Е. Д. Емцова, А. Н. Петров** О сохраняющихся величинах для движущейся чёрной дыры в телепараллельном эквиваленте ОТО | **E. D. Emtsova, A. N. Petrov** On conserved quantities for a moving black hole in TEGR | **77** |

| | | |
|---|---|---|
| **М. Л. Фильченков, Ю. П. Лаптев**<br>О проблеме времени в квантовой космологии | **M. L. Fil'chenkov, Yu. P. Laptev**<br>On The Temporal Problem In Quantum Cosmology | **89** |
| **И. В. Фомин, Е. С. Денцель**<br>Инфляционные модели на основе обобщенных точных космологических решений | **I. V. Fomin, E. S. Dentsel**<br>Inflationary models based on generalized exact cosmological solutions | **93** |
| **В. О. Гладышев, В. Л. Кауц, А. В. Каютенко, А. Н. Морозов, П. П. Николаев, И. В. Фомин, Е. А. Шарандин**<br>Анализ связанных гравитационных и электромагнитных волн | **V. O. Gladyshev, V. L. Kauts, A. V. Kayutenko, A. N. Morozov, P. P. Nikolaev, I. V. Fomin, E. A. Sharandin**<br>The analysis of coupled gravitational and electromagnetic waves | **99** |
| **М. В. Гордин, Д. А. Базлев, В. О. Гладышев, В. Л. Кауц, А. В. Каютенко, П. П. Николаев, И. В. Фомин, Е. А. Шарандин**<br>Использование реликтового излучения для построения новой системы навигации | **M. V. Gordin, P. P. Petrov, P. P. Petrov, V. L. Kauts, A. V. Kayutenko, P. P. Nikolaev, I. V. Fomin, E. A. Sharandin**<br>Using relic radiation to construct new navigation system | **108** |
| **Л. В. Грунская, В. В. Исакевич, Д. В. Исакевич**<br>Физические основы свойства восприимчивости электромагнитного поля Земли к гравитационно-волновому излучению двойных звездных систем | **L. V. Grunskaya, V. V. Isakevich, D. V. Isakevich**<br>Physical Basis of Sensitivity of the Earth's Electromagnetic Field to Gravitation | **117** |
| **А. К. Гутьеррес-Пинерес, Э. Кеведо**<br>Обобщение процедуры согласования $C^3$ | **A. C. Gutierrez-Pineres, H. Quevedo**<br>Generalization of the $C^3$ matching procedure | **127** |
| **Г. Н. Измайлов, В. В. Озолин**<br>Имитация извлечения кинетической энергии из черной дыры Керра–Ньюмана | **G. N. Izmailov, V. V. Ozolin**<br>Simulation of kinetic energy extraction from a Kerr – Newman black hole | **133** |
| **В. В. Кассандров**<br>Алгебродинамика: в поисках истинной алгебраической “Мировой” структуры | **V. V. Kassandrov**<br>The algebrodynamics: in search of the ultimate algebraic “World” structure | **147** |
| **Л. Х. Кауффман**<br>Уравнение Дирака и фермионная алгебра | **L. H. Kauffman**<br>The Dirac Equation and a Fermionic Algebra | **154** |
| **Р. Кернер**<br>Обобщенные модели Калуцы - Клейна с лагранжианами Гаусса - Бонне | **R. Kerner**<br>Generalized Kaluza-Klein models with Gauss-Bonnet lagrangians | **166** |
| **Г. Д. Манучарян, И. В. Фомин, В. О. Гладышев, Д. А. Литвинов**<br>О детектировании высокочастотных реликтовых гравитационных волн | **G. D. Manucharyan, I. V. Fomin, V. O. Gladyshev, D. A. Litvinov**<br>On the detection of high-frequency relic gravitational waves | **188** |
| **Б. Э. Мейерович**<br>Движение в гравитационном поле чёрной дыры в синхронной системе координат | **B. E. Meierovich**<br>Motion in the gravitational field of a black hole in a synchronous coordinate system | **199** |

| | | |
|---|---|---|
| **В. В. Монахов**<br>Невозможность существования майорановских спиноров как физических частиц | **V. V. Monakhov**<br>The Impossibility Of The Existence Of Majorana Spinors As Physical Particles | **211** |
| **Р. С. Накибов, А. В. Урсулов**<br>Орбиты массивных частиц в сферически симметричном гравитационном поле с учетом космологической постоянной | **R. S. Nakibov, A. V. Ursulov**<br>Orbits of massive particles in a spherically symmetric gravitational field in view of cosmological constant | **218** |
| **И. М. Пинто**<br>Снижение теплового шума зеркал в детекторе гравитационных волн. Краткий обзор и некоторые новые результаты | **I. M. Pinto**<br>Reducing Thermal Noise in the Mirrors of Gravitational Wave Detectors. A Short Review and Some New Results | **229** |
| **К. Ромеро, М. П. Дуарте**<br>Возвращение поля Прока | **C. Romero, M. P. Duarte**<br>The Coming Back of the Proca Field | **247** |
| **С. Салума, А. Н. Тауфик**<br>Стандартно-мерные системы преобразований для специальной теории относительности | **S. Salouma, A. N. Tawfik**<br>Standard-Dimensional Transformation Systems for Special Relativity | **251** |
| **О. В. Сандакова, В. Ф. Панов, Е. В. Кувшинова**<br>Различные инфляционные космологической модели с вращением | **O. V. Sandakova, V. F. Panov, E. V. Kuvshinova**<br>Various inflationary cosmological models with rotation | **271** |
| **С. Ю. Седов**<br>О теории гравитации Вейля-Дирака и ее развитии | **S. Yu. Sedov**<br>On Weyl-Dirac gravitation theory and its development | **277** |
| **В. Н. Тимофеев**<br>Рассеяние электронов на червоточине в борновском приближении | **V. N. Timofeev**<br>Electron Scattering on a Wormhole in the Born Approximation | **290** |
| **Э. Трелл**<br>Ауфбау дифференциальной геометрии Ли атомов и молекул | **E. Trell**<br>Lie differential geometry aufbau of the atoms and molecules | **299** |
| **В. Г. Георгиев, А. Маедер**<br>Парадигма масштабно-инвариантного вакуума: основные результаты и текущий прогресс плюс BBNS результаты | **V. G. Gueorguiev, A. Maeder**<br>The Scale Invariant Vacuum Paradigm: Main Results plus the Current BBNS Progress | **314** |
| **И. Л. Жогин**<br>Внегалактические ТэВ-ные фотоны и предел спектра нулевых колебаний | **I. L. Zhogin**<br>Extragalactic TeV Photons and the Zero-point Vibration Spectrum Limit | **327** |
| **В. М. Журавлев**<br>Новая теория тяготения, осцилляции звезд и 11-летний цикл активности Солнца | **V. M. Zhuravlev**<br>New theory of gravity, stellar oscillations and the 11-year cycle of solar activity | **333** |

# ГРАВИТАЦИЯ, КОСМОЛОГИЯ И ФУНДАМЕНТАЛЬНЫЕ ПОЛЯ

***

## ИТОГИ XXIII МЕЖДУНАРОДНОЙ НАУЧНОЙ КОНФЕРЕНЦИИ “ФИЗИЧЕСКИЕ ИНТЕРПРЕТАЦИИ ТЕОРИИ ОТНОСИТЕЛЬНОСТИ ПИРТ-2023”

В период с 3 по 6 июля 2023 г. в МГТУ им. Н.Э. Баумана состоялась XXIII Международная научная конференция по современным проблемам теории относительности, космологии и астрофизики «Физические интерпретации теории относительности PIRT-2023».

Конференция PIRT - это международное научное мероприятие, которое возникло в 1988 году и вначале проводилось в Имперском колледже в Лондоне один раз в два года, а с 2003 года проводится в Бауманском Университете в Москве. Председателем Международного организационного комитета является ректор МГТУ Н.Э. Баумана Михаил Гордин, со-председателем – руководитель НУК «Фундаментальные науки», профессор Владимир Гладышев. Председателем Международного академического комитета являлся Академик РАН Алексей Старобинский.

Основными целями конференции XXIII конференции PIRT являлись: обсуждение современных обобщений теории относительности, ее наблюдаемых следствий; экспериментальная проверка теории относительности; методы регистрации гравитационных волн; эффекты релятивистской электродинамики и оптики движущихся сред; а также астрофизические наблюдения и космические эксперименты.

Программа конференции была посвящена последним достижениям в области теории гравитации, космологии, астрофизики, привлекла более 180 исследователей из 27 стран. Более 60 участников из 5 стран выступили с докладами в конференц-зале МГТУ им. Н.Э. Баумана, остальные участники и слушатели конференции принимали участие дистанционно в Зум. Для гостей конференции была организованы широкая культурная программа.

С докладами на конференции выступили президент Российского гравитационного общества, Академик РАН Алексей Старобинский, член-корр. РАН, зав. каф. «Физика» Андрей Морозов, профессор математики в Иллинойском университете в Чикаго Луис Кауффман, профессор Университета Неаполя «Федерико II» Инноченцо Пинто и другие.

Одновременно с конференцией была организована работа IV Международной летней школы «Гравитация, космология и астрофизика ISGCA-2023». Основными целями школы являлись: обсуждение современных достижений в области исследования Вселенной и знакомство с основными идеями и методами исследования в теории гравитации и космологии. В Школе приняли участие более 100 слушателей из 26 стран. На ISGCA-2023 выступили с лекциями широко известные учёные. Студенты Школы смогли лично послушать лекции и задать свои вопросы таким известным учёным, как Академику РАН Алексею Старобинскому, профессору МГУ Сергею Вятчанину, профессору Института Технологии и Науки Бирла Бивудутте Мишре и другим.

Рабочими языками Конференции были русский и английский, осуществлялся синхронный перевод всех докладов. Предварительно Издательством МГТУ им. Н.Э. Баумана были изданы тезисы докладов.

Организаторы и участники уверены, что Конференция и Летняя Школа будут способствовать повышению уровня образования в области теории гравитации, астрофизики и космологии, развитию и укреплению международных научных связей.

# RESULTS OF THE XXIII INTERNATIONAL SCIENTIFIC CONFERENCE "PHYSICAL INTERPRETATIONS OF RELATIVITY THEORY PIRT-2023"

Between July 3rd and July 6th, 2023, the Bauman Moscow State Technical University held the 23rd International Scientific Conference on Modern Problems of the Relativity Theory, Cosmology and Astrophysics, known as "Physical Interpretations of the Relativity Theory: PIRT-2023".

The PIRT conference is an international scientific event originating in 1988, first held biennially at Imperial College London and later, since 2003, at the Bauman Moscow State Technical University.

The Chairman of the International Organizing Committee is Mikhail Gordin, Rector of Bauman Moscow State Technical University, while the Co-Chairman is Professor Vladimir Gladyshev, Head of Scientific Educational Complex of Fundamental Sciences. The Chairman of the International Academic Committee was Alexey Starobinsky, Academician of the Russian Academy of Sciences.

The 23rd PIRT conference primarily aimed to discuss the following topics: modern generalizations of the relativity theory and its observed consequences; experimental verification of the relativity theory; methods for gravitational wave recording; effects of relativistic electrodynamics and optics in moving media; astrophysical observations and space-based experiments.

The conference program focused on the latest achievements in the theory of gravity, cosmology and astrophysics, which attracted over 150 researchers from 27 countries. Over 60 participants from 5 countries gave their presentations in the conference hall of the Bauman Moscow State Technical University; other participants and listeners attended the conference remotely via Zoom. An extensive cultural program was arranged for the conference attendees.

The luminaries who delivered their presentations at the conference include: Alexey Starobinsky, Academician of the Russian Academy of Sciences, President of the Russian Gravitational Society; Andrey Morozov, Corresponding Member of RAS, Head of the Physics Department; Louis Kauffman, Professor of Mathematics in the University of Illinois at Chicago; Innocenzo Pinto, Professor, University of Naples "Federico II"; and many more.

The 4th "Gravitation, Cosmology and Astrophysics ISGCA-2023"International Summer School was in action simultaneously with the conference. The main goals of the school were to discuss modern advances in the study of the Universe and to familiarize the participants with the main ideas and methods of research in the theory of gravity and cosmology. The School was attended by over a hundred students from 26 countries. Eminent scientists delivered their lectures at the ISGCA-2023. Students of the School had a chance to listen to lectures in person and pose their questions to such celebrated scientists as Alexei Starobinsky, Academician of the Russian Academy of Sciences; Sergey Vyatchanin, Professor, Lomonosov Moscow State University; Bivudutta Mishra, Professor, Birla Institute of Technology and Science; and many more.

The working languages of the Conference were Russian and English, with all presentations simultaneously interpreted. The Publishing House of Bauman Moscow State Technical University had published the presentation summaries in advance.

The organizers and participants are confident that the Conference and the Summer School will contribute to raising the quality of education concerning the theory of gravity, astrophysics and cosmology, as well as to developing and strengthening international scientific collaboration.

# ПАМЯТИ А.А. СТАРОБИНСКОГО

21 декабря 2023 г. ушёл из жизни выдающийся учёный-астрофизик, академик РАН Старобинский Алексей Александрович.

Алексей Александрович был одним из крупнейших физиков-теоретиков, известный всему миру работами в области классической и квантовой теории гравитации, космологии и релятивистской астрофизики. Совместно с Я. Б. Зельдовичем Алексей Александрович рассчитал количество частиц и среднее значение тензора энергии-импульса квантовых полей в однородной анизотропной космологической модели. Вместе с ним же продемонстрировал Стивену Хокингу, что в соответствии с принципом неопределённости квантовой механики вращающиеся чёрные дыры должны порождать и излучать частицы. Совместно с Ю. Н. Парийским и другими обнаружил флуктуации температуры реликтового излучения. Совместно с Аланом Гутом и Андреем Линде является основоположником теории ранней Вселенной с де-ситтеровской (инфляционной) стадией. Наиболее важными его результатами в этой области являются: первый расчёт спектра гравитационных волн, генерируемых на инфляционной стадии, первая последовательная модель инфляционного сценария, первый (одновременно, но независимо от Хокинга и Гута) количественно правильный расчёт спектра возмущений плотности, теория стохастической инфляции, теория разогрева материи во Вселенной после конца инфляционной стадии, теория перехода от квантового описания первичных неоднородностей к классическому.

С 1997 года ученый был членом-корреспондентом РАН, с 2011 года академик РАН, с 2010 года — член Немецкой национальной академии наук «Леопольдина». В 2017 году он был избран иностранным членом Национальной академии наук США.

Учёный награжден медалью ордена «За заслуги перед Отечеством» II степени (2009), медалью СССР «За трудовую доблесть» (1986), удостоен Золотой медали А.Д. Сахарова РАН (2016), медали А.А. Фридмана Пермского государственного университета (2013), памятной медали имени В.Я. Струве (2019), памятной медали ЦК КПРФ «300 лет М. В. Ломоносову», лауреат премии им. А.А. Фридмана РАН (1996), лауреат премии МАИК «Наука/Интерпериодика» (2004). Алексей Александровичу вручены самые престижные международные награды: премия Кавли по астрофизике от Норвежской Академии естественных и гуманитарных наук, Министерства образования и науки Норвегии и фонда Кавли — высшая награда в мировой астрофизике (2014, вместе с А. Гутом и А.Д. Линде); премия Дирака (2019, Италия, вместе с В.Ф. Мухановым и Р.А. Сюняевым) — считается самой престижной наградой в области теоретической и математической физики; Международная премия фонда Грубера (США) — высшая мировая награда в области космологии (2013, вместе с В.Ф. Мухановым); медаль Амальди от Итальянского Общества по общей теории относительности и гравитационной физике SIGRAV (2012, вместе с В.Ф. Мухановым); Международная премия фонда Томалла (Швейцария) за выдающийся вклад в общую теорию относительности и гравитацию (2009, вместе с В.Ф. Мухановым); звание Офицера национального Ордена Академических Пальм (2017, Франция); медаль О. Клейна от Шведской королевской академии наук с предложением прочитать Мемориальную лекцию Оскара Клейна (2010); Международная премия по теоретической физике Исаака Померанчука (2021).

Алексей Александрович подготовил 4 профессора (в т. ч. члена трех национальных Академий наук Индии) и 16 докторов, PhD и кандидатов наук. Является автором более 300 научных работ.

Алексей Александрович был членом редколлегии журналов «Письма в ЖЭТФ», «Письма в Астрономический журнал», «Gravitation and Cosmology», «International Journal of Modern Physics D», «Journal of Cosmology and Astroparticle Physics», «Classical and Quantum Gravity», «General Relativity and Gravitation», «Physical Review D», а также входил в состав научных комитетов большинства известных международных конференций в области гравитации, космологии и астрофизики. С 2017 года являлся президентом Российского гравитационного общества.

С 2023 года Алексей Александрович председательствовал в Международном научном комитете конференции «Физические интерпретации теории относительности PIRT-2023», объединяющей ученых из разных стран и континентов, и являлся руководителем Международной молодежной летней школы по гравитации, космологии и астрофизике ISGCA-2023, которые традиционно проводятся в МГТУ им. Н.Э. Баумана при поддержке РАН, МГУ им. М.В.Ломоносова и других российских и зарубежных университетов.

Одним из последних научных событий, которые организовал Алексей Александрович стала осенняя Международная научная конференция «Пространство. Время. Цивилизация. STC-2023», которая проводилась в Египте совместно РАН, МГТУ им. Н.Э. Баумана и Институтом технологий и науки Бирла, Пилани (Birla Institute of Technology and Science, Pilani). На открытии конференции Алексей Александрович отметил, что все доклады объединяет общенаучный подход, который сочетает теоретическую точку зрения логики и разума с точкой зрения экспериментального использования того, что сейчас называют таким модным словом, как "артефакты это те объекты, которые дошли до нас из прошлого. Используя эти артефакты плюс нашу логику, мы узнаем прошлое нашей Вселенной, нашей цивилизации. И, конечно, общая проблема, которая абсолютна одинакова для историков и археологов с одной стороны, и для космологов с другой стороны это, то, что мы должны проверять и доказывать, что не так легко, что эти артефакты действительно подлинные, что они не возникли в более поздние времена.

Эти слова подчеркивают широту интересов Алексея Александровича, его веру в безграничный процесс познания и объединяют многих исследователей вокруг его личности Ученого и Человека.

*Международный научный и организационный комитеты конференции PIRT*

**IN MEMORY OF A.A. STAROBINSKY**

On December 21, 2023 the outstanding scientist-astrophysicist, academician of the Russian Academy of Sciences Starobinsky Alexey Alexandrovich passed away.

Alexei Alexandrovich was one of the greatest theoretical physicists, known worldwide for his works in the field of classical and quantum theory of gravitaty, cosmology and relativistic astrophysics. Together with Ya. B. Zeldovich, Alexey Alexandrovich calculated the number of particles and the mean value of the energy-momentum tensor of quantum fields in the homogeneous anisotropic cosmological model. Together with him he demonstrated to Stephen Hawking that according to the uncertainty principle of quantum mechanics rotating black holes should generate and emit particles. Together with Yu. N. Parijsky and others, he discovered fluctuations in the temperature of relic radiation. Together with Alan Guth and Andrei Linde he is the founder of the theory of the early Universe with a de-sitter (inflationary) stage. His most important results in this field are: the first calculation of the spectrum of gravitational waves generated at the inflationary stage, the first consistent model of the inflationary scenario, the first (simultaneously but independently of Hawking and Guth) quantitatively correct calculation of the density perturbation spectrum, the theory of stochastic inflation, the theory of matter warming up in the Universe after the end of the inflationary stage, the theory of transition from the quantum description of primary inhomogeneities to the classical one.

The scientist has been a corresponding member of the Russian Academy of Sciences since 1997, an academician of the Russian Academy of Sciences since 2011, and a member of the German National Academy of Sciences "Leopoldina"since 2010. In 2017, he was elected a foreign member of the US National Academy of Sciences.

The scientist was awarded the Medal of the Order "For Merit to the Fatherland"II degree (2009), the USSR Medal "For Labor Valor"(1986), awarded the Gold Medal of A.D. Sakharov RAS (2016), the A.A. Friedman Medal of Perm State University (2013), the V.Y. Struve Commemorative Medal (2019), the CPRF Central Committee Commemorative Medal "300 years of M.V. Lomonosov laureate of the

A.D. Friedman Prize. A.A. Friedman of the Russian Academy of Sciences (1996), laureate of the MAIC Prize "Science/Interperiodica"(2004). Alexey Aleksandrovich has been awarded the most prestigious international awards: the Kavli Prize in Astrophysics from the Norwegian Academy of Natural Sciences and Humanities, the Norwegian Ministry of Education and Science, and the Kavli Foundation - the highest award in world astrophysics (2014, together with A. Guth and A.D. Lin. Guth and A. D. Linde); Dirac Prize (2019, Italy, together with V. F. Mukhanov and R. A. Syunyaev) - considered the most prestigious award in theoretical and mathematical physics; Gruber Foundation International Prize (USA) - the world's highest award in cosmology (2013, together with V. F. Mukhanov); Amaldi Medal from the Italian Society for General Relativity and Gravitational Physics SIGRAV (2012, together with V.F. Mukhanov); International Prize of the Thomall Foundation (Switzerland) for outstanding contributions to general relativity and gravitation (2009, together with V.F. Mukhanov); title of the International Prize of the Thomall Foundation (Switzerland) for outstanding contributions to general relativity and gravitation (2009, together with V.F. Mukhanov). Mukhanov); title of Officer of the National Order of Academic Palms (2017, France); O. Klein Medal from the Royal Swedish Academy of Sciences with an invitation to deliver the Oskar Klein Memorial Lecture (2010); Isaac Pomeranchuk International Prize in Theoretical Physics (2021).

Alexey Alexandrovich has prepared 4 professors (including members of three national academies of sciences of India) and 16 doctors, PhDs and candidates of sciences. He is the author of more than 300 scientific papers.

Alexey Aleksandrovich was a member of the editorial board of the journals "Letters in ZhETF "Letters in Astronomical Journal "Gravitation and Cosmology "International Journal of Modern Physics D "Journal of Cosmology and Astroparticle Physics "Classical and Quantum Gravity "General Relativity and Gravitation "Physical Review D as well as a member of the scientific committees of most well-known international conferences in the field of gravitation, cosmology and astrophysics. Since 2017, he has been the President of the Russian Gravitational Society.

Since 2023, Alexey Alexandrovich has chaired the International Scientific Committee of the conference "Physical Interpretations of Relativity Theory PIRT-2023 which brings together scientists from different countries and continents, and was the head of the International Youth Summer School on Gravitation, Cosmology and Astrophysics ISGCA-2023, which are traditionally held at Bauman Moscow State Technical University with the support of the Russian Academy of Sciences, Lomonosov Moscow State University and other Russian and foreign universities.

One of the latest scientific events organized by Alexey Aleksandrovich was the autumn International Scientific Conference "Space. Time. Civilization. STC-2023 which was held in Egypt jointly by RAS, Bauman Moscow State Technical University and Birla Institute of Technology and Science, Pilani. At the opening of the conference Alexey Alexandrovich noted that all the reports unite the general scientific approach, which combines the theoretical point of view of logic and reason with the point of view of experimental use of what is now called such a fashionable word as "artifacts these are those objects that have reached us from the past. Using these artifacts plus our logic, we learn the past of our universe, of our civilization. And, of course, the common problem, which is exactly the same for historians and archaeologists on the one hand, and for cosmologists on the other hand, is that we have to verify and prove, which is not easy, that these artifacts are really authentic, that they did not originate in later times.

These words emphasize the breadth of Alexei Alexandrovich's interests, his belief in the boundless process of cognition and unite many researchers around his personality of a Scientist and a Man.

*International Scientific and Organizing Committees PIRT conferences*

УДК 537.8



## КВАЗИКЛАССИЧЕСКОЕ ОПИСАНИЕ ЭЛЕКТРОМАГНИТНОГО ИЗЛУЧЕНИЯ УСКОРЕННЫХ ЗАРЯДОВ*

Адорно Т. К.[a,b,1], Бреев А. И.[b,2], Гитман Д. М.[c,d,b,3]

[a] Факультет физики, Сианьский университет Цзяотун-Ливерпуль, 111 Ren'ai Road, Сучжоу, район науки и образования озера Душу, промышленный парк Сучжоу, Сучжоу, 215123, Китай.

[b] Томский государственный университет, пр. Ленина 36, Томск, 634050, Россия.

[c] Физический институт им. П. Н. Лебедева, Ленинский проспект 53, 119991, Москва, Россия.

[d] Институт физики, Университет Сан-Паулу, улица Матан, 1371, Сан-Паулу 05508-090, Бразилия.

Мы рассматриваем наши недавние результаты по электромагнитному излучению, создаваемому распределениями зарядов, в рамках квазиклассического подхода. В этом подходе токи, генерирующие излучение, рассматриваются классически, при этом точно сохраняется квантовая природа излучения. Величины, имеющие отношение к проблеме излучения, вычисляются с помощью вероятностей перехода, квантовые состояния которых электромагнитного поля имеют четко определенное число фотонов и являются решениями соответствующего уравнения Шредингера. Мы получим полную энергию и скорости, излучаемых точечных зарядов, ускоренными электромагнитными полями, и сравним полученные результаты с результатами, полученными в классической электродинамике. .

*Ключевые слова*: Классическая электродинамика, электромагнитное излучение, квантовая механика, уравнение Шредингера.

## SEMICLASSICAL DESCRIPTION OF THE ELECTROMAGNETIC RADIATION BY ACCELERATED CHARGED DISTRIBUTIONS

Adorno T. C.[a,b,1], Breev A. I.[b,2], Gitman D. M.[c,d,b,3]

[a] Department of Physics, Xi'an Jiaotong-Liverpool University, 111 Ren'ai Road, Suzhou Dushu Lake Science and Education Innovation District, Suzhou Industrial Park, Suzhou, 215123, P. R. China.

[b] Department of Physics, Tomsk State University, Lenin Ave. 36, Tomsk 634050, Russia.

[c] P. N. Lebedev Physical Institute 53 Leninskiy prospekt, 119991 Moscow, Russia.

[d] Instituto de Física, Universidade de São Paulo, Rua do Matão, 1371, São Paulo 05508-090, Brazil.

We review our recent results on the electromagnetic radiation produced by charge distributions in the framework of a semiclassical approach. In this approach, currents, generating the radiation are considered classically, while the quantum nature of the radiation is kept exactly. Pertinent quantities to the radiation problem are calculated with the aid of transition probabilities, whose quantum states of the electromagnetic field have well-defined number of photons and are solutions of the corresponding Schrödinger's equation. We summarize the calculation of the total energy and and rates radiated by point charges accelerated by electromagnetic fields and compare our results with those obtained in classical electrodynamics.

*Keywords*: Classical electrodynamics, electromagnetic radiation, quantum mechanics, Schrödinger equation.

PACS: 03.50.De, 03.70.+k, 03.65.Sq, 03.50.-z

DOI: 10.17238/issn2226-8812.2023.3-4.12-20

*The work of T. C. Adorno was supported by the XJTLU Research Development Funding, award no. RDF-21-02-056 and the work of A. I. Breev and D. M. Gitman was supported by Russian Science Foundation, grant no. 19-12-00042. D. M. Gitman thanks CNPq for permanent support.

[1]E-mail: Tiago.Adorno@xjtlu.edu.cn

[2]E-mail: breev@mail.tsu.ru

[3]E-mail: gitman@if.usp.br

## Introduction

It is known that a change in the state of motion of charged particles is usually accompanied by electromagnetic radiation. The most prominent examples are the radiation of accelerated charges performing rectilinear or circular motions. While the accurate description of the process should be carried out in the framework of $QED$ (as described in Refs. [1, 2, 3], for instance) there are numerous cases where the direct application of the $QED$ formalism leads to technical difficulties. In such cases, one usually resorts to the classical approximation, which is as follows: the motion of charged particles is considered within the framework of classical (non-relativistic or relativistic) mechanics, then using Maxwell's equations, the electromagnetic field generated by this motion is restored (for example, in the form of Liénard-Wiechert potentials), and finally, the observed electromagnetic radiation generated by the motion of the charges is calculated as the energy flux determined by the Poynting-Heaviside theorem, see, e.g., Refs. [4, 5, 6, 7, 8]. However, it must be noted that such a way of calculating electromagnetic radiation hinges on certain assumptions; in our opinion, the most adequate discussion on this matter is in Stratton's book [9].

In this work we summarize our recent results [10, 11] on an alternative approach to calculate electromagnetic radiation by charged distributions, which does not suffer from the technical difficulties associated with the application of QED nor the assumptions underlying the classical theory. We call such a formulation the semiclassical approach. In this approach, currents generating the radiation are considered classically, whereas the quantum nature of the radiation is taken into account exactly. This possibility is based on the exact construction of quantum states of the electromagnetic field interacting with the mentioned classical currents and subsequent consistent application of $QED$ methods for calculating the radiation. Universal formulas describing multiphoton radiation were derived. The approach does not require knowledge of the exact solutions of relativistic wave equations with external fields; hence technical difficulties associated with using the Furry picture do not arise. Moreover, the semiclassical approach can be applied to any trajectory performed by the particle, even including cases with backreaction, as these can be accounted for by solving the Lorentz equations with radiation-reaction terms. We note that in the framework of the semiclassical approach, one can directly calculate the radiation emitted from any trajectory of a charged particle, whereas, in QED, the technics of calculating photon transition amplitudes (say in the Furry picture) is adopted only for charge motions caused by external electromagnetic fields. However, a univocal correspondence between every charge trajectory and a corresponding electromagnetic field does not exist. The efficacy of the semiclassical approach was demonstrated in calculating synchrotron [10] and undulator [12] radiations. In this work we consider the Minkowski spacetime, $\eta_{\mu\nu} = \operatorname{diag}(+1,-1,-1,-1)$, parameterized by coordinates $x^{\mu} = \left(x^0 = ct, \mathbf{r}\right)$. Boldface letters denote three-dimensional vectors, e.g. $\mathbf{r} = \left(x^i,\ i = 1,2,3\right)$, and three-dimensional differentials denote volume integration measures, e.g., $d\mathbf{r} = dx^1 dx^2 dx^3$. Gaussian units are used.

## 1. Semiclassical description of electromagnetic radiation induced by classical currents

The state vector $|\Psi(t)\rangle$ of the quantized electromagnetic field interacting with a classical current satisfies the Schrödinger equation and an initial condition $|\Psi\rangle_{\mathrm{in}}$ at the initial time instant $t_{\mathrm{in}}$,

$$i\hbar\partial_t |\Psi(t)\rangle = \hat{H}(t) |\Psi(t)\rangle , \quad |\Psi(t_{\mathrm{in}})\rangle = |\Psi\rangle_{\mathrm{in}} . \tag{1.1}$$

Here, $\hat{H}(t)$ is the Hamiltonian of the quantized electromagnetic field $\hat{A}^{\mu}(x) = \left(A^0(x), \hat{\mathbf{A}}(\mathbf{r})\right)$ interacting with a classical four-current $j^{\mu}(x) = \left(j^0(x), \mathbf{j}(x)\right)$. The potential $\hat{\mathbf{A}}(\mathbf{r})$ splits into a transverse $\hat{\mathbf{A}}_{\perp}(\mathbf{r})$ and longitudinal parts $\hat{\mathbf{A}}_{\parallel}(\mathbf{r})$:

$$\begin{aligned}
&\hat{\mathbf{A}}(\mathbf{r}) = \hat{\mathbf{A}}_{\perp}(\mathbf{r}) + \hat{\mathbf{A}}_{\parallel}(\mathbf{r}) \ , \\
&\hat{\mathbf{A}}_{\perp}(\mathbf{r}) = \delta_{\perp}\hat{\mathbf{A}}(\mathbf{r}) , \quad \hat{\mathbf{A}}_{\parallel}(\mathbf{r}) = (1-\delta_{\perp})\hat{\mathbf{A}}(\mathbf{r}) \ , \\
&\operatorname{div}\hat{\mathbf{A}}_{\perp}(\mathbf{r}) = 0, \quad \operatorname{curl}\hat{\mathbf{A}}_{\parallel}(\mathbf{r}) = 0 \ ,
\end{aligned}$$

in which $\delta_{\perp}^{sp} = \delta^{sp} - \Delta^{-1}\partial^{s}\partial^{p}$ denotes the transverse projection operator, $(\delta_{\perp}\hat{A}(\mathbf{r}))^{s} = \delta_{\perp}^{sp}A^{p}(\mathbf{r})$ (see Refs. [3, 13]). Sticking to the Coulomb gauge – in which the longitudinal degree of freedom of $\hat{\mathbf{A}}(\mathbf{r})$ is absent and only transverse photons are present – $\hat{\mathbf{A}}(\mathbf{r}) = \hat{\mathbf{A}}_{\perp}(\mathbf{r})$, and the scalar potential $A^{0}(x)$ is a non operatorial solution of the Poisson equation,

$$\Delta A^{0}(x) = -\frac{4\pi}{c}j^{0}(x) \rightarrow A^{0}(x) = \frac{1}{c}\int \frac{j^{0}(t,\mathbf{r}')}{|\mathbf{r}-\mathbf{r}'|}d\mathbf{r}' \,, \tag{1.2}$$

while the operator of the vector potential $\hat{\mathbf{A}}(\mathbf{r})$ reads:

$$\begin{aligned}
&\hat{\mathbf{A}}(\mathbf{r}) = \sqrt{4\pi\hbar c}\sum_{\lambda=1}^{2}\int\left[\hat{c}_{\mathbf{k}\lambda}\mathbf{f}_{\mathbf{k}\lambda}(\mathbf{r}) + \hat{c}_{\mathbf{k}\lambda}^{\dagger}\mathbf{f}_{\mathbf{k}\lambda}^{*}(\mathbf{r})\right]d\mathbf{k}\,,\\
&\mathbf{f}_{\mathbf{k}\lambda}(\mathbf{r}) = \frac{e^{i\mathbf{kr}}\boldsymbol{\epsilon}_{\mathbf{k}\lambda}}{\sqrt{2k_{0}(2\pi)^{3}}}\,, \quad k^{\mu} = \left(k_{0} = \frac{\omega}{c}, \mathbf{k}\right), \quad k_{0} = |\mathbf{k}|\,.
\end{aligned} \tag{1.3}$$

Here, $\hat{c}_{\mathbf{k}\lambda}^{\dagger}$ and $\hat{c}_{\mathbf{k}\lambda}$ are creation and annihilation operators of free photons with wave vector $\mathbf{k}$ and polarizations $\lambda$,

$$\left[\hat{c}_{\mathbf{k}\lambda}, \hat{c}_{\mathbf{k}'\lambda'}^{\dagger}\right]_{-} = \delta_{\lambda\lambda'}\delta(\mathbf{k}-\mathbf{k}')\,, \quad [\hat{c}_{\mathbf{k}\lambda}, \hat{c}_{\mathbf{k}'\lambda'}]_{-} = \left[\hat{c}_{\mathbf{k}\lambda}^{\dagger}, \hat{c}_{\mathbf{k}'\lambda'}^{\dagger}\right]_{-} = 0\,, \tag{1.4}$$

while $\boldsymbol{\epsilon}_{\mathbf{k}\lambda}$ are complex polarization vectors that obey the orthogonality and completeness relations:

$$\boldsymbol{\epsilon}_{\mathbf{k}\lambda}\boldsymbol{\epsilon}_{\mathbf{k}\lambda'}^{*} = \delta_{\lambda\lambda'}\,, \quad \boldsymbol{\epsilon}_{\mathbf{k}\lambda}\mathbf{k} = 0, \quad \sum_{\lambda=1}^{2}\epsilon_{\mathbf{k}\lambda}^{i}\epsilon_{\mathbf{k}\lambda}^{j*} = \delta^{ij} - n^{i}n^{j}\,, \quad n^{i} = \frac{k^{i}}{|\mathbf{k}|}\,. \tag{1.5}$$

The Hamiltonian $\hat{H}(t)$ reads:

$$\begin{aligned}
\hat{H}(t) &= \hat{H}_{\gamma} + \frac{1}{c}\int\left[\frac{1}{2}j_{0}(x)A^{0}(x) - \mathbf{j}(x)\hat{\mathbf{A}}(\mathbf{r})\right]d\mathbf{r}\,,\\
\hat{H}_{\gamma} &= \hbar c\sum_{\lambda=1}^{2}\int k_{0}\hat{c}_{\mathbf{k}\lambda}^{\dagger}\hat{c}_{\mathbf{k}\lambda}d\mathbf{k}\,.
\end{aligned} \tag{1.6}$$

One can demonstrate that a solution of equation (1.1) can be written as

$$|\Psi(t)\rangle = U(t,t_{\mathrm{in}})\,|\Psi\rangle_{\mathrm{in}}\,, \tag{1.7}$$

where the evolution operator $U(t,t_{\mathrm{in}})$ has the form [10, 11],

$$\begin{aligned}
&U(t,t_{\mathrm{in}}) = e^{i\phi(t,t_{\mathrm{in}})}U_{\gamma}(t,t_{\mathrm{in}})\,\mathcal{D}(y)\,,\\
&\mathcal{D}(y) = \exp\sum_{\lambda=1}^{2}\int\left[y_{\mathbf{k}\lambda}(t,t_{\mathrm{in}})\,\hat{c}_{\mathbf{k}\lambda}^{\dagger} - y_{\mathbf{k}\lambda}^{*}(t,t_{\mathrm{in}})\,\hat{c}_{\mathbf{k}\lambda}\right]d\mathbf{k}\,,\\
&y_{\mathbf{k}\lambda}(t,t_{\mathrm{in}}) = i\sqrt{\frac{4\pi}{\hbar c}}\int_{t_{\mathrm{in}}}^{t}dt'\int\mathbf{j}(x')\,\mathbf{f}_{\mathbf{k}\lambda}^{*}(x',t_{\mathrm{in}})\,d\mathbf{r}'\,.
\end{aligned} \tag{1.8}$$

and $\phi(t,t_{\mathrm{in}})$ is a phase.

With this solution we can calculate transition amplitudes and probabilities between states with a definite number of photons. For example, the transition probability that the vacuum state $|0\rangle = |\Psi\rangle_{\mathrm{in}}$ evolves to a state with $N$ photons

$$|\{N\}\rangle = \frac{1}{\sqrt{N!}}\prod_{a=1}^{N}\hat{c}_{\mathbf{k}_{a}\lambda_{a}}^{\dagger}|0\rangle\,, \tag{1.9}$$

after a time interval $\Delta t = t - t_{\mathrm{in}}$ reads [11]:

$$\begin{aligned} P\left(\{N\};t,t_{\mathrm{in}}\right) &= \left|\langle\{N\}\left|\Psi\left(t\right)\rangle\right|^{2} \\ &= \frac{1}{N!}\prod_{a=1}^{N}\left|y_{\mathbf{k}_a\lambda_a}\left(t,t_{\mathrm{in}}\right)\right|^{2}\exp\left[-\sum_{\lambda=1}^{2}\int\left|y_{\mathbf{k}\lambda}\left(t,t_{\mathrm{in}}\right)\right|^{2}d\mathbf{k}\right]. \end{aligned} \tag{1.10}$$

From the above probability and the energy of $N$ photons

$$W\left(\{N\}\right) = \hbar c\sum_{a=1}^{N}k_{0,a}\,, \quad k_{0,a} = \left|\mathbf{k}_a\right|\,, \tag{1.11}$$

the observe that the total electromagnetic energy of $N$ photons radiated by the current, $W\left(N;t,t_{\mathrm{in}}\right)$, is the sum of energies (1.11) weighted by the probability $P\left(\{N\};t,t_{\mathrm{in}}\right)$:

$$\begin{aligned} W\left(N;t,t_{\mathrm{in}}\right) &= \prod_{a=1}^{N}\sum_{\lambda_a=1}^{2}\int d\mathbf{k}_a W\left(\{N\}\right)P\left(\{N\};t,t_{\mathrm{in}}\right) \\ &= \frac{W\left(1;t,t_{\mathrm{in}}\right)}{\left(N-1\right)!}\left[\sum_{\lambda=1}^{2}\int\left|y_{\mathbf{k}\lambda}\left(t,t_{\mathrm{in}}\right)\right|^{2}d\mathbf{k}\right]^{N-1}. \end{aligned} \tag{1.12}$$

The prefactor $W\left(1;t,t_{\mathrm{in}}\right)$ denotes the electromagnetic energy of one photon radiated by the external current

$$W\left(1;t,t_{\mathrm{in}}\right) = \hbar cP\left(0;t,t_{\mathrm{in}}\right)\sum_{\lambda=1}^{2}\int k_0\left|y_{\mathbf{k}\lambda}\left(t,t_{\mathrm{in}}\right)\right|^{2}d\mathbf{k}\,. \tag{1.13}$$

Finally, summing Eq. (1.12) over all the photons, we obtain the *total* electromagnetic energy radiated by the external current:

$$W\left(t,t_{\mathrm{in}}\right) = \sum_{N=1}^{\infty}W\left(N;t,t_{\mathrm{in}}\right) = \hbar c\sum_{\lambda=1}^{2}\int k_0\left|y_{\mathbf{k}\lambda}\left(t,t_{\mathrm{in}}\right)\right|^{2}d\mathbf{k}\,. \tag{1.14}$$

With these results, we may define the rate at which energy is emitted from the source by differentiating Eq. (1.14) with respect to time:

$$w\left(t,t_{\mathrm{in}}\right) = \frac{\partial W\left(t,t_{\mathrm{in}}\right)}{\partial t} = 2\hbar c\mathrm{Re}\sum_{\lambda=1}^{2}\int k_0\left[y_{\mathbf{k}\lambda}\left(t,t_{\mathrm{in}}\right)\frac{\partial}{\partial t}y^{*}_{\mathbf{k}\lambda}\left(t,t_{\mathrm{in}}\right)\right]d\mathbf{k}\,. \tag{1.15}$$

Equations (1.14) and (1.15) can be alternatively expressed in terms of the current density distribution $\mathbf{j}\left(\mathbf{r}\right)$. To this end, we substitute the function $y_{\mathbf{k}\lambda}\left(t,t_{\mathrm{in}}\right)$ given by Eq. (1.8) into Eqs. (1.14), (1.15) and simplify the summations over $\lambda$ with the aid the identities (1.5) to finally obtain:

$$\begin{aligned} W\left(t,t_{\mathrm{in}}\right) &= 4\pi^{2}\int\left|\mathbf{n}\times\left[\mathbf{n}\times\tilde{\mathbf{j}}\left(k;t,t_{\mathrm{in}}\right)\right]\right|^{2}d\mathbf{k}\,, \\ w\left(t,t_{\mathrm{in}}\right) &= 2\left(2\pi\right)^{3/2}\mathrm{Re}\int e^{-ik_0ct}\left\{\tilde{\mathbf{j}}^{*}\left(\mathbf{k};t\right)\tilde{\mathbf{j}}\left(k;t,t_{\mathrm{in}}\right)\right. \\ &- \left.\left[\mathbf{n}\tilde{\mathbf{j}}^{*}\left(\mathbf{k};t\right)\right]\left[\mathbf{n}\tilde{\mathbf{j}}\left(k;t,t_{\mathrm{in}}\right)\right]\right\}d\mathbf{k}\,. \end{aligned} \tag{1.16}$$

where

$$\tilde{\mathbf{j}}\left(k;t,t_{\mathrm{in}}\right) = \frac{1}{\sqrt{2\pi}}\int_{t_{\mathrm{in}}}^{t}e^{ik_0ct'}\tilde{\mathbf{j}}\left(\mathbf{k};t'\right)dt'\,, \quad \tilde{\mathbf{j}}\left(\mathbf{k};t'\right) = \frac{1}{\left(2\pi\right)^{3/2}}\int e^{-i\mathbf{k}\mathbf{r}'}\mathbf{j}\left(x'\right)d\mathbf{r}'\,. \tag{1.17}$$

The total energy, in particular, coincides with the classical result [6, 7] in the limits $t_{\mathrm{in}} \to -\infty$, $t \to +\infty$, namely,

$$W\left(+\infty,-\infty\right) = W_{\mathrm{cl}} = 4\pi^{2}\int\left|\mathbf{n}\times\left[\mathbf{n}\times\tilde{\mathbf{j}}\left(k\right)\right]\right|^{2}d\mathbf{k}\,, \tag{1.18}$$

$$\tilde{\mathbf{j}}\left(k\right) = \frac{1}{\sqrt{2\pi}}\int_{-\infty}^{+\infty}e^{ik_0ct'}\tilde{\mathbf{j}}\left(\mathbf{k};t'\right)dt'\,. \tag{1.19}$$

Here $\tilde{\mathbf{j}}\left(k\right)$ denotes the ordinary four-dimensional Fourier transform of the current density $\mathbf{j}\left(x\right)$.

## 2. Electromagnetic energies and rates radiated by accelerated charges

### 2.1. Point charge in a constant and homogeneous magnetic field

Consider a point charge (with algebraic charge $q$ and mass $m$) moving with velocity $\mathbf{v}(t)$ along a circular trajectory with radius $\mathbf{R}$ in a constant and homogeneous magnetic field $\mathbf{B} = (0,0,B)$. The corresponding current density has the form

$$j^0(x) = q\delta(\mathbf{r} - \mathbf{r}(t)) , \quad \mathbf{j}(x) = qc\boldsymbol{\beta}(t)\,\delta(\mathbf{r} - \mathbf{r}(t)) , \quad \boldsymbol{\beta}(t) = \frac{\mathbf{v}(t)}{c} , \tag{2.1}$$

where the position $\mathbf{r}(t)$ and the velocity read [8]

$$\mathbf{r}(t) = (R\cos\Omega t, R\sin\Omega t, 0) , \quad \mathbf{v}(t) = \Omega R(-\sin\Omega t, \cos\Omega t, 0) , \quad \Omega = \frac{eB}{mc} . \tag{2.2}$$

Plugging this current into Eq. (1.8) we find,

$$y_{\mathbf{k}\lambda}(t, t_{\mathrm{in}}) = -\frac{iqc}{2\pi}\frac{e^{-ik_0ct_{\mathrm{in}}}}{\sqrt{\hbar c k_0}}\int_{t_{\mathrm{in}}}^{t} e^{i\Phi(t')}\boldsymbol{\beta}(t')\,\boldsymbol{\epsilon}^*_{\mathbf{k}\lambda}dt', \quad \Phi(t') = k_0ct' - \mathbf{kr}(t') . \tag{2.3}$$

Setting $t_{\mathrm{in}} = 0$ and choosing a reference frame whose origin coincides with the center of the particle's circular trajectory, such that the wave vector $\mathbf{k}$ is parameterized by the polar $\theta$ and azimuthal $\varphi$ spherical angles, $\mathbf{k} = \left(|\mathbf{k}_\perp|\cos\varphi,\, |\mathbf{k}_\perp|\sin\varphi,\, k_\parallel\right)$, $|\mathbf{k}_\perp| = k_0\sin\theta$, $k_\parallel = k_0\cos\theta$, we obtain:

$$\begin{aligned}
y_{\mathbf{k}1}(t) &= y_{\mathbf{k}1}(t,0) = -\frac{iqR\cos\theta}{2\pi\sqrt{\hbar c k_0}}Y_{\mathbf{k}}(\varphi) \\
&\times \int_{\tau_i}^{\tau_i+\Omega t}\exp\left[i\left(\frac{ck_0}{\Omega}\tau - |\mathbf{k}_\perp|\,R\sin\tau\right)\right]\cos\tau d\tau , \\
y_{\mathbf{k}2}(t) &= y_{\mathbf{k}2}(t,0) = -\frac{iqR}{2\pi\sqrt{\hbar c k_0}}Y_{\mathbf{k}}(\varphi) \\
&\times \int_{\tau_i}^{\tau_i+\Omega t}\exp\left[i\left(\frac{ck_0}{\Omega}\tau - |\mathbf{k}_\perp|\,R\sin\tau\right)\right]\sin\tau d\tau , \\
Y_{\mathbf{k}}(\varphi) &= \exp\left[i\frac{ck_0}{\Omega}(\varphi - \pi/2)\right] .
\end{aligned} \tag{2.4}$$

To obtain these integrals, we performed a changed of variables $\Omega t' = \tau - \tau_i$, $\tau_i = \pi/2 - \varphi$, and used the following representation of the polarization vectors $\boldsymbol{\epsilon}_{\mathbf{k}1} = (\cos\varphi\cos\theta, \sin\varphi\cos\theta, -\sin\theta)$, $\boldsymbol{\epsilon}_{\mathbf{k}2} = (-\sin\varphi, \cos\varphi, 0)$. Next, using the plane-wave expansions of the Bessel functions $J_n(z)$ given by Eqs. (9.56) in [8] and performing additional manipulations as described in [10], the total electromagnetic energy (1.14) radiated by the point charge has the form [10]

$$\begin{aligned}
W(t) &= \frac{q^2\Omega^2}{2\pi}\sum_{n=-\infty}^{+\infty}\int_0^\infty dk_0\left(\frac{2}{ck_0 - n\Omega}\right)^2\sin^2\left(\frac{ck_0 - n\Omega}{2}t\right) \\
&\times \int_0^\pi \sin\theta\left[n^2J_n^2(|\mathbf{k}_\perp|\,R)\cot^2\theta + k_0^2R^2J_n'^2(|\mathbf{k}_\perp|\,R)\right]d\theta .
\end{aligned} \tag{2.5}$$

Differentiating the energy (2.5) we obtain the rate (1.15) at which energy is emitted by the source:

$$\begin{aligned}
w(t) &= \frac{q^2\Omega^2}{2\pi}\sum_{n=-\infty}^{+\infty}\int_0^\infty dk_0\frac{2\sin\left[(ck_0 - n\Omega)\,t\right]}{ck_0 - n\Omega} \\
&\times \int_0^\pi \sin\theta\left[n^2J_n^2(|\mathbf{k}_\perp|\,R)\cot^2\theta + k_0^2R^2J_n'^2(|\mathbf{k}_\perp|\,R)\right]d\theta .
\end{aligned} \tag{2.6}$$

The above expression is a generalization of the well-known Schott's formula [14], owing to the explicit dependence on time. In the semiclassical formulation, the quantum transition interval $\Delta t = t - t_{\mathrm{in}} = t$

determines the interval where radiation is formed; in other words, $\Delta t$ is the radiation formation interval. This feature is absent in the classical theory. However, in the limit where the interval $t \to \infty$ we obtain Schott's classical formula [14]:

$$
\begin{aligned}
w &= \lim_{t\to\infty} w(t) = \frac{q^2\Omega^2}{2\pi} \sum_{n=-\infty}^{+\infty} n^2 \\
&\times \int_0^{\pi} \sin\theta \left[ J_n^2\left(\frac{n\Omega R}{c}\sin\theta\right)\cot^2\theta + \left(\frac{\Omega R}{c}\right)^2 J_n'^2\left(\frac{n\Omega R}{c}\sin\theta\right)\right] d\theta\,. \quad (2.7)
\end{aligned}
$$

## 2.2. Point charge in a constant and homogeneous electric field

Consider the point charge accelerated by a constant and homogeneous electric field, $\mathbf{E} = (0, 0, E)$. The current density describing the point charge is given by Eq. (2.1). Its trajectory and velocity with initial data $\underline{\mathbf{r}} = \mathbf{r}(0) = (\underline{x}, \underline{y}, \underline{z})$, $\underline{\mathbf{v}} = \mathbf{v}(0) = (\underline{v}_x, \underline{v}_y, \underline{v}_z)$ read:

$$
\begin{aligned}
&\mathbf{r}_\perp(t) = \tilde{\mathbf{r}}_\perp + \frac{\underline{\mathbf{u}}_\perp}{\varepsilon}\operatorname{arc\,sinh}\left(\frac{\varepsilon t + \underline{u}_\parallel/c}{\varrho}\right), \quad \boldsymbol{\beta}_\perp(t) = \frac{\underline{\mathbf{u}}_\perp/c}{\sqrt{\varrho^2 + \left(\varepsilon t + \underline{u}_\parallel/c\right)^2}}, \\
&r_\parallel(t) = \underline{r}_\parallel + \frac{c}{\varepsilon}\sqrt{\varrho^2 + \left(\varepsilon t + \underline{u}_\parallel/c\right)^2}, \quad \beta_\parallel(t) = \frac{\varepsilon t + \underline{u}_\parallel/c}{\sqrt{\varrho^2 + \left(\varepsilon t + \underline{u}_\parallel/c\right)^2}}, \\
&\varepsilon = \frac{qE}{mc}, \quad \varrho = \frac{\sqrt{m^2c^2 + \underline{\mathbf{P}}_\perp^2}}{mc}, \quad \underline{\mathbf{P}}_\perp = m\underline{\mathbf{u}}_\perp, \quad \underline{\mathbf{u}} = \frac{c\underline{\boldsymbol{\beta}}}{\sqrt{1-\underline{\boldsymbol{\beta}}^2}}\,. \quad (2.8)
\end{aligned}
$$

Here, $\tilde{\mathbf{r}}_\perp = \underline{\mathbf{r}}_\perp - (\underline{\mathbf{u}}_\perp/\varepsilon)\operatorname{arc\,sinh}\left(\underline{u}_\parallel/\varrho c\right)$ and the indexes "$\perp$", "$\|$" here label components "perpendicular", "parallel" to the external field, respectively. Using the above solutions, we substitute $t'$ by $\eta'$

$$
t' = -\frac{\underline{u}_\parallel}{\varepsilon c} + \frac{\varrho}{\varepsilon}\sinh\eta'\,, \quad (2.9)
$$

and introduce three auxiliary variables $z$, $\xi$, $\nu$,

$$
z = \frac{c\varrho}{\varepsilon}|\mathbf{k}_\perp|\,, \quad \xi = \frac{1}{2}\ln\left(\frac{|\mathbf{k}| + k_\parallel}{|\mathbf{k}| - k_\parallel}\right), \quad \nu = \frac{\mathbf{k}_\perp\underline{\mathbf{u}}_\perp}{\varepsilon}, \quad |\mathbf{k}_\perp| \neq 0\,, \quad (2.10)
$$

to rewrite the phase $\Phi(t')$ (2.3) as follows

$$
\Phi(\eta') = z\sinh(\eta' - \xi) - \nu\eta' + \tilde{\mathcal{C}}\,, \quad (2.11)
$$

where $\tilde{\mathcal{C}}$ is a phase. As a result, the complex function (2.3) admits the representation

$$
\begin{aligned}
y_{\mathbf{k}\lambda}(t, t_{\text{in}}) &= -i\frac{qc}{2\pi}\frac{e^{-ik_0ct_{\text{in}}}e^{i\tilde{\mathcal{C}}}}{\varepsilon\sqrt{\hbar\omega}}\boldsymbol{\epsilon}^*_{\mathbf{k}\lambda}\mathbf{I}_\nu(t, t_{\text{in}})\,, \\
\mathbf{I}_\nu(t, t_{\text{in}}) &= \left(\frac{\underline{\mathbf{u}}_\perp}{c}I_\nu^{(1)}(t, t_{\text{in}})\,, \varrho I_\nu^{(2)}(t, t_{\text{in}})\right)\,, \quad (2.12)
\end{aligned}
$$

where

$$
\begin{aligned}
&I_\nu^{(1)}(t, t_{\text{in}}) = \int_{\eta_{\text{in}}}^{\eta} e^{i\left[z\sinh\left(\eta'-\xi\right)-\nu\eta'\right]}d\eta'\,, \\
&I_\nu^{(2)}(t, t_{\text{in}}) = \int_{\eta_{\text{in}}}^{\eta} e^{i\left[z\sinh\left(\eta'-\xi\right)-\nu\eta'\right]}\sinh\eta' d\eta'\,, \\
&\eta = \eta(t) = \operatorname{arc\,sinh}\left(\varepsilon t/\varrho + \underline{u}_\parallel/\varrho c\right), \quad \eta_{\text{in}} \equiv \eta(t_{\text{in}})\,. \quad (2.13)
\end{aligned}
$$

By performing a supplementary change of variable $u' = \eta' - \xi$ we may express the above integrals in terms of an "incomplete" Macdonald function,

$$K_{i\nu}(z;t,t_{\text{in}}) = \frac{e^{-\pi\nu/2}}{2}\int_{u_{\text{in}}}^{u} e^{i\phi(u')}du', \quad \phi(u') = z\sinh u' - \nu u' . \tag{2.14}$$

Finally, calculating the modulus square of Eq. (2.12) and summing the result over the photon polarizations with the aid of the identities (1.5), the total electromagnetic energy radiated by the particle (1.14) takes the form [11]:

$$\begin{aligned} W(t,t_{\text{in}}) &= \left(\frac{qc}{\varepsilon\pi}\right)^2 \int e^{\pi\nu}\left\{\left[\left(1-\frac{\nu^2}{z^2}\right)\varrho^2 - 1\right]\left|K_{i\nu}(z;t,t_{\text{in}})\right|^2\right. \\ &+ \left.\varrho^2\left|S_{i\nu}(z;t,t_{\text{in}})\right|^2\right\}d\mathbf{k}, \end{aligned} \tag{2.15}$$

where

$$\begin{aligned} S_{i\nu}(z;t,t_{\text{in}}) &= K'_{i\nu}(z;t,t_{\text{in}}) - \frac{1}{z}\frac{k_\parallel}{|\mathbf{k}|}\dot{K}_{i\nu}(z;t,t_{\text{in}}) , \\ K'_{i\nu}(z;t,t_{\text{in}}) &= \partial_z K_{i\nu}(z;t,t_{\text{in}}) , \end{aligned}$$

and

$$\begin{aligned} \dot{K}_{i\nu}(z;t,t_{\text{in}}) &= \partial_\xi K_{i\nu}(z;t,t_{\text{in}}) \\ &= \begin{cases} e^{-\pi\nu/2}\frac{e^{i(z\sinh u_{\text{in}} - \nu u_{\text{in}})} - e^{i(z\sinh u - \nu u)}}{2} & \text{if } -\infty < t_{\text{in}} < t < +\infty , \\ 0 & \text{if } t = -t_{\text{in}} = +\infty . \end{cases} . \end{aligned}$$

This compact expression corresponds to a generalization of the classical differential energy due to its dependence on time; cf. Eq. (16) in Ref. [15]. In the limit $t \to \infty$, $t_{\text{in}} \to -\infty$, we recover the result obtained by Nikishov and Ritus in classical theory [15]:

$$W = \lim_{\Delta t\to\infty} W(t,t_{\text{in}}) = \left(\frac{qc}{\varepsilon\pi}\right)^2 \int e^{\pi\nu}\left\{\left[\left(1-\frac{\nu^2}{z^2}\right)\varrho^2 - 1\right]K^2_{i\nu}(z) + \varrho^2 K'^2_{i\nu}(z)\right\}d\mathbf{k} .$$

It remains to discuss the energy rate emitted by the accelerated particle. Differentiating Eq. (2.15) with respect to time we find:

$$\begin{aligned} w(t,t_{\text{in}}) &= \left(\frac{qc}{\pi}\right)^2 \frac{1}{\varepsilon\varrho}\int \frac{e^{\pi\nu/2}}{\cosh\eta}\left\{\left[\left(1-\frac{\nu^2}{z^2}\right)\varrho^2 - 1\right]\text{Re}\left[e^{i\phi(u)}K^*_{i\nu}(z;t,t_{\text{in}})\right]\right. \\ &+ \left.\frac{|\mathbf{k}_\perp|}{|\mathbf{k}|}\left(\sinh\eta - \frac{\nu}{z}\frac{k_\parallel}{|\mathbf{k}_\perp|}\right)\varrho^2\text{Re}\left[ie^{i\phi(u)}S^*_{i\nu}(z;t,t_{\text{in}})\right]\right\}d\mathbf{k} . \end{aligned} \tag{2.16}$$

This equation is our main result. It expresses the electromagnetic energy radiated by the particle within the quantum transition interval $\Delta t = t - t_{\text{in}}$. Similarly to the total energy (2.15), Eq. (2.16) corresponds to a generalization of the classical energy rate radiated by the particle accelerated by the electric field. The computation of the rate simplifies considerably if we set $t_{\text{in}} \to -\infty$ and restrict ourselves to the case where the particle is subjected to the initial condition $\underline{\mathbf{v}}_\perp = \mathbf{0}$. In this case, $\varrho = 1$, $\nu = 0$, and the energy rate (2.16) assumes the form

$$\begin{aligned} &w(t)|_{\underline{\mathbf{v}}_\perp=\mathbf{0}} = \frac{2(qc)^2}{\pi\varepsilon}\tanh\eta \\ &\times\int_0^\infty d|\mathbf{k}_\perp|\,\mathbf{k}^2_\perp \int \frac{\cos(z\sinh u)\,\text{Im}K'_0(z;t) - \sin(z\sinh u)\,\text{Re}K'_0(z;t)}{\sqrt{\mathbf{k}^2_\perp + k^2_\parallel}}dk_\parallel . \end{aligned} \tag{2.17}$$

where $K'_0(z;t) = K'_0(z;t,-\infty)$. In the limit $t \to +\infty$, the integral

$$K_{i\nu}(z;t) \equiv K_{i\nu}(z;t,-\infty) = \frac{e^{-\pi\nu/2}}{2}\int_{-\infty}^{u} e^{i\phi(u')}du' . \tag{2.18}$$

becomes the Macdonald function and $\mathrm{Im}K_0'(z;+\infty)=0$, $\mathrm{Re}K_0'(z;+\infty)=K_0'(z)$. Thus, performing a supplementary change of variables and using the identity $K_0'(z)=-K_1(z)$ we finally obtain

$$w|_{\mathbf{v}_\perp=\mathbf{0}}=\lim_{t\to\infty}w(t)|_{\mathbf{v}_\perp=\mathbf{0}}=\frac{q^2\varepsilon^2}{c}\int_0^\infty K_1(z)\,z^2dz=2\frac{q^2}{c^3}a^2\,,\quad a=\frac{qE}{m}\,. \tag{2.19}$$

Except by a factor of 1/3, this result coincides with Larmor's formula for the total energy rate radiated by a uniformly accelerated charged particle [7, 16]. The absence of this factor was also pointed out in the framework of the classical theory by Nikishov and Ritus in Ref. [15].

## 3. Conclusion

In this work we addressed the problem of the electromagnetic radiation produced by charge distributions in a semiclassical approach, in which the radiation field is quantum while current densities–sources of radiation–are regarded classically. In this formulation, pertinent electromagnetic quantities, such as energies and energy rates radiated by currents, are calculated with the aid of transition probabilities between states with a well-defined number of photons. Assuming the vacuum as the initial state, we calculated time-dependent one-photon, multi-photon, total electromagnetic energies and the rate at which the radiation is emitted from the source. We discovered that our formulas for the total energy and rate are compatible with the corresponding classical results in the limit where the quantum transition interval tends to infinity. To illustrate the use of the semiclassical approach, we summarized our recent results on the synchroton radiation [10] and the radiation by a charged particle in rectilinear accelerated motion [11]. We conclude this work by emphasizing that the semiclassical approach offers an alternative description of physical systems interacting with background fields. Despite being an approximation compared to QED, the semiclassical formulation exactly incorporates the quantum character of the electromagnetic field. For this reason, this theory allows extracting information about electromagnetic properties stemming from the interaction between radiation and matter beyond the reach of classical electrodynamics.

## Список литературы/References


1. Heitler, W. *The quantum theory of radiation.* Courier Corporation, 1984.
2. Schweber, Silvan S. *An introduction to relativistic quantum field theory.* Courier Corporation, 2013.
3. N. N. Bogoliubov and D. V. Shirkov, *Introduction to the Theory of Quantized Fields*, 3rd Ed. (John Wiley & Sons, New York 1980).
4. Poynting, J. H. "On the transfer of energy in the electromagnetic field."Proceedings of the Royal Society of London 36.228-231 (1883): 186-187.
5. Heaviside, O. "The induction of currents in cores."Electrician 13, 1884, 133.
6. L. D. Landau and E. M. Lifshitz, *The classical theory of fields* (Pergamon Press, Oxford 1971).
7. J. D. Jackson, *Classical Electrodynamics* (John Wiley & Sons, New York 1999).
8. A. A. Sokolov, I. M. Ternov, *Synchrotron Radiation* (Academic Verlag, Berlin 1968); *Radiation from relativistic electrons*(American Institute of Physics, New York 1986).
9. J. A. Stratton, *Electromagnetic Theory* (McGraw-Hill, New York 1941).
10. V. G. Bagrov, D. M. Gitman, A. A. Shishmarev and A. J. D. Farias, Quantum states of an electromagnetic field interacting with a classical current and their applications to radiation problems, *J. Synchrotron Rad.* **27**, 902 (2020).
11. T. C. Adorno, A. I. Breev, A. J. D. Farias, and D. M. Gitman, Electromagnetic radiation of accelerated charged particle in the framework of a semiclassical approach, *Ann. Phys.* (Berlin) **2023**, 2300118, 2023.

12. A. A. Shishmarev, A. D. Levin, V. G. Bagrov, D. M. Gitman, Semiclassical Description of Undulator Radiation, *JETPh* **132**, (2) 247 (2021).
13. W. Greiner, J. Reinhardt, *Field Quantization* (Springer, Berlin 1996).
14. G. A. Schott, On the radiation from moving systems of electrons, and on the spectrum of canal rays, *Phil. Mag.* **13**, 657 (1907).
15. A. I. Nikishov and V. I. Ritus, Radiation spectrum of an electron moving in a constant electric field, *Zh. Eksp. Teor. Fiz.* **56**, 2035 (1969) [*Sov. Phys. JETP* **29**, 1093 (1969)].
16. J. Larmor, On the theory of the magnetic influence on spectra; and on the radiation from moving ions, *Phil. Mag.* **44**, No. 271, 503 (1897).

**Авторы**

**Тьяго Карлос Адорно де Фрейтас**, к.ф.-м.н., доцент, Факультет физики, Сианьский университет Цзяотун-Ливерпуль, 111 Ren'ai Road, Сучжоу, район науки и образования озера Душу, промышленный парк Сучжоу, Сучжоу, 215123, Китай.
E-mail: Tiago.Adorno@xjtlu.edu.cn

**Александр Игоревич Бреев**, к.ф.-м.н., доцент кафедры теоретической физики ФФ, Томский государственный университет, пр. Ленина 36, Томск, 634050, Россия.
E-mail: breev@mail.tsu.ru

**Дмитрий Максимович Гитман**, д.ф.-м.н., профессор, Физический институт им. П. Н. Лебедева, Ленинский проспект 53, 119991, Москва, Россия; Институт физики, Университет Сан-Паулу, улица Матан, 1371, Сан-Паулу 05508-090, Бразилия; Томский государственный университет, пр. Ленина 36, Томск, 634050, Россия.
E-mail: gitman@if.usp.br

**Просьба ссылаться на эту статью следующим образом:**

Адорно Т. К., Бреев А. И., Гитман Д. М. Квазиклассическое описание электромагнитного излучения ускоренных зарядов. *Пространство, время и фундаментальные взаимодействия.* 2023. № 3-4. С. 12–20.

**Authors**

**Tiago Carlos Adorno de Freitas**, Ph.D., Assistant Professor, Department of Physics, Xi'an Jiaotong-Liverpool University, 111 Ren'ai Road, Suzhou Dushu Lake Science and Education Innovation District, Suzhou Industrial Park, Suzhou, 215123, P. R. China.
E-mail: Tiago.Adorno@xjtlu.edu.cn

**Alexander Igorevich Breev**, Ph.D., Associate Professor, Department of Physics Tomsk State University Lenin Ave. 36, Tomsk 634050, Russia.
E-mail: breev@mail.tsu.ru

**Dmitri Maximovich Gitman**, Ph.D., Full Professor, P. N. Lebedev Physical Institute 53 Leninskiy prospekt, 119991 Moscow, Russia; Instituto de Física, Universidade de São Paulo, Rua do Matão, 1371, São Paulo 05508-090, Brazil; Department of Physics Tomsk State University Lenin Ave. 36, Tomsk 634050, Russia.
E-mail: gitman@if.usp.br

**Please cite this article in English as:**

Adorno T. C., Breev A. I., Gitman D. M. Semiclassical description of the electromagnetic radiation by accelerated charged distributions. *Space, Time and Fundamental Interactions*, 2023, no. 3-4, pp. 12–20.

УДК 530.12; 530.51



## МОДЕЛЬ ОТКРЫТОЙ ВСЕЛЕННОЙ С КОСМОЛОГИЧЕСКОЙ ПОСТОЯННОЙ КАК ЗАДАЧА О ДВИЖЕНИИ ЧАСТИЦЫ В СИЛОВОМ ПОЛЕ

Баранов А. М.[a,1], Савельев Е. В.[b,2]

[a] ФГБОУ ВПО Красноярский государственный педагогический университет им.В.П.Астафьева (КГПУ), г. Красноярск, 660049, Россия
[b] ООО “ПРОФИЛЬ - 2С", Москва, 123007, Россия

Рассмотрена возможность нахождения точных космологических решений уравнений Эйнштейна с космологической постоянной для открытой модели вселенной путем сведения проблемы к эквивалентной задаче о движении массивной частицы в силовом поле. Взятая космологическая модель заполнена материей в приближении идеальной жидкости с отличными от нуля давлением и космологической постоянной, вообще говоря. Метрика четырехмерного пространства-времени берется в форме Фока как метрика, конформная метрике Минковского с зависимостью от одной переменной, квадрат которой есть произведение опережающего и запаздывающего времен. Использование механической интерпретации для уравнений тяготения приводит к возможности рассмотрения различных силовых полей, в частности потенциальных, с последующей физической интерпретацией получаемых точных космологических решений. Прежде всего, рассматривается движение свободной частицы единичной массы (механическая сила отсутствует), то есть частица движется по инерции. Конформный множитель космологической конформно-плоской метрики есть четвертая степень найденного закона движения. Этот случай при отсутствии космологической постоянной соответствует точному космологическому решению без давления, совпадающему с известным решением Фридмана для открытой Вселенной. Затем рассматривается силовой потенциал в виде линейной функции. Полученное точное космологическое решение, асимптотически описывает как некогерентную пыль, так и ультрарелятивистскую материю, которую можно было бы интерпретировать как равновесное излучение. Далее в качестве потенциала выбирается квадратичная функция без линейного члена и постоянной. Такой потенциал можно интерпретировать как потенциал свободного осциллятора отвечающего линейной по смещению силе (силе Гука). Решение соответствующего уравнения движения записывается в виде функции косинуса с некоторой начальной фазой, связанной с отношением параметров, определяющих пылевидную и ультрарелятивистскую материю. Этот вывод становится очевиден после асимптотического рассмотрения давления и плотности энергии. Космологическая модель оказывается обобщением решения Фридмана с равновесным излучением и веществом, которые заполняют вселенную. Рассмотрены примеры моделей при наличии космологического члена.

*Ключевые слова*: Открытые космологические модели, «механический» подход к конструированию космолологических моделей, космологическая постоянная.

## THE OPEN UNIVERSE MODEL WITH THE COSMOLOGICAL CONSTANT AS A PARTICLE MOVEMENT TASK IN A FORCE FIELD

Baranov A. M.[a,1], Saveljev E. V.[b,2]

[a] Krasnoyarsk State Pedagogical University named after V.P.Astafyev, Krasnoyarsk, 60049, Russia
[b] LLC "PROFILL - 2S", Moscow, 123007, Russia

The possibility of deriving of exact cosmological solutions of the Einstein equations with the cosmological constant for the open universe model by reducing the problem to an equivalent task of the movement of a mass particle in the force field is considered. Taken cosmological model is filled by substance in an approximation of the perfect fluid with nonzero pressure and cosmological constant, generally speaking. A four-dimensional space-time metric is taken in Fock's form as the metric, conformal to the Minkowski metric. This metric depends on one variable. A square of the variable is a product of advanced and retarded times. The using of mechanical interpretation of

[1]E-mail: alex_m_bar@mail.ru
[2]E-mail: profill07@mail.ru

the gravitation equations leads to a possibility of consideration of various force fields, in particular the potential fields, with the subsequent physical interpretation of found exact cosmological solutions. First of all the movement of free particle with an unit mass (a mechanical force is absent) is considered, that is to say the particle moves on inertia. The fourth degree of finded law of movement is a conformal factor of cosmological conformally-flat metric. This case corresponds to the exact cosmological solution without cosmological constant and pressure, coinciding with known the Friedman solution for the open universe. After that the force potential is taken in the form of linear function. Found exact cosmological solution asymptotically describes both an incoherent dust, and the ultra-relativistic matter which could be interpreted as an equilibrium radiation. Further a square-law function without a linear term and a stationary value is taken as a potential. Such potential can be interpreted as potential of the free oscillator corresponding to linear shift force (Hooke's force). The solution of corresponding equation of motion is written in the form of a cosine function with some initial phase related to the correlation of parameters which define dust-like and ultra-relativistic matter. The cosmological model is the generalization of Friedman's model with the equilibrium radiation and substance which fill the universe. Examples of models in the presence of the cosmological constant are considered.

*Keywords*: The open universe models, a "mechanical" approach to the construction of cosmological models, the cosmological constant.

PACS: 04.20.-q; 98.80.Jk

DOI: 10.17238/issn2226-8812.2023.3-4.21-29

**Введение**

В настоящей работе в псевдоримановом 4D пространстве, конформном 4D пространству Минковского с метрикой в записи Фока [1]

$$ds^2 = g_{\mu\nu}dx^\mu dx^\nu = \exp(2\sigma)\,\eta_{\mu\nu}dx^\mu dx^\nu, \tag{0.1}$$

где $\eta_{\mu\nu} = diag(1,-1,-1,-1)$; $\sigma = \sigma(S)$; $S^2 = \eta_{\mu\nu}x^\mu x^\nu = t^2 - r^2$; $\mu,\nu = 0,1,2,3$; рассматривается возможность моделирования открытых космологических моделей Вселенной без указания конкретного уравнения состояния путем введения функции состояния, которая для каждого значения $S$ представляет собой уравнение состояния. Скорость света и гравитационная постоянная Ньютона взяты равными единице. Уравнения Эйнштейна с источником в приближении тензора энергии импульса (ТЭИ) идеальной паскалевой жидкости и с космологическим членом записываются как [2]

$$G_{\mu\nu} + \varkappa\lambda g_{\mu\nu} = -\varkappa T_{\mu\nu} = -\varkappa(\varepsilon\cdot u_\mu u_\nu + p\cdot b_{\mu\nu}) \tag{0.2}$$

или

$$G_{\mu\nu} = -\varkappa(T_{\mu\nu} + \lambda g_{\mu\nu}) = -\varkappa((\varepsilon + p)\cdot u_\mu u_\nu - (p-\lambda)\cdot g_{\mu\nu}), \tag{0.3}$$

где $\varepsilon$ – плотность энергии, $p$ – давление , $\lambda$ – космологическая постоянная, $\lambda > 0$.

Трехмерное пространство, ортогональное к временной конгруэнции и определяемое 3-проектором $b_{\mu\nu} = u_\mu u_\nu - g_{\mu\nu}$ с четырехмерной скоростью $u_\mu = (exp(\sigma))\cdot b_\mu$ ; $b_\mu = S_{,\mu}$ ; $b_\nu b^\nu = 1$ , является сферически симметричным.

После расщепления уравнений Эйнштейна путем проектирования их на временноподобное направление и пространственноподобную 3-площадку система уравнений сводится к уравнениям (штрихом обозначена производная по $S$)

$$\exp(-2\sigma)(\frac{2}{S}\sigma' + (\sigma')^2) = \varkappa(\varepsilon + \lambda), \tag{0.4}$$

$$2\,\exp(-2\sigma)(\sigma'' + \frac{2}{S}\sigma' + \frac{1}{2}(\sigma')^2) = -\varkappa(p-\lambda). \tag{0.5}$$

Следует отметить, что если при $\lambda = 0$ воспользоваться уравнением состояния $p = -\varepsilon$ (физический вакуум [3]), то решением приведенных уравнений оказывается вакуумно-подобным (решение де-Ситтера для метрики (0.1); см. [4, 5]): $\exp(2\sigma) = (1 - A\cdot S^2)^{-2}$, $A = \varkappa\,\varepsilon/12 = const$ .

Если же наоборот, положить $\lambda \neq 0$; $\varepsilon = p = 0$, то получим тоже самое решение с $A = \varkappa\lambda/12 = const$.

## 1. «Механический» подход

Тогда возникает вопрос: нужно ли вообще учитывать в полевых уравнениях лямбда-член для введения физического вакуума?

Для этого рассмотрим случай $\lambda = 0$ и введем замену $\sigma = 2\ln y$. После этого система полевых уравнений запишется как

$$12 \cdot y'(y' + \frac{1}{S}y) = \varkappa\varepsilon \cdot y^6; \tag{1.1}$$

$$4 \cdot (y'' + \frac{2}{S}y') = -\varkappa p \cdot y^5. \tag{1.2}$$

Далее произведем замены: $y = f_1(1/S) \equiv f_1(\chi)$ и $y = f_2(S)/S$, тогда полевое уравнение с давлением $p$ преобразуется к общем виду

$$\frac{d^2Y}{d\chi^2} = F(\chi, Y, p) \tag{1.3}$$

или

$$F(\chi, Y, p) = -\varkappa\frac{Y^5}{4\chi^4}p. \tag{1.4}$$

В этой записи считаем, что переменная $\chi$ может быть как переменной $1/S$, так и переменной $S$, а функция $Y$ как функцией $f_1$, так и $f_2$ .

Если переменную $\chi$ считать новой «временной» переменной, а функцию $Y$ своеобразной обобщенной пространственной «координатой» («переменной»), то получаем возможность интерпретировать выше приведенное уравнение как уравнение Ньютона (2-й закон Ньютона) для одномерного движения частицы единичной массы под действием силы $F(\chi, Y, p)$.

Мы легко найдем конформный множитель $\exp(2\sigma) = Y^4$ и интересующие нас величины в открытой космологической модели, если будем знать силу F и проинтегрируем "уравнение движения". При этом конкретному «механическому» движению частицы единичной массы будет соответствовать конкретная эволюция Вселенной. Силовая функция может зависеть и от скорости, например, при описании осциллятора с диссипацией.

Считая переменную $\chi$ новой «временной» переменной, а функцию $Y$ своеобразной обобщенной пространственной «координатой» («переменной»), получаем возможность интерпретировать выше приведенное уравнение как уравнение Ньютона (2-й закон Ньютона) для одномерного движения частицы единичной массы под действием силы $F(\chi, Y, p)$, зная которую, и интегрируя уравнение, легко находим конформный множитель $\exp(2\sigma) = Y^4$ и интересующие нас величины в открытой космологической модели. При этом конкретному «механическому» движению частицы единичной массы будет соответствовать конкретная эволюция Вселенной. Силовая функция может зависеть и от скорости, например, при описании осциллятора с диссипацией.

Таким образом, появляется возможность *замены проблемы моделирования эволюции открытой Вселенной на эквивалентную ей задачу о механическом движении частицы единичной массы в некотором силовом поле.*

Наиболее распространенными являются потенциальные силовые поля, когда $F = -\dfrac{dU}{dY}$. Тогда получаем уравнение «движения» в виде $\varkappa p = 4\dfrac{\chi^4}{Y^5}\dfrac{dU}{dY}$ , и давление оказывается напрямую связанным с выбором потенциальной функции $U$.

Следует отметить, что второе полевое уравнение в этом случае становится определением плотности энергии $\varepsilon$.

Остановимся теперь подробней на первой замене с $\chi = \dfrac{1}{S}$ и $Y = f_1$ .

**2. Открытая космологическая модель Фридмана**

Движение по инерции есть простейший пример движения, для которого сила $F = 0$. Тогда в такой «механистической» интерпретации открытая космологическая модель Фридмана [6] с давлением $p = 0$ будет отвечать равномерному движению и решению $Y = 1 - A\chi \equiv 1 - \dfrac{A}{S}$ ; $A > 0$ , где постоянная $A$ с одной стороны есть постоянная «скорость» (в данной интепретации), а с другой, это постоянная связанная с плотностью вещества, заполняющую фридмановскую Вселенную.

Конформный множитель совпадает с известным выражением для открытой фридмановской модели [1, 7]

$$\exp(2\sigma) = Y^4 = \left(1 - \frac{A}{S}\right)^4. \tag{2.1}$$

**3. Фридмана-подобная модель с излучением**

Другой пример -– это квадратичный потенциал для осциллятора

$$U = \frac{B^2 Y^2}{2} + U_0, \tag{3.1}$$

где $B^2$ – аналог коэффициента жесткости осциллятора.

Из уравнения «движения» сразу получаем решение

$$Y(\chi) = \sqrt{(1 + A^2/B^2)} \cdot \cos(B\chi + \alpha_0) = \frac{\cos(B\chi + \alpha_0)}{\cos\alpha_0}, \tag{3.2}$$

согласованное с решением Фридмана для открытой космологической модели и асимптотическим поведение на бесконечности ($S \to \infty$); при этом $\tan^2(\alpha_0) = \dfrac{A^2}{B^2}$ и

$$p \approx 4B^2\chi^4 = \frac{1}{3}\,\varepsilon_{rad}; \tag{3.3}$$

$$\varepsilon \approx \varepsilon_{dust} + \varepsilon_{rad}. \tag{3.4}$$

Таким образом, в асимптотике получаем реликтовое космологическое равновесное излучение.

**4. Функция состояния космологической модели с излучением**

Введем функцию состояния $\beta = \dfrac{p}{\varepsilon}$, которая после введения безразмерной переменной $z = B\chi$ может быть представлена как

$$\beta(z) = \frac{1}{3}\frac{z \cdot ctg(\varphi(z))}{(1 + z \cdot tg(\varphi(z)))}, \tag{4.1}$$

где $\varphi(z) = z + \alpha_0$.

Функция состояния имеет два корня:

$$z_1 = \frac{\pi}{2} - \alpha_0\,; \qquad z_2 = 0. \tag{4.2}$$

Поведение функции состояния $\beta$ может быть представлено в зависимости от переменной $1/z$ (см. Fig1) и переменной $z$ (см. Fig2) следующими графиками:

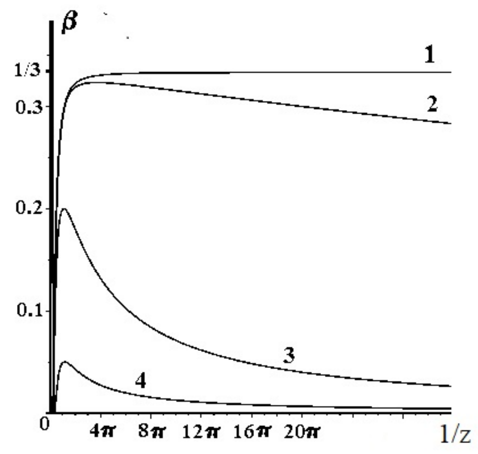


**Рис. 1.** Поведение функции состояния $\beta(z)$ открытой космологической модели в зависимости от $1/z$ в присутствии только равновесного излучения (1) и в присутствии массовой материи и излучения (2, 3).

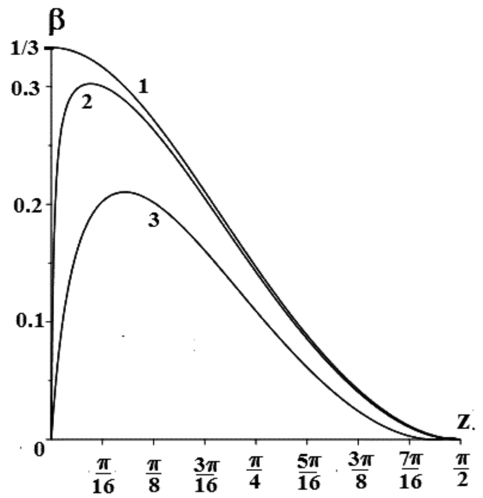


**Рис. 2.** Поведение функции состояния $\beta(z)$ открытой космологической модели в зависимости от $z$ в присутствии только равновесного излучения (1) и в присутствии массовой материи и излучения (2, 3).

## 5. «Квази-де ситтеровская» модель

Перейдем теперь к рассмотрению случая с $Y = f_2(S)$ , то есть теперь

$$\exp(2\sigma) = \frac{Y^4}{S^4} = y^4. \tag{5.1}$$

Выберем убывающий параболический потенциал

$$U = -\frac{\Omega^2 Y^2}{2}, \tag{5.2}$$

где $\Omega = const$ (аналог собственной частоты осциллятора).

Квадратура уравнения «движения» запишется в виде

$$Y = \frac{\sqrt{2E}\cdot\sinh(\Omega S)}{\Omega} \quad \text{или} \quad y = \frac{\sqrt{2E}\cdot\sinh(\Omega S)}{\Omega S}, \tag{5.3}$$

где $E = const$ (аналог энергии).

Тогда для давления

$$\varkappa p = \frac{\Omega^2}{E^2} \left(\frac{\Omega S}{\sinh(\Omega S)}\right)^2 \to -\frac{\Omega^2}{E^2}, \quad when\ S \to 0. \tag{5.4}$$

С другой стороны, для плотности энергии получаем

$$\varkappa\varepsilon = 3 \cdot |p| \coth(\Omega S)^2 \left(1 - \frac{\tanh(\Omega S)}{\Omega S}\right) \to \frac{\Omega^2}{E^2}, \quad when\ S \to 0. \tag{5.5}$$

Следовательно, в «начале» ($S = 0$) выбранный потенциал (5.2)) требует состояния физического вакуума, $p_{vac} = -\varepsilon_{vac}$. Поэтому в окрестности «начала» должно быть состояние де Ситтера с конформным фактором

$$\exp(2\sigma) = y^4 = \frac{1}{\left(1 - \widetilde{A} \cdot S^2\right)^2}. \tag{5.6}$$

Тогда функция состояния в этом случае запишется как

$$\beta(S) = \frac{p}{\varepsilon} = \frac{1}{3} \frac{(\Omega S) \cdot \tanh(\Omega S)^2}{(\Omega S - \tanh(\Omega S))} \tag{5.7}$$

с $\lim\limits_{S\to 0} \beta(S) = -1$ и $\lim\limits_{S\to\infty} \beta(S) = -\dfrac{1}{3}$.

Соответствующие графики поведения этой функции принимают следующий вид вблизи «окрестности» нуля (начала) (Fig.3) и асимптотически на бесконечности (Fig.4)

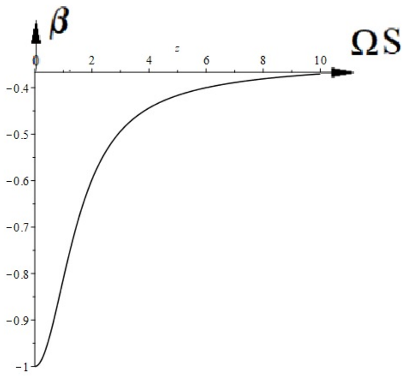


**Рис. 3.** Поведение функции состояния $\beta$ открытой космологической модели де Ситтера в зависимости от переменной $\Omega S$ вблизи «окрестности» начала.

Таким образом, данное решение описывает чисто вакуумное состояние. Все это указывает на то, что «механический» подход не позволяет получить единое космологическое решение, объединяющее обычную «горячую» модель Вселенной и вакуумное решение.

В данном случае имеем как бы внешнюю задачу (для фридмана-подобных решений) и обособленную внутреннюю задачу (квази де ситтеровское решение), то есть получаем «разрыв» в полном описании Вселенной.

Следовательно, удалось обойтись без $\lambda$-члена для введения вакуумного состояния, которое было получено в виде точного решения уравнений Эйнштейна без космологического члена. Это решение в «начале» эволюции модели ($S = 0$ ) совпадаем с решением де Ситтера (уравнение состояния $p_{vac} = -\varepsilon_{vac}$).

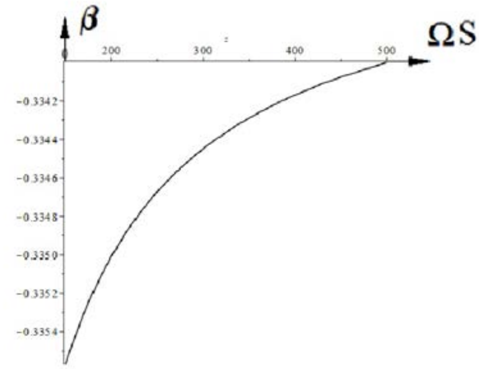


**Рис. 4.** Поведение функции состояния $\beta$ открытой космологической модели де Ситтера в зависимости от переменной $\Omega S$ асимптотически на бесконечности.

### 6. Введение космологической постоянной в «механическую» модель

Вернемся к случаю учета космологического члена, то есть теперь выберем $\lambda \neq 0$.

Если ввести новые величины для плотности энергии $\mathcal{E} = \varepsilon + \lambda$ и давления $P = p - \lambda$ (в этом можно убедиться путем проектирования ТЭИ из уравнения (0.3) на временноподобное направление и на 3-площадку, ортогональную этому временноподобному направлению), то гравитационные уравнения (0.3) можно переписать как

$$G_{\mu\nu} = -\varkappa \widehat{T}_{\mu\nu}, \tag{6.1}$$

где источником гравитационного поля оказывается новый ТЭИ для «идеальной паскалевой жидкости» с учетом $\lambda-$члена

$$\widehat{T}_{\mu\nu} = \mathcal{E} \cdot u_\mu u_\nu + P \cdot b_{\mu\nu}. \tag{6.2}$$

Другими словами, введение космологического члена не меняет структуры ТЭИ для идеальной паскалевой жидкости, если $\lambda-$член связать с источником гравитационного поля.

Уравнения Эйнштейна (1.1)-(1.2) тогда могут быть переписаны с $\widehat{T}_{\mu\nu}$ из формулы (6.2). Уравнение «движения» (1.3)-(1.4) в этом случае переписывается с учетом нового давления $P$, а «определение» плотности энергии (1.1) через $\mathcal{E}$.

**A**. Если теперь рассмотреть отсутствие силы $F(\chi, Y, P) = 0$ (выбрать потенциал $U = const$), что соответствует «инерциальному» движению частицы единичной массы, то получим $P = 0$ (Фридмана-подобная космологическая модель в данном случае) или $p = \lambda = const$. Следует отметить, что $p$ – физически наблюдаемое давление. В пределе $S \to \infty$, когда плотность энергии $\mathcal{E} = 0$, то $\varepsilon = -\lambda$ или $p = -\varepsilon$.

Соответствующее формальное решение уравнения «движения» равно $Y = c - a \cdot \chi$ , где $c$ и $a$ суть некоторые произвольные постоянные. Без ограничения общности можно записать $\widehat{Y} = 1 - \widehat{A} \cdot \chi$, введя $\widehat{Y} = Y/c$; $\widehat{A} = a/c$ ; $\widehat{\sigma} = \sigma - \ln(c)$, что допускают гравитационные уравнения, куда входит только производная от $\sigma$. Следовательно, судя по полученному решению, имеем открытую «модель Фридмана», с учетом космологической постоянной. В самом деле, величина $\varkappa\lambda$ имеет следующий порядок величины: $\varkappa\lambda \approx 10^{-56}\,\dfrac{1}{\text{см}^2}$, то есть требование движения по инерции гипотетической частицы требует реализации космологической модели с $\varkappa p$ порядка величины $\varkappa\lambda$. Поэтому из-за такой малости космологического члена $\varkappa p \approx 0$, то есть фактически реализуется открытая модель Фридмана.

**B**. Перейдем к рассмотрению случая с потенциалом гармонического осциллятора (3.1), но с новым коэффициентом жесткости $\widehat{B}$,

$$\widehat{U} = \frac{\widehat{B}^2 \widehat{Y}^2}{2} = b^2 \frac{B^2 Y^2}{2} = b^2 \cdot U, \tag{6.3}$$

где $b = const$, то есть вводится масштабированная потенциальная функция $U$ из (3.1).

Тогда решение уравнение для осциллятора можно записать аналогично как (3.2)

$$Y(z) = \sqrt{(1 + A^2/\widehat{B}^2)} \cdot \cos(z + \gamma_0) = \frac{\cos\varphi(z)}{\cos\gamma_0}, \tag{6.4}$$

где теперь $z = \dfrac{\widehat{B}}{S}, \quad \varphi(z) = z + \gamma_0$

Теперь сравним функции состояния $\beta$ при отсутствии $\lambda-$члена и его учете. Во втором случае получим

$$\widehat{\beta} = \frac{P}{\mathcal{E}} = \frac{p - \lambda}{\varepsilon + \lambda} = \beta \left( \frac{1 - \lambda/p}{1 + \lambda/\varepsilon} \right) = \frac{z}{3} \left( \frac{1 + \dfrac{3\lambda}{z}\Phi(z)}{\tan\varphi(z) \cdot (1 + z\tan\varphi(z)) - \lambda\Phi(z)} \right), \tag{6.5}$$

где

$$\Phi(z) = \frac{\varkappa \widehat{B}^2}{12 z^3} Y(z)^4. \tag{6.6}$$

Очевидно, что при $\lambda = 0$ получаем соотношение (4.1). Кроме того, при $z = 0$ ($S \to \infty$) имеем $\widehat{\beta} = -1$. Как и в случае с моделью Фридмана при учете космологической постоянной, предельным фоном на $S = \infty$ оказывается субстанция с уравнением состояния физического вакуума.

## 7. Заключение

Проанализирована возможность полуения точных космологических решений уравнений Эйнштейна с космологическим членом и необходимость введения этого члена для получения решений уравнений Эйнштейна для описания физического вакуума.

При этом путем сведения проблемы нахождения точных решений гравитационных уравнений для открытой модели вселенной к эквивалентной задаче о движении массивной частицы в силовом поле получен ряд результатов. Тензор энергии-импульса исследуемых космологических моделей берется в приближении идеальной жидкости с отличными от нуля давлением. Для записи метрики использована метрика в форме Фока, конформная метрике Минковского. механической интерпретации для уравнений тяготения приводит к возможности рассмотрения различных силовых полей, в частности потенциальных, с последующей физической интерпретацией получаемых точных космологических решений. В частности, такая интерпретация (без космологического члена) позволяет рассматривать открытую модель Фридмана как соответствующую инерциальному движению материальной частицы (силовое воздействие отсутствует). При наличии упругой силы (силы Гука) рассмотрение свободного осциллятора приводит к обобщению решения Фридмана при наличии равновесного излучения.

Кроме того, в «механическом» подходе не удается построить единое космологическое решение, объединяющее как «горячую» модель Вселенной и вакуумное решение. Приведены примеры конструирования моделей с космологическим членом: решение Фридмана и его обобщение с излучением. В этих случаях показано, что предельным фоном на $S = \infty$ оказывается материя с уравнением состояния физического вакуума.

## Список литературы/References

1. Fock V.A. *The Theory of Space, Time and Gravitation.* New York:, Pergamon Press, 1964. 460 p.

2. Einstein A. Zum kosmologischen Problem der allgemeinen Relativitätstheorie. *Akad. Wiss., phys-math.* 1931, pp. 235-237.
3. Gliner É.B. Algebraic properties of the energy-momentum tensor and vacuum-like states of matter. *Sjviet Physics JETP*. 1965. V. 22, no. 2, pp. 378-382.
4. Baranov A.M., Saveljev E.V. Exact solutions of the conformally flat Universe. I. The evolution of model as the problem about a particle movement in a force field. *Space, Time and Fundamental Interactions*. 2014. no.1, pp. 37-46 (in Russian).
5. Baranov A.M., Saveljev E.V. Exact solutions of the conformally flat Universe. I. The evolution of model as the problem about a particle movement in a force field. *Space, Time and Fundamental Interactions*. 2020, no. 3, pp. 27–36.
6. Friedman A.A. Über die Möglichkeit einer Welt mit konstanter negativer Krümmung des Raumes. *Z. Phys.*. 1924. V. 21, Lief., no. 1, pp. 326–333.
7. Mitskievich N.V. *Physical Fields in General Relativity.* Moskow: Nauka, 1969. 563 p. (in Russian)

**Авторы**

**Баранов Александр Михайлович**, д.ф.-м.н., профессор, кафедра физики и методики обучения физике, ФГБОУ ВПО Красноярский государственный педагогический университет им.В.П.Астафьева (КГПУ), ул. Ады Лебедевой, 89, г. Красноярск, 660049, Россия
E-mail: alex_m_bar@mail.ru

**Савельев Евгений Викторович**, к.ф.-м.н., доцент, ООО “ПРОФИЛЬ - 2С”, 78, Хорошевское шоссе, Москва, 123007, Россия.
E-mail: profill07@mail.ru

**Просьба ссылаться на эту статью следующим образом:**

Баранов А. М., Савельев Е. В. Модель открытой вселенной с космологической постоянной как задача о движении частицы в силовом поле . *Пространство, время и фундаментальные взаимодействия.* 2023. № 3-4. С. 21–29.

**Authors**

**Baranov Alexandre Mikhailovich**, Doctor of Physics and Mathematics, Professor, Department “Physics and Methods of Physics Training”, Krasnoyarsk State Pedagogical University named after V.P.Astafyev, 89 Ada Lebedeva St., Krasnoyarsk, 660049, Russia
E-mail: alex_m_bar@mail.ru

**Saveljev Evgeniy Viktorovich**, Candidate of Phys.-Mat. Sci, Assistent Professor, LLC "PROFILL - 2S", 78, Khoroshevskoe sh., Moscow, 123007, Russia.
E-mail: profill07@mail.ru

**Please cite this article in English as:**

Baranov A. M., Saveljev E. V. The open universe model with the cosmological constant as a particle movement task in a force field . *Space, Time and Fundamental Interactions*, 2023, no. 3-4, pp. 21–29.

УДК 521.9, 52.08



# ФИЛЬТРАЦИЯ ЭФФЕКТА ГРАВИТАЦИОННОГО СДВИГА ЧАСТОТЫ ДЛЯ СИГНАЛОВ РАДИОСВЯЗИ СО СПУТНИКАМИ ЗЕМЛИ

Белоненко А. В.[a,1], Гурин Ф. С.[a,2], Руденко В. Н.[a,3], Гусев А. В.[a,4], Кулагин В. В.[a,5], Попов С. М.[a,6], Манучарян Г. Д.[b,a,7]

[a] ГАИШ МГУ, Университетский пр., 13, Москва, 119992, Россия.

[b] МГТУ им. Н.Э. Баумана, г. Москва, 105005, Россия.

В статье представлен конкретный метод измерения гравитационного сдвига частоты радиосигналов связи между космическим кораблем и наземными станциями слежения. Он основан на алгоритме максимального правдоподобия и использует предел Крамера-Рао для оценки точности обнаружения параметров сигнала. Численный пример иллюстрирует эффективность метода. Оно осуществляется с использованием банка данных, полученных в ходе миссии «Радиоастрон». Внимание сосредоточено на компенсации релятивистского эффекта Доплера и частотных шумов используемых в эксперименте стандартов.

*Ключевые слова*: ОТО, тест ППЭ, РадиоАстрон.

# FILTERING OF THE GRAVITATIONAL FREQUENCY SHIFT EFFECT FOR RADIO COMMUNICATION SIGNALS WITH THE EARTH SATELLITES

Belonenko A. V.[a,1], Gurin F. S.[a,2], Rudenko V. N.[a,3], Gusev A. V.[a,4], Kulagin V. V.[a,5], Popov S. M.[a,6], Manucharyan G. D.[b,a,7]

[a] SAI MSU, Moscow,119992, Russia.

[b] Bauman Moscow State Technical University, Moscow, 105005, Russia.

The paper presents a some specific method of the gravitational frequency shift measurement for communication radio signals between the spacecraft and ground tracking stations. It is based on the maximum likelihood algorithm and utilizes the Cramér-Rao bound to estimate the accuracy of signal parameter determination. It is carried out with the bank of data obtained during the “Radioastron” mission. Attention is concentrated at a compensation of the relativistic Doppler effect and frequency noises of the standards used in the experiment.

*Keywords*: Test of general relativity, Einstein Equivalence Principle, RadioAstron.

PACS: 95.10, 95.55

DOI: 10.17238/issn2226-8812.2023.3-4.30-37

## Introduction

A possible violation of the equivalence principle can be checked by measuring by checking the deviation of the predicted gravitational “redshift” from the measured one:

$$\frac{\Delta f_{grav}}{f} = \frac{\Delta U}{c^2}(1+\varepsilon), \tag{0.1}$$

[1]E-mail: av.belonenko@physics.msu.ru
[2]E-mail: fedor.gurin@mail.ru
[3]E-mail: rvn@sai.msu.ru
[4]E-mail: mta-kuskovo@mail.ru
[5]E-mail: victorvkulagin@yandex.ru
[6]E-mail: serg@sai.msu.ru
[7]E-mail: gevorgbek.manucharyan@gmail.com

where $\Delta f_{grav}/f$ - is the gravitational clock shift, $\Delta U$ is the difference in the gravitational potential between them, $c$ is the speed of light, and $\varepsilon$ is the phenomenological parameter of GR violation. High-precision measurement of the violation parameter is the goal of the experiment described in this paper. If the epsilon parameter turns out to be zero, we can consider the theory correct. To carrying out such an experiment, the RadioAstron satellite was used[4], equipped with a highly stable frequency and time standard, as well as on-board equipment for data exchange with tracking stations. For the first time, the idea of a space experiment to measure gravitational "redshift" was implemented in a specialized Gravity-Probe A mission[3]. Compensation of the Doppler effect was carried out online, due to the simultaneous operation of the one-way and two-way modes. The result of the experiment was the confirmation of the theory with an accuracy of $1.4 \times 10^{-4}$. The best result in the space experiment was obtained in the GALILEO experiment [5][6]. In this paper we present a description of the compensation of various noise coherent effects in the measurement of the gravitational frequency shift with the Radioastron spacecraft. The hardware complex of the spacecraft allowed operating in two communication modes: "1-way" and "2-way". "1-way" (satellite → GTS (ground tracking station)) communication mode is a signal based on the onboard H-maser frequency standard. "2-way" (GTS→satellite→GTS ) the mode is synchronized by the ground H-maser frequency standard. The scheme of these operating modes is shown in the figure: A spacecraft launched into an evolving high eccentricity orbit around Earth with geocentric distances

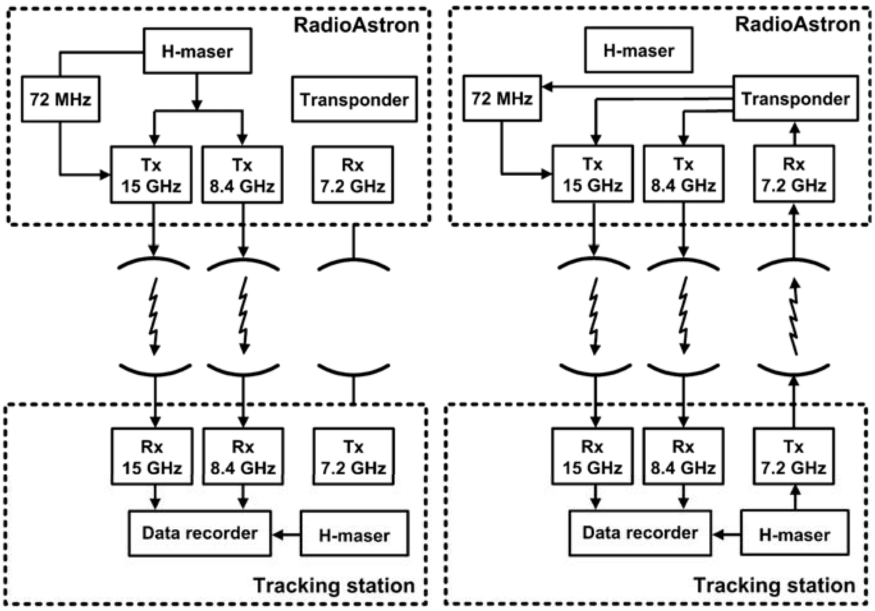


(a) 1way Mode (b) 2way Mode

**Рис. 1.** Scheme of operating modes

reaching 353000km, see fig. 2.

The total duration of the operation of the satellite operation was occupied the period from the launch in 2011 to 2018. Special gravity sessions of approximately an hour duration with interleaved "1-way" and "2-way" mode were held from 2015 to 2018, when the onboard hydrogen frequency standard finished working. The presence of two signal transmission modes allowed for complete compensation of the first-order Doppler effect by interpolating the signal in 2way mode over sections of 1way mode. The signal was transmitted at two frequencies (8.4 GHz and 15GHz), the initial frequency estimation of the signal at the station was conducted using a regular frequency counter, which computed the signal spectrum with short signal interval divisions every 40 milliseconds and estimated the signal frequency with an accuracy of up to 2 mHz. These data were used in [7], in which the influence of the frequency noise of the on board frequency standard was considered. This article will consider the method of phase detection of the signal, the evaluation of its accuracy, as well as the technical features of processing gravitational sessions.

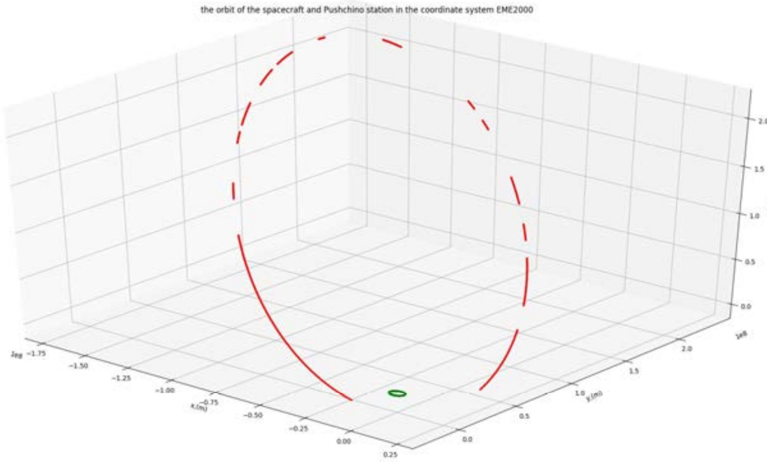


**Рис. 2.** The geocentric distance of the spacecraft (red), constructed using the data from the reconstructed orbit. The presence of gaps in the data is due to the absence of data from the reconstructed orbit.

## 1. Phase detector and Cramer-Rao bound

The concept of the experiment was based on the use of two modes of SC (spacecraft)-GTS communication to compensate for the dominant Doppler effect of the 1st order. The signal was transmitted from a ground tracking station at a frequency of 7.2075 GHz, taking into account the correction for the expected 1st Doppler effect, so as to get into the SC reception band. Then, after heterodyning, the signal was sent back to the GTS already at a frequency of 8.4 GHz and 15 GHz. At the station, the signal was again subjected to heterodyn with a frequency sampling of 32 MHz and 2-bit amplitude quantization. The signal was recorded in RDF (Radioastron Data Format) format similar to the Mark5b standard. The signal in 1w and 2w mode was recorded continuously in one file for each

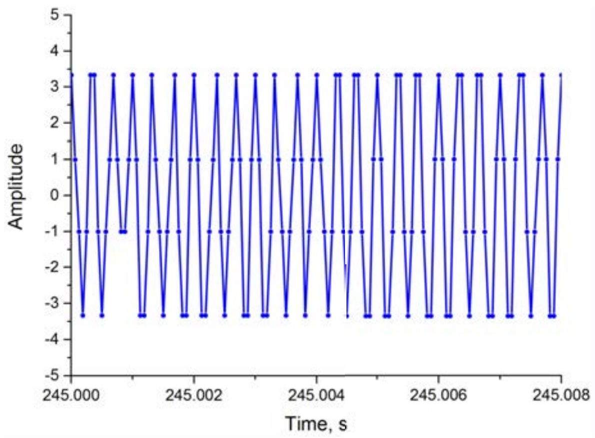


**Рис. 3.** Digital signal, 2-bit quantization, decrease SNR less than 1%

session, so it was necessary to divide the input recording into separate files according to their operating modes. For this task we used the library baseband[1] and information about switching the operating mode from the session's cyclogram. Recording in 1w mode lasted 80 seconds, in 2w mode 120 seconds. The phase detection algorithm assumes a narrowing of the signal band and the use of a bandpass filter. At

[1]https://doi.org/10.5281/zenodo.1214268

the output, we obtained a recording of a narrowband signal with a sampling frequency of 4 kHz and with subtracted frequency drift, which was then used in the phase detection algorithm. To extract the

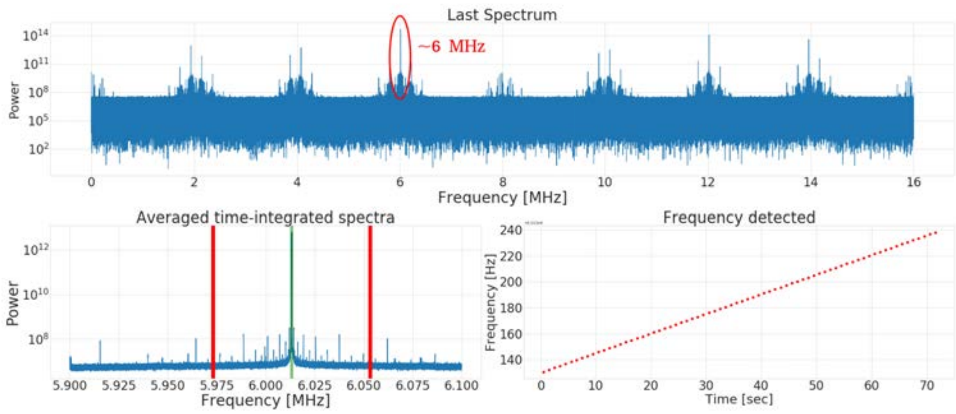


**Рис. 4.** The upper graph shows one of the spectra plotted on a one-second interval, at a frequency of about 6 MHz; the main tone is highlighted by which the signal frequency is determined. The lower-left graph shows the average signal spectrum over all intervals. In the red borders, we consider that there is noise, in the green borders, the signal. The lower right graph shows the dependence of frequency on time, each point corresponds to a frequency determined by the maximum in the spectrum.

phase from the temporal recording of the signal, it is necessary to convert it into an analytical form, which was done using the Hilbert transform. Next, we isolated the quadrature components of the signal by computing the signal's phase and unwrapping it.[2]. As a result, we estimated the instantaneous phase of the signal, which needs to be fitting by a polynomial, the degree of which was chosen taking into account the maneuverability of the SC and the frequency noise of the SHM (spacecraft H-Maser). To calculate the errors of the coefficients of the resulting polynomial, we used the Cramer-Rao bound.[10] Let's consider a mixture of signal and noise at the input of the receiver

$$y(t) = S(t, \mathbf{a}) + n(t), \quad 0 < t < T, \tag{1.1}$$

$S(t, \mathbf{a})$ is a useful narrowband signal, the spectrum of which is concentrated in a narrow band:

$$\Delta\omega = (\omega_2 - \omega_1) \ll \omega_0 = (\omega_1 + \omega_2)/2 \tag{1.2}$$

$$< n(t)n(t+\tau) >= N\delta(\tau) - \text{gaussian white noise} \tag{1.3}$$

Primary information processing (discrete time):

$$\left.\begin{array}{ccc} y(t) & \rightarrow & ||\Psi_0 \dots \Psi_m||^T \\ \Psi_k & = & \varphi_d(t_k) + \eta(t_k) + \varphi_n(t_k) \end{array}\right\} SNR = \frac{A^2}{\sigma^2} \gg 1 \tag{1.4}$$

where $\varphi_d(t_k)$ Doppler frequency shift on the k interval, $\eta(t_k)$ - frequency noise, $\sigma^2$ - varianc of additive noise $n(t)$ in the band $(\omega_1, \omega_2)$.

In matrix form:

$$\begin{array}{c} \vec{\Psi} = ||\Psi_0 \dots \Psi_m||^{\mathrm{T}} = \vec{S}_\varphi + \vec{n}_\varphi \\ \vec{S}_\varphi \quad = ||\varphi_d(t_0) \dots \varphi_d(t_m)||^T - \text{is a useful signal} \end{array} \tag{1.5}$$

depending on the vector parameter $\mathbf{a} = ||a_0, \ \dots \ , a_L||^{\mathrm{T}}$,

$$\varphi_d(t) = \sum_{i=0}^{L} a_i t^i \tag{1.6}$$

[2] https://numpy.org/doc/stable/reference/generated/numpy.unwrap.html

$\vec{n}_f$ - discrete Gaussian noise, with a correlation matrix $\vec{K}_\varphi$:

$$\vec{K}_\varphi = [K_{\varphi,ij}] = \frac{1}{2}[D(t_i) + D(t_j) - D(t_i - t_j)] + \frac{\sigma^2}{A^2}\delta_{ij}, \tag{1.7}$$

where $D(\tau)$ is a structural function, $\delta_i j$ is a Kronecker symbol. In the linear signal model , the elements of the Fisher information matrix are written:

$$I_{ij} = -\left\langle \frac{\partial^2 \ln \Lambda(y|\mathbf{a})}{\partial a_i \partial a_j} \right\rangle = \frac{1}{2}\frac{\partial^2 a}{\partial a_i \partial a_j} \tag{1.8}$$

$$I_{ij} = ||t_0^i \dots t_m^i|| \vec{K}_m \begin{Vmatrix} t_0^j \\ \vdots \\ t_m^j \end{Vmatrix} \tag{1.9}$$

Fischer information matrix:

$$I = \begin{Vmatrix} I_{11} & I_{12} & I_{13} \\ I_{21} & I_{22} & I_{23} \\ I_{31} & I_{32} & I_{33} \end{Vmatrix} \to I^{-1} = \begin{Vmatrix} \sigma^{\mathbf{2}}_{\mathbf{11}} & \cdot & \cdot \\ \cdot & \sigma^{\mathbf{2}}_{\mathbf{22}} & \cdot \\ \cdot & \cdot & \sigma^{\mathbf{2}}_{\mathbf{33}} \end{Vmatrix} \tag{1.10}$$

The formulas 1.9, 1.10 define the Cramer-Rao variance of unknown parameters in the presence of frequency noise, which are taken into account in the structural function $D(\tau)$. After processing all the accumulated data that does not have artifacts in the record, sessions with an SNR greater than 50 db. they give an estimate of the variance of the coefficients of the polynomial at a level less than $2 \times 10^{-4}$, which in turn gives a potential possibility to estimate the error of $\varepsilon$ no less than $4 \times 10^{-5}$.

## 2. Relativistic Doppler effect

To calculate the second-order Doppler effect, it is necessary to know the coordinates, speed and acceleration of the Pushchino station and spacecraft in the EME2000 system. Since these data are provided in the ITRF system, it was necessary to transform to the EME2000 coordinate system, in which the coordinate and velocity of the spacecraft are given. Geodetic coordinates have been converted to EME2000 using the SOFA library [11]. We used the pysofa2 python library[3] which had to be supplemented with the necessary function wrappers. Using the *pvtob* function, the coordinates and velocity of the Pushchino station in CIRS were obtained, then the transition matrix from GCRS to CIRS was called using the *c2ixys* function, transposed using the *tr* function built into the sofa library and multiplied by the coordinates and velocities of the Pushchino station in CIRS. We get the coordinates in GCRS, and then we get the matrix (frame bias) using the *pn06* function, multiply by the coordinates in GCRS and get the coordinates in EME2000. The EME2000 coordinate system is close to GCRS, the difference between these coordinate systems on the Earth's surface is 0.7 m. The difference consists in determining the position of the earth's axis of rotation (z axis). The acceleration of the station was obtained by taking the numerical derivative.

The coordinates and velocity of the Pushchino station in CIRS, *pvtob*

↓

The transition matrix from GCRS to CIRS, *c2ixys* → *tr* → *pn06*

The compensatory switching scheme allowed for the compensation of the effect without taking the acceleration of the spacecraft into account.[12] In the 1-way mode, the received signal on the GTS had a frequency offset:

$$\frac{\Delta f_{1w}}{f_{nominal}} = -\frac{\dot{D}}{c} + \frac{\Delta U}{c^2} + \frac{|\vec{v}_e - \vec{v}_s|^2}{2c^2} + \frac{\vec{D} \cdot \vec{a}_s}{c^2} + \frac{\Delta f_{ion}}{f^2} + \frac{\Delta f_{3rd}}{f_{nominal}} \tag{2.1}$$

[3]https://pypi.org/project/pysofa/

where $\dot{D}$ is the rate of change in the magnitude of the range vector $\vec{D}$, also called range rate, and $\vec{a}_s$ is the acceleration of the spacecraft. $\frac{\Delta f_{3rd}}{f_{nominal}}$ includes effects of the third order of smallness, including the effect of the movement of the phase center.

In the “2-way” mode, the formula for the signal frequency offset had the form:

$$\frac{\Delta f_{2w}}{f_{nominal}} = -2\frac{\dot{D}}{c} + 2\frac{|\vec{v}_e - \vec{v}_s|^2}{2c^2} + 2\frac{\vec{D}\cdot\vec{a}_s}{c^2} - 2\frac{\vec{D}\cdot\vec{a}_e}{c^2} + \frac{\Delta f_{2w,ion}}{f^2} + \frac{\Delta f_{2w,3rd}}{f_{nominal}} \tag{2.2}$$

where $\vec{a}_e$ acceleration of the ground tracking station and $\frac{\Delta f_{2w,3rd}}{f_{nominal}}$ small effects similar to 2.1. The characteristic of this mode is the absence of the gravitational frequency shift we need, while the signal “2-way” undergoes a double Doppler and troposphere frequency shift compared to “1-way”, and also contains doubled contributions of propagation atmospheric noise and a number of instrumental effects. This makes it possible to compensate for these effects using complex data processing “1-way” and “2-way” and, that avoid the need to evaluate these effects from orbital data.

The combination of “1-way” and “2-way” communication modes gives:

$$\frac{\Delta f_{1w}}{f_{nominal}} - \frac{1}{2}\cdot\frac{\Delta f_{2w}}{f_{nominal}} = \frac{\Delta U}{c^2} - \frac{|\vec{v}_e - \vec{v}_s|^2}{2c^2} + \frac{\vec{D}\cdot\vec{a}_s}{c^2} + \frac{\Delta f_{ion}}{f^2} + \frac{\Delta f_{3rd}}{f_{nominal}} \tag{2.3}$$

In the last term, the residual effects of the troposphere, ionosphere, the movement of the phase center and the Doppler effect of the third order of smallness remain. To achieve the desired accuracy, it is necessary to take into account the relative frequency shifts up to $10^{-15}$, including the third-order terms of $\frac{v}{c}$

To compensate for the relativistic Doppler effect, we need to know the parameters that are given in this formula:

$$\frac{\Delta f_{Doppler}}{f} = -\frac{|\vec{v}_e - \vec{v}_s|^2}{2c^2} + \frac{(\vec{D}\cdot\vec{a}_e)}{c^2} \tag{2.4}$$

The calculation of the effect for one complete orbit allows us to estimate the limiting values for the contribution of the relativistic Doppler effect to the frequency shift see 5.

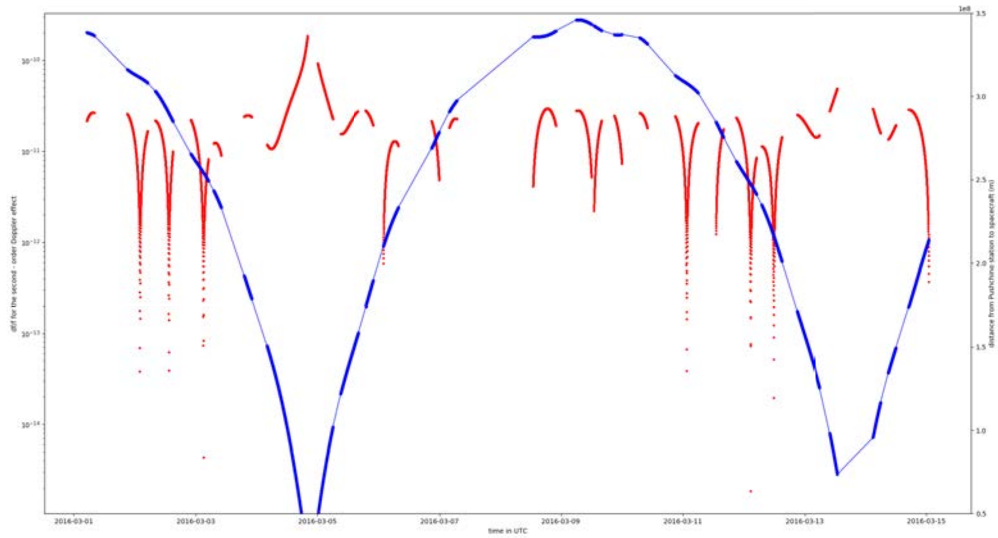


**Рис. 5.** Relativistic Doppler effect (red) against the background of geocentric distance (blue), gravity sessions were chosen in such a way as to avoid measurements near the perigee of the orbit.

The error in determining the velocity (1.4 mm/s) and coordinates (300 m) SC [13] allows us to compensate for the effect with accuracy $\Delta f/f < 10^{-15}$.

### 3. Measurements and conclusions

Result of processing some selected gravitational sessions are presented in the Table 1:

**Таблица 1.** Results of individual gravity sessions

| session code | SNR, db | “Redshift” offset, Hz | Cramer-Rao error, Hz | relative accuracy |
|---|---|---|---|---|
| raks17bb | 55.0 | 4.641 | 0.00041514 | 8.945e-05 |
| raks17bj | 56.0 | 5.002 | 0.00036288 | 7.255e-05 |
| raks17bk | 55.8 | 5.608 | 0.00036805 | 6.563e-05 |

The frequency of the signal obtained by this method requires further post-processing, which will include compensation for the shift of the ionosphere [14], the drift of frequency standards. The results presented in Table 1 demonstrate for the selected sessions the possibility of measuring the raw redshift effect with relative accuracy exceeding $10^{-4}$. After accumulating and processing all the measurement sessions conducted, this result could be improved, as expected. Combining sessions conducted in one orbit period provides a potential possibility to compensate for the drift of frequency standards and reduce the bound of the GR violation parameter to the level of $10^{-5}$, however, it has to be addressed.

### Список литературы/References

1. C. Misner, K. Thorne, J. Wheeler, *FRE* 1973 1 pp.236
2. N.S. Kardashev, et al, *ASR* 2013 no.57 pp.153-194
3. R. F. C. Vessot, M. W. Levine, *PRT*, 1980 no.45 pp.20-34
4. D.A. Litvinov, V.N. Rudenko, et al, *PLA*, 2018 no.3822192
5. S. Herrmann et al, *PRT*, 2018 no. 121 pp.231102
6. P. Delva et al, *PRT*, 2018 no.121 pp.231101
7. N.V.Nunes, N.Bartel et al, *ADV* 2020 no.65 pp.790-799
8. Molera Calves G. 2012, Ph.D. dissertation, Aalto University, Pub. No. 42/2012 http://lib.tkk.fi/Diss/2012/isbn9789526045818
9. P.Touboul et al,*PRT*, 2022 no.129 pp.121-126
10. A.V.Belonenko et al, *GAS*, 2021 no.27.4 pp.383-391
11. IAU SOFA Board, IAU SOFA Software Collection Issue 2021-01-25 http://www.iausofa.org
12. M. V. Sazhin et al, *Astron. Rep.* , 2010 no.54 pp. 959–973
13. M.V. Zakhvatkin et al, *Advances in Space Research*, 2021 no.65 pp.798-212
14. A.V.Belonenko et al, *Gravitational and cosmology*, 2020 no.26.2 pp.128-125

### Авторы

**Белоненко Алексей Вячеславович**, аспирант, ГАИШ МГУ, Университетский пр., 13, Москва, 119992, Россия.
E-mail: av.belonenko@physics.msu.ru

**Федор Сергеевич Гурин**, студент, ГАИШ МГУ, Университетский пр., 13, Москва, 119992, Россия.
E-mail: fedor.gurin@mail.ru

**Валентин Николаевич Руденко**, профессор, заведующий кафедры, ГАИШ МГУ, Университетский пр., 13, Москва, 119992, Россия.
E-mail: rvn@sai.msu.ru

**Гусев Андрей Викторович** , снс, ГАИШ МГУ, Университетский пр., 13, Москва, 119992, Россия.
E-mail: mta-kuskovo@mail.ru

**Кулагин Виктор Владимирович** , снс, ГАИШ МГУ, Университетский пр., 13, Москва, 119992, Россия.
E-mail: victorvkulagin@yandex.ru

**Попов Сергей Михайлович** , снс, заведующий кафедры, ГАИШ МГУ, Университетский пр., 13, Москва, 119992, Россия.
E-mail: serg@sai.msu.ru

**Манучарян Геворг Дереникович** , ассистент кафедры “Физика”, Московский государственный технический университет им. Н.Э. Баумана, ул. 2-я Бауманская, д. 5, с. 1, г. Москва, 105005, Россия. Инженер, ГАИШ МГУ, Университетский пр., 13, Москва, 119992, Россия.
E-mail: gevorgbek.manucharyan@gmail.com

**Просьба ссылаться на эту статью следующим образом:**
Белоненко А. В., Гурин Ф. С., Руденко В. Н., Гусев А. В., Кулагин В. В., Попов С. М., Манучарян Г. Д. Фильтрация эффекта гравитационного сдвига частоты для сигналов радиосвязи со спутниками Земли. *Пространство, время и фундаментальные взаимодействия.* 2023. № 3-4. С. 30–37.

**Authors**

**Belonenko Alexei Vacheslavovich**, Ph.D.,dk, SAI MSU, Universitetskiy st., 13, Moscow, 119992, Russia.
E-mail: av.belonenko@physics.msu.ru

**Gurin Fedor Sergeevich**, mag, dk, SAI MSU, Universitetskiy st., 13, Moscow, 119992, Russia.
E-mail: fedor.gurin@mail.ru

**Rudenko Valentin Nikolaevich**, prof, zavkaf, SAI MSU, Universitetskiy st., 13, Moscow, 119992, Russia.
E-mail: rvn@sai.msu.ru

**Gusev Andrei Victorovich**, senior staff scientist, SAI MSU, Universitetskiy st., 13, Moscow, 119992, Russia.
E-mail: mta-kuskovo@mail.ru

**Kulagin Victor Vladimirovich**, senior staff scientist, SAI MSU, Universitetskiy st., 13, Moscow, 119992, Russia.
E-mail: victorvkulagin@yandex.ru

**Popov Sergei Mihailovich**, senior staff scientist, SAI MSU, Universitetskiy st., 13, Moscow, 119992, Russia.
E-mail: serg@sai.msu.ru

**Manucharyan Gevorg Derenikovich**, assistant of Physics department, Bauman Moscow State Technical University, 2nd Baumanskaya st., 5c1, Moscow, 105005, Russia. Engineer, SAI MSU, Universitetskiy st., 13, Moscow, 119992, Russia.
E-mail: gevorgbek.manucharyan@gmail.com

**Please cite this article in English as:**
Belonenko A. V., Gurin F. S., Rudenko V. N., Gusev A. V., Kulagin V. V., Popov S. M., Manucharyan G. D. Filtering of the gravitational frequency shift effect for radio communication signals with the Earth satellites. *Space, Time and Fundamental Interactions*, 2023, no. 3-4, pp. 30–37.

УДК 524.8, 533.9, 620.9



# ЭЛЕКТРОН КЕРРА – НЬЮМАНА КАК АДАПТИВНАЯ СИСТЕМА

Буринский А. Я.[a,1], Измайлов Г. Н.[b,2]

[a] ИБРАЭ РАН, г. Москва, 115191, Россия.

[b] Московский авиационный институт (национальный исследовательский университет), Волоколамское ш., д. 4, г. Москва, 125993, Россия.

В предыдущей работе, развивая модель электрона как черной дыры Керра-Ньюмана (КН), мы установили двулистность суперврающегося (параметр Лоренца $\gamma \sim 1$) решения КН, интерпретируя *одетый* электрон КН как сгусток электрон-позитронного вакуума, охваченный (одетый) электронной и позитронной петлями Вильсона, затягиваемыми гравитацией. В то время как *голый* электрон КН отвечал за волновые свойства электрона, и формировался как безмассовая кольцевая струна, которая сжималась в точку и приобретала массу при релятивистском вращении. Мы получаем и анализируем новые решения КН с волновым излучением и обнаруживаем, что они соответствуют черно-белой дыре, которая не только поглощает энергию своею черной стороной, но также излучает ее своей обратной (белой) стороной, генерируя согласованные струнные возбуждения электронно-позитронного вакуума.

*Ключевые слова*: Черная дыра, квантовая гравитация, электрон, петля Вилсона.

# KERR – NEWMAN ELECTRON AS AN ADAPTIVE SYSTEM

Burinskii A. Ya.[a,1], Izmailov G. N.[b,2]

[a] IBRAE RAN, Moscow, 115191, Russia.

[b] Moscow Aviation Institute (National Research University), Volokolamskoye sh., 4, Moscow, 125993, Russia.

In a previous paper, developing the Kerr-Newman (KN) model of the electron as a black hole, we established the birefringence of the superrotating (Lorentz parameter $\gamma \sim 1$) KN solution, interpreting the KN electron as an electron-positron vacuum clot encompassed (clothed) by electron and positron Wilson loops tightened by gravity. While the *naked* electron of the KN was responsible for the wave properties of the electron, and was formed as a massless circular string, which was compressed into a point and acquired mass at relativistic rotation. We obtain and analyse new wave-radiating solutions of the KN and find that they correspond to the black-white hole, which not only absorbs energy by its black side, but also radiates it by its back (white) side, generating coordinated string excitations of the electron-positron vacuum.

*Keywords*: Black hole, quantum gravitation, electron, Wilson loop.

PACS: 11.27.+d, 04.20.Jb, 04.70.Bw

DOI: 10.17238/issn2226-8812.2023.3-4.38-47

## Введение

Проблема объединения гравитации и квантовой теории является, по-видимому, главной нерешенной проблемой современной теоретической физики. Одним из подходов к решению проблемы взаимодействия гравитации и квантовой теории является теория суперструн, в которой элементарные частицы представлены собственными частотами протяженных объектов - струнами конечных размеров – суперструнами. Базовые выводы хорошо известны и до сих пор широко обсуждаются, хотя и подвергаются критике поскольку не подтверждаются и не приносят новых результатов. Альтернативой теории суперструн является петлевая квантовая гравитация. Как отметил один

[1]E-mail: burinskii@mail.ru

[2]E-mail: izmailov@mai.ru

из основателей теории суперструн Дж. Шварц: "... с 1974 года теория суперструн перестала рассматриваться как физика частиц ... "и "... реалистичные модели элементарных частиц до сих пор кажутся далееекой мечтой ... "[1]. Третья парадигма – рассматривать черные дыры (источник гравитации) как элементарные частицы – предлагалась неоднократно с 1980 года, и с 1990-х годов она привлекла также внимание в теории суперструн. Интерес к поиску связи между черными дырами, струнами и элементарными частицами возобновился в сравнительно недавних работах [2, 3, 4, 5], и продолжается до настоящего времени [6].

Особенность этой парадигмы – в интерпретации элементарной квантовой частицы (электрона) как сверхвращающейся (параметр $\gamma \sim 1$) черной дыры Керра – Ньюмана(КН) [3, 8, 9, 10, 10, 11, 12, 13, 14, 15, 16, 17, 19, 20]. Обсуждаемое нами в [1] решение для совместимой с КЭД моделью электрона как заряженной и сверхвращающейся черной дыры (ЧД) Керра – Ньюмана (КН), имеет согласно [30**?** ] следующий вид: появляются две различные метрики формы Керра – Шильда с твистом конгруэнции Керра: $g^{+}_{\mu\nu} = \eta_{\mu\nu} + Hk^{+}_{\mu}k^{+}_{\nu}$ и $g^{-}_{\mu\nu} = \eta_{\mu\nu} + Hk^{-}_{\mu}k^{-}_{\nu}$, связанные с запаздывающим полем электрона и опережающим полем позитрона, где $\eta_{\mu\nu}$ метрика плоского вспомогательного пространства Минковского (-+++), $H = (2mr - e^2)/r^2 + a^2\cos^2\theta$, $k_\mu$ и $k^{+}_{\nu}$ – запаздывающая и опережающая конгруэнции Керра, связанные с полем излучения и полем входящей радиации. Развивая работу [30**?** ], мы анализируем точное решение, полученное Дебнеем, Керром и Шильдом (ДКШ) для с волнового электромагнитного поля и обнаруживаем, что оно было проинтегрировано в ДКШ не до конца, а только в предположении отсутствия электромагнитного излучения. Однако, при наличии излучения электронные (левые) и позитронные (правые) моды возбуждения кольцевой струны Керра не являются взаимно коррелированными в общем случае.

Это направление вновь оказывается связанным со струнной моделью, но это уже классическая релятивистская струна в 4-х измерениях, которая существенно отличается от суперструн многомерной квантовой гравитации.

Образование черных дыр связано с гравитационным эффектом затягивания пространства, который никогда ранее не рассматривался в физике частиц. Этот эффект оказывается действительно нетривиален и очень важен для понимания физической картины взаимодействия гравитации с квантовой теорией, поскольку он придает электрону дополнительную магнитную массу-энергию, порождаемую петлями Вильсона,– гравитационным затягиванием пространства во вращающуюся черную дыру КН [26].

Противоречие между квантовой теорией и гравитацией проявляются наиболее остро в теории электрона. Квантовая теория Дирака представляет электрон как точечный математический объект: гибрид волны и частицы, в то время как гравитация, требует протяженного распределения материи в пространствовремени. Предположение, что частицы являются черными дырами было впервые высказано независимо рядом известных физков, Нобелевскими лауреатами: Абдус Саламом (Abdus Salam), Франком Вильчеком (Frank Wilczek) и Геральд т Хофтом (Gerald 't Hooft).

Однако, эти ранние идеи касались только решения Э. Шварцшильда, свойства которого очень далеки от свойств решения Керра для релятивистки вращающегося гравитационного поля, и практически не имели отношения к модели вращающейся черной дыры КН. Подход к черной дыры Керра как модели электрона начинается с работы Б. Картера [3] (1968), который обнаружил, что решение Керра – Ньюмена (метрика Керра с зарядом) имеет гиромагнитное отношение ($g = 2$) такое же, как у модели электрона Дирака.

В отличие от гравитационного радиуса решения Швацшильда $l_s = \frac{gm}{c^2}$, эффективная зона гравитационного взаимодействия в решении КН определяется радиусом керровского сингулярного кольца

$$a = \frac{J}{mc}, \tag{0.1}$$

который обратно пропорционален массе $m$ и прямо пропорционален угловому моменту решения Керра $J$.

Для параметров электрона с массой $m$ и спином $J = \hbar/2$, параметр $a$ является половиной длины волны Комптона $a = \frac{\hbar}{2mc}$, и обычные аргументы об исключительной роли планковской длины (см., например, [22]) оказываются недействительными при их применении к вращающейся гравитации Керра.

К числу дополнительных неожиданностей, связанных с моделью электрона как черной дыры Керра –Ньюмена (КН), являлась ее "неточечность". Связанная с электроном, длина волны Комптона возникла как бесплатное приложение, обусловленное параметром вращения решения Керра (0.1). В координатах Керра – Шильда, связанных с ассиптотически плоским пространством Минковского, решение КН описывается как классическое гравитационное поле кольцевой струны половины компτоновского радиуса $a$.

На комптоновский размер электрона указывал также В. Израэль [10], и позднее К. А. Лопез [11] и др., и это совсем не безобидный факт, поскольку комтоновский масштаб $10^{-11}$ см, являясь естественным масштабом для физики частиц, превышает планковский масштаб $10^{-33}$см на 22 порядка, на котором основаны как квантовая петлевая гравитация, так и теория суперструн.

Вслед за Картером, модель электрона КН была детально рассмотрена в фундаментальной работе Дж.С. Дебнея, К.Р. Керра и А. Шильда (DKS) [8] и далее в важных работах [10] и [11], а также в моделях [12, 13, 23], основанных на идее Дж. Уиллера "массы без массы "и аналогии сингулярного кольца Керра с классической струной Нильсена–Олесена [24], возникающей в виде сингулярной нити в теории сверхпроводимости.

Эти работы были учтены в последующей серии работ [15, 16, 17], в которой модель электрона рассматривалась как сверхпроводящий "мешок имеющий форму очень тонкого сверхпроводящего диска Керра с толщиной $\approx a/137$ и радиусом $a$, равным половине комптоновской длины волны электрона, см. Рис.1. Диск Керра, искажая пространство, образует вакуумный сгусток – "ядро"электрона, окаймленное двумя петлями Вильсона (электронной и позитронной), которые формируются гравитационным затягиванием электромагнитного поля. Модель электрона КН согласована с классической гравитацией по своей природе, как точное решение системы уравнений Эйнштейна-Максвелла [8], и исследование структуры этой модели связано с разрешением известных ранее непреодолимых противоречий между гравитацией и квантовой теорией. В частности, утверждений:

**(1)** точечный, бесструктурный электрон квантовой теории *не совместим* с гравитацией;

**(2)** протяжённый гравитирующий электрон *не совместим* с квантовой теорией.

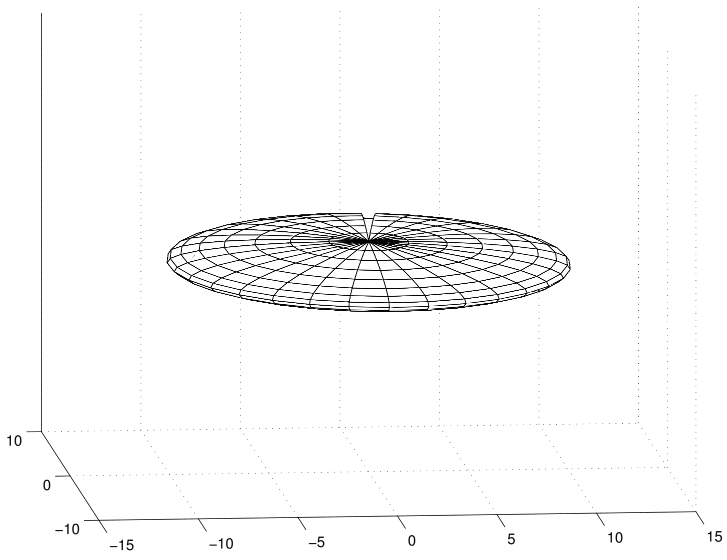


**Рис. 1.** Дискообразное ядро электрона КН, однозначно определяемое формой решения КН и эллипсоидальной системой координат Керра-Шильда [8].

Плоскость, в которой лежит сингулярное кольцо Керра, служит границей расщепления пространства на два листа, и решение КН с параметрами электрона *не является на самом деле черной дырой,* потому что для типичных вращающихся элементарных частиц $a^2 \gg e^2+m^2$, что приводит к условию исчезновения горизонтов черной дыры, а это значит, что обнаженное сингулярное кольцо Керра оказывается голым. Как следствие, тензор энергии-импульса сингулярного кольца Керра расходится, и сверхвращающееся кольцо Керра несёт бесконечную энергию, которая нуждается в регуляризации (и даже в перенормировке) в соответствии с КЭД.

Введенный Лопезом параметр обрезания $r_e$, определяет приращение векторного потенциала КН вдоль замкнутых петель Вильсона [25, 26, 27], что ведущее к балансу между гравитационным и электромагнитным взаимодействиями, определяя регуляризированную массу частицы как результат нелинейного гравито-электромагнитного взаимодействия. Электрон Лопеза, образует диск толщиной $2r_e$ и радиусом $a$, равным половине длины волны Комптона (0.1), см. Рис.1.
При этом, ядро регуляризованного электрона приобретает внутреннюю метрику пространства Минковского,сохраняя *внешнее* гравитационное и электромагнитное поле решения КН.

Кроме того, параметр обрезания $r_e$, порождает две граничные поверхности диска Керра $r_e^\pm$, электронную и позитронную (см. Рис.3,4), которые формируются суперсимметричным фазовым переходом механизма Хигса [28] и играют важную роль в формировании единой квантовой вакуумной системы. При этом, как было показанно в [29, 30] соответствующие петли Вильсона формируют сильную магнитную связь между электронной и позитронной частями вакуумного ядра.

При этом, появление двух различных механизмов формирования массы-энергии электрона, объясняет физический смысл отдельного анализа голого и одетого электрона.

*Голый электрон* строится путем регуляризации классического стационарного решения КН в виде *кольцевой безмассовой релятивистской струны,* которая приобретает массу и сжимается в точечный электрон за счет релятивистского вращения. Волновые возбуждения струны порождают квантовую волновую функцию электрона в представлении В. Гейзенберга, удовлетворяющую уравнению Э. Шредингера.

*Одетый электрон* порождается суперсимметричной моделью Гинзбурга-Ландау, в процессе фазового перехода к регуляризованному вакуумному состоянию. Масса-энергия одетого электрона рождается из бесконечной энергии регуляризованного сингулярного электрона Керра под влиянием полей Хиггса, формирующих фазовый переход к сверхпроводящему ядру – области сильного магнитного взаимодействия электронного и позитронного вакуума.

Модифицируя исходное решение КН, Израэль и Лопез [4,5] отсекали отрицательный лист решения КН. В докладе [1] обсуждалась иная модификация решения КН, с заменой отрицательного листа решения на зеркальный лист, с одновременным отражением конгруэнции от тяжелого ядра электрона, формируемого полями Хиггса. Зеркальный лист интерпретируется как позитронный лист электронно-позитронного вакуума одетого электрона согласно КЭД, [1]. Эта интерпретация поддерживается также известной старой интерпретацией о порождении заряда электрона стационарным ЭМ полем запаздывающего потенциала и законом сохранения заряда электронно-позитронного вакуума. Запишем уравнение Эйнштейна в метрике Керра – Шильда [8]

$$R_{\mu\nu} = -\frac{8\pi G}{c^4} T_{\mu\nu}, \tag{0.2}$$

где $R_{\mu\nu}$ - тензор Риччи, определяемый симметричным метрическим тензором $g_{\mu\nu}; T_{\mu\nu}$ - тензор энергии-импульса материи; c – скорость света в вакууме; G – гравитационная постоянная Ньютона. В уравнении (3) правая часть описывает энергию стационарных гравитационного и электромагнитного полей, формирующих кольцевую релятивистскую безмассовую струну голого электрона, порожденную увлечением вектор-потенциала (frame-dragging) гравитационным полем КН с твистом конгруэнции Керра, рис.1.
Это решение имеет соответствующий экспериментальным данным $g$-фактор (равный 2) для электрона [3, 8], и описывает структуру электрона КН, моделируя непертурбативный гравитирующий

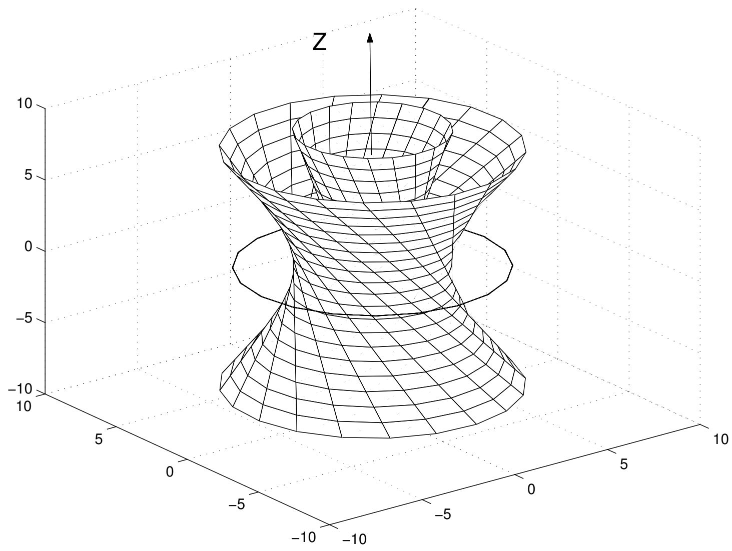


**Рис. 2.** Конгруенция Керра переходит аналитически через сингулярное кольцо Керра на отрицательный лист метрики КН.

электрон [3, 10, 11] и процесс взаимодействия электрона с полями Хиггса и гравитацией, который регуляризует электронно-позитронный вакуум согласно КЭД [30]. Заметим, что полученное в фундаментальной работе Керра, Дебнея и Шильда [8] точное решение было доведено до конца лишь при условии отсутствии $\gamma = 0$ (см. [8] (5.51)), что как было выяснено позже в работе [][8] (АБ 2003) соответствует стационарному решению КН без излучения ЭМ поля. Решения КН с излучением, полученные в работе [8] для выходящей конгруэнции $k^+_\mu$ показали, что параметр $\gamma^+$ имеет смысл ЭМ излучения в направлении $k^+_\mu$, и соответствующая часть энергии излучения равна $T^{(rad)}_{\mu\nu} = |\gamma^+|^2(k\mu^+ k^+_\nu)/2$. Подобным образом, поглощение ЭМ поля, входящего с направления $k^-$, описывается заменой $\gamma^+$ на $\gamma^-$, и конгруэнции $k^+_\mu$ на $k^-_\mu$. Следовательно, точное решение КН является стационарным и рассмотренная в [1] модель электрона как кольцевой струны Керра не излучает и не поглощает энергию ЭМ поля. Это является существенным недостатком рассмотренной ранее модели, которая в остальных отношениях очень важна, поскольку описывает согласованное с КЭД стационарное кольцевое состояние как голой, так и одетой релятивистской струны электрона, а также, связанной с ядром электрона позитронной струны электрона, и обе струны взаимодействуют с гравитацией и с полями Хиггса путем формирования двух магнитно-связанных петель Вильсона [1].

Решение уравнений для случая ненулевого параметра $\gamma$ было доведено до конца в серии работ [8, 9] (АБ 2002-2004 гг.) для полей Керра – Шильда, включающих как поле излучения, так и поле входящей радиации. Эти решения, для волновых полей $\gamma^+$ и $\gamma^-$, существенно отличаются тем, что в них появляется дополнительная аксиальная сингулярная струна в виде суммы двух полуструн, формируемых как сумма входящего и выходящего аксиальных лучей, направление которых, $k^+$ или $k^-$ задается соответствующими комплексными угловыми координатами $Y^+ = e^{i\varphi(s)}\,\mathrm{tg}(\theta_s/2)$ и $Y^- = e^{-i\varphi(s)}\,\mathrm{ctg}(\theta_s/2)$.

Вектор-потенциал ЭМ поля в электронной петле $A^+_\mu = -((Y^+, \tau^+)/(r + ia\cos\theta))k^+_\mu$ приобретает дополнительную зависимость от $Y^+$(поворот по углу $\varphi$), порождая излучение электрона КН, и одновременно воздействуя на аксиальный входящий луч $k^-_\mu$ позитронной петли, возбуждая входящее ЭМ поле, как обратную связь осциллирующей электронно-позитронной системы. Эта корреляция между возбуждениями ЭМ поля в электронной и позитронной петлях, настраивает связь между положениями и направлениями соответствующих полуструн и индуцируемыми вблизи них полями, включая частоту колебаний и их фазы, сопоставляя исходящему электронно-

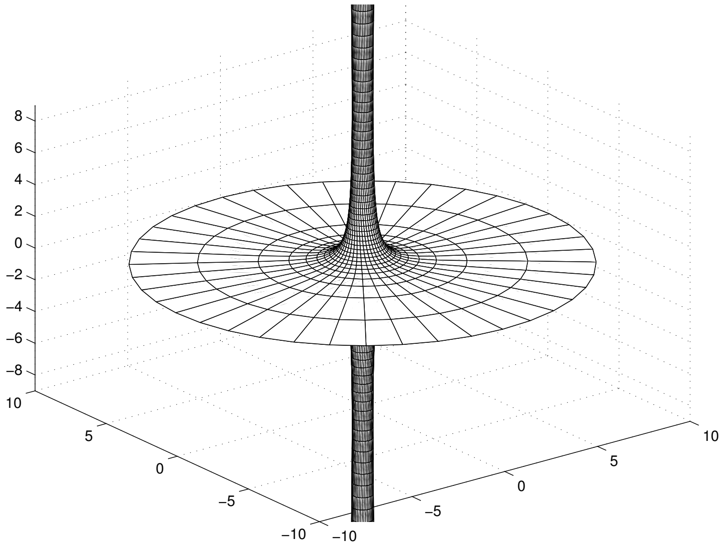


**Рис. 3.** Аксиальный сингулярный луч, направляющий выходящее ЭМ поле, в решениях с излучением $\gamma^+$.

му лучу левую моду осцилляции с левой комплексной полуструной, а входящему позитронному лучу — правую комплексную полуструну, устанавливая между ними связь струнной операцией, известной как ориентифолдизация.

Таким образом, общее решение КН, учитывающее как ЭМ поле излучения, связанное с параметром $\gamma^+$, так и входящее ЭМ поле с параметром $\gamma^-$, связывает правые и левые моды возбуждения электронной и позитронной петли. Аксиальный луч, совместно с кольцевой сингулярностью Керра действуют как узко направленная антенна, которая усиливает излучаемое ЭМ поле, а также отраженный сигнал входящего ЭМ поля, поступающий в соответствующую позитронную ветвь решения КН. Нами выдвигается гипотеза, что непертурбативный электрон КН является аналогом минимальной адаптивной системы, которая способна просматривать и оценивать окружающую обстановку передачей и приемом электромагнитного излучения и вырабатывать обратную связь (сигнал ошибки) для управления направлением движения электрона согласно принципу наименьшего действия. В хорошо известном квантовом опыте с двумя щелями, волна де Бройля, сопутствующая падающей частице (волны-пилота), дифрагирует на щелях, а затем создает интерференционную картину сложения двух частей первоначальной волны, свидетельствуя о загадочной сверх информированности электрона о состоянии щелей. Непертурбативная модель электрона КН, снабженная аксиальной структурой излучающей и принимающей ЭМ поле, показывает, что волновая функция электрона Дирака генерируется ЭМ полем, связанным с релятивистским вращением электрона. Аксиальная сингулярная струна генерирует устойчиво направленное ЭМ поле, которое излучается кольцевой электронной струной, действующей как узконаправленная передающая антенна. Отраженное от пластины с двумя параллельными щелями ЭМ поле принимается "позитронной"струной решения КН, действующей как приемная антенна для входящего ЭМ сигнала. При этом, аксиальная струнная система, подчиненная структуре ориентифолда, автоматически согласует излучаемый и приходящий сигнал по направлению, частоте и фазе, формируя согласованную приемо-передающую систему. Предположительно, интерференция скоррелированных переданного и принятого сигналов может формировать обратную связь и вырабатывать сигнал ошибки. Таким образом, в модели ЭМ поля электрона КН, являющейся развитием модели волны-пилота де Бройля – Бома, электрон "прощупывает"ЭМ полем окружающее пространство, и "видит"топологию пластины. Иначе говоря, он действует как простейшая самоорганизующаяся адаптивная система, выбирая оптимальный путь в соответствии с принципом наименьшего действия.

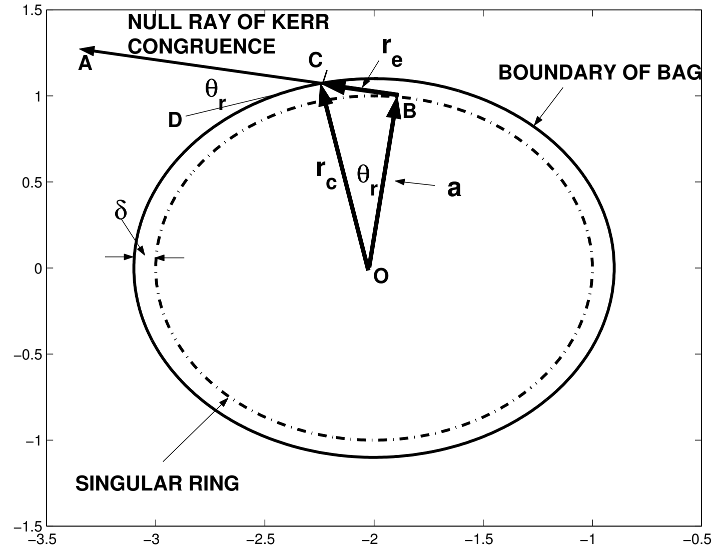


**Рис. 4.** Сингулярное кольцо электрона КН модифицируется добавлением аксиальной струны, в виде двух полуструн, согласуемых исходящим и входящим излучением

## Заключение

Выше было показано, что понимание важности взаимодействия в модели электрона КН привело к определяемого вакуумным вкладом в виде двух сопряжённых петель Вильсона с зеркальными сторонами решения КН. Была выдвинута гипотеза, что непертурбативный электрон КН является аналогом минимальной адаптивной системы, которая способна просматривать и оценивать окружающую обстановку передачей и приемом электромагнитного излучения и вырабатывать обратную связь (сигнал ошибки) для управления направлением движения электрона согласно принципу наименьшего действия. Отметим также, что новая точка зрения на решение Керра - Ньюмана устанавливает тесную связь геометрии КН с теорией твисторов и теорией суперструн на комптоновском масштабе в соответствии с основным соотношением решения КН $a = J/2m$, увеличивая реальный масштаб гравитационного взаимодействия с релятивистским электроном с предполагаемой ранее планковской длины $10^{-33}$ см до комптоновской длины $10^{-11}$ см, т.е. на 22 порядка.

В новой модели КН электрона проявляется физический смысл используемого в КЭД разделения массы-энергии элекрона на массу "голого"электрона, отвечающего за его волновые свойства, и гравитационно "одетого"электрона, генерирующего самосжимаемую массу-энергию сгустка "ядра"окружающего электрон поля, асоциируемого с "темной энергией". Сделан вывод, что все основные проблемы, связанные с совместимостью структуры гравитации со строением элементарных частиц находят решение в модели Керра – Ньюмана для сверхвращающейся (фактор Лоренца $\sim 1$) ЧД с излучением, показывая совместимость модели электрона КН с квантовой теорией в представлении Гейзенберга, а также с моделью элементарной частицы, основанной на классической модели кольцевой струны Керра-Ньюмана как решения уравнений Максвелла – Эйнштейна.

## Список литературы/References

1. Schwarz J., The Early History of String Theory and Supersymmetry, *CALT-68-2858 arXiv:1201.0981*
2. Dabholkar A., Gauntlett J. P., Harvey J. A., Waldram D., Strings as Solitons and Black Holes as Strings, *Nucl.Phys.* **B474** 85 (1996).
3. Carter B. Global structure of the Kerr family of gravitational fields *Phys. Rev.* 1968. Vol. **174**. P. 1559.

4. Sen A. , Macroscopic Charged Heterotic String. *Nucl.Phys. B* 388 457 (1992), [arXiv:hep-th/9206016].
5. Burinskii A., Some properties of the Kerr solution to low-energy string theory. *Phys. Rev. D* 52 5826 (1995), [arXiv:hep-th/9504139].
6. Arkani-Hamed N.1, Dimopoulos S., Dvali G. and Kaloper N., Infinitely Large New Dimensions,*Phys.Rev.Lett.* 84 586 (2000) DOI: 10.1103/PhysRevLett.84.586 [hep-th/9907209].
7. Kerr R.P. Gravitational field of a spinning mass as an example of algebraically special metrics, *Phys. Rev. Letters.* 1963. Vol. 11. P. 237.
8. Debney G. C., Kerr R. P., Schild A. Solutions of the Einstein and Einstein-Maxwell equations, *J. Math. Phys.* 1969. Vol. 10. P. 1842.
9. Newman E.T., Janis A.I. Note on the Kerr Spinning-Particle Metric. *J. Math. Phys.* 1965. Vol. 6. P. 915. doi:10.1063/1.1704350.
10. Israel W. Source of the Kerr metric, *Phys. Rev. D.* 1970. Vol. 2. P. 641.
11. López C.A. An Extended Model Of The Electron In General Relativity, *Phys. Rev. D* 1984. Vol. 30. P. 313.
12. Burinskii A.Ya. Microgeons with spin. *Sov. Phys. JETP* 1974. Vol. 39. P. 193.
13. Ivanenko D.D. and Burinskii A.Ya., Gravitational strings in the models of elementary particles, *Izv. Vuz. Fiz.* 1974. Vol. 5. P. 135.
14. Arcos H.I., Pereira J.G., Kerr-Newman solution as a Dirac particle. *Gen. Rel. Grav.* 2004. Vol. 36. P. 2441.
15. Burinskii A., Gravitating lepton bag model *JETP (Zh. Eksp. Teor. Fiz.)* 2015. Vol. 148(8). P. 228. arXiv:1505.03439.
16. Burinskii A. Stability of the lepton bag model based on the Kerr-Newman solution *JETP (Zh. Eksp. Teor. Fiz.)* 2015. Vol. 148. P. 937.
17. Burinskii A. Source of the Kerr-Newman solution as a supersymmetric domain-wall bubble: 50 years of the problem *Phys Lett. B* 2016. Vol. 754. P. 99.
18. Dymnikova I. 2006, Spinning superconducting electrovacuum soliton *Phys. Lett.* B 639 368
19. Schmekel B.S. Quasi-Local Energy of a Charged Rotating Object Described by the Kerr-Newman Metric *Phys. Rev.D* 2019. Vol. 100. P. 124011.
20. Arkani-Hamed N., Huang Y-t. and O'Connell D. Kerr Black Holes as Elementary Particles *J. High Energ. Phys.* - 2020. - Vol. 46.
21. Misner Ch. W., Thorne K. S., Wheeler J.A. *Gravitation.* San Francisco: Freeman W. H. and Company. 1973.
22. *Baez J. C. Higher Dimensional Algebra and Planck Scale Physics.* Physics Meets Philosophy at the Planck Length,eds. Craig Callender and Nick Huggett, Cambridge U. Press 2001. P. 177-195. arXiv:gr-qc/9902017.
23. Burinskii A. Orientifold D-String in the Source of the Kerr Spinning Particle *Phys. Rev.D* 2003. Vol. 68. P. 105004.
24. Nielsen H.B. and Olesen P. Vortex-line models for dual strings. *Nucl. Phys. B.* 1973. Vol. 61. P. 45.
25. Burinskii A. The Kerr-Newman Black Hole Solution as Strong Gravity for Elementary Particles, *Grav.Cosmol.* 2020. Vol. 26. P. 87.
26. Burinskii A 2018, Supersymmetric bag model for unification of gravity with spinning particles *Phys. of Part. and Nucley* 49(5) 958
27. Burinskii A 2020, Spinning Particle as Kerr-Newman "Black Hole"*Physics of Particles and Nuclei Letters*, 17 (5) 724
28. Wess J. and Bagger J. *Supersymmetry and Supergravity.* Princeton Univ. Press, New Jersey - 1983.

29. Burinskii A. A Bare and Gravitationally Dressed Electron Formed from Kerr–Newman Black Hole, *Physics of Particles and Nuclei*, 2023, Vol. 54, No. 6, pp. 1033–1038.
30. Burinskii A. Gravitating Electron Based on Overrotating Kerr-Newman Solution *Universe* 2022. Vol. 8. P. 553. https://doi.org/10.3390/universe8110553
31. Burinskii A., The Dirac Electron Consistent with Proper Gravitational and Electromagnetic Field of the Kerr-Newman Solution *Galaxies* 2021. Vol. 9. P. 18. doi:10.3390/galaxies9010018.
32. Burinskii A 2022 Appell's Correspondence Unifies Gravity with Quantum Theory, *Gravitation and Cosmology*, 2022, Vol. 28, No. 4, 342 (2022). Pleiades Publishing, Ltd. DOI: 10.1134/S0202289322040065
33. Wang H.-Y., A Theory of Dark Energy that Matches Dark Matter, *Physics Essays* 35(2), 152 (2022), http://dx.doi.org/10.4006/0836-1398-35.2.152
34. Appell P., Quelques remarques sur la th'eorie des potentiels multiforms. *Math. Ann.* 30 (1887), 155–156;
35. Whittacker E.T. and Watson G.N., *A Course of Modern Analysis,* Cambrige Univ. Press London/New York,p.400, 1969 .
36. Hamity V. An interior of the Kerr metric *Phys. Lett. A* 1986. Vol. 56. P. 77.
37. Ландау Л.Д., Лифшиц Е.М. *Теоретическая физика т. II Теория Поля.* Наука 1973. пар.89. Landau L. D. and Lifshitz E. M. *The Classical Theory of Fields.* Pergamon, Oxford. 1975.
38. Weisskopf V.F. Recent Developments in the Theory of the Electron. *Rev. Mod. Phys.* 1949. Vol. 21. P. 305.
39. Bardeen W.A., Bars I., Hanson A. and Peccei R.D. Study of the longitudinal kink model of the string *Phys. Rev. D* 1976. Vol. 13. P. 2364.
40. A. Patrascioiu 1974 Quantum Dynamiks of a Massless Relativistic Strings (*Nucl.Phys.* B81 525 (1974)
41. Bjorken J.D. and Drell S.D. *Relativistic Quantum Fields*, McGraw-Hill Book Company 1965. Vol. 2.
42. Burinskii A. Regularized Kerr-Newman Solution as a Gravitating Soliton *J. Phys. A: Math. Theor.* 2010. Vol. 43. P. 392001. [arXiv: 1003.2928].
43. Burinskii A 2003 Complex Kerr geometry and nonstationary Kerr solution *Phys. Rev. D.* 67 124024 (2003)
44. Burinskii A 2004 Twstor Analiticity and Three Stringy Systems of the Kerr Spinning Particle, *Phys. Rev. D.* 70 086006 (2004)
45. Burinskii A 2004 Axial Stringy System of the Kerr Spinning Particle *Grav.Cosmol.* 10 50 (2004),
46. Burinskii A 2004 Two Stringy Systems of the Kerr Spinning Particle, In:*Proc. of the 26th Workshop on Fundamental Problems of High-Energy Physics and Field Theory*, Ed. V.A.Petrov, p.87-100, IHEP, Protvino, 2003 , arXiv: hep-th/0402114
47. Burinskii A. Stringlike structures in Kerr-Schild geometry: N=2 string, twistors and Calabi-Yau twofold, *Theor. and Math. Phys.* 177(2) (2013) 1492.
48. R. Penrose Twistor Algebra *J. Math. Phys.* 1967. Vol. 8. P. 345.
49. Burinskii A. Wonderful Consequences of the Kerr Theorem *Grav. Cosmol.* 2005. Vol. 11. P. 301; Burinskii A. Multiparticle Kerr-Schild Solutions... *Grav. Cosmol.* 2007. Vol. 4. P. 437.
50. Logunov A A, Petrov V A 1988 *How does an electron work?* (in Russian). Moscow.: Pedagogic
51. Lind R. W. and Newman E. T., Complexification of the algebraically special gravitational field *J. Math. Phys.* 15 1103 (1974).
52. Гинзбург В.Л. и Ландау Л.Д. К Теории Сверхпроводимости *ЖЭТФ.* 1950. Vol. 20. P. 1064.
53. Lomdahl P.S., Olsen O.H. and Samuelsen M.R. *Phys. Rev. A* 1984. Vol. 29. P. 350.

54. Wheeler John A. *Neutrinos, Gravitation and Geometry.* Tipografia Compositori 1960.
55. Green M.B., Schwarz J. and Witten E. Superstring Theory *Cambridge Univ. Press* 1987. Vol. I.
56. Goddard P., Goldstone J. , Rebbi C. and Thorn C.B. Quantum Dynamics of a Massless Relativistic String *Nuclear Physics* 1973. Vol. B56. P. 109-135.
57. Burinskii A. Appell's Correspondence Unifies Gravity with Quantum Theory *Gravitation and Cosmology* 2022. Vol. 28 №4. P. 342-351. DOI: 10.1134/S0202289322040065.
58. Ахиезер А.И. и Берестецкий В.Б. *Квантовая Элктродинамика.* М: Наука. 1951.

**Авторы**

**Буринский Александр**, Лаборатория теоретической физики, ИБРАЭ РАН, ул. Большая Тульская, д. 52, г. Москва, 115191, Россия.
E-mail: burinskii@mail.ru

**Измайлов Георгий Николаевич**, д.ф.-м.н., профессор, Московский авиационный институт (национальный исследовательский университет), Волоколамское ш., д. 4, г. Москва, 125993, Россия.
E-mail: izmailov@mai.ru

**Просьба ссылаться на эту статью следующим образом:**

Буринский А. Я., Измайлов Г. Н. Электрон Керра – Ньюмана как адаптивная система. *Пространство, время и фундаментальные взаимодействия.* 2023. № 3-4. С. 38–47.

**Authors**

**Burinskii Alexander**, Theor. Phys. Lab., IBRAE RAN, B. Tulskaya str., 52, 115191, Moscow, Russia.
E-mail: burinskii@mail.ru

**Izmailov George Nikolaevich**,Dr. Sci., Professor, Moscow Aviation Institute (National Research University), Volokolamskoye sh., 4, Moscow, 125993, Russia.
E-mail: izmailov@mai.ru

**Please cite this article in English as:**

Burinskii A. Ya., Izmailov G. N. Kerr – Newman electron as an adaptive system. *Space, Time and Fundamental Interactions*, 2023, no. 3-4, pp. 38–47.

УДК 539.12,530.2,53.02



## О ЛЕПТОНАХ В ТЕОРИИ ПРОСТРАНСТВЕННО-ВРЕМЕННОЙ ПЛЁНКИ

Черницкий А. А.[a,b,1]

[a] Санкт-Петербургский Государственный Химико-Фармацевтический Университет, г. Санкт-Петербург, 197376, Россия.

[b] Фридмановская Лаборатория Теоретической Физики, г. Санкт-Петербург, Россия.

В данной работе мы продолжаем исследование задачи нахождения тороидальных солитонных решений уравнения пространственно-временной плёнки, которые могут представлять заряженные лептоны. Введена квази-цилиндрическая комплексная тороидальная система координат с вращением и получено уравнение пространственно-временной плёнки в этой системе. Предложен способ нахождения решения в виде формального ряда по обратным степеням радиуса тороидального кольца. Обсуждается начальное приближение для этого метода.

*Ключевые слова*: Пространственно-временная плёнка, space-time film, лептон, lepton, полевая модель заряженного лептона, field model of charged lepton.

## ABOUT LEPTONS IN SPACE-TIME FILM THEORY

Chernitskii A. A.[a,b,1]

[a] St. Petersburg State Chemical and Pharmaceutical University, St. Petersburg, 197376, Russia.

[b] A. Friedmann Laboratory for Theoretical Physics, St.-Petersburg, Russia

In the present work, we continue the investigation of the problem for finding the toroidal soliton solutions of space-time film equation, which can represent the charged leptons. The quasi-cylindrical complex toroidal coordinate system with rotation is introduced and the appropriate equation of space-time film is obtained. We propose the way for finding the solutions in the form of formal series in negative powers of the radius of the toroidal ring. The initial approximation for this method is discussed.

*Keywords*: Space-time film, lepton, field model of charged lepton.

PACS: 12.10.Dm, 12.10.-g,12.60.-i

DOI: 10.17238/issn2226-8812.2023.3-4.48-53

### Introduction

In the given work, we continue to consider possible toroidal solutions of the space-time film (STF) equation [1] associated with leptons [3, 4].

Earlier we have obtained the exact solutions of STF equation in the form of twisted or spiral solitons which are rectilinearly moving with the speed of light [1]. These spiral light-like solitons are characterized by the twist parameter $m$. It was shown that the solitons of the first twist order ($m = 1$) can be associated with photons. We suppose that the light-like solitons of higher twist orders $m > 1$ can be associated with various neutrinos.

Moreover, the static solution in the form of charged cylindrical shell were obtained in the work [1].

The toroidal solutions under consideration are circinate combinations of the charged cylindrical shell and the twisted light-like solitons.

[1] E-mail: alexander.chernitskii@pharminnotech.com, AAChernitskii@mail.ru

## 1. Equation of space-time film in coordinates with rotation

The action for space-time film has the following form [1]:

$$\mathcal{A}=\int\limits_{\overline{V}}\pounds\,\mathrm{d}\overline{V}\ ,\quad \pounds\doteqdot\sqrt{\left|1+\chi^{2}\,\mathfrak{m}^{\mu\nu}\,\frac{\partial\Phi}{\partial x^{\mu}}\,\frac{\partial\Phi}{\partial x^{\nu}}\right|} \tag{1.1}$$

where $\mathrm{d}\overline{V}\doteqdot\sqrt{|\mathfrak{m}|}\ (\mathrm{d}x)^{4}$ is a four-dimensional volume element,, $\mathfrak{m}\doteqdot\det(\mathfrak{m}_{\mu\nu})$, $\Phi$ is the scalar field function, $\mathfrak{m}_{\mu\nu}$, $\mathfrak{m}^{\mu\nu}$ are components of metric tensor for an arbitrary coordinate system in flat space-time. The Greek indexes take the values $\{0,1,2,3\}$. $x^{0}\doteqdot\mathfrak{c}\,t$ is the time coordinate, where $t$ is time and $\mathfrak{c}$ is the velocity of light in free space.

Here we consider the signature of metric $\{-,+,+,+\}$, that is we have $-\mathfrak{m}^{00}=\mathfrak{m}^{11}=\mathfrak{m}^{22}=\mathfrak{m}^{33}=1$ in Cartesian coordinates. In the base work [1], the opposite metric $\{+,-,-,-\}$ was also considered. But the investigation of the gravitational interaction in the framework of STF theory shows that the signature must be $\{-,+,+,+\}$ [2].

The stationary condition for the action (1.1) gives the following equation:

$$\frac{1}{\sqrt{|\mathfrak{m}|}}\,\frac{\partial}{\partial x^{\mu}}\,\frac{\sqrt{|\mathfrak{m}|}\,\mathfrak{m}^{\mu\nu}}{\pounds}\,\frac{\partial\Phi}{\partial x^{\nu}}=0\ , \tag{1.2}$$

Let us consider the class of four-dimensional space-time coordinate systems having the azimuthal coordinate or azimuth angle $\varphi$, called also horizontal angle. Let us introduce the following coordinate transformation for such coordinate systems:

$$\breve{\theta}=\varphi-\tilde{\omega}\,x^{0}\ ,\quad \breve{\vartheta}=\varphi+\tilde{\omega}\,x^{0}\ . \tag{1.3}$$

The coordinates $\breve{\theta}$ and $\breve{\vartheta}$ can be called right and left phase coordinates accordingly. The positive parameter $\tilde{\omega}>0$ meaning of the angular velocity. It is evident that a function depending from one phase coordinate $\breve{\theta}$ or $\breve{\vartheta}$ is right- or left-rotating field configuration relatively vertical axis $x^{3}$ or $z$.

The densities of energy $\mathcal{E}$ and vertical component of angular momentum $\mathcal{J}_{z}$ have the following form in the coordinate system with rotation:

$$\mathcal{E}=\frac{1}{4\pi}\left(\frac{\tilde{\omega}^{2}}{\pounds}\left(\frac{\partial\Phi}{\partial\breve{\theta}}-\frac{\partial\Phi}{\partial\breve{\vartheta}}\right)^{2}+\frac{1}{\chi^{2}}\left(\pounds-1\right)\right)\ , \tag{1.4a}$$

$$\mathcal{J}_{z}=\frac{\tilde{\omega}}{4\pi\,\pounds}\left(\left(\frac{\partial\Phi}{\partial\breve{\theta}}\right)^{2}-\left(\frac{\partial\Phi}{\partial\breve{\vartheta}}\right)^{2}\right)\ , \tag{1.4b}$$

Here we consider the rational toroidal coordinate system [3, 4]. This system is obtained from the usual toroidal one $\{x^{0},\kappa,\upsilon,\varphi\}$ with the help of the following change of the variable $\kappa$ $(0\leqslant\kappa\leqslant\infty)$: $\bar{\kappa}=\mathrm{e}^{\kappa}-1$. This system is convenient because its components of metrical tensor are the rational functions of the variable $\bar{\kappa}$:

$$\mathfrak{m}_{00}=-1\ ,\quad \mathfrak{m}_{\bar{\kappa}\bar{\kappa}}=\frac{\rho_{\circ}^{2}}{4\,\bar{\mathcal{K}}^{2}}\ ,\quad \mathfrak{m}_{\upsilon\upsilon}=\frac{\left(\bar{\kappa}+1\right)^{2}\rho_{\circ}^{2}}{4\,\bar{\mathcal{K}}^{2}}\ ,\quad \mathfrak{m}_{\varphi\varphi}=\frac{\bar{\kappa}^{2}\left(\bar{\kappa}+2\right)^{2}\rho_{\circ}^{2}}{16\,\bar{\mathcal{K}}^{2}}\ , \tag{1.5a}$$

$$\bar{\mathcal{K}}\doteqdot\frac{1}{4}\left(2+\bar{\kappa}\left(\bar{\kappa}+2\right)-2\left(\bar{\kappa}+1\right)\cos\upsilon\right)=\left(\bar{\kappa}+1\right)\,\sin^{2}\!\left(\frac{\upsilon}{2}\right)+\frac{\bar{\kappa}^{2}}{4}\ . \tag{1.5b}$$

where $\rho_{\circ}$ is the radius of the singular ring of the coordinate system.

We will consider, in particular, the field configurations with singularity on the toroidal surface $\kappa=\breve{\kappa}=\mathrm{const}$ or $\bar{\kappa}=\breve{\bar{\kappa}}=\mathrm{const}$. The large $\breve{\rho}_{\circ}$ and small $\bar{\bar{\rho}}$ radii of the toroid is given by the formulas

$$\breve{\rho}_{\circ}=\rho_{\circ}\,\coth\breve{\kappa}=\rho_{\circ}\left(\frac{1}{\breve{\bar{\kappa}}}+\frac{1+\breve{\bar{\kappa}}}{2+\breve{\bar{\kappa}}}\right)\ ,\quad \bar{\bar{\rho}}=\rho_{\circ}\,\mathrm{csch}\,\breve{\kappa}=\rho_{\circ}\left(\frac{1}{\breve{\bar{\kappa}}}+\frac{1}{2+\breve{\bar{\kappa}}}\right)\ . \tag{1.6}$$

As we see, the large radius of the toroid $\breve{\rho}_{\circ}$ is not coincide with the radius of the singular ring $\rho_{\circ}$ of toroidal coordinate system.

Then we use the rational toroidal coordinates with rotation $\{\breve{\theta}, \overset{*}{\breve{\theta}}, \bar{\kappa}, \upsilon\}$. The metrical tensor for this coordinate system is not diagonal. But the metrical tensor for the truncated systems $\{\breve{\theta}, \bar{\kappa}, \upsilon\}$ and $\{\overset{*}{\breve{\theta}}, \bar{\kappa}, \upsilon\}$ is diagonal.

In the present work, we take the following relation between the parameter of angular velocity and the large radius of the toroid:

$$\tilde{\omega} = \frac{1}{\rho_{\circ}} \; . \tag{1.7}$$

Let us introduce also the coordinates $\{\breve{\rho}, \breve{\varphi}, \breve{z}\}$, which can be named quasi-cylindrical toroidal (QCT) ones. We will consider two variants of such coordinates in accordance with the following formulas:

$$\breve{\rho} = \frac{2\,\rho_{\circ}}{\bar{\kappa}} \; , \qquad 0 \leqslant \breve{\rho} < \infty \; , \quad \breve{\varphi} = -\upsilon \; , \quad \breve{z} = \rho_{\circ}\,\varphi \; , \tag{1.8a}$$

$$\breve{\rho} = \rho_{\circ}\, \operatorname{sech}\kappa \; , \quad 0 \leqslant \breve{\rho} \leqslant \rho_{\circ} \; , \quad \breve{\varphi} = -\upsilon \; , \quad \breve{z} = \rho_{\circ}\,\varphi \; . \tag{1.8b}$$

The coordinate systems (1.8a) and (1.8b) can be called unlimited and limited QCT accordingly.

Metrical tensor for these coordinate system passes to metrical tensor of cylindrical system when $\rho_{\circ} \to \infty$.

Also we introduce the complex quasi-cylindrical toroidal coordinates by the formulas

$$\breve{\xi} \doteqdot \breve{\rho}\, \mathrm{e}^{\mathrm{i}\,\breve{\varphi}} \; , \quad \overset{*}{\breve{\xi}} \doteqdot \breve{\rho}\, \mathrm{e}^{-\mathrm{i}\,\breve{\varphi}} \; . \tag{1.9}$$

Next step is the transformation to phase-complex coordinates $\{\breve{\theta}, \overset{*}{\breve{\theta}}, \breve{\xi}, \overset{*}{\breve{\xi}}\}$ in the nonlinear equation of the model. The obtained equation is reduced to the following form:

$$\left(1 + 2\,\chi^2\,\frac{\partial\Phi}{\partial\breve{\xi}}\,\frac{\partial\Phi}{\partial\overset{*}{\breve{\xi}}}\right)\frac{\partial^2\Phi}{\partial\breve{\xi}\,\partial\overset{*}{\breve{\xi}}} - \chi^2\left(\left(\frac{\partial\Phi}{\partial\overset{*}{\breve{\xi}}}\right)^2\frac{\partial^2\Phi}{(\partial\breve{\xi})^2} + \left(\frac{\partial\Phi}{\partial\breve{\xi}}\right)^2\frac{\partial^2\Phi}{(\partial\overset{*}{\breve{\xi}})^2}\right) = \sum_{l=1}^{1_{max}} \frac{1}{\rho_{\circ}^{l}}\, Q_l\!\left(\chi, \breve{\xi}, \overset{*}{\breve{\xi}}, \frac{\partial\Phi}{\partial q_i}, \frac{\partial^2\Phi}{\partial q_j\,\partial q_k}\right) , \tag{1.10}$$

where $\{q_i\} = \{\breve{\theta}, \overset{*}{\breve{\theta}}, \breve{\xi}, \overset{*}{\breve{\xi}}\}$. For variant (1.8a) $1_{max} = 14$, the functions $Q_l$ depend on integral and half-integral powers of variables $\{\breve{\xi}, \overset{*}{\breve{\xi}}\}$, they are polynomials of the rest arguments. For variant (1.8b) $1_{max} = 7$, the functions $Q_l$ are polynomials of all arguments.

It is evident that the right side of the equation (1.10) vanishes for $\rho_{\circ} \to \infty$. Notable that the left side of the equation does not contain the derivatives with respect to variables $\{\breve{\theta}, \overset{*}{\breve{\theta}}\}$. This property is the consequent of the condition (1.7), because that the derivatives with respect to phases are small for $\rho_{\circ} \to \infty$.

Here we will consider a rotated field configurations depending from the three variables $\{\breve{\theta}, \bar{\kappa}, \upsilon\}$. For such solutions we have the following notable expressions:

$$\mathcal{E} = \tilde{\omega}\,\mathcal{J}_z + \frac{1}{4\pi\,\chi^2}\,(\pounds - 1) \; , \quad \mathcal{J}_z = \frac{\tilde{\omega}}{4\pi\,\pounds}\left(\frac{\partial\Phi}{\partial\breve{\theta}}\right)^2 \tag{1.11}$$

Energy and angular momentum of a soliton-particle are

$$\mathbb{E} \doteqdot \int\limits_V \mathcal{E}\,\mathrm{d}V \; , \quad \mathbb{J} \doteqdot \int\limits_V \mathcal{J}_z\,\mathrm{d}V \; , \tag{1.12}$$

where $V$ is the three-dimensional space without of the interior of the singular shell, in particular, toroidal one.

## 2. Charged lepton as toroidal soliton

Here we use the following dimensionless function and parameter for a solution:

$$\underline{\Phi} \doteqdot \frac{\rho_{\circ}}{\bar{e}}\,\Phi\,, \quad \varepsilon \doteqdot \frac{\bar{e}^2\,\chi^2}{\rho_{\circ}^4}\,, \tag{2.1}$$

where $\bar{e}$ is the elementary electrical charge. The parameter $\varepsilon$ used here differs by sign from one introduced in works [3, 4], where the field model with two metric signatures were considered.

Using these designations and relation (1.7), we have the following expressions for spin and energy densities for a rotating solution:

$$\mathcal{J}_z = \frac{\bar{e}^2}{4\pi\,\rho_{\circ}^3\,\pounds}\left(\frac{\partial\underline{\Phi}}{\partial\breve{\theta}}\right)^2\,, \quad \mathcal{E} = \tilde{\omega}\,\mathcal{J}_z + \frac{\bar{e}^2}{4\pi\,\rho_{\circ}^4\,\varepsilon}\left(\pounds - 1\right)\,. \tag{2.2}$$

We take the following empirical conditions for leptons:

$$\mathbb{E} = \hbar\,\omega\,, \quad \mathbb{J} = \frac{\hbar}{2}\,. \tag{2.3}$$

Also we take that the length of the singular ring of the toroidal coordinate system is multiple to Compton wave-length $\lambda\!\!\!^{-}_{\circ}$ of a charged lepton:

$$2\pi\,\rho_{\circ} = n\,\lambda\!\!\!^{-}_{\circ} \quad\Longrightarrow\quad \rho_{\circ} = \frac{n}{\omega} \quad\Longrightarrow\quad \omega = n\,\tilde{\omega}\,. \tag{2.4}$$

Using (2.3) and (2.4) we have the following conditions for charged leptons:

$$\tilde{\mathbb{J}} \doteqdot \frac{1}{\bar{e}^2}\,\mathbb{J} = \frac{\bar{e}^2}{4\pi\,\rho_{\circ}^3}\int\limits_V \frac{1}{\pounds}\left(\frac{\partial\underline{\Phi}}{\partial\breve{\theta}}\right)^2 \mathrm{d}V = \frac{\alpha^{-1}}{2}\,, \tag{2.5a}$$

$$\tilde{\mathcal{A}} \doteqdot \frac{1}{\bar{e}^2}\left(\rho_{\circ}\,\mathbb{E} - \mathbb{J}\right) = \int\limits_V \frac{1}{4\pi\,\rho_{\circ}^3\,\varepsilon}\left(\pounds - 1\right)\mathrm{d}V = \alpha^{-1}\left(n - \frac{1}{2}\right)\,, \tag{2.5b}$$

where $\alpha$ is fine structure constant, $\alpha^{-1} \approx 137$, $\tilde{\mathbb{J}}$ is dimensionless spin, $\tilde{\mathcal{A}}$ is dimensionless time density of regularized action.

Using relations(2.5) let us write the following expression for energy of a charged toroidal lepton:

$$\mathbb{E} = \frac{\bar{e}^2}{\rho_{\circ}}\left(\tilde{\mathbb{J}} + \tilde{\mathcal{A}}\right) = \frac{n\,\bar{e}^2}{\alpha\,\rho_{\circ}}\,. \tag{2.6}$$

## 3. Initial approximation to toroidal solution for charged lepton

We can try to find a solution in the form of formal series in the negative powers of the radius $\rho_{\circ}$ of the toroidal ring. The equation of space-time film in phase-complex quasi-cylindrical toroidal coordinates (1.10) is suitable for this purpose. The left side of this equation is coincide with the equation for which the exact solutions were obtained in work [1].

For the solution associated with a charged lepton, it is naturally to take the initial approximation in the form of combination of the charged tubular shell and twisted lightlike soliton.

The exact solutions in [1] were obtained with the help of transformation to new complex coordinates (tilde ones), in which the equation becomes linear. The transformation matrix to new coordinates depends on the solution. The obtained elementary solutions have singular cylindrical surface in the tilde coordinates. But a combination of the elementary solutions have more complicated singular surface in the tilde coordinates. And the singular surfaces transformed to the base cylindrical coordinates have a complicated form even for the elementary solutions. Thus the singular surface of the desired solution is not an exact toroid. In this case we must consider the small toroid radius $\bar{\bar{\rho}}$ in (1.6) as some mean quantity.

If we take the initial approximation in the form of referred combination of exact solutions for initial nonlinear equation in (1.10), then the behaviour of such field configuration at space infinity will not be correct. It is natural to consider that the desired solution at infinity is similar to an appropriate solution of linear equation. But dynamical solutions of wave equation in toroidal coordinates are not known. We can consider the rotating static solution as an approximation to such solution.

The necessary static solution of linearized equation of the field model under consideration follows from the known solution of the Laplace equation in toroidal coordinates [5]:

$$\underline{\Phi} = \sqrt{\bar{\mathcal{K}}}\;\dot{\bar{\Phi}}_{nm}\,\Big(C_1\,\cos(n\,\varphi) + C_2\,\sin(n\,\varphi)\Big)\Big(C_3\,\cos(m\,\upsilon) + C_4\,\sin(m\,\upsilon)\Big)\;, \tag{3.1a}$$

$$\dot{\bar{\Phi}}_{nm} \doteqdot \frac{2^{1-2|m|+|n|}\,\bar{\kappa}^{|n|}}{(\bar{\kappa}+1)^{|m|}\,(\bar{\kappa}+2)^{1-2|m|+|n|}}\;\mathcal{F}_{\frac{1}{2}-|m|,\frac{1}{2}-|m|+|n|;|n|+1}\left(\frac{\bar{\kappa}^2}{(\bar{\kappa}+2)^2}\right) \tag{3.1b}$$

$$= \bar{\kappa}^{|n|}\left(1 - \frac{|n|+1}{2}\,\bar{\kappa} + \mathcal{O}\big(\bar{\kappa}^2\big)_{\bar{\kappa}\to 0}\right)\;, \tag{3.1c}$$

where $n$ and $m$ are integer numbers, $\varphi = \big(\breve{\theta} + \bar{\bar{\theta}}\big)/2$, $\mathcal{F}_{\alpha,\beta;\gamma}(z) \doteqdot {}_2F_1(\alpha,\beta;\gamma;z)$ is a hypergeometric function, $\{C_1, C_2, C_3, C_4\}$ are arbitrary real constants.

Let us consider the following rotating static solution as an approximation to dynamical solution of the linear wave equation in toroidal coordinates:

$$\underline{\Phi}_{(0)} = \sqrt{\bar{\mathcal{K}}}\left(\dot{\bar{\Phi}}_{00} + a_{nm}\,\dot{\bar{\Phi}}_{nm}\,\sin(n\,\theta - m\,\upsilon)\right)\;, \tag{3.2}$$

where the functions $\dot{\bar{\Phi}}_{nm}$ are defined in (3.1b).

Here in (3.2), the function $\dot{\bar{\Phi}}_{00}$ is the static part which defines the charge of the particle. The dynamic part with amplitude $a_{nm}$ defines the wave or quantum behaviour of the particle.

Let us consider the asymptotic behaviour of the dynamic part in (3.2) near ring of the quasi-cylindrical toroidal coordinates (1.8). We have the following asymptotic expression for this dynamic part:

$$\underline{\Phi} \sim \frac{1}{\breve{\rho}^{|m|}}\,\sin(n\,\breve{\theta} + m\,\breve{\varphi})\;,\quad \breve{\rho}\to 0\;. \tag{3.3a}$$

where $|m| > 0$, $|n| > 0$, and according to (1.3), (1.7), (1.8) we have

$$\breve{\theta} = \tilde{\omega}\,\big(\breve{z} - x^0\big)\;. \tag{3.3b}$$

This is a solution of the linear wave equation in cylindrical coordinates $\{x^0, \breve{\rho}, \breve{\varphi}, \breve{z}\}$. This twisted wave propagates with the speed of light along the ring of the toroidal system.

Let us consider the asymptotic behaviour for the dynamic part of the rotating static solution near the origin of the cylindrical coordinates system $\{\rho, \varphi, z\}$ with the vertical axis $z$ and the horizontal angle $\varphi$. In these coordinates we have the following asymptotic expression for the dynamic part:

$$\underline{\Phi} \sim \rho^{|n|}\,\sin\!\Big(n\,\varphi + \tilde{\omega}\,\big(2\,m\,z - n\,x^0\big)\Big)\;,\quad \rho\to 0\;,\quad z\to 0\;. \tag{3.4}$$

where $|m| > 0$, $|n| > 0$.

The function (3.4) is also the asymptotic form of a solution of the linear wave equation in cylindrical coordinates $\{x^0, \rho, \varphi, z\}$. This twisted wave propagates with the phase velocity $n/(2\,m)$ along $z$ axis and presents so called Bessel beam.

For the special case

$$n = 2\,m\;, \tag{3.5}$$

the function (3.4) is a twisted wave propagating with the speed of light. This case needs a separate consideration.

## 4. Conclusions

In the present work, we have continued the investigation of the problem for finding the toroidal soliton solutions of space-time film equation, which can represent the charged leptons.

The quasi-cylindrical complex toroidal coordinate system with rotation is introduced and the appropriate equation of space-time film is obtained. We propose the way for finding the solutions in the form of formal series in negative powers of the radius of the toroidal ring. The initial approximation for this method is discussed.

## Список литературы/References


1. Chernitskii A.A. Lightlike shell solitons of extremal space-time film. *J. Phys. Commun.*, 2018, 2, 105013.
2. Chernitskii A.A. Gravitation in theory of space-time film and galactic soliton. *J. Phys.: Conf. Ser.*, 2021, 2081, 012016.
3. Chernitskii A.A. About toroidal model of leptons in space-time film theory. *JPS Conf. Proc.*, 2022, 37, 020608.
4. Chernitskii A.A. On leptons in theory of space-time films. *Phys. Part. Nucl.*, 2023, 54 no. 4, pp. 685–692.
5. Morse P.M. and Feshbach H. *Methods of Theoretical Physics*, volume II. New York Toronto London, McGraw-Hill Book Company Inc., 1953.


## Авторы


**Черницкий Александр Александрович**, к.ф.-м.н., доцент, Санкт-Петербургский Государственный Химико-Фармацевтический Университет, ул. Проф. Попова, д. 14, г. Санкт-Петербург, 197376, Россия.
E-mail: alexander.chernitskii@pharminnotech.com, AAChernitskii@mail.ru



**Просьба ссылаться на эту статью следующим образом:**
Черницкий А. А. О лептонах в теории пространственно-временной плёнки. *Пространство, время и фундаментальные взаимодействия.* 2023. № 3-4. С. 48–53.


## Authors


**Chernitskii Alexander Aleksandrovich**, Ph.D., Associate Professor, St. Petersburg State Chemical and Pharmaceutical University, Prof. Popov st., 14, St. Petersburg, 197376, Russia.
E-mail: alexander.chernitskii@pharminnotech.com, AAChernitskii@mail.ru



**Please cite this article in English as:**
Chernitskii A. A. About leptons in space-time film theory. *Space, Time and Fundamental Interactions*, 2023, no. 3-4, pp. 48–53.

УДК 530.12, 530.122



## СПИНЫ СВЕРХМАССИВНЫХ ЧЕРНЫХ ДЫР

Докучаев В. И.[a,1]

[a] Институт ядерных исследований РАН, Москва 117312, Проспект 60-летия Октября 7а, Россия.

Формы изображений черных дыр, наблюдаемые удаленным телескопом (наблюдателем), зависят от распределения излучающего вещества вокруг черных дыр. Возможны два принципиально различных случая: (1) яркий стационарный фон позади черной дыры (излучение фотонов вне фотонных сфер). В этом случае наблюдается класссическая тень черной дыры, которая является сечением захвата фотонов в гравитационном поле черной дыры. (2) яркий аккреционный поток вблизи горизонта событий черной дыры (излучение фотонов внутри фотонных сфер). В этом случае наблюдается темная тень черной дыры, которая является гравитационно-линзированным изображением части глобуса самого горизонта событий черной дыры. Размер и форма этого темного изображения (темного пятна) зависят от массы и спина черной дыры. Существование горячей аккрецируемой материи иблизи горизонта событий предсказывается механизмом Блэндфорда-Знайека. Основной особенностью этого механизма является существование электрического тока, генерируемого в аккреционной плазме и протекающего через черную дыру. Этот ток очень сильно нагревает аккрецируемое вещество вблизи горизонта событий черной дыры, обеспечивая доминирующий вклад в светимость черной дыры. Размеры и форма темных пятен на изображениях, полученных коллаборацией Телескоп Горизонта Событий, свидетельствуют о быстром вращении сверхмассивных черных дыр SgrA* (спин 0.65<a<0.9) и M87* (спин a>0.75).

*Ключевые слова*: Черные дыры, общая теория относительности, гравитационное линзирование.

## SPINS OF SUPERMASSIVE BLACK HOLES

Dokuchaev V. I.[a,1]

[a] Institute for Nuclear Research of the Russian Academy of Sciences, prospekt 60-letiya Oktyabrya 7a, Moscow 117312, Russia.

Shapes of black hole images, viewed by a distant observer, depend on the distribution of emitting matter around black holes. There are two distinctive astrophysical cases: (1) Luminous stationary background behind the black hole (emission of photons outside the photon spheres). In this case the dark classical black hole shadow is viewed, which is a capture photon cross-section in the black hole gravitational field. (2) Luminous accretion inflow near the black hole event horizon (emission of photons inside the photon spheres). In this case the dark event horizon shadow is viewed, which is a lensed image of the event horizon globe. The existence of hot accreting matter in the vicinity of black hole event horizons is predicted by the Blandford-Znajek mechanism. The basic feature of this mechanism is the existing of electric current embracing the black hole and heating the accretion disk very near the black hole event horizon providing the main contribution to the black hole luminosity. We used the numerically calculated sizes of dark spots in the EHT images of supermassive black holes SgrA* and M87* for inferring their spins, $0.65 < a < 0.9$ and $a > 0.75$, respectively.

*Keywords*: Black holes, general relativity, gravitational lensing.

PACS: 04.70.Bw, 98.35.Jk, 98.62.Js

DOI: 10.17238/issn2226-8812.2023.3-4.54-62

## Introduction

The blistering technological progress in astronomical and astrophysical experiments provides the successful opportunity for formulation of the “Standard Astronomical and Astrophysical Model” quite like the “The Standard Model of Particle Physics”. The supermassive black holes with masses $M >$

[1]E-mail: dokuchaev@inr.ac.ru

$10^6 M_\odot$ (where $M_\odot$ is the Sun mass), reside either in the centers of galaxies or at the intergalactic space, are the indispensable components of this "Standard Model". Nowadays we have the clear qualitative understanding of the astrophysical properties of supermassive black holes owing to the huge amount of the observational data and theoretical predictions in the framework of the General Relativity [1, 2, 3, 3, 4, 5, 6, 7, 8, 9, 10, 10, 11, 12, 13, 14, 16, 17, 18, 19, 20, 21, 22, 23, 24, 25, 26, 27, 28, 30, 31, 33, 34, 35, 36, 37, 38, 39, 40**?** ].

The existence of hot accreting matter in the vicinity of black hole event horizons is predicted by the Blandford-Znajek mechanism [38], which is confirmed by recent General Relativistic MHD numerical simulations at the most powerful supercomputers. The basic feature of the Blandford-Znajek mechanism is the existing of electric current embracing the black hole and heating the accretion disk very near the black hole event horizon providing the main contribution to the black hole luminosity. This luminosity exceeds in many orders the corresponding luminosity from the stationary background behind the black hole. A dark spot at the black hole image in the Blandford-Znajek mechanism is a lensed image of the event horizon globe. This luminosity exceeds in many orders the corresponding luminosity from the stationary background behind the black hole.

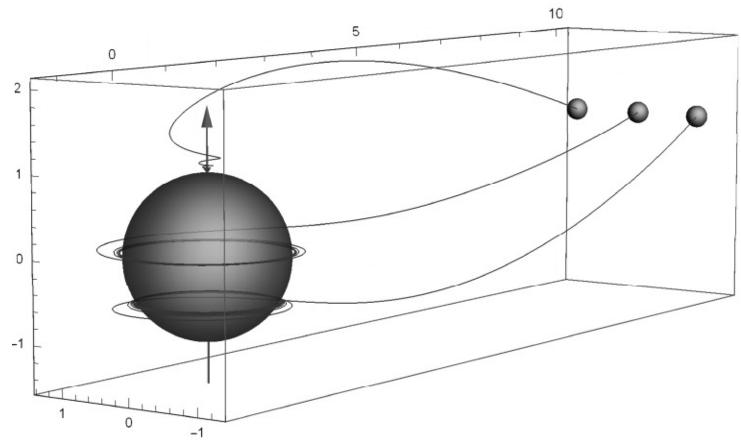


**Рис. 1.** The examples of $3D$ numerically calculated trajectories of massive test particles, infalling into the fast rotating black hole with spin $a = 1$. Particles are winding on the event horizon in the direction of the black rotation by approaching to the black hole. The dark grey sphere is the globe of the black hole event horizon. Arrow shows the direction of the black hole spin (for details see [41, 42, 43, 44, 45, 46, 47, 48, 49]).

The theoretical framework for understanding the black hole physics is the classical Einstein theory of gravity (the General Relativity) providing also the quasi-classical description of the amazing Hawking black hole evaporation. The major discoveries of last decade, related with the black holes are the direct detection of gravitational waves by the laser interferometers [1] and direct observation of the supermassive black hole images by the Event Horizon collaboration [2, 3, 4, 5, 6, 7, 8, 9, 10, 11, 12, 13, 14]. There are the plentiful publications describing the astrophysical and physical properties of black holes, including the supermassive ones. See, e. g., the subjectively chosen list of textbooks, monographs and review articles [3, 10, 16, 17, 18, 19, 20, 21, 22, 23, 24, 25, 26, 27, 28, 30, 31, 32, 33, 34, 35, 36, 37, 38, 39, 40].

In this paper we describe mainly the theoretical physical concepts and observational astrophysical data related with the rotation of supermassive black holes, which is crucially important for different physical phenomena: a huge energy emission from the accreting matter, a generation of giant relativistic jets or production of High Energy Cosmic Rays (HECRs).

The numerous observational astrophysical data indicating in favour of the fast rotation of supermassive black holes in the Active Galactic Nuclei (AGNs) were obtained initially by the interferometric radio-telescopes. It was the discovery of the extremely long relativistic jets from the Active Galactic Nuclei [50, 51, 52, 53, 54]. The relativistic jets from the Active Galactic Nuclei are the

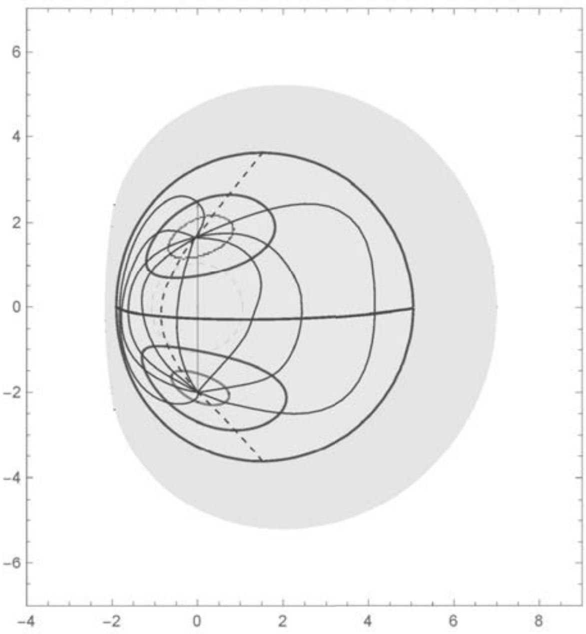


**Рис. 2.** A reconstruction of the lensed event horizon globus of SgrA* with distant observer a little bit above the black hole equatorial plane. The closed curves are meridians and parallels on the lensed event horizon globe. The dashed curve is the null meridian. The grey region is the position of the classical black hole shadow projected at the celestial sphere. Arrow shows the direction of the black hole spin. The dashed ring is the size of the event horizon in the imaginary Euclidean space without gravity. For more details see [41, 42, 43, 44, 45, 46, 47, 48, 49].

inevitable sources of the observable High Energy Cosmic Rays, including photons, protons, neutrinos and, possibly, the hypothesized dark matter particles [55, 56, 57, 58, 59, 60].

A dark spot at the black hole image in the Blandford-Znajek mechanism is a lensed image of the event horizon globe. We calculate numerically the form of dark spots at the black hole images by using Carter equations of motion [17] of test articles in the Kerr metric [10]. For more details see [41, 42, 43, 44, 45, 46, 47, 48, 49].

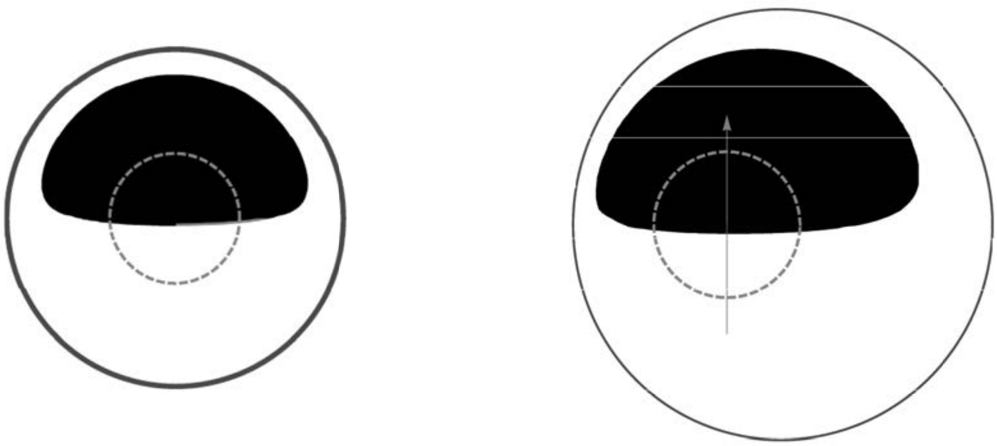

**Рис. 3.** Superposition of the observable image of SgrA* with the modelled dark spot at the value of spin $a = 0$ (left) and $a = 0.65$ (right). The closed curve is the position of the outer boundary of the classical black hole shadow at the celestial sphere. The dashed ring is the size of the event horizon in the imaginary Euclidean space without gravity.

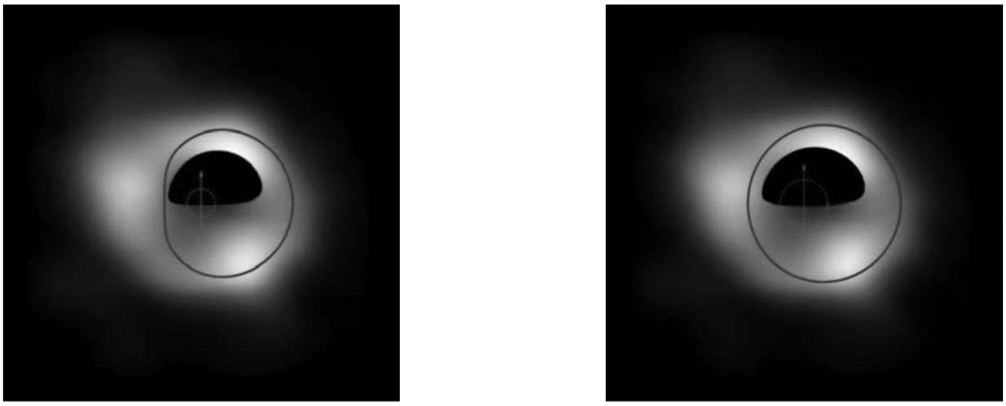

**Рис. 4.** The superposition of the Event Horizon Telescope image of supermassive black hole SgrA* with the corresponding numerically modelled dark spot in the case of $a = 1$ (left panel) and $a = 0.75$ (right panel). The closed curve is the position of the outer boundary of the classical black hole shadow at the celestial sphere. The dashed ring is the size of the event horizon in the imaginary Euclidean space without gravity. Arrow shows the direction of the black hole spin.

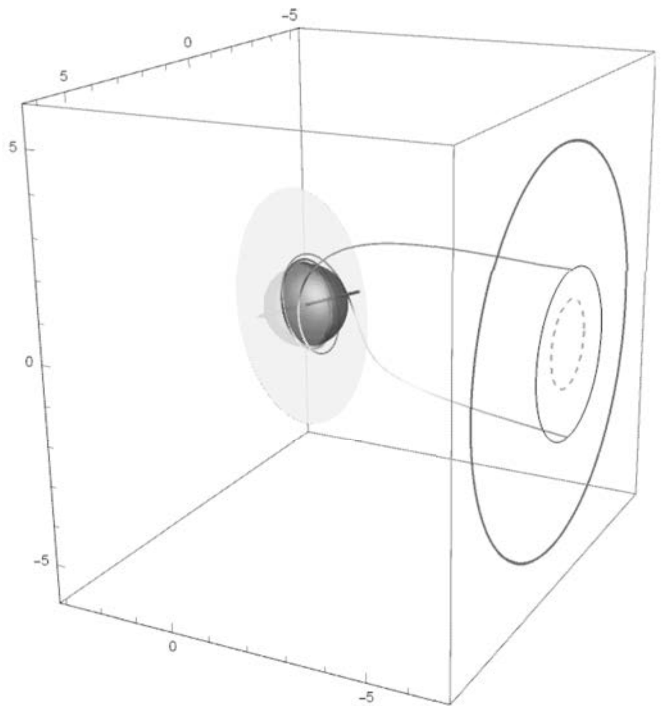


**Рис. 5.** Spin orientation of the supermassive black hole M87* athe center of the giant elliptical galaxy M87 with respect to the distant observer at the Earth. Arrow shows the direction of the black hole spin. The grey disk is a thin accretion disk in the equatorial plane of this black hole. The biggest closed curve at the right side of the box is a outer boundary of the projection of classical black hole shadow at the celestial sphere. The smaller closed curve is the outer boundary of the dark spot, which in this case is a gravitationally lensed equator of the event horizon globe. The inner part of the dark spot is a gravitationally lensed south hemisphere of the black hole globe. The dashed ring is the size of the event horizon in the imaginary Euclidean space without gravity. Arrow shows the direction of the black hole spin.

The very promising physical idea for the explanation of the relativistic jet formation and energy extraction from the fast-rotating black holes was formulated by the Blandford and Znajek [38]. This idea nowadays is called the "Blandford-—Znajek mechanism" and confirmed by the numerous General Relativistic Magneto-Hydro-Dynamical (GRMHD) supercomputer simulations [53, 54, 55, 56].

The crucial point of the "Blandford-—Znajek mechanism" is the electric current, generated in the accreting plasma and flowing through the event horizon of fast-rotating black hole. The accreting plasma under these conditions is continuously heated by the electric current up to the very vicinity of the black hole event horizon. Correspondingly, the heated plasma ensures the strong radiation emission from the very vicinity of the black hole event horizon. Additionally, it is generated the emission of the electromagnetic radiation in the form of the Pointing energy flux $P$ along the black hole rotation axis: $P = (1/4)c[EH]$ with $c$ — velocity of light and, respectively, the electric and magnetic fields $E$ and $H$, generated by the accreting plasma around the black hole.

It must be checked that in the classical Shakura-—Sunyaev alpha-model of the accretion disc [57] the strong emission of accreting plasma is absent inside the region without the stable motion due to a fast cooling-down of the accreting plasma.

All observational data and theoretical physical ideas are in accordance with the fast rotation of supermassive black holes in the "Standard Astronomical and Astrophysical Model".

## 1. Recovering the spins of supermassive black holes from the form of their images

The angular momenta of black holes in the General Relativity are described by the classical Kerr metric [10], depending on two parameters: the dimensional spin a, valued in the range $0 \leq a \leq 1$ and the black hole mass M (if $0 \leq a \leq 1$), or the mass of naked singularity (if $a > 1$).

The images (or silhouettes) of supermassive black holes M87* at the center of the giant galaxy M87 and SgrA* at the center of our Galaxy, obtained recently by the Event Horizon Telescope collaboration [2, 3, 4, 5, 6, 7, 8, 9, 10, 11, 12, 13, 14], open the unique possibility for the recovering spin values of these black holes. In accordance with the theoretical predictions for Einstein gravity and for modified gravity theories both the form and size of the dark spots at the central parts of the observed images strongly depend on the black hole spin value.

The simplest possible image is the classical black hole shadow, which is the capture photon cross section in the strong black hole gravitational field. The corresponding equation for the outer boundary of the classical black hole shadow can be written in the following parametric form $(\lambda, q) = (\lambda(r), q(r))$, [18, 27]:

$$\lambda = \frac{-r^3 + 3r^2 - a^2(r+1)}{a(r-1)}, \quad q^2 = \frac{r^3[4a^2 - r[(r-3)]^2]}{a^2(r-1)^2}. \tag{1.1}$$

Here $\lambda$ and $q$ are the orbital parameters of photon trajectories, related with the horizontal and vertical impact parameters $\alpha$ and $\beta$, respectively, for the projection of the Kerr black hole shadow on the celestial sky, viewed by a distant observer at the black hole equatorial plane [22, 23].

The very intriguing possibility for the described spin measurement is in detection of the photon ring structures just outside and inside the classical black hole shadow. This detection is a main task of the projected Millimetron Space Observatory [58, 59].

At last, the additional possibility to measure the supermassive black hole spins is related with the Lense-Thirring orbital shift of the short-period S-stars orbiting supermassive black hole Sgr A* [60] and with the observations of wobbling and rotation of relativistic jet near black hole event horizons [61, 62, 63].

At all Figures of this paper the linear unit is $GM/c^2 = 1$, where $G$ — Newtonian constant, $M$ — black hole mass, $c$ — velocity of light. Correspondingly, the projection of the classical black hole shadow on the celestial sphere is drawing by grey color. It is also sometimes shown the closed curve of the outer boundary of this classical black hole shadow. Arrow shows the direction of the black hole spin. The dashed ring is the size of the event horizon in the imaginary Euclidean space without gravity.

See in Figure 1 the examples of $3D$ numerically calculated trajectories of massive test particles, infalling into the fast rotating black hole with spin $a = 1$. Particles are winding on the event horizon in the direction of the black hole rotation by approaching to the black hole. The dark grey sphere is the globe of the black hole event horizon.

Figure 2 shows a reconstruction of the lensed event horizon globus of the supermassive black hole SgrA* with distant observer a little bit above the black hole equatorial plane. The closed curves are meridians and parallels on the lensed event horizon globe. The dashed curve is the null meridian. The grey region is the projection of the classical black hole shadow on the celestial sphere. For more details see [41, 42, 43, 44, 45, 46, 47, 48, 49].

Figures 3 demonstrates the numerically calculated forms of dark spots for the case of supermassive black hole SgrA* with a distant observer at the black hole equatorial plane and with the spin values $a = 0$ and $a = 0.65$, respectively. The closed curve is the position of the outer boundary of the classical black hole shadow at the celestial sphere.

Figure 4 shows the the superposition of the Event Horizon Telescope image of supermassive black hole SgrA* with the corresponding numerically modelled dark spot in the case of $a = 1$ (left panel) and $a = 0.75$ (right panel). Again, the closed curve is the position of the outer boundary of the classical black hole shadow at the celestial sphere.

superposition of the Event Horizon Telescope image of supermassive black hole SgrA* with the corresponding dark spot in the case of $a = 1$ (left panel) and $a = 0.75$ (right panel).

At last, Figure 5 demonstrates the $3D$ position and orientation of the supermassive black hole M87* with respect to the distant observer at the Earth.

Finally, we used the numerically calculated sizes of dark spots in the EventHorizon Telescope images of SgrA* and M87* for inferring their spins, $0.65 < a < 0.9$ and $a > 0.75$, respectively. For more details see [49].

## Conclusion

The supermassive black holes are the important ingredients of the "Standard Astronomical and Astrophysical Model". Nowadays all observational data and theoretical physical ideas are in accordance with the fast rotation of supermassive black holes.

The gravitationally lensed images (silhouettes) of event horizons are always projected at the celestial sphere inside the awaited positions of the classical black hole shadows. We used the numerically calculated sizes of dark spots in the EHT images of supermassive black holes SgrA* and M87* for inferring their spins, $0.65 < a < 0.9$ and $a > 0.75$, respectively.

It would be possible to reconstruct the dark spot forms at the images of supermassive black holes SgrA* and M87* with the projected Millimetron Space Observatory, by using the model of geometrically thin accretion disk highlighting black hole in the vicinity of its event horizon. This reconstruction also provides the possibility for spin determinations of these supermassive black holes.

**Acknowledgments:** I am very grateful to E. O. Babichev, V. A. Berezin, Yu. N. Eroshenko and N. O. Nazarova for stimulating discussions.

## Список литературы/References

1. Abbott B.P. et al. (LIGO Scientific Collaboration and Virgo Collaboration). Observation of Gravitational Waves from a Binary Black Hole Merger. *Phys. Rev. Lett.*, 2016, 116, 061102, 16pp.
2. Akiyama, K. et al. Event Horizon Telescope Results. I. The Shadow of the Supermassive Black Hole. *Astrophys. J.*, 2019, 875, L1, 17pp.
3. Akiyama, K. et al. First M87 Event Horizon Telescope Results. II. Array and Instrumentation. *Astrophys. J.*, 2019, 875, L2, 28 pp.
4. Akiyama, K. et al. First M87 Event Horizon Telescope Results. III. Data Processing and Calibration *Astrophys. J.*, 2019, 875, L3, 32 pp.
5. Akiyama, K. et al. First M87 Event Horizon Telescope Results. IV. Imaging the Central Supermassive Black Hole. *Astrophys. J.*, 2019, 875, L4, 52 pp.

6. Akiyama, K. et al. First M87 Event Horizon Telescope Results. V. Physical Origin of the Asymmetric Ring. *Astrophys. J.*, 2019, 875, L5, 31 pp.
7. Akiyama, K. et al. First M87 Event Horizon Telescope Results. VI. The Shadow and Mass of the Central Black Hole. *Astrophys. J.*, 2019, 875, L6, 44 pp.
8. Event Horizon Telescope Collaboration et al. First Sagittarius A* Event Horizon Telescope Results. I. The Shadow of the Supermassive Black Hole in the Center of the Milky Way. *ApJL*, 2022, 930, L12, 21pp.
9. Event Horizon Telescope Collaboration et al. First Sagittarius A* Event Horizon Telescope Results. II. EHT and Multiwavelength Observations, Data Processing, and Calibration. *ApJL*, 2022, 930, L13, 31pp.
10. Event Horizon Telescope Collaboration et al. First Sagittarius A* Event Horizon Telescope Results. III. Imaging of the Galactic Center Supermassive Black Hole. *ApJL*, 2022, 930, L14, 64pp.
11. First Sagittarius A* Event Horizon Telescope Results. IV. Variability, Morphology, and Black Hole Mass. *ApJL*, 2022, 930, L15, 52pp.
12. Event Horizon Telescope Collaboration et al. First Sagittarius A* Event Horizon Telescope Results. V. Testing Astrophysical Models of the Galactic Center Black Hole *ApJL*, 2022, 930, L16, 49pp.
13. Event Horizon Telescope Collaboration et al. First Sagittarius A* Event Horizon Telescope Results. VI. Testing the Black Hole Metric. *ApJL*, 2022, 930, L17, 44pp.
14. Broderick A.E. et al. Characterizing and Mitigating Intraday Variability: Reconstructing Source Structure in Accreting Black Holes with mm-VLBI. *ApJL*, 2022, 930, L21, 30pp.
15. Kerr R.P. Gravitational Field of a Spinning Mass as an Example of Algebraically Special Metrics. *Phys. Rev. Lett.*, 1963, 11, 237-238.
16. Zel'dovich Ya.B.; Novikov I. D. Relativistic astrophysics. II. *Sov. Phys. Usp.*, 1966, 8, 522-577.
17. Carter B. Global Structure of the Kerr Family of Gravitational Fields. *Phys. Rev.*, 1968, 174, 1559-1571.
18. Bardeen J.M. Stability of Circular Orbits in Stationary, Axisymmetric Space-Times. *Astrophys. J.*, 1970, 161, 103-109.
19. Lynden-Bell D., Rees M.J. On quasars, dust and the Galactic Centre. *MNRAS*, 1971, 152. 461-475.
20. Zel'dovich Ya.B., Novikov I.D. Relativistic Astrophysics: Stars and Relativity Vol. 1 (Chicago: Univ. of Chicago Press), 1971 522pp.
21. Bardeen J.M.; Press W.H., Teukolsky S.A. Rotating Black Holes: Locally Nonrotating Frames, Energy Extraction, and Scalar Synchrotron Radiation. *Astrophys. J.*, 1972, 178, 347-370.
22. Cunningham C.T., Bardeen J.M. The Optical Appearance of a Star Orbiting an Extreme Kerr Black Hole. *Astrophys. J.*, 1972, 173, L137-L142.
23. Cunningham C.T., Bardeen J.M. The Optical Appearance of a Star Orbiting an Extreme Kerr Black Hole. *Astrophys. J.*, 1973, 163, 237-264.
24. Novikov I.D., Thorne K.S. in Black Holes (Eds C DeWitt, B S DeWitt) (New York: Gordon and Breach, 1973) 108 pages.
25. Bardeen J.M., Carter B., Hawking S.W. The four laws of black hole mechanics. *Commun. Math. Phys.*, 1973 31, 161-170.
26. Misner C.W., Thorne K.S., Wheeler J.A. (WH Freeman, San Francisco, CA), 1973, 1304 pages.
27. Bardeen J.M. Timelike and null geodesics in the Kerr metric. In: DeWitt C., DeWitt B.S. (eds.) Black Holes (Gordon and Breach, New York), 1973 pp. 217-239.
28. Zel'dovich Ya.B. Neutron Stars and "Black Holes". *Sov. Phys. Usp.*, 1974, 16, 559-560.
29. Landau L.D., Lifshitz E.M. The Classical Theory of Fields (Oxford: Pergamon Press), 1975, 402 pages.

30. Rees M.J. Relativistic jets and beams in radio galaxies. *Nature*, 1978, 275, 516-517.
31. Eichler D., Smith M. Why is M87 jet one sided in appearance? *Nature*, 1983, 303, 779-781.
32. Rees M.J. Black Hole Models for Active Galactic Nuclei. *Annu. Rev. Astron. Astrophys.*, 1984 22, 471-506.
33. Begelman M.C., Blandford R.D., Rees M.J. Theory of extragalactic radio sources. *Rev. Mod. Phys.*, 1984, 56, 255-351
34. Chandrasekhar S. The Mathematical Theory of Black Holes (Oxford: Clarendon Press), 1983, 646 pages.
35. Carter, B. Global Structure of the Kerr Family of Gravitational Fields *Phys. Rev.*, 1968, 174, 1559-1571.
36. Dokuchaev V.I. Birth and life of massive black holes *Sov. Phys. Usp.*, 1991, 34, 447-470.
37. Frolov V.P., Novikov I.D. Black Hole Physics: Basic Concepts and New Developments (Dordrecht: Kluwer Acad. Publ.), 1998, 770 pp.
38. Blandford R. D., Znajek R.L. Electromagnetic extraction of energy from Kerr black holes. *MNRAS*, 1973, 179, 433-456.
39. Beskin V.S. MHD flows in compact astrophysical objects: accretion, winds and jets (Extraterrestrial Physics & Space Sciences, Springer), 2010
40. Galtsov D.V. Particles and Fields in the Vicinity of Black Holes (Moscow Univ. Press: Moscow, Russia), 1986 288 pages (in Russian).
41. Dokuchaev V.I.; Nazarova N.O. Gravitational lensing of a star by rotating black hole. *JETP Letters*, 2017, 106, 637-642.
42. Dokuchaev V.I., Nazarova N.O., Smirnov V.P. Event horizon silhouette: Implications to supermassive black holes M87* and SgrA*. *Gen. Relativ. Gravit.*, 2019, 51, 81, 17pp.
43. Dokuchaev V.I., Nazarova N.O. Event horizon image within black hole shadow *J. Exp. Theor. Phys.*, 2019, 128, 578-585
44. Dokuchaev V.I., Nazarova N.O. Brightest point in accretion disk and black hole spin: Implication to the image of black hole M87*. *Universe*, 2019, 5, 183, 13pp.
45. Dokuchaev V.I. To see invisible: image of the event horizon within the black hole shadow *Intern. J. Mod. Phys. D*, 2019, 28, 1941005, 16pp.
46. Dokuchaev V.I., Nazarova N.O. Silhouettes of invisible black holes. *Phys. Usp.*, 2020, 63, 583-600.
47. Dokuchaev V.I., Nazarova N.O. Visible shapes of black holes M87* and SgrA* *Universe*, 2020 Universe 6, 154, 27pp.
48. Dokuchaev V.I., Nazarova N.O. Motion of bright spot in jet from black hole viewed by a distant observer, 2020, `https://youtu.be/7j8f_vlTul8`.
49. Dokuchaev V.I. Spins of Supermassive Black Holes M87* and SgrA* Revealed from the Size of Dark Spots in Event Horizon Telescope Images. *Astronomy*, 2023, 2, 141-152.
50. Loeb A., Waxman E. The cumulative background of high energy neutrinos from starburst galaxies. *JCAP*, 2007, 03, 011.
51. Plavin A., Kovalev Y.Y., Kovalev Yu.A., Troitsky S.V. Observational evidence for the origin of high-energy neutrinos in parsec-scale nuclei of radio-bright active galaxies. *Astrophys. J.*, 2020, 894, 101, 13pp.
52. Kovalev Y. Y., Plavin A. V., Pushkarev A.B. Troitsky S.V. Probing Neutrino Production in Blazars by Millimeter VLBI *Galaxies*, 2023, 11, 84, 8pp.
53. Tchekhovskoy A., McKinney J.C., Narayan R. General Relativistic Modeling of Magnetized Jets from Accreting Black Holes. *J. Phys. Conf. Ser.*, 2012, 372, 012040, 8pp.
54. McKinney J.C., Tchekhovskoy A., Blandford R.D. General relativistic magnetohydrodynamic

simulations of magnetically choked accretion flows around black holes. *MNRAS*, 2012, 423, 3083-3117.

55. Ressler S. M., Tchekhovskoy A., Quataert E., Chandra M., Gammie C.F. The Disc-Jet Symbiosis Emerges: Modeling the Emission of Sagittarius A* with Electron Thermodynamics. *MNRAS*, 2017, 467, 3604-3619.
56. Ryan B.R., Ressler S.M. Dolence J.C, Tchekhovskoy A., Gammie C, Quataert E. The Radiative Efficiency and Spectra of Slowly Accreting Black Holes from Two-temperature GRRMHD Simulations *ApJL*, 2017, 844 L24, 7pp.
57. Shakura N. I.; Sunyaev R. A. 1973 Astronomy and Astrophysics 24, 337
58. ShatskiyA. A.; Novikov I. D.; Kardashev N.S. 2011 Phys. Usp. 54, 381 (2011)
59. Likhachev S. F.; Rudnitskiy A. G.; Shchurov M. A.; Andrianov A. S.; Baryshev A. M.; Chernov S. V.; Kostenko V. I. 2022 MNRAS 511, 668
60. Iorio L. 2023 Is it possible to measure the Lense-Thirring orbital shifts of the short-period S-star S4716 orbiting Sgr A*. Preprint gr-qc/2306.17432
61. Broderick, A.E.; Loeb, A. Imaging the Black Hole Silhouette of M87: Implications for Jet Formation and Black Hole Spin. *Astrophys. J.*, 2009, 697, 1164-1179.
62. Sob'yanin D.N. Black hole spin from wobbling and rotation of the M87 jet and a sign of a magnetically arrested disc. *MNRAS*, 2018, 479, L65-L69.
63. Reynolds C.S. Observing black holes spin. *Nat. Astron.*, 2019, 3, 41-47.

**Авторы**

**Докучаев Вячеслав Иванович**, д.ф.-м.н., ведущий научный сотрудник, Институт ядерных исследований РАН, Москва 117312, Проспект 60-летия Октября 7а, Россия.
E-mail: dokuchaev@inr.ac.ru

**Просьба ссылаться на эту статью следующим образом:**

Докучаев В. И. Спины сверхмассивных черных дыр. *Пространство, время и фундаментальные взаимодействия.* 2023. № 3-4. С. 54–62.

**Authors**

**Dokuchaev Vyacheslav Ivanovich**, Ph.D., Leading scientific researcher, Institute for Nuclear Research of the Russian Academy of Sciences, prospekt 60-letiya Oktyabrya 7a, Moscow 117312, Russia.
E-mail: dokuchaev@inr.ac.ru

**Please cite this article in English as:**

Dokuchaev V. I. Spins of supermassive black holes. *Space, Time and Fundamental Interactions*, 2023, no. 3-4, pp. 54–62.

УДК 53.01, 52-43, 52-423



## СВОЙСТВА АККРЕЦИОННЫХ ДИСКОВ В ГИБРИДНОЙ МЕТРИЧЕСКОЙ-ПАЛАТИНИ F(R)-ГРАВИТАЦИИ*

Дядина П. И.[a,1], Авдеев Н. А.[a,2]

[a] ГАИШ МГУ, Москва, 119234, Россия.

Гибридная метрическая-Палатини f(R)-гравитация на данный момент является одной из перспективных модифицированных теорий гравитации, основной задачей которой является объяснение ускоренного расширения Вселенной. Однако любая теория должна быть проверена на различных наблюдательных данных. В данной работе гибридная f(R)-гравитация будет рассмотрена в сильном поле черных дыр, а именно будет построен поток энергии и светимость от тонких аккреционных дисков, формирующихся вокруг таких объектов. Данное исследование позволит выявить возможные отличия от общей теории относительности в объяснении наблюдательных данных, что впоследствии поможет понять, насколько рассматриваемая теория релевантна. В частности, одним из результатов работы является то, что аккреционные диски в гибридной f(R)-гравитации тусклее, чем предсказывает общая теория относительности.

*Ключевые слова*: модифицированные теории гравитации, аккреционные диски, черные дыры, гравитация.

## PROPERTIES OF ACCRETION DISKS IN HYBRID METRIC-PALATINI F(R) GRAVITY

Dyadina P. I.[a,1], Avdeev N. A.[a,2]

[a] SAI MSU, Moscow, 119234, Russia.

Hybrid metric-Palatini f(R)-gravity is currently one of the most promising modified theories of gravity, the main task of which is to explain the accelerated expansion of the Universe. However, any theory must be tested in wide range of observational data from different objects. In this work, hybrid f(R)-gravity are tested in the strong field of black holes, namely, the energy flux and luminosity from thin accretion disks that form around such objects in this model are constructed. This study identifies possible differences from the general relativity in explaining observational data, which subsequently help to understand how relevant the theory is. One of the results of the work is that accretion disks in hybrid f(R)- gravity are dimmer than predicted by general relativity.

*Keywords*: modified theories of gravity, accretion disks, black holes, gravity.

PACS: 95.30.Sf , 97.10.Gz, 04.50.Kd

DOI: 10.17238/issn2226-8812.2023.3-4.63-76

### Введение

На данный момент в современной физике остро стоят проблемы ускоренного расширения Вселенной [1, 2] и наличия темного вещества, которое проявляется в наблюдениях на масштабе галактик и их скоплений [3, 4]. Помимо этого, до сих пор нет теории, которая позволяла бы описывать гравитацию на квантовом уровне. Проблемы в ранней Вселенной также приводят к необходимости поиска подходящей модели, которая бы адекватно описывала инфляцию [5, 6, 7]. Одним из наиболее распространенных методов решения этих вопросов является модификация общепринятой теории гравитации — общей теории относительности (ОТО). Существуют разные методы расширения ОТО, однако один из самых распространенных подходов — это f(R)-теории [8].

*Дядина П.И. благодарит Российский научный фонд за поддержку данной работы (грант № 22-72-00022).

[1]E-mail: guldur.anwo@gmail.com

[2]E-mail: naavdeev1995@mail.ru

Модели f(R)-гравитации представляют собой обобщение действия Эйнштейна-Гильберта путем замены скаляра Риччи на произвольную функцию этой величины. Семейство f(R)-теорий делится на два подкласса: метрический и Палатини. В рамках первого единственной переменной является метрика, во втором же аффинная связность рассматривается величиной, независящей от метрики. Однако оба подхода не лишены недостатков [9, 10]. Этот последний факт привел к появлению модели гибридной метрической-Палатини f(R)-гравитации [11]. Данная теория объединяет в себе метрический и Палатини подходы, при этом не включает их недостатки. Действие модели совмещает в себе действие Эйнштейна-Гильберта и произвольную функцию от скаляра Риччи Палатини. Гибридная f(R)-гравитация исследовалась на широком диапазоне масштабов и гравитационных режимов. Подробный обзор всех исследований данной модели приведен в работе [12]. Основным же преимуществом гибридной f(R)-гравитации является то, что она позволяет описывать как ускоренное расширение Вселенной, так и масштабы Солнечной системы без использования экранирующих механизмов. Также важно отметить тот факт, что теория имеет скалярно-тензорное представление, что облегчает ее рассмотрение и анализ.

Недавно было найдено первое (и на данный момент единственное) численное статическое сферически-симметричное решение типа черная дыра в гибридной f(R)-гравитации [13]. Данное решение было получено в двух случаях: в случае отсутствия потенциала $V(\phi) = 0$ и с учетом потенциала хиггсовского типа $V(\phi) = -\frac{\mu^2}{2}\phi^2 + \frac{\zeta}{4}\phi^4$. Одним из методов проверки адекватности такого решения может быть рассмотрение свойств аккреционных дисков вокруг таких черных дыр. Аккреция — это процесс падения материи на черную дыру. Данный процесс очень чувствителен к особенностям теории гравитации, что позволяет его использовать для наложения ограничений на рассматриваемые гравитационные модели. Исторически первая модель аккреции была создана Н. Шакурой и Р. Сюняевым [14]. Первая же модель, учитывающая релятивистские эффекты, была разработана И. Новиковым и К. Торном [15, 16]. В данной работе мы будем использовать численное сферически-симметричное решение для вычисления потока энергии и светимости от тонкого аккреционного диска. В работе используется модель Новикова-Торна. Также будет произведено сравнение полученных результатов с предсказаниями ОТО, что позволит сделать выводы о жизнеспособности теории и адекватности полученного ранее сферически-симметричного решения.

Статья разделена на пять разделов. В первом разделе дается описание гибридной $f(R)$-модели и ее скалярно-тензорного представления. Во втором разделе мы представляем модель Новикова-Торна. В третьем разделе представлены результаты численного расчета свойств аккреции в гибридной $f(R)$-гравитации. В четвертом разделе обсуждаются полученные результаты. В заключении суммируются наши выводы.

На протяжении всей статьи греческие индексы $(\mu, \nu, ...)$ пробегают $0, 1, 2, 3$, и принимается сигнатура $(-, +, +, +)$. Все расчеты выполняются в системе СГС.

## 1. Гибридная f(R)-гравитация

Действие гибридной метрической-Палатини f(R)-гравитации состоит из члена Эйнштейна-Гильберта и произвольной функции кривизны Палатини [11]:

$$S = \frac{1}{2k^2} \int d^4x\sqrt{-g}\,[R + f(\mathfrak{R})] + S_m, \tag{1.1}$$

где $k^2 = 8\pi G$, $G$ — ньютоновская гравитационная постоянная, $R$ и $\mathfrak{R} = g^{\mu\nu}\mathfrak{R}_{\mu\nu}$ — метрическая и Палатини кривизна соответственно, $g$ — определитель метрического тензора, $S_m$ — действие материи. Здесь Палатини кривизна $\mathfrak{R}$ определяется как функция $g_{\mu\nu}$ и независимо определяемых символов Кристоффеля $\hat{\Gamma}^{\alpha}_{\mu\nu}$.

Как и в случае чисто метрических и Палатини f(R)-теорий, действие (1.1) может быть представлено в терминах скалярного поля (более подробный вывод представлен в работах [11]):

$$S = \frac{1}{2k^2} \int d^4x \sqrt{-g} \left[ (1+\phi)R + \frac{3}{2\phi} \partial_\mu \phi \partial^\mu \phi - V(\phi) \right] + S_m, \tag{1.2}$$

где $\phi$ — это скалярное поле, и $V(\phi)$ — это скалярный потенциал. В действии (1.2) скалярное поле неминимально связано с материей, а кинетический член является неканоническим. Уравнения поля, получаемые из (1.2), имеют следующий вид citeHarko2012:

$$(1+\phi)R_{\mu\nu} = k^2 \left( T_{\mu\nu} - \frac{1}{2} g_{\mu\nu} T \right) - \frac{3}{2\phi} \partial_\mu \phi \partial_\nu \phi + \frac{1}{2} g_{\mu\nu} \left[ V(\phi) + \nabla_\alpha \nabla^\alpha \phi \right] + \nabla_\mu \nabla_\nu \phi, \tag{1.3}$$

$$\nabla_\mu \nabla^\mu \phi - \frac{1}{2\phi} \partial_\mu \phi \partial^\mu \phi - \frac{\phi[2V(\phi) - (1+\phi)V_\phi]}{3} = -\frac{k^2}{3} \phi T, \tag{1.4}$$

где $T_{\mu\nu}$ и $T$ — это тензор энергии-импульса и его след соответственно.

## 2. Модель тонкого аккреционного диска

Аккреционный диск — это астрофизическая структура, образующаяся вблизи массивного объекта и представляющая собой диффузный материал, вращающийся вокруг центрального тела. В данной статье рассматриваются только тонкие аккреционные диски. Первая модель таких дисков была разработана Н. Шакурой и Р. Сюняевым [14] и позднее расширена И. Новиковым, К. Торном и Д. Пейджем [15, 16] с учетом релятивистских эффектов. Тонкий аккреционный диск характеризуется тем, что его вертикальный размер $h$ пренебрежимо мал по сравнению с горизонтальным размером $h << r$. В таких структурах частицы движутся по кеплеровским орбитам, аккреционный диск расположен в экваториальной плоскости компактного тела, а скорость аккреции $\dot{M}_0$ предполагается постоянной во времени. Дополнительным условием является то, что в стационарной диске аккрецирующее вещество находится в термодинамическом равновесии.

В данной работе рассматривается статическая сферически-симметричная черная дыра. Метрика такой черной дыры задается следующим образом:

$$ds^2 = g_{00} dt^2 + g_{11} dr^2 + g_{22} d\theta^2 + g_{33} d\varphi^2, \tag{2.1}$$

где элементы $g_{00}, g_{11}, g_{22}, g_{33}$ зависят только от радиальной координаты $r$. Кроме того, используется экваториальное приближение $|\theta - \pi/2| << 1$. Чтобы определить основные характеристики аккреционного диска, необходимо определить приведенную энергию $\tilde{E}$, приведенный момент импульса $\tilde{L}$ и угловую скорость $\Omega$ [15]:

$$\tilde{E} = g_{00} \dot{t} = -\frac{g_{00}}{\sqrt{-g_{00} - g_{33}\Omega^2}}, \tag{2.2}$$

$$\tilde{L} = g_{22} \dot{\varphi} = \frac{g_{33}\Omega}{\sqrt{-g_{00} - g_{33}\Omega^2}}, \tag{2.3}$$

$$\Omega = \frac{d\varphi}{dt} = \sqrt{\frac{-g_{00,r}}{-g_{33,r}}}. \tag{2.4}$$

Здесь $\tilde{E} = E/m_0c^2$ и $\tilde{L} = L/m_0c$, где $E$ представляет собой полную энергию частицы на орбите, $m_0c^2$ — энергия покоя такой частицы, $L$ — ее момент импульса.

Одной из основных характеристик аккреционного диска является усредненный по времени поток энергии, излучаемый с поверхности диска. Поток излучения на единицу площади можно выразить через удельную энергию, угловой момент и угловую скорость частиц, вращающихся в диске, следующим образом:

$$F(r) = -\frac{\dot{M}_0}{4\pi\sqrt{-g}} \frac{\Omega_{,r}}{(\tilde{E} - \Omega\tilde{L})^2} \int_{r_{isco}}^{r} (\tilde{E} - \Omega\tilde{L}) \tilde{L}_{,r} r dr, \tag{2.5}$$

где $\dot{M}_0$ — скорость аккреции, $r_{isco}$ — радиус последней устойчивой орбиты.

Стационарная модель тонкого диска подразумевает, что аккрецирующее вещество находится в термодинамическом равновесии, а значит для описания излучения с поверхности диска применима модель абсолютно черного тела, а поток энергии может быть получен из закона Стефана-Больцмана: $F(r) = \sigma T(r)^4$, где $\sigma$ — постоянная Стефана-Больцмана. Следовательно, наблюдаемая светимость может быть определена следующим образом [17]:

$$L(\nu) = \frac{2h}{c^2} \cos\gamma \int_{r_i}^{r_f} \int_0^{2\pi} \frac{\nu_e^3 r d\varphi dr}{\exp\left(h\nu_e/kT\right) - 1}, \tag{2.6}$$

где $d$ — расстояние до источника, $\gamma$ — угол наклона диска, $r_i$ и $r_f$ — радиусы внутреннего и внешнего края диска соответственно; $\nu_e = \nu(1+z)$ обозначает частоту излучения, а красное смещение определяется как:

$$1 + z = \frac{1 + \Omega r \sin\varphi \sin\gamma}{\sqrt{-g_{00} - g_{33}\Omega^2}}, \tag{2.7}$$

где мы пренебрегаем искривлением света [18].

## 3. Свойства аккреционного диска

В данной работе мы исследуем свойства аккреционных дисков вокруг статических сферически-симметричных черных дыр в гибридной f(R)-гравитации. Само решение было найдено в работе [13]. В рамках же своего исследования мы повторили результаты, приведенные в статье [13], используя численные методы Python's scipy library. Результат оказался тождественным, поэтому мы не приводим его в своей работе и отсылаем интересующегося читателя к статье [13].

Для получения потока энергии от аккреционного диска и его светимости мы рассматриваем два случая: случай без потенциала $V = 0$ и с потенциалом хиггсовского типа $V = -\frac{\mu^2}{2}\phi^2 + \frac{\zeta}{4}\phi^4$. Кроме того, при получении необходимых характеристик аккреции нами были использованы реальные наблюдательные данные системы MAXI J1820+070 [19], такие как масса $M$ и скорость аккреции $\dot{M}$. Эта система выбрана из-за малого значения параметра Керра $a = 0,14$, который наиболее близок к черной дыре Шварцшильда.

В работе мы исследовали разные наборы свободных параметров в зависимости от выбранного случая (с потенциалом или без). В следующих двух подразделах мы подробно расскажем о выборе диапазонов параметров для первого и второго случая, а также полученных в рамках выбора результатах.

### 3.1. Случай $V = 0$

В случае $V = 0$ метрика гибридной f(R)-гравитации включает два параметра модели: начальное значение скалярного поля $\phi_0$ и начальное значение его производной $u_0$. Мы рассматриваем три случая:

1. фиксированное значение $\phi_0 = 1$ и диапазон $u_0 = [4 \times 10^{-9}; 6.4 \times 10^{-8}]$,

2. фиксированное значение $u_0 = 5.12 \times 10^{-7}$ и диапазон $\phi_0 = [0.5; 8]$,

3. связь между $\phi_0$ и $u_0$, полученная в результате постньютоновского анализа. Это соотношение имеет следующий вид:

$$u_0 = \frac{2GM\phi_0}{3c^2r^2}. \tag{3.1}$$

Его можно получить из выражения для скалярного возмущения $\varphi = \frac{-2GM\phi_0 e^{-m_\phi r}}{3c^2r}$ [20]. В данном случае мы рассматриваем $\phi_0 < 4 \times 10^{-5}$ [21]. Это ограничение на начальное значение скалярного поля было найдено с использованием данных эксперимента Кассини [22].

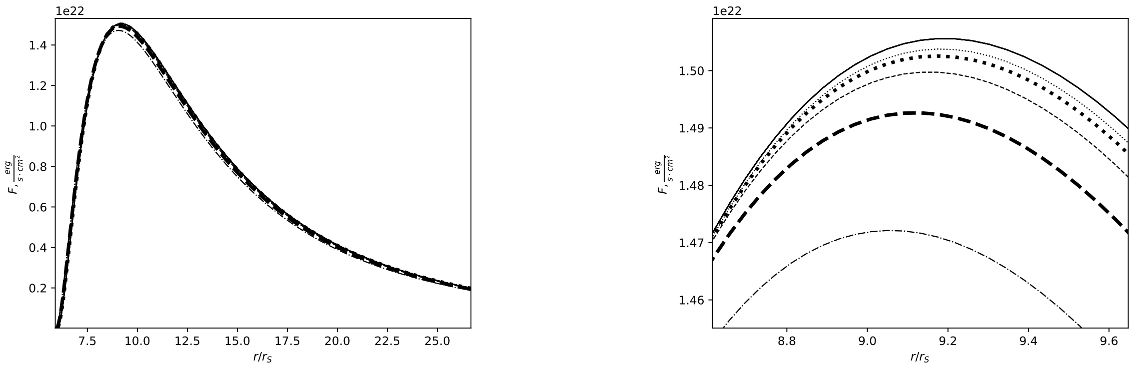


a) b)

**Рис. 1.** Случай $V = 0$. Поток энергии $F(r)$ с учетом $\dot{M} = 2.21 \times 10^{18} g/s$ и $M = 8.48 M_\odot$ для различных значений $u_0$ и фиксированного $\phi_0 = 1$ как функции $r/r_s$. b) Версия в масштабе. Сплошная линия соответствует черной дыре Шварцшильда. Начальное значение производной скалярного поля принимается следующим: $u_0 = 4 \times 10^{-9}$ (пунктирная линия), $u_0 = 8 \times 10^{-9}$ (жирная пунктирная линия), $u_0 = 1.6 \times 10^{-8}$ (штриховая линия), $u_0 = 3.2 \times 10^{-8}$ (жирная штриховая линия), $u_0 = 6.4 \times 10^{-8}$ (штрих-пунктирная линия).

Первые два случая выбраны в связи с тем, что такие черные дыры изучались в статье [13], где было получено сферически-симметричное решение. Выбор последнего случая обусловлен следующей причиной: мы берем начальное значение скалярного поля на достаточно большом расстоянии от черной дыры, а так как на этом расстоянии гравитационное поле достаточно слабое, мы можем использовать результаты постньютоновского (ППН) анализа.

Как итог для случая без потенциала были получены графики потока энергии как функции нормированной радиальной координаты $r/r_s$, где $r_s$ — радиус Шварцшильда, и светимости как функции частоты излучения. Поток энергии для всех трех рассмотренных выше различных наборов параметров представлен на графиках 1, 2, 3 соответственно.

Светимость, в соответствии с приведенными выше наборами свободных параметров, представлена на рис. 4, 5, 6.

Далее мы представим результаты для случая с потенциалом, а после перейдем к обсуждению результатов.

### 3.2. Случай $V = -\frac{\mu^2}{2}\phi^2 + \frac{\zeta}{4}\phi^4$

В статье [13] авторы рассматривают единственный случай с потенциалом, и этот потенциал имеет форму типа потенциала Хиггса:

$$V = -\frac{\mu^2}{2}\phi^2 + \frac{\zeta}{4}\phi^4, \tag{3.2}$$

где $\mu^2$ и $\zeta$ — константы. Теперь переопределим константы $\mu^2$ и $\zeta$ так, чтобы они приняли безразмерный вид [13]:

$$v(\phi) = \alpha\phi^2 + \beta\phi^4, \tag{3.3}$$

где

$$\alpha = -\frac{1}{4}\left(\frac{2GnM_{BH}}{c^2}\right)^2 \mu^2, \qquad \beta = \frac{1}{2}\left(\frac{2GnM_{BH}}{c^2}\right)^2 \zeta^2. \tag{3.4}$$

Потенциал типа Хиггса дает четырехпараметрические $(\alpha, \beta, \phi_0, u_0)$ решения уравнений статического гравитационного поля в гибридной f(R)-гравитации. Авторы статьи [13] ограничиваются исследованием роли констант $\alpha$ и $\beta$, сохраняя фиксированными $\phi_0$ и $u_0$. Однако мы рассматриваем более широкий круг возможных комбинаций параметров:

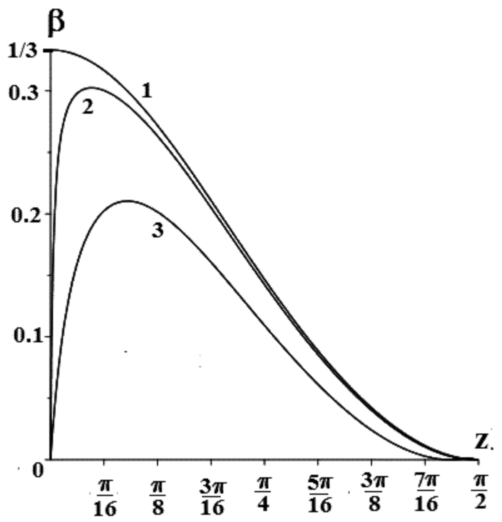


**Рис. 2.** Случай $V = 0$. Поток энергии $F(r)$ с учетом $\dot{M} = 2.21 \times 10^{18} g/s$ и $M = 8.48 M_\odot$ для различных значений $\phi_0$ фиксированного $u_0 = 5.12 \times 10^{-7}$ как функции $r/r_s$. Сплошная линия соответствует черной дыре Шварцшильда. Начальное значение скалярного поля принимается следующим: $\phi_0 = 0.5$ (пунктирная линия), $\phi_0 = 1$ (жирная пунктирная линия), $\phi_0 = 2$ (штриховая линия), $\phi_0 = 4$ (жирная штриховая линия), $\phi_0 = 8$ (штрих-пунктирная линия).

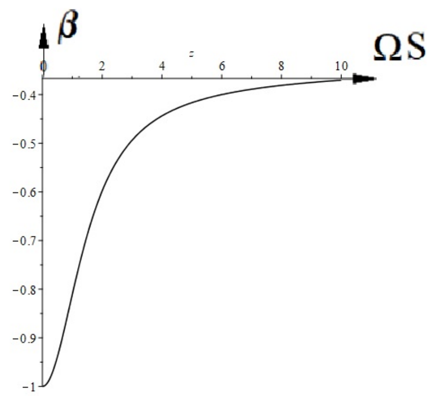


**Рис. 3.** Случай $V = 0$. Поток энергии $F(r)$ с учетом $\dot{M} = 2.21 \times 10^{18} g/s$ и $M = 8.48 M_\odot$ для значений $\phi_0 = 4 \times 10^{-5}$ и $u_0 = 2.2 \times 10^{-17}$ как функции $r/r_s$. Сплошная линия соответствует черной дыре Шварцшильда.

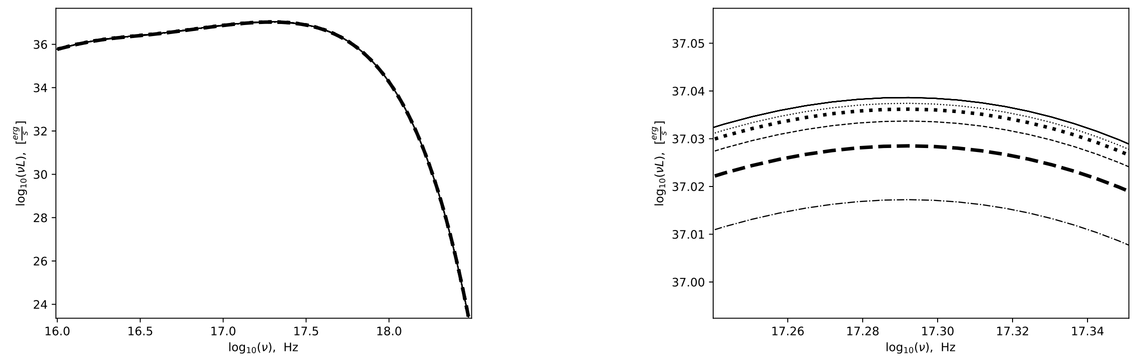


a) b)

**Рис. 4.** Случай $V = 0$. Спектр излучения $\nu L(\nu)$ с учетом $\dot{M} = 2.21 \times 10^{18} g/s$ и $M = 8.48 M_\odot$ для различных значений $u_0$ и фиксированного $\phi_0 = 1$ как функции $\nu$. b) Версия в масштабе. Сплошная линия соответствует черной дыре Шварцшильда. Начальное значение производной скалярного поля принимается следующим: $u_0 = 4 \times 10^{-9}$ (пунктирная линия), $u_0 = 8 \times 10^{-9}$ (жирная пунктирная линия), $u_0 = 1.6 \times 10^{-8}$ (штриховая линия), $u_0 = 3.2 \times 10^{-8}$ (жирная штриховая линия), $u_0 = 6.4 \times 10^{-8}$ (штрих-пунктирная линия).

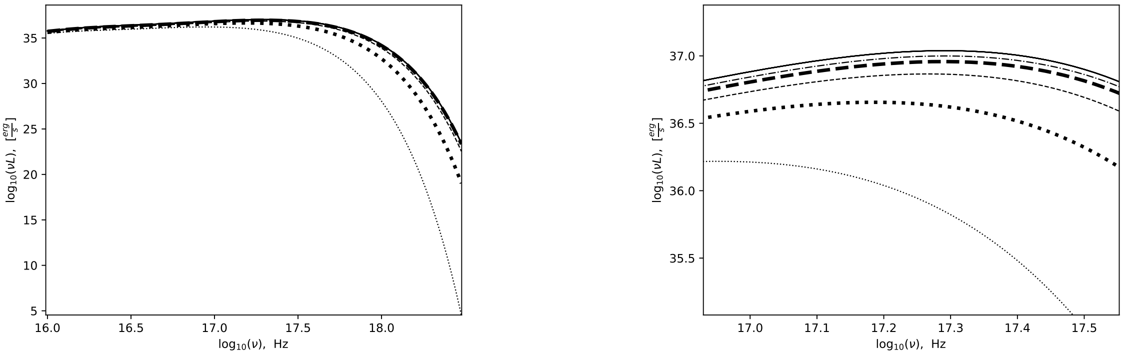


a) b)

**Рис. 5.** Случай $V = 0$. Спектр излучения $\nu L(\nu)$ с учетом $\dot{M} = 2.21 \times 10^{18} g/s$ и $M = 8.48 M_{\odot}$ для различных значений $\phi_0$ и фиксированного $u_0 = 5.12 \times 10^{-7}$ как функции $\nu$. b) Версия в масштабе. Сплошная линия соответствует черной дыре Шварцшильда. Начальное значение скалярного поля принимается следующим: $\phi_0 = 0.5$ (пунктирная линия), $\phi_0 = 1$ (жирная пунктирная линия), $\phi_0 = 2$ (штриховая линия), $\phi_0 = 4$ (жирная штриховая линия), $\phi_0 = 8$ (штрих-пунктирная линия).

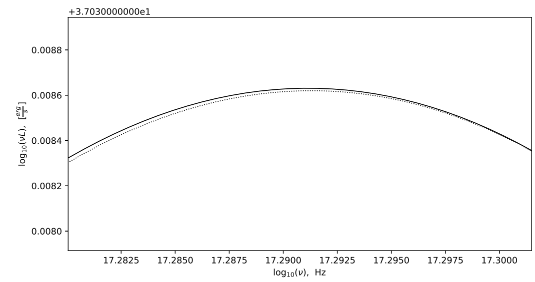


**Рис. 6.** Случай $V = 0$. Спектр излучения $\nu L(\nu)$ с учетом $\dot{M} = 2.21 \times 10^{18} g/s$ и $M = 8.48 M_{\odot}$ для значений $\phi_0 = 4 \times 10^{-5}$ и $u_0 = 2.2 \times 10^{-17}$ как функции $\nu$. Сплошная линия соответствует черной дыре Шварцшильда.

1. Фиксируем $u_0 = 10^{-8}, \phi_0 = 1, \beta = 10^{-10}$, и берем диапазон $\alpha = [-10^{-6}; -4 \times 10^{-5}]$.

2. Фиксируем $u_0 = 10^{-8}, \phi_0 = 1, \alpha = -10^{-10}$, и изменяем $\beta = [2 \times 10^{-10}; 14 \times 10^{-10}]$.

3. Случай на основе данных Солнечной системы. Предположим, что масса скалярного поля определяется как [20, 23]

$$m_{\varphi}^2 = [2V_0 - V_{\phi} - (1 + \phi)\phi V_{\phi\phi}]/3|_{\phi=\phi_0}, \tag{3.5}$$

где индекс $\phi$ обозначает производную по скалярному полю. Тогда $m_{\varphi}^2$ имеет связь с параметрами $\alpha$ и $\beta$:

$$m_{\varphi}^2 = [-4/3\alpha\phi_0 - 16/3\beta\phi_0^3 - 10/3\beta\phi_0^4] \times 2\left(\frac{c^2}{2GM_{BH}}\right)^2. \tag{3.6}$$

Сохраняем связь между $u_0$ и $\phi_0$, которая известна из ППН-анализа как производная от $\varphi = \frac{-2GM\phi_0 e^{-m_\phi r}}{3c^2 r}$ по отношению к $r$. В результате получаем

$$u_0 = -\frac{2GM\phi_0 e^{-m_\phi r} m_\phi}{3c^2 r} - \frac{2GM\phi_0 e^{-m_\phi r}}{3c^2 r^2}. \tag{3.7}$$

В данном случае мы изменяем $\alpha = [-10^{-6}; -4 \times 10^{-5}]$ и фиксируем $\beta = 10^{-20}$, $\phi_0 = 4 \times 10^{-5}$.

Первые два случая соответствуют черным дырам, рассмотренным в работе [13]. Однако мы немного расширили диапазон параметров $\alpha$ и $\beta$, чтобы лучше проиллюстрировать изменения в характеристиках аккреции. Третий случай основан на постньютоновском анализе, связях и ограничениях, полученных из Солнечной системы.

Полученные результаты для потока энергии для случая с потенциалом представлены на рис. 7, 8, 9.

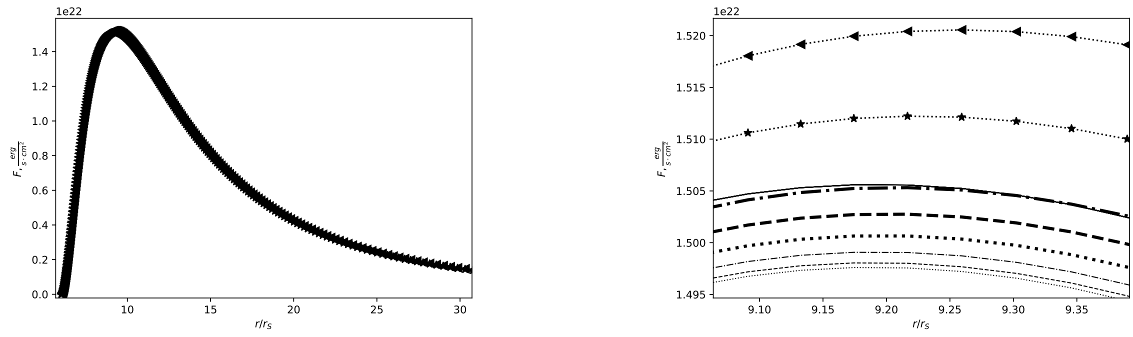


a) b)

**Рис. 7.** Случай с потенциалом. Поток энергии $F(r)$ с учетом $\dot{M} = 2.21 \times 10^{18} g/s$ и $M = 8.48 M_{\odot}$ для различных значений $\alpha$ и фиксированных $\phi_0 = 1$, $u_0 = 10^{-8}$, $\beta = 10^{-10}$ как функция $r/r_s$. b) Версия в масштабе. Сплошная линия соответствует черной дыре Шварцшильда. Параметр $\alpha$ принимает следующие знаечния: $\alpha = -4 \times 10^{-5}$ (линия с треугольниками), $\alpha = -3 \times 10^{-5}$ (линия со звездочками), $\alpha = -2.1 \times 10^{-5}$ (жирная штрих-пунктирная линия), $\alpha = -1.7 \times 10^{-5}$ (жирная штриховая линия), $\alpha = -1.3 \times 10^{-5}$ (жирная пунктирная линия), $\alpha = -9 \times 10^{-6}$ (штрих-пунктирная линия), $\alpha = -5 \times 10^{-6}$ (штриховая линия), $\alpha = -10^{-6}$ (пунктирная линия).

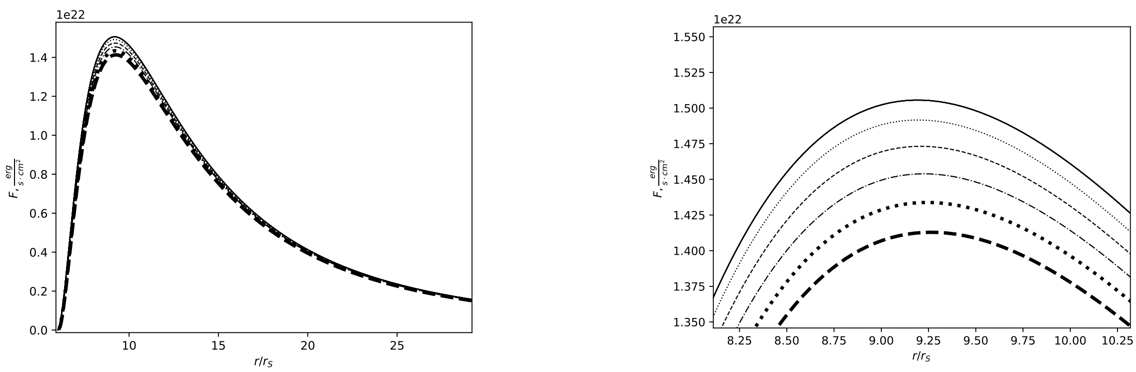


a) b)

**Рис. 8.** Случай с потенциалом. Поток энергии $F(r)$ с учетом $\dot{M} = 2.21 \times 10^{18} g/s$ и $M = 8.48 M_{\odot}$ для различных значений $\beta$ и фиксированных $\phi_0 = 1$, $u_0 = 10^{-8}$, $\alpha = -10^{-10}$ как функция $r/r_s$. b) Версия в масштабе. Сплошная линия соответствует черной дыре Шварцшильда. Параметр $\beta$ принимает значения: $\beta = 2 \times 10^{-10}$ (пунктирная линия), $\beta = 5 \times 10^{-10}$ (штриховая линия), $\beta = 8 \times 10^{-10}$ (штрих-пунктирная линия), $\beta = 1.1 \times 10^{-9}$ (жирная пунктирная линия), $\beta = 1.4 \times 10^{-9}$ (жирная штриховая линия).

Результаты для светимости в случае с потенциалом хиггсовского типа отображены на графиках 10, 11, 12.

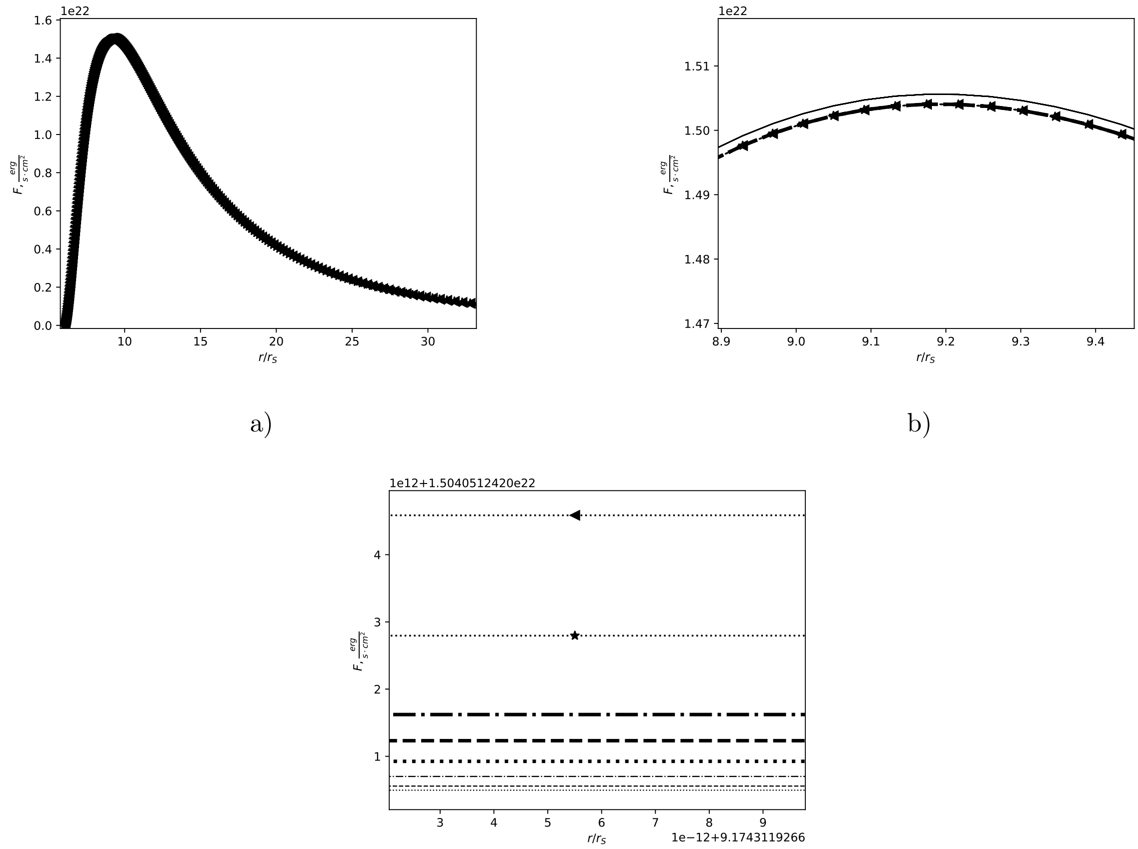


a) b)

c)

**Рис. 9.** Случай с потенциалом. Поток энергии $F(r)$ с учетом $\dot{M} = 2.21 \times 10^{18} g/s$ и $M = 8.48 M_{\odot}$ для различных значений $\alpha$ и фиксированного $\phi_0 = 4 \times 10^{-5}$, $\beta = 10^{-20}$ как функция $r/r_s$. Связи (3.6) и (3.7) между параметрами учтены. b) Сплошная линия соответствует кривой Шварцшильда, объединенная линия соответствует различным параметрам $\alpha$. c) Версия в масштабе. Параметр $\alpha$ принимает значения: $\alpha = -4 \times 10^{-5}$ (линия с треугольниками), $\alpha = -3 \times 10^{-5}$ (линия со звездочками), $\alpha = -2.1 \times 10^{-5}$ (жирная штрих-пунктирная линия), $\alpha = -1.7 \times 10^{-5}$ (жирная штриховая линия), $\alpha = -1.3 \times 10^{-5}$ (жирная пунктирная линия), $\alpha = -9 \times 10^{-6}$ (штрих-пунктирная линия), $\alpha = -5 \times 10^{-6}$ (штриховая линия), $\alpha = -10^{-6}$ (пунктирная линия).

## 4. Обсуждение результатов

В данной работе исследуются свойства тонких аккреционных дисков вокруг статических сферически-симметричных черных дыр в гибридной метрической-Палатини f(R)-гравитации. В качестве основы для нашего исследования было использовано численное решение типа черная дыра, полученное в статье [13]. Для изучения свойств аккреции была применена стационарная модель Новикова-Торна и наблюдательные данные системы MAXI J1820+070 [19]. В нашей работе рассмотрены два типа решений: без потенциала $V = 0$ и с потенциалом хиггсовского типа $V = -\frac{\mu^2}{2}\phi^2 + \frac{\zeta}{4}\phi^4$. В качестве характеристик аккреционного диска мы численно получаем поток энергии и светимость аккреционного диска. Численное решение типа черная дыра, полученное в статье [13], имеет определенный набор свободных параметров. Этот набор определяется, в том числе, наличием потенциала. В случае отсутствия потенциала $V = 0$ к этим параметрам относятся начальное значение скалярного поля $\phi_0$ и его производной $u_0$. В случае потенциала хиггсовского типа имеется два дополнительных параметра: $\alpha$ и $\beta$.

В случае $V = 0$ были найдены следующие особенности аккреционных дисков гибридной f(R)-

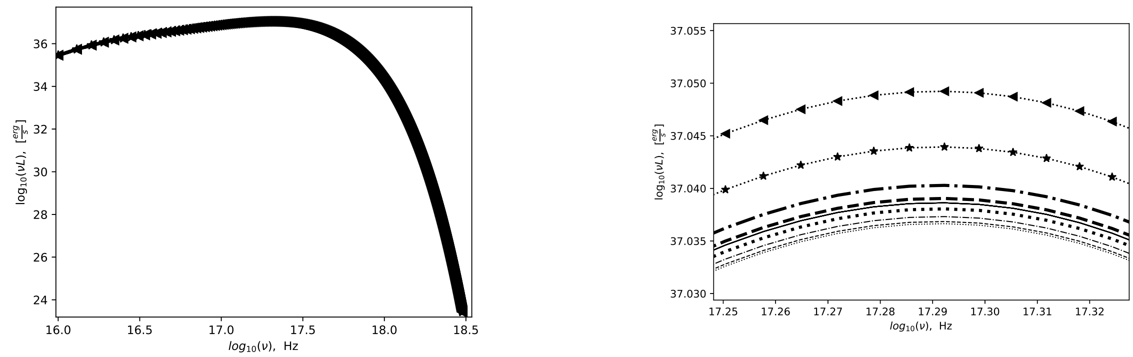


a) b)

**Рис. 10.** Случай с потенциалом. Спектр излучения $\nu L(\nu)$ с учетом $\dot{M} = 2.21 \times 10^{18} g/s$ and $M = 8.48 M_\odot$ для различных значений $\alpha$ и фиксированных $\phi_0 = 1$, $u_0 = 10^{-8}$, $\beta = 10^{-10}$ как функция $\nu$. b) Версия в масштабе. Сплошная линия соответствует черной дыре Шварцшильда. Параметр $\alpha$ принимает значения: $\alpha = -4 \times 10^{-5}$ (линия с треугольниками), $\alpha = -3 \times 10^{-5}$ (линия со звездочками), $\alpha = -2.1 \times 10^{-5}$ (жирная штрих-пунктирная линия), $\alpha = -1.7 \times 10^{-5}$ (жирная штриховая линия), $\alpha = -1.3 \times 10^{-5}$ (жирная пунктирная линия), $\alpha = -9 \times 10^{-6}$ (штрих-пунктирная линия), $\alpha = -5 \times 10^{-6}$ (штриховая линия), $\alpha = -10^{-6}$ (пунктирная линия).

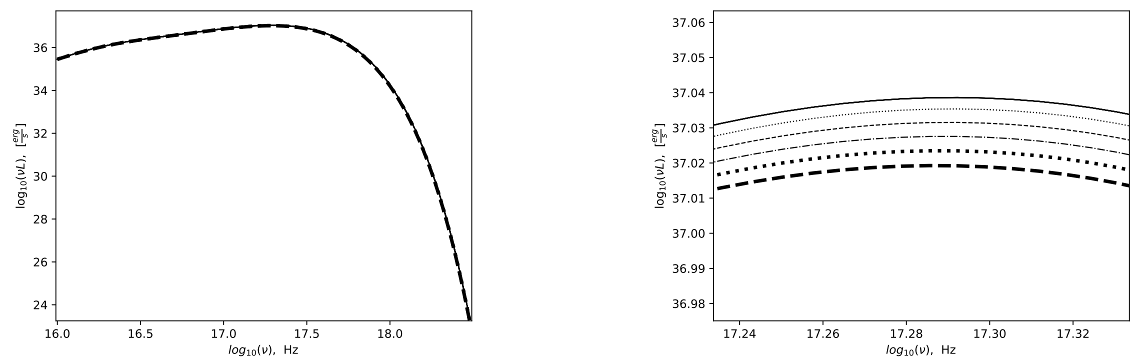


a) b)

**Рис. 11.** Случай с потенциалом. Спектр излучения $\nu L(\nu)$ с учетом $\dot{M} = 2.21 \times 10^{18} g/s$ и $M = 8.48 M_\odot$ для различных значений $\beta$ и фиксированных $\phi_0 = 1$, $u_0 = 10^{-8}$, $\alpha = -10^{-10}$ как функция $\nu$. b) Версия в масштабе. Сплошная линия соответствует черной дыре Шварцшильда. Параметр $\beta$ принимает значения: $\beta = 2 \times 10^{-10}$ (пунктирная линия), $\beta = 5 \times 10^{-10}$ (штриховая линия), $\beta = 8 \times 10^{-10}$ (штрих-пунктирная линия), $\beta = 1.1 \times 10^{-9}$ (жирная пунктирная линия), $\beta = 1.4 \times 10^{-9}$ (жирная штриховая линия).

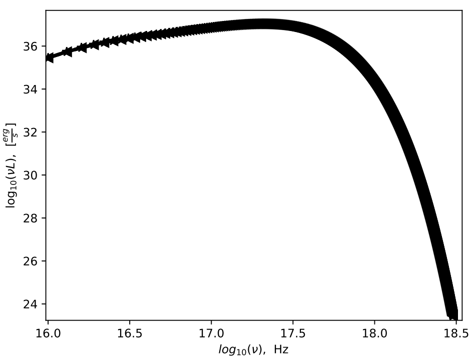


a)

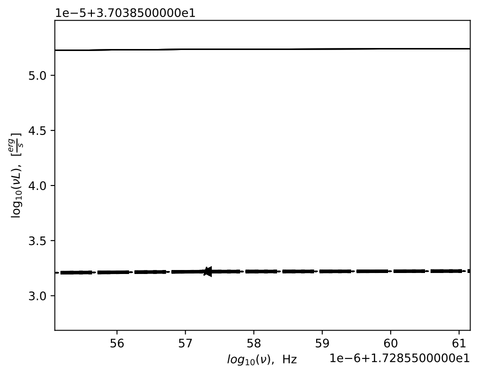


b)

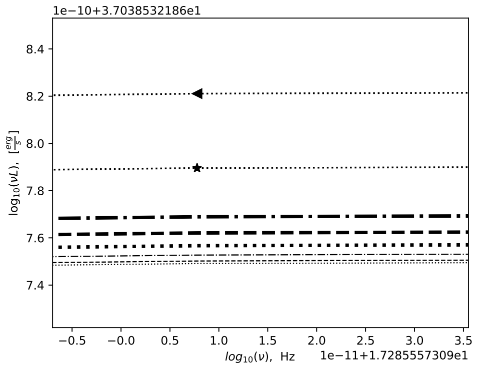


c)

**Рис. 12.** Случай с потенциалом. Спектр излучения $\nu L(\nu)$ с учетом $\dot{M} = 2.21 \times 10^{18} g/s$ и $M = 8.48 M_{\odot}$ для различных значений $\alpha$ и фиксированных $\phi_0 = 4 \times 10^{-5}$, $\beta = 10^{-20}$ как функция $\nu$. Связи (3.6) и (3.7) между параметрами учтены. b) Сплошная линия соответствует кривой Шварцшильда, объединенная линия соответствует различным параметрам $\alpha$. c) Версия в масштабе. Параметр $\alpha$ принимает значения: $\alpha = -4 \times 10^{-5}$ (линия с треугольниками), $\alpha = -3 \times 10^{-5}$ (линия со звездочками), $\alpha = -2.1 \times 10^{-5}$ (жирная штрих-пунктирная линия), $\alpha = -1.7 \times 10^{-5}$ (жирная штриховая линия), $\alpha = -1.3 \times 10^{-5}$ (жирная пунктирная линия), $\alpha = -9 \times 10^{-6}$ (штрих-пунктирная линия), $\alpha = -5 \times 10^{-6}$ (штриховая линия), $\alpha = -10^{-6}$ (пунктирная линия).

модели. Результаты, близкие к ОТО, можно получить, если взять достаточно большие значения $\phi_0$ для больших $u_0$ или малые значения $u_0$ для малых $\phi_0$. Однако первый результат кажется нереалистичным, поскольку скалярное поле должно принимать свое фоновое значение на большом расстоянии от черной дыры, а это значение значительно меньше единицы [21], [20], [24]. Поэтому $\phi_0 > 1$ выглядит неестественно.

Другой подход к выбору начальных параметров $\phi_0$ и $u_0$ возникает на основе постньютоновского анализа. Вдали от черной дыры, где мы выбираем значения свободных параметров, гравитационное поле слабое, что позволяет применить постньютоновский подход. В рамках постньютоновского анализа скалярное поле рассматривается как сумма фонового значения и его возмущения $\phi = \phi_0 + \varphi$. Фоновое значение $\phi_0$ является постоянной величиной, в отличие от возмущения $\varphi$. Таким образом, взяв производную от скалярного поля $\phi$ по расстоянию на бесконечности, мы просто получим значение $u_0$. В результате получаем уравнение связи (3.1) между $u_0$ и $\phi_0$. Если такая связь установлена и значения $\phi_0$ взяты в пределах, полученных в рамках эксперимента Кассини [22], то полученные поток энергии и светимость практически не отличаются от результатов, полученных для черной дыры Шварцшильда (см. рисунки (3), (6)). В этом случае $u_0$ принимает небольшие значения ($\sim 10^{-11}$), что еще раз говорит в пользу выбора малых значений исходных параметров ввиду их естественности.

В случае потенциала типа Хиггса теория включает четыре свободных параметра: $u_0$, $\phi_0$, $\alpha$ и $\beta$. Параметры $\alpha$ и $\beta$ вшиты в структуру самого потенциала. Сначала мы рассматриваем все параметры как независимые величины. Большое значение модуля $\alpha$ и $\phi_0 > 1$ приводят к ситуации, когда максимальный поток энергии и светимость могут превысить соответствующие кривые для черной дыры Шварцшильда. Такая ситуация противоречит следующей идее: большие значения $\phi_0$ не согласуются с данными, полученными из других наблюдений [21], [20], [24]. Этот факт приводит нас к выводу, что такое сочетание нереалистично. Далее с увеличением параметра $\beta$ наблюдается уменьшение максимума потока энергии, хотя и незначительное, однако ни один параметр $\beta$ не дает кривой, превосходящей результаты для черной дыры Шварцшильда.

Затем мы рассматриваем набор параметров, основанный на ограничениях, полученных из наблюдений в Солнечной системе. Используя связь между параметрами, возникающую из постньютоновского анализа, мы показываем, что все параметры должны быть малыми. С увеличением модуля $\alpha$ наблюдается уменьшение максимума потока энергии.

## 5. Выводы

В данной работе мы исследовали тонкие аккреционные диски вокруг черных дыр в гибридной f(R)-гравитации. В этом исследовании мы опирались на численное статическое сферически-симметричное решение [13]. В результате мы получили поток энергии и светимость для тонких аккреционных дисков, возникающих вокруг таких черных дыр. Мы показали, что в гибридной метрической f(R)-гравитации Палатини аккреционные диски вокруг звездных статических сферически-симметричных черных дыр более тусклые, чем в ОТО. Это отличает гибридную f(R)-гравитацию от метрической f(R)-теории, согласно которой тонкие аккреционные диски вокруг таких черных дыр более горячие и яркие [25].

Одним из наиболее важных следствий исследования является то, что в условиях ограничений, налагаемых на параметры теории другими методами [20, 21, 24, 26], гибридная f(R)-гравитация показывает свою полную жизнеспособность, а результаты для потока энергии и светимости близки к ОТО. Еще одним преимуществом гибридной f(R)-гравитации является то, что реалистичные режимы аккреции реализуются в широком диапазоне параметров без их тонкой настройки. Кроме того, существование реалистичных режимов аккреции указывает на адекватность численного решения черной дыры, полученного в статье [13].

В данной статье мы рассмотрели случай статической сферически-симметричной черной дыры. Это важный первый шаг в исследовании аккреции в гибридной f(R)-гравитации. Несмотря на то, что вероятность реализации этого типа черных дыр в природе крайне мала, важно понимать потенциальное существование адекватных режимов аккреции для этого типа объектов. Следующим шагом этого исследования будет рассмотрение аккреции в случае черных дыр типа Керра. Это позволит сравнить предсказания гибридной f(R)-гравитации с наблюдениями. Данное исследование прольет свет на реалистичность теории и послужит основой для введения ограничений на свободные параметры гибридной f(R)-гравитации, в том числе через исследование аккреционных дисков вокруг вращающихся черных дыр.

### Список литературы/References


1. Perlmutter S. et al. Measurements of $\Omega$ and $\Lambda$ from 42 high-redshift supernovae. *Astrophys. J.*, 1999, vol. 517, no. 2, pp. 565-586.
2. Riess A.G. et al. Observational evidence from supernovae for an accelerating universe and a cosmological constant. *Astron. J.*, 1998, vol. 116, no. 3, pp. 1009-1038.
3. Oort J.H. The force exerted by the stellar system in the direction perpendicular to the galactic plane and some related problems. *Bulletin of the Astronomical Institutes of the Netherlands*, 1932, vol. 6, p. 249.
4. Zwicky F. Die Rotverschiebung von extragalaktischen Nebeln. *Helvetica Physica Acta*, 1933, vol. 6, pp. 110-127.
5. Starobinsky A. A new type of isotropic cosmological models without singularity. *Physics Letters B*, 1980, vol. 91, no. 1, pp. 99-102.
6. Guth A.H. Inflationary universe: A possible solution to the horizon and flatness problems. *Phys. Rev.*, 1981, vol. 23, no. 2, pp. 347-356.
7. Linde A. A new inflationary universe scenario: A possible solution of the horizon, flatness, homogeneity, isotropy and primordial monopole problems. *Physics Letters B*, 1982, vol. 108, no. 6, pp. 389-393.
8. Nojiri S., Odintsov S., Oikonomou V. Modified gravity theories on a nutshell: Inflation, bounce and late-time evolution. *Physics Reports*, 2017, vol. 692, pp. 1-104.
9. Chiba T. $1/r$ gravity and scalar-tensor gravity. *Physics Letters B*, 2003, vol. 575, no. 1-2, pp. 1-3.
10. Koivisto T., Kurki-Suonio H. Cosmological perturbations in the palatini formulation of modified gravity. *Classical and quantum gravity*, 2006, vol. 23, no. 7, pp. 2355-2369.
11. Harko T., Koivisto T.S., Lobo F.S.N., Olmo G.J. Metric-palatini gravity unifying local constraints and late-time cosmic acceleration. *Phys. Rev. D*, 2012, vol. 85, no. 8, p. 084016.
12. Harko T., Lobo F.S.N. Beyond Einstein's general relativity: Hybrid metric-palatini gravity and curvature-matter couplings. *International Journal of Modern Physics D*, 2020, vol. 29, no. 13, p. 2030008.
13. Danila B., Harko T., Lobo F.S., Mak M.K. Spherically symmetric static vacuum solutions in hybrid metric-Palatini gravity. *Phys. Rev. D*, 2019, vol. 99, no. 6, p. 064028.
14. Shakura N.I., Sunyaev R.A. Black holes in binary systems. observational appearance. *Astronomy and Astrophysics*, 1973, vol. 24, pp. 337-355.
15. Page D.N., Thorne K.S. Disk-accretion onto a black hole. time-averaged structure of accretion disk. *Astrophys. J.*, 1974, vol. 191, pp. 499-506.
16. Novikov I.D., Thorne K.S. *Astrophysics of black holes.* N.Y.: Gordon and Breach, 1973. pp. 343-450.
17. Torres D.F. Accretion disc onto a static non-baryonic compact object. *Nuclear Physics B*, 2002, vol. 626, no. 1-2, p. 377-394.
18. Luminet J.P. Image of a spherical black hole with thin accretion disk. *Astronomy and Astrophysics*, 1975, vol. 79, pp. 228-235.

19. Zhao X. et al. Estimating the black hole spin for the X-ray binary MAXI J1820+070. *Astrophys. J.*, 2021, vol. 916, no. 2, p. 108.
20. Dyadina P.I., Labazova S.P., Alexeyev S.O. Post-Newtonian limit of hybrid metric-Palatini f(R)-gravity. *Journal of Experimental and Theoretical Physics*, 2019, vol. 129, no. 5, pp. 838-848.
21. Leanizbarrutia I., Lobo F.S., Saez-Gomez D. Crossing SNe Ia and BAO observational constraints with local ones in hybrid metric-Palatini gravity. *Phys. Rev. D*, 2017, vol. 95, no. 8, p. 084046.
22. Bertotti B., Iess L., Tortora P. A test of general relativity using radio links with the Cassini spacecraft. *Nature*, 2003, vol. 425, pp. 374-376.
23. Capozziello S., Harko T., Koivisto T., Lobo F., Olmo G. Hybrid metric-Palatini gravity. *Universe*, 2015, vol. 1, no. 2, pp. 199-238.
24. Dyadina P.I., Avdeev N.A., Alexeyev S.O. Horndeski gravity without screening in binary pulsars. *Monthly Notices of the Royal Astronomical Society*, 2018, vol. 483, no. 1, pp. 947-963.
25. Perez D., Romero G.E., Bergliaffa S.E.P. Accretion disks around black holes in modified strong gravity. *Astronomy and Astrophysics*, 2013, vol. 551, p. A4.
26. Avdeev N.A., Dyadina P.I., Labazova S.P. Test of hybrid metric-Palatini f(R)-gravity in binary pulsars. *Journal of Experimental and Theoretical Physics*, 2020, vol. 131, no. 4, p. 537-547.

**Авторы**

**Дядина Полина Игоревна**, к. ф.-м. н., научный сотрудник, Государственный астрономический институт имени П.К. Штернберга Московского государственного университета имени М.В.Ломоносова, Университетский проспект, 13, г. Москва, 119234, Россия.
E-mail: guldur.anwo@gmail.com

**Авдеев Никита Алексеевич**, ведущий инженер, Государственный астрономический институт имени П.К. Штернберга Московского государственного университета имени М.В.Ломоносова, Университетский проспект, 13, г. Москва, 119234, Россия.
E-mail: naavdeev1995@mail.ru

**Просьба ссылаться на эту статью следующим образом:**

Дядина П. И., Авдеев Н. А. Свойства аккреционных дисков в гибридной метрической-Палатини f(R)-гравитации. *Пространство, время и фундаментальные взаимодействия.* 2023. № 3-4. С. 63–76.

**Authors**

**Dyadina Polina Igorevna**, Ph.D., researcher, Sternberg Astronomical Institute, Moscow State University, Universitetsky pr., 13, Moscow 119234, Russia.
E-mail: guldur.anwo@gmail.com

**Avdeev Nikita Alexeevich**, lead engineer, Sternberg Astronomical Institute, Moscow State University, Universitetsky pr., 13, Moscow 119234, Russia.
E-mail: naavdeev1995@mail.ru

**Please cite this article in English as:**

Dyadina P. I., Avdeev N. A. Properties of accretion disks in hybrid metric-palatini f(R) gravity. *Space, Time and Fundamental Interactions*, 2023, no. 3-4, pp. 63–76.

УДК 530.12



# О СОХРАНЯЮЩИХСЯ ВЕЛИЧИНАХ ДЛЯ ДВИЖУЩЕЙСЯ ЧЁРНОЙ ДЫРЫ В ТЕЛЕПАРАЛЛЕЛЬНОМ ЭКВИВАЛЕНТЕ ОТО *

Емцова Е. Д.[a,1], Петров А. Н.[b,2]

[a] Казанский федеральный университет, г. Казань, 420008, Россия.

[b] Астрономический институт им. П.К.Штернберга МГУ им. М.В.Ломоносова, г. Москва, 119992, Россия.

В рамках телепараллельного эквивалента (ТЭ) ОТО, где полевыми переменными являются компоненты тетрад, выведены масса и импульс для движущейся (равномерно относительноситительно удаленных наблюдателей) черной дыры Шварцшильда (ЧДШ). Используется формализм, разработанный авторами ранее, для построения сохраняющихся величин в ТЭ ОТО, где токи и суперпотенциалы как координатно ковариантны, так и инвариантны относительно локальных лоренцевых вращений тетрад. Это преимущество достигнуто благодаря введению инерциальной спиновой связности (ИСС) и использованию теоремы Нётер с сохранением векторов смещений в окончательных выражениях. Набор пар (ИСС и тетрад), связанных гладкими преобразованиями, мы назвали калибровкой, это класс эквивалентности. Величина ИСС внешняя, поэтому мы определяем её благодаря введённому нами обобщенному принципу «выключения гравитации». Но, даже этот разумный принцип приводит к различным определениям ИСС для одной и той же тетрады, что ведет к различным результатам. Здесь, на примере движущейся ЧДШ мы 1) демонстрируем преимущества нашего полностью ковариантного формализма, 2) а также изучаем неопределенность в определении ИСС. В расчетах используются аналогии с движущимся материальным шаром в пространстве Минковского и только «статическая» калибровка. Получены ожидаемые масса и импульс. Затем сравниваются «статическая» и «движущаяся» калибровки. Найдено, что они совпадают. То есть, в случае движущейся ЧДШ, нет ожидаемой двусмысленности, и в обоих случаях получены те же масса и импульс.

*Ключевые слова*: телепараллельная гравитация, сохраняющиеся величины, черные дыры; teleparallel gravity, conserved quantities, black holes.

## ON CONSERVED QUANTITIES FOR A MOVING BLACK HOLE IN TEGR

Emtsova E. D.[a,1], Petrov A. N.[b,2]

[a] Kazan Federal University, Kazan, 420008, Russia.

[b] Sternberg Astronomical Institute, MV Lomonosov Moscow State University, Moscow, 119992, Russia.

In the framework of the Teleparallel Equivalent of General Relativity (TEGR), where the field variables are tetrad components, mass and momentum for a moving (uniformly with respect to distant observers) Schwarzschild black hole (SBH) are constructed. A formalism developed by the authors earlier for constructing conserved quantities in TEGR, where currents and superpotentials are covariant with respect both to coordinate transformations and to local Lorentz rotations of tetrads is applied. This advantage has been reached by introducing inertial spin connection (ISC) and using the Noether theorem with preservation of a displacement vector in final expressions. A set of pairs (tetrad and related ISC) connected by smooth transformations we call as a “gauge”, it is the equivalence class. The quantity ISC is an external one, therefore we define it with making the use of the introduced by us generalized “turning off gravity” principle. But, even this a reasonable principle leads to different values of ISCs for the same tetrad that leads to different results. Here, on the example of the moving SBH we 1) demonstrate advantages of our fully covariant formalism, 2) study the ambiguity in definition of ISC as well. In calculations, we the use analogies with a moving mater ball in Minkowski space only in the “static gauge”.

*Участие Е.М.Емцовой поддержано грантом РНФ №21-12-00130, участие А.Н.Петрова поддержано грантом: Междисциплинарная научно-образовательная школа Московского университета «Фундаментальные и прикладные исследования космоса».

[1]E-mail: ed.emcova@physics.msu.ru

[2]E-mail: alex.petrov55@gmail.com

Expected mass and momentum have been obtained. Next we compare “static gauge” and “moving gauge”. It was found that they coincide. In the result, in the case of a moving SBH aforementioned ambiguity is absent because in both the cases the same mass and momentum are obtained.

*Keywords*: teleparallel gravity, conserved quantities, black holes.

PACS: 04.70.Bw, 11.30.-j

DOI: 10.17238/issn2226-8812.2023.3-4.77-88

**Introduction**

Last decades teleparallel gravity attracts a lot of attention, see, for example, [1, 2, 3] and numerous references therein. Except expanded telerarallel theories one continues actively to consider Teleparallel Equivalent of General Relativity (TEGR) [1] where the tetrad components present field variables, and non-zero torsion determines non-zero gravitational field. In many such researches, black hole solutions are the most popular models for application of various formalisms. Among such solutions, the Schwarzschild black hole (SBH) is considered more frequently than others, see [4, 5, 6, 7, 8] and references therein, and is used to calculate the mass of a black hole as a conserved global charge or derive energy density of the gravitational field measured by an observer.

Many of approaches (see, for example, [7, 8]) look as not so satisfactory ones. The reason is that they lead either to non-covariant with respect to coordinate transformations, or non-invariant with respect to local Lorentz rotations conserved currents or charges. However, using Noether's theorem, a fully covariant formalism has been developed. One can recall the series of the papers [9, 10, 11], where fully covariant conserved quantities are constructed in the formalism of differential forms. Unfortunately this approach did not obtain a development. Recently, in [12, 13, 14, 15] we have developed a fully covariant approach for constructing conserved quantities in TEGR in the more popular tensorial presentation. Namely, this formalism is applied in the present paper.

Concerning the Schwarzschild solution, for the best of our knowledge it was not considered in TEGR as a moving black hole. By this, the first goal here is to calculate the global conserved energy and momentum for the moving SBH [16] with making the use of the method [12, 13]. Of course, it is not an end in itself because such quantities can be easily obtained by other appropriate methods [17]. Here, we only demonstrate possibilities of our covariant formalism [12, 13] and its advantages. We note that in such calculations analogies with calculating the mass and momentum of a moving matter ball in Minkowski space are used.

In order to obtain the covariance of the both types one needs, first, to introduce an inertial spin connection (ISC) that is not dynamical quantity and is not determined by the theory itself. In [12, 13, 14, 15], the unified principle of “turning off” gravity is used to determine ISC for a concrete solution. It is based on the fact that in the absence of gravity, only inertial effects remain. In this case, the curvature tensor vanishes and then the Levi-Civita spin connection (L-CSC) is to be able to express only inertial effects and should be equal to the ISC. Second, to obtain the full covariance one needs to preserve in expressions a displacement vector $\xi$ after applying the Noether theorem as well. This application is based on diffeomorphisms induced by an arbitrary smooth vector field $\xi$, and then one needs to choose $\xi$ in a physically meaningful way. Thus, $\xi$ can be chosen as Killing vector fields of the reference geometry, proper vectors of observers, etc.

A plenty of pairs of tetrads and related ISCs, which are connected by smooth transformations of both the types we call as a “gauge” (really it is the equivalence class). Thus, for a concrete gauge conserved quantities are the same. However, even the reasonable principle of “turning off” gravity leads to different definitions of ISCs for the same tetrad that leads to different gauges, the same to construction of different conserved quantities. This problem in detail has been studied in [14, 15] on the example of the Schwarzschild solution. Here (it is the second goal of the paper), on the example of the moving SBH we analyze the ambiguity in definition of ISC (the same, in definition of a gauge) as well. First, we introduce a so-called "static gauge". Expected mass and momentum have been obtained. Then, we introduce a so-called "moving gauge" Comparing "static gauge" and "moving gauge", we find that they coincide. In the result, in the case of a moving SBH aforementioned ambiguity is absent because in both cases the same mass and momentum are obtained.

This paper is based on our presentation at the conference PIRT-2023 [18], which unites the results of our previous works [19, 20]. The results of these papers look as very disparate ones, although evidently that they have to be given uniformly, representing a new quality. Thus, here we close this gap.

The paper is organized as follows. In section 1, a short description of elements of TEGR and of constructing fully covariant conserved quantities is given. Besides, the notion of gauges and ambiguities in their definitions are outlined. In section 2, a construction of conserved quantities for an uniformly moving matter ball in Minkowski space is presented. In section 3, a "static gauge" for the SBH solution in isotropic coordinates is introduced. In section 4, basing on the static isotropic gauge and analogy with the matter ball in Minkowski space the total energy and momentum for the moving SBH are calculated. In section 5, the fully covariant formalism in TEGR itself is applied to construct the aforementioned conserved quantities, and a "moving gauge" is defined and compared with the static gauge.

At last, in the paper, we use abbreviations as follows. GR — general relativity; TEGR — teleparallel equivalent of general relativity; SBH — Schwarzschild black hole; ISC — inertial spin connection; L-CSC — Levi-Civita spin connection; SSG — static Schwarzschild gauge; LG — Lemaitre gauge; SIG — static isotropic gauge.

## 1. Preliminaries

### 1.1. Elements of TEGR and fully covariant formalism

One of the ways to present the gravitational Lagrangian of TEGR is [1]

$$\overset{\bullet}{\mathcal{L}} = \frac{h}{2\kappa}\left(\overset{\bullet}{K}{}^{\rho}{}_{\mu\nu}\overset{\bullet}{K}{}_{\rho}{}^{\nu\mu} - \overset{\bullet}{K}{}^{\nu}{}_{\rho\nu}\overset{\bullet}{K}{}^{\mu\rho}{}_{\mu}\right), \tag{1.1}$$

that is equivalent to the Hilbert Lagrangian up to a divergence with the Einstein constant $\kappa$. Unlike metric presentation of GR, dynamical variables in TEGR are components of the tetrad field $h^a{}_\rho$, which are connected with the metric by $g_{\mu\nu} = \eta_{ab}h^a{}_\mu h^b{}_\nu$ and $h \equiv \det h^a{}_\rho$, where $\eta_{ab}$ is the Minkowski metric. Greek indexes are spacetime components, Latin indexes $a, b, c, \ldots$ are tetrad components, Latin indexes $i, j, k, \ldots$ are space components. The contortion tensor in (1.1) is defined as a difference

$$\overset{\bullet}{K}{}^{a}{}_{b\nu} = \overset{\bullet}{A}{}^{a}{}_{b\nu} - \overset{\circ}{A}{}^{a}{}_{b\nu}, \tag{1.2}$$

where

$$\overset{\bullet}{A}{}^{a}{}_{b\nu} = -h_b{}^\rho \overset{\bullet}{\nabla}_\nu h^a{}_\rho \tag{1.3}$$

is the ISC, and

$$\overset{\circ}{A}{}^{a}{}_{b\nu} = -h_b{}^\rho \overset{\circ}{\nabla}_\nu h^a{}_\rho \tag{1.4}$$

is the L-CSC. Tetrad indexes are replaced by spacetime indexes and inversely by contracting with $h^a{}_\mu$ or $h_a{}^\mu$, for example, $\overset{\bullet}{K}{}^{\rho}{}_{\mu\nu} = \overset{\bullet}{K}{}^{a}{}_{b\nu}h_a{}^\rho h^b{}_\mu$. Here and below, $\bullet$ means that a quantity is constructed with the use of the teleparallel connection $\overset{\bullet}{\Gamma}{}^\alpha{}_{\mu\nu}$ of zero curvature, whereas $\circ$ means that a quantity is constructed with the use of the Levi-Chivita connection $\overset{\circ}{\Gamma}{}^\alpha{}_{\mu\nu}$, like the covariant derivatives $\overset{\bullet}{\nabla}_\nu$ and $\overset{\circ}{\nabla}_\nu$.

Simultaneous transformations of tetrads and ISCs under local Lorentz rotations are:

$$h'^a{}_\mu = \Lambda^a{}_b h^b{}_\mu, \tag{1.5}$$

$$\overset{\bullet}{A}{}'^{a}{}_{b\mu} = \Lambda^a{}_c \overset{\bullet}{A}{}^{c}{}_{d\mu}\Lambda_b{}^d + \Lambda^a{}_c\partial_\mu\Lambda_b{}^c, \tag{1.6}$$

where $\Lambda^b{}_d(x)$ is a matrix of a local Lorentz transformation. The L-CSC $\overset{\circ}{A}{}^{a}{}_{b\nu}$ is transformed analogously to (1.6). Then it is evidently that $\overset{\bullet}{K}{}^{\rho}{}_{\mu\nu}$ defined in (1.2) is invariant under local Lorentz transformations.

Because $\overset{\bullet}{A}{}^{c}{}_{d\mu}$ represents the inertial effects it can be suppressed by (1.6) with appropriate $\Lambda^{a}{}_{b}$ [12, 13]. By the next a local Lorentz transformation $\Lambda^{*a}{}_{b}$ it can be represented in the form:

$$\overset{\bullet}{A}{}''^{a}{}_{b\mu} = \Lambda^{*a}{}_{c}\partial_{\mu}\Lambda^{*}{}_{b}{}^{c}\,. \tag{1.7}$$

In [12, 13], considering the invariance of (1.1) under a diffeomorphism induced by an arbitrary smooth vector field $\xi$, one derives the conservation law for the current $\overset{\bullet}{\mathcal{J}}{}^{\alpha}(\xi)$:

$$\partial_{\alpha}\overset{\bullet}{\mathcal{J}}{}^{\alpha}(\xi) = \overset{\circ}{\nabla}_{\alpha}\overset{\bullet}{\mathcal{J}}{}^{\alpha}(\xi) = 0. \tag{1.8}$$

Here, it is not necessary to derive a concrete structure of the current itself. It is more convenient to use its representation through the superpotential:

$$\overset{\bullet}{\mathcal{J}}{}^{\alpha}(\xi) = \partial_{\beta}\overset{\bullet}{\mathcal{J}}{}^{\alpha\beta}(\xi) = \overset{\circ}{\nabla}_{\beta}\overset{\bullet}{\mathcal{J}}{}^{\alpha\beta}(\xi). \tag{1.9}$$

Noether's current $\overset{\bullet}{\mathcal{J}}{}^{\alpha}(\xi)$ is the vector density of the weight $+1$, Noether's superpotential $\overset{\bullet}{\mathcal{J}}{}^{\alpha\beta}(\xi)$ is the antisymmetric tensor density of the weight $+1$ for which the explicit expression is

$$\overset{\bullet}{\mathcal{J}}{}^{\alpha\beta}(\xi) = \frac{h}{\kappa}\overset{\bullet}{S}{}_{\sigma}{}^{\alpha\beta}\xi^{\sigma}, \tag{1.10}$$

where the teleparallel superpotential is

$$\overset{\bullet}{S}{}_{\sigma}{}^{\alpha\beta} = \overset{\bullet}{K}{}^{\alpha\beta}{}_{\sigma} + \delta^{\beta}_{\sigma}\overset{\bullet}{K}{}^{\theta\alpha}{}_{\theta} - \delta^{\alpha}_{\sigma}\overset{\bullet}{K}{}^{\theta\beta}{}_{\theta}. \tag{1.11}$$

Both $\overset{\bullet}{\mathcal{J}}{}^{\alpha}(\xi)$ and $\overset{\bullet}{\mathcal{J}}{}^{\alpha\beta}(\xi)$ are locally Lorentz invariant, that invariant with respect to simultaneous transformations (1.5) and (1.6).

The conservation law (1.8) allows us to construct a conserved integral quantity:

$$\mathcal{P}(\xi) = \int_{\Sigma} d^{3}x\overset{\bullet}{\mathcal{J}}{}^{0}(\xi), \tag{1.12}$$

where $\Sigma$ is a hypersurface of constant time $t = x^{0} = \text{const}$. In the case of spherical symmetry, when $r = x^{1}$, the conservation law (1.9) allow us to represent (1.12) as a conserved charge:

$$\mathcal{P}(\xi) = \oint_{\partial\Sigma} d^{2}x\overset{\bullet}{\mathcal{J}}{}^{01}(\xi) = \frac{1}{\kappa}\oint_{\partial\Sigma} d^{2}x\, h\,\overset{\bullet}{S}{}_{\sigma}{}^{01}\xi^{\sigma}, \tag{1.13}$$

where $\partial\Sigma$ is a boundary of $\Sigma$, and can be considered both at finite $r = r_0$ and at $r \to \infty$. By the construction, it is evidently that (1.12) or (1.13) are scalars with respect to the both aforementioned types of transformations. At last, the interpretation of (1.8), (1.10), (1.12) and (1.13) depend on a choice of $\xi^{\sigma}$.

### 1.2. Ambiguity in determining gauges

Here, we describe in more detail the aforementioned above problem related to an ambiguity in determining gauges. At the earlier stage of development of teleparallel theory the problem of non-covariance of classical pseudotensors [17] has been suggested by Møller [21] in order to construct covariant conserved quantities in GR in the tetrad form. However, it turns out that these quantities are not invariant/covariant with respect to local Lorentz rotations of tetrad vectors. As shown in the previous subsection, the incorporation of ISC and $\xi^{\sigma}$ into conserved quantities gives a possibility to construct them in fully covariant form [12, 13]. An ambiguity in the definition of ISC by the principle of "turning off" gravity has been outlined in Introduction.

In the framework of the covariant formalism [12, 13] the notion of "gauges" has been introduced [14]. It can be formulated as follows [20]:

*For the given tetrad-ISC pair* $(h_a{}^\mu, \overset{\bullet}{A}{}^a{}_{b\mu})$ *it is considered the equivalence class of pairs related either by smooth coordinate transformations* $(h_a{}^\mu, \overset{\bullet}{A}{}^a{}_{b\mu}) \sim (h_a{}^{\mu'}, \overset{\bullet}{A}{}^a{}_{b\mu'})$ *and/or local Lorentz transformations* $(h_a{}^\mu, \overset{\bullet}{A}{}^a{}_{b\mu}) \sim (h_{a'}{}^\mu, \overset{\bullet}{A}{}^{a'}{}_{b'\mu})$*. Any member of the equivalence class is viewed as the same* gauge *by the definition of* [14], *and any such pair leads to the same results in the calculation of conserved quantities.*

Then, the ambiguity in determining ISCs leads to an ambiguity in determining gauges themselves. This problem has been studied in detail in [14, 15] on the example of the SBH. It was clarified, that a diagonal tetrad and related ISC induced by the standard static Schwarzschild metric, *static Schwarzschild gauge* (SSG), is appropriate for calculating the total mass of SBH. On the other hand, the SSG fails in describing a freely falling observer for whom correspondence with the equivalence principle is lost. Conversely, a diagonal tetrad and related ISC induced by the Lemaitre metric, *Lemaitre gauge* (LG), is appropriate for correspondence with the equivalence principle, but it does not lead to acceptable mass for SBH. In this a concrete case, we have resolved this problem introducing a generalized Lemaitre metric and related *generalized Lemaitre gauge*. However, it is a particular case only, and more wide study of the problem is required.

Thus, here, we are continuing to study the problem of ambiguity in definition of gauges on the example of a SBH moving with a constant (with respect to distant static observers) velocity [16]. From the start, we use a calculation of the total mass for the static SBH in isotropic coordinates using an appropriate gauge (static gauge). By the aforementioned logic, calculations for the moving SBH can be carried out successfully when its own (separate) appropriate gauge (moving gauge) is found. We find it and clarify a connection between both the gauges. Besides, we compare them with SSG in [14].

## 2. A moving matter ball

It turns out that in order to demonstrate advantages of our fully covariant formalism [12, 13] it is very fruitful to use analogies with properties of special relativity. We recall them beginning from the Minkowski space with metric:

$$ds^2 = -dt^2 + dx^2 + dy^2 + dz^2. \tag{2.1}$$

We denote $(t, x, y, z) = (x^0, x^i) = (x^\alpha)$, where $i = 1, 2, 3$. To define a reference frame, we add to (2.1) static observers with proper vectors

$$\xi^\alpha = (-1, 0, 0, 0). \tag{2.2}$$

Assume that the matter in the Minkowski space has energy-momentum tensor $\Theta^\alpha{}_\beta$, which is differentially conserved, $\partial_\alpha \Theta^\alpha{}_\beta = 0$. Then, if one defines the current $\mathcal{J}^\alpha = \Theta^\alpha{}_\beta \xi^\beta$, one finds that it is conserved, $\partial_\alpha \mathcal{J}^\alpha = 0$, as well. Its components present the energy density $\mathcal{J}^0 = \Theta^0{}_0 \xi^0$ and the momentum density $\mathcal{J}^i = \Theta^i{}_0 \xi^0$ measured by the introduced above observers (2.2). To define integral (global) conserved quantities on has to integrate $\mathcal{J}^0$ to obtain the total energy (mass)

$$E = \int_\Sigma dxdydz \mathcal{J}^0, \tag{2.3}$$

and integrate $\mathcal{J}^i$ to obtain the total momentum

$$P^i = \int_\Sigma dxdydz \mathcal{J}^i, \tag{2.4}$$

over the space section in (2.1) $\Sigma := t = \text{const}$. The current in TEGR defined as $\overset{\bullet}{\mathcal{J}}{}^\alpha(\xi)$ generalizes the simplest definition in Minkowski space and its components have the analogous interpretation for observers with proper vectors $\xi^\alpha$.

Assuming the static spherically symmetric distribution of matter, one has for the current

$$\mathcal{J}^\alpha_s = [\rho(r),\ 0,\ 0,\ 0]\,, \tag{2.5}$$

(subscript '$s'$ means 'static') with $\rho(r) = \mathcal{J}_s^0(r) = \Theta^0{}_0(r)\xi^0$. It is just the energy density, where $r^2 \equiv x^2+y^2+z^2$ with

$$x = r\sin\theta\cos\phi; \quad y = r\sin\theta\sin\phi; \quad z = r\cos\phi. \tag{2.6}$$

Let the matter distribution on the hypersurface $\Sigma$ be bounded by $\partial\Sigma$ that presents a sphere $r = r_0$. Then the total mass (energy) of such an object is calculated as

$$E_s = \int_\Sigma dxdydz\mathcal{J}_s^0(r) = \int_\Sigma dxdydz\rho(r) = \int_0^{2\pi}\int_0^\pi\int_0^{r_0} d\phi d\theta dr\sin\theta\, r^2\rho(r) = \mathcal{M}. \tag{2.7}$$

Let an absolutely identical matter ball be moving with the constant velocity $v$ along the axis $\mathbf{x}$ relatively to the frame $\{x^\alpha\}$ connected with (2.1). The proper coordinates of the moving object are connected with those in (2.1) by the Lorentz transformation:

$$\overline{t} = \gamma(t - vx); \quad \overline{x} = \gamma(x - vt); \quad \overline{y} = y; \quad \overline{z} = z, \tag{2.8}$$

where, as usual, $\gamma \equiv (1-v^2)^{-\frac{1}{2}}$. In analogy with the reference frame $\{x^\alpha\}$ determined by (2.1) the moving ball has a *proper* (its own) reference frame $\{\overline{x}^\alpha\}$.

Let us give the simplest illustration before real calculations. Let the moving sphere be filled by $N$ point particles with masses $m$ at the rest in the proper frame $\{\overline{x}^\alpha\}$. Then the total mass in $\{\overline{x}^\alpha\}$ is $\mathcal{M}_s = Nm$. After that, let us find the mass and momentum of such a moving object in the frame $\{x^\alpha\}$. First, the moving sphere undergoes relativistic compression and its volume decreases $\gamma$ times. Second, by effects of special relativity, energy and momentum of each particle with mass $m$ becomes $\gamma m$, and $\gamma vm$. At last, third, because the number of particles $N$ is conserved the concentration of particles increases in $\gamma$ times. It is evidently that the first and third factors are compensated. Then, the total mass and momentum of the moving object becomes $\mathcal{M}_m = N(\gamma m) = \gamma\mathcal{M}_s$ and $\mathcal{P}_m^1 = N(\gamma vm) = \gamma v\mathcal{M}_s$.

Turning to the case of continuous matter distribution one can carry out the same. In the proper frame $\{\overline{x}^\alpha\}$ of the moving ball the current has the form:

$$\mathcal{J}_s^{\overline{\alpha}} = [\rho(\overline{r}),\ 0,\ 0,\ 0]\,, \tag{2.9}$$

where $\overline{r}^2 = \overline{x}^2 + \overline{y}^2 + \overline{z}^2$ and $\rho(\overline{r})$ is the same function like in (2.5). Now, let us transform from the frame $\{\overline{x}^\alpha\}$ to the frame $\{x^\alpha\}$. Then, first, the factor of the relativistic compression of the sphere is to be taken into account in boundaries of integration. Second, the components of the vector (2.9) after Lorentz transformations (2.8) become

$$\mathcal{J}_m^\alpha = [\gamma\rho(\overline{r}), \gamma v\rho(\overline{r}),\ 0,\ 0] \tag{2.10}$$

in the frame $\{x^\alpha\}$ in coordinates $(t,x,y,z)$, where $\overline{r}^2 = \gamma^2(x-vt)^2 + y^2 + z^2$ (subscript '$m'$ means 'moving'). Third, due to the relativistic compression the densities (that is the components of (2.10)) have to be multiplied by $\gamma$ under the integration in the compressed boundaries. Again the first and third factors are compensated.

Finally for the total mass of the moving matter ball one has

$$E_m = \int_\Sigma dxdydz\left(\gamma\mathcal{J}_m^0(\overline{r})\right) = \gamma\int_\Sigma dx'dydz\rho(r') = 4\pi\gamma\int_0^{r_0} dr'\, r'^2\rho(r') = \gamma\mathcal{M}, \tag{2.11}$$

where the boundary $\partial\Sigma$ of $\Sigma$ is defined as $\gamma^2x^2 + y^2 + z^2 = r_0^2$. Without the loss of generality we set $t = 0$ . After the simple redefinition $x' = \gamma x$ one has $x'^2 + y^2 + z^2 = r'^2$ and the boundary $\partial\Sigma$ is defined as usual $r' = r_0$, thus the last integration in (2.11) repeats exactly (2.7). Keeping in mind (2.4) and following the logic in calculations (2.11) one finds for the total momentum

$$P_m^1 = \int_\Sigma dxdydz\left(\gamma\mathcal{J}_m^1(\overline{r})\right) = \gamma v\int_\Sigma dx'dydz\rho(r') = 4\pi\gamma v\int_0^{r_0} dr'\, r'^2\rho(r') = \gamma v\mathcal{M}. \tag{2.12}$$

The results (2.11) and (2.12) are in the full correspondence with the conclusions of special relativity. The analogies with the above calculus based on the covariant formalism of [12, 13] will be used to calculate the global mass and momentum of the moving SBH.

### 3. Static isotropic gauge for Schwarzschild solution

Before studying a moving SBH it is more convenient to consider the Schwarzschild metric in isotropic coordinates, like in [16]:

$$ds^2 = -\alpha^2(r)dt^2 + \psi^4(r)(dx^2 + dy^2 + dz^2), \tag{3.1}$$

where $\alpha(r) \equiv (1 - \frac{M}{2r})/(1 + \frac{M}{2r})$, $\psi(r) \equiv 1 + \frac{M}{2r}$ and again $x^2 + y^2 + z^2 = r^2$.

Let us derive the necessary TEGR expressions. The most convenient is to choose the tetrad in diagonal form:

$$h^a{}_\mu = \mathrm{diag}\left[\alpha(r), \psi^2(r), \psi^2(r), \psi^2(r)\right]. \tag{3.2}$$

Non-zero components of L-CSC (1.4) calculated for (3.1) and (3.2) are:

$$\overset{\circ}{A}{}^{\hat 0}{}_{\hat i 0} = -\overset{\circ}{A}{}^{\hat i}{}_{\hat 0 0} = \frac{Mx^i}{r^3}\frac{1}{\psi^4(r)}; \quad \overset{\circ}{A}{}^{\hat i}{}_{\hat k i} = -\overset{\circ}{A}{}^{\hat k}{}_{\hat i i} = \frac{Mx^k}{r^3}\frac{1}{\psi(r)}, \tag{3.3}$$

where the indexes with "hat" are tetrad components and indexes without "hat" are spacetime components; here, $x^i \equiv (x^1, x^2, x^3) \equiv (x, y, z)$. "Turning-off gravity" for L-CSC (3.3) and related curvature leads to $M \to 0$. Then L-CSC vanishes giving for all the components of ISC

$$\overset{\bullet}{A}{}^a{}_{b\mu} = 0. \tag{3.4}$$

For the L-CSC (3.3) and zero ISC (3.4) the formulae (1.2) and (1.11) give the teleparallel superpotential, non-zero components of which are:

$$\overset{\bullet}{S}{}_0{}^{0i} = -\overset{\bullet}{S}{}_0{}^{i0} = \frac{2Mx^i}{r^3}\frac{1}{\psi^5(r)}; \quad \overset{\bullet}{S}{}_i{}^{ik} = -\overset{\bullet}{S}{}_i{}^{ki} = \frac{M^2x^k}{2r^4}\frac{1}{\alpha(r)\psi^6(r)}. \tag{3.5}$$

To calculate the total mass of the Schwarzschild black hole, it is more convenient to take the spherical coordinates. Therefore, let us provide the standard coordinate transformation (2.6) after that the metric (3.1) acquires the form:

$$ds^2 = -\alpha^2(r)dt^2 + \psi^4(r)\left[dr^2 + r^2(d\theta^2 + \sin^2\theta d\phi^2)\right]. \tag{3.6}$$

Again we chose the diagonal tetrad, this time for the metric (3.6):

$$h^a{}_\mu = \mathrm{diag}\left[\alpha(r), \psi^2(r), r\psi^2(r), r\psi^2(r)\sin\theta\right]. \tag{3.7}$$

For the metric (3.6) and tetrad (3.7), the non-zero components of L-CSC (1.4) are

$$\begin{aligned}\overset{\circ}{A}{}^{\hat 0}{}_{\hat 1 0} = \overset{\circ}{A}{}^{\hat 1}{}_{\hat 0 0} = \tfrac{M}{r^2}\tfrac{1}{\psi^4(r)}; \quad \overset{\circ}{A}{}^{\hat 1}{}_{\hat 2 2} = -\overset{\circ}{A}{}^{\hat 2}{}_{\hat 1 2} = \tfrac{M}{r}\tfrac{1}{\psi(r)} - 1;\\ \overset{\circ}{A}{}^{\hat 1}{}_{\hat 3 3} = -\overset{\circ}{A}{}^{\hat 3}{}_{\hat 1 3} = -\alpha(r)\sin\theta; \quad \overset{\circ}{A}{}^{\hat 2}{}_{\hat 3 3} = -\overset{\circ}{A}{}^{\hat 3}{}_{\hat 2 3} = -\cos\theta,\end{aligned} \tag{3.8}$$

where now $x^i \equiv (x^1, x^2, x^3) \equiv (r, \theta, \phi)$.

"Turning off" gravity by $M \to 0$ in (3.8) gives ISC, non-zero components of which are:

$$\overset{\bullet}{A}{}^{\hat 1}{}_{\hat 2 2} = -\overset{\bullet}{A}{}^{\hat 2}{}_{\hat 1 2} = -1; \quad \overset{\bullet}{A}{}^{\hat 1}{}_{\hat 3 3} = -\overset{\bullet}{A}{}^{\hat 3}{}_{\hat 1 3} = -\sin\theta; \quad \overset{\bullet}{A}{}^{\hat 2}{}_{\hat 3 3} = -\overset{\bullet}{A}{}^{\hat 3}{}_{\hat 2 3} = -\cos\theta. \tag{3.9}$$

Then, formulae (1.2) and (1.11) for the L-CSC (3.8) and ISC (3.9) give non-zero components of $\overset{\bullet}{S}{}_\sigma{}^{\alpha\beta}$:

$$\overset{\bullet}{S}{}_0{}^{01} = -\overset{\bullet}{S}{}_0{}^{10} = -\frac{2M}{r^2}\frac{1}{\psi^5(r)}; \quad \overset{\bullet}{S}{}_2{}^{12} = -\overset{\bullet}{S}{}_2{}^{21} = \overset{\bullet}{S}{}_3{}^{13} = -\overset{\bullet}{S}{}_3{}^{31} = -\frac{M^2}{2r^3}\frac{1}{\alpha(r)\psi^6(r)}. \tag{3.10}$$

It is necessary to compare the pair (3.2) and (3.4) with the pair (3.7) and (3.9). Let us apply the transformations (1.5) and (1.6) to the tetrad (3.7) and ISC (3.9), where

$$\Lambda^a{}_b = \begin{pmatrix} 1 & 0 & 0 & 0 \\ 0 & \sin\theta\cos\phi & \cos\theta\cos\phi & -\sin\phi \\ 0 & \sin\theta\sin\phi & \cos\theta\sin\phi & \cos\phi \\ 0 & \cos\theta & -\sin\theta & 0 \end{pmatrix}. \tag{3.11}$$

Then the tetrad (3.7) goes to the tetrad (3.2) (after the coordinate transformations (2.6)), whereas the transformed ISC vanishes that is becomes (3.4). Thus, in the framework of the fully covariant formalism [12, 13] in terminology of [14, 15] these pairs represent the same gauge, we call it the "static isotropic gauge" (SIG).

It is useful to compare the SIG introduced here with the SSG in [14]. The isotropic coordinates in (3.6) are connected with the static Schwarzschild coordinates in [14], with $R$ radial coordinate, by the relation $R = r(1 + M/2r)^2$. Applying this transformation to the components of the tetrad (3.7), one obtains the components of the diagonal tetrad in [14] in the SSG; the components of the ISC (3.9) do not change and coincide with those in [14]. Thus the SIG here and the SSG in [14] are the same gauge presented in different coordinates.

## 4. Calculations in analogy with the matter ball in Minkowski space

Let us calculate the global mass of the SBH. First of all, it is necessary to determine the observers in the same way as (2.2) in the Minkowski space. A spacetime with metric (3.1), or (3.6), and with the 4-vectors of static observers

$$\xi^\sigma = \left[-\alpha^{-1}(r),\ 0,\ 0,\ 0\right] \tag{4.1}$$

presents a static reference frame $\{x^\alpha\}$. Then, (1.10) with (3.10) gives the non-zero component of the Noether superpotential

$$\overset{\bullet}{\mathcal{J}}{}_s^{01} = -\overset{\bullet}{\mathcal{J}}{}_s^{10} = 2\kappa^{-1} M\psi(r)\sin\theta; \tag{4.2}$$

and (1.9) gives the Noether current in the form:

$$\overset{\bullet}{\mathcal{J}}{}_s^{\alpha} = \left[2\kappa^{-1}M\psi'(r)\sin\theta,\ 0,\ 0,\ 0\right]. \tag{4.3}$$

Because $\overset{\bullet}{\mathcal{J}}{}_s^{\alpha}$ is a vector density, see (1.8) and (1.9), the energy density in (4.3) presented in spherical coordinates can be rewritten as $\overset{\bullet}{\mathcal{J}}{}_s^{0} = \overset{\bullet}{\rho}(r) r^2\sin\theta$, where $\overset{\bullet}{\rho}(r)$ is the energy density in the Cartesian coordinates of (3.1), compare with (2.5). Thus, substituting (4.3) and (4.2) into (1.12) and (1.13) we get

$$E_s = \lim_{r_0\to\infty}\int_\Sigma dxdydz\overset{\bullet}{\rho}(r) = \lim_{r_0\to\infty}\int_\Sigma drd\theta d\phi\overset{\bullet}{\mathcal{J}}{}_s^{0} = \lim_{r_0\to\infty}\oint_{\partial\Sigma} d\theta d\phi\overset{\bullet}{\mathcal{J}}{}_s^{01} = M, \tag{4.4}$$

where the boundary $\partial\Sigma$ of $\Sigma$ presents a sphere $r = r_0$ again, and then one takes the limit $r_0 \to \infty$. The result (4.4) can be interpreted as the global mass of the static SBH, since at $r_0 \to \infty$ the 4-vector (4.1) asymptotically tends to the timelike Killing vector in the form (2.2). If the charge (4.4) is calculated at finite $r = r_0$, it can be interpreted as the energy measured by observers resting at $r = r_0$ and inside $r = r_0$. The acceptable result (4.4) shows us that the choice of the gauge as SIG corresponds to the problem of calculating the global mass. It is not surprisingly because SIG and SSG being identical ones give the same result $M$.

Following [16] we construct the related description of the SBH moving with a constant velocity $v$ with respect to distant observers. It has its own frame $\{\bar{x}^\alpha\}$ with the barred metric (3.1). Then, to describe the moving SBH in the frame $\{x^\alpha\}$ the authors of [16] apply the transformations (2.8) to the *barred* metric (3.1) and obtain the metric:

$$ds^2 = -\frac{\alpha^2\psi^4}{\gamma^2(\psi^4 - \alpha^2v^2)}dt^2 + \gamma^2(\psi^4 - \alpha^2 v^2)(dx + \beta dt)^2 + \psi^4(dy^2 + dz^2). \tag{4.5}$$

Here, $\beta = -v(1 - \alpha^2/\psi^4)(1 - \alpha^2v^2/\psi^4)^{-1}$, where $\alpha = \alpha(\bar{r})$ and $\psi = \psi(\bar{r})$ with $\bar{r}^2 = \bar{x}^2 + \bar{y}^2 + \bar{z}^2 = \gamma^2(x - vt)^2 + y^2 + z^2$. Thus, $\bar{r} = \text{const}$ presents a compressed sphere (ellipsoid) moving in the frame $\{x^\alpha\}$ with the constant velocity $v$ in direction $x$.

Let us turn to the *proper* reference frame of the moving SBH $\{\overline{x}^\alpha\}$ defined by the *barred* metric (3.1) and related observers analogous to (4.1). Repeating all the steps done for the static SBH and preserving the SIG (that has to be accented), we get in the coordinates $(\bar{t}, \bar{x}, \bar{y}, \bar{z})$:

$$\overset{\bullet}{\mathcal{J}}{}_{s}^{\bar{\alpha}}(\bar{r}) = \left[\overset{\bullet}{\rho}(\bar{r}),\ 0,\ 0,\ 0\right], \tag{4.6}$$

where the dependence $\overset{\bullet}{\rho}(\bar{r})$ is exactly the same as defined for (4.3) and $\bar{r}^2 = \bar{x}^2 + \bar{y}^2 + \bar{z}^2$. We emphasize that in the frame $\{\bar{x}^\alpha\}$ we, of course, repeat the result (4.4): $\overline{E}_s = M$ for the global mass.

Because the gauge is already chosen, and the solution (4.5) is obtained from the barred metric (3.1) with the use of (2.8), the covariant formalism [12, 13] allows us to transform the components of the current (4.6) with the use of (2.8) to the frame $\{x^\alpha\}$:

$$\overset{\bullet}{\mathcal{J}}{}_{m}^{\alpha}(\bar{r}) = \left[\gamma\overset{\bullet}{\rho}(\bar{r}),\ \gamma v\overset{\bullet}{\rho}(\bar{r}),\ 0,\ 0\right]. \tag{4.7}$$

Formally (4.7) coincides with the current (2.10) for a matter ball in Minkowski space. Likewise, the integration for the components of (4.7) actually repeats the integration in (2.11) and (2.12). The only difference is that according to (1.13) one has to go to the surface integration like in (4.4), and then take the limit $r' = r_0 \to \infty$. Finally, we get the global mass for the moving black hole:

$$E_m = \gamma M \tag{4.8}$$

and the global momentum for the moving black hole

$$P^1_m = \gamma v M \tag{4.9}$$

the same as (2.11) and (2.12) for the moving matter ball. Note that inner surfaces are ignored in all surface integrations. This position is in a correspondence with Einstein's point of view [1] that energy of an isolated system is determined by external boundary conditions only.

## 5. A direct application of the fully covariant formalism in TEGR and a "moving gauge"

Up to now, to construct conserved quantities for the moving SBH we have used analogies in Minkowski space. By this, it was taken into account the fully covariance of our formalism [12, 13], but the formalism itself was not applied totally. In this section, we do it.

In the proper frame $\{\bar{x}^\alpha\}$ for the related SIG, the components $\overset{m}{S}{}_{\bar{\sigma}}{}^{\bar{\alpha}\bar{\beta}}$ of $S$-tensor in (1.10) are exactly the components (3.5) in the *barred* form only. Due to the fully covariant formalism we represent the components $\overset{m}{S}{}_{\bar{\sigma}}{}^{\bar{\alpha}\bar{\beta}}$ as $\overset{m}{S}{}_{\sigma}{}^{\alpha\beta}$ in the frame $\{x^\alpha\}$ with the use of the coordinate transformation (2.8). Of course, the components of $\overset{m}{S}{}_{\sigma}{}^{\alpha\beta}$, being very cumbersome ones, differ from the components of $\overset{\bullet}{S}{}_{\sigma}{}^{\alpha\beta}$ in (3.5) if both of them are in the same frame $\{x^\alpha\}$.

To calculate total energy for the moving SBH in the frame $\{x^\alpha\}$ we use again the general formulae (1.12) and (1.13). Note that under integration we use only (1.12) with zero curent component, not (2.4) or (2.12). Thus

$$E_m = \lim_{r\to\infty}\int_{\Sigma_r} dxdydx\, \overset{\bullet}{\mathcal{J}}{}_{m}^{0}(\xi) = \lim_{r\to\infty}\int_{\Sigma_r} dxdydz\, \partial_k \overset{\bullet}{\mathcal{J}}{}_{m}^{0k}(\xi). \tag{5.1}$$

Here, for the sake of simplicity we use $r$ instead of $r_0$ under limits. To evaluate this expression, we exploit the following. First, we have already carried out the easier calculation for the static case in isotropic coordinate system in SIG gauge. Second, since we consider $r \to \infty$, terms which make no contribution to this limit may be neglected. Thus, the integration (5.1) takes place on a $t = \text{const}$ slice, and without the loss of generality we set $t = 0$, after that on this slice we make the coordinate transformation $x = \bar{x}/\gamma, y = \bar{y}, z = \bar{z}$. From here the relations $r^2 = \bar{r}^2/\gamma^2 + v^2(\bar{y}^2 + \bar{z}^2)$ and $\bar{r}^2 = r^2 + \gamma^2 v^2 x^2$ follow easily. Therefore one can replace $r \to \infty$ by $\bar{r} \to \infty$ and similarly on the slice $t = \text{const}$, and, thus, (5.1) is rewritten as

$$E_m = \lim_{\bar{r}\to\infty}\frac{1}{\gamma}\int_{\Sigma_{\bar{r}}} d\bar{x}d\bar{y}d\bar{z}\, \partial_k \overset{\bullet}{\mathcal{J}}{}_{m}^{0k}(\xi). \tag{5.2}$$

Here, the limit is carried out for the surface $\partial\Sigma_{\bar r}$ defined by $\bar r = \mathrm{const}$. The integrand in (5.2) is rewritten as

$$\partial_k \overset{\bullet}{\mathcal{J}}{}^{0k}_{m}(\xi) = \partial_\beta \overset{\bullet}{\mathcal{J}}{}^{0\beta}_{m}(\xi) = \frac{1}{\kappa}\partial_\beta \left(h(x^\alpha)\overset{m}{S}_\sigma{}^{0\beta}\xi^\sigma\right) = \frac{1}{\kappa}\partial_{\bar\beta} \left(h(\bar r)\overset{m}{S}_\sigma{}^{0\bar\beta}\xi^\sigma\right). \tag{5.3}$$

Because determinant of the Lorentz transformations (2.8) is equal to unit one can transform $h(x^\alpha) = \det h^a{}_\mu$ simply to $h(\bar r) = \det h^a{}_{\bar\mu}$. Thus the last equality is holding due to the covariance of the divergence which involves the correct density weight. As an observer we can choose again the static observer with the proper vector (4.1) for which $\xi^\sigma \to (-1,0,0,0)$ at $r, \bar r \to \infty$. Finally, to carry out the calculation of (5.2), we need the asymptotic behavior at $r, \bar r \to \infty$ of the quantity

$$\overset{m}{S}_0{}^{0\bar\beta}\xi^0 = \overset{m}{S}_{\bar\sigma}{}^{\bar\alpha\bar\beta}\frac{\partial x^0}{\partial \bar x^{\bar\alpha}}\frac{\partial \bar x^{\bar\sigma}}{\partial x^0}\xi^0 = -\overset{m}{S}_{\bar 0}{}^{\bar 0\bar\beta}\frac{\partial t}{\partial \bar t}\frac{\partial \bar t}{\partial t} + \text{neglectable terms}. \tag{5.4}$$

The last terms are not important due to asymptotic behaviour in (3.5) presented in barred coordinates. Taking into account (2.8) we rewrite (5.3) as

$$\partial_k \overset{\bullet}{\mathcal{J}}{}^{0k}_{m}(\xi) = \gamma^2 \partial_{\bar k} \overset{\bullet}{\mathcal{J}}{}^{\bar 0\bar k}_{s}(\xi) + \text{neglectable terms} \tag{5.5}$$

and substitute it into (5.2)

$$E_m = \gamma \lim_{\bar r\to\infty}\int_{\Sigma_{\bar r}} d\bar x d\bar y d\bar z\, \partial_{\bar k} \overset{\bullet}{\mathcal{J}}{}^{\bar 0\bar k}_{s}(\xi) = \gamma \lim_{\bar r\to\infty}\oint_{\partial\Sigma_{\bar r}} d\bar\theta d\bar\phi\, \overset{\bullet}{\mathcal{J}}{}^{\bar 0\bar 1}_{s}(\xi) = \gamma E_s = \gamma M. \tag{5.6}$$

Calculations are carried out with the use of barred coordinates $(\bar x, \bar y, \bar z)$ introduced now on the slice $t = \mathrm{const}$. The last integral is written in spherical coordinates, in fact, repeating the calculation (4.4), that gives the energy $E_s$ of the static SBH.

The formulae (1.12) and (1.13) for defining global conserved quantities are quite universal and a choice of vector $\xi^\alpha$ determines their interpretation. Thus, formulae (5.1)-(5.3) are left universal up to the choice of vector $\xi^\alpha$. In order to calculate the momentum expression of for the moving SBH we choose $\xi^\alpha = (0, \xi^1, 0, 0)$ when $\xi^1 \to 1$ at $r \to \infty$ that specifies an $x$-translation Killing vector at $r \to \infty$. In this case we need to derive an asymptotics of the expression:

$$\overset{m}{S}_1{}^{0\bar\beta}\xi^1 = \overset{m}{S}_{\bar\sigma}{}^{\bar\alpha\bar\beta}\frac{\partial x^0}{\partial \bar x^{\bar\alpha}}\frac{\partial \bar x^{\bar\sigma}}{\partial x^1}\xi^1 = \overset{m}{S}_{\bar 0}{}^{\bar 0\bar\beta}\frac{\partial t}{\partial \bar t}\frac{\partial \bar t}{\partial x} + \text{neglectable terms}. \tag{5.7}$$

Again, the last terms are not important due to asymptotic behaviour in (3.5) presented in barred coordinates. Note that sign 'minus' in barred (3.5) for $\overset{m}{S}_{\bar 0}{}^{\bar 0\bar i}$ and sign 'minus' in $\partial\bar t/\partial x = -v\gamma$ are compensated, and the leading term in (5.7) is positive. Taking into account (2.8), we rewrite (5.3) for the asymptotically $x$-translation vector $\xi$ as

$$\partial_k \overset{\bullet}{\mathcal{J}}{}^{0k}_{m}(\xi) = v\gamma^2 \partial_{\bar k} \overset{\bullet}{\mathcal{J}}{}^{\bar 0\bar k}_{s}(\xi) + \text{neglectable terms}. \tag{5.8}$$

Thus, analogously to (5.6) one has for the total momentum of the moving SBH:

$$P_m = v\gamma \lim_{\bar r\to\infty}\int_{\Sigma_{\bar r}} d\bar x d\bar y d\bar z\, \partial_{\bar k} \overset{\bullet}{\mathcal{J}}{}^{\bar 0\bar k}_{s}(\xi) = v\gamma \lim_{\bar r\to\infty}\oint_{\partial\Sigma_{\bar r}} d\bar\theta d\bar\phi\, \overset{\bullet}{\mathcal{J}}{}^{\bar 0\bar 1}_{s}(\xi) = v\gamma E_s = v\gamma M. \tag{5.9}$$

One can see that the results (5.6) and (5.9) are acceptable from the point of view of relativistic theory.

Returning to gauges introduced in [14], we recall that both SSG (connected with a static tetrad) and different from it LG (connected with a freely falling tetrad) are not in the same equivalence class, but nonetheless are both obtained by the "switching off" gravity principle. However, in [15], we have shown that the static tetrad of SSG *after a radial boost* together with the *unchanged* related ISC leads to the LG itself. Here, to construct the 'moving gauge' in a more economical way we follow the logic of [15] and provide the boost

$$(\Lambda_{boost})^{a'}{}_b = \begin{pmatrix} \gamma & v\gamma & 0 & 0 \\ v\gamma & \gamma & 0 & 0 \\ 0 & 0 & 1 & 0 \\ 0 & 0 & 0 & 1 \end{pmatrix}, \tag{5.10}$$

for the tetrad (3.2) that transforms it to the tetrad moving correspondingly to the moving SBH. At the same time we *preserve* zero ISC. On the other hand, to be staying in the framework of SIG, simultaneously with changing the tetrad we have to apply the global boost (5.10) to zero ISC in correspondence with (1.6). We see that the zero ISC is left to be zero. Thus, the "moving gauge" and the SIG are the same unique gauge. This means that the acceptable results for both the total energy and the total momentum for the moving SBH, in fact, have been obtained in the framework of the related appropriate "moving gauge". Of course, the aforementioned "moving gauge" can be obtained by the "switching off" gravity principle for the moving (boosted) tetrad.

**Conclusion**

The formalism for constructing conserved quantities in TEGR [12, 13] has been applied to the SBH moving with a constant velocity with respect to distant static observers. These conserved quantities are calculated by two ways: first, in analogy with the matter ball model in Minkowski space; second, by the technology of the TEGR itself. The expected energy and momentum are obtained in both the cases. The acceptable results follow due to the fully covariance of the formalism. However there is ambiguity in the definition of gauges. To avoid an ambiguity in such calculations an appropriate gauge defined by a pair of tetrad and related inertial spin connection has to be defined [14, 15]. Such a gauge is found for the moving SBH and we stress that the SIG is the unique gauge both for the static and moving tetrads, and SIG is just the SSG introduced in [14].

**Список литературы/References**


1. Aldrovandi R., Pereira J.G. *Teleparallel Gravity: An Introduction.* Dordrecht, Heidelberg, New York, London: Springer, 2013.
2. Kršsák M., van den Hoogen R.J., Pereira J.G., Boehmer C.G., Coley A.A. Teleparallel Theories of Gravity: Illuminating a Fully Invariant Approach. *Class. Quantum Grav.*, 2019, vol. 36, no. 18, 183001.
3. Bahamonde S., Dialektopoulos K.F., Escamilla-Rivera C., Farrugia G., Gakis V., Hendry M., Hohmann M., Said J.L., Mifsud J., Valentino E.D. Teleparallel gravity: From theory to cosmology. *Rep. Prog. Phys.*, 2023, vol. 86, no. 2, 026901.
4. Mikhail F.I., Wanas M.I., Hindawi A., Lashin E.I. Energy-Momentum Complex in Møller's Tetrad Theory of Gravitation. *Int. J. Theor. Phys.*, 1993, vol. 32, no. 9, pp. 1627–1642.
5. Maluf J.W. Accelerated observers and gravitational radiation. *Grav. Cosmol.*, 2005, vol. 11, no. 3, pp. 284–288.
6. Maluf J.W. The teleparallel equivalent of general relativity. *Annalen der Phys.*, 2013, vol. 525, no. 5, pp. 339–357.
7. Maluf J.W., Faria F.F., Ulhoa S.C. On reference frames in spacetime and gravitational energy in freely falling frames. *Class. Quantum Grav.*, 2007, vol. 24, no. 10), pp. 2743–2754.
8. Lucas T.G., Obukhov Y.N., Pereira J.G. Regularizing role of teleparallelism. *Phys. Rev. D*, 2009, vol. 80, no. 6, 064043.
9. Obukhov Y.N., Rubilar G.F. Covariance properties and regularization of conserved currents in tetrad gravity. *Phys. Rev. D*, 2006, vol. 73, no. 12, 064043.
10. Obukhov Y.N., Rubilar G.F. Invariant conserved currents in gravity theories with local Lorentz and diffeomorphism symmetry. *Phys. Rev. D*, 2006, vol. 74, no. 6, 064002.
11. Obukhov Y.N., Rubilar G.F., Pereira J.G. Conserved currents in gravitational models with quasi-invariant Lagrangians: Application to teleparallel gravity. *Phys. Rev. D*, 2006, vol. 74, no. 10, 104007.
12. Emtsova E.D., Petrov A.N., Toporensky A.V. Conserved Currents and Superpotentials in Teleparallel Equivalent of General Relativity. *Class. Quantum Grav.*, 2020, vol. 37, no. 9, 095006.

13. Emtsova E.D., Petrov A.N., Toporensky A.V. On conservation laws in teleparallel gravity. *J. Phys.: Conf. Ser.*, 2020, vol. 1557, 012017.
14. Emtsova, E.D., Krššák, M., Petrov, A.N., Toporensky, A.V.: On conserved quantities for the Schwarzschild black hole in teleparallel gravity. *Eur. Phys. J. C*, 2021, v. 81, no. 8, 743.
15. Emtsova, E.D., Krššák, M., Petrov, A.N., Toporensky, A.V.: On the Schwarzschild solution in TEGR. *J. Phys.: Conf. Ser.*, 2021, vol. 2081, 012017.
16. Hartle, J.B., Thorne, K.S., Price, R.H.: Gravitational interaction of a black hole with distant bodies. In: Thorne, K.S., MacDonald D.A. (eds.) *Black Holes: The Membrane Paradigm*, pp. 146–180. Yale University Press, New Haven/London, 1986.
17. Petrov, A.N., Kopeikin, S.M., Lompay, R.R., Tekin, B. *Metric Theories of Gravity: Perturbations and Conservation Laws.* Berlin, de Gruyter, 2017.
18. Emtsova E.D., Petrov A.N. On Conserved Quantities for a Moving Black Hole in TEGR. Physical Interpretations of Relativity Theory: XXIII International Scientific Conference, Moscow, July 3–6, 2023, Abstracts, p. 48.
19. Emtsova E.D., Petrov A.N. A moving black hole in TEGR as a moving matter ball. *Space, time and fundamental interactions*, 2022, no 39, pp. 18–25.
20. Emtsova E.D., Petrov A.N. On gauges for a moving black hole in TEGR. *Gen. Relat. Grav.*, 2022, vol. 54, 114.
21. Møller, C. Further remarks on the localization of the energy in the general theory of relativity. *Ann. Phys.*, 1961, vol. 12, no. 1, pp. 118–133.
22. Einstein, A.: Der Energiesatz in der allgemeinen Relativitätstheorie. *Sitzungsber. preuss. Akad. Wiss.*, 1918, no. 1, pp. 448–459.

**Авторы**

**Емцова Елена Дмитриевна**, к.ф.-м.н., ведущий инженер НИЛ КОСМОЛОГИЯ, Казанский федеральный университет, ул. Кремлевская, д. 18, г. Казань, 420008, Россия.
E-mail: ed.emcova@physics.msu.ru

**Петров Александр Николаевич**, д.ф.-м.н., ведущий научный сотрудник, Астрономический институт им. П.К.Штернберга МГУ им. М.В.Ломоносова, Университетский пр-кт, д. 13, г. Москва, 119992, Россия.
E-mail: alex.petrov55@gmail.com

**Просьба ссылаться на эту статью следующим образом:**

Емцова Е. Д., Петров А. Н. О сохраняющихся величинах для движущейся чёрной дыры в телепараллельном эквиваленте ОТО. *Пространство, время и фундаментальные взаимодействия.* 2023. № 3-4. С. 77–88.

**Authors**

**Emtsova Elena Dmitrievna**, Ph.D., leading engineer NIL COSMOOGY, Kazan Federal University, Kremlevskaya st., 18, Kazan, 420008, Russia..
E-mail: ed.emcova@physics.msu.ru

**Petrov Alexander Nikolaevich**, Sc.H., Leading Scientific Researcher, Sternberg Astronomical Institute, MV Lomonosov Moscow State University, Universitetskii pr-kt, 13, Moscow, 119992, Russia.
E-mail: alex.petrov55@gmail.com

**Please cite this article in English as:**

Emtsova E. D., Petrov A. N. On conserved quantities for a moving black hole in TEGR. *Space, Time and Fundamental Interactions*, 2023, no. 3-4, pp. 77–88.

УДК 115.4



## О ПРОБЛЕМЕ ВРЕМЕНИ В КВАНТОВОЙ КОСМОЛОГИИ *

Фильченков М. Л.[a,1], Лаптев Ю. П.[a,2]

[a] Учебно-научный институт гравитации и космологии РУДН, г. Москва, 117198, Россия.

Рассмотрена проблема времени в квантовой космологии в рамках квантовой геометродинамики. Хотя время явно не присутствует в квантовой космологии, оно появляется в классической космологии. Классический мир оказывается запрограммированным на квантовом уровне.

*Ключевые слова*: геометродинамика, космология.

## ON THE TEMPORAL PROBLEM IN QUANTUM COSMOLOGY

Fil'chenkov M. L.[a,1], Laptev Yu. P.[a,2]

[a] Institute of Gravitation and Cosmology, Peoples' Friendship University of Russia, 6 Miklukho-Maklay Street, Moscow 117198, Russia.

The time problem in quantum cosmology has been considered in the framework of quantum geometrodynamics. Although time is not present in quantum cosmology explicitly, it emerges in classical cosmology. The classical world proves to be programmed on the quantum level.

*Keywords*: geometrodynamics, cosmology .

PACS: 98.80.-k

DOI: 10.17238/issn2226-8812.2023.3-4.89-92

### Introduction

The four-dimensional space-time is split into time and a three-dimensional of instantaneous configurations, forming a a space-time of 3-geometries being considered in quantum cosmology. On the other hand, its classical limit describes the Universe's time. Therein lies the temporal problem in quantum cosmology, which was considered by philosophers, mainly on the level of interpretations [1]. Consider it in the framework of quantum geometrodynamics.

### 1. Wheeler-DeWitt's Equation

In quantum cosmology, the Universe's wave function is described in space of 3-geometries [2], i.e. $\frac{\partial\psi(^3G)}{\partial t} = 0$ is assumed. Hence we obtain Wheeler-DeWitt's equation $\hat{H}\psi = 0$. Since each 3-geometry describes a spatial configuration at a certain instant, time is present in 3-geometry implicitly. The combination of 3-geometries describes an implicit dependence of the superspace on time. The 3-geometries are space-loke cross-sections of the4-dimensional space-time, whose realization probability is determined by the absolute value squared of the wave function.

For a homogeneous isotropic Universe Friedmann's first equation

$$\frac{1}{2}\left(\frac{da}{d\eta}\right)^2 - \frac{4\pi G\varepsilon a^2}{3c^2} = -\frac{kc^2}{2} \tag{1.1}$$

is describable in the form of Hamiltonian connection

$$H = \frac{p_a^2}{2} + \frac{ka^2}{2} - \frac{4\pi G\varepsilon a^4}{3c^2} = 0, \tag{1.2}$$

*This research was founded by RUDN University scientific project No. FSSSF2023-0003.

[1]E-mail: fmichael@mail.ru

[2]E-mail: yplaptev@rambler.ru

where $\varepsilon$ is the energy density, $a$ is the scale factor, $k = 0, \pm 1$ the model parameter, $p_a = \frac{da}{d\eta}$ the generalized momentum, $\eta$ the conformal time, related to synchronous one $t$ by the formula $cdt = ad\eta$.

Hence it follows that the Lagrangian

$$L = \frac{p_a^2}{2} - \frac{ka^2}{2} + \frac{4\pi G\varepsilon a^4}{3c^2} = 0 \tag{1.3}$$

and the generalized momentum

$$p_a = \sqrt{\frac{8\pi G\varepsilon a^4}{3c^4} - ka^2}. \tag{1.4}$$

Replacing the quantity $p_a$ in the Hamiltonian connection by the operator $\hat{p}_a = \frac{l_{pl}^2}{i}\frac{d}{da}$, we obtain Wheeler-DeWitt's equation in the minisuperspace of scale factors [3]

$$\frac{d^2\psi}{da^2} - V(a)\psi = 0, \tag{1.5}$$

where

$$V(a) = \frac{1}{l_{pl}^4}\left(ka^2 - \frac{8\pi G\varepsilon a^4}{3c^4}\right). \tag{1.6}$$

From the relation $Ld\eta = p_a da$ we find the dependence of the synchronous time on the scale factor

$$t = \frac{1}{cl_{pl}^2}\int \frac{ada}{\sqrt{-V}}. \tag{1.7}$$

## 2. WKB Approximation of Quantum Geometrodynamics

Consider a WKB approximation of quantum geometrodynamics. The WKB wave function has the form $\psi \sim e^{\frac{iS}{\hbar}}$, where the action reads

$$S = \hbar\int \sqrt{-V}da. \tag{2.1}$$

Find a relation between $t(a)$ and $S(a)$ in the form

$$t = \frac{\hbar}{cl_{pl}^2}\int \frac{ada}{\frac{dS}{da}}. \tag{2.2}$$

Since time is determined by the WKB wave function, the classical world proves to be programmed on the quantum level [3].

For the multicomponent medium with

$$\varepsilon(a) = \varepsilon_0 \sum_n B_n \left(\frac{r_0}{a}\right)^n, \tag{2.3}$$

where $n = 3(1+w)$, $\sum_n B_n = 1$, $\frac{1}{r_0^2} = \frac{8\pi G\varepsilon_0}{3c^4}$, $r_0$ is de Sitter's horizon. In the case of a barotropic equation of state we have $p = w\varepsilon$. Consider the dependence of the scale factor on time and the corresponding ones for the WKB wave function phase on the scale factor for one-component media with $k = 0$. The scale factor

$$a(t) = r_0\left(\frac{nct}{2r_0}\right)^{\frac{2}{n}-1} \text{for } n \neq 0, \tag{2.4}$$

the wave function phase

$$\frac{S}{\hbar} = \frac{r_0^{\frac{n}{2}} a^{3-\frac{n}{2}}}{(3-\frac{n}{2})l_{pl}^2} \text{for } n \neq 6, \tag{2.5}$$

Consider these formulae for de Sitter's vacuum, i.e. for $w = -1$, $n = 0$:

$$a(t) = r_0 e^{\frac{ct}{r_0}}, \ \frac{S}{\hbar} = \frac{a^3}{3r_0 l_{pl}^2}. \tag{2.6}$$

De Sitter's vacuum responsible for the first inflation is unstable, since the sound velocity $v_s = \sqrt{\left(\frac{\partial p}{\partial \rho}\right)_s}$ is imaginary in this case.

At $t \sim 10^{-33}s$ from the singularity there occurs the Big Bang being accompanied by creation of ultrarelativistic particles and radiation with the equation of state $w = \frac{1}{3},\ n = 1$. In this case we obtain:

$$a(t) = r_0\sqrt{\frac{2ct}{r_0}},\ \frac{S}{\hbar} = \frac{r_0 a}{l_{pl}^2}. \tag{2.7}$$

## 3. Time Emergence in Quantum Cosmology

Reduce Wheeler-DeWitt's equation in minisuperspace of 3-geometries, allowing for the relation

$$V(a) = \frac{2m_{pl}}{\hbar^2}[U(a) - E], \tag{3.1}$$

to the equation of stationary Schrödinger type

$$\frac{d^2\psi}{da^2} - \frac{2m_{pl}}{\hbar^2}[U(a) - E] = 0, \tag{3.2}$$

where

$$E = \frac{m_{pl}c^2}{2}\left(\frac{r_o}{l_{pl}}\right)^2 B_4. \tag{3.3}$$

This equation describes the Universe, behaving as an ultrarelativistic planckeon in the field formed by types of matter with $w \neq \frac{1}{3}$, to which corresponds the potential energy $U(a)$. The Universe's birth from de Sitter's vacuum, as a result of quantum fluctuation, is interpreting as a tunnelling of the planckeon from the pre-de Sitter's stage through a potential barrier [4].

The tunnelling probability is given by Gamow's formula

$$D = \exp\left(-|\frac{2}{\hbar}\int\limits_{a_1}^{a_2}\sqrt{E-U}da|\right), \tag{3.4}$$

where $U(a_1) = U(a_2) = E$.

## 4. Conclusion

In quantum geometrodynamics, the Universe wave function is implicitly dependent on time in the minisuperspace of scale factors, whereas the WKB wave function phase depends on the scale factor, describing the Universe evolution. A relation between the a certain instant, dependence of the scale factor on time and the dependence of the wave function phase on the scale factor has been found for one-component media. Each 3-geometry describes the spatial configuration at a certain instant, which means that the superspace of scale factors contains time implicitly.

## Acknowledgement

We are grateful to the Organizing Committee of PIRT-2023 Conference for the invitation. This research was founded by RUDN University scientific project No. FSSSF2023-0003

## Список литературы/References

1. A.Yu. Sevalnikov, *Metaphysics*No. 1(17), p. 136 (2013).
2. J.A. Wheeler, *Einsteins Vision.* Berlin: Springer–Verlag, 1968.
3. M.L. Fil'chenkov, Yu.P. Laptev. *Quantum Gravity.* Moscow: Lenand, 2016.
4. E.P. Tryon, *Nature*, v. 246, 396 (1973).

**Авторы**

**Фильченков Михаил Леонидович**, д.ф.-м.н., доцент Учебно-научного института гравитации и космологии РУДН, Россия.
E-mail: fmichael@mail.ru

**Лаптев Юрий Павлович**, к.ф.-м.н.
E-mail: yplaptev@rambler.ru

**Просьба ссылаться на эту статью следующим образом:**
Фильченков М. Л., Лаптев Ю. П. О проблеме времени в квантовой космологии. *Пространство, время и фундаментальные взаимодействия.* 2023. № 3-4. С. 89–92.

**Authors**

**Fil'chenkov Mikhail Leonidovich**, D.Sc.
E-mail: fmichael@mail.ru

**Laptev Yuri Pavlovich**, Ph.D.
E-mail: yplaptev@rambler.ru

**Please cite this article in English as:**
Fil'chenkov M. L., Laptev Yu. P. On The Temporal Problem In Quantum Cosmology. *Space, Time and Fundamental Interactions*, 2023, no. 3-4, pp. 89–92.

УДК 530.12, 531.51



## ИНФЛЯЦИОННЫЕ МОДЕЛИ НА ОСНОВЕ ОБОБЩЕННЫХ ТОЧНЫХ КОСМОЛОГИЧЕСКИХ РЕШЕНИЙ*

Фомин И. В.[a,1], Денцель Е. С.[a,2]

[a] МГТУ им. Н.Э. Баумана,, г. Москва, 105005, Россия.

В данной работе предложен метод построения неограниченного числа точных решений уравнений космологической динамики для случая гравитации Эйштейна и телепараллельного эквиввалента общей относительности. Точные космологические решения полученные, в рамках данного подхода, подразумевают сложные типы эволюции скалярного поля и динамики расширения вселенной. В качестве примера рассмотрены решения уравнений космологической динамики в виде рядов, каждый член которых и весь ряд являются точными решениями. Показано, что при определенном выборе параметров, полученные решения соответствуют корректной динамике расширения вселенной на различных стадиях ее эволюции.

*Ключевые слова*: телепараллельная гравитация, общая теория относительности, скалярные поля, точные решения.

## INFLATIONARY MODELS BASED ON GENERALIZED EXACT COSMOLOGICAL SOLUTIONS

Fomin I. V.[a,1], Dentsel E. S.[a,2]

[a] Bauman Moscow State Technical University, Moscow, 105005, Russia.

This paper proposes a method for constructing an unlimited number of exact solutions to the equations of cosmological dynamics for the case of Einstein gravity and the teleparallel equivalent of general relativity. The exact cosmological solutions obtained within the framework of this approach imply complex types of evolution of the scalar field and the dynamics of the expansion of the universe. As an example, solutions to the equations of cosmological dynamics in the form of series are considered, each term of which and the entire series are exact solutions. It is shown that with a certain choice of parameters, the solutions obtained correspond to the correct dynamics of the expansion of the universe at various stages of its evolution.

*Keywords*: teleparallel gravity, general relativity, scalar fields, exact solutions.

PACS: 04.50.-h

DOI: 10.17238/issn2226-8812.2023.3-4.93-98

### Introduction

Within the framework of constructing current cosmological models, the stage of cosmological inflation is important, since during this stage various physical processes occur that determine the further evolution of the universe [1, 5].

Various gravity theories are used to construct models of cosmological inflation, including Einstein gravity (GR) and the teleparallel equivalent of general relativity (TERG) [3, 4, 5].

Teleparallel gravity is a special case of metric-affine gravity, an important feature of which is the use of non-Riemannian geometry. Unlike Einstein gravity, teleparallel gravity does not have geodesic line equations. Force equations describe the motion of particles under the influence of gravity, and instead of metrics, dynamic tetrads are used. Just as the Levi-Civita connection which provides a way to naturally

*Работа Фомина И.В. выполнена при поддержке гранта РНФ № 22–22–00248.

[1]E-mail: ingvor@inbox.ru

[2]E-mail: edentsel@yandex.ru

differentiate vector fields on a Riemann manifold, in teleparallel gravity the Weizenbock connection with torsion and zero curvature is used [5].

It can also be noted that to construct and analyze cosmological models, different methods are used including exact and approximate solutions of the cosmological dynamic equations [5]. A review of various methods for constructing exact cosmological solutions for the case of Einstein gravity is given in [5, 6]. We also note that all these methods can be used in constructing exact solutions of the equations of cosmological dynamics based on TEGR [7].

However, it should be noted that these methods make it possible to construct a limited number of exact solutions to the equations of cosmological dynamics in explicit form. Also, in the context of construction of the exact solutions of the cosmological dynamics equations in explicit form, as a rule, fairly simple types of evolution of scalar fields or types of cosmological dynamics are considered.

In this paper, we propose a method for constructing an unlimited number of exact solutions of cosmological dynamic equations with a complex form of the volution of a scalar field and a complex form of the cosmological dynamics based on the generating function of a special type for the case of GR and TERG.

It is also shown that in the case of a special choice of the constant parameters of the cosmological models obtained by the method, they correctly describe the dynamics of the expansion of the universe at different stages of its evolution.

## 1. Cosmological models based on the teleparallel gravity

Teleparallel gravity is a well-known modification of Einstein gravity, in which tetrads $e^a_\mu$ or components of the tetrad field $\mathbf{e}_a(x^\mu)$ are used instead of a metric.

The tetrads form an orthogonal coordinate basis for which $e^a_\mu e^\nu_a = \delta^\nu_\mu$ and $e^a_\mu e^\mu_b = \delta^a_b$. They relate the space-time metric $g_{\mu\nu}$ and the Minkowski tangent space metric $\eta_{ab} = diag(-1, 1, 1, 1)$ as follows [5, 8]

$$g_{\mu\nu} = e^a_\mu e^b_\nu \eta_{ab}. \tag{1.1}$$

Characteristic quantities of teleparallel gravity: torsion scalar $T = S_\rho{}^{\mu\nu} T^\rho{}_{\mu\nu}$, superpotential $S_\rho{}^{\mu\nu}$ and the distortion tensor $K^{\mu\nu}_{\ \ \rho}$, which are specified in the components of the tetrad field [5, 8]

$$T^\rho{}_{\mu\nu} = e^\rho_a \left(\partial_\mu e^a_\nu - \partial_\nu e^a_\mu + \omega^a_{b\mu} e^b_\nu - \omega^a_{b\nu} e^b_\mu\right), \tag{1.2}$$

$$S_\rho{}^{\mu\nu} = \frac{1}{2}\left(K^{\mu\nu}_{\ \ \rho} + \delta^\mu_\rho T^{\theta\nu}_{\ \ \theta} - \delta^\nu_\rho T^{\theta\mu}_{\ \ \theta}\right), \tag{1.3}$$

$$K^{\mu\nu}_{\ \ \rho} = -\frac{1}{2}\left(T^{\mu\nu}_{\ \ \rho} - T^{\nu\mu}_{\ \ \rho} - T_\rho{}^{\mu\nu}\right), \tag{1.4}$$

where $\omega^a_{b\mu} = \Lambda^a_d(x)\partial_\mu \Lambda^d_b(x)$ is the spin connection, $\Lambda^a_d(x)$ is the local Lorentz transformations.

To construct and analyze models of cosmological inflation with a non-minimal connection between the scalar field and torsion, let us consider in the system of units $8\pi G = c = 1$ the following action [8]

$$S = \int d^4x e \left[f(T, \phi) + \omega(\phi) X\right], \tag{1.5}$$

where $f(T, \phi)$ is some arbitrary function of the scalar field $\phi$ and torsion $T$, $\omega(\phi)$ is the kinetic function, $X = -\frac{1}{2}\partial_\mu\phi\partial^\mu\phi$ is the kinetic energy of the scalar field and $e = det\left(e^a_\mu\right) = \sqrt{-g}$.

To describe inflation dynamics in the case of a spatially flat Friedman-Robertson-Walker (FRW) metric

$$ds^2 = -dt^2 + a^2\delta_{ij}dx^i dx^j, \tag{1.6}$$

where $a = a(t)$ is the scale factor, the following tetrad is considered

$$e^a_\mu = diag(1, a, a, a), \tag{1.7}$$

taking into account the Weizenbock connection

$$\omega^a_{\ b\mu} = 0. \tag{1.8}$$

In this case, the background dynamics equations corresponding to the action (1.5) are written as follows [8]

$$f(T,\phi) - \omega(\phi)X - 2Tf_{,T} = 0, \tag{1.9}$$

$$f(T,\phi) + \omega(\phi)X - 2Tf_{,T} - 4\dot{H}f_{,T} - 4H\dot{f}_{,T} = 0, \tag{1.10}$$

$$-\omega_{,\phi}X - 3\omega(\phi)H\dot{\phi} - \omega(\phi)\ddot{\phi} + f_{,\phi} = 0, \tag{1.11}$$

where $H = \frac{\dot{a}}{a}$ is the Hubble parameter, $T = 6H^2$ is the torsion scalar and $f_{,T} = \frac{\partial f}{\partial T}$.

Also note that the canonical scalar fields correspond to the case $\omega > 0$, for phantom fields $\omega < 0$, based on the possibility of the following redefinition of the fields $\varphi = \int \sqrt{\omega(\phi)}\, d\phi$.

The choice of the function $f = f(T,\phi)$ determines the form of the theory of gravity in the cosmological models under consideration.

In works [9, 10], exact solutions of the system of equations (1.9)–(1.11) were obtained for an arbitrary Hubble parameter with a function $f(T,\phi) = -G(\phi)\sqrt{T} - V(\phi)$, where $G = G(\phi)$ is the coupling function of the scalar field and torsion.

Now, we consider the special case

$$f(T,\phi) = -T - V(\phi), \tag{1.12}$$

corresponding to the teleparallel equivalent of general theory of relativity (TEGR), where $V = V(\phi)$ is the potential of the scalar field, the equations of cosmological dynamics (1.9)–(1.11) for $\omega = 1$ reduces to the case of cosmological inflation based on Einstein gravity

$$3H^2 = \frac{1}{2}\dot{\phi}^2 + V(\phi), \tag{1.13}$$

$$-3H^2 - 2\dot{H} = \frac{1}{2}\dot{\phi}^2 - V(\phi), \tag{1.14}$$

$$\ddot{\phi} + 3H\dot{\phi} + V_{,\phi} = 0, \tag{1.15}$$

where $V_{,\phi} = \frac{dV}{d\phi}$ and a dot represents a derivative with respect to the cosmic time $t$.

Also, we note that for the case of inflationary models based on general relativity one has the same dynamical equations [**?** ], for this reason, the methods for constructing generalized solutions of the system of equations (1.13)-(1.15) are the same for the cases of GR and TEGR.

## 2. Generalized exact solutions of cosmological dynamic equations

Since only two equations in system (1.13)-(1.15) are independent, they can be rewritten as follows

$$V(t) = 3H^2 + \dot{H}, \tag{2.1}$$

$$\dot{\phi}^2 = -2\dot{H}. \tag{2.2}$$

In order to get exact solutions for the case of complex dynamics, let us consider a scalar field $\phi = \phi(t)$ and a Hubble parameter $H = H(t)$ as follows

$$\phi(t) = \pm A \ln\left[\frac{E\dot{\sigma}}{(C\sigma(t)+F)^2}\right] \mp ABt + \phi_0, \tag{2.3}$$

$$H(t) = A^2 \ln\left[\frac{u(t)^{K/2}\dot{\sigma}^B}{(C\sigma(t)+F)^{2B}}\right] + \frac{2A^2C\dot{\sigma}}{C\sigma(t)+F} - \frac{A^2B^2}{2}t + \lambda, \tag{2.4}$$

where functions $\sigma = \sigma(t)$ and $u = u(t)$ are related as follows

$$\left(\frac{\ddot{\sigma}}{\dot{\sigma}}\right)^2 + K\frac{\dot{u}}{u} = 0, \sigma \neq const, \tag{2.5}$$

and $A, B, C, E, F, K, \lambda, \phi_0$ are arbitrary parameters.

By direct substitution, one can verify that system (2.3)–(2.5) fully correspond to the cosmological dynamics equation (2.2).

The main feature of the proposed representation of the equations of cosmological dynamics is the specific choice of the generating function $\sigma = \sigma(t)$, which leads to the possibility of constructing an unlimited number of exact solutions.

As the example of prosed approach, we consider the function $\sigma(t)$ in the following form

$$\sigma(t) = \sigma_0 \int \frac{t^p dt}{(t+m)^q} = -\frac{\sigma_0 t^p}{(q-1)(t+m)^{q-1}} + \frac{\sigma_0 p}{q-1}\int \frac{t^{p-1}dt}{(t-m)^{q-1}}, \tag{2.6}$$

where $\sigma_0 = const$ and $\sigma(t)$ may be represented as the series

$$\sigma(t) = \sigma_0 \int \frac{t^p dt}{(t+m)^q} = -\sigma_0 \sum_{k=0}^{p} C_p^k \frac{(-m)^{p-k}}{(q-k-1)(t+m)^{q-k-1}}, \tag{2.7}$$

where $C_p^k = \frac{p!}{k!(p-k)!}$.

The representation (2.7) of $\sigma(t)$ allow us to construct unlimited number of exact cosmological solutions in the explicit form.

By substituting (2.7) into (2.5), we get

$$u(t) = u_0 (t+m)^{-\frac{2pq}{Km}} t^{\frac{2pq}{Km}} \exp\left(\frac{(p^2+q^2)t + p^2 m}{Kt(t+p)}\right), \tag{2.8}$$

where $u_0$ is an arbitrary constant.

Thus, from (2.3)–(2.5) and (2.6)–(2.8) we obtain explicit exact expressions for the scalar field and the Hubble parameter

$$\phi(t) = A\ln\left(\frac{E\sigma_0 t^p}{(t+m)^q\left(C\sigma_0\left(\int \frac{t^p}{(t+m)^q}dt\right)+F\right)^2}\right) - ABt + \phi_0, \tag{2.9}$$

$$H(t) = A^2 \ln\left(\frac{\left(\frac{\sigma_0 t^p}{(t+m)^q}\right)^B \left(u_0 (t+m)^{-\frac{2pq}{Km}} t^{\frac{2pq}{Km}} \exp\left(\frac{(p^2+q^2)t+p^2 m}{Kt(t+m)}\right)\right)^{K/2}}{\left(C\sigma_0\left(\int \frac{t^p}{(t+m)^q}dt\right)+F\right)^{2B}}\right) - \frac{A^2B^2t}{2} + \lambda, \tag{2.10}$$

or, in the other form

$$\phi(t) = A\ln\left(\frac{E\left(\sum\limits_{k=0}^{p} C_p^k (-m)^{p-k}(t+m)^{k-q}\right)}{\left(C\left(-\sum\limits_{k=0}^{p} C_p^k \frac{(-m)^{p-k}}{(q-k-1)(t+m^{q-k-1})}\right)+F\right)^2}\right) - ABt + \phi_0, \tag{2.11}$$

$$H(t) = A^2 \ln\left[\frac{\left(C_1 \prod\limits_{k=0}^{p} exp\left(\frac{k-q}{t+m}\right)\right)^{K/2}\left(\sum\limits_{k=0}^{p} C_p^k (-m)^{p-k}(t+m)^{k-q}\right)^B}{\left(C\left(-\sum\limits_{k=0}^{p} C_p^k \frac{(-m)^{p-k}}{(q-k-1)(t+m^{q-k-1})}\right)+F\right)^{2B}}\right] + \tag{2.12}$$

$$+\frac{2A^2C\left(\sum\limits_{k=0}^{p} C_p^k (-m)^{p-k}(t+m)^{k-q}\right)}{C\left(-\sum\limits_{k=0}^{p} C_p^k \frac{(-m)^{p-k}}{(q-k-1)(t+m^{q-k-1})}\right)+F} - \frac{A^2B^2t}{2} + \lambda,$$

where a sum of a series itself and any summand are the exact solutions of equation (2.2).

Also, from (2.1) and solutions (2.13) we can reconstruct the type of the potential evolution in explicit form. However, due to the fact that the expression for the evolution of the potential is quite cumbersome, the form of function $V = V(t)$ is shown in Fig. ?? for the certain values of the constant parameters of the inflationary model.

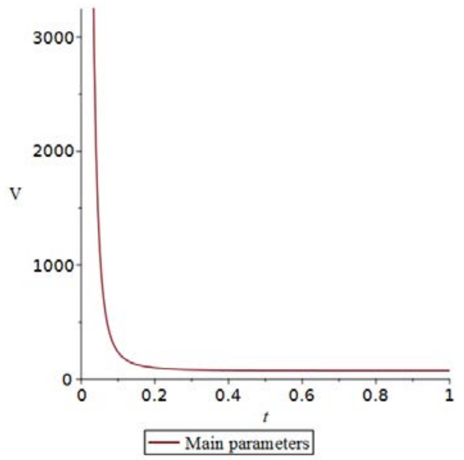


**Рис. 1.** The potential evolution $V(t)$ for parameters $p = 2, q = 3, m = 1, A = 1, B = 0.01, C = 1, K = 1, u_0 = 1, F = 1, E = 11, \phi_0 = 10.6, \lambda = 1$.

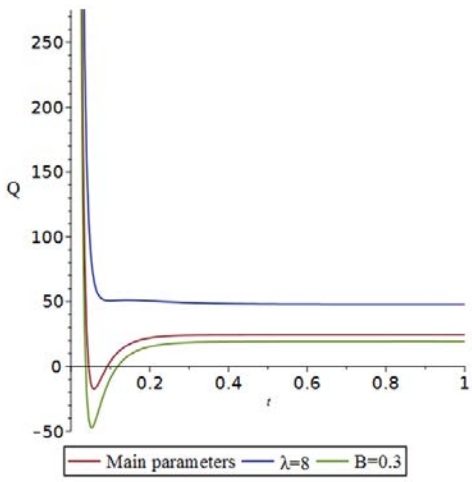


**Рис. 2.** The relative acceleration $Q$ for parameters $p = 2, q = 3, m = 1, A = 1, B = 0.01, C = 1, K = 1, u_0 = 1, F = 1, E = 11, \phi_0 = 10.6, \lambda = 1$.

We will also check the cosmological model basad on the solutions (2.11)–(2.13) with the selected parameters for exit from the inflationary stage and the presence of a stage of the second accelerated expansion of the universe.

For this purpose, we define the relative acceleration of the expansion of the universe as follows

$$Q = \frac{\ddot{a}}{a} = H^2 + \dot{H}, \tag{2.13}$$

where $Q > 0$ corresponds to the accelerated expansion of the universe and $Q < 0$ corresponds to the decelerated expansion of the universe.

From Fig. ?? one can see that the obtained solutions for the selected parameters correspond to both the exit from inflation and the second accelerated expansion of the universe.

We also note that these properties of cosmological models based on solutions (2.11)–(2.13) can be obtained for other values of constant parameters.

## Conclusion

In this paper, we proposed a new method for constructing an unlimited number of exact solutions to the equations of cosmological dynamics for the case of Einstein gravity and the teleparallel equivalent of general relativity.

The specificity of the method is the reduction of dynamic equations to a special form and the choice of a generating function $\sigma = \sigma(t)$, which allows one to obtain an unlimited number of exact solutions.

Topical issues for further development of this approach are the construction of exact solutions with the scalar field potential in explicit form $V = V(\phi)$, the correspondence of the cosmological models obtained by these method to observational constraints on the values of the parameters of cosmological perturbations, and the analysis of approximate solutions following from physically motivated approximations.

## Список литературы/References

1. D. Baumann, L. McAllister, *Inflation and String Theory*, Cambridge Monographs on Mathematical Physics (Cambridge University Press, 2015), https://doi.org/10.1017/CBO9781316105733
2. S. Chervon, I. Fomin, V. Yurov, A. Yurov, *Scalar Field Cosmology*, Series on the Foundations of Natural Science and Technology, Volume 13 (WSP, Singapur, 2019), https://doi.org/10.1142/11405
3. Nojiri S. and Odintsov S. D. Modified non-local-F(R) gravity as the key for the inflation and dark energy. *Phys. Lett. B*, 2008, vol. 659, p. 821.
4. Clifton T., Ferreira P. G., Padilla A. and Skordis C. Modified Gravity and Cosmology. *Phys. Rept.*, 2012, vol. 513, p. 1.
5. Yi-Fu Cai, Capozziello S., Mariafelicia De Laurentis, Saridakis E. f(T) teleparallel gravity and cosmology. *Rep. Prog. Phys.*, 2016, vol. 2, no. 1, p. 106901.
6. Chervon S. V., Fomin I. V. and Beesham A. The method of generating functions in exact scalar field inflationary cosmology. *Eur. Phys. J. C*, 2018, vol. 78, no.4, p. 301.
7. Fomin I. V. Methods for constructing and verifying inflationary models of the early universe. *Space, Time and Fundamental Interactions*, 2022, no. 40, pp. 50–63.
8. Gonzalez-Espinoza M., Otalora G. Generating primordial fluctuations from modified teleparallel gravity with local Lorentz-symmetry breaking. *Phys. Rev. B*, 2020, vol. 809, p. 135696.
9. Dentsel E. S., Fomin I. V. Generalized exact solutions in cosmological models with non-minimal coupling of scalar field and torsion. *Space, Time and Fundamental Interactions*, 2022, no. 40, pp. 110–118.
10. Dentsel E. S., Fomin I. V. Exact solutions in cosmological models with non-minimal coupling of scalar field and torsion. *Space, Time and Fundamental Interactions*, 2023, no. 1, pp. 46–50.

### Авторы

**Фомин Игорь Владимирович**, д. ф.-м. н., профессор кафедры физики, Московский государственный технический университет имени Н.Э. Баумана, 2-я Бауманская ул., д. 5, г. Москва, 105005, Россия.
E-mail: ingvor@inbox.ru

**Денцель Евгений Станиславович**, ассистент кафедры «Физика», МГТУ им. Н.Э. Баумана, ул. 2-я Бауманская, д. 5, стр. 1, г. Москва, 105005, Россия.
E-mail: edentsel@yandex.ru

**Просьба ссылаться на эту статью следующим образом:**
Фомин И. В., Денцель Е. С. Инфляционные модели на основе обобщенных точных космологических решений. *Пространство, время и фундаментальные взаимодействия.* 2023. № 3-4. С. 93–98.

### Authors

**Fomin Igor Vladimirovich**, Doctor of Physical and Mathematical Sciences, Professor of Physics Department of Bauman Moscow State Technical University, 2-nd Baumanskaya street, 5, Moscow, 105005, Russia.
E-mail: ingvor@inbox.ru

**Dentsel Evgenii Stanislavovich**, assistant of Physics department, Bauman Moscow State Technical University, 2-nd Baumanskaya st., 5/1, Moscow, 105005, Russia.
E-mail: edentsel@yandex.ru

**Please cite this article in English as:**
Fomin I. V., Dentsel E. S. Inflationary models based on generalized exact cosmological solutions. *Space, Time and Fundamental Interactions*, 2023, no. 3-4, pp. 93–98.

УДК 530.121



## АНАЛИЗ СВЯЗАННЫХ ГРАВИТАЦИОННЫХ И ЭЛЕКТРОМАГНИТНЫХ ВОЛН*

Гладышев В. О.[a,1], Кауц В. Л.[a,2], Каютенко А. В.[a,3], Морозов А. Н.[a,4], Николаев П. П.[a,5], Фомин И. В.[a,6], Шарандин Е. А.[a,7]

[a] МГТУ им. Н.Э. Баумана, г. Москва, 105005, Россия.

Рассматривается метод исследования связанных с электромагнитным полем гравитационных волн в резонаторах Фабри-Перо посредством детектирования свободных поперечных гравитационных волн в окружающем пространстве. Представлены внутренние решения уравнений гравитационного поля, описывающие связанные гравитационные волны и метод расчета характеристик свободных гравитационных волн. Также представлены оценки параметров источника и детектора для реализации экспериментов такого типа.

*Ключевые слова*: гравитационные волны, электромагнитные волны, резонатор Фабри-Перо.

## THE ANALYSIS OF COUPLED GRAVITATIONAL AND ELECTROMAGNETIC WAVES

Gladyshev V. O.[a,1], Kauts V. L.[a,2], Kayutenko A. V.[a,3], Morozov A. N.[a,4], Nikolaev P. P.[a,5], Fomin I. V.[a,6], Sharandin E. A.[a,7]

[a] Bauman Moscow State Technical University, Moscow, 105005, Russia.

A method for studying gravitational waves coupled with an electromagnetic field in the Fabry-Perot resonators by detecting free transverse gravitational waves in the surrounding space is considered. Internal solutions of the gravitational field equations describing bound gravitational waves and a method for calculating the characteristics of free gravitational waves are presented. Estimates of the source and detector parameters for implementing experiments of this type were also presented.

*Keywords*: gravitational waves, electromagnetic waves, the Fabry-Perot resonator.
PACS: 04.30.-w
DOI: 10.17238/issn2226-8812.2023.3-4.99-107

### Introduction

Currently, various astrophysical processes and cosmological perturbations in the early universe are considered as sources of gravitational wave radiation [1]. Gravitational waves resulting from the merger of black holes and neutron stars were discovered in the LIGO and Virgo experiments [2, 3] based on the interference method proposed in [4]. Relic gravitational waves, which is one of the types of cosmological perturbations at the inflationary stage of the evolution of the early universe, are described both on the basis of Einstein gravity [5] and its modifications [6, 9] have not yet been discovered due to their small amplitude, which is less than the sensitivity of modern detectors [8].

*Работа Фомина И.В. выполнена при поддержке гранта РНФ № 22–22–00248.
[1]E-mail: vgladyshev@mail.ru, gladyshev@bmstu.ru
[2]E-mail: kauts@bmstu.ru
[3]E-mail: akayutenko@bmstu.ru
[4]E-mail: amor59@mail.ru, amor@bmstu.ru
[5]E-mail: ppn@bmstu.ru
[6]E-mail: ingvor@inbox.ru
[7]E-mail: shar@bmstu.ru

Various laboratory sources of gravitational waves are also considered, based both on the interaction of electromagnetic radiation and matter [9, 10], and considering the electromagnetic field as a source of gravitational waves [11, 12].

Thus, gravitational-wave fluctuations of the space-time metric are induced by both matter perturbations and an alternating electromagnetic fields $\delta T_{\mu\nu} = \delta T^{(M)}_{\mu\nu} + \delta T^{(EM)}_{\mu\nu}$, and the predominance of the first or second factor is associated with the specifics of the process of generating gravitational waves.

According to estimates given in [9, 10], the interaction of a short pulse of powerful laser radiation and matter $\delta T^{(M)}_{\mu\nu} \gg \delta T^{(EM)}_{\mu\nu}$ makes it possible to generate high-frequency gravitational waves with an amplitude on the order $h_0 \sim 10^{-40}$ forthe realistic parameters of this experiment, which is much less than the sensitivity limit of modern detectors $h_0 \sim 10^{-21} - 10^{-22}$ [2, 3].

In [13, 14, 15, 16] exact wave solutions of the equations of the gravitational field in linearized General Relativity were obtained for the case of gravitational waves induced by electromagnetic waves in vacuum, dielectric media and an external magnetic field. In these works, a Fabry-Perot resonator filled with electromagnetic radiation was considered as a source of gravitational waves, and the characteristics of external transverse gravitational waves were calculated based on the characteristics of gravitational waves coupled with the electromagnetic field inside the resonator.

Also, the analysis of the processes of generating gravitational wave radiation through electromagnetic fields of a special configuration in a vacuum, dielectric media and an external magnetic field, carried out in [15, 16], implies the possibility of obtaining gravitational waves with controlled characteristics in laboratory conditions.

The coupled states of gravitational and electromagnetic waves were considered as the basis for this analysis. These states were considered earlier both: within the framework of the analysis of gravitational and electromagnetic waves in the vicinity of astrophysical objects [17], and within the framework of the problem of generating gravitational waves in terrestrial conditions [18].

In this work, we consider the possibility of detecting free gravitational waves induced by a system of coupled gravitational-electromagnetic fields when separating a gravitational wave from such a system. Direct detection of free gravitational waves in the vicinity of a region filled with coupled gravitational-electromagnetic fields makes it possible to determine the characteristics of gravitational waves associated with the electromagnetic field.

## 1. Coupled gravitational and electromagnetic waves

Weak gravitational waves are considered based on the linearized Einstein gravity theory as small perturbations of Minkowski space-time [1]

$$g_{\mu\nu} = \eta_{\mu\nu} + h_{\mu\nu}, \quad |h_{\mu\nu}| \ll 1, \tag{1.1}$$

where $\eta_{\mu\nu}$ is the metric tensor of Minkowski space-time with nonzero components $\eta_{00} = 1$, $\eta_{11} = \eta_{22} = \eta_{33} = -1$ and $\mu, \nu = 0, 1, 2, 3$.

In this case, the Einstein equations

$$G_{\mu\nu} \equiv R_{\mu\nu} - g_{\mu\nu} R = \kappa T_{\mu\nu}, \tag{1.2}$$

taking into account the harmonic gauge, can be written as follows [1]

$$\Box h_{\mu\nu} = \Delta h_{\mu\nu} - \frac{1}{c^2}\frac{\partial^2 h_{\mu\nu}}{\partial t^2} = \left(T_{\mu\nu} - \frac{1}{2}\eta_{\mu\nu} T\right), \tag{1.3}$$

where $G$ is the gravitational constant, $c$ is the velocity of light in vacuum, $\kappa = \frac{16\pi G}{c^4}$ is the Einstein constant and $T_{\mu\nu}$ is the energy-momentum tensor.

For gravitational waves propagating in direction $x^1 = x$, non-zero components of tensor $h_{\mu\nu}$ determine three possible types [19]:

- $h_{22}$, $h_{23}$, $h_{33}$ – transverse–transverse ($TT$),
- $h_{12}$, $h_{13}$, $h_{20}$, $h_{30}$ – longitudinal–transverse ($LT$),
- $h_{11}$, $h_{10}$, $h_{00}$ – longitudinal–longitudinal ($LL$).

However, in empty space ($T_{\mu\nu} = 0$), $LT$ and $LL$–waves do not lead to a deviation from the flat Minkowski space-time and can be eliminated by additional coordinate transformations [19]. Also, one has three possible polarizations for $TT$-waves, namely $h_{23}$, $h_{22} - h_{33}$ and $h_{22} + h_{33}$. However, equations (1.3) in empty space lead to condition $h_{22} + h_{33} = 0$, and, thus, transverse-traceless gravitational waves with only two polarizations $h_{23}$ and $h_{22} - h_{33}$ can propagate, which corresponds to so called transverse-traceless gauge [1].

Nevertheless, one can consider the possibility of the existence of coupled states of electromagnetic and gravitational waves for which $LT$ and $LL$–types of the metric perturbations are non-zero and $h_{22} + h_{33} \neq 0$ on the basis of Einstein-Maxwell equations written in a general form.

The gravitational field equations (1.2) in the gauge-invariant form can be written as follow [20]

$$\nabla^2\Theta = -\kappa\rho, \tag{1.4}$$

$$\nabla^2\Phi = \frac{\kappa}{2}\left(\rho + 3P - 3\dot{S}\right), \tag{1.5}$$

$$\nabla^2\Xi_i = -2\kappa S_i, \tag{1.6}$$

$$\Box h_{ij}^{\mathrm{TT}} = -2\kappa\sigma_{ij}, \tag{1.7}$$

where $h_{ij}^{\mathrm{TT}}$ corresponds to the $TT$-waves, gauge-invariant potentials $\Theta$, $\Phi$, $\Xi_i i$ define the remaining possible modes $h_{00}$, $h_{0j}$ and $\rho$, $P$, $S$, $S_i$, $\sigma_{ij}$ are defined by the components of the energy-momentum tensor $T_{\mu\nu}$ of the source of gravitational field.

For the case of empty space these equations are reduced to the following form

$$\nabla^2\Theta^{\mathrm{vac}} = 0, \tag{1.8}$$

$$\nabla^2\Phi^{\mathrm{vac}} = 0, \tag{1.9}$$

$$\nabla^2\Xi_i^{\mathrm{vac}} = 0, \tag{1.10}$$

$$\Box h_{ij}^{\mathrm{TT,vac}} = 0. \tag{1.11}$$

As one can see, in empty space, only equation (1.11) has wave solutions corresponding to the free $TT$-waves.

Nevertheless, for a specific source, under conditions

$$\rho \sim \frac{\partial^2}{\partial t^2}\Theta, \tag{1.12}$$

$$\left(\rho + 3P - 3\dot{S}\right) \sim \frac{\partial^2}{\partial t^2}\Phi, \tag{1.13}$$

$$S_i \sim \frac{\partial^2}{\partial t^2}\Xi_i, \tag{1.14}$$

expressions (1.4)–(1.6) correspond to the Poisson type wave equations.

Solutions of these equations describe gravitational waves coupled with this specific source, which are not a product of the choice of coordinate system.

Electromagnetic waves in a Fabry-Perot resonator were considered as such a specific source in works [14, 15, 16]. Based on solutions to the gravitational field equations in these works, the characteristics of coupled gravitational waves inside the resonator were obtained. Also, in [14, 15, 16] a procedure for reconstructing characteristics of free gravitational $TT$-waves in the empty space was defined, that we will consider in more detail.

### 2. Decoupling of gravitational and electromagnetic waves

Let us consider coupled gravitational waves induced by a system of the flat electromagnetic waves (or one wave) in a Fabry-Perot resonator along a some direction $x$ as follows

$$h_{\mu\nu} = A_{\mu\nu}\left(U_s, E_k, \omega_k, L, x\right)\left\{\alpha\cos\left[\omega_g\left(t - \frac{x}{c}\right) + \varphi_{\mu\nu}\right] + \beta\cos\left[\omega_g\left(t + \frac{x}{c}\right) + \varphi_{\mu\nu}\right]\right\}, \quad (2.1)$$

where $A_{\mu\nu} = A_{\mu\nu}\left(E_k, \omega, L, x\right)$ are the amplitudes of the coupled gravitational waves, $U_s$ $(s = 1, 2, 3, ...)$ are the characteristics of additional constant or variable fields (for example, magnetic fields or the medium with some dielectric and magnetic properties) inside resonator, $E_k$ is the electric field strength and $\omega_k$ is the frequency for each electromagnetic wave $(k = 1, 2, 3, ...)$, $L$ is the Fabry-Perot resonator length, the constants parameters $\alpha$ and $\beta$ depend on the configuration of the resulting electromagnetic field, $\omega_g = \omega_g(\omega_k, U_s)$ is the frequency of the coupled gravitational waves and $\varphi_{\mu\nu}$ are a some additional phases.

Examples of such solutions of the gravitational field equations were considered in [14, 15, 16] for the case of a single electromagnetic wave [14], a system of electromagnetic waves and in the presence of a constant magnetic field and dielectric media as well [15, 16].

When electromagnetic part of the coupled gravitational-electromagnetic waves are reflected from the walls of the resonator (or absorbed by the walls of the resonator), gravitational and electromagnetic waves are decoupled, since gravitational waves interact extremely weakly with matter [1].

In empty space $T_{\mu\nu} = 0$, solutions of equations (1.3) can be written in the form of plane gravitational $TT$-waves [1]

$$h_{22} = -h_{33} = h_0\cos\left[\omega_g\left(t \mp \frac{x}{c}\right)\right], \quad (2.2)$$

where $h_0$ and $\omega_g$ are the amplitude and frequency of gravitational waves in empty space, the upper sign corresponds to the case of wave propagation in the positive direction, for the lower sign wave propagates in the opposite direction.

Thus, internal solutions (2.1) for a given energy-momentum tensor $T_{\mu\nu}$ correspond to the gravitational field coupled with the source, and solution (2.2) in the form of plane transverse gravitational waves is external one. Consequently, the comparison of the characteristics of coupled and free gravitational waves presupposes the choice of a certain type of sources of the gravitational field.

The connection between internal and external solutions is determined from the condition of continuity of the energy density flux of gravitational waves [14, 15, 16]

$$ct^{01} = -\frac{c}{4\kappa}\left(\partial_0 h_{ij}\partial_1 h^{ij}\right), \qquad i, j = 1, 2, 3, \quad (2.3)$$

at the boundary between the region filled with the source and empty space $\left(ct^{01}\right)_{in} = \left(ct^{01}\right)_{out}$.

When considering the process of generating gravitational waves by means of Fabry-Perot resonators filled with electromagnetic waves, the method of theoretical analysis of this process can be represented as follows:

1. Obtaining internal gravitational-wave solutions of equations (2.1) for a given source;
2. Calculation of the energy density flux $ct^{01}$ of gravitational waves based on the obtained solutions;
3. Reconstruction of the characteristics of free gravitational waves in empty space based on the solutions (2.1) and (2.2) with condition $\left(ct^{01}\right)_{in} = \left(ct^{01}\right)_{out}$;
4. Assessment of the possibility of detecting external gravitational waves.

Thus, the analysis of gravitational waves coupled with the electromagnetic field is of interest both from the point of view of their difference from free gravitational waves in empty space, and for assessing the possibility of creating emitters of fundamentally observed gravitational waves.

In works [14, 15, 16], coupled gravitational waves induced by a system of standing electromagnetic waves in a Fabry-Perot resonator were considered

$$h_{00} = h_{11} = -\frac{4GE_1E_2}{c^3\tilde{\omega}}\left(\frac{L}{2}+x\right)\sin\left(\tilde{\omega}\left(t-\frac{x}{c}\right)\right) - \frac{4GE_1E_2}{c^3\tilde{\omega}}\left(\frac{L}{2}-x\right)\sin\left(\tilde{\omega}\left(t+\frac{x}{c}\right)\right), \quad (2.4)$$

$$h_{01} = h_{10} = \frac{4GE_1E_2}{c^3\tilde{\omega}}\left(\frac{L}{2}+x\right)\sin\left(\tilde{\omega}\left(t-\frac{x}{c}\right)\right) - \frac{4GE_1E_2}{c^3\tilde{\omega}}\left(\frac{L}{2}-x\right)\sin\left(\tilde{\omega}\left(t+\frac{x}{c}\right)\right), \quad (2.5)$$

$$h_{22} = -\frac{4\alpha GE_1E_2}{c^2\tilde{\omega}^2}\left[\cos\left(\tilde{\omega}\left(t-\frac{x}{c}\right)\right)+\cos\left(\tilde{\omega}\left(t+\frac{x}{c}\right)\right)\right], \quad (2.6)$$

$$h_{33} = -\frac{4\beta GE_1E_2}{c^2\tilde{\omega}^2}\left[\cos\left(\tilde{\omega}\left(t-\frac{x}{c}\right)\right)+\cos\left(\tilde{\omega}\left(t+\frac{x}{c}\right)\right)\right], \quad (2.7)$$

and corresponding transverse gravitational waves in the surrounding space were defined as follows

$$h_{22} = -h_{33} = \pm\frac{2GE_1E_2}{c^2\tilde{\omega}^2}\cos\left(\tilde{\omega}\left(t-\frac{x}{c}\right)\right), \quad (2.8)$$

where $\tilde{\omega} = |\omega_2 - \omega_1| = \omega_g$ is the difference frequency of electromagnetic waves.

Thus, the space-time metric in the vicinity of an electromagnetic resonator filled with two standing electromagnetic waves can be defined as

$$ds^2 = c^2dt^2 - dx^2 - \left[1 - h_0\cos\left(\tilde{\omega}\left(t\mp\frac{x}{c}\right)\right)\right]dy^2 - \left[1 + h_0\cos\left(\tilde{\omega}\left(t\mp\frac{x}{c}\right)\right)\right]dz^2, \quad (2.9)$$

i.e. it contains only components of one type of polarization

$$h_+(x,t) = h_0\cos\left(\tilde{\omega}\left(t\mp\frac{x}{c}\right)\right). \quad (2.10)$$

Within the framework of the problem of generating and detecting gravitational waves, the controlled parameters of the source are the electric field strengths $E_1 = E_2 = E_0$ in the resonator and their difference frequency $\tilde{\omega}$, and the controlled parameter of the detector is the amplitude of detectable gravitational waves $h_0$, which is restricted by detector sensitivity.

After substitution of expression for electric field strengths

$$E_0^2 = \frac{8\pi}{c}I_L \times Q = \frac{8\pi}{c}\left(\frac{P_S}{S}\right)\times Q, \quad (2.11)$$

and $\omega_g = 2\pi f_{gw}$ into (2.8) we obtain the amplitude of gravitational waves

$$h_0 = \left(\frac{4G}{\pi c^3}\right)\times\left(\frac{I_L}{f_{gw}^2}\right)\times Q, \quad (2.12)$$

where $Q$ is the quality factor of the resonator, $I_L$ is the laser radiation intensity, $P_L$ is the laser radiation power and $S$ is the cross-sectional area of the beam.

For the quality factor of the electromagnetic resonator $Q \simeq 10^6$, the continuous laser radiation power $P_L \simeq 10^3\ W$ and the cross-sectional area of the beam $S \simeq 10^{-4}\ m$ we obtain following amplitude of decoupled gravitational waves in empty space

$$h_0 \simeq 3\times 10^{-23}\times\left(\frac{\mathrm{Hz}}{f_{gw}}\right)^2. \quad (2.13)$$

Thus, indirect analysis of the states of coupled gravitational and electromagnetic waves in the Fabri-Perot resonator can be performed by detecting decoupled gravitational waves in the surrounding space.

As one can see, the frequency of detected gravitational waves or the difference frequency of standing electromagnetic waves in the resonator for the successful implementation of such an experiment must be determined by the sensitivity of the detector.

## 3. The detection of decoupled gravitational waves

As a possible method for detecting decoupled gravitational waves we consider their influence on an external magnetic field.

The equations of electrodynamics for arbitrary space-time geometry can be written as follows

$$\partial_\mu F^{\mu\nu} + \frac{1}{\sqrt{-g}}\partial_\mu\left(\sqrt{-g}\right)F^{\mu\nu} = \mu_0 j^\nu, \tag{3.1}$$

$$\frac{\partial F_{\beta\gamma}}{\partial x^\alpha} + \frac{\partial F_{\gamma\alpha}}{\partial x^\beta} + \frac{\partial F_{\alpha\beta}}{\partial x^\gamma} = 0, \tag{3.2}$$

where components of the tensor of electromagnetic field is

$$F_{0k} = \frac{1}{c}\partial_t A_k - \partial_k A_0 \equiv \frac{E_k}{c}, \tag{3.3}$$

$$F_{jk} = \partial_j A_k - \partial_k A_j \equiv -\epsilon_{ijk}B^i. \tag{3.4}$$

Considering the magnetic field $\vec{B} = (0, B^y, B^z)$ for the case of the unperturbed Minkowski space-time, in the gravitational wave field for metric (2.9) its components are determined from equations (3.1)–(3.2) as follows [21]

$$\tilde{B}^y = B^y\left(\frac{1+h_+}{\sqrt{1-h_+^2}}\right), \tag{3.5}$$

$$\tilde{B}^z = B^z\left(\frac{1+h_+}{\sqrt{1-h_+^2}}\right). \tag{3.6}$$

Thus, the relative change in the magnetic field

$$\frac{\delta B}{B} = \frac{\tilde{B} - B}{B} = -1 + \frac{1+h_+}{1-h_+} \simeq 2h_+ \sim h_0. \tag{3.7}$$

Taking into account the sensitivity of SQUID magnetometers $(\delta B)_{\min} \sim 10^{-18}\ T$ [22, 23] and the magnetic field $B \simeq 10\ T$, from (2.13) and (3.7) we can estimate the frequency the detectable decoupled gravitational waves as follows

$$f_g = \tilde{f} \leq 2 \times 10^{-2}\ Hz. \tag{3.8}$$

Thus, the main problem in implementing this approach is the formation of the system of standing electromagnetic waves in the resonator at the difference frequency $\tilde{f} \leq 2 \times 10^{-2}\ Hz$ and generating sufficiently strong magnetic fields.

Similar estimates can be made for other methods of detecting gravitational waves [24]. However, increasing the power of laser radiation and the sensitivity of gravitational wave detectors make it possible in the future to increase the difference frequency $\tilde{f} = f_g$ and consider such experiments as feasible ones.

## Conclusion

In this work, we considered coupled gravitational and electromagnetic waves in the Fabri-Perot resonators. It has been shown that coupled gravitational waves can appear not as gauge artifacts generated by a special choice of coordinate system, but as actual physical effects.

To study such gravitational-electromagnetic waves, a method for detecting decoupled gravitational waves in the surrounding space was proposed. A system of standing electromagnetic waves and associated gravitational waves was considered as a source of decoupled gravitational waves. For realistic parameters of the experiment on the generation and observation of such decoupled gravitational waves, restrictions

$\tilde{f} \leq 2 \times 10^{-2}\ Hz$ were obtained on the difference frequency of standing electromagnetic waves, which leads to the significant difficulties in implementation.

Nevertheless, this result can be interpreted as technical, rather than fundamental, problems in implementing such experiment based on the proposed approach, which can be solved both by using opportunities to increase the characteristics of the source and improving the sensitivity of gravitational wave detectors.

Also, as a perspective for studying the considered states of coupled gravitational and electromagnetic waves, we can note the analysis of their propagation in the expanding universe and their possible influence on the stochastic gravitational waves background at the present era.

**Список литературы/References**

1. Maggiore M. *Gravitational Waves: Volume 1: Theory and Experiments.* Oxford: Oxford University Press, 2007, 576 p.
2. Abbott B. P. et al. [LIGO Scientific and Virgo Collaborations]. GW151226: Observation of Gravitational Waves from a 22-Solar-Mass Binary Black Hole Coalescence, *Phys. Rev. Lett.*, 2016, vol. 116, p. 241103.
3. Abbott B. P. et al. [LIGO Scientific and Virgo and Fermi-GBM and INTEGRAL Collaborations]. Gravitational Waves and Gamma-rays from a Binary Neutron Star Merger: GW170817 and GRB 170817A, *Astrophys. J. Lett.*, 2017, vol. 848, L13.
4. Gertsenshtein M. E. and Pustovoit V.I. On the Detection of Low Frequency Gravitational Waves, *Sov. Phys. JETP*, 1962, vol. 16, p. 433.
5. S. Chervon, I. Fomin, V. Yurov, A. Yurov, *Scalar Field Cosmology*, Series on the Foundations of Natural Science and Technology, Volume 13 (WSP, Singapur, 2019), https://doi.org/10.1142/11405
6. Manucharyan G. D., Fomin I. V. Corrections to standard inflationary models induced by Gauss - Bonnet scalar, *Space, Time and Fundamental Interactions*, 2022, no. 40, pp. 119–131
7. Chervon S. V., Fomin I. V. Reconstruction of Scalar-Torsion Gravity Theories from the Physical Potential of a Scalar Field, *Symmetry*, 2023, vol. 15, p. 291.
8. Morozov A. N., Golyak I. S., Fomin I. V., Chervon S. V. Detectors of high-frequency gravitational waves based on the gravitational-optical resonance, *Space, Time and Fundamental Interactions*, 2022, no. 41, pp. 49–61.
9. Kadlecová H., Klimo O., Weber S. and Korn G. Gravitational wave generation by interaction of high power lasers with matter using shock waves, *Eur. Phys. J. D*, 2017, vol. 71, p. 89.
10. Fomin I. V.,Gladyshev V. O., Gorelik V. S.,Kauts V. L., Kaytenko A. V. and Sharandin E. A. Laboratory sources of gravitational waves, *J. Phys. Conf. Ser.*, 2020, vol. 1705, p. 012004. doi:10.1088/1742-6596/1705/1/012004
11. Grishchuk L. P. and Sazhin M. V. Emission of gravitational waves by an electromagnetic cavity, *Zh. Eksp. Teor. Fiz.*, 1973, vol. 65, pp. 441-454.
12. Kolosnitsyn N. I. and Rudenko V. N. Gravitational Hertz experiment with electromagnetic radiation in a strong magnetic field, *Phys. Scripta*, 2015, vol. 90, p. 074059.
13. Morozov A. N. and Pustovoit V. I. Generation and registration of coupled high-frequency gravitational waves, *Herald of the Bauman Moscow State Technical University, Series Natural Sciences*, 2020, vol. 1, p. 46.
14. Morozov A. N., Pustovoit V. I., Fomin I. V. On the gravitational waves coupled with electromagnetic waves. *Space, Time and Fundamental Interactions*, 2020, no. 2, pp. 53–63.
15. Morozov A. N., Pustovoit V. I., Fomin I. V. Bound gravitational waves in a dielectric medium and a constant magnetic field, *Eur. Phys. J. Plus*, 2020, vol. 135, p. 950.
16. Morozov A. N., Pustovoit V. I., Fomin I. V. Generation of Gravitational Waves by a Standing

Electromagnetic Wave, *Grav. Cosmol.*, 2021, vol. 27, pp. 24-29.

17. Fabbri R. Electromagnetic and Gravitational Waves in the Background of a Reissner-Nordstrom Black Hole, *Nuovo Cim. B*, 1977, vol. 40, pp. 311-329.
18. Morozov A. N., Fomin I. V., Gladyshev V.O., et al. Method for generating gravitational waves by means of a standing electromagnetic wave system, *Herald of the Bauman Moscow State Technical University, Series Natural Sciences*, 2020, no. 6 (105), pp. 90-105.
19. Eddington A. S. The propagation of gravitational waves, *Proc. Roy. Soc. Lond. A.* 1922, vol. 102, p. 268.
20. Flanagan E. E. and Hughes S. A. The Basics of gravitational wave theory, *New J. Phys.*, 2005. vol. 7, p. 204.
21. Cabral F. and Lobo F. S. N. Gravitational waves and electrodynamics: New perspectives, *Eur. Phys. J. C.* 2017, vol. 77, p. 237.
22. Clarke J. SQUIDs: then and now, *Int. J. Mod. Phys. B*, 2010, vol. 24, pp. 3999-4038.
23. Storm J. H., Hömmen P., Drung D. and Körber R. An ultra-sensitive and wideband magnetometer based on a superconducting quantum interference device, *Appl. Phys. Lett.*, 2017, vol. 110, p. 072603.
24. Aggarwal N., Aguiar O. D., Bauswein A. *et al.* Challenges and opportunities of gravitational-wave searches at MHz to GHz frequencies, *Living Rev. Rel.*, 2021, vol. 24, p. 4.

**Авторы**

**Гладышев Владимир Олегович**, д. ф.-м. н., декан факультета «Фундаментальные науки», профессор кафедры физики, Московский государственный технический университет имени Н.Э. Баумана, 2-я Бауманская ул., д. 5, г. Москва, 105005, Россия.
E-mail: vgladyshev@mail.ru, gladyshev@bmstu.ru

**Кауц Владимир Леонидович**, к. ф.-м. н., доцент кафедры физики, Московский государственный технический университет имени Н.Э. Баумана, 2-я Бауманская ул., д. 5, г. Москва, 105005, Россия.
E-mail: kauts@bmstu.ru

**Каютенко Александр Викторович**, начальник ОТЭ НУК «Фундаментальные науки» , МГТУ им. Н.Э. Баумана, ул. 2-я Бауманская, д. 5, стр. 1, г. Москва, 105005, Россия.
E-mail: akayutenko@bmstu.ru

**Морозов Андрей Николаевич**, профессор, д. ф.-м. н., член-корреспондент Российской Академии Наук, заведующий кафедры физики, Московский государственный технический университет имени Н.Э. Баумана, 2-я Бауманская ул., д. 5, г. Москва, 105005, Россия.
E-mail: amor59@mail.ru, amor@bmstu.ru

**Николаев Павел Петрович**, к. ф.-м. н., доцент кафедры физики, Московский государственный технический университет имени Н.Э. Баумана, 2-я Бауманская ул., д. 5, г. Москва, 105005, Россия.
E-mail: ppn@bmstu.ru

**Фомин Игорь Владимирович**, д. ф.-м. н., профессор кафедры физики, Московский государственный технический университет имени Н.Э. Баумана, 2-я Бауманская ул., д. 5, г. Москва, 105005, Россия.
E-mail: ingvor@inbox.ru

**Шарандин Евгений Анатольевич**, к. ф.-м. н., доцент кафедры физики, Московский государственный технический университет имени Н.Э. Баумана, 2-я Бауманская ул., д. 5, г. Москва, 105005, Россия.
E-mail: shar@bmstu.ru

**Просьба ссылаться на эту статью следующим образом:**
Гладышев В. О., Кауц В. Л., Каютенко А. В., Морозов А. Н., Николаев П. П., Фомин И. В., Шаран-

дин Е. А. Анализ связанных гравитационных и электромагнитных волн. *Пространство, время и фундаментальные взаимодействия.* 2023. № 3-4. С. 99–107. **Authors**

**Gladyshev Vladimir Olegovich**, Doctor of Physical and Mathematical Sciences, Head of the Faculty of Fundamental Sciences, Professor of Physics Department of Bauman Moscow State Technical University, 2-nd Baumanskaya street, 5, Moscow, 105005, Russia.
E-mail: vgladyshev@mail.ru, gladyshev@bmstu.ru

**Kauts Vladimir Leonidovich**, Candidate of Physical and Mathematical Sciences, Associate Professor of Physics Department of Bauman Moscow State Technical University, 2-nd Baumanskaya street, 5, Moscow, 105005, Russia.
E-mail: kauts@bmstu.ru

**Kayutenko Alexander Victirovich**, Head of OTE Scientific Educational Complex «Fundamental Sciences» , Bauman Moscow State Technical University, 2-nd Baumanskaya st., 5/1, Moscow, 105005, Russia.
E-mail: akayutenko@bmstu.ru

**Morozov Andrey Nikolaevich**, Professor, Doctor of Physical and Mathematical Sciences, Corresponding Member of the Russian Academy of Sciences, Head of Physics Department of Bauman Moscow State Technical University, 2-nd Baumanskaya street, 5, Moscow, 105005, Russia.
E-mail: amor59@mail.ru, amor@bmstu.ru

**Nikolaev Pavel Petrovich**, Candidate of Physical and Mathematical Sciences, Associate Professor of Physics Department of Bauman Moscow State Technical University, 2-nd Baumanskaya street, 5, Moscow, 105005, Russia.
E-mail: ppn@bmstu.ru

**Fomin Igor Vladimirovich**, Doctor of Physical and Mathematical Sciences, Professor of Physics Department of Bauman Moscow State Technical University, 2-nd Baumanskaya street, 5, Moscow, 105005, Russia.
E-mail: ingvor@inbox.ru

**Sharandin Eugenyi Anatolievich**, Candidate of Physical and Mathematical Sciences, Associate Professor of Physics Department of Bauman Moscow State Technical University, 2-nd Baumanskaya street, 5, Moscow, 105005, Russia.
E-mail: shar@bmstu.ru

**Please cite this article in English as:**
Gladyshev V. O., Kauts V. L., Kayutenko A. V., Morozov A. N., Nikolaev P. P., Fomin I. V., Sharandin E. A. The analysis of coupled gravitational and electromagnetic waves. *Space, Time and Fundamental Interactions*, 2023, no. 3-4, pp. 99–107.

УДК 530.12



## ИСПОЛЬЗОВАНИЕ РЕЛИКТОВОГО ИЗЛУЧЕНИЯ ДЛЯ ПОСТРОЕНИЯ НОВОЙ СИСТЕМЫ НАВИГАЦИИ

Гордин М. В.[a,1], Базлев Д. А.[a,2], Гладышев В. О.[a,3], Кауц В. Л.[a,4], Каютенко А. В.[a,5], Николаев П. П.[a,6], Фомин И. В.[a,7], Шарандин Е. А.[a,8]

[a] МГТУ им. Н.Э. Баумана, г. Москва, 105005, Россия.

Рассматривается метод ориентации и навигации космической техники на основе кинетической дипольной компоненты анизотропии космического микроволнового фона. Приводится анализ и оценки локальной анизотропии пространства-времени. Производится оценка точности предложенного метода навигации.

*Ключевые слова*: Реликтовое излучение, системы навигации, космический микроволновой фон.

## USING RELIC RADIATION TO CONSTRUCT NEW NAVIGATION SYSTEM

Gordin M. V.[a,1], Petrov P. P.[a,2], Petrov P. P.[a,3], Kauts V. L.[a,4], Kayutenko A. V.[a,5], Nikolaev P. P.[a,6], Fomin I. V.[a,7], Sharandin E. A.[a,8]

[a] Bauman Moscow State Technical University, Moscow, 105005, Russia.

The method of orientation and navigation of space technology based on the kinetic dipole component of the anisotropy of the space microwave background is considered. The analysis and estimations of local space-time anisotropy are given. The accuracy of the proposed navigation method is evaluated..

*Keywords*: Relic radiation, navigation systems, cosmic microwave background.

PACS: 04.20.-q

DOI: 10.17238/issn2226-8812.2023.3-4.108-116

### Введение

Совершенствование и создание новых систем ориентации и навигации космической техники предполагает увеличение сроков активного существования ЛА, снижение массогабаритных характеристик и энергопотребления, наращивание числа решаемых функциональных задач.

За последние десятилетия в РФ и за рубежом в теоретической физике получен ряд новых фундаментальных результатов. В их числе открытие анизотропии реликтового микроволнового излучения [1, 2]. Спектр реликтового излучения соответствует спектру излучения абсолютно черного тела с температурой 2,725 К [3]. Его максимум приходится на частоту 160,2 ГГц, что соответствует длине волны 1,9 мм. Распределение температуры на небесной сфере постоянно во времени и представляет собой стабильное навигационное поле, которое можно использовать при решении навигационных задач.

Подобно существующим звездным датчикам, использующим в качестве эталона карту звездного неба, карта реликтового излучения могла бы стать эталоном на устройствах автономной

[1]E-mail: gordinmv@bmstu.ru
[2]E-mail: email2@inbox.ru
[3]E-mail: email2@inbox.ru
[4]E-mail: kauts@bmstu.ru
[5]E-mail: akayutenko@bmstu.ru
[6]E-mail: ppn@bmstu.ru
[7]E-mail: ingvor@inbox.ru
[8]E-mail: shar@bmstu.ru

навигации космических аппаратов. Важной отличительной особенностью такой системы является потенциально высокая помехозащищенность и стабильность измеряемых параметров во времени.

Кроме потенциальных мультипольных компонент анизотропии реликтового излучения, связанных с эффектами в гравитационных полях очень больших масштабов [4], существует также и кинетическая дипольная составляющая, которая обусловлена движением наблюдателя относительно реликтового излучения [5].

Наличие данного эффекта позволяет использовать кинетическую дипольную компоненту анизотропии космического микроволнового фона для целей ориентации и навигации космической техники.

## 1. Оценки локальной анизотропии пространства

В работах [6-8] рассматривалась локальная анизотропия пространства, определенная малыми возмущениями метрики. Локальная анизотропия определяется волновыми решениями уравнений Эйнштейна для слабых возмущений метрики Минковского со специальными условиями, наложенными на тензор возмущений. Следствием является зависимость скорости света от направления наблюдения.

В работе [8] было показано, что экспериментальная регистрация представленной зависимости позволяет определить компоненты тензора метрических возмущений и, таким образом, определить метрику анизотропного пространства-времени.

Запишем метрику Минковского с малыми анизотропными возмущениями

$$ds^2 = g_{\mu\nu}dx^\mu dx^\nu = (\eta_{\mu\nu} + h_{\mu\nu})\, dx^\mu dx^\nu, | \quad h_{\mu\nu}| \ll 1, \tag{1.1}$$

где метрический тензор невозмущенного пространства Минковского определяется следующим образом $\eta_{\mu\nu} = (1, -1, -1, -1)$ и малые анизотропные возмущения метрики запишем как

$$h_{\mu\nu} = \begin{pmatrix} h_{tt} & h_{tb} \\ h_{at} & h_{ab} \end{pmatrix}, \tag{1.2}$$

где $h_{tb} = h_{bt}$, греческие индексы пробегают значения

$$0, 1, 2, 3$$

и латинские индексы пробегают значения $1, 2, 3$, $x^0 = ct$, $x^a = (x, y, z)$.

Решения уравнений Эйнштейна в вакууме,

$$R_{\mu\nu} - \frac{1}{2}g_{\mu\nu}R = 0, \tag{1.3}$$

для данного случая, записываются в виде плоских волн следующего вида

$$h_{\mu\nu} = \sum_{s=+,\times} A^{(s)}_{\mu\nu} e^{ik_\mu x^\mu}, \tag{1.4}$$

где $A^{(s)}_{\mu\nu}$ - тензоры поляризации, $\mathbf{k} = k(\cos\theta, \sin\theta, 0)$ - пространственная компонента четырехвектора $k_\mu$,$\theta$ - угол между выбранным направлением и волновым вектором $\mathbf{k}$, и скорость света в пространстве Минковского с малыми анизотропными возмущениями определяется как

$$c(\theta) = c - \frac{c}{2}(h_{tt} + 2h_{tb}k^b + h_{ab}k^a k^b) + O(h^2), \tag{1.5}$$

или

$$\frac{\delta c(\theta)}{c} \approx -\frac{1}{2}\left(h_{tt} + 2h_{t1}\cos\theta + 2h_{t2}\sin\theta + h_{11}\cos^2\theta + h_{22}\sin^2\theta + h_{12}\sin 2\theta\right), \tag{1.6}$$

где $\delta c(\theta) = c(\theta) - c$.

Для невозмущенной метрики $h_{\mu\nu} = 0$, и скорость света не зависит от направления $c(\theta) = c$.

Вначале рассмотрим метрику вращающейся оптически прозрачной среды (диска) в цилиндрических координатах [8]

$$g_{\mu\nu} = \begin{pmatrix} 1 + \frac{\omega^2 r^2 n^2}{c^2} & 0 & \frac{\omega^2 r^2 n^2}{c^2} & 0 \\ 0 & -1 & 0 & 0 \\ \frac{\omega^2 r^2 n^2}{c^2} & 0 & -r^2 & 0 \\ 0 & 0 & 0 & -1 \end{pmatrix}, \tag{1.7}$$

с учетом показателя преломления $n$.

В таких средах фазовая скорость распространения света нелинейно зависит от векторного поля скоростей движения вследствие анизотропных свойств сил, связывающих атомы решетки.

Для метрики (1) ненулевые компоненты тензора метрических возмущений

$$h_{tt} = h_{t2} = h_{2t} = \frac{\omega^2 r^2 n^2}{c^2}, \tag{1.8}$$

и, таким образом, из выражения (6) получим

$$\frac{\delta c(\theta)}{c} = \frac{\omega^2 r^2 n^2}{c^2} \left(\sin\theta - 1/2\right). \tag{1.9}$$

В работе [9] рассматривается возможность использования двухлучевого интерферометра для лабораторного обнаружения пространственной анизотропии и представлен эксперимент по наблюдению оптической анизотропии света во вращающемся оптически прозрачном диске. В интерферометре свет от лазера с длиной волны $\lambda = 0.632991 \pm 1 \times 10^{-7} \mu m$проходил через вращающийся оптический диск диаметром D = $62mm$.

Достигнутая в экспериментах точность позволила зарегистрировать угловые вариации в положении интерференционных полос при фиксированной скорости вращения оптического диска. Оптический путь в проекции на вектор скорости среды равнялся $4.1 \times 10^{-2} m$. Отношение измеренной вариации интерференционной полосы к оптическому пути соответствует верхнему пределу на анизотропию скорости света $\delta c(\theta)/c < 2.3 \times 10^{-10}$.

Для рассмотрения дипольной и квадрупольной компонент анизотропии пространства Минковского на тензор метрических возмущений $h_{\mu\nu}$ накладываются следующие условия

$$h_{\mathrm{tt}}{=}h_{\mathrm{t}2}{=}h_{12}{=}\ 0{,}h_{11}{=}\ -h_{22}. \tag{1.10}$$

В результате, выражение (6) записывается в следующем виде

$$\frac{\delta c(\theta)}{c} = h_{t1}\cos\theta + \frac{1}{2} h_{11} \cos 2\theta = (v/c)\cos\theta + (v^2/2c^2)\cos 2\theta, \tag{1.11}$$

где $h_{t1} = v/c$ и $h_{11} = -h_{22} = v^2/c^2$, где $v$- скорость движения наблюдателя относительно некоторой неподвижной системы отсчета.

Первое слагаемое в выражении (11) соответствует дипольной компоненте анизотропии, второе - квадрупольной.

Таким образом, метрику анизотропного пространства-времени без учета источников гравитационных полей можно определить как

$$ds^2 = c^2 dt^2 + 2\frac{v}{c} dx dy - \left(1 - \frac{v^2}{c^2}\right) dx^2 - \left(1 + \frac{v^2}{c^2}\right) dy^2 - dz^2. \tag{1.12}$$

Также отметим, что гравитирующие объекты с симметричным распределением массы не влияют на анизотропию скорости света [8].

В работе [10] представлены результаты эксперимента по поиску дипольной анизотропии скорости света, определяемой движением Земли относительно реликтового излучения v/c = 0.000122.

Верхняя граница локальной анизотропии пространства оценена следующим образом $\delta c(\theta)/c < 1 \times 10^{-14}$.

Таким образом, пространство-время на Земле и в околоземном пространстве можно рассматривать как изотропное с высокой степенью точности, что соответствует случаю $h_{\mu\nu} = 0$ для метрики (1).

## 2. Дипольная анизотропия космического микроволнового фона

Выражение (11) совпадает с выражением для экспериментально наблюдаемой анизотропии температуры космического микроволнового фона

$$\frac{\delta T(\theta)}{T} = (v/c)\cos\theta + (v^2/2c^2)\cos 2\theta + O(v^3/c^3), \tag{2.1}$$

где $v$- скорость движения наблюдателя относительно реликтового излучения, и дипольная компонента анизотропии определяется первым слагаемым.

Дипольная анизотропия реликтового излучения проявляется в том, что яркостная температура изменяется вдоль выделенного направления относительно своего среднего значения, достигая максимального значения в направлении созвездия Льва (экваториальные координаты alpha = 11h 12m и delta = –7,1° (epoch J2000); галактические координаты l = 264,26° и b = 48,22°). Разница между наиболее холодной и горячей областью составляет 6,706 мК и вызвана доплеровским смещением частоты излучения из-за движения Солнечной системы относительно реликтового фона со скоростью примерно 370 км/с в сторону созвездия Льва.

В работе [11] приведены оценки погрешностей определения угловой координаты и скорости от направления, в котором производится измерение спектральной плотности мощности реликтового излучения. Погрешность определения угла $d\theta$

$$d\theta = -\frac{dT(1-\beta\cos\theta)^2}{T_0\beta\sqrt{1-\beta^2}\sin\theta}, \tag{2.2}$$

где $\theta$ - угол между вектором движения $v$ и направлением наблюдения, $T_0$ - температура реликтового излучения в системе координат, которая покоится относительно излучения, $dT$ - точность измерения температуры реликтового излучения, $\beta$ - модуль отношения скорости к скорости света $v/c$.

Скорость движения Солнца в направлении созвездия Льва составляет $v = 370$км/с, т.е. $\beta \sim 10^{-3} \ll 1$. Тогда

$$d\theta \;\; \frac{dT}{T_0\beta}\frac{1}{\sin\theta} \tag{2.3}$$

Минимальная погрешность $d\theta$ при предельно достижимой современными приборами точности измерения температуры $\sim 10^{-7}$К [2,12] составит около $3 \times 10^{-3}$ радиан ( 6 угловых секунд). При этом точность измерения будет оставаться высокой в широком диапазоне углов. За исключением диапазона углов $\theta = 0° \pm 6°$ и $\theta = 180° \pm 6°$ будет наблюдаться увеличение погрешности не более чем на порядок.

Ошибка вычисления скорости летательного аппарата

$$dv = \frac{c\sqrt{1-\beta^2}\,(1-\beta\cos\theta)^2\,dT}{T_0\left[(1-\beta^2)\cos\theta - \beta\,(1-\beta\cos\theta)\right]}. \tag{2.4}$$

Учитывая, что $\beta \ll 1$

$$dv \sim \frac{cdT}{T_0\cos\theta}. \tag{2.5}$$

При точности измерения температуры $\sim 10^{-7}$К минимальная ошибка определения скорости составит около 11 м/с и не превысит десятикратной минимальной величины во всем диапазоне углов, за исключением $\theta = 90° \pm 6°$ и $\theta = 270° \pm 6°$.

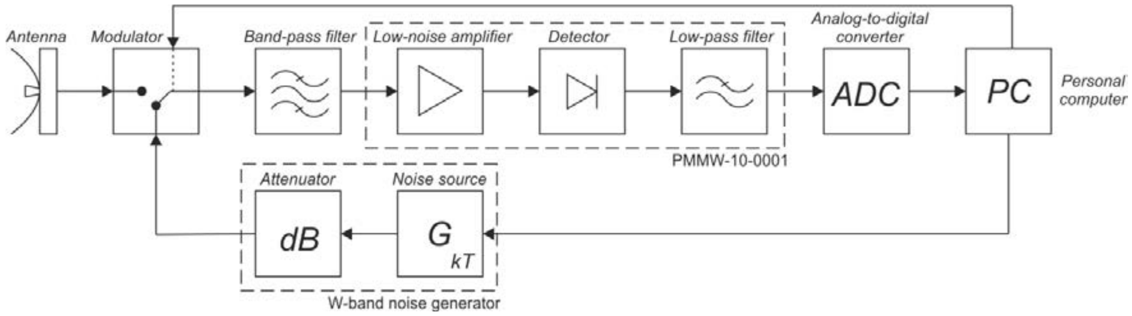


**Рис. 1.** Структурная схема радиометра.

Сделанные оценки точности определения угловых координат и скорости движения позволяют утверждать о принципиальной возможности и перспективности создания систем ориентации и навигации по карте реликтового излучения.

## 3. Схема экспериментальной установки

Для экспериментального исследования возможности создания систем ориентации по карте реликтового фона был разработан макет мобильного полноповоротного радиометра, структурная схема которого приведена на рисунке 1, а также программное обеспечение для работы с ним.

Радиометр собран по модуляционной схеме с оптико-механическим обтюратором в квазиоптическом тракте и встроенным опорным генератором шума для проведения самокалибровки. Его антенная система с шириной диаграммы направленности $1,2^{\circ}$ реализована по классической схеме Кассегрена. Основное параболическое зеркало антенны имеет диаметр 200 мм, гиперболический контрефлектор – диаметр 16 мм. В качестве облучателя используется пирамидальный рупор. Ширина диаграммы направленности была выбрана, с одной стороны, исходя из необходимости эффективного усреднения излучения точечных источников на небесной сфере, а с другой – исходя из условия обеспечения разрешающей способности по углу места и азимуту.

Квазиоптический тракт модулятора имеет в своем составе два скрещенных металлических волновода квадратного сечения $14{\times}14$ мм длиной 50 мм с расположенным в точке пересечения под углом $45^{\circ}$ к апертуре вращающимся металлическим диском, имеющим два четвертных секторальных выреза. Одну половину времени приемный тракт нагружен на прямой (антенный) канал, другую – на боковой (нагружен на генератор шума), посредствам зеркального отражения. Частота модуляции равна 30 Гц. Временные отрезки длительностью 3,2 мс, соответствующие области частичного перекрытия квазиоптического сечения при вращении диска, из обработки исключаются.

Усилительно-детекторный тракт радиометра был основан на использовании модуля Farran PMMW-10-0001, который имеет на входе малошумящий широкополосный усилитель. Эквивалентная шумовая температура в рабочей полосе частот (от 75 до 110 ГГц) этого модуля не превышает 450 К, а постоянная времени его фильтра нижних частот равна 1 мкс. Оцифровка выходного сигнала производится с помощью дифференциального 24-битного АЦП, выполненного на микросхеме Analog Devices AD7766.

В качестве высокостабильного опорного источника яркостной температуры используется широкополосный полупроводниковый генератор шума разработки НИФТИ ННГУ, сигнал которого ослабляется аттенюатором до уровня, соответствующего эквивалентной шумовой температуры 350 К, приведенной к входу приемного модуля.

Для исключения систематической ошибки измерений за счет теплового излучения полос поглощения молекулярного кислорода с максимумами поглощения вблизи частот 60 и 120 ГГц в волноводный тракт радиометра может быть установлен полосовой фильтр.

С целью повышения стабильности измерений при длительных наблюдениях в радиометре ре-

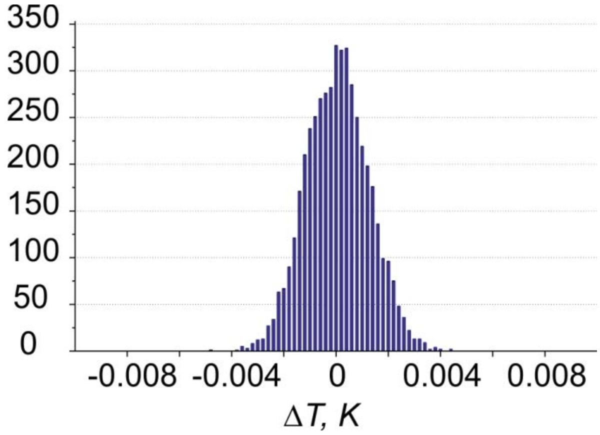


**Рис. 2.** Гистограмма распределения измерений яркостной температуры при времени накопления 60 секунд.

ализована система термостабилизации приемно-усилительного модуля и генератора шума. Дополнительно имеется общая термостабилизация радиометра с принудительной циркуляцией воздуха внутри всего объема.

Для наблюдения в выделенной области небесной сферы радиометр установлен на опорно-поворотном устройстве Радант AZ1000VX, позволяющем проводить сканирование и сопровождение по азимутальной координате в диапазоне от 0° до 360° и угломестной координате в диапазоне 0° до 90°.

Для определения потенциальной разрешающей способности радиометра при времени накопления 60 секунд были произведены длительные измерения уровня сигнала с опорного источника яркостной температуры. Гистограмма для распределения нестабильности регистрируемой яркостной температуры приведена на рисунке 2. Разрешающая способность разработанного радиометра составила величину порядка 1 мК при времени накопления сигнала 1 мин. На этом основании можно предположить, что при установке в точке с хорошим астроклиматом, радиометрический комплекс потенциально способен зарегистрировать дипольную составляющую яркостной температуры реликтового излучения и обеспечить точность определения угловых координат $\sim 15°$. Увеличение точности в данной реализации радиометра возможно посредством увеличения времени накопления.

Разработанное программное обеспечение позволяет осуществлять удаленное управление радиометром, сбор и обработку экспериментальных данных. Программа управления опорно-поворотным устройством поддерживает работу в горизонтальной, экваториальной и галактической системах координат. Помимо наведения радиометра на заданное направление имеется возможность проведения сканирования в произвольном диапазоне углов и слежение за выбранными небесным объектом.

Созданный радиометр может быть использован в длительном цикле измерений для исследования микроволнового астроклимата в области высокоточных радиометрических измерений. Также в дальнейшем планируется проведение экспериментальных исследований зависимости шумовой температуры от высоты в горных районах и на летающих лабораториях.

## 4. Заключение

В статье рассматривался метод определения ориентации по измерению спектральной плотности мощности на фоне дипольной анизотропии реликтового микроволнового излучения и решения задачи навигации по кинетической дипольной компоненте анизотропии реликтового излучения, возникающей в результате движения детектора относительно данного излучения. Данный метод основан на измерении температурного поля микроволнового космического излучения движущимся объектом.

Для экспериментального исследования влияния атмосферы на точность измерения температуры космического излучения создан макет мобильного радиометра с возможностью удаленного управления, Макет имеет временную стабильность и точностные характеристики, достаточные для выделения дипольной составляющей реликтового излучения и, тем самым, позволяет решать задачи автономной ориентации. Сделанные оценки точности предложенного метода навигации и проведенные экспериментальные исследования показали принципиальную возможность создания перспективных систем автономной ориентации и навигации по карте реликтового излучения.

**Список литературы/References**


1. Струков И.А., Брюханов А.А., Скулачев Д.П., Сажин М.В. Анизотропия фонового радиоизлучения. *Письма в Астрономический журнал.* 1992. Т. 18, № 5. С. 387—395.
2. Inoue, K.T. Local Voids as the Origin of Large-Angle Cosmic Microwave Background Anomalies: The Effect of a Cosmological Constant. *Astrophysical Journal*, 2007, 664 (2): 650–659.
3. Чернин А.Д. Как Гамов вычислил температуру реликтового излучения, или немного об искусстве теоретической физики. *Успехи физических наук*, 1994, Т. 164, №8, С.889-896.
4. Насельский П. Д., Новиков Д. И., Новиков И. Д. *Реликтовое излучение Вселенной.* М.: Наука, 2003. — 390 с.
5. Y. Akrami et al. [Planck], Planck intermediate results. LVI. Detection of the CMB dipole through modulation of the thermal Sunyaev-Zeldovich effect: Eppur si muove II. *Astron. Astrophys.* Vol. 644, (2020). A100.
6. Mansouri R. and Sexl S.U. A Test Theory of Special Relativity: I. Simultaneity and Clock Synchronization. *Gen. Rel. Grav.* 8 – 1977. – P.497.
7. Sfarti A. Light Speed Anisotropy Constraints via Measurement of Relativistic Light Aberration. *ARPN Journal of Science and Technology*, Vol. 4, No. 6 – 2014.
8. Фомин И.В. Скорость света в анизотропном пространстве-времени. *Известия вузов. Физика.* 2016.Т. 59 , № 1. С. 36 – 40.
9. Гладышев В.О., Тиунов П.С., Леонтьев А.Д, Гладышева Т.М., Шарандин Е.А. Исследование анизотропии пространства скоростей электромагнитного излучения в движущейся среде. *Журнал технической физики*, Т.82, №11, – 2012. – с.54-63.
10. Gurzadyan V.G., et.al A new limit on the light speed isotropy from the GRAAL experiment at ESRF. *Proc.12th M.Grossmann Meeting on General Relativity*, v. B, World Sci., – 2012. – P.1495.
11. Гладышев В.О.*, Портнов Д.И.*, Базлев Д.А.**, Скобелев М.М. Метод ориентации летательного аппарата в космическом пространстве на основе измерения пространственных вариаций спектральной плотности мощности реликтового излучения. *Вестник Московского государственного технического университета им. Н.Э. Баумана. Серия Естественные науки*, 2017. № 5 (74). С. 49-56.
12. Strukov I. A. et al. The Relikt-1 experiment - New results. *Monthly Notices of the Royal Astronomical Society.* 1992. V. 258. P. 37-40. (Bibcode: 1992MNRAS.258P..37S.)


**Авторы**


**Гордин Михаил Валерьевич**, кандидат технических наук, ректор, МГТУ им. Н.Э. Баумана, ул. 2-я Бауманская, д. 5, с. 1, г. Москва, 105005, Россия.
E-mail: gordinmv@bmstu.ru

**Базлев Д А**, к.ф.-м.н., профессор, второй университет, ул. Другая, д. 01, г. Новый, 012340, Россия; доцент, первый университет, ул. Такая, д. 00, г. Первый, 000000, Россия.

E-mail: email2@inbox.ru

**Гладышев Владимир Олегович**, д.ф.-м.н., декан факультета “Фундаментальные науки”, профессор кафедры “Физика”, Московский государственный технический университет им. Н.Э. Баумана, ул. 2-я Бауманская, д. 5, с. 1, г. Москва, 105005, Россия.
E-mail: email2@inbox.ru

**Кауц Владимир Леонидович**, к. ф.-м. н., доцент кафедры физики, Московский государственный технический университет имени Н.Э. Баумана, 2-я Бауманская ул., д. 5, г. Москва, 105005, Россия.
E-mail: kauts@bmstu.ru

**Каютенко Александр Викторович**, начальник ОТЭ НУК «Фундаментальные науки» , МГТУ им. Н.Э. Баумана, ул. 2-я Бауманская, д. 5, стр. 1, г. Москва, 105005, Россия.
E-mail: akayutenko@bmstu.ru

**Николаев Павел Петрович**, к. ф.-м. н., доцент кафедры физики, Московский государственный технический университет имени Н.Э. Баумана, 2-я Бауманская ул., д. 5, г. Москва, 105005, Россия.
E-mail: ppn@bmstu.ru

**Фомин Игорь Владимирович**, д. ф.-м. н., профессор кафедры физики, Московский государственный технический университет имени Н.Э. Баумана, 2-я Бауманская ул., д. 5, г. Москва, 105005, Россия.
E-mail: ingvor@inbox.ru

**Шарандин Евгений Анатольевич**, к. ф.-м. н., доцент кафедры физики, Московский государственный технический университет имени Н.Э. Баумана, 2-я Бауманская ул., д. 5, г. Москва, 105005, Россия.
E-mail: shar@bmstu.ru

**Просьба ссылаться на эту статью следующим образом:**
Гордин М. В., Базлев Д. А., Гладышев В. О., Кауц В. Л., Каютенко А. В., Николаев П. П., Фомин И. В., Шарандин Е. А. Использование реликтового излучения для построения новой системы навигации. *Пространство, время и фундаментальные взаимодействия.* 2023. № 3-4. С. 108–116.

**Authors**

**Gordin Mikhail Valerievich**, PhD, rector of Bauman Moscow State Technical University, 2nd Baumanskaya st., 5 build. 1, Moscow, 105005, Russia.
E-mail: gordinmv@bmstu.ru

**Petrov Petr Petrovich**, Ph.D., Professor, Second University, Another st., 01, New-City, 012340, Russia; Associate Professor, First University, Takaya st., 00, First-City, 000000, Russia.
E-mail: email2@inbox.ru

**Gladyshev Vladimir Olegovich**, Ph.D.,Head of the Fundamental Sciences faculty, Professor of Physics department, Bauman Moscow State Technical University, 2nd Baumanskaya st., 5c1, Moscow, 105005, Russia.
E-mail: email2@inbox.ru

**Kauts Vladimir Leonidovich**, Candidate of Physical and Mathematical Sciences, Associate Professor of Physics Department of Bauman Moscow State Technical University, 2-nd Baumanskaya street, 5, Moscow, 105005, Russia.
E-mail: kauts@bmstu.ru

**Kayutenko Alexander Victirovich**, Head of OTE Scientific Educational Complex «Fundamental Sciences» , Bauman Moscow State Technical University, 2-nd Baumanskaya st., 5/1, Moscow, 105005, Russia.
E-mail: akayutenko@bmstu.ru

**Nikolaev Pavel Petrovich**, Candidate of Physical and Mathematical Sciences, Associate Professor of Physics Department of Bauman Moscow State Technical University, 2-nd Baumanskaya street, 5, Moscow, 105005, Russia.
E-mail: ppn@bmstu.ru

**Fomin Igor Vladimirovich**, Doctor of Physical and Mathematical Sciences, Professor of Physics Department of Bauman Moscow State Technical University, 2-nd Baumanskaya street, 5, Moscow, 105005, Russia.
E-mail: ingvor@inbox.ru

**Sharandin Eugenyi Anatolievich**, Candidate of Physical and Mathematical Sciences, Associate Professor of Physics Department of Bauman Moscow State Technical University, 2-nd Baumanskaya street, 5, Moscow, 105005, Russia.
E-mail: shar@bmstu.ru

**Please cite this article in English as:**
Gordin M. V., Petrov P. P., Petrov P. P., Kauts V. L., Kayutenko A. V., Nikolaev P. P., Fomin I. V., Sharandin E. A. Using relic radiation to construct new navigation system. *Space, Time and Fundamental Interactions*, 2023, no. 3-4, pp. 108–116.

УДК [530.12+530.145](082)



# ФИЗИЧЕСКИЕ ОСНОВЫ СВОЙСТВА ВОСПРИИМЧИВОСТИ ЭЛЕКТРОМАГНИТНОГО ПОЛЯ ЗЕМЛИ К ГРАВИТАЦИОННО-ВОЛНОВОМУ ИЗЛУЧЕНИЮ ДВОЙНЫХ ЗВЕЗДНЫХ СИСТЕМ

Грунская Л. В.[a,1], Исакевич В. В.[b,2], Исакевич Д. В.[b,3]

[a] Владимирский государственный университет, г. Владимир, 600000, Россия.
[b] ООО Собственный вектор, Владимир, 600005, Россия.

Компоненты вертикальной составляющей напряжённости электрического поля Земли, спектрально локализованные на гармониках частот обращения релятивистских двойных звёздных систем, имеющие значимую амплитуду и большую спектральную локализацию, чем компоненты, локализованные на других частотах, открыты с использованием айгеноскопии (анализа амплитудных спектров собственных векторов матриц смешанных вторых моментов на конечном интервале анализа) на экспериментальном материале многолетних временных рядов напряжённости электрического поля Земли в инфранизкочастотном диапазоне.

*Ключевые слова*: Собственный вектор, ковариационная матрица, спектральная локализация, электрическое поле Земли, гравитационные волны, релятивистские двойные звёздные системы.

# PHYSICAL BASIS OF SENSITIVITY OF THE EARTH'S ELECTROMAGNETIC FIELD TO GRAVITATION

Grunskaya L. V.[a,1], Isakevich V. V.[b,2], Isakevich D. V.[b,3]

[a] Vladimir State University, Vladimir, 600000, Russia.
[b] Eigenvector LLC, Vladimir, 600005, Россия.

Components of the Earth's electric field vertical strength which are spectrally localized at the multiplied rotation frequencies of relativistic binary star systems, have significant amplitude and sharper spectral localization than at the other frequencies, have been discovered at the experimental material of multy-year time series of the Earth's electric field strength in the infralow frequency band using eigenoscopy (second mixed moments eigenvectors' amplitude spectra analysis at finite analysis span).

*Keywords*: Eigenvector, covariance matrix, spectral localization, Earth electric field, gravitational waves, relativistic binary star systems.
PACS: 04.20.-q
DOI: 10.17238/issn2226-8812.2023.3-4.117-126

## Introduction

The task solved in the current work is to reveal the influence of the gravitational waves irradiated by relativistic binary star systems (RBSS) to the Earth electric field vertical strength ($E_z$).

Components of the electric field vertical strength (in the infralow frequency range and in the near-terrestrial atmosphere layer) which are spectrally localized at the frequencies of the gravitational-wave irradiation from two groups of the RBSS listed in [1]. The first group consists of the small-eccentricity RBSS which have an orbital period from 14 to 207 hours; the expected gravitational waves from a small-eccentricity RBSS are irradiated mainly at the double orbital frequency. The second group consists of

[1]E-mail: grunsk@vlsu.ru
[2]E-mail: eigenoscope@yandex.ru
[3]E-mail: eigenoscope@yandex.ru

**Таблица 1.** Four time series of vertical component of the Earth's electric field strength in the near-ground layer of atmosphere which have been analyzed

| No. | Observation station | Total sample count | Duration, days | Duration, months | Duration, years |
|---|---|---|---|---|---|
| 1 | Voeikovo | 170000 | 7083 | 236 | 20 |
| 2 | Dusheti | 120000 | 5000 | 167 | 14 |
| 3 | Verkhnee Dubrovo | 120000 | 5000 | 167 | 14 |
| 4 | VlSU experimental base | 36000 | 1500 | 50 | 4 |

the high-eccentricity RBSS; the expected gravitational waves from these RBSS are irradiated mainly at the higher multiples of their orbital frequencies.

The conducted research of the electric field components which are spectrally localized at the frequencies of gravitational-wave irradiation from the RBSS are based on the long-time series of the electric field vertical strength at four spatially separated observation stations.

As it is known the Earth-ionosphere resonator has no lower cutoff frequency; therefore all the infralow frequency components of the electric field vertical strength in near-terrestrial layer of the atmosphere, that may be observed at any point of the Earth surface, are formed by the global processes occurring in this resonator. Obviously this resonator may be considered as a part of the Solar system influenced by many factors including the gravitational waves irradiated by RBSS.

Preliminary use of standard spectral analyzers lead to the following result: time series of electric field in the near-terrestrial atmosphere layer are identified by these analyzers as a noise; therefore the gravitational-waves influence of RBSS cannot be revealed with these analyzers.

We've got two choices: the first one is to abandon the problem; the second one (that is our choice) is to solve the problem using some non-standard way of analysis. Following the principle of having a specific analyzer for each problem formulated by L.I. Mandelshtam [2], we chose the way of search of analysis means which should solve a problem of revealing the influence of gravitational waves from RBSS to vertical component of the Earth's electric field strength in the near-ground atmosphere layer.

## 1. The used data

Four multi-year time series recorded at Rosgidromet observation stations (Voeikovo, Verkhnee Dubrovo, Dusheti) and the Vladimir state university General and Applied Physics Dept. experimental base has been used in the current work. All these time series have the same sampling time equal to 3600 sec; some data about the series is presented in Table 1.

Johnston's list [1] contains 43 small-eccentricity RBSS which irradiate GW at the second multiple of the orbital frequency. These frequencies constitute the first list of frequencies which are used for formation of the multisets' used in the research. This list will be named further as $\lfloor J2F43 \rfloor$. Six RBSS which have high eccentricity have been selected from the Johnston's list for the research at the higher multiples of theirs' orbital frequencies [1]. This list will be named further as $\lfloor JF6/288 \rfloor$. We consider some test multisets of frequencies which are not expected to show the gravitational-wave influence of RBSS on the Earth's electric field; these frequencies are not gravitational-wave frequencies contained in the multisets $\lfloor J2F43 \rfloor$ and $\lfloor JF6/288 \rfloor$ considered for revealing this influence. Among these multisets are multiset of the small-eccentricity RBSS orbital frequencies and of their third multiples; the listed small-eccentricity RBSS does not irradiate gravitation waves of these frequencies. The frequencies close to those listed in Table 2, row 2 are shifted by $\delta F$ and are not expected to show the gravitational-wave influence.

**Таблица 2.** The frequency multisets which are used in the current work

| No. | Designation | Number of frequencies |
|---|---|---|
| 1 | $\lfloor J2F43 \rfloor$ | 43 |
| 2 | $\lfloor JF6/288 \rfloor$ | 288 |
| 3 | $\lfloor JF43 \rfloor \oplus \lfloor J3F43 \rfloor$ | 86 |
| 4 | $\lfloor JF43 \rfloor \oplus \lfloor J3F43 \rfloor \oplus \lfloor J(F+\delta F)6/288 \rfloor$ | 374 |

## 2. Eigenoscopy of the $E_z$ time series at the selected frequencies

Eigenoscopy provides the following steps:

1. Covariance matrix of the time series is computed with the analysis span of 1000 samples.
2. Eigenvectors and eigennumbers of the covariance matrix are computed.
3. Amplitude spectra and coherence ratios (which is a ratio of the maximum amplitude value to the mean amplitude in the eigenvector amplitude spectrum) of all the eigenvectors are computed.
4. Spectral localization band which is a neighbourhood of main maximum of the amplitude spectrum by 0.707 level is computed.
5. Eigenpairs with spectral localization band containing the frequencies from Table 2 are found.
6. Multisets of coherence ratios and eigenvalues which correspond to the eigenvectors selected at the previous step are formed.

Analysis of statistically significant differences of multisets of coherence ratios and eigenvalues for the frequency multisets No.1 and No.3 have been performed with Bernoulli test (because of a small volume of these multisets). Comparative analysis of cumulative distribution functions for the frequency multisets No.2 and No.4 have been performed with Smirnov-Kolmogorov criterion.

Schemes of eigenoscopes which correspond to these two ways analysis are shown at Figure 1 and Figure 2.

Functional blocks of the eigenoscope scheme are described below.

Block No.1 converts the time series $|s\rangle = |s_1; s_2; \ldots; s_L\rangle$ of $L$ samples to the trajectory matrix $T_{M\times(L-M+1)} = \langle |S_1\rangle, |S_2\rangle, \ldots, |S_{L-M+1}\rangle|$ where $|S_i\rangle = |s_{(i-1)M+1}; s_{(i-1)M+2}; \ldots; s_{i+M-1}\rangle$ is an $i$-th segment which consists of $M$ consequent samples of the time series; total amount of the segments is $L-M+1$.

Block No.2 converts trajectory matrix to the density matrix

$$\varrho_{M\times M} = \frac{\sum\limits_{1}^{L-M+1} |S_i\rangle\langle S_i|}{\langle S_i|S_i\rangle} \tag{2.1}$$

Block No.3 computes eigenpairs (eigenvectors and eigennumbers) of the density matrix which are defined by the following relations

$$\langle\psi_i|\varrho_{M\times M} = \lambda_i\langle\psi_i|, i = 1,\ldots,M \text{ in bra form,} \tag{2.2}$$

$$\varrho_{M\times M}|\psi_i|\rangle = \lambda_i|\psi_i\rangle, i = 1,\ldots,M \text{ in cket form.} \tag{2.3}$$

Block No.4 computes amplitude spectra of the eigenvectors. Each of the eigenvectors is extended with $M \cdot U$ zero samples in order to increase spectral discernment. Amplitudes of fast Fourier transform (FFT) are computed for the extended eigenvectors

$$|\mathrm{FFT}(\||\psi_i\rangle; |0_{M\cdot U}\rangle\rangle| = |a_{1,i}; a_{2,i}; \ldots; a_{M(U+1),i}\rangle \tag{2.4}$$

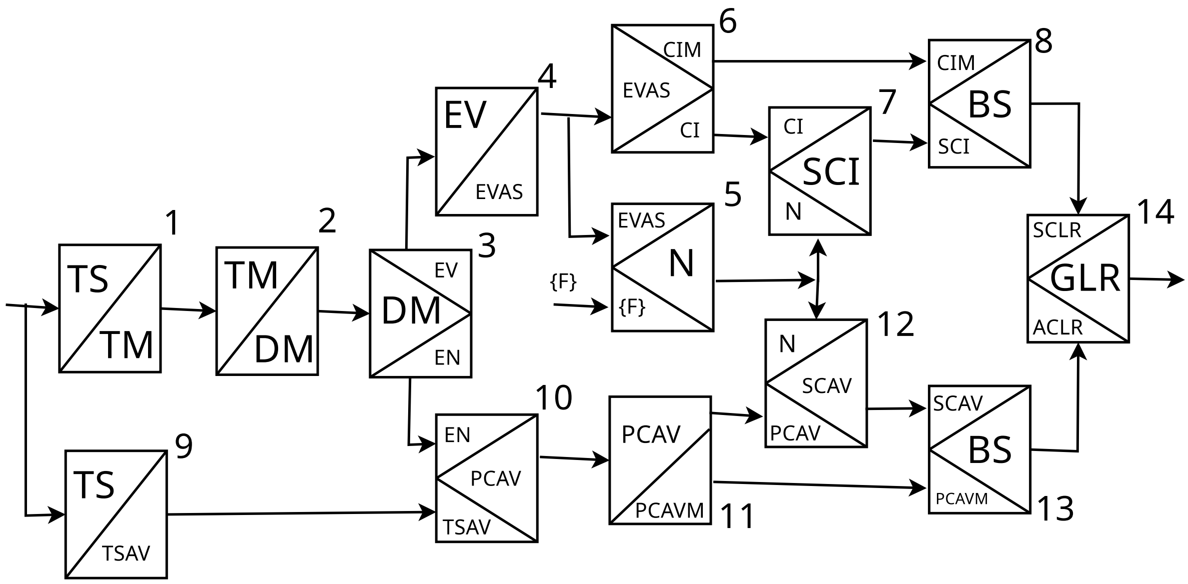


**Рис. 1.** Eigenoscope (utility models [1–4]): TS — Time series. TM — Trajectory matrix. DM — Density matrix. EV — Eigenvector. EN — Eigennumber. EVAS — Eigenvector amplitude spectrum. CI — Coherence ratio. CIM — Coherence ratio median. SCI — Selected eigenvectors coherence ratios. BS — Bernoulli scheme. SCLR — Spectral channel likelihood ratio. TSAV — Time series active value. PCAV — Principal components active values. PCAVM — Principal components active values median. SCAV — Selected components active values. ACLR — Amplitude channel likelihood ratio. GLR — Generalized likelihood ratio. $\{F\}$ — Frequency list.

First $H$ values of the amplitudes are used as the eigenvectors' normed amplitude spectra estimations:

$$\tilde{A}_i = \frac{|a_{1,i}; a_{2,i}; \dots; a_{H,i}\rangle}{\max_j a_{j,i}} = |\tilde{a}_{1,i}; \tilde{a}_{2,i}; \dots; \tilde{a}_{H,i}\rangle \tag{2.5}$$

where $H$ is an integer part of $M(U+1)/2$.

Block No.5 returns the list $N_{\text{SEV}}$ of eigenvectors which are spectrally localized near $F_j$, $j = 1, \dots, Q$ frequencies is formed in the following way. A set of discrete frequencies (frequency samples)

$$f_i^{(W)} =_{k=1, \tilde{a}_{k,i} > W}^{H} \{k\}, i = 1, \dots, M \tag{2.6}$$

is defined for each of the normed amplitude spectra $|\tilde{A}_i\rangle$ at which set $\tilde{a}_{k,i}$ exceeds the predefined level $W$ (usually $W = \sqrt{2}$). The upper and lower bounds $f_i^{min} = \min(f_i^{(W)})$, $f_i^{max} = \max(f_i^{(W)})$ of the set $f_i^{(W)}$ are defined and compared with the given discrete frequencies from the list $F_j, j = 1, \dots, Q$. If the listed frequency lays between the boundaries of $f_i^{(W)}$ then the eigenvector's number is listed at the output of the block. Therefore

$$N_{\text{SEV}} =_{i,j, f_i^{min} < F_j < f_i^{max}} \{i\} \tag{2.7}$$

Further $N_{\text{SEV}}$ will mean length of the eigenvectors' list. The lower output of the block No.6 gives coherence ratios for all the eigenvectors. Coherence ratio is computed as a ratio

$$I_i = H \cdot (\sum_{k=1}^{H} a_{k,i})^{?1}, i = 1, \dots, M \tag{2.8}$$

The upper output is the median value of the coherence ratio

$$I_{\text{med}} = q_{0.5}(I), I = \{I_i\} \tag{2.9}$$

Block No.7 forms set of the coherence ratios for the eigenvectors which are spectrally localized near the frequencies of interest listed in $F_j$, $j = 1, \dots, M$. The output set includes coherence ratios of the

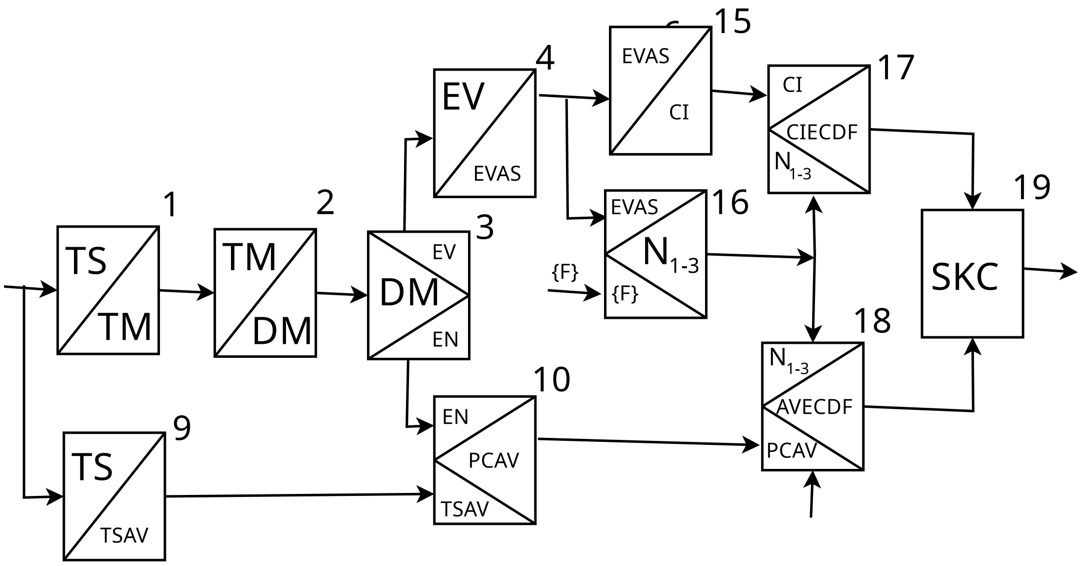


**Рис. 2.** Eigenoscope used for research at the frequencies of GW from RBSS with high eccentricity (RBSS 6/299 object): TS — Time series. TM — Trajectory matrix. DM — Density matrix. EV — Eigenvector. EN — Eigennumber. EVAS — Eigenvector amplitude spectrum. CI — Coherence ratio. TSAV — Time series active value. PCAV — Principal components active values. SCAV — Selected components active values. $\{F\}$ — Frequency list. CIECDF — Coherence ratios empirical cumulative distribution function. AVECDF — Principal components active values empirical cumulative distribution function. SKC — Smirnov-Kolmogorov criterion. N1-3 — sets of numbers of eigenvectors which are exposed to analysis.

eigenvectors which are listed in $N_{\mathrm{SEV}}$:

$$I_{\mathrm{SEV}} = \{I_i | i \in N_{\mathrm{SEV}}\} \tag{2.10}$$

Block No.8 implements Bernoulli scheme for the spectral processing channel. The Bernoulli scheme works in the following way. Test count $N_{\mathrm{test}} = n(N_{\mathrm{SEV}})$ is equal to the number of selected eigenvectors. Success count $N^{(\,I\,)}_{\mathrm{success}} = n(I_i | i \in N_{\mathrm{SEV}} \wedge I_i > I_{\mathrm{med}})$ is equal to number of the coherence ratios of the selected eigenvectors which exceed the median $I_{\mathrm{med}}$ of the coherence ratio estimated for all the eigenvectors. Random exceed (success) probability of coherence ratios over the median value is the false detection rate for anomalous spectral localization of $E_z$ near the listed frequencies of GW from RB. This probability is defined as

$$P^{(I)}_{\mathrm{false\ detection}}(N^{(I)}_{\mathrm{success}}, N_{\mathrm{test}}) = \frac{N^{(I)}_{\mathrm{test}}!}{2^{N_{\mathrm{test}}} N^{(I)}_{\mathrm{success}}! \cdot (N^{(I)}_{\mathrm{test}} ? N^{(I)}_{\mathrm{success}})!} \tag{2.11}$$

while the likelihood ratio is defined as

$$L^{(I)}(N^{(I)}_{\mathrm{success}}, N_{\mathrm{test}}) = \frac{(\lfloor N_{\mathrm{test}}/2 \rfloor)!}{N^{(I)}_{\mathrm{success}}! \cdot (N_{\mathrm{test}} ? N^{(I)}_{\mathrm{success}})!} \tag{2.12}$$

Block No.9 computes the active value $D$ for the time series according to the formula:

$$D = \sqrt{\langle D^2 \rangle}, \langle D^2 \rangle = \frac{\sum\limits_{t=1}^{L?M+1} \langle S_t | S_t \rangle}{M \cdot (L?M+1} \tag{2.13}$$

Block No.10 computes the active values of the principal components using the time series active value $D$ and the normed eigennumbers $\lambda_i$:

$$D_i = \sqrt{\lambda_i} \cdot D \tag{2.14}$$

Block No.11 gives median of the active values of the principal components:

$$D_{\text{med}} = q_{0.5}(D_i) \tag{2.15}$$

Block No.12 gives active values of the principal components which are spectrally localized near the frequencies listed in $F_j$, $j = 1, \ldots, M$ are defined by the following:

$$D_{\text{SEV}} = \{D_i | i \in N_{\text{SEV}}\} \tag{2.16}$$

Block No.13 implements Bernoulli scheme for the amplitude processing channel works in the following way. The test count for the amplitude channel is the same as for the spectral channel $N_{\text{test}} = n(N_{\text{SEV}})$. The success count is $N^{(D)}_{\text{success}} = n(D_i | i \in N_{\text{SEV}} \wedge D_i > D_{\text{med}})$. The false detection probability of anomalous $E_z$ principal components behavior near the frequencies of GW from RB is defined as

$$P^{(D)}_{\text{false detection}}(N^{(D)}_{\text{success}}, N_{\text{test}}) = \frac{N^{(D)}_{\text{test}}!}{2^{N_{\text{test}}} N^{(D)}_{\text{success}}! \cdot (N^{(D)}_{\text{test}} ? N^{(D)}_{\text{success}})!} \tag{2.17}$$

while the likelihood ratio is

$$L^{(D)}(N^{(D)}_{\text{success}}, N_{\text{test}}) = \frac{(\lfloor N_{\text{test}}/2 \rfloor)!}{N^{(D)}_{\text{success}}! \cdot (N_{\text{test}} ? N^{(D)}_{\text{success}})!} \tag{2.18}$$

Block No.14 according to generalized Bernoulli scheme for the spectral and the amplitude channels for all the reception points gives the following probability

$$P^{(\Sigma)}_{\text{false detection}}(N^{(\Sigma)}_{\text{success}}, N_{\text{test}}) = \frac{N^{(\Sigma)}_{\text{test}}!}{2^{N_{\text{test}}} N^{(\Sigma)}_{\text{success}}! \cdot (N^{(\Sigma)}_{\text{test}} ? N^{(\Sigma)}_{\text{success}})!} \tag{2.19}$$

and likelihood

$$L^{(\Sigma)}(N^{(\Sigma)}_{\text{success}}, N_{\text{test}}) = \frac{(\lfloor N_{\text{test}}/2 \rfloor)!}{N^{(\Sigma)}_{\text{success}}! \cdot (N_{\text{test}} ? N^{(\Sigma)}_{\text{success}})!} \tag{2.20}$$

where

$$N^{(\Sigma)}_{\text{test}} = \sum_g N^{(I)}_{\text{test},g} + \sum_g N^{(D)}_{\text{test},g} \tag{2.21}$$

$g$ is a number of the observation (reception) point. The output of Block No.15 is set of the coherence ratios for all the eigenvectors. The coherence ratio is computed as a ratio

$$I_i = H \cdot (\sum_{k=1}^{H} a_{k,i})^{?1}, i = 1, \ldots, M \tag{2.22}$$

Block No.16 gives lists $N_{1--3}$ which are the lists of eigenvectors' numbers used for further analysis. Set of discrete frequencies (frequency samples)

$$f^{(W)}_i =^{H}_{k=1, \tilde{a}_{k,i} > W} \{k\}, k = 1, \ldots, M \tag{2.23}$$

for which $|\tilde{A}_i\rangle$ exceeds the predefined level $W$ (usually $W = \sqrt{2}$) is defined for each of the normed amplitude spectra $|\tilde{A}_i\rangle$. Lower and upper boundaries $f^{min}_i = \min(f^{(W)}_i)$, $f^{max}_i = \max(f^{(W)}_i)$ of the set $f^{(W)}_i$ are defined which are compared with the discrete frequencies listed in $F_j$, $j = 1, \ldots, M$. If the frequency lays in the boundaries of $f^{(W)}_i$ then the eigenvector's number is listed at the output. The first output list $N_1$ is formed as an union of pairs' sets

$$N_1 =_{i,j,f^{min}_i < F_j < f^{max}_i} \{j, i\}, j = 1, \ldots, Q, i = 1, \ldots, M \tag{2.24}$$

The second one ($N_2$) is formed from $N_1$ by elimination of pairs with repeated $i$ and extracting the numbers of eigenvectors. The third list $N_3$ is formed from the numbers of these eigenvectors for which

$f_i^{(W)}$ lays in the multiple RBSS rotation frequencies' range that is the range from $\min_F = \min_{j=1,\ldots,Q} F_j$ to $\max_F = \max_{j=1,\ldots,Q} F_j$.

Coherence ratios' empirical cumulative distribution functions (CIECDFs) are computed for the coherence ratios listed in $N_1$, $N_2$ and $N_3$ correspondingly in Block No.17.

Principal components active values' empirical cumulative distribution functions (AVECDFs) are computed for the active values listed in $N_1$, $N_2$ and $N_3$ correspondingly in Block No.18.

The work of Block No.19 is following. The false detection probabilities are estimated from three CIECDFs using the Smirnov-Kolmogorov criterion. The false detection probabilities are estimated from three AVECDFs using the Smirnov-Kolmogorov criterion. The conclusion on presence or absence of the anomalous behavior of components which are spectrally localized near the frequencies of interest is based on the estimated false detection probabilities.

## 3. Interpretation of the results

Use of spectral eigenoscopy (which is a signal representation at the finite analysis span using the eigenvectors basis of the signal covariance matrix and the subsequent eigenvectors amplitude spectra analysis) has shown that the Earth electric field vertical strength (measured at the infra-low frequency range) contains non-correlated components; these components are spectrally localized at the gravitational-waves irradiation frequencies of relativistic binary star systems (gravitational-wave beacons) and significantly differ from the other components.

Two groups of the gravitational waves irradiation frequencies are considered in the current article. The first group consists of forty three RBSS having a small eccentricity and an orbital period greater than 14 hours and less than 207 hours. Small eccentricity of the RBSS in this group makes them likely irradiate gravitational waves mainly at their doubled orbital frequencies. The other group consists of six RBSS with high eccentricity and rather long orbital periods (17-231 Earth days); therefore they likely irradiate gravitational waves mainly at higher multiples of their orbital frequencies; total count of the considered multipled frequencies for these RBSS is 288.

Four long (multy-year) time series of the observed Earth electric field strength vertical projection in the infra-low frequency range have been processed in order to get the results; these time series are recorded at the corresponding observation stations Voeikovo, Verkhnee Dubrovo, Dusheti and at the experimental ground of the General and Applied Physics Department, Vladimir state university.

Non-correlated components of all these time series have been examined. Properties of the non-correlated components spectrally localized at the two groups of the considered gravitational wave frequencies differ from the corresponding properties of the non-correlated components spectrally localized at the other frequencies; the difference is statistically significant.

The results of the article make it possible to affirm that there is no reason to negate a gravitational-wave influence of the RBSS to the Earth electromagnetic field. The authors suppose that observation of the Earth electromagnetic field components at the RBSS gravitational-wave irradiation frequencies may start a multi-frequency gravitational-waves monitoring; this new direction of research may reveal new opportunities for research of the Earth and Universe.

The current research is made possible because previously was made the following [5, 6, 7, 8, 9, 10, 11]:

1. Found out that classical methods of spectral analysis do not reveal anomalies of the Earth electromagnetic field amplitude spectra at the RBSS gravitational-wave frequencies.

2. Found out that adding small harmonic components with the RBSS gravitational-wave frequencies to the observation time series leads to a sure detection of these components using the classical spectral analysis.

3. Fixed the absence of harmonic components at the gravitational-wave frequencies in the time series of Earth electric field vertical strength in the near-terrestrial atmosphere layer.

4. Found out that the searched signal is not harmonic but is a signal of unknown structure which is spectrally localized near the gravitational-wave frequency of RBSS.

5. Found out (by theoretical estimation) that tidal effects in the Earth atmosphere caused by the RBSS gravitational wave influence may cause only the vanishingly small variations of the Earth electric field vertical strength. As a result, a question arose about the other possible mechanisms of RBSS gravitational-waves influence on the electric field vertical strength in the near-terrestrial layer of atmosphere.

6. Performed an experimental study of using the covariance matrix eigenvectors basis for analyzing the Earth electric field vertical strength time series. It appeared that the analyzer using such a representation was not studied specially.

7. Introduced a special class of signal eigenvectors and components analyzers (eigenoscopes) to theory and practice. Set a task of eigenoscope properties systematic study and consolidating the priority for the use of this class of analyzers in the form of patents.

8. Performed the study of eigenvectors and eigennumbers typologies (behavior) for regular oscillations and stochastic signals depending on the source signal, the finite analysis span and the way of forming the observations ensemble.

9. Performed the study of eigenoscopes supersensitivity and superselectivity effects compared to the classical amplitude and energetic spectra analysis methods. Estimated the eigenoscopy precision depending on the quantization noise and the properties of the analyzed signal.

10. Developed the criteria of eigenvector spectral localization and of eigenvectorsamplitude spectra closeness to the RBSS gravitational wave irradiation frequencies. Estimated false detection probability.

11. Used Bernoulli test and Smirnov-Kolmogorov criterion to develop effective rules of statistical inference on abnormal behavior of the non-correlated components (eigenpairs) at the RBSS gravitational-wave irradiation frequencies.

12. Showed that for the Earth electric field vertical projection strength the observed rms values (more than 0.1 V/m) of non-correlated components spectrally localized at the RBSS gravitational waves irradiation frequencies may be explained using a theory of the Earth orbital perturbations caused by the RBSS gravitational waves; these perturbations lead to the Earth shift in relation to total charge of the atmosphere (in the ionosphere-terrestrial resonator).

13. Proved the existence of spatial (between the spatially separated observation stations) correlations of non-correlated components spectrally localized near the RBSS gravitational-waves frequencies.

The results of this work are based on the observation data of the Earth electric field donated by Y. M. Schwartz (Voeikovo, Verkhnee Dubrovo, Dusheti stations); on the data recorded at the experimental ground of Department of General and Applied Physics of Vladimir State University (lead by L. V. Grunskaya); on the RBSS list published by Johnston at his site [1] and on the innovative processing methods (called eigenoscopy) [3]. The results does not contain any explanations of the observed effects; though simple estimations [10] allow the assumption that the observed effects are the result the RBSS gravitational waves influence on the Earth-Sun gravitational antenna. Due to the different degrees of this influence on the Earth and on its atmosphere the observed effects may caused by the relative shift of the total storm charge in the global ground-ionosphere resonator.

### Conclusion

Significant (false detection probability is less than $10^{-9}$) difference of eigenvectors' coherence ratios and normed eigenvalues for the eigenvectors which are spectrally localized at the small-eccentricity RBSS double orbital frequencies (using Bernoulli test) and which are spectrally localized at the higher multiples of the high-eccentricity RBSS orbital frequencies (using Smirnov-Kolmogorov criterio) from those of the test multisets have been revealed.

It is known that: eigennumbers spectrum of the $E_z$ covariance matrix is similar to the one of covariance matrix of a partially-integrated noise; while the eigenvectors of it are spectrally localized near frequencies which are lowered with the eigennumber growth [5].

Also it is shown that a small perturbing monochromatic component which is spectrally localized at a given frequency and added to the partially integrated noise leads to a significant perturbation of the components with small eigennumbers without significant change of the dominant components if spectral localization of the perturbation is higher than of the noise. Pair of eigenvectors is observed the spectral localization of which is similar to spectral localization of the perturbation [12].

These two facts may explain the sensitivity of $E_z$ to perturbations from RBSS GW which show itself in the higher spectral localization of the covariance matrix' eigenvectors spectrally localized at the frequencies of interest.

### Список литературы/References

1. http://www.johnstonsarchive.net/relativity/binpulstable
2. Gorelik G.S. L. I. Mandelshtam i uchenie o rezonanse *Akademik L. I. Mandelshtam k 100-letiyu so dnya rozhdeniya*. Moscow, Nauka, 1979, pp.138–157.
3. Isakevich V.V., Isakevich D.V., Grunskaya L.V., R. F. Utility Model Patent No. 116,242 (30 September 2011).
4. Isakevich V.V., Isakevich D.V., R. F. Utility Model Patent No. 178, 399 (28 June 2017).
5. Isakevich D.V., Grunskaya L.V. *Russian Physics Journal* 2015, 58, pp. 1160–1166.
6. Grunskaya L.V., Isakevich V.V., Isakevich D.V., Lukyanov V.E. *Russian Physics Journal* 2017, 59, pp. 1373–1379.
7. Grunskaya L.V., Isakevich V.V., Isakevich D.V. *Gravitation and Cosmology* 2018, 24, pp. 384–392.
8. Grunskaya L.V., Isakevich V.V., Isakevich D.V. *Russian Physics Journal* 2019, 62, pp. 55–61.
9. Grunskaya L.V., Isakevich V.V., Isakevich D.V. *Russian Physics Journal* 2020, 63, pp. 34–42.
10. Grunskaya L.V., Isakevich V.V., Isakevich D.V. *Russian Physics Journal* 2021, 64, pp. 496–503.
11. Grunskaya L.V., Isakevich V.V., Isakevich D.V. *Russian Physics Journal* 2022, 65, pp. 440–449.
12. Grunskaya L.V., Isakevich V.V., Isakevich D.V. *Materials of IX All-Russian Scientific Conference on the Atmospheric Electricity* 2023, pp. 65–74.

### Авторы

**Грунская Любовь Валентиновна**, д.т.н., профессор, Владимирский государственный университет, ул. Горького, д. 87, г. Владимир, 600000, Россия.
E-mail: grunsk@vlsu.ru

**Исакевич Валерий Викторович**, к.т.н., доцент, ООО Собственный вектор, ул. Горького, д. 50, г. Владимир, 600005, Россия.
E-mail: eigenoscope@yandex.ru

**Исакевич Даниил Валерьевич**, ООО Собственный вектор, ул. Горького, д. 50, г. Владимир, 600005, Россия.
E-mail: eigenoscope@yandex.ru

**Просьба ссылаться на эту статью следующим образом:**
Грунская Л. В., Исакевич В. В., Исакевич Д. В. Физические основы свойства восприимчивости электромагнитного поля Земли к гравитационно-волновому излучению двойных звездных систем. *Пространство, время и фундаментальные взаимодействия.* 2023. № 3-4. С. 117–126. **Authors**

**Grunskaya Liubov Valentinovna**, Ph.D., Professor, Vladimir State University, Gorkogo st., 87, Vladimir, 600000, Russia.
E-mail: grunsk@vlsu.ru

**Isakevich Valery Victorovich**, Ph.D., Associate Professor, Eigenvector LLC, Gorkogo st., 50, Vladimir, 600005, Russia.
E-mail: eigenoscope@yandex.ru

**Isakevich Daniil Valeryevich**, Eigenvector LLC, Gorkogo st., 50, Vladimir, 600005, Russia.
E-mail: eigenoscope@yandex.ru

**Please cite this article in English as:**
Grunskaya L. V., Isakevich V. V., Isakevich D. V. Physical Basis of Sensitivity of the Earth's Electromagnetic Field to Gravitation. *Space, Time and Fundamental Interactions*, 2023, no. 3-4, pp. 117–126.

УДК 530.12



## ОБОБЩЕНИЕ ПРОЦЕДУРЫ СОГЛАСОВАНИЯ $C^3$

Гутьеррес-Пинерес А. К.[a,b,1], Кеведо Э.[c,d,2]

[a] Индустриальный университет Сантандера, Букараманга, CP 680002, Колумбия.
[b] Национальный автономный университет Мексики, Мехико, AP 70543, Мексика.
[c] Римский университет "Сапиенца", г. Рим, I-00185, Италия.
[d] Казахский национальный университет имени аль-Фараби, Алматы, 050040, Казахстан.

Для решения проблем, связанных с присутствием разрывов вдоль совпадающих гиперповерхностей, в данной работе мы представляем обобщение процедуры совпадения $C^3$, рассмотренной в предыдущих работах. Они требуют, чтобы решение уравнений Эйнштейна также описывало совпадающую гиперповерхность.

*Ключевые слова*: Условия соответствия, соответствие $C^3$, собственные значения кривизны.

## GENERALIZATION OF THE $C^3$ MATCHING PROCEDURE

Gutierrez-Pineres A. C.[a,b,1], Quevedo H.[c,d,2]

[a] Escuela de Fí sica, Universidad Industrial de Santander, CP 680002, Bucaramanga, Colombia.
[b] Instituto de Ciencias Nucleares, Universidad Nacional Autónoma de México, AP 70543, México, DF 04510, México.
[c] Dipartimento di Fisica and ICRA, Università di Roma "Sapienza I-00185, Roma, Italy.
[d] Institute of Experimental and Theoretical Physics, Al-Farabi Kazakh National University, Almaty 050040, Kazakhstan.

To handle the case in which discontinuities are present along the matching hypersurface, in this work, we present a generalization of the $C^3$ matching procedure discussed in previous works. It demands that a solution of Einstein's equations also describe the matching hypersurface.

*Keywords*: Matching conditions, $C^3$ matching, curvature eigenvalues.
PACS: 04.20.-q
DOI: 10.17238/issn2226-8812.2023.3-4.127-132

### Introduction

General relativity is a theory of the gravitational interaction and, in particular, should describe the gravitational field of relativistic compact objects. In this case, the spacetime can be split into two different parts, namely, the interior region described by an exact solution of Einstein's equations with a physically reasonable energy-momentum tensor and the exterior region, which corresponds to an exact vacuum solution. This implies that the spacetime can be considered as split into two regions with certain hypersurface $\Sigma$ at which the two regions should be matched.

This problem has been investigated for a long time [1]. In 1927, Darmois [2, 3] proposed that a physically meaningful matching can be obtained by demanding that the first and second fundamental forms (induced metric and extrinsic curvature, respectively) be continuous across $\Sigma$. Later on, in 1955, Lichnerowicz [4] proposed an alternative approach that turned out to be equivalent to the Darmois approach by choosing the underlying coordinates appropriately. If the fundamental forms are not

[1]E-mail: acgutierrez@correo.nucleares.unam.mx
[2]E-mail: quevedo@nucleares.unam.mx

continuous across the matching surface, Israel proposed in [5] to "cover" $\Sigma$ with a shell, whose energy-momentum tensor takes care of the discontinuities. In the case of compact objects, $\Sigma$ should be identified with the surface of the object, i.e., it is a time-like hypersurface. It then follows that at $\Sigma$, certain matching conditions should be imposed in order for the spacetime to be well defined.

Recently [6], we propose to use a $C^3$ criterion to find information about the location of the hypersurface $\Sigma$. It is defined in terms of the eigenvalues of the Riemann curvature tensor, which are invariant quantities. The idea is simple. Since the curvature tensor is a measure of the gravitational interaction, the curvature eigenvalues provide us with an invariant measure of the gravitational interaction. Since, for a compact object, one expects the spacetime to be asymptotically flat, the curvature eigenvalues should vanish at spatial infinite, and the behavior of the eigenvalues approaching the gravitational source could give some information about its borders.

In this work, we continue the investigation of the $C^3$ procedure. Based on Israel's formalism [5], we propose a general approach considering cases in which discontinuities are present along the matching surface $\Sigma$. It consists of demanding that a solution of Einstein equations also describe the 3-dimensional hypersurface $\Sigma$. In Section 1, we review in detail the main aspects of the $C^3$ matching procedure, whereas Section 2 is devoted to proposing a generalization of the $C^3$ matching procedure. Finally, in Section 3, we sum up our results.

## 1. $C^3$ matching procedure

The $C^3$ matching procedure is based on the analysis of the behavior of the Riemann curvature eigenvalues. This method was applied to study asymptotically flat spacetimes in [6]. Here, we employ the Cartan formalism of differential forms and local orthonormal tetrads to determine these eigenvalues. A local orthonormal tetrad is the simplest and most natural choice for an observer in order to perform local measurements of time, space, and gravity. So, let us choose the local ortho-normal tetrad $\vartheta^a$, $a = 0, ..., 3$ such that

$$ds^2 = g_{\mu\nu} dx^\mu \otimes dx^\nu = \eta_{ab} \vartheta^a \otimes \vartheta^b \ , \tag{1.1}$$

with $\eta_{ab} = \mathrm{diag}(-1, 1, 1, 1)$, and $\vartheta^a = e^a{}_\mu dx^\mu$. The first and second Cartan equations

$$d\vartheta^a = -\omega^a{}_b \wedge \vartheta^b \ , \tag{1.2}$$

$$\Omega^a{}_b = d\omega^a{}_b + \omega^a{}_c \wedge \omega^c{}_b = \frac{1}{2} R^a{}_{bcd} \vartheta^c \wedge \vartheta^d \tag{1.3}$$

allow us to compute the components of the Riemann curvature tensor $R_{abcd}$ in the local orthonormal frame $\vartheta^a$. Moreover, we define the Ricci tensor and the scalar curvature as $R_{ab} = R^c{}_{acb}$ and $R = R^a{}_a$, respectively. Furthermore, we introduce the bivector representation that consists in defining the curvature components $R_{abcd}$ as the components of a $6 \times 6$ matrix $\mathbf{R}_{AB}$ according to the convention proposed in [7] (Chapter 14, Section 14.1, pp. 333-334), which establishes the following correspondence between tetrad $ab$ and bivector indices $A$:

$$01 \to 1 \ , \quad 02 \to 2 \ , \quad 03 \to 3 \ , \quad 23 \to 4 \ , \quad 31 \to 5 \ , \quad 12 \to 6 \ . \tag{1.4}$$

Hence, the Riemann tensor can be represented as a symmetric matrix $\mathbf{R}_{AB}$ with 21 independent components. The algebraic Bianchi identity $R_{a[bcd]} = 0$, which in bivector representation reads

$$\mathbf{R}_{14} + \mathbf{R}_{25} + \mathbf{R}_{36} = 0 \tag{1.5}$$

reduces the number of independent components to 20. Furthermore, Einstein's equations, in geometric units such that $k = 8\pi G c^{-4}, G = c = 1$,

$$R_{ab} - \frac{1}{2} R \eta_{ab} = k \, T_{ab} \ , \tag{1.6}$$

can be written explicitly in terms of the curvature components $\mathbf{R}_{AB}$, resulting in a set of ten algebraic equations that relate the components of $\mathbf{R}_{AB}$ and $T_{ab}$. Consequently, only ten components $\mathbf{R}_{AB}$ are algebraic independent and can be arranged in the $6 \times 6$ curvature matrix in the following way

$$\mathbf{R}_{AB} = \begin{pmatrix} \mathbf{M}_1 & \mathbf{L} \\ \mathbf{L} & \mathbf{M}_2 \end{pmatrix}, \tag{1.7}$$

where

$$\mathbf{L} = \begin{pmatrix} \mathbf{R}_{14} & \mathbf{R}_{15} & \mathbf{R}_{16} \\ \mathbf{R}_{15} - kT_{03} & \mathbf{R}_{25} & \mathbf{R}_{26} \\ \mathbf{R}_{16} + kT_{02} & \mathbf{R}_{26} - kT_{01} & -\mathbf{R}_{14} - \mathbf{R}_{25} \end{pmatrix},$$

and $\mathbf{M}_1$ and $\mathbf{M}_2$ are $3 \times 3$ symmetric matrices

$$\mathbf{M}_1 = \begin{pmatrix} \mathbf{R}_{11} & \mathbf{R}_{12} & \mathbf{R}_{13} \\ \mathbf{R}_{12} & \mathbf{R}_{22} & \mathbf{R}_{23} \\ \mathbf{R}_{13} & \mathbf{R}_{23} & -\mathbf{R}_{11} - \mathbf{R}_{22} + k\left(\frac{T}{2} + T_{00}\right) \end{pmatrix},$$

$$\mathbf{M}_2 = \begin{pmatrix} -\mathbf{R}_{11} + k\left(\frac{T}{2} + T_{00} - T_{11}\right) & -\mathbf{R}_{12} - kT_{12} & -\mathbf{R}_{13} - kT_{13} \\ -\mathbf{R}_{12} - kT_{12} & -\mathbf{R}_{22} + k\left(\frac{T}{2} + T_{00} - T_{22}\right) & -\mathbf{R}_{23} - kT_{23} \\ -\mathbf{R}_{13} - kT_{13} & -\mathbf{R}_{23} - kT_{23} & \mathbf{R}_{11} + \mathbf{R}_{22} - kT_{33} \end{pmatrix},$$

with $T = \eta^{ab}T_{ab}$. This is the most general form of a curvature tensor that satisfies Einstein's equations with an arbitrary energy-momentum tensor. The eigenvalues $\lambda_n$ $(n = 1, \cdots, 6)$ of the matrix $\mathbf{R}_{AB}$ are known as the curvature eigenvalues.

The invariant character of the curvature eigenvalues allows us to apply them in many different physical situations and configurations. In particular, we here use the eigenvalues to match asymptotically flat solutions of the Einstein equation to its interior counterpart describing a material source of the gravitational field. In the $C^3$ matching approach, the matching surface $\Sigma$ is determined by the matching radius, $r_{match}$, defined as

$$r_{match} \in [r_{rep}, \infty) \ , \quad r_{rep} = \max\{r_l\} \ , \tag{1.8}$$

where $r_l$ $(l = 1, 2, ...)$, with $0 < r_l < \infty$, represents the set of solutions of the equation

$$\left.\frac{\partial \lambda_n^+}{\partial r}\right|_{r=r_l} = 0 \ , \tag{1.9}$$

with $\lambda_n^+$ being the curvature eigenvalues of the manifold $(\mathcal{M}^+, \mathbf{g}^+)$, which is assumed to be asymptotically flat, i.e., there exists a spatial coordinate $r$ such that

$$\lim_{r\to\infty} \mathbf{g}^+ = \eta \tag{1.10}$$

where $\eta$ represents the Minkowski metric.

**Theorem 1.1.** *Let $(\mathcal{M}^-, \mathbf{g}^-)$ and $(\mathcal{M}^+, \mathbf{g}^+)$ be an arbitrary and an asymptotically flat spacetime, which satisfy Einstein equations, and let $\lambda_n^-$ and $\lambda_n^+$ be the curvature eigenvalues of $(\mathcal{M}^-, \mathbf{g}^-)$ and $(\mathcal{M}^+, \mathbf{g}^+)$, respectively. Then, we say that $\mathcal{M}^-$ and $\mathcal{M}^+$ can be matched at the surface $\Sigma$, determined by the matching radius $r_{match}$ as defined in Eq.(1.8), if the necessary and sufficient condition*

$$[\lambda_n] \equiv \lambda_n^- - \lambda_n^+ = 0, \quad n = 1, \cdots, 6 \tag{1.11}$$

*is satisfied.*

From a pragmatical point of view, the interior region of compact objects corresponds to the spacetime $(\mathcal{M}^-, \mathbf{g}^-)$ whereas the exterior region is described by $(\mathcal{M}^+, \mathbf{g}^+)$. Then, $r_l$ represent the extrema of the exterior eigenvalues $\lambda_n^+$ and the repulsion radius $r_{rep}$ corresponds to the extremum $r_l$ with the maximum value. In other words, $r_{rep}$ is the value of $r$, where the first extremum of $\lambda_n^+$ is encountered when approaching the origin of coordinates $r = 0$ coming from infinity. The spacetimes $(\mathcal{M}^+, \mathbf{g}^+)$ and $(\mathcal{M}^-, \mathbf{g}^-)$ can be matched at the matching radius $r_{match}$, which can be chosen at any value of $r$ located between the repulsion radius $r_{rep}$ and infinity.

## 2. $C^3$ matching across spherically symmetric thin shells

In general relativity, the interior of spacetimes corresponding to a spherically symmetric perfect fluid can be described by the energy-momentum tensor

$$\mathbf{T}^{\alpha\beta} = (\rho + p)\mathbf{V}^{\alpha}\mathbf{V}^{\beta} + p\mathbf{g}^{\alpha\beta} \tag{2.1}$$

where $\rho$ and $p$ are the energy density and the pressure of the fluid, respectively, and $\mathbf{V}$ is the velocity of the fluid, which we choose as the comoving velocity $\mathbf{V}_{\alpha} = (-1, 0, 0, 0)$.

According to Birkhoff's theorem, the exterior spacetime must be described by the Schwarzschild metric

$$\mathbf{g}^{+} = -\left(1 - \frac{2m}{r}\right)\mathrm{d}\, t \otimes \mathrm{d}\, t + \left(1 - \frac{2m}{r}\right)^{-1}\mathrm{d}\, r \otimes \mathrm{d}\, r + r^2(\mathrm{d}\,\theta \otimes \mathrm{d}\,\theta + \sin^2\theta\, \mathrm{d}\,\phi \otimes \mathrm{d}\,\phi). \tag{2.2}$$

Furthermore, we choose the matching hypersurface as a sphere of constant radius. For the $C^3$ approach we only need to calculate the curvature eigenvalues. We choose the orthonormal tetrad $\vartheta^a$ as

$$\vartheta^0 = \left(1 - \frac{2m}{r}\right)^{1/2}\mathrm{d}\, t\ ,\ \vartheta^1 = \left(1 - \frac{2m}{r}\right)^{-1/2}\mathrm{d}\, r\ ,\ \vartheta^2 = r\,\mathrm{d}\,\theta\ ,\ \vartheta^3 = r\sin\theta\ \mathrm{d}\,\phi\ . \tag{2.3}$$

A straightforward computation shows that the curvature matrix $\mathbf{R}_{AB}$ is diagonal and the eigeinvalues are

$$\lambda_2^+ = \lambda_3^+ = -\lambda_5^+ = -\lambda_6^+ = m/r^3, \quad \lambda_1^+ = -\lambda_4^+ = -2m/r^3. \tag{2.4}$$

To perform the $C^3$ procedure, we first find the extrema of the exterior eigenvalues. As we can see, none of the Schwarzchild eigenvalues has an extremum. This means that there is no repulsion radius $r_{rep}$, which indicates in the approach the smallest sphere at which the matching can be carried out. Consequently, there is no repulsion region in the Schwarzschild spacetime that should be covered by an interior solution, which is the conceptual background of the $C^3$ approach. Then, the matching radius can be located anywhere outside the central singularity, i.e., $r_{match} \in (0, \infty)$.

In previous references (See [6, 8]), it was shown that in the case of spherically symmetric perfect fluids, the vanishing of the energy-momentum tensor on the matching surface is a necessary condition to perform the matching procedure; this suggests that the jump of the curvature eigenvalues across the matching surface vanishes. Recently, we have glimpsed particular solutions corresponding to perfect fluids in which this does not occur. In this work, we construct a formalism that allows the $C^3$ matching in the case of discontinuities across the matching surface, i.e., $\lambda_n^+ \neq \lambda_n^-$ on $\Sigma$ for at least one value of $n$.

We will use Israel's formalism [5] as a conceptual guide that allows the existence of discontinuities of the first and second fundamental forms by introducing an effective energy-momentum tensor on the matching surface $\Sigma$ so that it can be intepreted as a infinitesimal matter shell that join the interior and exterior spacetimes. To this end, let us consider the jump of the eigenvalues across $\Sigma$ as

$$[\lambda_n] = \lambda_n^- - \lambda_n^+\ . \tag{2.5}$$

In the case of a matching between an interior perfect fluid solution and the exterior Schwarzschild vacuum solution, we have shown that the $C^3$ procedure implies that $\rho$ and $p$ should be zero on $\Sigma$. When these conditions are not satisfied, let us define the surface density $\sigma$ and pressure $\pi$ as

$$\sigma = \rho|_{\Sigma}\ , \qquad P = p|_{\Sigma}\ . \tag{2.6}$$

Then, since in the case of discontinuities we have that $[\lambda_n] \neq 0$, it follows that $\sigma \neq 0$ and $P \neq 0$, in general. This is equivalent to saying that the explicit values of $[\lambda_n]$ should contain information about the physical quantities $\sigma$ and $P$. For this reason, we assume that $[\lambda_n]$ is arbitrary in value but finite.

The question is now whether $\sigma$ and $P$ can be used to construct a realistic matter shell on $\Sigma$. To this end, consider the jump of the Einstein tensor on $\Sigma$, i. e.,

$$[G_{ij}] = G^-_{ij} - G^+_{ij} \ , \quad G^\pm_{ij} = \frac{\partial x^\mu_\pm}{\partial \xi^i} \frac{\partial x^\nu_\pm}{\partial \xi^j} G^\pm_{\mu\nu} \ , \tag{2.7}$$

where $\xi^i$ are the coordinates of the surface $\Sigma$ and $x^\mu_\pm$ are the coordinates of the interior and exterior spacetimes, respectively. Then, $G^\pm_{ij}$ is the Einstein tensor induced on $\Sigma$. Furthermore, we introduce an energy-momentum tensor $S_{ij}$ on $\Sigma$ as

$$[G_{ij}] = kS_{ij} \ . \tag{2.8}$$

Certainly, it is always possible to introduce algebraically an energy-momentum tensor in this way. However, the essential point is whether $S_{ij}$ is physically meaningful. To guarantee the fulfillment of this condition, we demand that $S_{ij}$ be induced by the energy-momentum tensors of the interior and exterior spacetimes and be in agreement with their physical significance. Then, in the case of the perfect fluid we are considering here, we demand that

$$S_{ij} = [T_{ij}] = T^-_{ij} - T^+_{ij} = (\sigma + P)u_i u_j + P\gamma_{ij} \ , \tag{2.9}$$

where $T^\pm_{ij}$ are the energy-momentum tensors and $\gamma_{ij} = \gamma^\pm_{ij}$ is the metric tensor induced on $\Sigma$, respectively.

In summary, in the case of discontinuities, we will say that an interior spacetime can be matched with an exterior one along a boundary shell located on $\Sigma$, if there exist a density $\sigma$ and a pressure $P$, satisfying the induced Einstein equations (2.8) and (2.9) and the boundary condition (2.6).

In the case of spherical symmetry the coordinates on both sides of the boundary can be chosen as $x^\mu_\pm = (t, r, \theta, \phi)$ and on the matching surface as $\xi^i = (t, \theta, \phi)$. Then, all the components of the quantities $\partial x^\mu / \partial \xi^i$ are constant and the induced tensors can be calculated in a straightforward way. We obtain for the jump of the eigenvalues along the matching surface $r = r_{\rm match}$ the following expressions

$$[\lambda_2] = [\lambda_3] = [\lambda_4] = 0 \ , \quad [\lambda_1] = [\lambda_5] = [\lambda_6] = 4\pi\sigma \ , \tag{2.10}$$

which agrees with the result that on the matching surface the pressure vanishes. Furthermore, the jump of components of the induced Einstein tensor can be expressed as

$$[G_{ij}] = 2k[\lambda_1]u_i u_j = k\sigma u_i u_j \ , \quad u^i = (-1, 0, 0) \ . \tag{2.11}$$

It is then easy to see that on the matching surface $r = r_{\rm match}$, the induced Einstein equations for dust are satisfied, proving that, in fact, a realistic dust shell can be introduced that allows us to match, in the framework of the $C^3$ matching procedure, perfect fluids with the exterior Schwarzschild spacetime.

## 3. Conclusions

In this work, we have analyzed the problem of matching spherically symmetric solutions of Einstein equations. n particular, we limit ourselves to the case of interior solutions corresponding to perfect static fluids. We know that in specific perfect fluid solutions, the energy density shows a discontinuity across the matching surface; to handle the case in which discontinuities are present along the matching surface $\Sigma$, we propose in this work a generalization of the $C^3$ matching procedure. It consists of demanding that a solution of Einstein equations also describe the 3-dimensional hypersurface $\Sigma$. In fact, we consider the induced Einstein tensor on $\Sigma$ and show that it can be represented as a realistic energy-momentum tensor that describes the matter inside a boundary shell located on $\Sigma$. In the cases considered in this work, it turned out that the boundary corresponds to a dust shell. For more general interior solutions, we expect to obtain shells with more intricate internal structures.

### Список литературы/References

1. Lake K. Revisiting the Darmois and Lichnerowicz junction conditions. *Gen. Rel. Grav.*, 2017, **49** 134
2. Darmois G. “Les equations de la gravitation einsteinienne.” *Mémorial de Sciences Mathématiques, 1927, Fascicule XXV*
3. Darmois G. *Les équations de la gravitation einsteinienne.* (Gauthier-Villars, 1927.)
4. Lichnerowicz A. *Théories Relativistes de la Gravitation et de l Electromagnétisme* (Masson, Paris, 1955.)
5. Israel W. Singular hypersurfaces and thin shells in general relativity. *Il Nuovo Cimento B, 1966, (1965-1970)* **44** 1–14
6. Gutierrez-Pineres A. C., Quevedo H. $C^3$ matching for asymptotically flat spacetimes. *Class. Quantum Grav.*, 2019, **36** 135003
7. Misner C. W., Thorne K. S., Wheeler J. A. *Gravitation* (Princeton University Press, 2017.)
8. Gutierrez-Pineres A. C., Quevedo H 2022. Darmois matching and $C^3$ matching. *Class. Quantum Grav.* **39** 035015

### Авторы

**Гутьеррес-Пинерес К. Антонио**, Физический факультет, Индустриальный университет Сантандера, CP 680002, Букараманга, Колумбия.
E-mail: acgutierrez@correo.nucleares.unam.mx

**Кеведо Эрнандо**,Институт ядерных наук, Национальный автономный университет Мексики, AP 70543, Мехико, Мексика.
E-mail: quevedo@nucleares.unam.mx

### Просьба ссылаться на эту статью следующим образом:

Гутьеррес-Пинерес А. К., Кеведо Э. Обобщение процедуры согласования $C^3$. *Пространство, время и фундаментальные взаимодействия.* 2023. № 3-4. С. 127–132.

### Authors

**Gutierrez-Pineres Antonio C.**, Escuela de Fisica, Universidad Industrial de Santander, CP 680002, Bucaramanga, Colombia.
E-mail: acgutierrez@correo.nucleares.unam.mx

**Quevedo Hernando**, instituto de Ciencias Nucleares, Universidad Nacional Autónoma de México, AP 70543, Ciudad de México 04510, Mexico.
E-mail: quevedo@nucleares.unam.mx

### Please cite this article in English as:

Gutierrez-Pineres A. C., Quevedo H. Generalization of the $C^3$ matching procedure. *Space, Time and Fundamental Interactions*, 2023, no. 3-4, pp. 127–132.

УДК 524.8, 533.9, 620.9



## ИМИТАЦИЯ ИЗВЛЕЧЕНИЯ КИНЕТИЧЕСКОЙ ЭНЕРГИИ ИЗ ЧЕРНОЙ ДЫРЫ КЕРРА–НЬЮМАНА

Измайлов Г. Н.[a,1], Озолин В. В.[a,2]

[a] Московский авиационный институт (национальный исследовательский университет), Волоколамское ш., д. 4, г. Москва, 125993, Россия.

Рассматриваются некоторых теоретические и экспериментальные методы исследования преобразования кинетической энергии черной дыры в энергию релятивистских струй ионизованного газа, генерируемых заряженной вращающейся черной дырой после поглощения ею звездного вещества. Показан аналог эффекта увлечения системы отсчета при ее поступательном движении, который связан с явлением гравитомагнетизма при вращении массы. Сопоставлены уравнения Максвелла для электромагнитного поля и уравнения гравитационного поля, создаваемого не только поступательным движением массы, но и ее вращением. Показана экспериментальная достоверность эффекта Лензе – Тирринга в случае медленных вращений. Обращено внимание на эффекты влияния быстрых вращений массивных объектов (черных дыр) на движение пробных частиц. Представлены различные механизмы преобразования, в которых эффективность преобразования высока, и отсутствуют побочные отходы. Указана аналогия энергетики преобразования потенциальной энергии водяной струи в кинетическую энергию вращения гидротурбины энергетике исследуемых космических процессов. Отмечена как теоретическая, так и практическая значимость исследований.

*Ключевые слова*: Гравитомагнетизм, черная дыра, метрика Керра–Ньюмана, релятивистские струи, плазма, эффективность трансформации энергии.

## SIMULATION OF KINETIC ENERGY EXTRACTION FROM A KERR – NEWMAN BLACK HOLE

Izmailov G. N.[a,1], Ozolin V. V.[a,2]

[a] Moscow Aviation Institute (National Research University), Volokolamskoye sh., 4, Moscow, 125993, Russia.

This synopsis presents theoretical and experimental methods for studying the conversion of the kinetic energy of black holes into the energy of relativistic jets of ionized gas developing after the absorption of stellar matter by a rotating black hole. An analogue between the drag effect of the reference system during its translational motion and the phenomenon of gravitomagnetism during mass rotation is shown. Maxwell's equations for the electromagnetic field are compared with the equations for the gravitational field created not only by the translational motion of the mass, but also by its rotation. It is pointed out the Lense—Thirring effect experimental reliability in the case of slow rotations. Attention is drawn to the effects of rapid rotations of massive objects (black holes) on the motion of test particles. The high efficiency and lack of side waste for such transformation is noted. Various transformation mechanisms are discussed. An analogy is indicated between extracting the kinetic energy of a rotating black hole and converting it into the energy of a relativistic jet and converting the potential energy of a water jet into the kinetic energy of rotation of a hydraulic turbine (Francis turbine). The presented innovative methods are under development.

*Keywords*: Gravitomagnetism, black hole, Kerr–Newman metric, relativistic jets, plasma, magnetic reconnection, conversion energy efficiency.

PACS: 04.70-s, 95.30 Qd, 95.30 Sf

DOI: 10.17238/issn2226-8812.2023.3-4.133-146

[1]E-mail: izmailov@mai.ru

[2]E-mail: ozolinvv@mai.ru

**Введение**

Различие классической и современной точек зрения на природу гравитации привело к постановке современных прецизионных экспериментов и открытию принципиально новых возможностей передачи кинетической энергии. Вначале обсудим эти точки зрения.

И.Ньютон писал: *"Гравитация должна быть врожденной, присущей и существенной для Материи, чтобы одно тело могло воздействовать на другое на расстоянии через Вакуум, без посредства какой-либо другой вещи, через которую их Действие и Сила могут быть переданы от одного тела к другому"*. Таким образом, в теории гравитации Ньютона источником является только неподвижная масса. Напротив, А. Эйнштейн отрицал, что существует какая-либо фоновая евклидова система отсчета, простирающаяся по всему пространству. Нет и такой вещи, как сила гравитации, есть только структура самого пространствовремени. В общей теории относительности источником кривизны пространствовремени кроме *плотности массы (определяемой через полную энергию)* служит *плотность импульса, потоки энергии и импульса, давление и напряжения в среде.* То, что энергия гравитационного поля возвращается в виде создания добавки в гравитационное поле указывает на нелинейность уравнения в сильных гравитационных полях. На элементарном языке это звучит как "гравитация порождает гравитацию". [1, 2]. Общая теория относительности определяет несколько источников искривления пространствовремени в дополнение к массе, что отражено в уравнении поля Эйнштейна

$$R_{\mu\nu} - \frac{1}{2} g_{\mu\nu} R + \lambda g_{\mu\nu} = \frac{8\pi G}{c^4} T_{\mu\nu} \ . \tag{0.1}$$

В уравнении $R_{\mu\nu}$ - тензор Риччи, определяемый симметричным метрическим тензором $g_{\mu\nu}$, $R$ -скаляр, образованный из $R_{\mu\nu}$, $\lambda$ - космологическая постоянная (поправка А.А. Фридмана), $T_{\mu\nu}$ - тензор энергии-импульса материи; с - скорость света в вакууме, $G$ - гравитационная постоянная Ньютона. В ОТО тензор $g_{\mu\nu}$ соответствует присутствию гравитационных масс, что выражается в отличие от единиц диагональных элементов матрицы и неравенству нулю недиагональных. *Правая часть уравнения* — соответствует мере плотности энергии, импульса и наличия давления в среде — всего того, что создает гравитацию.

Включение импульса в качестве источника гравитации в предположении, что для слабой гравитации пространствовремя можно разбить на 3+1 пространство и время, приводит к предсказанию, что движущиеся или вращающиеся массы могут генерировать поля, аналогичные магнитным полям, создаваемым движущимися зарядами. Это явление известно как гравитомагнетизм. При этом, расщеп ление $4D$ пространствовремени на 3+1 предполагает, что трехмерное пространство искривлено, а не евклидово; его метрика $g_{jk}$ (в соответствующей системе координат) — это просто пространственная часть метрики $4D$ пространствовремени $\mathbf{g}_{\alpha\beta}$. В этом искривленном $3D$ - пространстве определены два гравитационных потенциала: "гравитоэлектрический" скалярный потенциал $\Phi$, который по сути является время-временной частью $\mathbf{g_{00}}$ пространствовременной метрики; и "гравитомагнитный" вектор ный потенциал $\vec{J}_g$, который по сути - времяпространственная часть $\mathbf{g_{0j}}$ пространствовременной метрики, что аналогично разделению электромагнитного четыре-вектора потенциала на электрический потенциал $\Phi = -\mathbf{A_0}$ и магнитный векторный потенциал $\vec{A} = A_j$. В адекватном приближении можно показать, что материя, движущаяся через гравитомагнитное поле, подвержена так называемым эффектам увлечения системы отсчета, что аналогично явлению действия электромагнитной индукции между движущимися зарядами.

Для демонстрации эффекта рассмотрим две неподвижные массивные пластины (продольные линии), между которыми на равных расстояниях расположена частица — центральная крупная точка посередине) (рис.1). Из-за симметрии установки результирующая сила, действующая на центральную частицу, равна нулю. Теперь предположим, что вместо неподвижных пластин есть потоки массивных частиц, которые имеют равные и противоположно направленные скорости -$\vec{v}$ и +$\vec{v}$ относительно покоящейся пробной частицы, находящейся посредине (рис.1).

Положим также, что скорости частиц малы ($v << c$). Опять же, вследствие зеркальной симметрии пробная частица останется неподвижной.

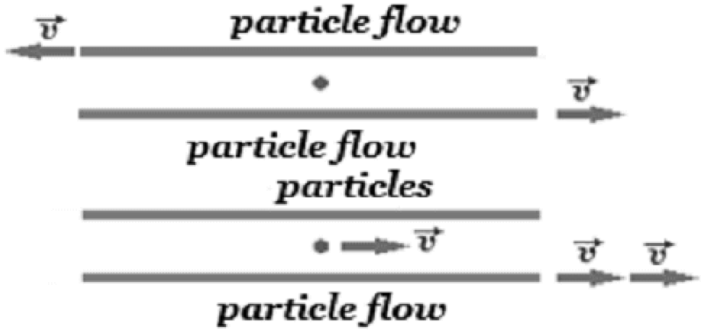


**Рис. 1.** Действие двух параллельных бесконечно протяженных потоков массивных частиц на пробную частицу.

Если наблюдатель расположил свою систему отсчета в верхнем потоке, то пробная частица имеет скорость $+\vec{v}$ вправо, а частицы нижнего потока имеют скорость $+2\vec{v}$. Поскольку теперь частицы нижнего потока движутся быстрее, то их массовая энергия стала больше, а у верхнего потока — меньше. Вследствие лоренцевого сокращения длины вдоль движения плотность частиц в нижнем потоке увеличилась. Возросло также и давление между частицами в нижнем потоке. В результате увеличилась активная масса частиц нижнего потока, их гравитационное поле увеличилось, и пробная частица должна сдвинуться вниз. Однако, хотя изменилась произвольно введенная система отчета, ситуация физически не изменилась. Поэтому пробная частица не притягивается к нижнему потоку из-за дополнительной, зависящей от скорости, силы, которая служит для отталкивания частицы, движущейся в том же направлении, что и нижний поток. Ситуация подобна действию силы Лоренца. Новая сила — сила Лензе – Тирринга имеет вид

$$\vec{F}_{LT} = m\vec{E}_g + m\vec{v} \times 2\vec{B}_g. \tag{0.2}$$

Этот зависящий от скорости гравитационный эффект называется гравитомагнетизмом [3].Аналогич ная логика была использована для демонстрации происхождения электромагнетизма [4]. Хорошо известно, что для статического гравитационного поля существует подобие - уравнение Пуассона потенциала электростатического поля

$$\nabla^2\Phi = -\frac{1}{\varepsilon_0}\rho, \tag{0.3}$$

где $\varepsilon_0$ электрическая постоянная, $\rho$ плотность заряда в точке наблюдения.

Изменения электромагнитных полей связаны. Если изменяется магнитное поле (или его поток), то создается вихревое электрическое поле (закон Фарадея). При изменении электрического поля возникает магнитное поле (закон Ампера - Максвелла). Трансформация полей объясняется в СТО использованием преобразования Лоренца. Р. Фейнман [4] (том II, в главах 13-6 его "Лекций по физике", доступных в Интернете) показал, как можно вывести магнитное поле, применяя преобразования Лоренца специальной теории относительности к движущимся зарядам.)

Согласно ОТО, гравитационное поле, создаваемое вращающимся объектом (или любой вращающейся массой-энергией), в частном предельном случае может быть описано уравнениями, которые имеют тот же вид, что и в классическом электромагнетизме. Исходя из основного уравнения ОТО, уравнения поля Эйнштейна, и предполагая слабое гравитационное поле или достаточно плоское пространствовремя, можно вывести гравитационные аналоги уравнений Максвелла для электромагнетизма, называемые "уравнениями GEM". Сопоставим уравнения GEM (гравитоэлектромагнетизма) с уравнениями Максвелла: [11] [12]

## 1. Уравнения гравитоэлектромагнетизма и электромагнетизма

Таблица 1

| **Уравнения гравитомагнетизма** | **Уравнения Максвелла** |
|---|---|
| $\vec{\nabla} \cdot \vec{E}_g = -4\pi G\rho_g$ | $\vec{\nabla} \cdot \vec{E} = (1/\varepsilon_0)\rho$ |
| $\vec{\nabla} \cdot \vec{B}_g = 0$ | $\vec{\nabla} \cdot \vec{B} = 0$ |
| $\vec{\nabla} \times \vec{E}_g = -\frac{\partial \vec{B}_g}{\partial t}$ | $\vec{\nabla} \times \vec{E} = -\frac{\partial \vec{B}}{\partial t}$ |
| $\vec{\nabla} \times \vec{B}_g = -\frac{4\pi G}{c^2}\vec{J}_g$ | $\vec{\nabla} \times \vec{B} = \frac{1}{\varepsilon_0 c^2}\vec{J} + \frac{1}{c^2}\frac{\partial E}{\partial t}$ |
| $\vec{\nabla} \cdot \vec{J}_g + \frac{\partial \rho_g}{\partial t} = 0$ | $\vec{\nabla} \cdot \vec{J} + \frac{\partial \rho}{\partial t} = 0$ |

- $\vec{E}_g$ — напряженность гравитостатического поля ($g$ - обычного гравитационного поля), в системе СИ м$\cdot c^{-2}$
- $\vec{E}$ — напряженность электрического поля, в системе СИ (кг/Кл)м$\cdot c^{-2}$
- $\vec{B}_g$ "индукция"гравимагнитного поля, в системе СИ с$^{-1}$
- $\vec{B}$ — индукция магнитного поля, в системе СИ (кг/Кл)$c^{-1}$
- $\rho_g$ — плотность массы, в системе СИ кг$\cdot$м$^{-3}$
- $\rho$ — плотность заряда, в системе СИ Кл$\cdot$м$^{-3}$
- $\vec{J}_g$ плотность тока массы или поток массы ($\vec{J}_g = \rho_g \vec{v}$, где $\vec{v}$— скорость потока массы), в системе СИ кг$\cdot$м$^{-2}\cdot$ с$^{-1}$
- $\vec{J}$ — плотность электрического тока, в системе СИ Кл$\cdot$м$^{-2}\cdot$ с$^{-1}$
- $G$ — гравитационная постоянная ($G$= 6,672 $\cdot 10^{-11}$кг$^{-1}\cdot$м$^3\cdot$с$^{-2}$)
- $\varepsilon_0$ — электрическая прстоянная вакуума ($\varepsilon_0 = 8,854 \cdot (10^{-12} \cdot$ кг$^{-1}$с$^2)$
- $c$ — скорость распространения гравитации и скорость света в вакууме ($c = 2,998 \cdot 10^8$ м $\cdot^{-1}$).

## 2. Экспериментальные подтверждения эффектов гравитоэлектромагнетизма

Таким образом, гравитация вокруг вращающегося тела (например, Земли) имеет три аспекта: поле $\vec{g}$, поле $\vec{B}_g$ и кривизна пространства — уравнения (4), (5), (6); каждый можно определить по прецессии гироскопа относительно далеких звезд.

*1.* Монопольный гравитоэлектрический момент определен массой тела $M$

$$\vec{g} = -\frac{GM}{r^2} \cdot \vec{e}_r. \tag{2.1}$$

*2.* Момент гравитомагнитного диполя - его угловым моментом вращения $\vec{L}$

$$\vec{B}_g = \frac{2G}{c^2} \frac{\left[\vec{L} - 3(\vec{L} \cdot \vec{e}_r) \cdot \vec{e}_r\right]}{r^3} \quad . \tag{2.2}$$

*3.* Кривизна пространства вокруг сферического тела постоянна во времени и может быть описана в пределе слабого поля Шварцшильда. Его пространственная метрика

$$ds^2 = (1 + \frac{r_g}{r})dr^2 + r^2(d\theta^2 + \sin^2 d\phi^2)\ , \quad r_g := \frac{2GM}{c^2} \ll r. \tag{2.3}$$

Аналогия гравитация $\Longleftrightarrow$ электромагнетизм особенно замечательна по своим достоинствам в случае систем со слабой гравитацией и малых скоростей ($v << c$): эксперименты LAGEOS [5], GRAVITY PROBE B [6], GINGER [7]. Для таких систем существенную роль играет "гравитоэлектрическое"поле $\vec{g}$ и "гравитомагнитное"поле $\vec{B_g}$, которое может быть образовано из $\vec{v}$ и $\vec{J_g}$ способом, похожим на разделение полей в электромагнетизме:

$$\vec{g} = -\vec{\nabla}\Phi, \quad \vec{B_g} = \vec{\nabla} \times \vec{J_g}, \quad \Phi = -\frac{1}{2}(1 + g_{00})c^2, \quad J_{g_j} = g_{0_j}. \tag{2.4}$$

В эксперименте $GravityProbeB$ измерялась прецессия спутника под действием гравитомагнитного поля — эффект Лензе - Тирринга с точностью лучшей, чем 1% [6]. Заметим, что если рассматривать гравитомагнитный эффект, испытываемый Землей при ее движении вокруг Солнца, то $\vec{g}_\odot$ - ньютоново ускорение свободного падения, создаваемое Солнцем, $\vec{B_g}$ — силовое поле, созданное вращением Солнца на орбите Земли, о котором Ньютон не догадывался, поскольку в динамике Солнечной системы его влияние на движение Земли в $10^9$ раз меньше, чем гравитостатическое влияние Солнца и примерно в $10^{12}$ меньше ньютонова ускорения свободного падения на Земле $\vec{g}_\oplus$.

### 3. Астрофизические подтверждения новых гравитационных эффектов

Этот подтвержденный гравитационный эффект достаточно слаб в поле Земли, тем не менее он должен проявляться в астрофизике как источник энергии и соответствующих сил для объяснения недавно обнаруженных струй из квазаров и ядер галактик. Примерами могут служить также слияние нейтронных звезд, слияния галактик, поглощение черной дырой (ЧД) галактики, излучение вращающейся ЧД. Для объяснения большинства астрофизических эффектов (таких как слияние нейтронных звезд и результирующее излучение струй - джетов; джетов релятивистких газов из черных дыр; струй релятивистского газа из эллиптической галактики Hercules A, причем измеренный размер джета около двух солнечных систем; анализ данных второго гравитационно-волнового события LIGO (GW 151226), показавший, что сверхновая может оказать сильное воздействие на созданную ею черную дыру (удар при коллапсе со скоростью $v_k$ ~50км/с) [8], — нужно новое понимание энергетики процессов генерации джетов. Опуская технические детали, отметим, что одним из последних ярких примеров истока кинетической энергии из чрной дыры явилось исторически первое изображение центральной сверхмассивной черной дыры M87, масса которой в 6,5 миллиардов раз больше солнечной и расположенной на расстоянии 55 миллионов световых лет от Земли, и изображение мощных струй, выходящих из сверхмассивной ЧД в центре галактики Мессье 87 (рис.2) [9, 10]. Чтобы понять, что струи питаются гравитационной энергией сверхмассивной ЧД в ядре эллиптической галактики потребовались значительные усилия со стороны теоретиков.

Метрика вращающейся и заряженной черной дыры в координатах Керра-Линдквиста [1] имеет вид

$$ds^2 = -\frac{\Delta}{\rho^2}\left(dt - a\sin^2\theta\, d\phi\right)^2 + \frac{\sin^2\theta}{\rho^2}\left((r^2 + a^2)d\phi - ac\, dt\right)^2 + \frac{\rho^2}{\Delta} + \rho^2 d\theta^2, \tag{3.1}$$

где $(r, \theta, \phi)$ - система обычных сферических координат, $a := J/Mc; \rho^2 := r^2 + a^2\cos^2\theta, \Delta := r^2 - r_S r + a^2 + r_Q^2; r_S := 2GM/c^2; r_Q^2 := MQ^2/4\pi\varepsilon_0 c^4$. $c$ – скорость света, $G$ – гравитационная постоянная,$\varepsilon_0$ – электрическая постоянная вакуума, $Q$ - заряд ЧД, $J$ – угловой момент ЧД, $M$ – масса ЧД.Все три параметра — $Q$, $M$, $r_S$ имеют размерность длины. При этом соблюдается условие $a^2 + r_Q^2 \leq r_S^2$, т.е. ЧД не имеет большого электрического заряда, а ее вращение незначительно. В дальнейшем все эффекты рассматриваются в этой метрике.

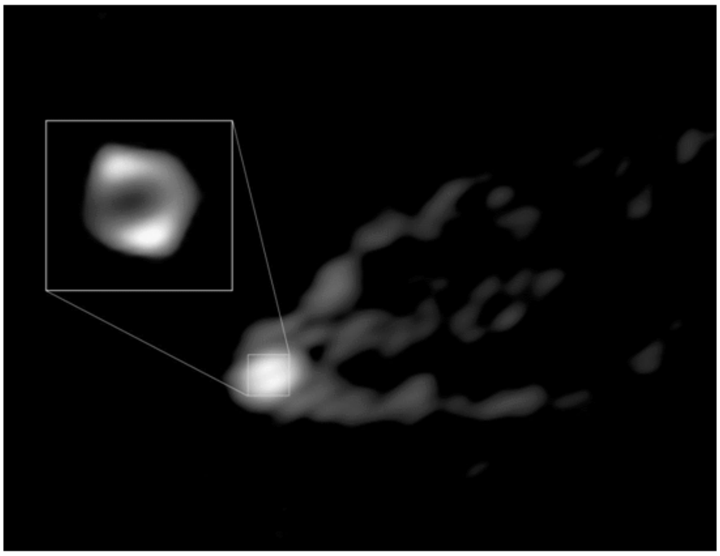

**Рис. 2.** рис. 2 Изображение мощных струй, выходящих из сверхмассивной черной дыры в центре галактики Мессье 87 ( масса ЧД в 6,5 миллиардов раз больше $M_{\odot}$) (Image credit: R.-S. Lu (SHAO), E. Ros (MPIfR), S. Dagnello (NRAO/AUI/NSF))

.

Рассмотрим теперь гравитомагнитные эффекты высшего порядка. Некоторые гравитомагнитные эффекты более высокого порядка могут воспроизводить эффекты, напоминающие взаимодействия более обычных поляризованных зарядов. Например, если два колеса вращаются вокруг общей оси, взаимное гравитационное притяжение между двумя колесами будет больше, если они вращаются в противоположных направлениях, чем в одном направлении. Это может быть выражено как притягивающий или отталкивающий гравитомагнитный компонент.

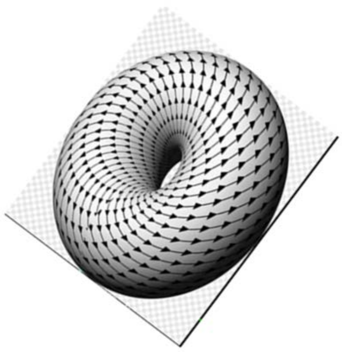

**Рис. 3.** Тор Клиффорда

Гравитомагнитные аргументы также предсказывают, что гибкая или жидкая тороидальная масса, подвергающаяся ускорению вращения вокруг малой оси (ускоряющее вращение "дымового кольца"), будет стремиться тянуть внешнюю массу через горловину (случай увлечения вращающейся системы отсчета, действующей через горловину) (рис. 3, 4). Теоретически эту конфигурацию можно использовать для ускорения объектов (через горловину) без воздействия на такие объекты каких-либо перегрузок.[11]

Рассмотрим тороидальную массу с двумя степенями вращения (вращение как по большой оси - синяя стрелка, так и по малой оси - красная стрелка, обе выворачиваются наизнанку и вращаются) (рис. 4). Это представляет собой "особый случай", в котором гравитомагнитные эффекты создают вокруг объекта киральное гравитационное поле, похожее на "кривой штопор". Обычно ожидается, что силы реакции на торможение на внутреннем и внешнем экваторе будут равными и противоположными по величине и направлению соответственно в более простом случае, включающем вращение только по малой оси. Когда оба вращения применяются одновременно, можно сказать, что эти два набора сил реакции возникают на разных глубинах в радиальном поле Кориолиса, которое простирается поперек вращающегося тора, что затрудняет установлению компенсации сил реакции вращений.

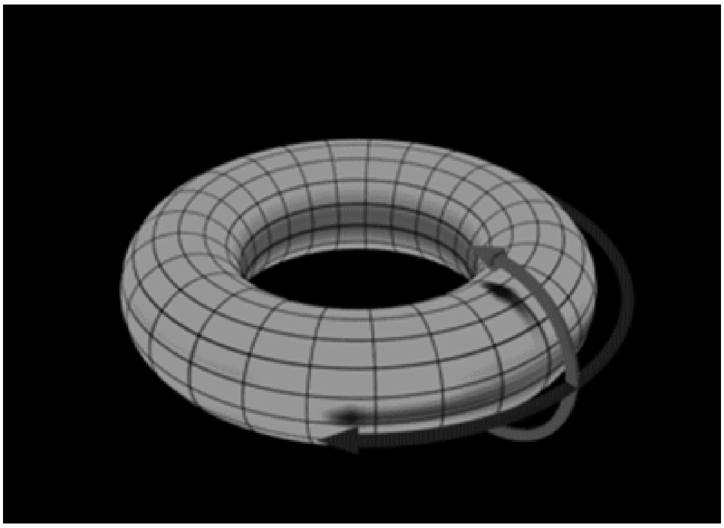

**Рис. 4.** Степени вращения вокруг тора

Моделирование этого сложного поведения как проблемы искривленного пространствовремени еще предстоит сделать, и считается, что это объясняет истечение релятивистских струй частиц из жерла вращающихся черных дыр (рис. 3-5). В работах [9, 10, 11, 12,] было высказано предположение, что такие гравитомагнитные силы лежат в основе генерации релятивистских струй (рис. 4), испускаемых некоторыми вращающимися сверхмассивными черными дырами [14].

## 4. Механизмы трансформации энергии вращающейся черной дыры

Согласно механизму Пенроуза [9] (рис.5, 6), если частица делится в эргосфере ЧД на два осколка, один из них упадет за горизонт событий, а второй, наоборот, будет выброшен за предел статичности в область, где тела уже не вращаются вокруг ЧД. При этом энергия выброшенного осколка будет больше, чем энергия изначальной частицы.

На рис.5 показано как рабочее тело падает (черная жирная линия) в эргосферу (серая область). В самой нижней точке орбиты тело делится на два осколка, причем выбрасывает один осколок назад, служа аналогом выброса топлива ракеты; однако для удаленного наблюдателя кажется, что оба осколка продолжают двигаться вперед из-за увлечения системы отсчета (хотя и с разной скоростью). "Топливо", замедляясь, падает (тонкая серая линия) на горизонт событий ЧД (черный диск). А второй осколок, разогнавшись, улетает (тонкая черная линия) с избытком энергии (что с лихвой компенсирует потери первого осколка и энергии,

затраченной на его выброс) (процесс аналогичен космическому маневру, использующему гравитационную энергию Солнца или массивных планет для разгона космических аппаратов при полетах к дальним планетам) [15]. Астрономы могут определить, находится ли в центре аккреционного диска ЧД или нейтронная звезда. Если спектр в излучении обнаруживается особенно горячую составляющую, она, вероятно, исходит от поверхности нейтронной звезды, нагретой уда-

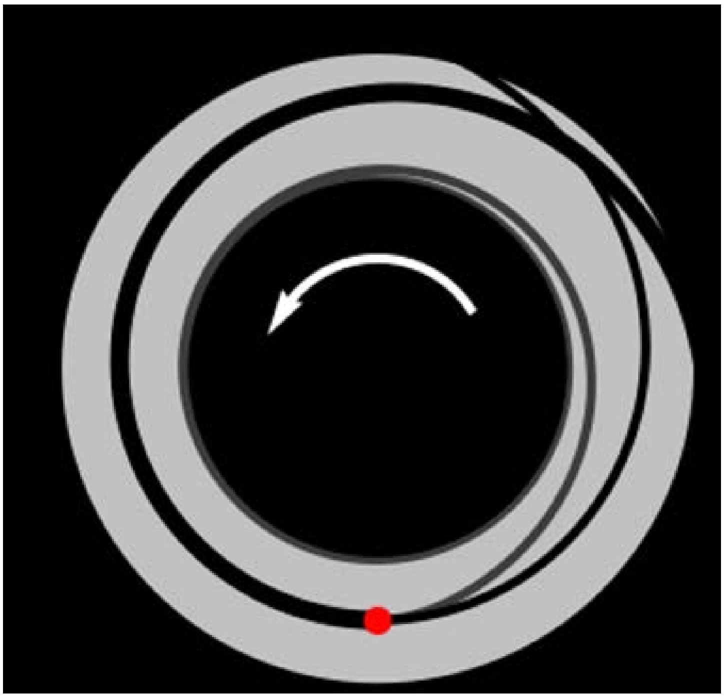

**Рис. 5.** Траектории частиц в процессе Пенроуза

ром аккрецирующего вещества. Если этого компонента нет, то, вероятно, поверхности вообще нет: газ падает пердикулярно горизонту (см. рис 6).

Процесс Пенроуза указывает на возможность получения энергии из ЧД, но его нельзя назвать хорошим практическим методом. Для его реализации необходимо, чтобы две новорожденные частицы обладали скоростью, превышающей половину скорости света. Ожидаемая частота таких событий настолько редка, что не позволит получить значительное количество энергии излучаемых частиц. Поэтому идет активный поиск других механизмов. Например, Стивен Хокинг показал, что черные дыры могут высвобождать энергию за счет теплового излучения. Еще одним способом извлечения энергии является процесс Блэнфорда-Знаека, основанный на электромагнитном взаимодействии. [16] Л. Комиссо из Колумбийского Университета и Ф. Асенхо из Университета А. Ибаньеса описали в своей статье[17] еще одну из альтернатив процессу Пенроуза. Черные дыры окружены горячей плазмой, частицы которой обладают магнитным полем. Основа нового механизма получения энергии из вращающихся ЧД - пересоединение силовых линий магнитного поля внутри эргосферы. Черная дыра при этом должна находиться во внешнем магнитном поле, иметь большой спин (a  1) и окружающую ее плазму с сильной намагниченностью. Нужными свойствами обладают, например, черные дыры, образовавшиеся в результате длинных и коротких гамма-всплесков и сверхмассивные ЧД в активных ядрах галактик. Магнитное пересоединение [18] ускоряет часть плазмы в направлении вращения дыры. Другая часть ускоряется в обратном направлении и падает за горизонт событий. Выделение энергии, как и в механизме Пенроуза, происходит, если поглощаемая плазма имеет отрицательную энергию, а ускоренная - "ускользает" из эргосферы. Отличие состоит в том, что для образования частиц с отрицательной энергией требуется диссипация энергии магнитного поля. В процессе, описанном Пенроузом, роль играет только инерция частиц.

Магнитное пересоединение - характерный процесс, который влияет на плазму, и этот процесс - причина вспышек на Солнце. Л. Комиссо и Ф. Асенхо считают, что магнитное пересоединение может быть также причиной вспышек рентгеновского излучения от черных дыр. [19] Девятичасовые вспышки задетектировали в 2019 году. [20]

По оценкам ученых Колумбийского университета (США, Columbia), прирост энергии опи-

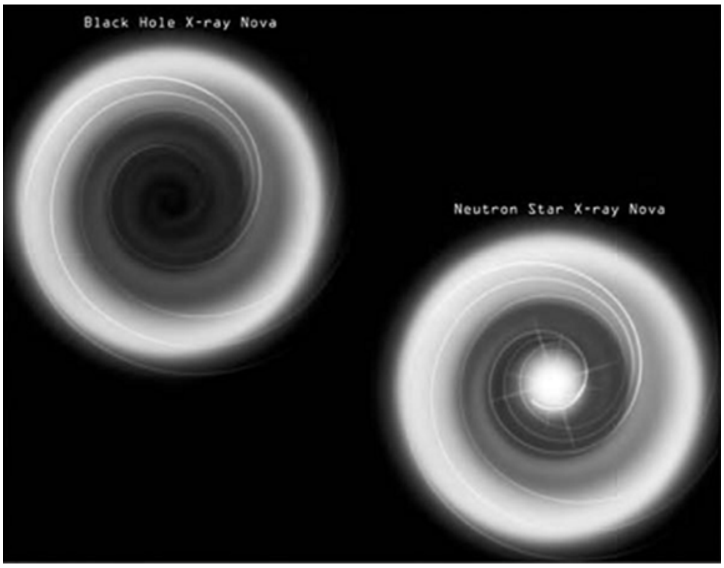


**Рис. 6.** Fig. 6. Показано отличие излучения рентгеновской новой, которая похожа на своего белого карлика за исключением того, что масса перетекает на компактный объект. Эти системы идеально подходят для необходимых здесь наблюдений, так как их можно сравнивать во время вспышки и в периоды затишья. Рисунок предоставлен NASA/CXC/M. Вайс.

санного процесса - 150 процентов. Это значит, что процесс позволяет получить в полтора раза больше энергии, чем нужно затратить на его реализацию. Достижение прироста больше 100 процентов возможно, потому что кинетическая энергия высвобожденных из эргосферы частиц плазмы увеличивается за счет энергии ЧД (подобно увеличению энергии КА при маневре в гравитационном поле планеты или звезды). Открытие нового механизма извлечения энергии из ЧД позволит астрономам лучше оценить их вращательный момент и понять, как они излучают энергию. До практического применения открытия еще далеко: необходимо выяснить, как долететь до черной дыры и разместить что-то в ее эргосфере, не угодив за горизонт событий. Максимальное количество энергии, возможное для распада одной частицы в результате исходного (или классического) процесса Пенроуза, составляет 20.7% от ее массы в случае незаряженной ЧД (при условии, что это лучший случай максимального вращения ЧД). Энергия берется из вращения черной дыры, поэтому существует ограничение на количество энергии, которую можно извлечь с помощью процесса Пенроуза и аналогичных стратегий (для незаряженной ЧД не более 29% ее первоначальной массы; большая эффективность возможна для заряженных вращающихся ЧД). Выяснено, что квазары и экстрагалактические компактные радиоисточники (массы $10^7 M_{\otimes}$) подпитываются струями газа из их ядер и магнитные поля (с мощностью $\sim 10^{44}$ Вт) [12-14]. На влияние энергии гравитомагнитного поля $B_g$ указывает, что происходит искажение плоскости вращения окружающего ядро газа. Оценка определяет период прецессии плоскости примерно в $10^4$ лет, коррелирующей с периодом прецессии гироскопа на орбите вокруг Земли (эффект Бардина – Петерсона) [14]. Нормальная компонента гравитомагнитного поля $B_{g\perp}$ ($\sim 1$ Тл), взаимодействуя с векторным потенциалом гравитомагнитного поля $\vec{J}_g$ , за пределами черной дыры вдоль ее горизонта создает электропотенциал гравитомагнитной батареи $E_{||}$[1, 16, 22]

$$\Delta U = \oint \vec{E}_{||} \cdot \vec{dl} = \oint \vec{J}_g \times \vec{B}_{g\perp} \cdot \vec{dl},$$

где $E_{||}$ is the tangential component of the electric field, which is not terminated at the horizon. Эта разность потенциалов толкает токи частиц до ультрарелятивистких скоростей вдоль замкнутого контура, опирающегося на горизонт черной дыры и простирающегося в область слабого $B_g$ поля. Передача энергии частицам подобна потоку энергии электромагнитного поля с помощью вектора

Умова-Пойнтинга. Для типичной модели черной дыры энергия, извлекаемая из черной дыры джетом оценивается величиной $W = 10^{37}$Дж $\cdot [\frac{L}{L_{max}}] \cdot [\frac{M}{10^9 M_\odot}]$, где $L/L_{max}$ - угловой момент черной дыры ("гравитомагнитный дипольный момент") в единицах максимально возможного углового момента $GM^2$ с ЧД, $M/(10^9 M_\odot)$ - масса дыры в единицах $10^9$ масс Солнца [16]. Таким образом, наряду с высокой мощностью процесса извлечения энергии из ЧД, его характерная эффективность высока; понимаются условия стабильности плазмы; кроме того, с прагматической точки зрения, отсутствуют необратимые отходы процесса – шлаки, угар, при сгорании ископаемого топлива; дополнительный нагрев рабочего механизма; радиоактивные отбросы и т.п. С другой стороны, есть прямая аналогия с гидротехническим устройством - гидротурбиной (Francis turbine) [23, 24], давно используемой для преобразования гравитационной энергии падающей воды в кинетическую энергию вращения турбины и последующего преобразования механической энергии в электрическую энергию в генераторе тока. Такие гидродинамические устройства широко используются в мировой практике создания гидроэлектростанций различной мощности от нескольких киловатт до сотен мегаватт с коэффициентом полезного действия более 95%. Конечно, для расчета потоков в гидротурбине используются уравнения гидродинамики. В данном случае важны уравнения магнитной гидродинамики.

## 5. Постановка современных лабораторных экспериментов

Встает вопрос о возможности реализации механизма передачи энергии в лабораторном эксперименте. Принципиально, малые девиации могут быть замечены либо с помощью интерферометрии (точность $\sim 10^{-22}$ отн. ед.), либо с помощью часов (точность $\sim 10^{-19}$ отн.ед.). Схемы обсуждаются в работах [25,26,27,28]. Измерение энергии в лабораторном эксперименте более проблематично. Так гравитомагнитный дипольный момент $L$ - угловой момент вращающегося маховика =10 т (момент инерции $\sim 20$ т$\cdot$ м$^2$), с угловой скоростью 63 $1/c$ равен $\sim 0.8 \cdot 10^9$ кг$\cdot$ м$^2 \cdot c^{-2}$. Оцениваемая энергия в экваториальной плоскости при использования описанного механизма в лаборатории $W_{lab} \sim 10^{-42}$ Дж за 1 секунду. Это безусловно мало, даже если сравнить с энергией квадрупольной гравитационной волны, регистрируемой интерферометрами LIGO – VIRGO – KAGRA ($10^{-3}$Вт/м$^2$). Возможно проведение более длительных экспериментов, или усложнение схемы эксперимента с использованием струй частиц, проходящих через тело со спином, может помочь поглотить большую часть энергии вращения. Моделирование сложного поведения потоков частиц как проблемы искривленного пространствовремени сложная научно-инженерная задача, начавшаяся с 2000-х годов. Предлагаются разные методы [17, 18, 29, 30]. Отметим последние работы [29, 30].

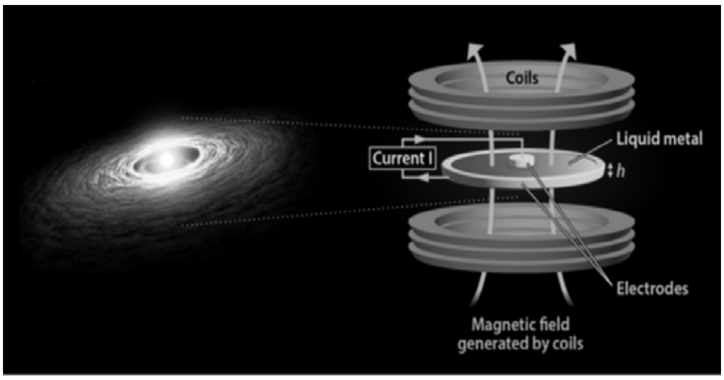


**Рис. 7.** Схема моделирования вращающейся черной дыры.

В одной из них [29] группа исследователей из Парижского университета Сорбонны сообщает о новом способе имитации ЧД и звездных аккреционных дисков. В своей статье, опубликованной в PRL, группа описывает использование магнитных и электрических полей для создания вращающегося диска из жидкого металла для имитации поведения материала, окружающего черные дыры и звезды, что приводит к развитию аккреционных дисков. Предыдущие исследования показали, что массивные объекты имеют гравитационное воздействие, которое притягивает газ, пыль и другие материалы. И поскольку такие массивные объекты вращаются, то материя, которую они притягивают, имеет тенденцию закручиваться вокруг объекта по мере своего приближения. Когда это происходит, гравитация, создаваемая веществом в закручивающейся массе, приводит к образованию единой структуры, то есть к возникновению тенденции образования аккреционного диска. Выявлены два вклада в локальный перенос углового момента: один от полоидальной рециркуляции, вызванной наличием границ, и другой от турбулентных флуктуаций в объеме. Последнее обеспечивает эффективный перенос углового момента независимо от молекулярной вязкости жидкости. В этой новой работе исследователи разработали метод создания аккреционного диска из частиц жидкого металла, вращающихся в воздухе. Чтобы имитировать действие реального аккреционного диска, исследователи применили радиальное электрическое поле к массе жидкого металла. Поле создавалось пропусканием тока между цилиндром и окружающим круглым электродом. Этот процесс удерживает металлические кусочки в плену, когда они вращаются вокруг центральной точки. В эксперименте, когда электромагнитная сила, приложенная к жидкому металлу, достаточно велика, соответствующая объемная инжекция углового момента создает турбулентный поток, характеризующийся усредненной по времени кеплеровской скоростью вращения $\Omega \sim r^{-3/2}$. Конечно, нет центрального тела, имитирующего звезду или черную дыру, - вместо этого действие управляется с помощью катушек выше и ниже заданной плоскости. Используя свой подход, исследователи смогли контролировать как степень турбулентности, так и скорость вращения диска. Они также добавили зонды, чтобы узнать больше об угловом моменте, и обнаружили, что он движется от внутренних частей диска к внешним краям турбулентными потоками, как предполагают некоторые ученые.

В другом эксперименте [30] более точно моделируется то, что происходит в этих плазменных дисках, что может помочь исследователям понять, как растут черные дыры и как коллапсирующее вещество образует звезды.

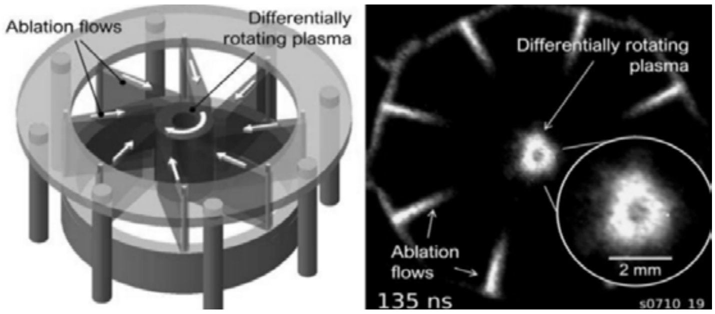


**Рис. 8.** Моделирование всасывания горячей плазмы в черную дыру и формирования аккомодационного диска. Рисунок из [30].

Когда вещество приближается к черным дырам, она нагревается, превращаясь в плазму - четвертое состояние материи, состоящее из заряженных ионов и свободных электронов. Она также начинает вращаться в структуре, называемой аккреционным диском. Вращение вызывает центробежную силу, выталкивающую плазму наружу, которая уравновешивается гравитацией ЧД, втягивающей ее вовнутрь. Эти светящиеся кольца орбитальной плазмы создают проблему: как растет ЧД, если материя застревает на орбите, а не падает в дыру? Ведущая теория состоит в том, что нестабильность магнитных полей в плазме вызывает трение, заставляющее ее терять энергию и падать в черную дыру. Основным способом проверки этого было использование жидких металлов, диск которых можно вращать, и наблюдение за тем, что происходит при приложении магнитных полей. Однако, поскольку металлы должны находиться внутри труб, они не являются истинным представлением свободно текущей плазмы. Теперь исследователи из Imperial College использовали свой мегаамперный генератор для экспериментов по плазменной имплозии ($MAGPIE$) для вращения плазмы с целью более точного представления аккреционного диска.

## 6. Ускоряемая плазма

Первый автор исследования [30], В. Валенсуэла-Вильясека отметил: "Понимание того, как ведут себя аккреционные диски, поможет нам не только увидеть причину роста черных дыр, но также и то, как газовые облака коллапсируют, образуя звезды, и даже как мы могли бы лучше создавать наши собственные звезды, повышая стабильность плазмы в термоядерных экспериментах". Команда из Империал Коллледж использовала машину MAGPIE, чтобы разогнать восемь плазменных струй и столкнуть их, образуя вращающийся столб [27]. Они обнаружили, что плазма во вращающемся кольце столба двигалась тем быстрее, чем ближе она находилась к внутренней части кольца, также подобно зависимости усредненной по времени кеплеровской скорости вращения $\Omega \sim r^{-3/2}$. А это является важной характеристикой аккреционных дисков во Вселенной. MAGPIE производит короткие импульсы плазмы, то есть был возможен только один оборот диска. Однако этот экспериментальный эксперимент показывает, как число оборотов можно увеличить с помощью более длинных импульсов, что позволит лучше охарактеризовать свойства диска. Более длительное время проведения эксперимента также позволит применить магнитные поля, чтобы проверить их влияние на трение в системе.

## 7. Заключение

Выше были рассмотрены различные подходы к объяснению и моделированию релятивистских струй, генерируемых вращающихся черных дыр при захвате приграничного вещества. Значимость исследований — не только в улучшении теории и конструкции термоядерного реактора, но и в определении возможности создания нового типа двигателя вещества, обладающего как высокой эффективностью, так и отсутствием продуктов, не используемых далее. С точки зрения создания теории таких двигателей, процитируем одного из исследователей в Принстонском университете ? В. Валенсуэла-Вильясеку [30]: "Мы только что начали смотреть на эти аккреционные диски [вокруг черных дыр] совершенно по-новому, включая наши эксперименты и снимки черных дыр с помощью Event Horizon Telescope. Это позволит нам проверить наши теории и посмотреть, совпадают ли они с астрономическими наблюдениями".

## Список литературы/References

1. Мизнер Ч., Торн К., Уилер Дж. *Гравитация.* М.: Изд. Мир. Редакция литературы по физике. Т. 3. С. 218. 510 с.; 1977. Misner C.W., Thorne K.S. and Wheeler J.A., *Gravitation.* San Francisco: W. H. Freeman and Co.; 1973.
2. Фейнман Р.Ф., Мориниго Ф.Б., Вагнер У.Г. *Фейнмановские лекции по гравитации. под ред. Б. Хатфилда.* Введение Дж. Прескилла и К.С. Торна, пер. с англ. А.Ф. Захарова М.: Янус-К; 2000. ISBN 5-8037-0049-5; Feynman R.P., F.B. Morinigo, W.G. Wagner, B. Hatfield (ed.) with foreword by J. Preskill and K.S. Thorne. *Feynman Lectures on Gravitation.* Addison Wesley Publishing Company. Advanced Book Program.
3. B.Schutz. *Gravity from the Ground Up: An Introductory Guide to Gravity and General Relativity*

*(Reprint ed.).* Cambridge: Cambridge University Press; 2004. ISBN 0-521-45506-5.

4. Фейнман Р., Лейтон Р., Сэндс М. *Фейнмановские лекции по физике. т.4 Электродинамика.* М.: Изд. АСТ; 2022. ISBN 9785171130121; Feynman R.P., Leighton R.B., Sands M.L. *The Feynman Lectures on Physics.* Addison-Wesley revised and extended edition in 2005. ISBN 978-0-465-02529-9.
5. Iorio, L. A comment on "A test of general relativity using the LARES and LAGEOS satellites and a GRACE Earth gravity model. Measurement of Earth's dragging of inertial frames,"by I. Ciufolini et al. *The European Physical Journal C.* 2017; 77 (2): p.73. arXiv:1701.06474. Bibcode:2017EPJC...77...73I. doi:10.1140/epjc/s10052-017-4607-1. S2CID 118945777
6. Everitt, C.W.T. et al. Gravity Probe B: Final Results of a Space Experiment to Test General Relativity. *Physical Review Letters.* 2011; 106 (22): p. 221101. arXiv:1105.3456. Bibcode:2011PhRvL.106v1101E. doi:10.1103/PhysRevLett.106.221101. PMID 21702590. S2CID 11878715.
7. Cartlidge, E. Underground ring lasers will put general relativity to the test. Physicsworld.com. Institute of Physics. 2016; Retrieved 2 July 2017.
8. O'Shaughnessy R., Gerosa D., and Wysocki D. Inferences about Supernova Physics from Gravitational-Wave Measurements: GW151226 Spin Misalignment as an Indicator of Strong Black-Hole Natal Kicks. *Phys Rev Lett.* 2017;119: p. 011101.
9. First M87 Event Horizon Telescope results. *The Astrophysical Journal Letters.* 2019; 875 (1).
10. *Black Hole Unmasked: Astronomers Capture First Image of Accretion Ring and Relativistic Jet. SciTechDaily.* 2023; CAS.
11. Penrose R. and Floyd R. M., Extraction of Rotational Energy from a Black Hole. *Nature Physical Science.* 1971; 229: p.177-185.
12. Begelman M. C., Blandford R. D. and Rees M. J., Theory of extragalactic radio sources. *Rev. Mod. Phys.* 1984; 56: p. 255-68. doi:https://doi.org/10.1103/RevModPhys.56.255.
13. R.K. Williams. Collimated escaping vortical polar e?e+ jets intrinsically produced by rotating black holes and Penrose processes. *The Astrophysical Journal.* 2004; 611 (2): p. 952-963. arXiv:astro-ph/0404135. Bibcode:2004ApJ...611..952W. doi:10.1086/422304. S2CID 1350543.
14. Bardeen J. M. and Petterson J. A., The Lense-Thirring Effect and Accretion Disks around Kerr Black Holes. *Astrophys. J. Letter.* 1975;195: p. 65-77. doi: 10.1086/181711.
15. Бобошина С.Б., Измайлов Г.Н.. Физические основы механики с приложениями к аэрокосмическим задачам.- М. : ЛЕЛАНД, 2020, 202 с. ISBN 978-5-97106740-5. Boboshina S.B., G.N. Izmaïlov. Fizicheskie osnovy mechaniki s prilozheniyami k aerokosmicheskim zadacham. Moscow: URSS; 2019. (in RUSSIAN).
16. Hartle, J.D. *Gravity: An Introduction to Einstein's General Relativity.* San Francisco: Addison Wesley; 2003. 582 p. ISBN 0-8053-8662-9.
17. Comisso L. and Asenjo F. A.. Magnetic reconnection as a mechanism for energy extraction from rotating black holes. *Phys. Rev. D.* 2002; 103: 023014.
18. Прист Э., Форбс Т. *Магнитное пересоединение. Магнитогидродинамическая теория и приложения.* М: ФИЗМАТЛИТ; 2005. - 592 с. ISBN 5-9221-0502-74; Priest E., Terry Forbes. *Magnetic Reconnection. MHD Theory and Applications.* Cambridge: Cambridge University Press; 2000. ISBN 0-521-48179-1.
19. Liu, T. Massive black holes flaring up time and again. *Nat Astron.* 2021; 5: S.438-439. https://doi.org/10.1038/s41550-021-01366-4.
20. Miniutti, G., Saxton, R.D., Giustini, M. et al. Nine-hour X-ray quasi-periodic eruptions from a low-mass black hole galactic nucleus. *Nature.* 2019; 573: S. 381-384. https://doi.org/10.1038/s41586-019-1556-x.
21. Hertog Th. *On the Origin of Time: Stephen Hawking's Final Theory.* Bantam, ISBN-13:978-

0593128442.

22. Shatskii, A.A. Unipolar induction of a magnetized accretion disk around a black hole. *Astron. Lett.* 2003; 29: S. 153-157. https://doi.org/10.1134/1.1558153/
23. https://en.wikipedia.org/wiki/Francis-turbine/
24. https://testbook.com/mechanical-engineering/francis-turbine/ .
25. Abramowicz M. A. and Fragile P. Chris. Foundations of Black Hole Accretion Disk Theory. *Living Rev. Relativity.* 2013: 16. http://www.livingreviews.org/lrr-2013-1.
26. Головашкин А.И., Жерихина Л.Н., Цховребов А.М., Измайлов Г.Н., Озолин В.В. Обычные СКВИД-интерферометры и интерферометры на волнах материи в сверхтекучем гелии: роль квантовых флуктуаций. *ЖЭТФ.* 2010: 138. вып. 2(8). С.373-380. Golovashkin A.I., Zherikhina L.N., Tskhovrebov A.M., Izmaïlov G.N., Ozolin V.V. Obychnye SKVID-interferometry i interferometry na volnakh materii v sverkh tekuchem helii: rol'kvantovykh fluktuatsii, *JETPh.* 2010:138. iss. 2(8). S.373-380.
27. Izmailov G.N. To the possibility of using clocks in gravitational antenna network. *J. Phys.: Conf. Series.* 2019. 1348 P.012005 doi:10.1088/1742-6596/1348/1/012005.
28. Жерихина Л.Н., Измайлов Г.Н., Озолин В.В.Возможности использования эффектов ОТО в космической навигации. *Альманах современной метрологии.* 2020: No 4 (24). С.24-35. Zherikhina L.N., Izmaïlov G.N., Ozolin V.V. Vozmozhnosti ispolzovaniya effectov OTO v kosmicheckoi navigatsii. *Almanakh sovremennoi metrologii.* 2020: №4 (24). S. 24-35.
29. Vernet M. et al, Angular Momentum Transport by Keplerian Turbulence in Liquid Metals. *Physical Review Letters.* 2022. doi: 10.1103/PhysRevLett.129.074501.
30. Valenzuela-Villaseca V. et al, Characterization of Quasi-Keplerian, Differentially Rotating, Free-Boundary Laboratory Plasmas. *Physical Review Letters.* 2023; 130: S. 195101. doi: https://doi.org/10.1103/PhysRevLett.130.195101.

**Авторы**

**Измайлов Георгий Николаевич**, д.ф.-м.н., профессор, Московский авиационный институт (национальный исследовательский университет), Волоколамское ш., д. 4, г. Москва, 125993, Россия.
E-mail: izmailov@mai.ru

**Озолин Владимир Викторович**, , к.ф.-м.н., доцент, Московский авиационный институт (национальный исследовательский университет), Волоколамское ш., д. 4, г. Москва, 125993, Россия.
E-mail: ozolinvv@mai.ru

**Просьба ссылаться на эту статью следующим образом:**

Измайлов Г. Н., Озолин В. В. Имитация извлечения кинетической энергии из черной дыры Керра–Ньюмана. *Пространство, время и фундаментальные взаимодействия.* 2023. № 3-4. С. 133–146.

**Authors**

**Izmailov George Nikolaevich**,Dr. Sci., Professor, Moscow Aviation Institute (National Research University), Volokolamskoye sh., 4, Moscow, 125993, Russia.
E-mail: izmailov@mai.ru

**Ozolin Vladimir Victorovich**, Ph.D., Associate Professor, Moscow Aviation Institute (National Research University), Volokolamskoye sh., 4, Moscow, 125993, Russia.
E-mail: ozolinvv@mai.ru

**Please cite this article in English as:**

Izmailov G. N., Ozolin V. V. Simulation of kinetic energy extraction from a Kerr – Newman black hole. *Space, Time and Fundamental Interactions*, 2023, no. 3-4, pp. 133–146.

УДК 530.12, 517.5



# АЛГЕБРОДИНАМИКА: В ПОИСКАХ ИСТИННОЙ АЛГЕБРАИЧЕСКОЙ "МИРОВОЙ" СТРУКТУРЫ

Кассандров В. В.[a,1]

[a] Институт гравитации и космологии, Российский университет дружбы народов, г. Москва, 117198, Россия.

Представлены основные принципы т.н. *алгебродинамического* подхода к построению единой теории поля, и его реализация на основе линейной алгебры *комплексных кватернионов*. Далее обсуждаются возможные реализации алгебродинамики на многообразии, оснащенном структурой группы Ли или ее специальными обобщениями – алгебрическими структурами (АС) с *единственной операцией*, заданной *единственным определяющим соотношением* для трех либо четырех элементов (аналогом требования ассоциативности для группы Ли). Заданная таким образом т.н. *инвариантная АС* оказывается эквивалентной группе Ли, однако допускает тем самым неканоническое введение последней с использованием единственного определяющего соотношения. На роль "Мировой" АС предложены и предварительно изучены еще два примечательных их типа, а именно т.н. *автоморфная* и *универсальная* АС. Фундаментальные физические поля $F(x)$ рассматриваются как нетривиальные отображения элементов АС отвечающие, в частности, умножению элемента "на себя", $F(x) = x \cdot x$.

*Ключевые слова*: Бикватернионы, группы Ли, инвариантная алгебраическая структура, автоморфная алгебраическая структура, универсальная алгебраическая структура, фундаментальные поля.

# THE ALGEBRODYNAMICS: IN SEARCH OF THE ULTIMATE ALGEBRAIC "WORLD" STRUCTURE

Kassandrov V. V.[a,1]

[a] Institute of gravitation and cosmology, Peoples' Friendship University of Russia, Moscow, 117198, Russia.

Principles of the so-called *algebrodynamical* approach to the construction of a unified field theory are presented, together with realization of the approach on the base of the linear algebra of *complex quaternions*. Then we discuss possible realizations of the algebrodynamics on a manifold equipped with the structure of a Lie group or its specific generalizations – algebraic structures (AS) defined by a *single operation* subject to a *single relation* containing three or four elements (analogous to the associativity requirement for a Lie group). Defined in such a way the so-called *invariant AS* turns out to be equivalent to a Lie group but allows thus for a non-canonical introduction of the latter which makes use of a single defining relation. The two more types of remarkable AS, the so-called *automorphic* and *universal* ones, are proposed for the role of the "World AS" and preliminary examined. Fundamental physical fields $F(x)$ are considered as *nontrivial mappings* of the elements of AS corresponding, in particular, to the multiplication of any element by itself, $F(x) = x \cdot x$.

*Keywords*: Biquaternions, Lie groups, invariant algebraic structure, automorphic algebraic structure, universal algebraic structure, fundamental fields).

PACS: 02.40.-k, 03.50.-z, 02.10.De

DOI: 10.17238/issn2226-8812.2023.3-4.147-153

## Introduction. The algebrodynamics

It is generally accepted that the most trustful approach to the construction of a unified field theory is the *geometrodynamics* (GD). Principles of GD have been formulated by Clifford, Einstein, Weyl and

[1]E-mail: vkassan@sci.pfu.edu.ru

Wheeler. In the GD paradigm all fundamental physical fields have purely geometrical origin, that is either are constructed from characteristics like curvature and torsion or are themselves vector (tensor) fields on the space-time manifold – geodesic, covariantly constant ones, etc.

However, the choice of the space-time geometry, – its dimension, topology, differential structure, – is completely phenomenological since none general criteria of such a choice appealing to the internal properties of space-time manifold have been established. Besides, even on a fixed geometrical background determination of the structures responsible for the physical fields themselves and their equations remains indefinite. Owing, in particular, to these factors the GD approach does not yet get substantial development.

On the other hand, it is known that algebraic structures defined on a manifold (the so-called "manifolds with a multiplication" [1, 2], naturally give rise to a corresponding geometry of the manifold. For example, a "Kleinian" group of the isometries defining metrical structure on the manifold should be isomorphic to the *group of the automorphisms* of the primary algebraic structure.

Importantly, among various classes of algebraic structures there exist representatives *exceptional* in their internal properties: three remarkable linear algebras (complex numbers, quaternions and octaves), five exceptional Lie groups $(F_4, G_2, E_6, E_7, E_8)$, etc. Finally, any algebraic structure naturally defines some *mappings* on the manifold so that corresponding functions can be regarded as physical fields subject to certain functional-differential equations. In view of the above stated considerations, such *algebrodynamical* (AD) approach seems to be more substantiated and promising than the GD one.

The most elaborated version of the AD approach is based on the exceptional *linear* algebra of quaternions, precisely, on its complexification – the algebra of *biquaternions* $\mathbb{B}$. In this framework, the complex vector space of $\mathbb{B}$ naturally maps into the interior of the light cone of the Minkowski space [3] realizing the isomorphism between the spinor Lorentz group $SL(2,\mathbb{C})$ and the group $SO(3,\mathbb{C})$, – the automorphism group of $\mathbb{B}$.

As for the mappings-fields $F(Z)$ – functions of the $\mathbb{B}$-variable $Z$, in our approach [4, 5] (see also [6, 7] and references therein), these functions have been defined by *the conditions of* $\mathbb{B}$*-differentiability*

$$dF = \Phi \cdot dZ \cdot \Psi, \tag{0.1}$$

$(\cdot)$ being multiplication in $\mathbb{B}$. Conditions (0.1) represent themselves a natural generalization of the *holomorphy* conditions for the functions of complex variable and lead, as opposed to the Cauchy-Riemann equations, to the *nonlinear* differential equation of *complex eikonal* (see, e.g., [4, 5, 6, 7] for detail). In this connection, *nonlinearity* responsible for the self-interaction of corresponding physical fields arises as a direct consequence of the *non-commutativity* property of the quaternion-type algebras in question.

Under the reduction $Z \mapsto X$ onto the Minkowski subspace defined by *Hermitian* matrices $X = X^+$, equations (0.1) become Lorentz invariant and, moreover, acquire natural spinor (twistor) and gauge (self-dual) structures. The first property allows to obtain general solution of (0.1) in the form of an implicit algebraic equation on the components of $\mathbb{B}$-field, while self-duality guarantees the fulfillment of the equations for gauge Maxwell and $SL(2,\mathbb{C})$ Yang-Mills fields on any solution to the primary system of equations corresponding to (0.1).

Finally, (elementary) *particles* can be identified with singular points of corresponding mappings-functions defined by the singular loci of the Maxwell and Yang-Mills field strengths. Their spacial distribution and temporary dynamics are fully controlled by the same primary conditions (0.1) of $\mathbb{B}$-differentiability.

Thus, one manages to construct a substantive algebraic field/particle theory making use only of the properties of the exceptional [1] linear algebra $\mathbb{B}$ and the conditions of differentiability of $\mathbb{B}$-functions treated as physical fields.

However, any *linear* algebra, apart of the principal multiplication of elements, carries two additional operations inherited from the structure of its basic vector space (addition of vectors and multiplication

[1]Precisely, of the direct sum of two exceptional algebras, complex numbers and Hamiltonian quaternions

of those by a number). Therefore, below we consider whether this linear structure could be replaced by a "nonlinear" one defined by a single operation of "multiplication" of the points of a manifold and inducing, in the turn, geometry of the latter.

## 1. Lie group as a simplest nonlinear algebraic structure

The most interesting and having a lot of applications algebraic structure [2] is, of course, the structure of a continuous group, *the Lie group.*

The structure of an abstract group is given by three well-known postulates: associativity, existence of the unit and inverse elements. It is completely determined by corresponding linear algebra, the Lie algebra, with a set of structure constants $C^{\rho}_{\mu\nu}$, skew symmetric in low indices and satisfying the known Yacobi identity. Classification of Lie groups obtained by Eli Cartan includes, besides some infinite series, 5 well-known exceptional groups.

Geometry of the Lie groups' manifolds is closely related to the existence of the so-called right- (left-) invariant vector fields $v^{\nu}_{\mu}(x)$, defined through the multiplication of an element $x$ by an inverse to the infinitesimally close to it element $y$, with coordinates $y^{\mu} = x^{\mu} + dx^{\mu}$,

$$f^{\mu} := (x \cdot y^{-1})^{\mu} = e^{\mu} + v^{\mu}_{\nu}(x)dx^{\nu}, \tag{1.1}$$

where $e^{\mu}$ are the coordinates of the unit element of the group. Making use of the properties of associativity and invertibility, one easily obtains that

$$v^{\mu}_{\nu}(f)df^{\nu} = v^{\mu}_{\nu}(x)dx^{\nu} = invariant, \tag{1.2}$$

while from the integrability conditions to the latter "invariance relation" (1.2) *the Maurer-Cartan equations* do follow,

$$\partial_{\mu}v^{\rho}_{\nu} - \partial_{\nu}v^{\rho}_{\mu} = C^{\rho}_{\alpha\beta}v^{\alpha}_{\mu}v^{\beta}_{\nu}. \tag{1.3}$$

As it was demonstrated in [4], the structure of vector fields allows for definition of the strength tensor of an effective field of the Yang-Mills type which, however, turns to zero by virtue of the Maurer-Cartan equations (1.3). Therefore, in [4, ch. 4] we proposed to consider matter as a sort of *invariant deformation of a fundamental algebraic structure.*

Below we shall discuss some promising algebraic structures which in a sense generalize the structure of a Lie group and pretend for the role of the "World structure". In this connection, we note that numerous known generalizations of the group structure via the denial of the associativity property or the existence of the unit element are too indefinite and do not lead to some noticeable new results (see, e.g., [8]). Similar situation takes place under the denial of the existence of the inverse operation, the "division", that is, under the transition to the structure of the so-called *semi-group.* Threfore, we need to formulate some alternative approach to define the algebraic "World structure" *exceptional in its internal properties.*

## 2. "Invariant" algebraic structure and a novel introduction of an abstract Lie group

Let us consider in more detail the property of invariance (1.2) of vector fields on a Lie group. In fact, the latter is based on the following relation valid for any three elements of the group

$$(x \cdot z^{-1}) \cdot (y \cdot z^{-1})^{-1} = (x \cdot y^{-1}), \tag{2.1}$$

to prove which one should exploit all of the three properties of the group multiplication, that is, associativity and existence of the unit and inverse elements.

In this connection, it seems promising to introduce a new algebraic structure on a manifold **M** defined by a *single* invariance postulate reproducing (2.1). Consider, therefore, an algebraic structure on

[2]For the first turn, this is related to the description of symmetries of systems or processes by continuous *groups of transformations.*

a manifold $\mathbf{M}$ for which only one operation is defined. Below, for convenience, instead of the habitual "multiplication" $(\cdot)$ we shall treat this operation as "substraction" and denote it hereafter as $(-)$. Besides usual topological assumptions of continuity and smoothness of the operation, to define the properties of the sought-for structure we require for any three elements $x, y, z \in \mathbf{M}$ the following relation to be fulfilled:

$$(x - z) - (y - z) = x - y, \tag{2.2}$$

that is, the property of invariance of the principal operation of substraction w.r.t. a *shift* by an arbitrary element $z$. We shall call the structure defined by (2.2) the *invariant algebraic structure (IAS)* and examine whether it induces a (non-associative) generalization of the Lie group structure.

Notice firstly that from (2.2) it follows immediately

$$(x - z) - (x - z) = x - x, \quad \Rightarrow G(x - z) = G(x), \tag{2.3}$$

where a mapping $G : x \mapsto (x - x)$ is introduced. Since $z$ is arbitrary element, from relation (2.3) it follows that $G(x) = \mathbf{0}$, where $\mathbf{0}$ is a *universal ("null") element* of the algebraic structure in question. Thus, existence of the null element (the direct analogue of the null (unit) element in the Lie group, see below) should not be postulated but follows from the principal relation (2.2) defining the IAS.

After this, one can automatically define, for any $x \in \mathbf{M}$, the element $\bar{x}$, *opposite* to $x$,

$$\bar{x} := \mathbf{0} - x, \tag{2.4}$$

and introduce a supplementary operation of "addition" $(+)$ for any pair of elements $x, y \in \mathbf{M}$,

$$x + y := x - \bar{y}. \tag{2.5}$$

The null element and introduced operations have the following properties for any elements $x, y, z, \ldots \in \mathbf{M}$. These properties are the consequences of the principal relation (2.2) and proved in the Appendix:

- (a) $\bar{\mathbf{0}} = \mathbf{0}$,
- (b) $x - \mathbf{0} = x$,
- (c) $\bar{\bar{x}} \equiv \mathbf{0} - \bar{x} = x$,
- (d) $x + \bar{x} = \mathbf{0}$,
- (e) $x + \mathbf{0} = \mathbf{0} + x = x$,
- (f) $\overline{x - y} = y - x$,
- (g) $(x - \bar{y}) - y = x$.

Using these properties, one can prove the associativity of the addition operation $(+)$,

$$(x + y) + z = x + (y + z). \tag{2.6}$$

Note that (2.6) can be equivalently represented in the form $(x - \bar{y}) - \bar{z} = x - (\overline{y - \bar{z}})$ or, using property (f),

$$(x - \bar{y}) - \bar{z} = x - (\bar{z} - y). \tag{2.7}$$

To prove (2.7), let us rewrite the principal relation (2.2) as

$$(x - \bar{y}) - \bar{z} = x - w, \tag{2.8}$$

where $\bar{z} := w - \bar{y}$. From the last definition one obtains $\bar{z} - y = (w - \bar{y}) - y$ or, using property (g), $\bar{z} - y = w$. Therefore, the principal relation (2.8) aquires the souught-for form (2.7), and the associativity property (2.6) is proved.

We come thus to the conclusion that the IAS is not essentially a presupposed generalization of the group. Nonetheless, we have obtained the following remarkable result. *The structure of "multiplication" for any Lie group can be uniquely introduced through a single operation of "substraction" which is completely defined by a single requirement of invariance (2.2).*

To conclude, it is quite evident that the operation $(+)$ completely reproducing the canonical multiplication in the Lie group structure allows for the inverse operation, so that the equations $a+x=b$ and $x+a=b$ have unique solutions $\forall a, b \in \mathbf{M}$. Specifically, from the first equation $x=b+\bar{a}$ while for the second the solution is $x=b+\bar{a}$. It is also easy to prove that the unique solution of the equation $a-x=b$ is given by $x=\bar{b}-\bar{a} \equiv \bar{b}+a$ while the solution of the equation $x-a=b$ is $x=b-\bar{a} \equiv b+a$.

Note finally that from the decomposition of $(x-y)$ in the vicinity of the null element which follows explicitly from (2.2),

$$(x-y)^{\mu} \sim x^{\mu}-y^{\mu}+b^{\mu}_{(\nu\rho)}(x^{\nu}-y^{\nu})y^{\rho}+c^{\mu}_{[\nu\rho]}x^{\nu}y^{\rho}+\ldots, \tag{2.9}$$

(where in the r.h.s. the sign $(-)$ has usual arithmetical sense) it follows that the IAS is determined by a set of structural constants $c^{\mu}_{[\nu\rho]}$ of some linear algebra subject to the Yacobi identity and isomorphic to a linear *Lie algebra*.

## 3. "Automorphic" algebraic structures and fundamental mappings - fields

As another possible candidate for the role of the "World algebraic structure" let us consider the defining relation of the following form:

$$(x-z)-(y-z)=(x-y)-z, \tag{3.1}$$

for any three elements of the sought-for struture $x, y, z \in \mathbf{M}$. The latter can be naturally called an *automorphic algebraic structure* (AAS), since the mapping $F : x \mapsto (x-z)$ is the automorphism of the AAS itself, that is,

$$F(x)-F(y)=F(x-y). \tag{3.2}$$

Remarkably, the AAS defining relation (3.1) is satisfied if one defines the principal operation of substraction $(-)$ through the "multiplication" $(\cdot)$ on a complementary structure of a Lie group. Specifically, one can set

$$x-y := y \cdot x^{-1} \cdot y. \tag{3.3}$$

Then the mapping $G : x \mapsto x-x$ becomes an identity, $G(x)=x$, one more relation takes place in addition

$$(y-x)-x=y \tag{3.4}$$

and, moreover, under some refined assumptions the structure of AAS comes into correspondence with the structure of a *symmetric space*. The latter can be algebraically defined through the postulate of "right- (left-) distributivity" like (3.1), inversibility (3.4) and idempotentivity $G(x) := x-x=x$ (see, e.g., [1, 9]).

In the turn, it is well known that the structure of symmetric spaces themselves is closely related to that of the Lie groups. On this base, the complete classification of symmetric spaces has been obtained by E. Cartan (see, e.g., [1, 2]).

Generally, however, the property of idempotentivity *does not* follow from the principal relation (3.1), whereas the alternative assumption on the mapping of *any* element $G(x)=x-x$ into a *universal (null) element* is immediately proved to be contradictory. Therefore, one can regard $G(x)$ as a nontrvial, *point dependent* mapping whose structure could define the AAS itself and corresponding geometry of the manifold as well. Physically, it would be natural to identify the form of this mapping with the structure of *fundamental fields* analogous to that of differentiable $\mathbb{B}$-functions in the framework of biquaternionic algebrodynamics (see section 1).

Thus, the AAS is richer in its internal properties than the group structure and only in a particular case reduces to the structure of a symmetric space in fact isomorphic to the Lie group structure. There exists a number of ways to define, on the AAS manifold, the structure of fundamental physical fields, the above proposed among them (see also [4, ch.3]). Corresponding differential equations for those fields as well as linear algebras defining the AAS, are the subject of further investigations.

## 4. "Universal" algebraic structure

IFinally, let us consider one more remarkable algebraic structure which can be defined by a single relation for any *four* elements $x, x', y, y' \in \mathbf{M}$,

$$(x' - y') - (x - y) = (x' - x) - (y' - y), \tag{4.1}$$

which corresponds, conditionally, to the following formulation by words: *"increment of differences equals to difference of increments"*. We shall call this structure *universal* algebraic structure (UAS).

Setting now $x' = x,\ y' = y$, one has for the function $G(x) = x - x$:

$$G(x - y) = G(x) - G(y). \tag{4.2}$$

This functional equation has two evident solutions, $G(x) = \mathbf{0}$ и $G(x) = x$, independently of the algebraic structure itself. In the first case, $G(x) = \mathbf{0}$, the UAS can reduce to the IAS and, thus, to the equivalent structure of a Lie group. In the second case, $G(x) = x$, the reduction to the structure of a symmetric space is possible. We, however, shall assume as above that the mapping $G : x \mapsto x - x$ is nontrivial and can be interpreted as a primary physical field.

We can speculate a bit about the properties of such fundamental structure. Specifically, the mapping $G$ can possess immobile $G(x_0) = x_0$ or, more generally, cyclic $G(G(...G(x_0))..) = x_0$ points. One can also presuppose the existence of domains on the basic manifold whose points are mapped in the procedure into vicinity of a universal (null) element. Note that, generally, such element can be not unique.

Possible physical interpretation of the cycles and the set of null elements arising in the procedure devotes special discussion. In any case, simplicity of the definition of UAS, its uniqueness and richness of possibilities makes it, from our point of view, *the most suitable candidate to the role of the "World algebraic structure"*.

## Conclusion

In the paper we have introduced a number of algebraic structures on a manifold very simple in the definition (through a single algebraic connection of the elements) and remarkable in their internal properties. The so-called invariant algebraic structure was proved to be isomorphic to the structure of a Lie group (which, therefore, can be introduced in an elegant, non-canonical way). The two other structures seem to be rather complicated and need further investigation as well as the introduction of physical fields and geometry of the manifold consistent with the properties of the primary algebraic structure. We think, nonetheless, that the novel types of structures proposed in the paper can stimulate the search of actually "World algebra" which could determine both the ultimate geometry of space-time and the dynamics of fundamental physical field(s).

## 5. Appendix

Let us prove the properties (a) – (g) of the IAS structure written out in section 3. Relation (a) follows directly from (2.2), that is, $\mathbf{0} \equiv \mathbf{0} - \mathbf{0} = (x - x) - (x - x) = x - x = \mathbf{0}$.

For relation (b) we take $z = \bar{y}$ and rewrite (2.2) in the form $(x - \bar{y}) - (\bar{y} - \bar{y}) = x - \bar{y}$, so that $(x - \bar{y}) - \mathbf{0} = x - \bar{y}$ or, taking $x = \mathbf{0}$, obtain $y - \mathbf{0} = y,\ \ \forall y \in \mathbf{M}$.

As for relation (c), one has $\bar{\bar{x}} \equiv \mathbf{0} - (\mathbf{0} - x) = (x - x) - (\mathbf{0} - x)$ and, in view of (2.2) and (b), $\bar{\bar{x}} = x - \mathbf{0} = x$.

For (d) one obtains immediately $x + \bar{x} = x - \bar{\bar{x}} = x - x = \mathbf{0}$.

Now, (e) follows as $x + \mathbf{0} = x - \bar{\mathbf{0}} = x - \mathbf{0} = x$ and, similarly, $\mathbf{0} + x = \mathbf{0} - \bar{x} = \bar{\bar{x}} = x$.

To prove (f) we take $z = x$ in (2.2) and rewrite it then as $\mathbf{0} - (y - x) = x - y$, that is, $\overline{y - x} = x - y$.

Finally, for (g) one obtains using (2.2) and (b): $(x - \bar{y}) - y = (x - \bar{y}) - (\mathbf{0} - \bar{y}) = x - \mathbf{0} = x$, $\forall x, y \in \mathbf{M}$.

## 6. Acknowledgement

The author is grateful to E. K. Loginov for his valuable consultation on the properties of (non-) associative algebras and loops and acknowledges support from Project no. FSSF-2023-0003

## Список литературы/References

1. Loos O. *Symmetric spaces.* NY-Amsterdam, W. A. Benjaman, 1969
2. Fedenko A. S. *Spaces with symmetries.* Minsk, Belarus State Univ. Press, 1977 (in Russian)
3. Kassandrov V. V. Algebrodynamics in complex space-time and physical meaning of hidden dimensions. *Gravit. & Cosmol..* 2005. 11, 354-358 ; arXiv: gr-qc/0602088
4. Kassandrov V. V. *Algebraic structure of space-time and the algebrodynamics.* Moscow, Peoples' Friendship Univ. Press, 1992 (in Russian)
5. Kassandrov V. V. Biquaternionic electrodynamics and Weyl-Cartan geometry of space-time. *Gravit. & Cosmol..* 1995. 1, 216-222; arXiv: gr-qc/0007027
6. Kassandrov V. V. Quaternionic analysis and the algebrodynamics In: "Space-time structure. Algebra and geometry", eds. D.G. Pavlov, Gh. Atanasiu, V. Balan. Moscow, Lilia-Print, 2007. P. 441-473; arXiv: 0710.2895
7. Kassandrov V. V. The algebrodynamics: quaternionic analysis, complex string and the "Unique" Worldline. *Space, time and fundamental interactions.* 2022. № 41. P. 31-48 (in Russian)
8. Belousov V. D. *Fundamentals of the theory of quazigroups and loops.* Moscow, Nauka, 1967 (in Russian)
9. Helgason S. *Groups and geometrical analysis.* NY, Academic Press, 1984

### Авторы

**Кассандров Владимир Всеволодович**, к.ф.-м.н., доцент, Институт гавитации и космологии, Российский университет дружбы народов, ул. Миклухо-Маклая, д. 6, г. Москва, 117198, Россия.
E-mail: vkassan@sci.pfu.edu.ru

### Просьба ссылаться на эту статью следующим образом:

Кассандров В. В. Алгебродинамика: в поисках истинной алгебраической “Мировой” структуры. *Пространство, время и фундаментальные взаимодействия.* 2023. № 3-4. С. 147–153. **Authors**

**Kassandrov Vladimir Vsevolodovich**, Ph.D., Associate Professor, Institute of gravitation and cosmology, Peoples' Friendship University of Russia, Miklukho-Maklaya st., 6, Moscow, 117198, Russia.
E-mail: vkassan@sci.pfu.edu.ru

### Please cite this article in English as:

Kassandrov V. V. The algebrodynamics: in search of the ultimate algebraic “World” structure . *Space, Time and Fundamental Interactions*, 2023, no. 3-4, pp. 147–153.

УДК 530.145



## УРАВНЕНИЕ ДИРАКА И ФЕРМИОННАЯ АЛГЕБРА

Кауффман Л. Х.[a,1]

[a] Иллинойский университет в Чикаго, 851 Саут Морган Стрит, Чикаго, Иллинойс, 60607-7045, США.

В данной работе рассматривается структура уравнения Дирака и дается новая трактовка уравнения Дирака в пространстве 1+1.

*Ключевые слова*: Алгебра Клиффорда, уравнение Дирака, доска Фейнмана.

## THE DIRAC EQUATION AND A FERMIONIC ALGEBRA

Kauffman L. H.[a,1]

[a] University of Illinois at Chicago, 851 South Morgan Street, Chicago, Illinois, 60607-7045, USA.

This paper examines the structure of the Dirac equation and gives a new treatment of the Dirac equation in 1+1 spacetime.

*Keywords*: Clifford algebra, Dirac Equation, Feynman checkerboard.
PACS: 03.65.Pm
DOI: 10.17238/issn2226-8812.2023.3-4.154-165

### 1. Introduction

This paper is a discussion of the structure of the Dirac equation, primarily in the case of one dimension of space and one dimension of time ($1+1$ spacetime). We reformulate the Dirac operator $\mathcal{D}$ so that there is a nilpotent element $U$, with $U^2 = 0$, in the Clifford algebra such that for a plane wave $\psi$, $\mathcal{D}\psi = U\psi$. This means that $U\psi$ is a solution to the Dirac equation since $\mathcal{D}(U\psi) = U^2\psi = 0 \times \psi = 0$. We explain this formulation in Section 2 of the paper, and use it in Section 3 to reformulate a nilpotent version of the Dirac equation for (1+1) spacetime in light cone coordinates. We can then give a solution to the Dirac equation by the method just indicated and we can compare this solution with the solutions already understood in relation to the Feynman checkerboard model. In the course of this reformulation we see that the transition to light cone coordinates corresponds to a rewriting of the Clifford algebra for the Dirac equation to a Fermionic algebra linked with a Clifford algebra. We obtain the following result (in summary).

We have the (1+1) Dirac equation in light cone coordinates $(l, r)$, using the light cone Dirac operator

$$\mathcal{D} = A\partial/\partial l + B\partial/\partial r - \alpha m.$$

The elements $A, B, \alpha$ satisfy the algebra relations:

$$AB + BA = 1, AB - BA = \alpha, A^2 = B^2 = 0, \alpha^2 = 1,$$

$$A\alpha = -A, \alpha A = A, B\alpha = B, \alpha B = -B.$$

Note that in this algebra the elements A and B form a Fermion algebra, each squaring to 0 and satisfying $AB + BA = 1$. The element $\alpha$ has square one, and can be regarded as a Clifford algebra element

[1] E-mail: kauffman@uic.edu

interacting with $A$ and $B$. This *special Fermion algebra* is the key to the calculations in this paper and we will study it further in subsequent work.

The rest of section 3 is a discussion of the relationship of our results in the paper with the Feynman checkerboard model and with our previous work on that model [1, 2].

The appendix discusses how the nilpotent and Majorana operators arise in three dimensions of space and one dimension of time. This appendix provides a link between our work and the work of Peter Rowlands [10]. The Majorana Dirac equation can be written as follows:

$$(\partial/\partial t + \hat{\eta}\eta\partial/\partial x + \epsilon\partial/\partial y + \hat{\epsilon}\eta\partial/\partial z - \hat{\epsilon}\hat{\eta}\eta m)\psi = 0$$

where $\eta$ and $\epsilon$ are the generators of a Clifford algebra with $\eta^2 = \epsilon^2 = 1$ and $\eta\epsilon + \epsilon\eta = 0$, and $\hat{\epsilon}, \hat{\eta}$ form a copy of this algebra that commutes with it. This combination of a Clifford algebra with itself is the underlying structure of Majorana Fermions. In the appendix we apply our methods to the Majorana Dirac Equation and give actual real solutions to the equation. These solutions make direct use of the Majorana Fermion Clifford algebra. This shows explicitly that Fermions and Majorana Fermions are related by the algebraic transformation between Fermion and Clifford algebra.

**Remark.** The more intricate algebra in this paper such as the special Fermion algebra described above can be regarded as coming from the patterns of the split quaternions seen as the Clifford algebra with generators $\alpha, \beta$ and relations $\alpha^2 = \beta^2 = 1, \alpha\beta + \beta\alpha = 0$. From these relations it follows that $(\alpha\beta)^2 = -1$ and if we write

$$U = \alpha\beta E + \alpha p + \beta m$$

where $E, p, m$ are scalars commuting with the algebra elements, then

$$U^2 = -E^2 + p^2 + m^2$$

since the cross terms all vanish in the product. Thus when $E^2 = p^2 + m^2$ we have a non-trivial nilpotent element $U$ in the Clifford algebra with $U^2 = 0$. This is the beginning of the key relationship of nilpotent algebra elements and Fermions as it occurs in the work of Peter Rowlands [10] and it is the keystone of the work in this paper as well.

## 2. The Dirac Equation

We begin by recalling how Dirac constructed his equation. By convention we take the speed of light to be equal to 1. Then energy $E$, momentum $p$ and mass $m$ are related through special relativity by the equation

$$E^2 = p^2 + m^2.$$

Dirac looked for an algebraic square root of $p^2+m^2$ so that he could have a linear operator corresponding to $E$ that would take the same role as the Hamiltonian in the Schrödinger equation.

We first take the case of one dimension of space and one dimension of time so that $p$ is a scalar. The quantum operator for momentum is

$$\hat{p} = -i\partial/\partial x,$$

the operator for energy is

$$\hat{E} = i\partial/\partial t,$$

and the operator for mass is

$$\hat{m} = m.$$

We can write an operator equation

$$\hat{E} = \alpha\hat{p} + \beta\hat{m},$$

where $\alpha$ and $\beta$ are elements of a a possibly non-commutative, associative algebra.

Then

$$\hat{E}^2 = \alpha^2\hat{p}^2 + \beta^2\hat{m}^2 + \hat{p}\hat{m}(\alpha\beta + \beta\alpha).$$

Hence we have $\hat{E}^2 = \hat{p}^2 + \hat{m}^2$ if we take

$$\alpha^2 = \beta^2 = 1,$$

$$\alpha\beta + \beta\alpha = 0.$$

The algebra so generated by $\alpha$ and $\beta$ is a simplest Clifford algebra.
**Remark.** Note that the Clifford algebra with generators $\alpha, \beta$ with relations as given above is often called the *split quaternions*. If we introduce a commuting (with $\alpha$ and $\beta$) square root of minus one, denoted $i$ with $i^2 = -1$, and let $I = i\alpha, J = i\beta, K = \beta\alpha$, then it is the case that $I^2 = J^2 = K^2 = IJK = -1$ and thus we obtain the quaternions from the split quaternions.
**Remark.** In general we take a Clifford algebra to be an associative algebra with abstract generators $e_1, e_2, \cdots, e_n$ so that $e_k^2 = 1$ for all $k$ and $e_r e_s + e_s e_r = 0$ whenever $r \neq s$. The generators are usually taken to be an orthonormal basis for a vector space over a field.
**Remark.** Clifford algebras and Fermion algebras are related to one another by a transformation that we illustrate here for the split quaternions. Let

$$U = (\alpha + i\beta)/2,$$

$$V = (\alpha - i\beta)/2.$$

then

$$U^2 = V^2 = (\alpha^2 - \beta^2 \pm i(\alpha\beta + \beta\alpha))/4 = 0,$$

$$UV + VU = (U + V)^2 = \alpha^2 = 1.$$

The relations $U^2 = V^2 = 0$ and $UV + VU = 1$ are characteristic of Fermion algebra and correspond to properties of creation and annihilation operators for Fermions. We will see that Fermion algebras arise naturally in relation to Clifford algebra formulations for the Dirac equation.
The Dirac equation is the operator equation

$$\hat{E}\psi = \alpha\hat{p}\psi + \beta\hat{m}\psi.$$

Thus the Dirac equation is the differential equation below.

$$i\partial\psi/\partial t = -i\alpha\partial\psi/\partial x + \beta m\psi.$$

We begin by discussing this version of the Dirac equation in $1 + 1$ spacetime, constructing solutions via light cone reformulaiton and we discuss the Feynman checkerboard model. In the Appendix, we explain how to extend these formulations to $(3 + 1)$ spacetime.

### 2.1. The Nilpotent Reformulation of the Dirac Equation

We can define the *Dirac operator* $\mathcal{O}$ as follows: Let $\mathcal{O} = i\partial/\partial t + i\alpha\partial/\partial x - \beta m$. Then the Dirac equation takes the form $\mathcal{O}\psi(x, t) = 0$.
Note that $\mathcal{O}e^{i(px-Et)} = (E - \alpha p - \beta m)e^{i(px-Et)}$.
We let $\Delta = (E - \alpha p - \beta m)$ and let

$$U = \alpha\beta\Delta = \alpha\beta E + \beta p - \alpha m,$$

so that

$$U^2 = -E^2 + p^2 + m^2 = 0.$$

(Note that $(\alpha\beta)^2 = \alpha\beta\alpha\beta = -\alpha\alpha\beta\beta = -1$ and that the cross terms cancel.)

**Remark.** It is of interest to note that in the split quaternions we have elements of the form

$$U = \alpha\beta E + \beta p - \alpha m$$

such that $U^2 = -E^2 + p^2 + m^2$ so that $U$ is nilpotent of order two exactly when $E^2 = p^2 + m^2$.
We now multiply the operator $\mathcal{O}$ by $\alpha\beta$ on the left, obtaining the operator

$$\mathcal{D} = \alpha\beta\mathcal{O} = i\alpha\beta\partial/\partial t + i\beta\partial/\partial x - \alpha m.$$

The Dirac equation is equivalent to the equation $\mathcal{D}\psi = 0$. Furthermore, we have have $\mathcal{D}(e^{i(px-Et)}) = Ue^{i(px-Et)}$. Thus for $\psi = e^{i(px-Et)}$, we have $\mathcal{D}(\psi) = U\psi$ and $\mathcal{D}(U\psi) = U^2\psi = 0$. Thus $U$ acts as a creation operator producing a solution to the Dirac equation.

This idea for reconfiguring the Dirac equation in relation to nilpotent algebra elements $U$ is due to Peter Rowlands [10]. Rowlands does this in the context of quaternion algebra. The solution to the Dirac equation that we have found is expressed in Clifford algebra. It can be articulated into specific vector solutions by using a matrix representation of the algebra.

### 2.2. Fermion Operators

We see that $U = \alpha\beta E + \beta p - \alpha m$ with $U^2 = 0$ is the essence of this plane wave solution to the Dirac equation. It is natural to compare this algebra structure with algebra of creation and annihilation operators that occur in quantum field theory.
If we let $\tilde{\psi} = e^{i(px+Et)}$ (reversing time), then we have $\mathcal{D}\tilde{\psi} = (\beta\alpha E + \beta p - \alpha m)\psi = U^\dagger\tilde{\psi}$, giving a definition of $U^\dagger$ corresponding to the anti-particle for $U\psi$.
We have $U = \alpha\beta E + \beta p - \alpha m$ and $U^\dagger = \beta\alpha E + \beta p - \alpha m$.
Note that here we have

$$(U + U^\dagger)^2 = (2\beta p + \alpha m)^2 = 4(p^2 + m^2) = 4E^2,$$

and

$$(U - U^\dagger)^2 = -(2\alpha\beta E)^2 = -4E^2.$$

We have that $U^2 = (U^\dagger)^2 = 0$ and $UU^\dagger + U^\dagger U = 4E^2$. Thus we have a direct appearance of the Fermion algebra corresponding to the Fermion plane wave solutions to the Dirac equation.

Normalizing by dividing by $2E$ we have $A = (\beta p - \alpha m)/E$ and $B = i\beta\alpha$. so that $A^2 = B^2 = 1$ and $AB + BA = 0$. then $U = (A + Bi)E$ and $U^\dagger = (A - Bi)E$, showing how the Fermion operators are expressed in terms of the simpler Clifford algebra of Majorana operators ($A$ and $B$ generating the split quaternions).

The decomposition of $U$and $U^\dagger$ into the corresponding Majorana Fermion operators with $A^2 = 1$ is exactly equivalent to $E^2 = p^2 + m^2$.

## 3. Spacetime in 1+1 Dimensions

We begin this section by discussing an algebra that is directly related to Clifford algebra. As we shall see, this algebra is also inherent in the Dirac equation when we use light cone coordinates.

### 3.1. Clifford algebra and Fermion algebra.

Suppose that we have a Clifford algebra generated by elements $\epsilon$ and $\eta$ with $\epsilon^2 = \eta^2 = 1$ and $\epsilon\eta + \eta\epsilon = 0$. Then we can define new elements $a$ and $b$ by the equations

$$\eta = a + b,$$

$$\epsilon\eta = a - b.$$

This means that

$$a = \frac{1}{2}(1 + \epsilon)\eta,$$

$$b = \frac{1}{2}(1 - \epsilon)\eta,$$

from which it follows that

$$a^2 = b^2 = 0, ab + ba = 1.$$

Note that we are given that the starting Clifford algebra is associative and so further identities such as

$$aba = a, bab = b, abab = ab, baba = ba$$

follow easily from the given identities. We call an associative algebra generated by $a, b$ with

$$a^2 = b^2 = 0, ab + ba = 1$$

a *Fermion algebra* since the annihilation, creation algebra for Fermions in quantum theory satisfies these identities. We see here that Clifford algebras (with an even number of generators) and Fermion algebras are interchangeable via the above transformations. This fact has been used by writers on Clifford algebras, [11] since it is useful to have projector properties such as $(ab)(ab) = ab$.
**Example.** In two by two matrix algebra, we can take

$$\epsilon = \begin{pmatrix} -1 & 0 \\ 0 & 1 \end{pmatrix}, \eta = \begin{pmatrix} 0 & 1 \\ 1 & 0 \end{pmatrix} = a + b.$$

Here

$$a = \begin{pmatrix} 0 & 0 \\ 1 & 0 \end{pmatrix}, b = \begin{pmatrix} 0 & 1 \\ 0 & 0 \end{pmatrix}.$$

Thus

$$ab = \begin{pmatrix} 0 & 0 \\ 0 & 1 \end{pmatrix}, ba = \begin{pmatrix} 1 & 0 \\ 0 & 0 \end{pmatrix}$$

so that

$$a^2 = b^2 = 0,$$

$$a + b = \eta,$$

$$a - b = \epsilon\eta,$$

$$ab + ba = 1,$$

$$ab - ba = \epsilon.$$

**Remark.** The above construction of Fermion algebra from Clifford algebra occurs without invoking an extra commuting square root of negative unity. It is common in physical applications to use a parallel construction involving $i$ where $i^2 = -1$ and $i$ commutes with all elements of the algebra. One can then define $\psi = \frac{1}{2}(\eta + i\epsilon)$ and $\psi^\dagger = \frac{1}{2}(\eta - i\epsilon)$. It follows that $\psi^2 = (\psi^\dagger)^2 = 0$ and $\psi\psi^\dagger + \psi^\dagger\psi = 1$, and one has a Fermion algebra with complex conjugation constructed in relation to a Clifford algebra. Another relation with a commuting $i$ occurs if we take

$$a = (i/2)(\alpha\beta + \beta)$$

$$b = (i/2)(\alpha\beta - \beta)$$

where $\alpha$ and $\beta$ form a Clifford algebra with $\alpha^2 = \beta^2 = 1$ and $\alpha\beta + \beta\alpha = 0$. Then $a$ and $b$ satisfy the Fermion relations and

$$ab + ba = 1,$$

$$ab - ba = \alpha,$$

but

$$a + b = i\alpha\beta,$$

$$a - b = i\beta.$$

Notice that $(i\alpha\beta)^2 = +1$ while $(i\beta)^2 = -1$. Thus we can regard this as a re-writing of the previous pattern with

$$i\alpha\beta = \eta$$

and

$$i\beta = \epsilon\eta$$

so that

$$\alpha = \beta\beta\alpha = -\beta\alpha\beta = i\beta[\alpha\beta = \epsilon\eta\eta = \epsilon.$$

This means that this Fermion algebra can occur with or without the explicit commuting square root of negative unity, $i$.

### 3.2. The Dirac Equation in Light Cone Coordinates

Light cone coordinates $r$ and $l$ are defined by

$$r = (x + t)/2$$

and

$$l = (x - t)/2.$$

Note that $4rl = x^2 - t^2$. Thus the light cone in $(x, t)$ Minkowski space (light speed $c = 1$) is descibed by the equations $r = 0$ or $l = 0$.

Recall the translation of operators to light cone coordinate operators.

$$\hat{E} = i\partial/\partial t = (i/2)(\partial/\partial r + \partial/\partial l)$$

$$\hat{p} = (1/i)\partial/\partial x = (1/2i)(\partial/\partial r - \partial/\partial l)$$

Here is the nilpotent version of the Dirac operator as we have formulated it.

$$\mathcal{D} = \alpha\beta\hat{E} + \beta\hat{p} - \alpha\hat{m}$$

We translate this operator into light cone coordinates.

$$\mathcal{D} = \alpha\beta((i/2)(\partial/\partial r + \partial/\partial l)) + \beta((1/2i)(\partial/\partial r - \partial/\partial l)) - \alpha m$$

$$\mathcal{D} = i[(\alpha\beta + \beta)/2]\partial/\partial l + i[(\alpha\beta - \beta)/2]\partial/\partial r - \alpha m$$

Thus

$$\mathcal{D} = A\partial/\partial l + B\partial/\partial r - \alpha m$$

$$A = (i/2)(\alpha\beta + \beta)$$

$$B = (i/2)(\alpha\beta - \beta)$$

As the reader can see, we arrive at algebraic coefficients that we have described above as the Fermion algebra associated with the Clifford algebra generated by $\alpha$ and $\beta$.

$$A + B = i\alpha\beta$$

$$A - B = i\beta$$

Further relations take the form:

$$AB + BA = 1, AB - BA = \alpha, A^2 = B^2 = 0, \alpha^2 = 1$$

$$A\alpha = -A, \alpha A = A, B\alpha = B, \alpha B = -B.$$

Thus

$$A\alpha + \alpha A = 0, B\alpha + \alpha B = 0$$

$$A\beta + \beta A = i, B\beta + \beta B = -i$$

### 3.3. Plane waves in light cone coordinates.

Let

$$\psi = e^{i(rX - lY)}$$

where

$$X = p - E$$

and

$$Y = p + E.$$

Note that $XY = -m^2$. This is the plane wave rewritten in light cone coordinates. Then with

$$\mathcal{D} = A\partial/\partial l + B\partial/\partial r - \alpha m,$$

$$\mathcal{D}\psi = U\psi$$

where

$$U = -iAX + iBY - \alpha m.$$

Thus

$$U^2 = ABXY + BAXY + m^2 = XY + m^2 = p^2 - E^2 + m^2 = 0.$$

Note that with

$$U^\dagger = -iAY + iBX - \alpha m$$

we have

$$(U^\dagger)^2 = 0$$

and

$$UU^\dagger + U^\dagger U = 4E^2$$

**Summary.** We have the (1+1) Dirac equation in light cone coordinates, using the light cone Dirac operator

$$\mathcal{D} = A\partial/\partial l + B\partial/\partial r - \alpha m.$$

The elements $A, B, \alpha$ satisfy the Fermionic algebra relations:

$$AB + BA = 1, AB - BA = \alpha, A^2 = B^2 = 0, \alpha^2 = 1,$$

$$A\alpha = -A, \alpha A = A, B\alpha = B, \alpha B = -B.$$

We can directly see the action of the light cone Dirac operator on a plane wave expressed in light cone coordinates. The plane wave is given by the formula

$$\psi = e^{i(rX - lY)}$$

where $X = p - E$ and $Y = p + E$. Thus $XY = -m^2$. Then $\mathcal{D}\psi = U\psi$ where $U = -iAX + iBY - \alpha m$, and $U^2 = 0$.

Note that with $U^\dagger = -iAY + iBX - \alpha m$ we have $(U^\dagger)^2 = 0$ and $UU^\dagger + U^\dagger U = 4E^2$. Thus we have rewritten the nilpotent Dirac operator and its equation directly in light cone coordinates, with the help of the Fermionic algebra.

### 3.4. Solving the 1+1 Dirac Equation

The (real valued) Majorana version of the Dirac operator

$$\mathcal{D} = A\partial/\partial l + B\partial/\partial r - \alpha m$$

that we have discussed above can be taken with the representation

$$A = \begin{pmatrix} 0 & 0 \\ 1 & 0 \end{pmatrix}, B = \begin{pmatrix} 0 & 1 \\ 0 & 0 \end{pmatrix}, \alpha = \begin{pmatrix} -1 & 0 \\ 0 & 0 \end{pmatrix}.$$

Then

$$AB = \begin{pmatrix} 0 & 0 \\ 0 & 1 \end{pmatrix}, BA = \begin{pmatrix} 1 & 0 \\ 0 & 0 \end{pmatrix}, AB - BA = \begin{pmatrix} -1 & 0 \\ 0 & 1 \end{pmatrix} = \alpha.$$

Letting $\Theta = rX - lY$, and $S = Sin(\Theta), C = Cos(\Theta)$, we have

$$U\psi = U(C + iS) = (AXS - BYS - \alpha mC) + i(-AXC + BYC - \alpha mS).$$

In the matrix representation we find

$$AXS - BYS - \alpha mC = \begin{pmatrix} mC & -YS \\ XS & -mC \end{pmatrix}.$$

And from this, letting

$$\psi_1 = mC, \psi_2 = XS$$

we have

$$\partial\psi_1/\partial r = -mXS = -m\psi_2$$

and

$$\partial\psi_2/\partial l = -XYC = m^2C = m\psi_1$$

Thus

$$\partial\psi_1/\partial r = -m\psi_2$$

$$\partial\psi_2/\partial l = m\psi_1$$

Note that these equations are satisfied by

$$\psi_1 = -mSin(-(E-p)r - (E+p)l),$$

$$\psi_2 = (E+p)Cos(-(E-p)r - (E+p)l)$$

exactly when $E^2 = p^2 + m^2$ as we have assumed. It is quite interesting to see these direct solutions to the Dirac equation emerge in this $1+1$ case. The solutions are fundamental and they are distinct from the usual solutions that emerge from the Feynman checkerboard model [1, 2]. It is the above equations that form the basis for the Feynman checkerboard model that is obtained by examining paths in a discrete Minkowski plane generating a path integral for the Dirac equation.

**Remark.** Note that a simplest instance of the above form of solution is obtained by writing

$$e^{i(r+l)} = cos(r+l) + isin(r+l) = \sum_{n=0}^{\infty}(\sqrt{-1})^n \sum_{i+j=n} \frac{r^i}{i!}\frac{l^j}{j!}.$$

Then with $\psi_2 = cos(r+l)$ and $\psi_1 = sin(r+l)$ we have $\partial\psi_1/\partial l = \psi_2$, $\partial\psi_2/\partial r = -\psi_1$, solving the Dirac equation in the case where $m = 1$.

**Remark.** Let $\psi_R = \sum_{k=0}^{\infty}(-1)^k \frac{r^{k+1}}{(k+1)!}\frac{l^k}{k!}$, $\psi_L = \sum_{k=0}^{\infty}(-1)^k \frac{r^k}{k!}\frac{l^{k+1}}{(k+1)!}$, $\psi_0 = \sum_{k=0}^{\infty}(-1)^k \frac{r^k}{k!}\frac{l^k}{k!}$. Then $\psi_1 = \psi_0 + \psi_L$ and $\psi_2 = \psi_0 - \psi_R$ give a solution to the Dirac equation in light cone coordinates as we have written it above with $m = 1 : \partial\psi_1/\partial l = \psi_2, \partial\psi_2/\partial r = -\psi_1$. These series are shown in [2] to be a natural limit of evaluations of sums of discrete paths on the Feynman checkerboard. The key to our earlier approach is that if one defines

$$C[\Delta]^x_k = \frac{(x)(x-\Delta)(x-2\Delta)\cdots(x-(k-1)\Delta)}{k!},$$

Then $C[\Delta]^x_k$ takes the role of $\frac{x^k}{k!}$ for discrete different derivatives with step length $\Delta$ and it can be interpreted as a choice coefficient. A Feynman path on a rectangle in Minkowski space can be interpreted as two choice of $k$ or $k+1$ points along the $r$ and $l$ edges of the rectangle. Thus the products in the limit expressions of the form $\frac{r^k}{k!}\frac{l^{k+1}}{(k+1)!}$ or $\frac{r^k}{k!}\frac{l^k}{k!}$ correspond to paths on the checkerboard with $k$ corners in a limit where there are infinitely many such paths. The details are in our paper [2]. The solutions we have given above, motivated by the Majorana algebra, are related in form to these path sum solutions. Our solutions contain more information, related to the factorization $(E-p)(E+p) = E^2 - p^2 = m^2$. In the usual checkerboard solution the propagators only know about the mass and not its factorization relative to energy and momentum. More work needs to be done to fully understand the relationship of solutions to the Dirac equation and path summations.

**Path Sum Derivation.**

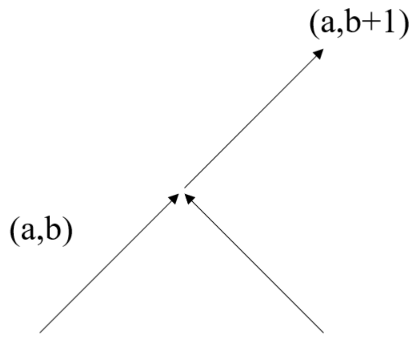


**Рис. 1.** Path Summation

Here we describe the Feynman checkerboard model where light-speed paths $p$ with corners, in Minkowski space, are each evaluated by $i^{c(p)}$ where $c(p)$ denotes the number of corners in the path. Let $(a,b)$ denote a point in discrete Minkowski spacetime in light cone coordinates. Thus $a$ denotes the number of steps taken to the left and $b$ denotes the number of steps taken to the right. We let $\psi_L(a,b)$ denote the sum over the paths that enter the point $(a,b)$ from the left and $\psi_R(a,b)$ the sum over the paths that enter $(a,b)$ from the right. View Figure 1.

It is clear from the diagram in the figure that

$$\psi_L(a,b+1) = \psi_L(a,b) + i\psi_R(a,b).$$

Thus we have a discrete version of the Dirac equation in light cone coordinates that is satisfied by the Feynman path summation. If we adjust the step sizes and take a limit we find

$$\partial\psi_L/\partial r = i\psi_R$$

and similarly

$$\partial\psi_R/\partial l = i\psi_L.$$

This pair of equations is the the Dirac Equation in light cone coordinates. When we take the the evalutation of a path to be $(-1)^{c(p)}$, we obtain the real version of the Dirac equation, as discussed above.

It remains to be seen how our plane wave solutions of the (1+1) Dirac equation in light cone coordinates are related to the Feynman path summation.

## 4. Appendix - Writing in the Full Dirac Algebra

We have written the Dirac equation in one dimension of space and one dimension of time. We now boost the formalism directly to three dimensions of space. We take an independent Clifford algebra generated by $\sigma_1, \sigma_2, \sigma_3$ with $\sigma_i^2 = 1$ for $i = 1, 2, 3$ and $\sigma_i \sigma_j = -\sigma_j \sigma_i$ for $i \neq j$. Now assume that $\alpha$ and $\beta$ as we have used them above generate an independent Clifford algebra that commutes with the algebra of the $\sigma_i$. Replace the scalar momentum $p$ by a 3-vector momentum $p = (p_1, p_2, p_3)$ and let $p \bullet \sigma = p_1\sigma_1 + p_2\sigma_2 + p_3\sigma_3$. We replace $\partial/\partial x$ with $\nabla = (\partial/\partial x_1, \partial/\partial x_2, \partial/\partial x_2)$ and $\partial p/\partial x$ with $\nabla \bullet p$. We then have the following form of the Dirac equation.

$$i\partial\psi/\partial t = -i\alpha\nabla \bullet \sigma\psi + \beta m\psi.$$

Let $\mathcal{O} = i\partial/\partial t + i\alpha\nabla \bullet \sigma - \beta m$ so that the Dirac equation takes the form $\mathcal{O}\psi(x,t) = 0$.
In analogy to our previous discussion we let $\psi(x,t) = e^{i(p\bullet x - Et)}$ and construct solutions by first applying the Dirac operator to this $\psi$. The two Clifford algebras interact to generalize directly the nilpotent solutions and Fermion algebra,that we have detailed for one spatial dimension, to this three dimensional case. To this purpose the modified Dirac operator is

$$\mathcal{D} = i\alpha\beta\partial/\partial t + \beta\nabla \bullet \sigma - \alpha m.$$

And we have that $\mathcal{D}\psi = U\psi$ where $U = \alpha\beta E + \beta p \bullet \sigma - \alpha m$. We have that $U^2 = 0$ and $U\psi$ is a solution to the modified Dirac Equation, just as before. And just as before, we can articulate the structure of the Fermion operators and locate the corresponding Majorana Fermion operators.

### 4.1. Majorana Fermions

There is more to do. We now discuss making Dirac algebra distinct from the one generated by $\alpha, \beta, \sigma_1, \sigma_2, \sigma_3$ to obtain an equation that can have real solutions. This was the strategy that Majorana [3] followed to construct his Majorana Fermions. A real equation can have solutions that are invariant under complex conjugation and so can correspond to particles that are their own anti-particles. We will describe this Majorana algebra in terms of the split quaternions $\epsilon$ and $\eta$. For convenience we use the matrix representation given below.

$$\epsilon = \begin{pmatrix} -1 & 0 \\ 0 & 1 \end{pmatrix}, \eta = \begin{pmatrix} 0 & 1 \\ 1 & 0 \end{pmatrix}.$$

Let $\hat{\epsilon}$ and $\hat{\eta}$ generate another, independent algebra of split quaternions, commuting with the first algebra generated by $\epsilon$ and $\eta$. Then a totally real Majorana Dirac equation can be written as follows:

$$(\partial/\partial t + \hat{\eta}\eta\partial/\partial x + \epsilon\partial/\partial y + \hat{\epsilon}\eta\partial/\partial z - \hat{\epsilon}\hat{\eta}\eta m)\psi = 0.$$

To see that this is a correct Dirac equation, note that

$$\hat{E} = \alpha_x\hat{p_x} + \alpha_y\hat{p_y} + \alpha_z\hat{p_z} + \beta m$$

(Here the "hats" denote the quantum differential operators corresponding to the energy and momentum.) will satisfy

$$\hat{E}^2 = \hat{p_x}^2 + \hat{p_y}^2 + \hat{p_z}^2 + m^2$$

if the algebra generated by $\alpha_x, \alpha_y, \alpha_z, \beta$ has each generator of square one and each distinct pair of generators anti-commuting. From there we obtain the general Dirac equation by replacing $\hat{E}$ by $i\partial/\partial t$, and $\hat{p_x}$ with $-i\partial/\partial x$ (and same for $y, z$).

$$(i\partial/\partial t + i\alpha_x\partial/\partial x + i\alpha_y\partial/\partial y + i\alpha_z\partial/\partial y - \beta m)\psi = 0.$$

This is equivalent to

$$(\partial/\partial t + \alpha_x \partial/\partial x + \alpha_y \partial/\partial y + \alpha_z \partial/\partial y + i\beta m)\psi = 0.$$

Thus, here we take

$$\alpha_x = \hat{\eta}\eta, \alpha_y = \epsilon, \alpha_z = \hat{\epsilon}\eta, \beta = i\hat{\epsilon}\hat{\eta}\eta,$$

and observe that these elements satisfy the requirements for the Dirac algebra. Note how we have a significant interaction between the commuting square root of minus one ($i$) and the element $\hat{\epsilon}\hat{\eta}$ of square minus one in the split quaternions. This brings us back to considerations about the source of the square root of minus one. Both viewpoints combine in the element $\beta = i\hat{\epsilon}\hat{\eta}\eta$ that makes this Majorana algebra work. Since the algebra appearing in the Majorana Dirac operator is constructed entirely from two commuting copies of the split quaternions, there is no appearance of the complex numbers, and when written out in $2\times 2$ matrices we obtain coupled real differential equations to be solved. This is a beginning of a new study of Majorana Fermions. For more information about this viewpoint, see [9]. In the next section we rewrite the Majorana Dirac operator, guided by nilpotents, obtaining solutions that directly use the Majorana Fermion operators.

### 4.2. Nilpotents, Majorana Fermions and the Majorana-Dirac Equation

Let $\mathcal{D} = (\partial/\partial t + \hat{\eta}\eta\partial/\partial x + \epsilon\partial/\partial y + \hat{\epsilon}\eta\partial/\partial z - \hat{\epsilon}\hat{\eta}\eta m)$. In the last section we have shown how $\mathcal{D}$ can be taken as the Majorana operator through which we can look for real solutions to the Dirac equation. Letting $\psi(x,t) = e^{i(p\bullet r - Et)}$, we have

$$\mathcal{D}\psi = (-iE + i(\hat{\eta}\eta p_x + \epsilon p_y + \hat{\epsilon}\eta p_z) - \hat{\epsilon}\hat{\eta}\eta m)\psi.$$

Let

$$\Gamma = (-iE + i(\hat{\eta}\eta p_x + \epsilon p_y + \hat{\epsilon}\eta p_z) - \hat{\epsilon}\hat{\eta}\eta m)$$

and

$$U = \epsilon\eta\Gamma = (i(-\eta\epsilon E - \hat{\eta}\epsilon p_x + \eta p_y - \epsilon\hat{\epsilon}p_z) + \epsilon\hat{\epsilon}\hat{\eta}m).$$

The element $U$ is nilpotent, $U^2 = 0$, and we have that $U = A + iB$, $AB + BA = 0$, $A = \epsilon\hat{\epsilon}\hat{\eta}m$, $B = -\eta\epsilon E - \hat{\eta}\epsilon p_x + \eta p_y - \epsilon\hat{\epsilon}p_z$, $A^2 = -m^2$, and $B^2 = -E^2 + p_x^2 + p_y^2 + p_z^2 = -m^2$.
Letting $\nabla = \epsilon\eta\mathcal{D}$, we have a new Majorana Dirac operator with $\nabla\psi = U\psi$ so that $\nabla(U\psi) = U^2\psi = 0$. Letting $\theta = (p \bullet r - Et)$, we have $U\psi = (A + Bi)e^{i\theta} = (A + Bi)(Cos(\theta) + iSin(\theta)) = (ACos(\gamma) - BSin(\theta)) + i(BCos(\theta) + ASin(\theta))$.
Thus we have found two real solutions to the Majorana Dirac Equation:

$$\Phi = ACos(\theta) - BSin(\theta),$$

$$\Psi = BCos(\theta) + ASin(\theta)$$

with $\theta = (p \bullet r - Et)$ and $A$ and $B$ the Majorana operators

$$A = \epsilon\hat{\epsilon}\hat{\eta}m,$$

$$B = -\eta\epsilon E - \hat{\eta}\epsilon p_x + \eta p_y - \epsilon\hat{\epsilon}p_z.$$

Note how the Majorana Fermion algebra generated by $A$ and $B$ comes into play in the construction of these solutions. This answers a natural question about the Majorana Fermion operators. Should one take the Majorana operators themselves seriously as representing physical states? Our calculation suggests that one should take them seriously.

In other work [4, 5, 6, 7] we review the main features of recent applications of the Majorana algebra and its relationships with representations of the braid group and with topological quantum computing. The present analysis of the Majorana Dirac equation first appears in our paper [9].

**Список литературы/References**


1. R. P. Feynman and A. R. Hibbs [1965] , *Quantum Mechanics and Path Integrals* McGraw Hill Companies, Inc, New York.
2. L. H. Kauffman and H. P. Noyes [1996], Discrete Physics and the Dirac Equation, *Physics Letters A*, 218 ,pp. 139-146.
3. E. Majorana [1937], A symmetric theory of electrons and positrons, *I Nuovo Cimento*, 14 (1937), pp. 171-184.
4. L. H. Kauffman [1991,1994,2001,2012], *Knots and Physics,* World Scientific Pub., Singapore.
5. Kauffman, Louis H. Knot logic and topological quantum computing with Majorana Fermions. In Logic and algebraic structures in quantum computing and information. *Lecture Notes in Logic, J. Chubb, J. Chubb, Ali Eskandarian, and V. Harizanov, editors* 124 (2016).
6. Kauffman, Louis H. Iterant algebra. *Entropy* 19.7 (2017): 347.
7. L. H. Kauffman [2018], Majorana Fermions and representations of the braid group. *Internat. J. Modern Phys. A* 33 (2018), no. 23, 1830023, 28 pp.
8. L. H. Kauffman and S. J. Lomonaco Jr. [2007], $q$-deformed spin networks, knot polynomials and anyonic topological quantum computation. *J. Knot Theory Ramifications* 16 (2007), no. 3, 267–332.
9. L. H. Kauffman and P. Rowlands [2021], The Dirac equation and the Majorana Dirac equation, *Aporia - 40-th Anniversary ANPA Proceedings 1979-2019*, Edited by John Ceres Amson, ANPA Pub. February 2021.
10. Rowlands, Peter. *Zero to Infinity: The foundations of physics.* Vol. 41. World Scientific, 2007.
11. Sobczyk, Garret. *Matrix Gateway to Geometric Algebra, Spacetime and Spinors.* Amazon Distribution GmbH, 2019.


**Авторы**


**Луи Хирш Кауффман**, профессор, Факультет математики, статистики и вычислительной техники, Иллинойский университет в Чикаго, 851 Саут Морган Стрит, Чикаго, Иллинойс, 60607-7045, США.

E-mail: kauffman@uic.edu


**Просьба ссылаться на эту статью следующим образом:**


Кауффман Л. Х. Уравнение Дирака и фермионная алгебра. *Пространство, время и фундаментальные взаимодействия.* 2023. № 3-4. С. 154–165.


**Authors**


**Louis Hirsch Kauffman**, professor, Department of Mathematics, Statistics and Computer Science, University of Illinois at Chicago, 851 South Morgan Street, Chicago, Illinois, 60607-7045, USA.

E-mail: kauffman@uic.edu


**Please cite this article in English as:**


Kauffman L. H. The Dirac Equation and a Fermionic Algebra. *Space, Time and Fundamental Interactions*, 2023, no. 3-4, pp. 154–165.

УДК 537.8, 530.12



# ОБОБЩЕННЫЕ МОДЕЛИ КАЛУЦЫ - КЛЕЙНА С ЛАГРАНЖИАНАМИ ГАУССА - БОННЕ

Кернер Р.[a,1]

[a] Университет Сорбонна, г. Париж, 75005, Франция.

Пятимерное обобщение эйнштейновской теории гравитации, впервые предложенное Т. Калуцей (1921) и улучшенное несколькими годами позже О. Клейном (1926), привело к модели Калуцы-Клейна, включающей электромагнетизм и гравитацию, и варианту теории гравитации Бранса-Дике, содержащему скалярное поле, взаимодействующее с метрическим тензорным полем. Однако ни одна из этих моделей не использовала возможности, открывающиеся при расширении вариационного принципа Эйнштейна-Гильберта за счет включения инварианта Гаусса-Бонне, который в 5 измерениях уже не является чистой дивергенцией и существенно модифицирует уравнения движения теории.

После напоминания основ модели Калуцы-Клейна, включая неабелев случай, мы даем краткий обзор многомерных космологических моделей со скалярными полями, порожденными калибровочными полями, вырожденными на структурной группе, включая обобщенный лагранжиан, содержащий член Гаусса-Бонне $R_{ABCD}R^{ABCD} - 4R_{AB}R^{AB} + R^2$.

Далее мы возвращаемся к 5-мерной модели Калуцы-Клейна, без скалярного поля и пренебрегая гравитацией, но с вариационным принципом, обогащенным членом Гаусса-Бонне. Это приводит в минковском пространстве-времени к интересному варианту нелинейной электродинамики. После обсуждения модифицированных уравнений Максвелла мы показываем, как может быть построен тороидальный солитон, и демонстрируем, что в нем проявляются наиболее существенные свойства электрона Дирака: электрический заряд, магнитный момент и спин. Он также предсказывает симметрию частица-античастица.

*Ключевые слова*: Теория Калуцы-Клейна, инварианты Гаусса-Бонне, нелинейная электродинамика, пучки волокон, космология в 10 измерениях.

# GENERALIZED KALUZA-KLEIN MODELS WITH GAUSS-BONNET LAGRANGIANS

Kerner R.[a,1]

[a] Sorbonne University, Paris, 75005, France.

The five-dimensional generalization of Einstein's theory of gravitation proposed first by Th. Kaluza (1921) and improved a few years later by O. Klein (1926) has led to the Kaluza-Klein model incorporating electromagnetism and gravitation, and a variant of the Brans-Dicke theory of gravity, containing a scalar field interacting with metric tensor field. However, neither of these models did use the possibilities offered by the enlargement of the Einstein-Hilbert variational principle via including the Gauss-Bonnet invariant, which in 5 dimensions is no more a pure divergence, and modifies substantially the equations of motion of the theory.

After recalling the basics of the Kaluza-Klein model, including the non-abelian case. we give a short review of multi-dimensional cosmological models with scalar fields generated by gauge fields defined on the structural group, including the generalized lagrangian containing the Gauss-Bonnet term $R_{ABCD}R^{ABCD} - 4R_{AB}R^{AB} + R^2$.

Then we turn our attention back to the 5-dimensional Kaluza-Klein model, without scalar field and neglecting gravity, but with variational principle enriched by the Gauss-Bonnet term, This leads, in the Minkowskian space-time, to an interesting variant of non-linear Electrodynamics. After discussing the modified Maxwell's equations, we show how a toroidal soliton can be constructed, and show that it displays the most essential features of Dirac's electron: electric charge, magnetic moment, and spin. It also predicts the particle-anti particle symmetry.

*Keywords*: Kaluza-Klein theory, Gauss-Bonnet invariants, Non-linear Electrodynamics, Fibre Bundles, Cosmology in 10 dimensions.

[1]E-mail: richard.kerner@sorbonne-universite.fr

PACS: 03.50.-z, 03.50.Kk, 04.50.+h, 04.50.Kd
DOI: 10.17238/issn2226-8812.2023.3-4.166-187

## 1. Introduction

After the advent of the Relativity Theory proposed by Einstein i 1905, and its geometrical interpretation by Hermann Minkowski a few years later, the fully relativistic interpretation of electromagnetism was achieved. The Maxwell-Faraday theory was reformulated in terms of four-vectors and one and two-forms defined on the four dimensional space-time manifold.

The Kaluza-Klein theory was an attempt to unify classical field theories of gravitation and electromagnetism on the basis of the idea of the extension of the four-dimensional Minowskian spacetime by adding an extra spatial dimension, thus passing to a five-dimensional spacetime with pseudo-Euclidean metric $g_{AB} = \text{diag}(+1, -1, -1, -1, -1)$. Curiously enough, the first to come with this idea was Gunnar Nordström (see [1]) who made his proposal of unification of gravitational and electromagnetic fields in 1914, one year before Einstein published his paper on General Relativity. In order to take gravitation into account Nordström added a fifth component to the electromagnetic vector potential. Note that he meant the Newtonian theory of gravity, represented by the scalar potential. Then the generalized Maxwell equations in five dimensions could be derived from a five-dimensional variational principle mimicking the lagrangian of the usual electromagnetism.

Introducing the five-dimensional vector potential

$$A_C = [A_\mu, A_5] = [A_\mu, \phi], \quad \text{with } \; B, C, .. = 1, 2, .., 5, \;\; \mu, \nu = 0, 1, 2, 3. \tag{1.1}$$

the Faraday-Maxwell field tensor could be generalized to five dimensons as follows:

$$F_{BC} = \partial_B A_C - \partial_C A_B, \quad \rightarrow \quad F_{\mu\nu} = \partial_\mu A_\nu - \partial_\nu A_\mu, \;\; F_{\mu 5} = -F_{5\mu} = \partial_\mu \phi - \partial_5 A_\mu. \tag{1.2}$$

$$\mathcal{L}_5 = -\frac{1}{4} F_{BC} F^{BC} = -\frac{1}{4} F_{\mu\nu} F^{\mu\nu} - \frac{1}{2} \partial_\mu \phi \partial^\mu \phi. \tag{1.3}$$

The homogeneous set of Maxwell's equations is satisfied by virtue of the definition (1.2), giving two independent identities, the usual one, valid also in four dimensional version:

$$\partial_\mu F_{\nu\lambda} + \partial_\nu F_{\lambda\mu} + \partial_\lambda F_{\mu\nu} = 0, \tag{1.4}$$

the extra set giving the following identities:

$$\partial_5 F_{\mu\nu} + \partial_\mu F_{\nu 5} + \partial_\nu F_{5\mu} = 0, \;\; \rightarrow \;\; \partial_5 F_{\mu\nu} = 0, \tag{1.5}$$

which reduces to a tautology due to the definition of Faraday's tensor; The last independent combination of three indices, $(5, \mu, 5)$, say, yields the following identity:

$$\partial_5 F_{\mu 5} + \partial_\mu F_{55} + \partial_5 F_{5\mu} = 0, \tag{1.6}$$

which is a tautology, too, because $F_{55} = 0$ and $F_{\mu 5} = -F_{5\mu}$ Therefore we cannot exclude in principle the dependence of the fifth component of our 5-dimensional vector potential (the scalar field $\phi$ included) on the fifth coordinate $x^5$. Let us however assume this for the sake of simplicity; then the differential system resulting from the variation of action with integrand given by (1.3) including the generalized current term $J^B A_B = j^\mu A_\mu + j^5 \phi$ is:

$$\partial_\mu F^{\mu\lambda} = -j^\lambda, \quad = -j^5, \tag{1.7}$$

reproducing the usual pair of Maxwell's equations with sources, which in appropriate units read:

$$\mathbf{rot\ H} = \mathbf{j} + \frac{\partial \mathbf{D}}{\partial t} \;\; \text{and} \;\; \text{div}\mathbf{D} = \rho \tag{1.8}$$

the fifth component yielding the d'Alembert equation for the gravitational potential $\phi$:

$$\frac{1}{c^2}\frac{\partial^2\phi}{\partial t^2} - \Delta\phi = \mu, \tag{1.9}$$

It is noticeable that in Nordström's 5-dimensional unification there is no interaction whatsoever between gravity and electromagnetism, they are described by totally independent potentials; on the other hand, the gravitational field is dynamical and can propagate with the speed of light. This was a step forward with respect to Newton's theory of gravitation, to which Nordström's model reduces in the case of a purely static field $\phi$.

The 5-dimensional unification of electromagnetism and gravity was proposed by Th. Kaluza after Einstein published his General relativity paper, and was based on the generalized Einstein's equations, involving the metric tensor as dynamical variable. After an approval letter from Einstein to whom Kaluza sent his results in 1919, got an approval letter, he published them in 1921 ([2]).

Kaluza's paper contained an extension of general relativity to five dimensions, with a metric tensor of 15 components, out of which ten were identified with the four-dimensional spacetime metric, four components with the electromagnetic vector potential, and one component with a hypothetical scalar field (sometimes called the "dilaton". The 5-dimensional variational principle yields the 4-dimensional Einstein field equations, with the electromagnetic energy-momentum tensor as source on the right-hand side, the Maxwell equations for the electromagnetic field, and an extra equation for the scalar field. In order to simplify the theory, Kaluza introduced the "cylinder condition" hypothesis assuming that no component of the five-dimensional metric depends on the fifth dimension.

After the advent of Quantum Mechanics, Oskar Klein ([3]) gave Kaluza's classical five-dimensional theory a quantum interpretation. He assumed that the fifth dimension was compact and microscopic, to explain the cylinder condition. Klein suggested that the geometry of the extra fifth dimension could take the form of a circle, with the radius of $10^{-30}$ cm. More precisely, the radius of the circular dimension is 23 times the Planck length, which in turn is of the order of $10^{-33}$ cm.

Kaluza's and Klein's ideas seemed attractive enough to Einstein, who published his comment on five-dimensional theories in 1927 ([4]).

Classical theory was completed in the 40-ties and the full field equations including the scalar field were obtained almost simultaneously Yves Thiry ([5], [6]), Pasqual Jordan ([7]) and W. Scherrer ([8].

Jordan's work led to the scalar-tensor theory of Brans-Dicke ([9]), who were apparently unaware of Thiry's or Scherrer's papers.

The full expressions for the curvature tensors in the complete Kaluza equations were given by Coquereaux and Esposito-Farese ([16]).

What seems really amazing is that although the Gauss-Bonnet invariant of second order was known since a long time, the fact that it can be used as a non-trivial integrand for variational principle in mora than four dimensions, in particular in the Kaluza-Klein theory. The second-order Gauss-Bonnet invariant is the unique quadratic combination of Riemann tensor's components that under variation yields only second-order differential equations. It is a pure divergence in 4 dimensions, but starting from fivr dimensions its variation contributes to the second-order Einstein differential equations, although in a very non-linear way.

The general definition of Gauss-Bonnet invariant of order $p$ is given in the followoing formula:

$$I_p = \frac{1}{2^p}\,\delta^{\mu_1\mu_2...\mu_p\nu_1\nu_2...\nu_p}_{\rho_1\rho_2...\rho_p\sigma_1\sigma_2...\sigma_p}\; R_{\mu_1\nu_1}{}^{\rho_1\sigma_1} R_{\mu_2\nu_2}{}^{\rho_2\sigma_2} ... R_{\mu_p\nu_p}{}^{\rho_p\sigma_p} \tag{1.10}$$

where the totally antisymmetric tensor of order $n$ is defined as the anti-symmetrized prodict of $n$ Kronecker's deltas:

$$\delta^{\mu_1\mu_2...\mu_n}_{\rho_1\rho_2...\rho_n} = \delta^{\mu_1}{}_{[\rho_1}\delta^{\mu_2}_{\rho_2}...\delta^{\mu_n}_{[\rho_n]} \tag{1.11}$$

An important feature of these invariants is that an invariant of order $p$, $I_p$, reduces to a pure divergence and do not contribute to the equations of motion under variation in dimensions lower than $2p$. Thus the first invariant, which is the Riemann scalar $R$, does not produce any equations in 2 dimensions: its integral over the entire manifold is constant and equal to $2\pi\chi$, where $\chi$ is the Euler-Poincaré characteristic (equal to 2 for a sphere, and 0 for a torus). The invariant $I_2$ is a pure divergence up to 4 dimensions, and $I_3$ is not a pure divergence only for manifolds whose dimension is higher than 6.

In 1971 Lovelock ([10]) presented an extension of Einstein's gravity to higher dimensions, with an enlarged lagrangian containing Gauss-Bonnet invariants. But to our knowledge, no one noticed that even in its original version the Kaluza-Klein five-dimensional theory can - and should - incorporate not only the usual Riemann curvature scalar, but also a non-trivial second order Gauss-Bonnet invariant. This possibility was never mentioned in modern expositions of the Kaluza-Klein theory that were written in early eighties by E. Witten ([11]), M. Duff ([13]), Th. Appelquist et al. ([12]) or by J. M. Overduin and P. S. Wesson ([14], [15]). The first extension of the Kaluza-Klein model incorporating the Gauss-Bonnet invariant of second order appeared in 1987 ([19])

**2. Kaluza-Klein theory revisited**

In the language of modern differential geometry, such a structure is called a *principal fibre bundle*, denoted by $P(M,G)$, where $M$ denotes a differential manifold (in this case a pseudo-Riemannian space-time), and $G$ is a compact and semi-simple Lie group (in this case the one-dimensional group $U(1)$, topologically equivalent to a circle. The canonical projection $\pi : P(M,G) \rightarrow M$ maps the points of $P(M,G)$ onto the points in $M$, $\pi(p) = x \in M$. The set of points in $P(M,G)$ that project on the same point $x \in M$ is called *a fibre*, and is isomorphic with the structure group $G$ (here it is the $U(1)$ group: $\pi^{-1}(x) \sim U(1)$.

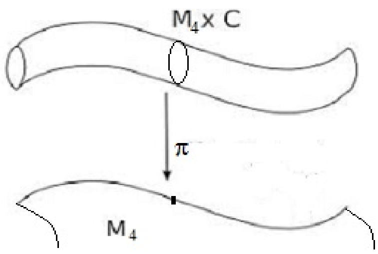


**Рис. 1.** Kaluza-Klein scheme.

The five-dimensional Kaluza-Klein space. The local coordinates are $x^A = (x^\mu, x^5)$; $A = 1,2,..5$, $\mu,\nu,.. = (0,i) = 0,1,2,3$, which under the projection $\pi$ reduce to points in the Minkowski space-time: $\pi(x^A) = \pi(x^\mu, x^5) = (x^\mu) \in M_4$.

In its first version proposed by Th. Kaluza, the fifth dimension was just an extra space coordinate, the entire space being isomorphic with $M_4 \times R^1 \sim [ct,x,y,z,x^5] \sim M_5$, a five-dimensional Minkowski space. the five-dimensional metric can be regarded upon as the composition of two independent metrics, the 4-dimensional Minkowskian one and the "vertical" one defining an invariant scalar product in fibres, which in this case can be taken as $g_{55} = 1$.

If one assumes, as Oskar Klein proposed, that the fifth dimension is topologically closed, then it can be considered as a circle with a very small radius. The dependence on the fifth dimension of functions defined on the "compactified" space must be then periodic, admitting a Fourier-like decomposition:

$$f(x^\mu, x^5) = \sum_{k=0}^{\infty} a_k(x^\mu) e^{ikmx^5}. \tag{2.1}$$

with dim (m) $= cm^{-1}$. Then the eigenvalues of the fifth component of quantum momentum operator, $p_5 = -i\hbar\partial_5$ are integer multiples of mass $m$.

Let us recall the form of the Kaluza-Klein metric tensor in the absence of scalar field, $g_55 = -1$:

$$\tilde{g}_{AB} = \begin{pmatrix} g_{\mu\nu} + A_\mu A_\nu & A_\mu \\ A_\nu & -1 \end{pmatrix} \tag{2.2}$$

or more explicitly,

$$\tilde{g}_{\mu\nu} = g_{\mu\nu} + A_\mu A_\nu, \;\; \tilde{g}_{5\mu} = \tilde{g}_{\mu 5} = A_\mu, \;\; \tilde{g}_{55} = -1. \tag{2.3}$$

with $A_\mu$ functions of space-time variables, identified as the 4-vector potential.

The inverse metric tensor $\tilde{g}^{AB}$ has the following components in 5-dimensional space-time:

$$\hat{g}^{AB} = \begin{pmatrix} g^{\mu\nu} & -A^\mu \\ -A^\nu & -1 + g_{\lambda\rho} A^\lambda A^\rho \end{pmatrix} \tag{2.4}$$

or more explicitly,

$$\hat{g}^{\mu\nu} = g^{\mu\nu}, \;\; \hat{g}^{5\mu} = \hat{g}^{\mu 5} = -A_\mu, \;\; \hat{g}^{55} = -1 + g_{\lambda\rho} A^\lambda A^\rho. \tag{2.5}$$

Nevertheless it turned out that this particular ansatz is still a solution to the full set of 15 equations, because in this case the last equation $R_{55} - g_{55} R = 0$ reduces to tautology $0 = 0$. This circumstance is often referred to as the "Kaluza-Klein miracle"

The explicit form of the remaining 14 equations in the 5-dimensional Einstein's general relativity theory is then:

$$R_{\mu\nu} - \frac{1}{2} g_{\mu\nu} R = \frac{1}{2} \eta^{\lambda\rho} F_{\mu\lambda} F_{\nu\rho} - \frac{1}{8} \, \eta_{\mu\nu} \eta^{\sigma\lambda} \eta^{\kappa\rho} \, F_{\sigma\kappa} F_{\lambda\rho} = -T_{\mu\nu} \tag{2.6}$$

$$R_{mu5} = \partial^\nu F^{\mu\nu} = 0, \quad \text{where} \quad F_{\mu\nu} = \partial_\mu A_\nu - \partial_\nu A_\mu. \tag{2.7}$$

### 2.1. Adding the scalar field $\Phi$

The full version of the Kaluza-Klein model englobes the gravitational field given 4-dimensional metric $g_{\mu\nu}(x)$, the electromagnetic field given by its 4-potential $A_\mu(x)$ and the scalar field $\Phi(x)$.

$$g_{\mu\nu} = \eta_{\mu\nu} = \mathrm{diag}(+1, -1, -1, -1), \;\; \mu, \nu, .. = 0, 1, 2, 3.$$

In this way we get the full set of 15 degrees of freedom present in the 5-dimensional Kaluza-Klein symmetric metric tensor $\hat{g}_{AB}$, $A, B, .. = 1, 2, ...5$.

In order to keep the fifth dimension spatial, $g_{55}$ should be strictly negative; this is why we shall give it the form $g_{55} = -\Phi^2$.

Several particular situations can be chosen for study now. We can consider a case with scalar field only, without the electromagnetic one. This will lead to a variant of the tensor-scalar theory of gravitation, similar to the one proposed by Brans and Dicke. Another choice is the classical Kaluza-Klein model uniting gravitation and electromagnetism, but without scalar field. This amounts to suppressing one degree of freedom out of 15, leaving only 14 degrees of freedom, the 4-dimensional space-time metric $g_{\mu\nu}$ and the 4-vector potential encoded in the components $\hat{g}_{\mu 5} = \hat{g}_{5\mu}$ of the 5-dimensional metric.

Finally, we may consider the electromagnetic and scalar fields interacting in a flat Minkowskian space-time, the gravitation field considered as being negligible.

The five-dimensional metric with scalar field $\Phi(x)$ as the single degree of freedom remains diagonal:

$$g_{AB} = \mathrm{diag}\left(+1, -1, -1, -1, -\Phi^2(x)\right). \tag{2.8}$$

In principle, the notation $\Phi(x)$ can mean the dependence of the scalar field not only on the space-time coordinates $(x^0 = ct, x^1, x^2, x^3)$ but also on the fifth coordinate $x^5$, so that in principle we may have not only $\partial_\mu \Phi \neq= 0$, but also $\partial_5 \Phi \neq= 0$.

However, supposing that the fifth dimension is the structural group $U(1)$ homeomorphic to a circle $S^1$, the dependence of $\Phi$ on $x^5$ can be only a periodic one:

$$\Phi(x^\mu, x^5) = \cos(n\, e\, x^5 + \delta) \cdot \phi(x^\mu), \;\; \text{so that} \;\; \partial_5^2 \Phi = -n^2 e^2 \Phi. \tag{2.9}$$

Let us derive the set of general formulas for metrics, connections and curvature in 5 dimensions, with all the 15 degrees of freesom present. The calculus in coordinates turns out to be quite complicated, but introduucing non-holonomic local frames simplifies the computations considerably.

The non-holonomic local frame is defined by means of the following set of 1-forms and vector fields: The 1-forms are:

$$\theta^\mu = dx^\mu, \quad \theta^5 = dx^5 + k\, A_\mu dx^\mu, \tag{2.10}$$

The dual vector fields, satisfying $\theta^A(\mathcal{D}_B) = \delta^A_B$ are:

$$\mathcal{D}_\mu = \partial_\mu - k\, A_\mu \partial_5, \quad \mathcal{D}_5 = \partial_5. \tag{2.11}$$

Let us introduce the following *transition matrices* $U^A_B$ and $\overset{-1}{U}{}^B_C$ such that $\theta^A = U^A_B dx^B,\ \mathcal{D}_C = \overset{-1}{U}{}^D_C \partial_D$, so that we can write:

$$U^\mu_\nu = \delta^\mu_\nu, \quad U^\mu_5 = 0, \ U^5_\mu = kA_\mu, \ U^5_5 = 1;$$

$$\overset{-1}{U}{}^\mu_\nu = \delta^\mu_\nu, \ \overset{-1}{U}{}^5_\nu = -kA_\nu, \ \overset{-1}{U}{}^\mu_5 = 0 \ \overset{-1}{U}{}^5_5 = 1. \tag{2.12}$$

The metric tensor expressed in the non-holonomic frame can be deduced from the 5-dimensional length element squared, and becomes thus as follows

$$ds^2 = g_{\mu\nu} dx^\mu dx^\nu - \Phi^2 \left[dx^5 + k\, A_\mu dx^\mu\right] \left[dx^5 + k\, A_\nu dx^\nu\right] \tag{2.13}$$

leading to the following $5 \times 5$ matrix representation:

$$g^{AB} = \begin{pmatrix} g_{\mu\nu} + k^2\Phi^2 A_\mu A_\nu & -k\Phi^2 A_\nu \\ -k\Phi^2 A_\mu & -\Phi^2 \end{pmatrix} \tag{2.14}$$

The inverse matrix becomes then:

$$g^{BC} = \begin{pmatrix} g^{\nu\lambda} & kA_\lambda \\ kA_\nu & -\Phi^{-2} + k^2 A^\nu A^\lambda \end{pmatrix} \tag{2.15}$$

One easily checks that

$$g_{AB} g^{BC} = \delta^A_C.$$

The simplest and most elegant way to evaluate the connection coefficients and the components of the Riemann tensor is to use the non-holonomic frame $\theta^A$ and its dual basis of derivations (vector fields) $\mathcal{D}_B, \ \ A, B = 1, 2...5$.We need to know the commutators of non-holonomic derivations. We have:

$$[\mathcal{D}_A, \mathcal{D}_B] = C^E_{AB}\, \mathcal{D}_E, \tag{2.16}$$

where

$$C^5_{\mu\nu} = C_{\mu\nu 5} = -k\, F_{\mu\nu} = -k\, (\partial_\mu A_\nu - \partial_\nu A_\mu). \tag{2.17}$$

We have then the connection coefficients in the non-holonomic basis:

$$\hat{\Gamma}^C_{AB} = \frac{1}{2}\hat{g}^{CE}\left[\mathcal{D}_A g_{BE} + \mathcal{D}_B g_{AE} - \mathcal{D}_E g_{AB}\right] + \hat{g}^{CE}\left[C_{EAB} + C_{EBA} - C_{BAE}\right] \tag{2.18}$$

where "hat" refers to the components with respect to the anholonomic frame.

The only non vanishing connection coefficients are then the following:

$$\hat{\Gamma}^\mu_{\nu\lambda} = \Gamma^\mu_{\nu\lambda}, \ \ \hat{\Gamma}^\mu_{\nu 5} = \hat{\Gamma}^\mu_{5\nu} = -\frac{1}{2}kF^\mu{}_\nu, \ \ \hat{\Gamma}^5_{\nu\lambda} = -\hat{\Gamma}^5_{\lambda\nu} = \frac{1}{2}kF_{\lambda\nu}, \tag{2.19}$$

The Riemann tensor expressed in a non-holonomic frame is:

$$\hat{R}^C_{AB\ \ D} = \mathcal{D}_A \hat{\Gamma}^C_{BD} - \mathcal{D}_B \hat{\Gamma}^C_{AD} + \hat{\Gamma}^C_{AF}\hat{\Gamma}^F_{BD} - \hat{\Gamma}^C_{BF}\hat{\Gamma}^F_{AD} - C^F_{AB}\hat{\Gamma}^C_{FD} \tag{2.20}$$

The Ricci tensor and the curvature scalar in 5 dimensions are calculated as usual,

$$\hat{R}_A D = \hat{R}^C_{AC \quad D}, \qquad \hat{R} = \hat{g}^{AB} \hat{R}_{AB}. \tag{2.21}$$

The resulting expression for the five-dimensional curvature is quite simple indeed:

$$\hat{R} = \overset{4}{R} - \frac{1}{4}\Phi^2 \, F_{\mu\nu}F^{\mu\nu} - \frac{2}{3\Phi^2} g^{\mu\nu}\partial_\mu\Phi\partial_\nu\Phi. \tag{2.22}$$

Considered as the integrand of a 5-dimensional variational principle, this Lagrangian density will lead to the following Einstein's equations when varying with respect to the metric only:

$$\hat{R}_{AB} - \frac{1}{2}\hat{g}_{AB}\hat{R} = 8\pi G \left[ T^{(\Phi)}_{AB} + \frac{k^2}{16\pi G} T^{(F)}_{AB} \right] \tag{2.23}$$

where formally

$$T^{(\Phi)}_{AB} = \partial_A\Phi\partial_B\Phi - \frac{1}{2}\hat{g}_{AB}(\hat{g}^{CD}\partial_C\Phi\partial_D\Phi), \tag{2.24}$$

and

$$T^{(F)}_{AB} = F_{AC}F^C_{\ B} - \frac{1}{4}\hat{g}_{AB}(F_{CD}F^{CD}), \tag{2.25}$$

which in the case of the "n-th mode", i. e. the dependence $\Phi$ on $x^5$ in a periodic way, only to the space-time components different from zero:

$$T^{(\Phi)}_{\mu\nu} = \partial_\mu\Phi\partial_\nu\Phi - \frac{1}{2}\hat{g}_{\mu\nu} \left[ \hat{g}^{\lambda\rho}\partial_\lambda\Phi\partial_\rho\Phi - n^2e^2\Phi^2 \right], \tag{2.26}$$

(where we neglected the mixed terms with $F_{\mu\nu}$ ) and where

$$T^{(F)}_{\mu\nu} = F_{\mu\lambda}F^\lambda_{\ \nu} - \frac{1}{4}\hat{g}_{\mu\nu}(F_{\lambda\rho}F^{\lambda\rho}), \tag{2.27}$$

Variation with respect to the scalar field $\Phi$ and the 4-vector potential $A_\mu$ lead to the following equations of motion:

$$\frac{1}{\Phi}\partial_\mu \left[ \Phi \, F^{\mu\nu} \right] = 0, \tag{2.28}$$

and

$$(\Box\Phi + n^2e^2)\Phi = 0. \tag{2.29}$$

where the term $n^2e^2$ comes from the second derivative of $\Phi$ with respect to the circular coordinate $x^5$ and plays the role of a mass term for the Klein-Gordon scalar field equation.

## 3. Non-abelian generalization

An immediate and trivial generalization of the Kaluza-Klein model consists in adding more "external" dimensions, all of them repeating the same unit circle $S^1$ topology. In other words, instead of one cyclic dimension which can be also interpreted as a 1-dimensional Lie group $U(1)$, introduce a $K$-dimensional torus $T^K = S^1 \times S^1 \times ... \times S^1$.

The symmetry group of $T^K$ is $[U(1)]^K$, the Cartesian product of $K$ one-dimensional unitary groups $U(1)$. The corresponding Kaluza-Klein metric will be extended in a trivial way: let us label the extra dimensiona by $y^1, y^2, ...y^K$ , and the set of all the coordinates by $x^B = (x^\mu, y^a)$, $A, B, .. = 1, 2, ..., 4 + K$, $\mu, \nu = 0, 1, 2, 3$, $a, b = 1, 2, ..., K$.

As a result, we shall get $K$ distinct scalar fields $\Phi^a(x, y)$ and $K$ distinct 4-potentials $A^b_\mu(x^\lambda)$, which will contribute separately to the action principle without any mutual interaction. In the absence of gauge fields and with the Minkowskian space-time the Kaluza-Klein multidimensional metric tensor would take on the Kasner metric form:

$$\hat{g}_{AB} = \text{diag}\,[+1,-1,-1,-1,-\Phi_1^2(x,y),-\Phi_2^2(x,y),...-\Phi_K^2(x,y)] \tag{3.1}$$

Let us suppose that the extra dimensions form a compact manifold of dimension $N$, endowed with a positive defined metric tensor $g_{ab}$ When incorporated as a part of the global Kaluza-Klein metric, it will be taken with minus sign i order to comply with spatial nature of the extra dimensions. The extra dimensions can be thought of as a maximally symmetric manifold (an $N$-dimensional sphere) with its natural metric, or as a Lie symmetry group acting on it. The number of Killing vectors on the maximally symmetric space of dimension $N$ is $K = N(N+1)/2$

Let us denote the $K$ Killing vectors - left-invariant vector fields on the structural group - by $X_a, \;\; a = 1,2,...K$:

$$X_a = X_a \frac{\partial}{\partial y^b} \tag{3.2}$$

They satisfy the following commutation relations:

$$X_a^d \partial_d X_b^c - X_b^d \partial_d X_a^c = C_{ab}^f X_f^c \tag{3.3}$$

where the coefficients $C_{ab}^f = -C_{ba}^f$ are the structure constants of the Lie group generating the gauge symmetry. In what follows, we shall assume that the internal space is the group manifold itself.

The set of $K$ 1-forms $\omega^b = \omega_c^b dy^c$ dual to the invariant vector fields is defined as follows:

$$\omega^b(X_a) = \omega_e^b X_a^e = \delta_a^b, \quad \text{also} \quad X_e^a \omega_b^e = \delta_b^a. \tag{3.4}$$

The $\omega^a$ are called the Maurer-Cartan forms. They satisfy the Maurer-Cartan equation:

$$\partial_a \omega_b^f - \partial_b \omega_a^f + C_{cd}^f \omega_a^c \omega_b^d = 0. \tag{3.5}$$

The invariant metric of the extra space is given by the Cartan-Killing symmetric tensor

$$g_{ab} = C_{ac}^d C_{bd}^c. \tag{3.6}$$

The overall metric tensor $g_{AB}, \;\; A,B.. = (\mu, b) = 1,2,..(K+4)$ in the non-abelian case is then:

$$\begin{pmatrix} g_{\mu\nu} + g_{ab} A_\mu^a A^b \nu & g_{ab}\omega_d^a A_\nu^b \\ g_{ab}\omega_c^a A_\mu^b & g_{ab}\omega_c^a \omega_d^b \end{pmatrix}, \tag{3.7}$$

$$\begin{pmatrix} g^{\nu\lambda} & -g^{\nu\rho} X_d^b A_\rho^d \\ -g^{\rho\lambda} X_c^a A_\rho^c & g^{ab} + g^{\mu\rho} X_c^a X_d^b A_\mu^c A_\rho^d \end{pmatrix}, \tag{3.8}$$

As in the 5-dimensional case, the calculus of the Riemann and Ricci tensors is made best in the non-holonomic frame.

The full set of expressions can be found in an article published in 1981 (R.K., *Ann. Inst. H. Poincaré*, **34**, p. 437-463) Here we give the resulting $4+K$ dimensional scalar curvature $\overset{(4+K)}{R}$ serving as integrand in the variational principle:

$$\overset{(4+K)}{R} = \overset{(4)}{R} - \frac{1}{4} g_{ab} g^{ab} - \frac{1}{4} g_{ab}^{\mu\lambda} g^{\nu\rho} F_{mu\nu}^a F_{\nu\rho}^b, \tag{3.9}$$

where $F_{\mu\nu}^a$ is the gauge field tensor given by:

$$F_{\mu\nu}^a = \partial_\mu A_\nu^a - \partial_\nu A_\mu^a + C_{bd}^a A_\mu^b A_\nu^d. \tag{3.10}$$

The resulting equations are similar as in the 5-dimensional case, with Einstein's equations given by

$$\overset{(4)}{R}_{\mu\nu} - \frac{1}{2} \overset{(4)}{g}_{\mu\nu} \overset{(4)}{R} = -\frac{8\pi G}{c^4} T_{\mu\nu} \tag{3.11}$$

with the energy-momentum tensor given by:

$$T_{\mu\nu} = g_{ab} g^{\lambda\sigma} F_{\mu\lambda}^a F_{\nu\sigma}^b - \frac{1}{4} g_{ab} g^{\mu\nu} g^{\lambda\rho} F_{\mu\lambda}^a F_{\nu\rho}^b. \tag{3.12}$$

and the gauge field equations are:

$$g^{\mu\nu} \; D_\mu F_{\nu\lambda}^a = g^{\mu\nu} \left[ \partial_\mu F_{\nu\lambda}^a + C_{bd}^a A_\mu^c F_{\nu\lambda}^d \right] = 0 \tag{3.13}$$

## 4. Kaluza-Klein cosmology

A Generalized FRW metric can be easily introduced on the Kaluza-Klein manifold. In 1980 Chodos and Detwiler ([25]) proposed a Kasner-type cosmological solution in the 5-dimensional Kaluza-Klein space. The metric element for this model was

$$ds^2 = dt^2 - \sqrt{t}\left[dx^2 + dy^2 + dz^2\right] - \frac{1}{\sqrt{t}}\rho^2 d\chi^2. \tag{4.1}$$

where the last angular variable $\chi$ comes from the fifth cyclic dimension.

This metric can be generalized to more extra dimensions $D$; to be more precise:

$$ds^2 = dt^2 - \sum_{i=1}^{3} t^{2k_i}(dx^i)^2 - \sum_{a=4}^{3+D} t^{2k_a}(dy^a)^2 \tag{4.2}$$

satisfying the following conditions:

$$\sum_{i=1}^{3} k_i + \sum_{a=4}^{3+D} k_a = 1, \tag{4.3}$$

$$\sum_{i=1}^{3} k_i^2 + \sum_{b=4}^{3+D} k_b^2 = 1 \tag{4.4}$$

The Friedmann-Robertson-Walker metric can be naturally generalized if we assume that the extra space dimensions form a compact spherically symmetric manifold. Then the overall metric can be derived from the following line element squared:

$$ds^2 = dt^2 - R_d^2(t)\, g_{ij}dx^i dx^j - R_D^2(t) g_{ab} dy^a dy^b, \tag{4.5}$$

with two time-dependent scale factors, $R_d(t)$ for the space dimensions of our space-time, $d = 3$, and $R_D(t)$ for the $D$-dimensional internal $D$-dimensional compact space - most usually, a $D$-dimensional sphere.

This ansatz yields the following Ricci tensor:

$$R_{00} = -\left[3\frac{\ddot{R}_d}{R_d} + D\frac{\ddot{R}_D}{R_D}\right),$$

$$R_{ij} = \left[\frac{2k_d}{R_d^2} + \frac{d}{dt}\left(\frac{\dot{R}_d}{R_d}\right) + \frac{\dot{R}_d}{R_d}\left(3\frac{\dot{R}_d}{R_d} + D\frac{\dot{R}_D}{R_D}\right)\right] g_{ij},$$

$$R_{ab} = \left[\frac{2k_D}{R_D^2} + \frac{d}{dt}\left(\frac{\dot{R}_D}{R_D}\right) + \frac{\dot{R}_D}{R_D}\left(3\frac{\dot{R}_d}{R_d} + D\frac{\dot{R}_D}{R_D}\right)\right] g_{ab},$$

In 1985 D. Sahdev ([26]) obtained solutions of this system with several perfect fluids added on the right-hand side. The nice feature was that $R_d$ was increasing with time, and $R_D$ decreasing. However, instead of stabilizing at some small but finite value, as any reasonable physics would require, the internal radius $R_D$ tended to zero.

Other models attempting to stabilize asymptotically the internal radius $R_D$ were proposed by Matzner and Mezzacappa (see [23], by Copeland and Toms ([24]) and in six dimensions by Gleisser and Taylor (1985).

All those models were using the Einstein-Hilbert variational principle, with the integrand of the form

$$\delta \int \sqrt{\overset{(4+D)}{\hat{g}}_{AB}}\; \overset{(4+D)}{R}\; d^4x d^D y = 0$$

In 1988 we proposed a generalized non-abelian Kaluza-Klein model in 10 dimensions, with two gauge symmetry groups (B. Giorgini and R.Kerner, *Classical and Quantum Gravity*, **5** (1988), pp. 339-351) , which can be described as a double fibre bundle space, ([18])

$$P(P(V_4, SU(2)), SU(2)).$$

The lagrangian contained not only the usual Riemann scalar, but also the second-order and third-order Gauss-Bonnet invariants.

This situation gives place to three gauge fields, $A^A_b$, $A^A_\mu$ and $A^a_\nu$, with indices $A, B = 1, 2, 3$ relating to the upper gauge geoup $SU(2)$, indices $a, b = 1, 2, 3$ relating to the lower gauge group $SU(2)$,and $\mu, \nu.. = 0, 1, 2, 3$ the space-time indices on $V_4$. The three field tensors become then:

$$F^B_{\mu\nu} = \partial_\mu A^B_\nu - \partial_\nu A^B_\mu + C^B_{CD} A^C_\mu A^D_\nu,$$

$$F^B_{cd} = \partial_c A^B_d - \partial_d A^B_c + C^B_{DE} A^D_c A^E_d,$$

$$F^b_{\mu\nu} = \partial_\mu A^b_\nu - \partial_\nu A^b_\mu + C^b_{cd} A^c_\mu A^d_\nu.$$

Looking for cosmological solutions, only the scalar multiplet $A^B_c(x, y)$ is of interest, the two vector potentials put to zero.

Decomposing $A^B_c$ that is defined on the lower group space along the Maurer-Cartan forms:

$$A^B_c = \Phi^B_d(x^\mu)\omega^d_c, \tag{4.6}$$

the corresponding field tensor becomes:

$$F^E_{ab} = \left(C^E_{BD}\Phi^B_g\Phi^D_f - C^d_{gf}\Phi^E_d\right)\omega^g_a\omega^f_b. \tag{4.7}$$

due to the Maurer-Cartan identity fulfilled by $\omega^b_c$.

The generalized FRW metric in 10 dimensions was as follows:

$$\overset{10}{g}_{\alpha\beta} = \mathrm{diag}\left(1, -R^2(t)\delta_{ij}, -a^2(t)\delta_{ab}, -b^2(t)\delta_{AB}\right), \tag{4.8}$$

with $\alpha, \beta = 1, 2, ..., 10,\ i, j = 1, 2, 3,\ a, b = 1, 2, 3$ and $A, B = 1, 2, 3$.

The variational principle contained a linear combination of cosmological constant $\overset{10}{\Lambda}$, the scalar curvature $\overset{10}{R}$ and the 10-dimensional Gauss-Bonnet invariant $\overset{10}{GB}$.

The resulting differential equations determine the temporal behavior of three scale factors, the observable 3-dimensional space, and the two separate scale factors for two $SO(2)$ structural groups.

$$\int \sqrt{g}\,\left[\overset{10}{\Lambda} + \overset{10}{R} + \overset{10}{GB}\right] d^4x d^3\xi d^3\chi. \tag{4.9}$$

The equations are highly non-linear, but display several fixed points. Qualitative solutions were found with finite initial conditions for all three scale factors, leading asymptotically to Friedmann's solution for $R(t)$, while the internal scale factors behave differently: while $a(t)$ grows, $b(t)$ decreases, the exchange providing energy needed for the expansion of $R(t)$

### 5. Classical electrodynamics

Let us start by recalling the standard Maxwell's electromagnetism and fixing the notations. The simplest and the most elegant form of Maxwell's system is written in modern system of units as follows:

$$\frac{\partial \mathbf{B}}{\partial t} = -\boldsymbol{\nabla} \times \mathbf{E}, \quad \boldsymbol{\nabla} \cdot \mathbf{B} = 0, \tag{5.1}$$

$$\frac{\partial \mathbf{D}}{\partial t} + \mathbf{j} = \boldsymbol{\nabla} \times \mathbf{H}, \quad \boldsymbol{\nabla} \cdot \mathbf{D} = \rho, \tag{5.2}$$

It should be underlined that the pairs of fields ($\mathbf{E}$, $\mathbf{H}$) and ($\mathbf{D}$, $\mathbf{B}$) represent *different geometrical objects*. This can be better understood if we look at the integral form of Maxwell's equations:

$$-\frac{\partial}{\partial t}\oint_S \mathbf{B}\cdot \mathrm{d}\boldsymbol{\sigma} = \oint_{\partial S} \mathbf{E}\cdot \mathrm{dl}, \qquad \oint_{\partial V} \mathbf{B}\cdot\boldsymbol{\sigma} = 0. \tag{5.3}$$

$$\oint_S \left[\frac{\partial}{\partial t}\mathbf{D} + \mathbf{j}\right]\cdot \mathrm{d}\boldsymbol{\sigma} = \oint_{\partial S} \mathbf{H}\cdot \mathrm{dl}, \qquad \oint_{\partial V} \mathbf{D}\cdot\boldsymbol{\sigma} = Q. \tag{5.4}$$

Here $S$ is a surface and $\partial S$ its boundary, which is a closed line; $V$ is a volume and $\partial V$ is its boundary which is a closed surface. Correspondingly, we have vector fields and streams (2-forms). In the integral form of Maxwell's equations, the entities $\mathbf{E}$ and $\mathbf{H}$ are genuine vector fields which can be integrated along curves, whereas $\mathbf{B}$ and $\mathbf{D}$ are in fact 2-forms, defining *streams*.

The rate of change of fluxes of $\mathbf{D}$ and $\mathbf{B}$ through a surface is determined by the circulation of their conjugate fields $\mathbf{H}$ and $\mathbf{E}$ along the boundary, and vice versa.

A problem arises with number of equations versus number of functions: 8 equations for $4 \times 3 = 12$ components. The *constitutive relations* $\mathbf{E} = \mathbf{E}(\mathbf{D},\ \mathbf{B})$ and $\mathbf{H} = \mathbf{H}(\mathbf{D},\ \mathbf{B})$ reduce the number of variables to 6, thus making the system seemingly overdetermined.

Things become straightened up in a four-dimensional notation, with 4-vector potential defined as a vector in 4-dimensional space-time endowed wth Minkowskian metric $\eta_{\mu\nu} = \mathrm{diag}(+,-,-,-)$, $\mu,\nu,.. = 0,1,2,3$

We assume that the 6 variables corresponding to the fields $\mathbf{E}$ and $\mathbf{B}$ are the 6 independent components of an antisymmetric 2-covariant tensor (a 2-form) $F_{\mu\nu} = -F_{\nu\mu}$, with $F_{0k} = E_k$, $F_{ik} = \epsilon_{ikm}B_m$, $i,k,m = 1,2,3.$

The Poincaré's Lemma states that if a 2-form - e.g. $F = \frac{1}{2}F_{\mu\nu}dx^\mu \wedge dx^\nu$ - is defined on an open subset of Minkowskian space-time $M_4$, then it is an exterior differential of some 1-form, then $A = A_\mu dx^\mu$:

$$F = dA \quad \to \quad F_{\mu\nu} = \partial_\mu A_\nu - \partial_\nu A_\mu. \tag{5.5}$$

We have two independent relativistic invariant functions of Faraday's 2-form $F_{\mu\nu}$:

$$S = -\frac{1}{4}\eta^{\mu\lambda}\eta^{\nu\rho}F_{\mu\nu}F_{\lambda\rho} = \frac{1}{2}\left(\mathbf{E}^2 - \mathbf{B}^2\right), \tag{5.6}$$

$$P = -\frac{1}{8}\epsilon^{\mu\nu\lambda\rho}F_{\mu\nu}F_{\lambda\rho} = F_{\mu\nu}\hat{F}^{\mu\nu} = \mathbf{E}\cdot\mathbf{B}, \tag{5.7}$$

with

$$\hat{F}^{\mu\nu} = \frac{1}{2}\epsilon^{\mu\nu\lambda\rho}F_{\lambda\rho}$$

The choice of symbols is not accidental: $S$ stands for "scalar", and $P$ stands for "pseudo-scalar".

To ensure relativistic invariance, the variational principle should be derived from a Lagrangian depending on these two invariants, $\mathcal{L}(S,P)$. The equations of motion of the electromagnetic field form two groups: the homogeneous ones,

$$\partial_\mu F_{\nu\lambda} + \partial_\nu F_{\lambda\mu} + \partial_\lambda F_{\mu\nu} = 0, \tag{5.8}$$

which are the consequence of the fact that $F = dA \ \to \ dF = d^2A = 0$, and the equations resulting from variational principle applied to $\mathcal{L}$,

$$\partial_\mu G^{\mu\nu} = 0, \quad \text{with} \ \ G^{\mu\nu} = \frac{\partial \mathcal{L}}{\partial F_{\mu\nu}} \tag{5.9}$$

$$G^{\mu\nu} = \frac{\partial \mathcal{L}}{\partial S}F^{\mu\nu} + \frac{\partial \mathcal{L}}{\partial P}\hat{F}^{\mu\nu} \tag{5.10}$$

The dual Faraday tensor is given by definition:

$$G^{0i} = -G^{i0} = D^i, \quad G^{ik} = -G^{ki} = \epsilon^{ik}{}_l H^l \tag{5.11}$$

so the equations of motion become:

$$\frac{\partial \mathbf{D}}{\partial t} = \boldsymbol{\nabla} \times \mathbf{H}, \quad \boldsymbol{\nabla} \cdot \mathbf{D} = 0, \tag{5.12}$$

which coincide with Maxwell's second set of equations when the sources (the current density $\mathbf{j}$ and the charge density $\rho$) are put to zero.

The dynamical properties of the electromagnetic field are described by the energy-momentum tensor $T^{\mu\nu}$:

$$T^{\mu\nu} = F^{\mu}{}_{\lambda} G^{\lambda\nu} - \eta^{\mu\nu}\, \mathcal{L}, \tag{5.13}$$

$$T^{00} = \mathbf{E} \cdot \mathbf{D} - \mathcal{L}, \tag{5.14}$$

$$T^{0i} = (\mathbf{E} \times \mathbf{H})^i, \quad T^{i0} = (\mathbf{D} \times \mathbf{B})^i, \tag{5.15}$$

$$T^{ik} = -E^i D^k - H^i B^k + \delta^{ik}(\mathcal{L} + \mathbf{H} \cdot \mathbf{B}). \tag{5.16}$$

The energy-momentum tensor is symmetric and conserved:

$$T^{\mu\nu} = T^{\nu\mu}, \quad \partial_\mu T^{\mu\nu} = 0, \tag{5.17}$$

The proof uses the following identity:

$$F_{\mu\lambda} \hat{F}^{\lambda\nu} = \delta^{\nu}_{\mu} P, \tag{5.18}$$

The relations (5.17) result in the following conserved quantities

$$P^\mu = \int T^{\mu 0} \mathrm{d}\mathbf{r}^3, \;\; M^{\mu\nu} = \int (x^\mu T^{\nu 0} - x^\nu T^{\mu 0}) \mathrm{d}\mathbf{r}^3 \tag{5.19}$$

Let us also note that the energy-momentum tensor could be obtained directly as

$$T_{\mu\nu} = \frac{\partial(\sqrt{\mid g \mid}\mathcal{L}}{\partial g^{\mu\nu}} \tag{5.20}$$

yielding the same expressions for the Hamiltonian $T_{00}$ and the Poynting vector $P_k = T_{0k}$.

**6. Kaluza-Klein Electrodynamics**

Countless theories based on lagrangians depending on $F_{\mu\nu}F^{\mu\nu}$ and $(F_{\mu\nu}{}^*F^{\mu\nu})^2$ (the square is needed to keep the invariance under space reflections) can be produced if we lack a guiding principle to fix the form of the lagrangian. In the Kaluza-Klein theory, as well as in its improvements by P. Jordan and Y. Thiry was based on the Einstein-Hilbert variational principle in five-dimensional space, with lagrangian equal to $R$, the scalar curvature of the metric. This lagrangian is unique in four dimensions, because already the second invariant of the Riemann tensor,

$$I_2 = R_{ABCD} R^{ABCD} - 4\, R_{AB} R^{AB} + R^2 \tag{6.1}$$

turns out to be a pure divergence and does not modify the equations of motion.

The invariant (6.1) is the unique quadratic combination of the Riemann tensor leading under variation to the second-order equations. In five dimensions this invariant is no more a divergence, therefore there is no reason to exclude it in the full theory. This fixes the lagrangian in five dimensions, leaving the place for the arbitrariness only in the choice of one dimensional parameter.

This is the starting point for non-linear modification of the electrodynamics. In our calculations we shall discard the gravitational and scalar fields, both too weak to influence the behaviour of the electromagnetic field at short distances.

The invariant $I_2$ for the metric (2.2) is easily calculated and is found to be (discarding the pure divergence term equal to $\partial_\mu(F_{\rho\lambda}\partial^\mu F^{\rho\lambda}) - 2\partial^\nu(F_{\rho\lambda}\partial_\nu F^{\mu\lambda})$:

$$I_2 = \frac{3}{16}\,\left[(F_{\mu\nu}F^{\mu\nu})^2 - 2F_{\mu\lambda}F_{\nu\rho}F^{\mu\nu}F^{\lambda\rho}\right]. \tag{6.2}$$

For fixed Minkowskian metric $\eta_{\mu\nu}$ we can put $\sqrt{|\,g\,|} = 1$ and write the full lagragian as

$$\mathcal{L} = -\frac{1}{4}\,F_{\mu\nu}F^{\mu\nu} + \frac{3\varepsilon}{16e^2}\left[F_{\mu\nu}F^{\mu\nu})^2 - 2F_{\mu\lambda}F_{\nu\rho}F^{\mu\nu}F^{\lambda\rho}\right], \tag{6.3}$$

with $\varepsilon$ a numerical parameter to be determined.

The equations of motion in vacuo are then

$$\partial_\lambda\left[F^{\lambda\rho} - \frac{3\varepsilon}{16e^2}(F_{\mu\nu}F^{\mu\nu})F^{\lambda\rho} + \frac{3\varepsilon}{e^2}F_{\mu\nu}F^{\lambda\mu}F^{\rho\nu}\right]. \tag{6.4}$$

The identities

$$\partial_\mu F_{\lambda\rho} + \partial_\lambda F_{\rho\mu} + \partial_\rho F_{\mu\lambda} = 0 \tag{6.5}$$

hold by definition (2.7), too:

$$F_{\mu\nu} = \partial_\mu A_\nu - \partial_\nu A_\mu.$$

Both lagrangian and equations of motion are more transparent when expressed by means of the fields $\mathbf{E}$ and $\mathbf{B}$, $\mathbf{D}$ and $\mathbf{H}$:

$$\mathcal{L} = \frac{1}{2}(\mathbf{E}^2 - \mathbf{B}^2) + \frac{3\varepsilon}{2e^2}(\mathbf{E}\cdot\mathbf{B})^2. \tag{6.6}$$

The new term contains only the square of the second invariant of the electromagnetic field. The full set of modified Maxwell's equations is:

$$\operatorname{div}\mathbf{B} = 0, \qquad \mathbf{rot}\;\mathbf{E} = -\frac{\partial\mathbf{B}}{\partial t},\;\; \operatorname{div}\mathbf{D} = -\frac{3\varepsilon}{e^2}\,\mathbf{B}\cdot\mathbf{grad}(\mathbf{E}\cdot\mathbf{B}),$$

$$\mathbf{rot}\;\mathbf{H} = \frac{\partial\mathbf{D}}{\partial t} + \frac{3\varepsilon}{e^2}\left[\mathbf{H}\frac{\partial(\mathbf{E}\cdot\mathbf{B})}{\partial t} - \mathbf{E}\times\mathbf{grad}(\mathbf{E}\cdot\mathbf{B})\right]. \tag{6.7}$$

In what follows we shall use the units in which $c = 1$, and in which we can put in the vacuum $\mathbf{E} = \mathbf{D}$ and $\mathbf{H} = \mathbf{B}$. Therefore the equations in vacuum will be

$$\operatorname{div}\mathbf{B} = 0, \qquad \mathbf{rot}\;\mathbf{E} = -\frac{\partial\mathbf{B}}{\partial t},\;\; \operatorname{div}\mathbf{E} = -\frac{3\varepsilon}{e^2}\,\mathbf{B}\cdot\mathbf{grad}(\mathbf{E}\cdot\mathbf{B}),$$

$$\mathbf{rot}\;\mathbf{B} = \frac{\partial\mathbf{E}}{\partial t} + \frac{3\varepsilon}{e^2}\left[\mathbf{B}\frac{\partial(\mathbf{E}\cdot\mathbf{B})}{\partial t} - \mathbf{E}\times\mathbf{grad}(\mathbf{E}\cdot\mathbf{B})\right]. \tag{6.8}$$

When $\varepsilon$ is put equal to zero, the equations recover their usual Maxwellian form. Two other possibilities, up to a scale that can be incorporated in $e^2$, are $\varepsilon = +1$ or $-1$.

## 7. General properties

The non-homogeneous couple of equations,

$$\operatorname{div}\mathbf{E} = -\frac{3\varepsilon}{e^2}\,\mathbf{B}\cdot\mathbf{grad}(\mathbf{E}\cdot\mathbf{B}) \tag{7.1}$$

and

$$\mathbf{rot}\;\mathbf{B} = \frac{\partial\mathbf{E}}{\partial t} + \frac{3\varepsilon}{e^2}\left[\mathbf{B}\frac{\partial(\mathbf{E}\cdot\mathbf{B})}{\partial t} - \mathbf{E}\times\mathbf{grad}(\mathbf{E}\cdot\mathbf{B})\right] \tag{7.2}$$

can be implemented by adding the charge density $\rho$ to the right-hand side of (7.1) and the current density $\mathbf{j}$ to the right-hand side of (7.2)

However, even in the absence of these "external sources", the right-hand sides of the eqs. (7.1) and (7.2) behave like conserved induced charge and current densities; their conservation is independent of eventual other non-induced similar objects. As a matter of fact, let us compare:

$$\frac{\partial}{\partial t}(\text{div } \mathbf{E}) = -\frac{3\varepsilon}{e^2}\frac{\partial \mathbf{B}}{\partial t} \cdot \mathbf{grad}(\mathbf{E} \cdot \mathbf{B}) - \frac{3\varepsilon}{e^2}\mathbf{B} \cdot \mathbf{grad}\frac{\partial(\mathbf{E} \cdot \mathbf{B})}{\partial t} =$$

$$= -\frac{3\varepsilon}{e^2}(\mathbf{rot}\mathbf{E}) \cdot \mathbf{grad}(\mathbf{E} \cdot \mathbf{B}) - \frac{3\varepsilon}{e^2}\mathbf{B} \cdot \mathbf{grad}\frac{\partial(\mathbf{E} \cdot \mathbf{B})}{\partial t} \tag{7.3}$$

and

$$\text{div } \frac{\partial \mathbf{E}}{\partial t} = \text{div}(\mathbf{rot}\mathbf{B}) - \frac{3\varepsilon}{e^2}\text{div}\left(\mathbf{B}\ \frac{\partial(\mathbf{E} \cdot \mathbf{B})}{\partial t}\right) - \frac{3\varepsilon}{e^2}\text{div}(\mathbf{E} \times \mathbf{grad}(\mathbf{E} \cdot \mathbf{B})) =$$

$$= \frac{3\varepsilon}{e^2}(\text{div}\mathbf{B})\frac{\partial(\mathbf{E} \cdot \mathbf{B})}{\partial t} - \frac{3\varepsilon}{e^2}\mathbf{B} \cdot \mathbf{grad}\frac{\partial(\mathbf{E} \cdot \mathbf{B})}{\partial t} + \frac{3\varepsilon}{e^2}(\mathbf{rot}\mathbf{E}) \cdot \mathbf{grad}(\mathbf{E}2 \cdot \mathbf{B}). \tag{7.4}$$

because

$$\text{div}\mathbf{B} = 0, \quad \mathbf{rot}(\mathbf{grad}f) = 0, \quad \text{div}(\mathbf{a} \times \mathbf{b}) = \mathbf{b} \cdot (\mathbf{rot}\mathbf{a}) - \mathbf{a} \cdot (\mathbf{rot}\mathbf{b}),$$

therefore

$$\frac{\partial}{\partial t}\left[-\frac{3\varepsilon}{e^2}\mathbf{B} \cdot \mathbf{grad}(\mathbf{E} \cdot \mathbf{B})\right] + \text{div}\left[\frac{3\varepsilon}{e^2}\mathbf{B}\frac{\partial(\mathbf{E} \cdot \mathbf{B})}{\partial t} - \mathbf{E} \times \mathbf{grad}(\mathbf{E} \cdot \mathbf{B})\right] = 0. \tag{7.5}$$

We shall denote the induced charge density by $\rho_{ind}$:

$$\rho_{ind} = -\frac{3\varepsilon}{e^2}\mathbf{B} \cdot \mathbf{grad}(\mathbf{E} \cdot \mathbf{B}), \tag{7.6}$$

and the induced current density by $\mathbf{j}_{ind}$:

$$\mathbf{j}_{ind} = \frac{3\varepsilon}{e^2}\mathbf{B}\frac{\partial(\mathbf{E} \cdot \mathbf{B})}{\partial t} - \mathbf{E} \times \mathbf{grad}(\mathbf{E} \cdot \mathbf{B}) \tag{7.7}$$

with

$$\frac{\partial \rho_{ind}}{\partial t} + \text{div}(\mathbf{j}_{ind}) = 0. \tag{7.8}$$

The theory does not need any non-induced charges if we can prove the existence of charged stable static solutions, (solitons localized in space). If we form the sum:

$$\mathbf{B} \cdot \frac{\partial \mathbf{B}}{\partial t} + \mathbf{E} \cdot \frac{\partial \mathbf{E}}{\partial t} \tag{7.9}$$

we shall easily find another conservation law:

$$\frac{\partial}{\partial t}\left[\frac{1}{2}(\mathbf{E}^2 + \mathbf{B}^2) + \frac{3\varepsilon}{e^2}(\mathbf{E} \cdot \mathbf{B})^2\right] = \text{div } (\mathbf{E} \times \mathbf{B}) \tag{7.10}$$

The Poynting vector in this theory is the same as in the linear electrodynamics, whereas the energy density contains a new term, as compared with the classical theory:

$$\mathcal{H} = \frac{1}{2}(\mathbf{E}^2 + \mathbf{B}^2) + \frac{3\varepsilon}{e^2}(\mathbf{E} \cdot \mathbf{B})^2 \tag{7.11}$$

Note that the parameter $\varepsilon$ has to be positive, in order to ensure the positivity of the energy. From now on we shall set $\varepsilon = 1$, leaving only the coupling constant $e^2$ to be determined.

Whenever the fields $\mathbf{E}$ and $\mathbf{B}$ are orthogonal to each other, our system in vacuum (7.1, 7.2) coincides with Maxwell's equations. Such is the case of the electromagetic waves, which are also solutions to the equations (7.1, 7.2). Moreover, these solutions are stable with respect to perturbations. As a matter of fact, any deviation from the usual solution in which $\mathbf{E}$ is everywhere orthogonal to $\mathbf{B}$, leads automatically to the rise of the energy $\mathcal{H}$, ensuring stability.

## 8. Static solutions

Let us rewrite the equations (7.1 and 7.2 in the stationary case, when all the time derivatives vanish:

$$\mathrm{div}\,\mathbf{B} = 0, \qquad \mathbf{rot}\,\mathbf{E} = 0,$$
$$\mathrm{div}\,\mathbf{E} = -\frac{3}{e^2}\mathbf{B}\cdot\mathbf{grad}(\mathbf{E}\cdot\mathbf{B}), \quad \mathbf{rot}\,\mathbf{B} = -\frac{3}{e^2}\mathbf{E}\times\mathbf{grad}(\mathbf{E}\cdot\mathbf{B}). \tag{8.1}$$

It would be very interesting to obtain a static and non-singular solution of this system, having finite energy and behaving like a soliton.

This is excluded in the linear case, therefore, if such solution exists, both fields $\mathbf{E}$ and $\mathbf{B}$ must be different from zero and non-orthogonal at least in some finite domain of space. We should also impose the rapid enough vanishing of both fields at infinity. Spherical symmetry for $\mathbf{B}$ leads immediately to the singularity at the origin; so, if the condition div $\mathbf{B}$ is to be maintained everywhere, the lines of force of the field $\mathbf{B}$ have to be closed.

The lines of the local current

$$\mathbf{j}_{ind} = \mathbf{rot}\,\mathbf{B} = -\frac{3\varepsilon}{e^2}\,\mathbf{E}\times\mathbf{grad}(\mathbf{E}\cdot\mathbf{B})$$

must be closed, too. This suggests the axial symmetry in which the current would have only the azimuthal component, and the field $\mathbf{B}$ would be everywhere perpendicular to the azimuthal unit vector $\mathbf{e}_\varphi$ (in cylindrical coordinates $(\rho = \sqrt{x^2+y^2}),\ z,\ \varphi)$, i.e. $\mathbf{B}$ having its components along $\mathbf{e}_z$ and $\mathbf{e}_\rho$ only. Also the field $\mathbf{E}$ should have only the $z$ and $\rho$ components; then the Poynting vector $\mathbf{P} = \mathbf{E}\times\mathbf{B}$ will have only the azimuthal component.

Such a configuration has some remarkable symmetry properties:

The trilinear combinations on the right-hand sides of equations (8.1) produce induced charge and current densities.

The current having only the azimuthal component will produce magnetic field which at great distances is similar to that of a circular distribution of currents, i.e. the one of a magnetic dipole. At the same time, one can expect a non-vanishing charge concentration falling off quite rapidly with distance from the origin, at large distances $\mathbf{E}$ should be then similar to the Coulomb field of an electric point-like charge.

All these conditions put together lead to the following symmetry properties of the components $\mathbf{E}$ and $\mathbf{B}$:

$$E_z(\rho,z) = -E_z(\rho,-z); \quad E_\rho(\rho,z) = E_\rho(\rho,-z), \tag{8.2}$$

and

$$B_z(\rho,z) = B_z(\rho,-z); \quad B_\rho(\rho,z) = -B_\rho(\rho,-z). \tag{8.3}$$

Let us evaluate the behaviour of charge and current distributions far away from the origin. We can take the field of a magnetic dipole and of concentrated charge as zeroth approximation satisfying Maxwell's equations, then insert them into the right-hand sides of eqs. (8.1) and compute the first corrections, supposing that the fields $\mathbf{E}$ and $\mathbf{B}$ develop as:

$$\mathbf{E} = \overset{(0)}{\mathbf{E}} + \frac{1}{e^2}\overset{(1)}{\mathbf{E}} + ...., \quad \mathbf{B} = \overset{(0)}{\mathbf{B}} + \frac{1}{e^2}\overset{(1)}{\mathbf{B}} + .... \tag{8.4}$$

if we put

$$\overset{(0)}{\mathbf{E}} = \frac{Q\,\rho}{(\rho^2+z^2)^{\frac{3}{2}}}\mathbf{e}_\rho + \frac{Q\,z}{(\rho^2+z^2)^{\frac{3}{2}}}\mathbf{e}_z, \tag{8.5}$$

and

$$\overset{(0)}{\mathbf{B}} = \frac{3\mu\,\rho z}{4(\rho^2+z^2)^{\frac{5}{2}}}\mathbf{e}_\rho + \frac{\mu\,(2z^2-\rho^2)}{4(\rho^2+z^2)^{\frac{5}{2}}}\mathbf{e}_z, \tag{8.6}$$

where $Q$ is the total charge, $\mu$ the total magnetic moment.

As the first correction, we obtain

$$\operatorname{div} \overset{(1)}{\mathbf{E}} = \frac{3\mu^2 Q}{8(\rho^2+z^2)^{\frac{11}{2}}}(\rho^2+10z^2), \tag{8.7}$$

and

$$\mathbf{rot}\ \overset{(1)}{\mathbf{B}} = \frac{3\mu Q^2\ \rho}{2(\rho^2+z^2)^{\frac{9}{2}}}\mathbf{e}_\varphi \tag{8.8}$$

which shows that the charge density falls off as $R^{-9}$ and the current density as $R^{-8}$ ($R=\sqrt{\rho^2+z^2}$), i.e. very fast indeed.

The lines of force of the field $\mathbf{B}$ form a family of closed curves which can be transformed into a family of circles by a suitable coordinate transformation; the toroidal coordinates are best adapted to describe the situation.

Let us introduce toroidal coordinates $(\mu,\ \eta,\ \phi)$:

$$\rho = \frac{a\ \sinh\mu}{\cosh\mu-\cos\eta}, \quad z = \frac{a\ \sin\eta}{\cosh\mu-\cos\eta},\ \ \phi=\varphi, \tag{8.9}$$

with $0\le\phi\le 2\pi$, $\quad 0\le\eta\le 2\pi\quad$ and $0\le\mu\le\infty$; $\ a$ is the constant of dimension of length fixing the scale; $\mu,\ \eta$ and $\phi$ are dimensionless.

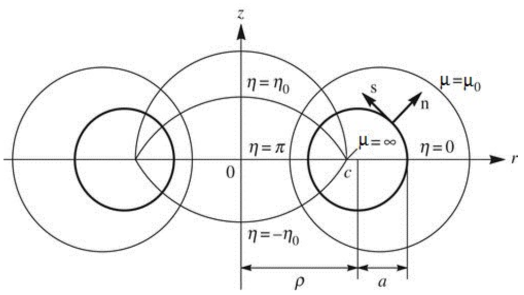


**Рис. 2.** Constant coordinate lines $\mu=$ Const. and $\eta=$ Const. in the $(\rho,z)$-plane.

A surface $\mu=\mu_0=$ Const. is a torus with he external radius $a\ \coth\mu_0$ and internal radius $a/\sinh\mu_0$. When $\mu\to\infty$ it reduces to a circle of radius $a$ in the $(x,y)$-plane. When $\mu\to 0$, the corresponding circle approaches the $z$-axis.

The lines of force of $\mathbf{B}$ coincide with circles $\mu=$ Const., i.e. in new coordinates (8.9)

$$\mathbf{B} = B_\eta(\mu,\eta)\ \mathbf{e}_\eta. \tag{8.10}$$

while $B_\mu(\mu,\eta)=0$. This determines the dependence of $\mathbf{B}$ on $\eta$:

$$\text{as}\quad B_\mu(\mu,\eta) = (\mathbf{rot}\mathbf{A})\cdot\mathbf{e}_\mu \quad\text{with}\quad \mathbf{A}=A_\phi(\mu,\eta)\mathbf{e}_\phi, \tag{8.11}$$

we have

$$B_\mu(\mu,\eta) = \frac{(\cosh\mu-\cos\eta)^2}{a\ \sinh\mu}\,\frac{\partial}{\partial\eta}\left(\frac{\sinh\mu}{\cosh\mu-\cos\eta}A_\phi\right) = 0. \tag{8.12}$$

Therefore

$$A_\phi(\mu,\eta) = (\cosh\mu-\cos\eta)\ G(\mu), \tag{8.13}$$

and

$$B_\eta(\mu,\eta) = -\frac{(\cosh\mu-\cos\eta)^2}{a\ \sinh\mu}\,\frac{\partial}{\partial\eta}\,(\sinh\mu\ G(\mu)) \tag{8.14}$$

with a yet unknown function $G(\mu)$.

Putting aside the problem of eventual singularity, we can at this point see quite well what the induced charge and current distributions look like. Consider one of the lines of force of **B**, i.e. a circle $\mu =_m u_0$, $\phi = \phi_0$ in the $(\rho, z)$ plane (Figure 1, left).

The symmetry properties of the field **E** impose the vanishing of its $\eta$-component for $z = 0$, i.e. for $\eta = 0$ or $\pi$, because $E_\eta(\eta) = -E_\eta(2\pi - \eta)$. On the other hand, $B_\eta(\eta) = B_\eta(2\pi - \eta) >$, so that the scalar product $\mathbf{E} \cdot \mathbf{B} = E_\eta B_\eta$ on the circle $\mu = \mu_0$ is an odd function of $\eta$ (Figure 1, right).

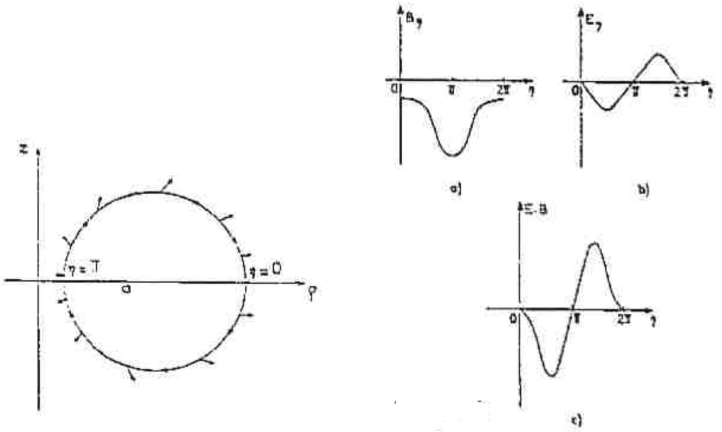


**Рис. 3.** Illustration for $\eta$

In order to obtain the charge distribution along this circle, we have to compute $-\mathbf{B} \cdot \mathbf{grad}(\mathbf{E} \cdot \mathbf{B})$, which reduces to the expression

$$-B_\eta \frac{(\cosh \mu - \cos \eta)}{a} \frac{\partial}{\partial \eta} (\mathbf{E} \cdot \mathbf{B}) \,. \tag{8.15}$$

The corresponding functions are displayed in Figure 3:

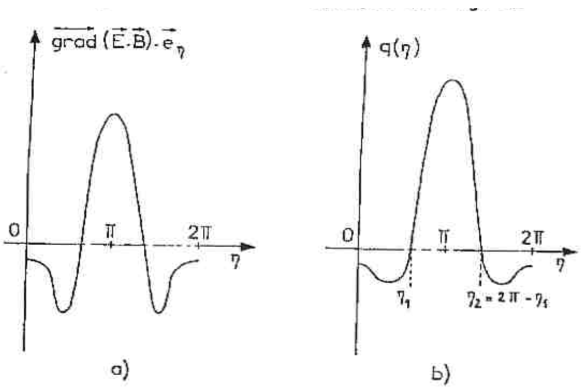


**Рис. 4.** a) The projection of $\mathbf{grad}(\mathbf{E} \cdot \mathbf{B})$ on the unit vector $\mathbf{e}_\eta$ as a function of $\eta$; b) The charge density distribution $q(\eta)$ as function of $\eta$

The charge density changes its sign between $\eta_1$ and $\eta_2 = 2\pi - \eta_1$. This phenomenon describes vacuum polarization: if at the core of the static solution there is an accumulation of charge density of a given sign, it must be surrounded by a cloud of charge density of opposite sign.

The value of $\eta_1$ at which the change of sign occurs depends on the line (i.e. the value of $\mu$). Reproducing similar reasoning for all circles $\mu =$ Const. we obtain the picture of the overall charge density (Figure 4):

The strongest vacuum polarization is on the $z$-axis and in the symmetry plane $(x, y)$, around the axially symmetric charge distribution at the core. If at any point of this distribution we wanted to

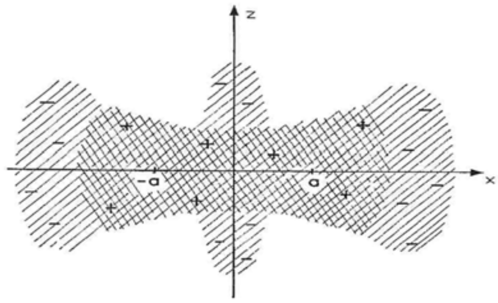


**Рис. 5.** The cross-section $(x, z, \phi = \text{Const.})$ of the charge density distribution.

interpret the azimuthal current density obtained from the last equation (8.1) as being produced by a rotational movement of the charge density around the $z$-axis, then it is easy to see, just comparing the units (remember that we chose the units in which $c = 1$), that the induced charge has to "move" with the speed of light. In reality, nothing is moving here: there is just a distribution of static fields $\mathbf{E}$ and $\mathbf{B}$ which produces this illusion, because the Poynting vector $\mathbf{E} \times \mathbf{B}$ has only the azimuthal component. Nevertheless, the illusion produced is the same as for the electron as a whole submitted to the *"zitterbewegung"* with the speed $c$ as it comes out from the relativistic Dirac equation describing the electron.

There is also another striking similarity between the predictions of this model and those of the Dirac equation. Both the lagrangian and the equations it led to (8.1) are invariant with respect to the independent changes of sign, $\mathbf{E} \to -\mathbf{E}$ and $\mathbf{B} \to -\mathbf{B}$.

This means that any static solution generates automatically three other ones, obtained by the inversions of $\mathbf{E}$ and $\mathbf{B}$. Now, the total charge is linear in $\mathbf{E}$, while the total magnetic moment is linear in $\mathbf{B}$; the Poynting vector is proportional to $\mathbf{E} \times \mathbf{B}$, and so will be the total kinetic angular momentum obtained by the integration of $\mathbf{r} \times (\mathbf{E} \times \mathbf{B})$ over the entire space.

The four solutions so obtained can be put together in the following Table 1:

| Solution | Energy | Charge | Magnetic $\mu$ | Spin |
|---|---|---|---|---|
| $\mathbf{E},\ \ \mathbf{B}$ | m | q | $\boldsymbol{\mu}$ | $\mathbf{S}$ |
| $\mathbf{E},\ -\mathbf{B}$ | m | q | $-\boldsymbol{\mu}$ | $-\mathbf{S}$ |
| $-\mathbf{E},\ \ \mathbf{B}$ | m | $-q$ | $\boldsymbol{\mu}$ | $-\mathbf{S}$ |
| $-\mathbf{E},\ -\mathbf{B}$ | m | $-q$ | $-\boldsymbol{\mu}$ | $\mathbf{S}$ |

Any static solution is, as a matter of fact, a quadruplet of solutions with the same rest mass. The first two solutions describe a particle with electric charge $q$ and magnetic moment $\boldsymbol{\mu}$ *parallel* to spin $\mathbf{S}$, in states with spin up or down (with respect to the $z$-axis).

The second pair of solutions describes a particle with the opposite charge $-q$ and magnetic moment *antiparallel* to the spin $\mathbf{S}$, also in two states with spin up or down. This result is identical with the predictions of Dirac's equation for the electron, which leads to the existence of the positron and a half-integer spin, too.

The bad news is that unfortunately a $C^\infty$-class solution of the system (8.1 does not exist. The proof is simple and goes as follows: Knowing that div $\mathbf{B} = 0$, we can write

$$\mathbf{B} \cdot \mathbf{grad}(\mathbf{E} \cdot \mathbf{B}) = \text{div}\ (\mathbf{B}\ (\mathbf{E} \cdot \mathbf{B})) \tag{8.16}$$

Similarly,

$$\mathbf{E} \times \mathbf{grad}(\mathbf{E} \cdot \mathbf{B}) = \mathbf{rot}(\mathbf{E}\ (\mathbf{E} \cdot \mathbf{B})), \tag{8.17}$$

because $\mathbf{rot}\ \mathbf{E} = 0$. This leads to

$$\text{div}\ \left(\mathbf{E} + \frac{3}{e^2}\ \mathbf{B}(\mathbf{E}\cdot\mathbf{B})\right) = 0, \quad \mathbf{rot}\ \left(\mathbf{B} - \frac{3}{e^2}\ \mathbf{E}(\mathbf{E}\cdot\mathbf{B})\right) = 0. \tag{8.18}$$

If the space we are working in has the topology of $R^3$, and all the functions are supposed to be $C^\infty$-smooth, then the Poincaré lemma states that

$$\mathbf{E} + \frac{3}{e^2}\ \mathbf{B}(\mathbf{E}\cdot\mathbf{B}) = \mathbf{rot}\ \mathbf{C}\ \ ;\ \ \text{and} \quad \mathbf{B} - \frac{3}{e^2}\ \mathbf{E}(\mathbf{E}\cdot\mathbf{B}) = \mathbf{grad}\psi. \tag{8.19}$$

with $\mathbf{C}(\mathbf{r})$ and $\psi(\mathbf{r})$ supposed to be $C^\infty$ smooth (vector and scalar, respectively) functions of $\mathbf{r}$.

Taking the scalar product of the first equation in (8.19) by $\mathbf{E}$ and of the second equation by $\mathbf{B}$ we get (supposing that $\mathbf{E} = -\mathbf{grad}V$):

$$\mathbf{E}^2 + \frac{3}{e^2}\ (\mathbf{E}\cdot\mathbf{B})^2 = \mathbf{E}\cdot\mathbf{rotC} = -(\mathbf{grad}V)\cdot\mathbf{rotC} = -\text{div}\ (V\mathbf{rotC}), \tag{8.20}$$

and

$$\mathbf{B}^2 - \frac{3}{e^2}\ (\mathbf{E}\cdot\mathbf{B})^2 = \mathbf{B}\cdot\mathbf{grad}\psi = \text{div}(\psi\ \mathbf{B}). \tag{8.21}$$

Combining equations (8.20) and (8.21) together, we have

$$\mathbf{E}^2 + \mathbf{B}^2 = \text{div}(\psi\mathbf{B} - V\ \mathbf{rot}\ \mathbf{C}). \tag{8.22}$$

If we want the total energy, as well as the total charge, to be finite, then both $\mathbf{E}$ and $\mathbf{B}$ must decrease at infinity at least as $R^{-2}$, so that the right-hand side of (8.22) must be of the order of $R^{-4}$, which means in turn that the vector field $\psi\ \mathbf{B} - V\ \mathbf{rot}\ \mathbf{C}$ is decreasing at infinity as $R^{-3}$. Applying the Gauss-Ostrogradsky theorem to a finite 3-volume $\Omega$ and its 2-dimensional boundary $\partial\Omega$:

$$\int_\Omega \text{div}(\psi\ \mathbf{B} - V\ \mathbf{rot}\ \mathbf{C})\ d^3\mathbf{r} = \int_{\partial\Omega} (\psi\ \mathbf{B} - V\ \mathbf{rot}\ \mathbf{C})\cdot \mathrm{d}\mathbf{\Sigma}, \tag{8.23}$$

we see that the integral of $\mathbf{E}^2 + \mathbf{B}^2$ over a spherical volume of radius $R$ behaves as $R^{-1}$, i.e. it vanishes when taken over the whole space. Both expressions $\mathbf{E}^2$ and $\mathbf{B}^2$ being positive, this means that $\mathbf{E} = 0$ and $\mathbf{B} = 0$, unless the solution is not $C^\infty$ and the Poincaré lemma does not hold at least on some line or surface.

The impossibility of obtaining a $C^\infty$ solution with finite energy can be also seen if we try to construct it by applying the method of successive approximations in toroidal coordinates.

Now the problem can be reduced down to two equations for two unknown functions, the azimuthal component of the vector potential $A_\phi$ and the scalar potential $V$. We can believe that in basic state the dependence on the azimuthal angle $\phi$ is trivial, therefore we may set

$$A_\phi = A_\phi(\mu,\eta) \quad \text{and} \quad V = V(\mu,\eta) \tag{8.24}$$

The dependence of both potentials on the toroidal angle $\eta$ must be of the form $\sin(k\eta)$ or $\cos(k\eta)$, $k = 1, 2, \ldots$; using the substitution

$$A_\phi = u(\eta)\ \sqrt{\cosh\mu - \cos\eta} = (\cosh\mu - \cos\eta)\ G(\mu) \tag{8.25}$$

we make the $\mu$-component of the magnetic field vanish, $B_\mu = 0$.

Along with another substitution

$$V = v(\eta)\ \sqrt{\cosh\mu - \cos\eta} \tag{8.26}$$

the laplacians appearing on the left-hand side of equations (8.1) will have their variables separated. For example, the equation

$$\text{div}\ \mathbf{E} = -\frac{3}{e^2}\ \mathbf{B}\cdot\mathbf{grad}(\mathbf{E}\cdot\mathbf{B}) \tag{8.27}$$

will take on the form:

$$\frac{1}{\sinh\mu}\frac{\partial}{\partial\mu}\left(\sinh\mu\frac{\partial v}{\partial\mu}\right)+\frac{\partial^2 v}{\partial\eta^2}+\frac{1}{4}v=$$

$$\frac{3}{a^2e^2}\frac{(\cosh\mu-\cos\eta)}{\sinh^2\mu}\left[\frac{\partial}{\partial\mu}(\sinh\mu\,G(\mu))\right]^2[W(\mu,\eta)], \tag{8.28}$$

with

$$W=[\cosh\mu-\cos\eta)\frac{\partial^2 v}{\partial\eta^2}+4\sin\eta\frac{\partial v}{\partial\eta}+\frac{(5\sin^2\eta+2\cosh\mu\cos\eta-\cos^2\eta)}{4(\cosh\mu-\cos\eta)}. \tag{8.29}$$

Similarly, the laplacian of the function $u(\mu,\eta)$ is equal to some non-linear terms mutiplied by $3/(a^2e^2)$. Developing functions $u$ and $v$ as e.g.

$$\sum_{n=1}^{\infty}[\overset{(1)}{v}_n(\mu)\sin(n\eta)+\overset{(2)}{v}_n(\mu)\cos(n\eta)]$$

the second derivatives in (8.28) will be replaced by $n^2v$, and the solutions of the *homogeneous equations*,nwhich correspond to the zeroth approximation ($\frac{2}{a^2e^2}=0$) are given as a series in spherical harmonics of half-integer order (cf. Morse and Feshbach).

$$P_{n+\frac{1}{2}}(\cosh\mu) \quad \text{and} \quad Q_{n-\frac{1}{2}}(\cosh\mu) \tag{8.30}$$

The functions $P_{n+\frac{1}{2}}$ display a logarithmic singularity for $\mu=\infty$, i.e. on the circle $\rho=a$, whereas the functions $Q_{n-\frac{1}{2}}$ have a logarithmic singularity for $\mu=0$ (i.e. $\rho,z\to\infty$).

In order to avoid singularity we may use the combination of both, but the price to pay is a discontinuity for some value of $\mu$ (on some toroidal surface). If we feed in such a solution to the right-hand side and use the Green functions in order to compute the first correction, we shall be faced with exactly the same problem, because any Green function has at least one singularity of the same kind.

The failure of producing a non-singular soliton is probably due to the fact that we have projected everything onto three space dimensions, discarding the fifth circular one. It seems possible to obtain solitons using the fifth dimension in a non-trivial way, like in the case of Kaluza-Klein monopoles of Sorkin and Gross and Perry.

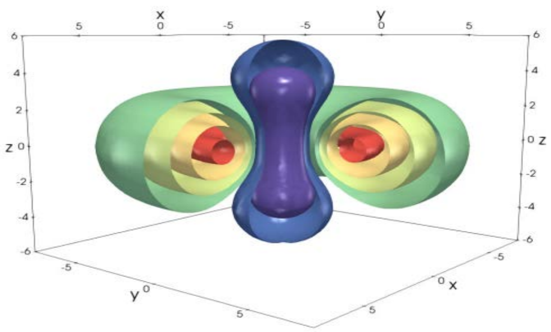


**Рис. 6.** The constant energy density surfaces in cartesian coordinates

Another development should include the non-abelian generalization of the Kaluza-Klein theory into more dimensions, in which also higher order invariants of the Riemann tensor might be included to the generalized lagrangian.

Recently toroidal solutions for the Higgs-'t Hooft $SU(2)\times U(1)$ monopole were produced numerically by M.S. Volkov *et al.*.

The constant energy density surfaces are represented in cartesian coordinates Fig. 6.

**Список литературы/References**


1. Nordström, Gunnar. Über die Möglichkeit, das elektromagnetische Feld und das Gravitationsfeld zu vereinigen. *Physikalische Zeitschrift* 15 (1914): 504-506.
2. Kaluza, Th. Zum unitätsproblem der physik. *Sitzungsber. Preuss. Akad. Wiss. Berlin (Math. Phys.)* 1921.arXiv: 1803.08616 (1921): 966-972.
3. Klein, O. Quantentheorie und fünfdimensionale Relativitätstheorie. *Zeitschrift für Physik* 37.12 (1926): 895-906.
4. Einstein, A. *Zu Kaluzas Theorie des Zusammenhanges von Gravitation und Elektrizität: erste-[zweite] Mitteilung.* Verlag der Akademie der Wissenschaften, in Kommission bei Walter de Gruyter u. Company, 1927.
5. Thiry, Y. Les équations de la théorie unitaire de Kaluza. *Comptes Rendus Acad. Sci.(Paris)* 226 (1948): 216.
6. M. Y. Thiry (1948) Sur la régularité des champs gravitationnel et électromagnétique dans les théories unitaires. *Compt. Rend. Acad. Sci. Paris* (in French). 226 pp.1881-1882.
7. J. Pascual. Fünfdimensionale kosmologie. *Astronomische Nachrichten* 276.5-6 (1948): 193-208.
8. Scherrer, W. Uber den Einfluss des metrischen Feldes auf ein skalares Materiefeld. *Helvetica Physica Acta* 22.5 (1949): 537-551.
9. Brans C., and Robert H. Dicke. Mach's principle and a relativistic theory of gravitation. *Physical review* 124.3 (1961): 925.
10. Lovelock D. The Einstein tensor and its generalizations. *Journal of Mathematical Physics* 12.3 (1971): 498-501.
11. Witten E. Search for a realistic Kaluza-Klein theory. *Nuclear Physics B* 186.3 (1981): 412-428.
12. Appelquist Th, Alan C. and Peter George Oliver Freund. *Modern Kaluza-Klein Theories.* (1987).
13. Duff M. J. Kaluza-Klein theory in perspective. *Proc. of the Symposium: The Oskar Klein Centenary, World Scientific, Singapore.* 1994.
14. Overduin J. M., and Paul S. W. Kaluza-klein gravity. *Physics reports* 283.5-6 (1997): 303-378.
15. Wesson P. S. *Five-dimensional physics: classical and quantum consequences of Kaluza-Klein cosmology.* World Scientific, 2006.
16. Coquereaux R. and Gilles E.F. The theory of Kaluza-Klein-Jordan-Thiry revisited. *Annales de l'IHP Physique théorique.* Vol. 52. No. 2. 1990.
17. Kerner R. Geometrical background for the unified field theories: the Einstein-Cartan theory over a principal fibre bundle. *Annales de l'institut Henri Poincaré. Section A, Physique Théorique.* Vol. 34. No. 4. 1981.
18. Kerner R. Multiple fiber bundles and gauge theories of higher order. *Journal of Mathematical Physics* 24.2 (1983): 356-360.
19. Kerner R. Electrodynamique non linéaire en théorie de Kaluza et Klein. *Comptes rendus de l'Académie des sciences. Série 2, Mécanique, Physique, Chimie, Sciences de l'univers, Sciences de la Terre* 304.12 (1987): 621-624.
20. Kerner R. Non-linear electrodynamics derived from the Kaluza-Klein theory. *arXiv preprint arXiv:2303.10603* (2023).
21. Bruno G., and Kerner R. Cosmology in ten dimensions with the generalised gravitational Lagrangian. *Classical and Quantum Gravity* 5.2 (1988): 339.
22. Ghosh S. G., and Sunil D. M. Cloud of strings for radiating black holes in Lovelock gravity. *Physical Review D* 89.8 (2014): 084027.
23. Matzner R. A. and Mezzacappa A. Three-dimensional closed universes without collapse in a five-

dimensional Kaluza-Klein theory. *Physical Review D* 32.12 (1985): 3114.

24. Copeland, Edmund J., and David J. Toms. Stability of self-consistent higher-dimensional cosmological solutions. *Physical Review D* 32.8 (1985): 1921.
25. Chodos, Alan, and Steven Detweiler. Where has the fifth dimension gone?. *Physical Review D* 21.8 (1980): 2167.
26. Sahdev, Deshdeep. Perfect-fluid higher-dimensional cosmologies. *Physical Review D* 30.12 (1984): 2495.
27. Srivastava, S. K. Some aspects of Kaluza-Klein cosmology. *Pramana* 49 (1997): 323-370.
28. Sorkin, Rafael D. Kaluza-klein monopole. *Physical Review Letters* 51.2 (1983): 87.
29. Gross, David J., and Malcolm J. Perry. Magnetic monopoles in Kaluza-Klein theories. *Nuclear Physics B* 226.1 (1983): 29-48.
30. Gervalle, Romain, and Mikhail S. Volkov. Electroweak multi-monopoles. *Nuclear Physics B* 987 (2023): 116112.

**Авторы**

**Ричард Кернер**, д.ф.-м.н., профессор, Сорбонский университет, пл. Жюсьё, d.4, г. Париж, 75005, Франция.
E-mail: richard.kerner@sorbonne-universite.fr

**Просьба ссылаться на эту статью следующим образом:**

Кернер Р. Обобщенные модели Калуцы - Клейна с лагранжианами Гаусса - Бонне. *Пространство, время и фундаментальные взаимодействия.* 2023. № 3-4. С. 166–187.

**Authors**

**Kerner Richard**, Ph.D., Professor, LPTMC, Sorbonne Universite - CNRS UMR 7600, Place Jussieu, 4, Paris, 75005, France.
E-mail: richard.kerner@sorbonne-universite.fr

**Please cite this article in English as:**

Kerner R. Generalized Kaluza-Klein models with Gauss-Bonnet lagrangians. *Space, Time and Fundamental Interactions*, 2023, no. 3-4, pp. 166–187.

УДК 530.12, 531.51



# О ДЕТЕКТИРОВАНИИ ВЫСОКОЧАСТОТНЫХ РЕЛИКТОВЫХ ГРАВИТАЦИОННЫХ ВОЛН*

Манучарян Г. Д.[a,b,1], Фомин И. В.[a,2], Гладышев В. О.[a,3], Литвинов Д. А.[c,4]

[a] МГТУ им. Н.Э. Баумана, г. Москва, 105005, Россия.

[b] ГАИШ МГУ им. М.В. Ломоносова, г. Москва, 119234, Россия.

[c] Астрокосмический центр Физического института им. П.Н. Лебедева РАН, г. Москва, 117997, Россия.

Рассмотрена специфика спектра реликтовых гравитационных волн, формирующихся на инфляционном и постинфляционном этапах эволюции ранней Вселенной, для космологических моделей, основанных на модифицированных теориях гравитации и гравитации Эйнштейна. Рассматривается возможность обнаружения высокочастотных реликтовых гравитационных волн с помощью процесса преобразования гравитонов в фотоны в постоянном и переменном магнитном поле. Проводится сравнение чувствительности детекторов этого типа с чувствительностью других существующих и перспективных детекторов высокочастотных гравитационных волн. На основе анализа оценки чувствительности различных типов детекторов высокочастотных гравитационных волн делается вывод о перспективах прямой верификации моделей космологической инфляции с помощью гравитационно-волновых антенн.

*Ключевые слова*: Общая теория относительности, модифицированные теории гравитации, гравитационные волны, гравитационно-волновые антенны.

# ON THE DETECTION OF HIGH-FREQUENCY RELIC GRAVITATIONAL WAVES

Manucharyan G. D.[a,b,1], Fomin I. V.[a,2], Gladyshev V. O.[a,3], Litvinov D. A.[c,4]

[a] Bauman Moscow State Technical University, Moscow, 105005, Russia.

[b] Sternberg Astronomical Institute, Moscow, 119234, Russia.

[c] Astro Space Center, Lebedev Physical Institute, Moscow, 117997, Russia.

The specificity of the spectrum of relic gravitational waves formed at the inflationary and post-inflationary stages of the evolution of the early universe is considered for cosmological models based on modified theories of gravity and Einstein gravity. The possibility of detecting high-frequency relic gravitational waves by using the process of converting gravitons into photons in a constant and alternating magnetic field is considered. The sensitivity of detectors of this type is compared with the sensitivity of other existing and prospective detectors of high-frequency gravitational waves. Based on the analysis of the sensitivity assessment of various types of high-frequency gravitational wave detectors, a conclusion is made about the prospects for direct verification of cosmological inflation models using gravitational-wave antennas.

*Keywords*: General relativity, modified gravity theories, gravitational waves, gravitational-wave detectors.

PACS: 04.50.-h

DOI: 10.17238/issn2226-8812.2023.3-4.188-198

## Introduction

Since the first detection of the emission of gravitational waves in 2015 [1] General Relativity (GR) has once again demonstrated its correctness in describing the large-scale structure of the Universe

*Работа Фомина И.В. поддержана грантом РНФ № 22–22–00248.

1E-mail: gevorgbek.manucharyan@gmail.com
2E-mail: ingvor@inbox.ru
3E-mail: vgladyshev@mail.ru
4E-mail: litvirq@gmail.com

and the validity of the geometric interpretation of gravitational interaction. Notwithstanding, General Relativity does not answer all the questions relating to the current accelerated expansion of the Universe and how to solve the problem of dark matter and dark energy. Various types of modifications of GR are considered to solve these types of problems, e.g. adding scalar fields to GR [2, 3] or modifying GR by adding dependencies of higher orders of space-time curvature [4, 5]. Although these frameworks may yield some interesting mathematical results, they require experimental verification.

The nature of the transition from the inflationary stage to the post-inflationary stage of the evolution of the universe has a significant impact on the spectrum of relict gravitational waves. Deviations of the state parameter of matter at the post-inflationary stage from the value corresponding to radiation $w_\gamma = 1/3$ during this transition corresponding to the presence of an additional stage of stiff energy domination, induce a significant increase in the energy density of relict gravitational waves in the high frequency range.

The value of the state parameter of the post-inflationary matter field can be determined as follows

$$w = -1 + \frac{4}{3}(1+\beta), \tag{0.1}$$

where $\beta = 0$ for the slow-roll inflation based on GR with post-inflationary radiation domination [6], $\beta = 1/2$ for quintessential inflation based on GR with post-inflationary domination of kinetic energy of a scalar field [7], $0 \leq \beta \leq 1/5$ for inflationary models based on the scalar-tensor gravity with the power-law connection between coupling function and the Hubble parameter [8], $0 \leq \beta \leq 1/2$ for the inflationary models based on the scalar-torsion gravity with the power-law connection between coupling function of a scalar field and torsion scalar and the Hubble parameter [9] and $-1/2 \leq \beta \leq 0$ for inflationary models based on the Einstein-Gauss-Bonnet gravity, where $\beta = \alpha_{GB}$ is a coupling constant between scalar field and the Gauss-Bonnet term [10, 11].

We also note that quintessential inflationary models based on Einstein gravity imply only one value of the stiff matter state parameter $w = 1$, while modified gravity theories imply a wider range of values for this parameter $1/3 < w \leq 1$. For this reason, analysis of the spectrum of relict gravitational waves leads to the possibility of determining the influence of modifications of Einstein gravity at the inflationary stage of the evolution of the universe.

In this paper, we consider the influence of stiff matter on the resulting spectrum of relict gravitational waves in the present era of the evolution of the universe and discuss the possibilities of direct registration of relict gravitational waves on the basis of the various detection methods.

To evaluate the possibility of direct detection, this paper discusses the classical and modified Gerzenshtein effect, which involves the conversion of gravitational wave (GW) emission into photons in the presence of constant and varying magnetic fields, respectively, as well as high-frequency gravitational-optical resonance in a multi-beam interferometer [12]. As it will be shown below, the latter is the most promising method for observing relic gravitational waves in laboratory conditions.

## 1. Energy contained in gravitational waves

The energy density of relic gravitational waves can be estimated [13] by a dimensionless value

$$\Omega_{\mathrm{GW}} \simeq \Omega^0_{\mathrm{GW}} \cdot \begin{cases} 1, & f < f_{\mathrm{RD}} \\ 1.27 \cdot \left(\frac{f}{f_{\mathrm{RD}}}\right)^{\alpha_S}, & f \geq f_{\mathrm{RD}} \end{cases} \tag{1.1}$$

where $\Omega^0_{\mathrm{GW}} = 10^{-15} \cdot r/h^2$, $r$ is the tensor – scalar ratio, $h \simeq 0.68$ is the dimensionless Hubble constant, parameter $\alpha_S$ is defined as

$$\alpha_S = 2\frac{3w-1}{3w+1}, \tag{1.2}$$

where $f_{\mathrm{RD}}$ is the frequency of the mode that corresponds to the size of the horizon at the beginning of the epoch of radiation domination in the present epoch. Taking into account the LIGO sensitivity

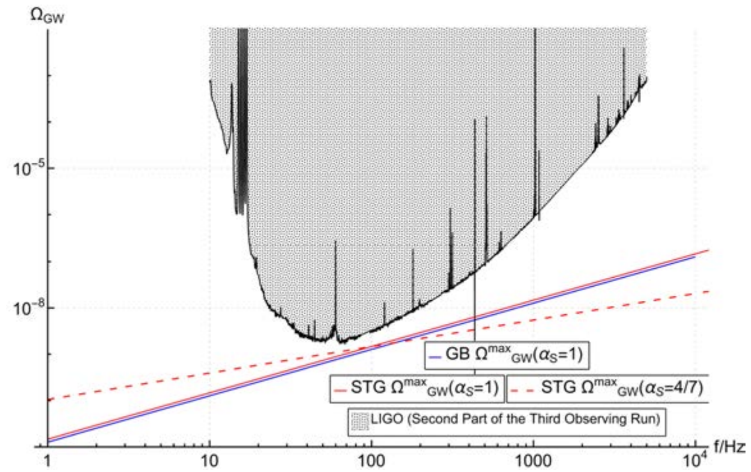


**Рис. 1.** Energy density of relic gravitational waves of the present models for different values of the post-inflationary matter state parameter in comparison with the region of operation of the LIGO gravitational-wave antenna [14]

it is not hard to obtain dependence between $f_{\mathrm{RD}}$ and parameter of matter state $w$. At 100Hz LIGO sensitivity is limited by dimensionless value $\Omega_{\mathrm{GW}} \lesssim \frac{1}{h^2}10^{-9}$ [14] (Fig.1) i.e.

$$f_{\mathrm{RD}}(w) = 100 \cdot \left(\frac{h^2 \cdot \Omega_{\mathrm{GW}}(100\mathrm{Hz})}{10^{-15} \cdot r}\right). \tag{1.3}$$

The cutoff frequency of the relic gravitational-wave background spectrum $f_{\mathrm{cutoff}}$ can be estimated taking into account the integral restriction on the energy density contained in relic gravitational waves [13]

$$\int_{f_{\mathrm{BBN}}}^{f_{\mathrm{cutoff}}} \Omega(f)\frac{df}{f} \lesssim 1 \times 10^{-6}, \tag{1.4}$$

where $f_{\mathrm{BBN}} < f_{\mathrm{RD}} < f_{\mathrm{cutoff}}$, $f_{\mathrm{BBN}} \simeq 1.8 \times 10^{-11}$Hz is the frequency of the mode corresponding to the size of the Universe, when primordial nucleosynthesis started. Given (1.1) and (1.4) it is not hard to obtain

$$f_{\mathrm{cutoff}}(w) \le f_{\mathrm{RD}}(w)\left(\alpha_S\left[\frac{1 \times 10^{-6}}{1.27 \times \Omega^0_{\mathrm{GW}}} - \frac{1}{1.27}ln\left(\frac{f_{\mathrm{RD}}(w)}{f_{\mathrm{BBN}}}\right)\right] + 1\right)^{\frac{1}{\alpha_S}} \tag{1.5}$$

this dependency allows us to evaluate the maximal possible energy density for given frequency of relic gravitational waves (or in other way the maximal energy density for given state parameter of post-inflationary matter of the Universe) which in it's turn allows evaluate the possibility of direct detection based on detectors sensitivity.

## 2. Detectors under consideration

First experimental scheme under consideration is one where detection is provided by the response of Gaussian beam (2.1) to high-frequency relic gravitational waves [15]

$$\psi = \frac{\psi_0}{\sqrt{1+(z/f)^2}}\left(-\frac{r^2}{W^2}\right)\exp\left[i\left((k_e z - \omega_e t) - tan^{-1}\frac{z}{f} + \frac{k_e r}{2R} + \delta\right)\right], \tag{2.1}$$

where $\psi$ is the electric field, $r^2 = x^2 + y^2$, $k_e = 2\pi/\lambda_e$, $f = 2\pi W_0^2/\lambda_e$, $W = W_0\left[1 + (z/f)^2\right]^{1/2}$, $R = z + f^2/z$, $\psi_0$ - maximum amplitude of the electric field, $W_0$ - beam radius, $\delta$ - phase additive. The following parameters are realized in the detector under analysis $W_0 = 0.05$m, $l = 0.1$m, $l_0 = 0.3$m, $\psi_0 = 3 \times 10^5$V/m, $\hat{B}^{(0)}_y = 30$T (constant magnetic field, applied to the region of space $-l/2 < z < l/2$).

As it is shown [15], the photon flux resulting from the interaction between the gravitational wave and the Gaussian beam is estimated to be

$$S^{\phi|(1)} = \frac{1}{\mu_0}\left(\tilde{E}_r^{(1)}\tilde{B}_z^{(0)}\right) = -\frac{1}{\mu_0}\left(\tilde{E}_x^{(1)}\tilde{B}_z^{(0)}\right)\cos\phi - \frac{1}{\mu_0}\left(\tilde{E}_y^{(1)}\tilde{B}_z^{(0)}\right)\sin\phi. \tag{2.2}$$

Above $S^{\phi|(1)}$ is the first order tangential photon flux, generated by perturbed electric field $\tilde{E}_r^{(1)}$ and constant magnetic field $\tilde{B}_z^{(0)}$ pointed radially and axially accordingly. In the case of $\omega_e = \omega_g$, and when considering the amplitude of the cross-polarisation of the gravitational wave in the plane $z = 0$, the average photon flux $S^{\phi|(1)}$ can be estimated as

$$\langle S_\times^\phi\rangle^{(1)}_{\omega_e=\omega_g} = \frac{h_\times \hat{B}_y^{(0)}\psi_0 lr}{4\mu_0 W_0^2} exp\left(-\frac{r^2}{W_0^2}\right)\sin^2\phi. \tag{2.3}$$

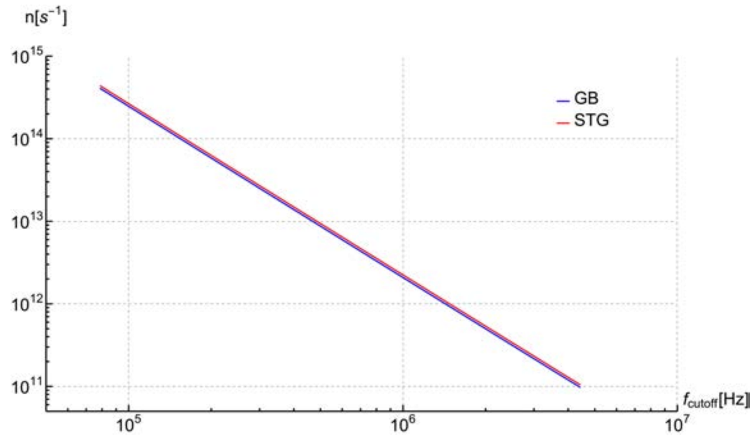


**Рис. 2.** Number of photons per second generated by the interaction of a Gaussian beam with a gravitational wave, for different cutoff frequencies $f_{\rm cutoff}(w)$, corresponding to different values of the state parameter of matter in the post-inflationary universe.

The number of generated photons per second in this case can be estimated as

$$n_\phi = \frac{1}{\hbar\omega_e}\int_0^{W_0}\int_{-l/2}^{l_0}\langle S_\times^\phi\rangle^{(1)}_{\omega_e=\omega_g,\phi=\pi/2} dzdr. \tag{2.4}$$

The theoretical photon formation frequency Fig.2 is presented for the gravitational wave frequency corresponding to the cutoff frequency, i.e., for each frequency the maximum permissible (taking into account the integral restriction (1.4)) amplitude of relic gravitational waves is taken. The photon formation frequency, as it is easy to see, at $4.4\times10^6$Hz is $n_\phi|_{4DEGB} \approx n_\phi|_{STG} \approx 10^{11}$Hz.

As it was shown by Mitskievich and Nesterov [16] during the propagation of gravitational and electromagnetic waves in parallel, the production of phase-shifted photons in the electromagnetic waves does not occur. Similarly, when the gravitational wave propagates perpendicularly to the plane of EM wave propagation, a phase shift is expected in the electromagnetic wave, which can be estimated as

$$\Delta\alpha = h\,(\Lambda - \sin[\Lambda])\sin[\Lambda - \delta], \tag{2.5}$$

where $\Lambda = \omega_g L/c$, $h$ - amplitude of gravitational wave, $\omega_g$ - circular frequency of the gravitational wave, $L$ - effective size of the space at which the gravitational wave interacts with the electromagnetic wave, $c$ - speed of light, $\delta$ - source wave phase. The geometric phase shift for the considered detector configuration is $\sim 2\times10^{-35}$ at $4.4\times10^6$Hz, which renders it impossible to record gravitational waves at laboratory-sized facilities. According to this, although the value $n_\phi|_{4DEGB} \approx n_\phi|_{STG} \approx 10^{11}$Hz is presented, the generated photons cannot be detected because of their small phase shift in respect to the alternating electromagnetic field available in the detector.

The second case considers a setup based on the modified Gertsenshtein effect, where it is implied that the gravitational wave interacts with the electromagnetic field inside a solenoid, where the magnetic field $\mathbf{B}^{(0)}$ is a superposition of the DC and AC components, namely [17]

$$\mathbf{B}^{(0)} = \overline{\mathbf{B}}^{(0)}(\mathbf{x}) + \tilde{\mathbf{B}}^{(0)}(\mathbf{x},t) = \begin{pmatrix} 0 \\ B_y^{(0)} \\ 0 \end{pmatrix} + \begin{pmatrix} 0 \\ -\tilde{B}_y^{(0)}\cos(\omega_B t) \\ 0 \end{pmatrix}, \qquad (2.6)$$

where $\omega_B$ is the frequency of the alternating magnetic field oscillation.

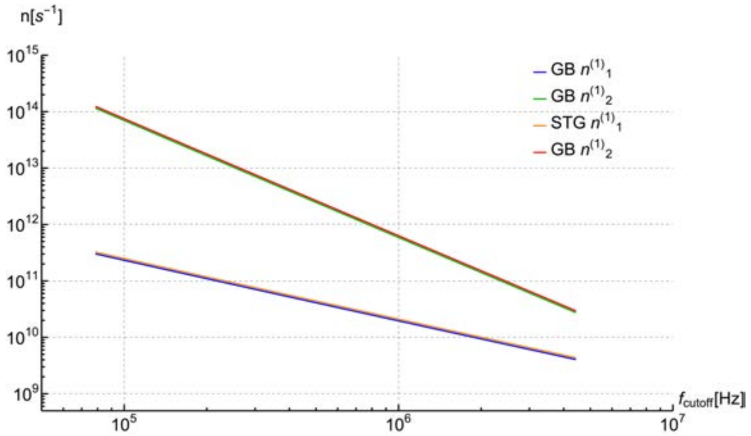


**Рис. 3.** Frequency of appearance of photons generated by the inverse Gertsenshtein effect.

As shown in [18], in the configuration when $\omega_g = \omega_B$ photon generation occurs at both the resonant and the dual frequency of the GW with characteristic frequency of formation

$$n_1^{(1)} = \frac{B_y^{(0)}\tilde{B}_y^{(0)} l\Xi}{4\mu_0\hbar} h_+, \qquad (2.7)$$

and

$$n_2^{(1)} = \frac{3\left(\tilde{B}_y^{(0)}\right)^2 c\Xi}{4\mu_0\hbar\omega_g} h_+, \qquad (2.8)$$

correspondingly, where $l$ is the effective distance traveled by the GW in the solenoid electromagnetic field, $\Xi$ is the area of the detector located so that the normal to its surface is $\mathbf{n}_\Xi \parallel \mathbf{k}_g$. In particular, we consider the setup in which the conditions $B_y^{(0)} = 30$T, $\tilde{B}_y^{(0)} = 0.1B_y^{(0)}$, $l = 0.1$m, $\Xi = 0.05\text{m}^2$ are realized. Here teoretical photon formation frequency for $\omega_g = 2\pi \times 4.4 \times 10^6$Hz is $n_1^{(1)}\Big|_{\text{STG}} \simeq n_1^{(1)}\Big|_{\text{4DEGB}} \simeq 4.1 \times 10^9$Hz and $n_2^{(1)}\Big|_{\text{STG}} \simeq n_2^{(1)}\Big|_{\text{4DEGB}} \simeq 2.8 \times 10^{10}$Hz (Fig.3).

The geometric phase shift of the generated photons (2.5) is $\sim 4.5 \times 10^{-35}$ making detection impossible despite the fact that antennas sensitivity [17] defined by minimal detectable GW amplitude (2.9) is enough for registration Fig.4.

$$h^{min} = \frac{1}{2\mathbb{S}}\left[\frac{\hbar\omega}{\Xi\tau} + 2\frac{\hbar\omega^2\Delta\omega}{2\pi c^2}\frac{1}{e^{\hbar\omega/k_B T} - 1} + \sqrt{\left(\frac{\hbar\omega}{\Xi\tau}\right)^2 + \frac{4}{\Xi\tau}\frac{\hbar^2\omega^3\Delta\omega}{2\pi c^2}\frac{1}{e^{\hbar\omega/k_B T} - 1}}\right], \qquad (2.9)$$

where $\mathbb{S} \approx \hbar\omega_g(n_1^{(1)} + n_2^{(1)})/h$, detector responce time $\tau = 10 \times 2\pi/\omega_g$, $\Delta\omega$ represents detector's sensitivity bandwidth.

Weak interacting small particle (WISP) detectors can also be considered as detectors of gravitational waves, since part of their design is well suited for registration of HFGW based on the inverse Gertsenshtein effect (in literature also appears as graviton-photon conversion (GRAPH)) [19].

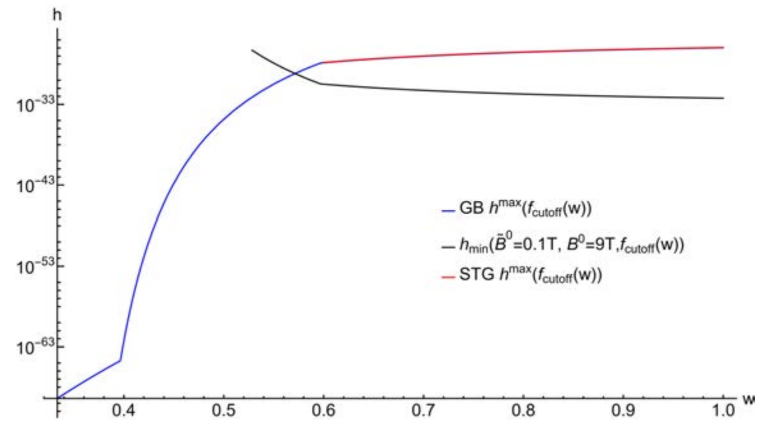


**Рис. 4.** The minimum GW amplitude $h_{min}$ required for registration based on the modified inverse Gertsenshtein effect and the maximum relic gravitational wave amplitude $h^{max}$ depending on the parameter of the post-inflationary matter state of the universe.

In this paper we consider both already realized WISP detectors (ALPS [20], OSQAR [21], CAST [22]) and promising ones (ALPS IIc [23], JURA [24], IAXO [25]). The sensitivity of detectors ALPS, OSQAR, CAST can be rated as

$$h_{min}(f) \simeq 1.16 \times 10^{-16} \times \left(\frac{1\text{T}}{B}\right)\left(\frac{1\text{m}}{L}\right)\sqrt{\left(\frac{N_{\text{exp}}}{1\text{Hz}}\right)\left(\frac{1\text{m}^2}{A}\right)\left(\frac{1\text{Hz}}{\Delta f}\right)\left(\frac{1}{\epsilon_\gamma}\right)}. \tag{2.10}$$

The above experiments were ultimately aimed at registration of $N_{\text{exp}}$ photons in the frequency range $\Delta f$ on detectors with a quantum efficiency $\epsilon_\gamma$ and a cross-sectional area of the photon generation region A. For the experimental setups considered above, these characteristics are given in Table 2, the quantum efficiency of the CCD matrices used as a function of the frequency of the incident radiation - in Fig.5

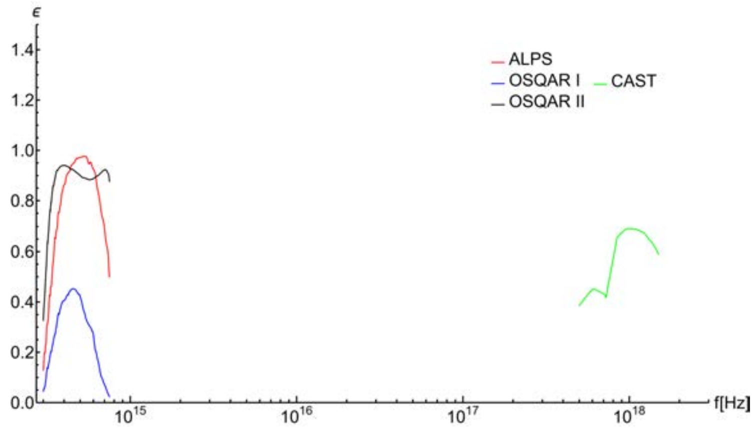


**Рис. 5.** Quantum efficiency of ALPS [20], OSQAR (2 matrices) [21] and CAST [22] CCD matrices used in the experiments as a function of radiation frequency.

The sensitivity of prospective detectors ALPS IIc, JURA, IAXO can be estimated as [19]

$$h_{min}(f) \simeq 2.8 \times 10^{-16}\left(\frac{1\text{T}}{B}\right)\left(\frac{1\text{m}}{L}\right)\sqrt{\left(\frac{1}{\mathcal{F}}\right)\left(\frac{N_{dark}}{1\text{Hz}}\right)\left(\frac{1\text{m}^2}{A}\right)\left(\frac{1\text{Hz}}{\Delta f}\right)\left(\frac{1}{\epsilon_\gamma}\right)}. \tag{2.11}$$

Table 2 presents all the necessary detector characteristics required for calculation. As the plants in this case have not yet been realized, we assume to use the theoretical value of quantum efficiency at wavelength 1024nm and the number of thermal photons $N_{dark}$ instead of experimental values for quantum efficiency and frequency of photon formation.

| | $N_{\rm exp}$(mHz) | $A$(m$^2$) | B(T) | L(m) | $\Delta f$(Hz) |
|---|---|---|---|---|---|
| ALPS | 0.61 | $0.5 \times 10^{-3}$ | 5 | 9.00 | $9 \times 10^{-14}$ |
| OSQAR I | 1.76 | $0.5 \times 10^{-3}$ | 9 | 14.3 | $5 \times 10^{-14}$ |
| OSQAR II | 1.14 | $0.5 \times 10^{-3}$ | 9 | 14.3 | $1 \times 10^{-15}$ |
| CAST | 0.15 | $2.9 \times 10^{-3}$ | 9 | 9.26 | $1 \times 10^{-18}$ |

**Таблица 1.** Characteristics of the experimental setups ALPS [26], OSQAR (2 matrices) [27] and CAST [28], necessary for estimation of the minimum detectable GW amplitude on them

| | $\epsilon_\gamma(\lambda = 1064$nm) | $N_{dark}$(Hz) | $A$(m$^2$) | B(T) | L(m) | $\mathcal{F}$ |
|---|---|---|---|---|---|---|
| ALPS IIc | 0.75 | $\approx 10^{-6}$ | $\approx 2 \times 10^{-3}$ | 5.30 | 120 | 40 000 |
| JURA | 1 | $\approx 10^{-6}$ | $\approx 8 \times 10^{-3}$ | 13.0 | 960 | 100 0000 |
| IAXO | 1 | $\approx 10^{-4}$ | $\approx 21$ | 2.50 | 25 | - |

**Таблица 2.** Characteristics of the experimental facilities ALPS IIc [23], JURA [24] and IAXO [25] required for estimation of the minimum detectable GW amplitude on them

Thus, as can be seen in Fig.6, none of the considered WISP detectors has sensitivity for HFGW registration.

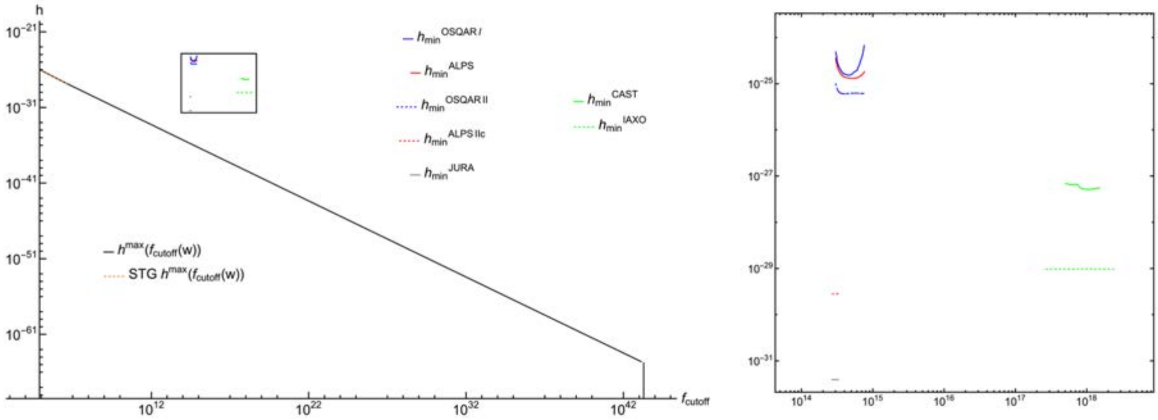


**Рис. 6.** Maximum amplitude of relic gravitational waves ($h^{max}$) and minimum GW amplitude required for registration at different WISP detectors ($h_{min}$).

The last discussed method of registering relic gravitational waves is gravitational-optical resonance. Gravitational-optical resonance in a multibeam interferometer is possible under the condition that an integer number of half-waves of GWs fit into the resonator length [29, 30]:

$$L = \frac{nc}{2f_g}, \quad n = 1, 2, 3, ..., \tag{2.12}$$

where $L$ is the length of the resonator, $c$ is the speed of light.

With such a resonator configuration that $L = c/2f_g$, the energy response of the Fabry-Perot interferometer to the passage of a gravitational wave can be estimated as [29, 30]

$$\delta W(t) = \frac{\mathcal{F}L}{\lambda_e} W_0 h_c(t), \tag{2.13}$$

where $\delta W$ is the change in laser power transmitted by the interferometer, $\mathcal{F}$ is the quality factor of the Fabry-Perot interferometer, $\lambda_e$ is the laser wavelength, and $W_0$ is the laser power at the input to the interferometer.

In terms of the spectral density of variation of the power generated by the passage of a GW through an interferometer, (2.13) can be written as [12]

$$S_{\delta W}(f) = \frac{\mathcal{F}^2 L^2}{\lambda_e^2} W_0^2 S_h(f), \tag{2.14}$$

where $S_h(f)$ is the spectral density of the gravitational-wave radiation. Taking into account the possibility of averaging the spectral density of the detector response over the time period $T$, it is shown [12] that for the described detection method, the minimum amplitude of the registered GW is estimated as follows

$$h_c = 2\left(\frac{\mathcal{F}}{T}\right)^{1/4} \left(\frac{\lambda_e}{\mathcal{F} W_0 c}\right) \sqrt{\tilde{S}_{\delta W}(f)} f^{5/4}, \tag{2.15}$$

where

$$\tilde{S}_{\delta W}(f) = \frac{\sqrt{cT}\mathcal{F}^{3/2} L^{3/2}}{\lambda_e^2} W_0^2 S_h(f) \tag{2.16}$$

is the time-averaged amplified spectral density of the Fabry-Perot interferometer response.

The shot photon noise, which determines the lower limit of detector sensitivity, is defined as [12]

$$h_{\text{Shot}} = 2f \left(\frac{\lambda_e}{\mathcal{F} W_0 c}\right) \left[\frac{\tilde{S}_{\delta W}(f)}{T}\right]^{1/2}. \tag{2.17}$$

For the setup in which the conditions $\lambda_e = 1.064\mu$m, $\mathcal{F} = 10^6$, $W_0 = 10^3$W are realized with signal averaging time $T = 1411$s and such a photodetector (DET10N2) that is able to detect $\tilde{S}_{\delta W} = 4 \times 10^{-28} W^2/Hz$, with $L = 27.5$m cavity is considered: Fig.7.

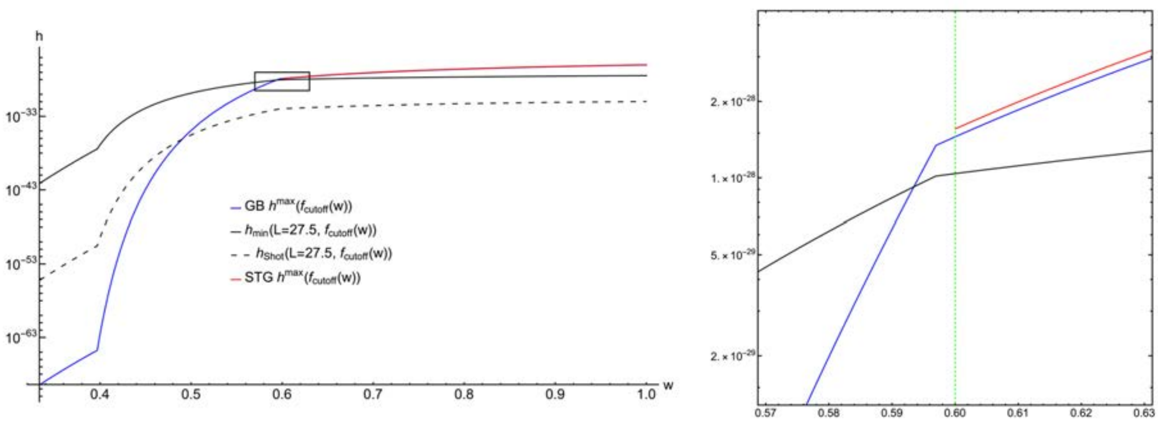


**Рис. 7.** The minimum detectable amplitude (black solid line) and limitation on the detector sensitivity from below, taking into account the shot photon noise (black hatched line), for the considered setup and the maximum GW amplitude depending on the parameter of the post-inflationary matter state of the Universe $w$. The green hatched line corresponds to 4.4 MHz.

From the presented analysis, it can be concluded that the high-frequency gravitational-optical resonance presents the most promising experimental scheme for detecting HFGWs. The gravitational-wave antenna based on the modified inverse Gertsenshtein effect is the next most promising option, provided that we can solve the issue of the small geometrical phase-shift between the generated and existing photons in the detection area.

## 3. Conclusion

Thus, when evaluating the possibility of directly registering relic gravitational waves, it has been established that detecting their interaction with a Gaussian beam at the frequency of 4.4MHz is impossible due to the small phase shift between the photons (with theoretical formation frequency $n_\phi \simeq 10^{11}s^{-1}$) of the Gaussian beam and those converted as a result of the GW-EM interaction. It was estimated that the theoretical frequency of photon formation, based on the modified inverse Herzenstein effect, is approximately $4.1 \times 10^9 s^{-1}$ for $\omega_e = \omega_g$, and $2.8 \times 10^{10} s^{-1}$ for $\omega_e = 2\omega_g$ at $\omega_g = 8.8\pi \times 10^6$rad/s. The considered setup based on the modified Herzenstein effect sets also a small $\left(\Delta\alpha \sim 4.5 \times 10^{-35}\right)$ geometric phase shift, which makes it technically impossible to register GW signals. Also has been shown that it is impossible to detect relic gravitational waves directly using the already created nor prospective WISP detectors. This is because, for the best of them, the minimum necessary amplitude of relic GW for detection is higher than predicted by the model by five orders of magnitude.

Among the considered installations for direct experimental verification of the correctness of the considered modifications of GR, it has been established that only the detector based on gravitational-optical resonance has the necessary sensitivity and is technically feasible (mirror mass is $M \simeq 6.4 \times 10^{-7}$kg, signal averaging time is $T \simeq 1411$s, cavity length is $L \simeq 27.5$m).

**Список литературы/References**


1. Abbott B. P., Abbott R., Abbott T., Abernathy M., Acernese F., Ackley K., Adams C., Adams T., Addesso P., Adhikari R. and others, Observation of gravitational waves from a binary black hole merger, *Physical review letters* **116**(6), 061102, 2016.
2. Gibbons G., Cosmological evolution of the rolling tachyon. *Physics Letters B* 537(1-2), 1–4, 2002.
3. Caldwell R. R., A phantom menace? Cosmological consequences of a dark energy component with super-negative equation of state. *Physics Letters B* 545(1-2), 23–29, 2002.
4. Nojiri S. and Odintsov S. D., Modified non-local-F (R) gravity as the key for the inflation and dark energy. *Physics Letters B* 659(4), 821–826, 2008.
5. Clifton T., Ferreira P. G., Padilla A. and Skordis C., Modified gravity and cosmology. *Physics reports* 513(1-3), 1–189, 2012.
6. Chervon S., Fomin I., Yurov V. and Yurov A. *Scalar Field Cosmology.* Series on the Foundations of Natural Science and Technology. WSP: Singapore, 2019.
7. Gangopadhyay M. R., Myrzakul S., Sami M. and Sharma M. K. Paradigm of warm quintessential inflation and production of relic gravity waves. *Phys. Rev. D* 103 (4), 043505, 2021.
8. Fomin I. V., Chervon S. V., Morozov A. N. and Golyak I. S. Relic gravitational waves in verified inflationary models based on the generalized scalar–tensor gravity. *The European Physical Journal C* 82(7), 642, 2022.
9. Chervon S. V. and Fomin I. V. Reconstruction of Scalar-Torsion Gravity Theories from the Physical Potential of a Scalar Field, *Symmetry* 15 (2), 291, 2023.
10. Fomin I. Gauss–Bonnet term corrections in scalar field cosmology, *Eur. Phys. J. C* 80 (12), 1145, 2020.
11. Manucharyan G. D., Fomin I. V. Corrections to standard inflationary models induced by Gauss - Bonnet scalar. *Space, Time and Fundamental Interactions*, (40) 119—131, 2022.
12. Morozov A. N., Golyak I. S., Fomin I. V. and Chervon S. V. Detectors of high-frequency gravitational waves based on the gravitational-optical resonance. *Space, Time and Fundamental Interactions*(41), 49–61, 2022.
13. Tanin E. H. and Tenkanen T., Gravitational wave constraints on the observable inflation. *Journal of Cosmology and Astroparticle Physics* 2021(01), 053, 2021.
14. LSC, *LIGO Document Control Center Portal*, 2021.
15. Li F.-Y., Tang M.-X. and Shi D.-P. Electromagnetic response of a Gaussian beam to high-frequency relic gravitational waves in quintessential inflationary models. *Physical Review D* 67(10), 104008, 2003.

16. Mitskievich N. V. and Nesterov A. I. Possible gravitational radiation detection using the geometric phase of a light beam. *General Relativity and Gravitation* 27, 361–366, 1995.
17. Zheng H. and Wei L. Experimental system to detect the electromagnetic response of high-frequency gravitational waves. *Physical Review D* 106(10), 104003, 2022.
18. Zheng H., Wei L., Wen H. and Li F. Electromagnetic response of gravitational waves passing through an alternating magnetic field: A scheme to probe high-frequency gravitational waves. *Physical Review D* 98(6), 064028, 2018.
19. Ejlli A., Ejlli D., Cruise A. M., Pisano G. and Grote H. Upper limits on the amplitude of ultra-high-frequency gravitational waves from graviton to photon conversion. *The European Physical Journal C* 79(12), 1032, 2019.
20. Ehret K., et. al. New ALPS results on hidden-sector lightweights, *Physics Letters B* 689(4-5), 149–155, 2010.
21. Ballou R., et. al. New exclusion limits on scalar and pseudoscalar axionlike particles from light shining through a wall, *Physical Review D* **92**(9), 092002, 2015.
22. Anastassopoulos V., et. al. New CAST limit on the axion-photon interaction, *arXiv preprint arXiv:1705.02290*, 2017.
23. Bähre R., et. al. Any light particle search II—technical design report, *Journal of Instrumentation* 8(09), T09001, 2013.
24. Beacham J., et. al. Physics beyond colliders at CERN: beyond the standard model working group report, *Journal of Physics G: Nuclear and Particle Physics* 47(1), 010501, 2019.
25. Armengaud E., et. al. Conceptual design of the international axion observatory (IAXO), *Journal of Instrumentation* 9(05), T05002, 2014.
26. Ehret K., et. al. Resonant laser power build-up in ALPS—A “light shining through a wall” experiment, *Nuclear Instruments and Methods in Physics Research Section A: Accelerators, Spectrometers, Detectors and Associated Equipment* 612(1), 83–96, 2009.
27. Pugnat P., et. al. Search for weakly interacting sub-eV particles with the OSQAR laser-based experiment: results and perspectives, *The European Physical Journal C* 74, 1–7, 2014.
28. Garza J. G., *Micromegas for the search of solar axions in CAST and low-mass WIMPs in TREX-DM.* PhD thesis. Universidad de Zaragoza, 2016.
29. Rudenko V. N. and Sazhin M. V. Laser interferometer as a gravitational wave detector, *Soviet Journal of Quantum Electronics* 10(11), 1366, 1980.
30. Golyak I., Morozov A., Nazolin A., Tabalin S., Esakov A. and Fomin I. Information - Measuring Complex to Detect High Frequency Gravitational Waves. *Radio Engineering* 2, 13–23, 2021.

**Авторы**

**Манучарян Геворг Дереникович**, ассистент кафедры “Физика”, Московский государственный технический университет им. Н.Э. Баумана, ул. 2-я Бауманская, д. 5, с. 1, г. Москва, 105005, Россия. Инженер, ГАИШ МГУ, Университетский пр., 13, Москва, 119992, Россия.
E-mail: gevorgbek.manucharyan@gmail.com

**Фомин Игорь Владимирович**, д.ф.-м.н., профессор кафрдры “Физика”, Московский государственный технический университет им. Н.Э. Баумана, ул. 2-я Бауманская, д. 5, с. 1, г. Москва, 105005, Россия.
E-mail: ingvor@inbox.ru

**Гладышев Владимир Олегович**, д.ф.-м.н., декан факультета “Фундаментальные науки”, профессор кафедры “Физика”, Московский государственный технический университет им. Н.Э. Баумана, ул. 2-я Бауманская, д. 5, с. 1, г. Москва, 105005, Россия.
E-mail: vgladyshev@mail.ru

**Литвинов Дмитрий Александрович**, к.ф.-м.н., научный сотрудник, лаборатория “Астрофизика высокого разрешения”, Астрокосмический центр Физического института им. П.Н. Лебедева РАН, Профсоюзная 84/32, г. Москва, 117997, Россия.
E-mail: litvirq@gmail.com

**Просьба ссылаться на эту статью следующим образом:**
Манучарян Г. Д., Фомин И. В., Гладышев В. О., Литвинов Д. А. О детектировании высокочастотных реликтовых гравитационных волн. *Пространство, время и фундаментальные взаимодействия.* 2023. № 3-4. С. 188–198.

**Authors**
**Manucharyan Gevorg Derenikovich**, assistant of Physics department, Bauman Moscow State Technical University, 2nd Baumanskaya st., 5c1, Moscow, 105005, Russia.
E-mail: gevorgbek.manucharyan@gmail.com

**Fomin Igor Vladimirovich**, Ph.D., Professor of Physics department, Bauman Moscow State Technical University, 2nd Baumanskaya st., 5c1, Moscow, 105005, Russia.
E-mail: ingvor@inbox.ru

**Gladyshev Vladimir Olegovich**, Ph.D.,Head of the Fundamental Sciences faculty, Professor of Physics department, Bauman Moscow State Technical University, 2nd Baumanskaya st., 5c1, Moscow, 105005, Russia.
E-mail: vgladyshev@mail.ru

**Dmitry Alexandrovich Litvinov**, Ph.D., Researcher of the laboratory for High-Resolution Astrophysics, Astro Space Center, Lebedev Physical Institute, Profsoyuznaya 84/32, 117997, Moscow, Russia
E-mail: litvirq@gmail.com

**Please cite this article in English as:**
Manucharyan G. D., Fomin I. V., Gladyshev V. O., Litvinov D. A. On the detection of high-frequency relic gravitational waves. *Space, Time and Fundamental Interactions*, 2023, no. 3-4, pp. 188–198.

УДК 530.12



## ДВИЖЕНИЕ В ГРАВИТАЦИОННОМ ПОЛЕ ЧЁРНОЙ ДЫРЫ В СИНХРОННОЙ СИСТЕМЕ КООРДИНАТ

Мейерович Б. Э. [a,1]

[a] Институт физических проблем имени П. Л. Капицы, г. Москва, 119334, Россия.

Рассматривается движение пробного тела, или частицы, в гравитационном поле чёрной дыры, граничащей с тёмной материей. Статическое гравитационное поле предельно сжатой материи определяется путем решения уравнений Эйнштейна и Клейна-Гордона в синхронной системе координат. Предельно сжатое состояние материи в виде конденсата квантовой Бозе-жидкости энергетически более выгодно, чем вырожденный ферми-газ. Важным отличием от черных дыр Шварцшильда и Керра является отсутствие сингулярности в центре. В регулярном гравитационном поле, в зависимости от прицельного параметра, существуют траектории, ведущие сквозь "горизонт событий"внутрь чёрной дыры, а не только пролетающие мимо. При нулевой температуре в зависимости от парного взаимодействия бозонов, конденсат состоит из компонентов сверхтекучей и обычной (не сверхтекучей) квантовой жидкости. Задача о движении пробного тела внутри черной дыры решается аналитически в предельном случае, когда на фоне доминирующей гравитации, трением о не сверхтекучую компоненту Бозе-конденсата можно пренебречь.

*Ключевые слова*: Чёрная дыра, тёмная материя, синхронные координаты.

## MOTION IN THE GRAVITATIONAL FIELD OF A BLACK HOLE IN A SYNCHRONOUS COORDINATE SYSTEM

Meierovich B. E. [a,1]

[a] P. L. Kapitza Institute for Physical Problems, Moscow, 119334, Russia.

Motion of a test body, or a particle, in the gravitational field of a black hole bordering dark matter is considered. The static gravitational field of extremely compressed matter is determined by solving the Einstein and Klein-Gordon equations in the synchronous coordinate system. An extremely compressed state of matter in the form of a condensate of a quantum Bose liquid is energetically more favorable than a degenerate Fermi gas. An important difference from the Schwarzschild and Kerr black holes is the absence of a singularity in the center. In a regular gravitational field, depending on the impact parameter, there are trajectories leading through the “event horizon” into the black hole, and not just passing by. At zero temperature, depending on the pair interaction of bosons, the condensate consists of components of a superfluid and an ordinary (non-superfluid) quantum liquid. The problem of the motion of a test body inside a black hole is solved analytically in the limiting case when, against the background of dominant gravity, friction with the non-superfluid component of the Bose condensate can be neglected.

*Keywords*: Black hole, dark matter, synchronous coordinates.

PACS: 04.30, 98.62, 95.36

DOI: 10.17238/issn2226-8812.2023.3-4.199-210

### Introduction

In a synchronous coordinate system, a static regular solution to the system of Einstein and Klein-Gordon equations for the gravitational field of extremely compressed matter was found [1]. A maximally compressed black hole bordering dark matter claims to be the state that the gravitational collapse can lead to. [2].

In a synchronous reference frame ([3], §97) a spherically symmetric static metric

$$ds^2 = \left(dx^0\right)^2 - e^{2F_1\left(x^1\right)}\left(dx^1\right)^2 - e^{2F_2\left(x^1\right)}\left(d\theta^2 + \sin^2\theta\, d\varphi^2\right) \tag{0.1}$$

[1] E-mail: meierovich@mail.ru

contains two functions $F_1\left(x^1\right)$ and $F_2\left(x^1\right)$, depending on one coordinate $x^1$. Substitution

$$dr = e^{F_1\left(x^1\right)}dx^1, \quad r\left(x^1\right) = \int^{x^1} e^{F_1\left(x^1\right)}dx^1, \quad F_2\left(x^1\right) = F_2\left(r\left(x^1\right)\right) \tag{0.2}$$

changes (1) to the metric

$$ds^2 = c^2dt^2 - dr^2 + g_{22}\left(r\right)\left(d\theta^2 + \sin^2\theta\, d\varphi^2\right), \quad g_{22}\left(r\right) = -e^{2F_2(r)}. \tag{0.3}$$

containing only one metric function $F_2\left(r\right)$. It simplifies the solution to the system of Einstein and Klein-Gordon equations. In this case, the solution turns out to be more general, since it is valid for an arbitrary function $F_1(x^1)$ [1]. Unlike the Schwarzschild metric [4], the synchronous coordinate $r$ is the real distance from the center.

In synchronous coordinates, as well as in Schwarzschild coordinates, in the equilibrium state of the extremely compressed Bose condensate, there are two gravitational radii $r_g$ and $r_h$, on which the conditions of the “Existence and Uniqueness Theorem” ([5], §3) are not satisfied. There is a difference between these two coordinate systems. In the Schwarzschild coordinates ([3] formula (100.14)) the metric component $g^{11}\left(r\right) = 0$ at $r = r_g$ and $r = r_h$, so that in the interval $r_g < r < r_h$ the signature of the metric tensor is violated. And in the synchronous coordinate system (3) $g_{11}\left(r\right) = -1$ does not vanish anywhere. The metric signature does not change. In synchronous coordinates, the Einstein and Klein-Gordon equations are reduced to a second order system (and not to the fourth order as in the Schwarzschild ones). Taking into account the elasticity of the condensate in the $\lambda\psi^4$ model, the metric component $g_{22}\left(r\right)$ in (3) is derived analytically (formula (36) in [1]).

Considering the structure of the static equilibrium state of a supermassive black hole, it is natural to use the fact that gravity dominates over all other types of interactions. At the same time, today we have no reason to believe that a strong gravitational field affects the basic quantum properties of particles. That is, regardless of gravity, fermions remain fermions, and bosons remain bosons. It would seem that with dominant gravity, an ensemble of particles of a gravitating object can be considered a quantum ideal gas. However, without taking elasticity into account, the wave function of the Bose condensate diverges logarithmically at the center [2]. The singularity disappears due to the presence of arbitrarily weak repulsion of colliding particles [6].

## 1. Black hole and dark matter in synchronous coordinates

In a synchronous reference frame, a static solution to the Einstein and Klein-Gordon equations exists if matter is compressed by its own gravitational field to the ultrarelativistic limit $p = -\varepsilon/3$. The pressure $p$ turns out to be negative because gravitational forces are aimed to compress the Bose condensate, and not to expand it. The equation defining the metric component $g_{22}\left(r\right) = -e^{2F_2(r)}$ is reduced to the form (formula (22) in [1]):

$$\frac{de^{F_2(r)}}{dr} = \sqrt{1 - \kappa\left|p\right|\left(e^{F_2(r)}\right)^2}. \tag{1.1}$$

Here $\kappa = \left(8\pi/c^4\right)k, \quad k = 6.67\times10^{-8}\,cm^3/\left(g\cdot\sec^2\right)$ – gravitational constant. The regular at the center solution to equation (4) is

$$g_{22}\left(r\right) = -e^{2F_2(r)} = -\frac{1}{\kappa\left|p\right|}\sin^2\left(\sqrt{\kappa\left|p\right|}r\right). \tag{1.2}$$

Solution (5) is unique only inside the sphere $0 < r < r_g$.

$$r_g = \frac{\pi}{2\sqrt{\kappa\left|p\right|}} \tag{1.3}$$

is the inner gravitational radius. At $r = r_g$ metric component

$$g_{22}\left(r_g\right) = -1/\kappa\left|p\right|. \tag{1.4}$$

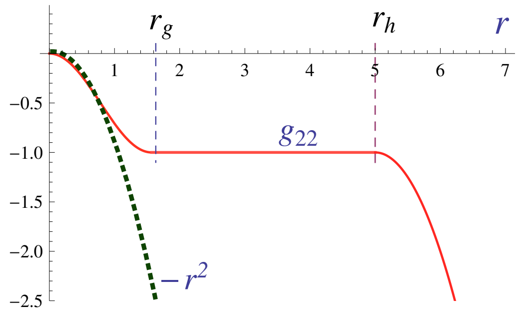


**Рис. 1.** Red line is metric component (1.7)

In the region $r > r_g$, the solution (5) to equation (4) with the boundary condition (7) is not unique [5]. The constant

$$g_{22}\left(r\right) = -\frac{1}{\kappa\left|p\right|} = -\left(\frac{2}{\pi}r_g\right)^2, \; r \geq r_g \tag{1.5}$$

is also a solution to equation (4) with the boundary condition (7). In a spherical volume of radius $r_h$, the mass of the condensate $M = \frac{3c^2}{2k}r_h$ in the solution (1.5) is bigger than the mass in the solution (5) [1].

The sphere $r = r_h$ is the boundary of a black hole with dark matter. The gravitational properties of dark matter are adequately described using a longitudinal vector field [7]. The covariant divergence of the longitudinal vector field is a scalar that satisfies the same Klein-Gordon equation as the scalar wave function of the Bose condensate ([8] §30). However, the rest mass of a dark matter quantum can be many orders of magnitude less than the rest mass of Standard Model bosons. Using the condition of continuity of the function $F_2\left(r\right)$ and its derivative at the interface $r = r_h$, a solution to the system of Einstein and Klein-Gordon equations was found. It determines the component $g_{22}\left(r\right)$ of the metric tensor outside the black hole [1]:

$$g_{22}\left(r\right) = -\left(\frac{2}{\pi}r_g\right)^2 - \left(r - r_h\right)^2, \quad r > r_h. \tag{1.6}$$

In synchronous coordinates, in the $\lambda\psi^4$ model, the metric component $g_{22}\left(r\right)$ of the regular static gravitational field of interdependent black hole and dark matter is:

$$g_{22}\left(r\right) = \begin{cases} -\frac{4}{\pi^2}r_g^2\sin^2\left(\frac{\pi}{2}\frac{r}{r_g}\right), & r < r_g, \\ -\frac{4}{\pi^2}r_g^2, & r_g \leq r \leq r_h, \\ -\frac{4}{\pi^2}r_g^2 - \left(r - r_h\right)^2, & r_h < r. \end{cases} \tag{1.7}$$

$g_{22}\left(r\right)$ is determined by two parameters – gravitational radii $r_g$ and $r_h$. The graph of function $g_{22}\left(r\right)$ is the red line in Figure 1 [1]. The dotted line is $g_{22}\left(r\right) = -r^2$ in Schwarzschild coordinates.

The parameters $r_g = 1$ and $r_h = 5$ were chosen for clarity. In reality $r_h$ can be many orders of magnitude greater than $r_g$.

Wave function of dark matter

$$\phi^r\left(r\right) = \frac{2}{\pi}\frac{\bar{\lambda}r_g}{\sqrt{\kappa}}\left[\left(\frac{2r_g}{\pi}\right)^2 + \left(r - r_h\right)^2\right]^{-1}, \quad r \geq r_h \tag{1.8}$$

decreases rapidly with distance from the black hole [1].

Below in this article I consider the motion of a test body, or a particle, in the gravitational field with metric (3), where the component $g_{22}\left(r\right)$ (1.7) is presented in Figure 1.

## 2. Test body in the gravitational field of a black hole and dark matter

### 2.1. General approach to a trajectory in synchronous coordinates

Consider the motion of a particle with mass $m$ in a gravitational field in the synchronous reference frame (3). Let us choose the orientation of the metric so that the trajectory and the center are in the plane $\theta = \pi/2$. In a static spherically symmetric gravitational field $x^0 = ct$ and $\varphi$ are cyclic coordinates. Accordingly, the associated energy $E$ and angular moment $M$ of a moving body are integrals of motion. The action $S(t, r, \varphi)$ satisfies the Hamilton-Jacobi equation (formula (9.19) in [3])

$$g^{ik}\left(\frac{\partial S}{\partial x^i}\frac{\partial S}{\partial x^k}\right) - m^2c^2 = 0$$

and allows separation of variables:

$$S(t, r, \varphi) = -\frac{E}{c}x^0 + M\varphi + S_r(r).$$

Metric (3) in the plane $\theta = \pi/2$

$$ds^2 = c^2dt^2 - dr^2 + g_{22}(r)\,d\varphi^2.$$

From the Hamilton-Jacobi equation

$$\frac{E^2}{c^2} - \left(\frac{\partial S_r}{\partial r}\right)^2 + \frac{M^2}{g_{22}(r)} - m^2c^2 = 0$$

we get the action

$$S(t, r, \varphi) = -Et + M\varphi \pm \int\sqrt{\frac{E^2}{c^2} - m^2c^2 + \frac{M^2}{g_{22}(r)}}dr. \tag{2.1}$$

The partial derivative of action (2.1) with respect to the angular moment $M$ determines the trajectory of motion in polar coordinates $r, \varphi$:

$$\frac{\partial S}{\partial M} = \varphi \pm M\int\frac{dr}{g_{22}(r)\sqrt{\frac{E^2}{c^2} - m^2c^2 + \frac{M^2}{g_{22}(r)}}} = const. \tag{2.2}$$

By differentiating (2.1) with respect to energy $E$

$$\frac{\partial S}{\partial E} = -t \pm \frac{E}{c^2}\int\frac{dr}{\sqrt{\frac{E^2}{c^2} - m^2c^2 + \frac{M^2}{g_{22}(r)}}} = const \tag{2.3}$$

the dependence of the radius on time $r(t)$ is determined.

The dark matter wave function (1.8) rapidly decreases with distance from the center. Far from the black hole, the trajectory of a test particle is a straight line on the plane. At infinity, the distance $\rho$ between the trajectory and the parallel straight line passing through the center is called the impact parameter. The impact parameter (impact factor) $\rho$ is a constant connecting the conserved angular momentum $M$ and energy $E$ with the momentum $P$ of the test body far from the black hole:

$$M = P\rho, \quad \frac{E^2}{c^2} - m^2c^2 = P^2, \quad \frac{E}{P} = \frac{c^2}{v}. \tag{2.4}$$

$v$ is the speed of a test body along the trajectory. Taking into account (1.7) and (2.4), trajectory (2.2) is determined by three parameters of length dimension $-$ gravitational radii $r_g, r_h$, and impact parameter $\rho$:

$$\varphi(r) \pm \rho\int\frac{dr}{\sqrt{g_{22}(r)\left(g_{22}(r) + \rho^2\right)}} = const. \tag{2.5}$$

The trajectory does not depend on the speed $v$ of the test body. The distance to the center as a function of time (2.3) depends on the speed $v$:

$$t(r) \pm \frac{1}{v}\int\frac{\sqrt{g_{22}(r)}dr}{\sqrt{g_{22}(r) + \rho^2}} = const. \tag{2.6}$$

### 2.2. Trajectory outside a black hole

Outside a black hole, the test body moves through dark matter. To date, no direct interaction between ordinary matter and dark matter has been detected. We observe manifestations of dark matter only due to gravity. The test body outside the black hole moves in the common gravitational field of the black hole and dark matter.

According to (1.7), $g_{22}(r) = -\left(\left(\frac{2}{\pi}r_g\right)^2 + (r-r_h)^2\right)$ at $r > r_h$. The trajectory of the test body (2.5) outside the black hole

$$\varphi(r) = \pm\rho\int\frac{dr}{\sqrt{\left(\left(\frac{2}{\pi}r_g\right)^2 + (r-r_h)^2\right)\left(\left(\frac{2}{\pi}r_g\right)^2 + (r-r_h)^2 - \rho^2\right)}} + const, \quad r > r_h. \tag{2.7}$$

Outside the black hole $r > r_h$ the bracket $\left(\left(\frac{2}{\pi}r_g\right)^2 + (r-r_h)^2 - \rho^2\right)$ under the root vanishes at $r = r_{\min}$,

$$r_{\min} = r_h + \sqrt{\rho^2 - \left(\frac{2}{\pi}r_g\right)^2} = r_h + \rho\sqrt{1-a^2}. \tag{2.8}$$

Here the dimensionless parameter

$$a = \frac{2r_g}{\pi\,\rho}. \tag{2.9}$$

The point on the trajectory closest to the center (turning point) (2.8), where the movement towards the center changes to the movement away from the center, exists provided that $a \le 1$. That is, the ratio of the impact parameter $\rho$ to the internal gravitational radius $r_g$

$$\frac{\rho}{r_g} \ge \frac{2}{\pi} = 0.63662 \tag{2.10}$$

The trajectory of a test body does not touch the black hole under the condition $a < 1$.

The integral in (2.7) reduces to an elliptic integral of the first kind ([9], p. 918):

$$F(\xi, k) = \int_0^{\xi}\frac{d\alpha}{\sqrt{1-k^2\sin^2\alpha}} = \int_0^{\sin\xi}\frac{dx}{\sqrt{(1-x^2)(1-k^2x^2)}}.$$

Namely, to the formula 3.152 6 on page 260 in [9]:

$$\int_b^u\frac{dx}{\sqrt{(x^2+a^2)(x^2-b^2)}} = \frac{F(\xi, s)}{\sqrt{a^2+b^2}}, \quad \xi = \arcsin\sqrt{(a^2+b^2)(a^2+u^2)}, \quad s = \frac{a}{\sqrt{a^2+b^2}}.$$

Outside the black hole, the trajectory is given by the formula:

$$\varphi(r) = \pm F\left(\arcsin\left[\rho\left(\left(\frac{2}{\pi}r_g\right)^2 + (r-r_h)^2\right)^{-1/2}\right], \frac{2r_g}{\pi\rho}\right) + const, \quad r > r_h. \tag{2.11}$$

However, it is easier to present a graph of the trajectory $r(\varphi)$ based on the equation

$$\frac{dr}{d\varphi} = \pm\frac{1}{\rho}\sqrt{\left[\left(\frac{2}{\pi}r_g\right)^2 + (r-r_h)^2\right]\left[\left(\frac{2}{\pi}r_g\right)^2 + (r-r_h)^2 - \rho^2\right]}, \quad r > r_h. \tag{2.12}$$

One can see that equation (2.12) is satisfied by an independent of $\varphi$ constant $r(\varphi) = r_{\min}$ (2.8). It means that a circle with the radius $r_{\min}$ is a trajectory of the test body. I draw your attention to the fact that one would not immediately notice how the trajectory $r(\varphi) = r_{\min}$ is contained in formula (2.11). According to the existence and uniqueness theorem ([5], §3), this solution to equation (2.12) with a boundary condition $r(\varphi_0) = r_{\min}$ exists, but it is not unique even for an arbitrary $\varphi_0$. It is natural to look for other solutions to equation (2.12) with the same boundary condition $r(\varphi_0) = r_{\min}$ in the form

$$r(\varphi_0 + \delta\varphi) = r_{\min} + \gamma(\delta\varphi)^p \tag{2.13}$$

with a small $\delta\varphi$ different from zero. In the linear approximation, function (2.13) satisfies equation (2.12) if $p = 2$ and

$$\gamma\left(\gamma - \frac{1}{2}\sqrt{\rho^2 - \left(\frac{2}{\pi}r_g\right)^2}\right) = 0. \tag{2.14}$$

Solution with $\gamma = 0$ is the circle of radius $r_{\min}$: $r(\varphi) = r_{\min}$. A solution, different from this circle, is obtained by numerical integration of equation (2.12) with the boundary condition

$$r(\varphi_0 + \delta\varphi) = r_{\min} + \frac{1}{2}\sqrt{\rho^2 - \left(\frac{2}{\pi}r_g\right)^2}(\delta\varphi)^2, \quad \delta\varphi << 1. \tag{2.15}$$

It is convenient to choose the origin of the angular coordinate $\varphi = 0$ so that the turning point, where both solutions coincide, lies on the horizontal axis at the distance (2.8) from the center.

The expression under the radical (2.15) must be positive. If the ratio $\rho/r_g$ is large, then the trajectory does not differ much from a straight line. In Figure 2a, the red circle is the boundary of the black hole with dark matter. Ratio $r_h/r_g = 10$. The blue circle is a trivial solution $r(\varphi) = r_{\min}$. The blue line tangent to the blue circle is the numerical solution to equation (2.12) with boundary condition (2.15). Ratio $\rho/r_g = 5$. With the decrease of $\rho/r_g$, both solutions approach the surface of the black hole. In Figure 2b $r_h/r_g = 10$, $\rho/r_g = 1$. As it approaches the lower boundary (2.10), the trajectory envelops the black hole. In Figure 2c $\rho/r_g = 0.651$. But this is not the limit. In the limit $\rho/r_g \to 2/\pi = 0.63662$ (2.10) the trajectory is completely wound around the black hole. At $\rho/r_g = 2/\pi$ both solutions merge into one circle on the surface of the black hole.

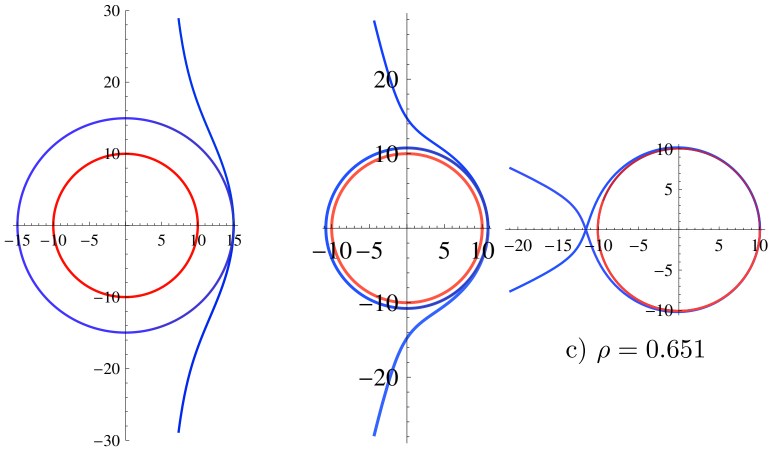


a) $\rho = 5$ b)$\rho = 1$ c) $\rho = 0.651$

Fig. 2. Trajectories with parameters $\frac{\rho}{r_g} \geq \frac{2}{\pi}$, $r_g = 1$, $r_h = 10$

In reality, the internal gravitational radius $r_g$ of a black hole can be many orders of magnitude smaller than the surface radius $r_h$. The presence of an internal gravitational radius $r_g$, no matter how small it may be, qualitatively changes the picture of motion of test bodies in the gravitational field of a black hole. If we put $r_g = 0$ in formulas (2.11) and (2.12), we get

$$\varphi(r) = \pm\arctan\sqrt{\frac{(r - r_h)^2}{\rho^2} - 1},$$

whence

$$r(\varphi) = r_h + \frac{\rho}{|\cos\varphi|}, \quad r > r_h. \tag{2.16}$$

For $r_g = 0$ and finite values $r_h > 0$, $\rho > 0$ we exclude the range of parameters $\rho/r_g \leq 2/\pi = 0.63662$ from consideration. The range of applicability for formula (2.16) is not only $r_g << r_h$, but also $r_g << \rho$.

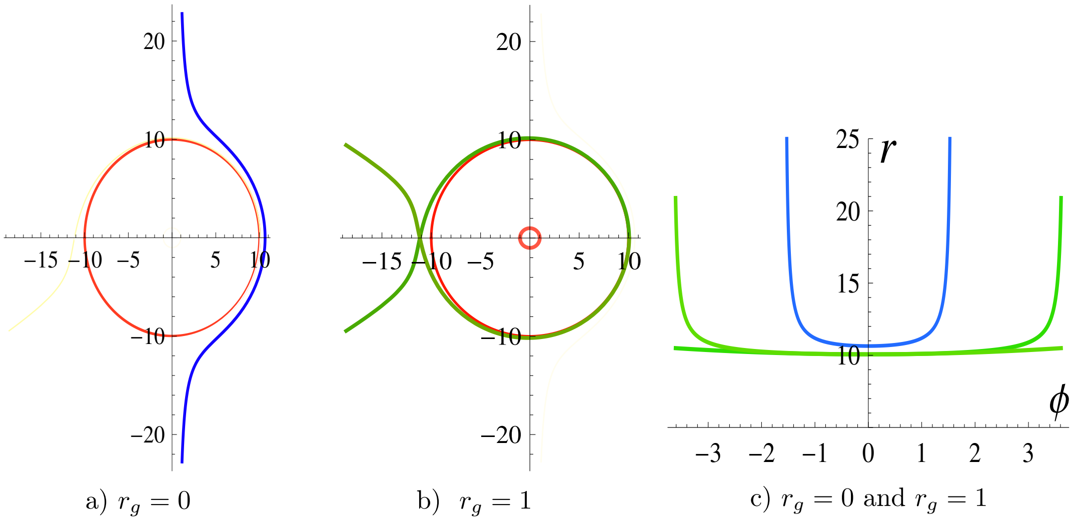


Fig. 3 The trajectories with $r_g = 0$ (blue lines) and $r_g = 1$ (green lines) . $r_h = 10$, $\rho = 0.64$

The trajectory with parameters $r_g = 0, r_h = 10, \rho = 0.64$ is presented in Figure 3a. For the same parameters $r_h = 10, \rho = 0.64$, but $r_g = 1$ the trajectory is shown in Figure 3b. For comparison, trajectories with $r_g = 0$ (blue curve) and $r_g = 1$ (green curve) are combined on a single graph in Figure 3c in Cartesian coordinates.

When $r_g = 0$ it follows from equation (2.12) that for any values $r_h > 0$ and $\rho > 0$ there is a turning point (2.8)

$$r_{\min} = r_h + \rho, \quad r_g = 0,$$

located outside a black hole. It means that at $r_g = 0$ there is no path along which anything could get inside a black hole. A "point-like" Schwarzschild's black hole (with a singularity at the center) [4] has only one gravitational radius $r_h$. For this reason, the surface radius $r_h$ of a Schwarzschild black hole was considered to be an event horizon.

### 2.3. About the trajectory inside a black hole

Regularity at the center of a black hole without mass limitation occurs in the presence of an internal gravitational radius $r_g$ [6]. When $r_g > 0$ the point closest to the center on the trajectory outside a black hole (2.8) exists if the parameter $a < 1$ (2.9). In this case, the impact parameter (impact factor) $\rho > \frac{2}{\pi} r_g$ (2.10). For $a > 1$, the impact factor is $\rho < \frac{2}{\pi} r_g$, and the bracket $\left(\left(\frac{2}{\pi} r_g\right)^2 + (r - r_h)^2 - \rho^2\right)$ in the denominator (2.7) does not vanish outside the black hole. Therefore, there is no turning point outside the black hole, if $\rho < \frac{2}{\pi} r_g$. Naturally, trajectories with an impact parameter $\rho < \frac{2}{\pi} r_g$ inevitably lead inside the sphere $r = r_h$. In principle, this fact opens up the possibility of studying not only the surface, but also the internal physical properties of black holes.

The fate of a test particle inside a black hole is more complicated than outside. Outside a black hole, no interactions, other than the gravitational one, has been observed between ordinary and dark matter. Inside a black hole $r < r_h$, the test particle falls into the Bose condensate of ordinary (not dark) matter. Deriving the metric tensor component (1.7), I took into account that gravity dominates over all other interactions of black hole bosons. Bosons were considered as an extremely compressed ideal Bose gas. At zero temperature, the condensate of extremely compressed bosons can be in the state of a quantum liquid having the property of superfluidity ([8], Chapter 3). In an ideal superfluid liquid, the motion of a test body would occur without dissipation. But in an ideal liquid with no elasticity, the wave function of the condensate diverges logarithmically at the center [2]. Even arbitrarily small elasticity can be sufficient for regularity at the center. But in the presence of elasticity, a condensate is no longer an ideal liquid. Even at absolute zero, a Bose liquid contains both superfluid and normal components. Due to friction with the normal component, the motion of a test particle becomes dissipative. In this article, I consider the motion inside a black hole in the limiting case when the friction with the normal component can be neglected due to the dominating gravity. So, the test body moves with no violation of conservation of energy and angular momentum. I would like to note that the considered limit is the basis, deviations from which contain information about the properties of a black hole.

### 2.4. Motion within the spherical layer $r_g \leq r \leq r_h$

At $\rho < (2/\pi)\, r_g$ the metric component (1.7) in the spherical layer between the gravitational radii

$$g_{22}(r) = -\left(\frac{2}{\pi} r_g\right)^2, \quad r_g < r < r_h$$

does not depend on $r$. There is no turning point in the spherical layer $r_g \leq r \leq r_h$. $\varphi(r)$ (2.5) is a linear function:

$$\varphi(r) = \pm\frac{\pi}{2\sqrt{a^2-1}}\frac{r}{r_g} + \varphi_0, \quad r_g \leq r \leq r_h \tag{2.17}$$

The test particle inevitably falls inside the black hole if the parameter (2.9) $a = \frac{2r_g}{\pi\,\rho} > 1$. Moving from $r = r_g$ to $r = r_h$, the angular variable increases by

$$\varphi(r_h) - \varphi(r_g) = \frac{\pi}{2r_g}\frac{r_h - r_g}{\sqrt{a^2-1}}. \tag{2.18}$$

Trajectory $r(\varphi)$ (2.17)

$$r(\varphi) = \frac{2r_g}{\pi}\sqrt{a^2-1}\,(\varphi - \varphi_0), \quad r_g \leq r \leq r_h \tag{2.19}$$

is the spiral with a step

$$\Delta r = r(\varphi + 2\pi) - r(\varphi) = 4\sqrt{a^2-1}\,r_g. \tag{2.20}$$

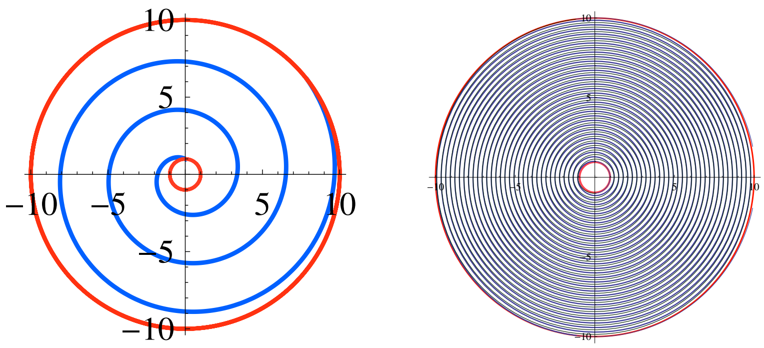


a) $\rho = 0.5$ b) $\rho = 0.635$

Fig. 4. Spirals within the layer $r_g \leq r \leq r_h$. $r_g = 1$, $r_h = 10$

In Figure 4, there are two spiral trajectories within the layer $r_g < r < r_h$ between the red spheres. I chose gravitational radii $r_g = 1$ and $r_h = 10$ for clarity. In Figure 4a impact parameter $\rho = 0.5$. As $\rho$ increases, the helix pitch (2.20) decreases. For comparison, at $\rho = 0.635$ (with $a = 1.00255$ very close to unity), spiral (2.19) with the same gravitational radii $r_g = 1$ and $r_h = 10$ is shown in Figure 4b.

### 2.5. Trajectory within the central area $r < r_g$

If we neglect dissipative processes during the motion of a test body through the Bose condensate of a black hole, then the dependence $\varphi(r)$ in the central area $r < r_g$ is determined by formulas (1.7) and (2.5):

$$\varphi(r) = \pm\frac{1}{a\rho}\int_{r_{\min}}^{r}\frac{dr}{\sin\left(\frac{\pi}{2}\frac{r}{\rho}\right)\sqrt{a^2\sin^2\left(\frac{\pi}{2}\frac{r}{r_g}\right)-1}}, \quad r < r_g. \tag{2.21}$$

Minimum distance $r_{\min}$ from the trajectory to the center

$$r_{\min} = a\rho\arcsin(1/a), \quad r < r_g. \tag{2.22}$$

$a = \frac{2}{\pi}\frac{r_g}{\rho}$ is the same parameter (2.9). For particles falling inside a black hole, $a > 1$.

Integrating (2.21)

$$\varphi(r) = \pm\arctan\sqrt{\frac{a^2-1}{\cos^2\left(\frac{\pi}{2}\frac{r}{r_g}\right)} - a^2}, \quad 0 < r < r_g,$$

we find the trajectory $r(\varphi)$ in the central region:

$$r(\varphi) = \frac{2}{\pi}r_g\arccos\sqrt{\frac{a^2-1}{a^2+\tan^2\varphi}}, \quad 0 < r < r_g. \tag{2.23}$$

With increasing modulus of the angular coordinate $|\varphi|$ from zero to $\pi/2$, function $\tan^2\varphi$ in the denominator (2.23) varies from zero to infinity. The distance from the center $r(\varphi)$ increases from $r = r_{\min}$ (B.74) to $r = r_g$.

Trajectory (2.23) is not unique inside the sphere $r < r_g$. It becomes clear if formula (2.21) is presented in differential form:

$$\frac{dr}{d\varphi} = \pm a\rho\sin\left(\frac{\pi}{2}\frac{r}{r_g}\right)\sqrt{a^2\sin^2\left(\frac{\pi}{2}\frac{r}{r_g}\right)-1}, \quad r < r_g. \tag{2.24}$$

Obviously, the circle with radius $r_{\min}$ (B.74)

$$r(\varphi) = r_{\min} = const \tag{2.25}$$

is also a solution to equation (2.24). Equation (2.24) with the boundary condition $r(0) = r_{\min}$ is satisfied by two solutions (2.23) and (2.25). The blue circle in Figure 5 is the solution (2.25). The blue line connecting the top pole of the red circle to the bottom is the solution (2.23). Ratio $\rho/r_g = 0.5$, $r_g = 1$, radius of the blue circle (2.25) $r_{\min} = 0.57508$.

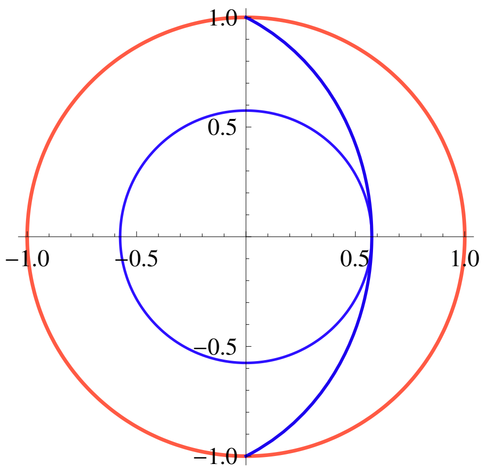


Fig. 5. Trajectories inside $r < r_g$. $r_g = 1$, $\rho = 0.5$.

In Figure 5, the blue line, connecting the upper and lower poles of the red circle, is the trajectory $r(\varphi)$ (2.23) inside a sphere of radius $r_g = 1$. Impact factor $\rho = 0.5$. The blue circle touching the blue line at point $r_{\min}$ (B.74) is also a possible trajectory inside the sphere $r < r_g$.

### 2.6. Time dependence $r(t)$ inside the sphere $r \leq r_g$

I choose the beginning of time at the moment of passing the turning point (B.74) $t\left(r_{\min}\right) = 0$. Equation (2.6) with metric component (1.7)

$$g_{22}\left(r\right) = -\frac{4}{\pi^2} r_g^2 \sin^2\left(\frac{\pi}{2}\frac{r}{r_g}\right), \quad r < r_g$$

and with a boundary condition $t\left(r_{\min}\right) = 0$ has two solutions. First, time-independent rotation in a circle with a constant radius $r_{\min}$. And, secondly, the “schedule” at what time the test body is at the distance $r$ from the center:

$$t\left(r\right) = \mp\frac{r_g}{v}\left[1 - \frac{2}{\pi}\arcsin\left(\sqrt{\frac{a}{a^2-1}}\right)\cos\left(\frac{2}{\pi}\frac{r}{r_g}\right)\right], \; r_{\min} < r < r_g. \tag{2.26}$$

Movement along the trajectory into the sphere $r < r_g$ begins from the gravitational radius $r_g$ (moment $t\left(r_g\right) = -r_g/v$ ), penetrates deep into the turning point $r_{\min}$ (at the moment $t\left(r_{\min}\right) = 0$), and returns back to $r_g$ (at the moment $t\left(r_g\right) = r_g/v$). The minus sign in (2.26) on the way towards the center, and the sign plus on the way back from the region $r < r_g$. The total time inside the sphere $r < r_g$ is $2r_g/v$, regardless of the impact parameter $\rho < (2/\pi)\, r_g$.

### 2.7. Complete trajectory

Trajectory (2.23) smoothly passes from the region $r < r_g$ to the region $r_g < r < r_h$,

$$\varphi\left(r\right) = \pm\frac{\pi}{2}\left(1 - \frac{r - r_g}{r_g\sqrt{a^2-1}}\right), \quad r_g < r < r_h, \tag{2.27}$$

if the constant $\varphi_0 = \pm\frac{\pi}{2}\left(1 - \frac{1}{\sqrt{a^2-1}}\right)$ in (2.17). At the boundary of a black hole and dark matter, the spiral trajectory ends with coordinates $r = r_h, \; \varphi = \varphi\left(r_h\right)$ (C.1). Being a solution to equation (2.12) with the boundary condition $\varphi\left(r_h\right) = \pm\frac{\pi}{2}\left(1 + \frac{r_h - r_g}{r_g\sqrt{a^2-1}}\right)$, the trajectory smoothly continues outside the black hole.

An example of a complete trajectory of a particle in the dominant gravitational field of a black hole and dark matter is presented in Figure 6. $r_g = 1, \; r_h = 10, \; \rho = 0.5$. The paths to and from the center are marked in different colors (blue and green). Spheres with radii $r_g$ and $r_h$ are highlighted in red.

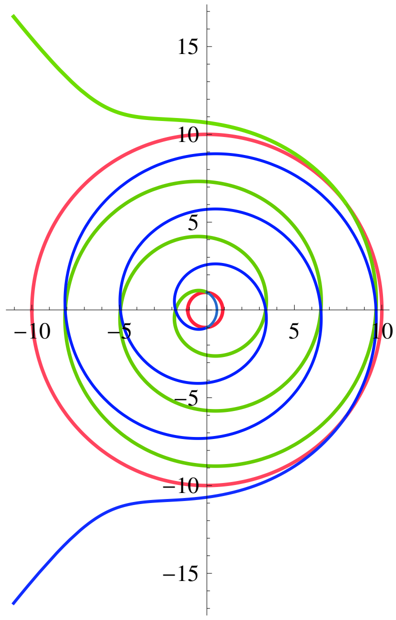


Fig. 6. Example of a complete trajectory. $r_g = 1,\ r_h = 10,\ \rho = 0.5$

The central sphere within the radius $r_g = 1$, magnified by the factor of 10, is shown in the previous Figure 5.

### 3. Real role of gravitational radii

In the Schwarzschild metric [4], a remote observer does not have the opportunity to reach the gravitational radius $r_h$ of a black hole in a finite time. On this basis, for more than a hundred years, there is an opinion that a singularity at the center is inevitable. But nobody cared, because the singularity is located beyond the event horizon $r_h$. In fact, the distance to the gravitational radius $r_h$, infinite in time, is exclusively a property of the Schwarzschild coordinate system. In a synchronous coordinate system, the static gravitational field of a black hole and dark matter does not have a singularity in the center. Regularity in the center occurs due to existence of the internal gravitational radius $r_g < r_h$. The possibility or impossibility of a test body to get inside a black hole depends on the ratio of the impact parameter $\rho$ and the internal gravitational radius $r_g$. At $\rho/r_g > 2/\pi$ the minimum distance of the trajectory to the center (2.8) exceeds the radius $r_h$ of the black hole surface. A test body flies past a black hole. And vice versa: when $\rho/r_g < 2/\pi$ there is no turning point outside a black hole. In this case, a test body inevitably falls inside the black hole, no matter how small the finite radius $r_g > 0$ is.

In the Schwarzschild [4] and Kerr [10] metrics there is a singularity at the center, and there is no internal gravitational radius $r_g$. If $r_g = 0$ and the impact factor $\rho \neq 0$, than the turning point $r_{\min} > r_h$ is located outside the black hole. Moving of a test particle towards the center changes to moving away at $r = r_{\min}$, not reaching the surface of the black hole. In this sense, the gravitational radius $r_h$ of the Schwarzschild and Kerr black holes appears to be an event horizon for a distant observer.

A regular at the center static solution to the system of Einstein and Klein-Gordon equations exists due to the arbitrarily low condensate elasticity [6]. The internal gravitational radius $r_g > 0$ in the regular solution depends on the elasticity of the condensate. In the Schwarzschild coordinate system, gravitational radii are separated by the fact that the component of the metric tensor $g^{rr} = 0$ at $r = r_g$ and $r = r_h$. The same solution in a synchronous coordinate system once again confirms that vanishing $g^{rr}$ at $r = r_g$ and $r = r_h$ is the exclusive property of the Schwarzschild coordinate system. A distinctive property of invariance of gravitational radii $r_g$ and $r_h$ is the fact that in any frame of reference, solutions to the set of Einstein and Klein-Gordon equations with boundary conditions at $r = r_g$ and $r = r_h$ exist, but are not unique.

## Conclusion

In the synchronous coordinate system, the existence of a regular static solution to the system of Einstein and Klein-Gordon equations is confirmed. This solution pretends to describe the extremely compressed state of a black hole surrounded by dark matter, to which gravitational collapse can lead. Moreover, with no limiting mass of a black hole. Unlike the singular in the center Schwarzschild's solution, regular solutions allow trajectories passing through the "event horizon" inside a black hole. Hence, a possibility opens up to study internal properties of black holes.

## Список литературы/References

1. Meierovich B.E. Black Hole and Dark Matter in the Synchronous Coordinate System. *Journal of Experimental and Theoretical* Physics, 2023,Vol. No. 5, pp585-592.
2. Meierovich B.E. Static state of a black hole supported by dark matter. *Universe*, 2019, No. 5, 198.
3. Landau L.D., Lifshitz E.M. *The Classical Theory of Fields.* (*Nauka*, Moscow, 1973) (In Russian).
4. Schwarzschild K. Uberdas Gravitationsfeld eines Massenprunktes nach der Tinsteinschen Theorue. *Sitzungsberichte der Koniglich Ireuischen Academie der Wissenschaften: Berlin, Germany, 1916, pp.189-196.*
5. Pontryagin L.S. *Ordinary Differential Equations.* (Fizmatlit, Moscow, 1961).
6. Meierovich B.E. Guessing the Riddle of a Black Hole. *Universe* 2020, 6, 113.
7. Meierovich. B.E. Galaxy rotation curves driven by massive vector fields. Key to the theory of the dark sector. *Phys. Rev. D* 2013, 87, 103510.
8. Landau L.D., Lifshitz E.M. *Statistical Physics Part 2.* (Fizmatlit, Moscow, 2000).
9. Gradshtein I.S., Ryzik I.M. *Tables of integrals, summs, etc...* (Fizmatlit, Moscow, 1963).
10. Kerr R.P. Gravitational field of a spinning mass as an example of an algebraically special matrics. *Phys. Rev. Lett*, 1963. 11, 237-238.

## Авторы

**Мейерович Борис Эдуардович**, д.ф.-м.н., в.н.с, Институт физических проблем имени П. Л. Капицы, ул. Косыгина, д. 2, г. Москва, 119334, Россия
E-mail: meierovich@mail.ru

## Просьба ссылаться на эту статью следующим образом:

Мейерович Б. Э. Движение в гравитационном поле чёрной дыры в синхронной системе координат. *Пространство, время и фундаментальные взаимодействия.* 2023. № 3-4. С. 199–210.

## Authors

**Meierovich Boris Eduardovich**, D.Sc., Advanced Research Fellow, P. L. Kapitza Institute for Physical Problems, Kosygina Str., 2, Moscow, 119334, Russia.
E-mail: meierovich@mail.ru

## Please cite this article in English as:

Meierovich B. E. Motion in the gravitational field of a black hole in a synchronous coordinate system. *Space, Time and Fundamental Interactions*, 2023, no. 3-4, pp. 199–210.

УДК 539.12.01



## НЕВОЗМОЖНОСТЬ СУЩЕСТВОВАНИЯ МАЙОРАНОВСКИХ СПИНОРОВ КАК ФИЗИЧЕСКИХ ЧАСТИЦ

Монахов В. В.[a,1]

[a] Санкт-Петербургский государственный университет, г. Санкт-Петербург, 198504, Россия.

Майорановские спиноры играют важную роль в современных физических теориях. Большинство механизмов генерации массы нейтрино основаны на наличии майорановского массового члена в лагранжиане. В частности, механизм "качелей" генерации массы нейтрино. Майорановские решения уравнения Дирака существуют. Однако мы доказали, что массовый член лагранжиана майорановского спинора равен нулю. Мы доказали, что майорановские решения имеют нулевую энергию и импульс как в массивном, так и в безмассовом случае. Это означает, что майорановские спиноры не могут соответствовать физически существующим частицам.

*Ключевые слова*: масса нейтрино; майорановские спиноры; майорановские фермионы; майорановская масса.

## THE IMPOSSIBILITY OF THE EXISTENCE OF MAJORANA SPINORS AS PHYSICAL PARTICLES

Monakhov V. V.[a,1]

[a] Saint Petersburg State University, Saint Petersburg, 198504, Russia.

Majorana spinors play an important role in modern physical theories. Most of the neutrino mass generation mechanisms are based on the presence of the Majorana mass term in the Lagrangian. In particular, the seesaw mechanism of neutrino mass generation. Majorana solutions of the Dirac equation exist. However, we have proven that Majorana spinor mass term of the Lagrangian is equal to zero. We have proven that Majorana solutions have zero energy and momentum for both the massive and massless cases. This means that Majorana spinors cannot correspond to physically existing particles.

*Keywords*: neutrino mass; Majorana spinors; Majorana fermions; Majorana mass.

PACS: 03.70.+k, 11.30.Er, 12.60.?i

DOI: 10.17238/issn2226-8812.2023.3-4.211-217

### Introduction

Majorana spinors [1] play an important role in modern physical theories. Most of the neutrino mass generation mechanisms are based on the presence of the Majorana mass term in the Lagrangian. In particular, the seesaw mechanism of neutrino mass generation is a leading candidate for explaining the smallness of the neutrino mass [2]. This mechanism is based on the assumption of the existence of two types of neutrinos with a common mass matrix. When such a matrix is diagonalized, light and heavy neutrinos with Majorana masses appear.

Majorana solutions of the Dirac equation certainly exist. However, we have proven that for the Majorana spinor the mass term of the Lagrangian is equal to zero not only in the so-called c-theory [3], but also in the q-theory (second quantization theory) [4]. Therefore, there was a need to carefully study the properties of Majorana spinors in quantum field theory.

[1] E-mail: v.v.monahov@spbu.ru

## 1. CHARGE CONJUGATION OPERATION AND MAJORANA SPINORS

A Majorana spinor is a charge-self-conjugate (or charge-anti-self-conjugate) solution of the Dirac equation

$$\gamma^\mu i\partial_\mu \Psi = m\Psi \tag{1.1}$$

Such solutions were found by Majorana [1].

Dirac spinor $\Psi_D$ is a superposition of charge-self-conjugate and charge-anti-self-conjugate Majorana spinors $\Psi_{M1}$ and $i\Psi_{M2}$

$$\Psi_D = \frac{1}{\sqrt{2}}(\Psi_{M1} + i\Psi_{M2}) \tag{1.2}$$

In the Majorana representation of Dirac gamma matrices $\gamma^\mu$ , the charge conjugation operator $(\cdot)^c$ is the same as the complex conjugation operator $(\cdot)^*$ , the gamma matrices are purely imaginary, and Majorana spinors $\Psi_{M1}$ and $\Psi_{M2}$ are real with respect to complex conjugation [1]

$$\begin{aligned} &(\cdot)^c = (\cdot)^*\,, \\ &\Psi^*_{M1} = \Psi_{M1}\,, \\ &\Psi^*_{M2} = \Psi_{M2}\,. \end{aligned} \tag{1.3}$$

In the Weyl (chiral) representation, the charge conjugation operation [5]

$$\begin{aligned} &(\cdot)^c = \eta_1\gamma^2(\cdot)^*\,, \\ &\Psi^c = (\cdot)^c\Psi = \eta_1\gamma^2\Psi^c \end{aligned} \tag{1.4}$$

in addition to complex conjugation, requires multiplication by $\eta_1\gamma^2$, where $\eta_1$ is an arbitrary phase factor. Usually it is considered equal to $i$ [3], [6]. In what follows, we will assume that $\eta_1 = i$.

In general case

$$\begin{aligned} \Psi_{M1} &= \frac{1}{\sqrt{2}}(\Psi_D + \Psi^c_D)\,, \\ \Psi_{M2} &= \frac{1}{i\sqrt{2}}(\Psi_D - \Psi^c_D)\,. \end{aligned} \tag{1.5}$$

and

$$\begin{aligned} &\Psi^c_{M1} = \Psi_{M1}\,, \\ &\Psi^c_{M2} = \Psi_{M2}\,. \end{aligned} \tag{1.6}$$

## 2. LAGRANGIAN, HAMILTONIAN AND COMPONENTS OF MAJORANA SPINORS

As already said, we have proven that for the Majorana spinor the mass term of the Lagrangian is equal to zero not only in the so-called c-theory [3], but also in the q-theory (second quantization theory) [4]. Wherein

$$\overline{\Psi}_{M1}\Psi_{M1} = \overline{\Psi}_{M2}\Psi_{M2} = 0\,. \tag{2.1}$$

The non-zero mass term $\mathscr{L}_M$ of the Lagrangian density arises only for the products of the fields of charge-self-conjugate and charge-anti-self-conjugate Majorana spinors, one of which is Dirac-conjugate

$$\mathscr{L}_M = -\frac{m}{2}(\,\overline{\Psi}_{M1} i\Psi_{M2} + (\overline{\Psi}_{M1} i\Psi_{M2})^+\,)\,. \tag{2.2}$$

The result is the Lagrangian density of the field of the Dirac spinor.

Left-chiral Dirac spinor in the Weyl representation can be represented as

$$\phi' = \begin{pmatrix} \phi'_1 \\ \phi'_2 \\ 0 \\ 0 \end{pmatrix} = \begin{pmatrix} \phi' \\ 0 \end{pmatrix}\,, \tag{2.3}$$

where

$$\phi' = \begin{pmatrix} \phi'_1 \\ \phi'_2 \end{pmatrix} . \tag{2.4}$$

From (1.4) and (2.3) it follows [3], [5] that

$$\Psi_{LM} = \frac{1}{\sqrt{2}}(\Psi_L + \eta_1\gamma^2\Psi_L^*) = \frac{1}{\sqrt{2}}\begin{pmatrix} \phi' \\ -\eta_1\sigma_2\phi'^* \end{pmatrix} . \tag{2.5}$$

A similar formula is obtained for the Majorana spinor obtained from the right-chiral Dirac spinor. For $\Psi_{M2}$ , the expression is similar

$$\Psi_{M2} = \frac{1}{i\sqrt{2}}(\Psi_L - \eta_1\gamma^2\Psi_L^*) = \frac{1}{\sqrt{2}}\begin{pmatrix} \phi'/i \\ -\eta_1\sigma_2(\phi'/i)^* \end{pmatrix} = \frac{1}{\sqrt{2}}\begin{pmatrix} \phi'' \\ -\eta_1\sigma_2\phi''^* \end{pmatrix} . \tag{2.6}$$

Thus, the most general expression for the components of the Majorana spinor is

$$\Psi_M = \frac{1}{\sqrt{2}}\begin{pmatrix} \phi \\ -\eta_1\sigma_2\phi^* \end{pmatrix} , \tag{2.7}$$

where

$$\phi = \begin{pmatrix} \phi_1 \\ \phi_2 \end{pmatrix} . \tag{2.8}$$

It is valid for Majorana spinors of both $\Psi_{M1}$ and $\Psi_{M2}$ types.

It follows from formula (2.7) that the two lower components (right-chiral) are expressed in terms of the two upper ones (left-chiral). Therefore, Majorana spinors have two times fewer independent components than Dirac spinors.

Matrix $\sigma_2$ rearranges the components with the spin projection up and down, and the ordering of the creation and annihilation operators for the left-chiral and right-chiral components of the Majorana spinor is the same. Because of this, Majorana spinors cannot have angular momentum projections and can only have helicity. In an implicit form, this was obtained in [5], and we indicate this explicitly. It follows from this that any physical system, which includes a Majorana spinor that does not interact with it, cannot also have a spin projection. Therefore, the Majorana spinor cannot exist as a physical particle.

The Lagrangian density $\mathscr{L}$ of the Majorana spinor $\Psi_M$ is

$$\mathscr{L} = \frac{1}{2}\overline{\Psi}_M\gamma^\mu i\partial_\mu\Psi_M + \frac{1}{2}(\overline{\Psi}_M\gamma^\mu i\partial_\mu\Psi_M)^+ - m\overline{\Psi}_M\Psi_M . \tag{2.9}$$

Corresponding Hamiltonian density $\mathscr{H}$ is

$$\mathscr{H} = \frac{\partial\mathscr{L}}{\partial\dot{\Psi}_M}\dot{\Psi}_M - \mathscr{L} = \frac{\partial\mathscr{L}}{\partial\dot{\Psi}_M}\dot{\Psi}_M = \overline{\Psi}_M\gamma^0 i\partial_0\Psi_M = \Psi_M^+ i\partial_0\Psi_M . \tag{2.10}$$

In the Majorana representation, charge conjugation coincides with complex conjugation. That is why formulas

$$\begin{aligned} (\cdot)^c\Psi_M &= \Psi_M^* = \Psi_M , \\ (\cdot)^c\Psi_M^+ &= (\Psi_M^+)^* = \Psi_M^+ \end{aligned} \tag{2.11}$$

are satisfied in this representation.

From (2.10) and (2.11) it follows that

$$(\cdot)^c\mathscr{H} = -\mathscr{H}(\cdot)^c \tag{2.12}$$

in the Majorana representation.

Majorana spinor field operator $\Psi_M$ is an eigenfunction of the charge conjugation operator $(\cdot)^c$. It follows from (2.12) that the Hamiltonian of the Majorana spinor cannot have nonzero eigenvalues. That is, the energy of the Majorana spinor must be identically equal to zero. In a similar way, one can prove that the spatial momentum of the Majorana spinor must be identically equal to zero. Therefore, the Majorana spinor cannot exist as a physical particle.

## 3. DIRAC AND MAJORANA SPINOR FIELD OPERATORS

Dirac spinor field operator is given by the standard formula [6]

$$\Psi_D = \sum_s \int \frac{d^3p}{(2\pi)^{3/2}} \sqrt{\frac{m}{E(p)}} \left( b_s(p) u_s(p) e^{-ip_\mu x^\mu} + d_s(p)^+ v_s(p) e^{ip_\mu x^\mu} \right), \tag{3.1}$$

where $b_s(p)$ is annihilation operator of the Dirac spinor with spatial momentum $p$ and spin projection numbering $s$ ($s = 1$ corresponds to the spin projection $+1/2$, $s = 2$ corresponds to the spin projection $-1/2$, or, as will be shown below, it is better to use helicity rather than spin projection), $d_s(p)^+$ is creation operator of the Dirac antispinor with spatial momentum $p$ and spin projection (or helicity) corresponding to the index $s$, $u_s(p)$ and $v_s(p)$ are corresponding spinor columns.

We will use the Dirac representation, since the structure of $u_s(p)$ and $v_s(p)$ is simpler in it. We choose as a basis in the rest frame

$$u_1(0) = \begin{pmatrix} 1 \\ 0 \\ 0 \\ 0 \end{pmatrix}, \quad u_2(0) = \begin{pmatrix} 0 \\ 1 \\ 0 \\ 0 \end{pmatrix}. \tag{3.2}$$

We have in the Dirac representation

$$i\gamma^2 = \begin{pmatrix} 0 & i\sigma_2 \\ -i\sigma_2 & 0 \end{pmatrix} = \begin{pmatrix} 0 & 0 & 0 & 1 \\ 0 & 0 & -1 & 0 \\ 0 & -1 & 0 & 0 \\ 1 & 0 & 0 & 0 \end{pmatrix}. \tag{3.3}$$

It is possible to define two more basis spinors $v_1(0)$ and $v_2(0)$ as

$$\begin{aligned} v_1(0) &= u_1(0)^c = i\gamma^2 u_1(0)^* = \begin{pmatrix} 0 \\ 0 \\ 0 \\ 1 \end{pmatrix}, \\ v_2(0) &= u_2(0)^c = i\gamma^2 u_2(0)^* = \begin{pmatrix} 0 \\ 0 \\ -1 \\ 0 \end{pmatrix}. \end{aligned} \tag{3.4}$$

In this case, relations

$$\begin{aligned} v_1(0)^c &= u_1(0), \\ v_2(0)^c &= u_2(0) \end{aligned} \tag{3.5}$$

are also satisfied.

Operator $(\cdot)^c$ commutes with Lorentz transformation generators $\gamma^{\mu\nu} = \frac{1}{2}(\gamma^\mu\gamma^\nu - \gamma^\nu\gamma^\mu)$. Therefore, relations

$$\begin{aligned} u_s(p)^c &= v_s(p), \\ v_s(p)^c &= u_s(p) \end{aligned} \tag{3.6}$$

are satisfied for all $p$ and $s = 1, 2$.

It follows from (3.4) that for negative-frequency states index $s$ in $v_s(0)$ corresponds to the spin projection opposite to the spin projection for $u_s(0)$. That is, it corresponds to helicity, not spin projection.

Operators $b_s(p)$, $b_s(p)^+$, $d_s(p)$ and $d_s(p)^+$ have canonical anticommutation relations

$$\begin{aligned}
&\{b_i(p)^+, b_j(p')\} = \delta^i_j \delta(p-p')\,,\\
&\{d_i(p)^+, d_j(p')\} = \delta^i_j \delta(p-p')\,,\\
&\{b_i(p), b_j(p')\} = \{d_i(p), d_j(p')\} = \{b_i(p), d_j(p')\} = \{b_i(p)^+, d_j(p')\} = 0\,.
\end{aligned} \tag{3.7}$$

Moreover, $b_s(p)^+ + b_s(p)$, $b_s(p)^+ - b_s(p)$, $d_s(p)^+ + d_s(p)$ and $d_s(p)^+ - d_s(p)$ are generators of the infinite-dimensional Clifford algebra. It is known that generators of the Clifford algebra can always be chosen to be real with respect to the complex conjugation operation [7]. Therefore, we can set

$$\begin{aligned}
b_s(p)^* &= b_s(p)\,,\\
d_s(p)^* &= d_s(p)\,.
\end{aligned} \tag{3.8}$$

From (3.1), (1.5) and (3.8) it follows that

$$\begin{aligned}
\Psi_{M1} = \frac{1}{\sqrt{2}} \sum_s \int \frac{d^3p}{(2\pi)^{3/2}} \sqrt{\frac{m}{E(p)}} (b_s(p) u_s(p) e^{-ip_\mu x^\mu} \;+\; d_s(p)^+ v_s(p) e^{ip_\mu x^\mu} \;+\\
b_s(p) u_s(p)^c e^{ip_\mu x^\mu} \;+\; d_s(p)^+ v_s(p)^c e^{-ip_\mu x^\mu})\,.
\end{aligned} \tag{3.9}$$

Let us define operators

$$\begin{aligned}
a_s(p) &= \frac{b_s(p) + d_s(p)^+}{\sqrt{2}}\,,\\
a'_s(p) &= \frac{b_s(p) - d_s(p)^+}{i\sqrt{2}}\,.
\end{aligned} \tag{3.10}$$

Therefore, from (3.9), ((3.6) and (3.10) we obtain

$$\Psi_{M1} = \sum_s \int \frac{d^3p}{(2\pi)^{3/2}} \sqrt{\frac{m}{E(p)}} (a_s(p) u_s(p) e^{-ip_\mu x^\mu} \;+\; a_s(p) v_s(p) e^{ip_\mu x^\mu})\,. \tag{3.11}$$

Similarly, we obtain the formula for $\Psi_{M2}$

$$\Psi_{M2} = \sum_s \int \frac{d^3p}{(2\pi)^{3/2}} \sqrt{\frac{m}{E(p)}} (a'_s(p) u_s(p) e^{-ip_\mu x^\mu} \;-\; a'_s(p) v_s(p) e^{ip_\mu x^\mu})\,. \tag{3.12}$$

Operators (3.10) have canonical anticommutation relations

$$\begin{aligned}
&\{a_i(p)^+, a_j(p')\} = \delta^i_j \delta(p-p')\,,\\
&\{a'_i(p)^+, a'_j(p')\} = \delta^i_j \delta(p-p')\,,\\
&\{a_i(p), a_j(p')\} = \{a'_i(p), a'_j(p')\} = \{a_i(p), a'_j(p')\} = \{a_i(p)^+, a'_j(p')\} = 0\,.
\end{aligned} \tag{3.13}$$

It should be noted that in (3.11) and (3.12) the same operators $a_s(p)$ and $a'_s(p)$ appear as in the negative-frequency terms as in the positive-frequency terms. This is because the charge conjugation operator contains complex conjugation, but does not contain transposition. In this case, due to (3.8),

$$\begin{aligned}
a_s(p)^* &= a_s(p)\,,\\
a'_s(p)^* &= -a'_s(p)\,.
\end{aligned} \tag{3.14}$$

## 4. ENERGY AND MOMENTUM OPERATORS OF MAJORANA SPINORS

Similarly to how it was done in [6] for the Dirac spinors, we obtain energy $P_0$ and spatial momentum $P_k$ operators of Majorana spinor $\Psi_{M1}$

$$\begin{aligned}
P_0 &= \sum_s \int d^3p\, p_0 (a_s(p)^+ a_s(p) - a_s(p)^+ a_s(p)) = 0\,,\\
P_k &= \sum_s \int d^3p\, p_k (a_s(p)^+ a_s(p) - a_s(p)^+ a_s(p)) = 0\,.
\end{aligned} \tag{4.1}$$

The same results are obtained for $\Psi_{M2}$

$$\begin{aligned} P_0 &= \sum_s \int d^3p\, p_0 (a'_s(p)^+ a'_s(p) - a'_s(p)^+ a'_s(p)) = 0\,, \\ P_k &= \sum_s \int d^3p\, p_k (a'_s(p)^+ a'_s(p) - a'_s(p)^+ a'_s(p)) = 0\,. \end{aligned} \tag{4.2}$$

Formulas (2.11), (2.12), (4.1) and (4.2) are true not only for massive but also for massless Majorana fields.

## 5. Discussion

Thus, we have proven that Majorana spinors have identically zero energy and momentum for both massive and massless cases. This means that Majorana spinors cannot correspond to physically existing particles.

The reason for the problems with spin projection, energy and momentum of Majorana spinors is due to the charge conjugation operation (1.3), (1.4). Majorana [1] and Kramers [8] defined operators (1.2) and (1.3) within the framework of the so-called c-theory, which preceded the theory of second quantization. For Dirac spinors, such a conjugation makes sense only in combination with the theory of "holes" in the Dirac Sea (fermions with negative energy). Majorana tried to construct a theory of fermions that did not require the concept of the Dirac Sea.

However, in quantum field theory, the theory of "holes" in the Dirac Sea was replaced by the use of fermion creation and annihilation operators. Therefore, in the theory of Dirac spinors, the positive-frequency components received the fermion annihilation operator as an additional factor, and the negative-frequency components received the antifermion creation operator.

Due to the fulfillment of equations (1.2) and (1.3), Majorana spinors have half the number of degrees of freedom than a Dirac spinor. Therefore, the approach that is suitable in the case of the Dirac fermion does not work in the case of the Majorana fermion.

It should be noted that charge conjugation operator $C$, defined by formulas (1.3) and (1.4), has another fundamental drawback. This operator contains complex conjugation and is therefore anti-unitary. But operator $CPT$ must be anti-unitary, operator $P$ must be unitary, operator $T$ must be anti-unitary, and therefore operator $C$ must be unitary [6], [9].

The Schwinger charge conjugation operator [10] is also used in the literature. In comparison with operators (1.3) and (1.4), it adds transposition of the creation and annihilation operators. However, it also contains complex conjugation and is therefore anti-unitary. Therefore, the question of constructing a consistent theory of charge-self-conjugate fermions and the see-saw mechanism based on it remains open.

## Conclusion

Majorana spinors exist as solutions of the Dirac equation. However, we have proven that Majorana mass term in quantum field theory (QFT) must vanish and Majorana spinors can not have spin projections. Also, we have proven that the charge conjugation operator anticommutes both with energy and spatial momentum operators of Majorana spinors, that is why Majorana spinors cannot have non-zero energy and momentum. We confirmed this conclusion by deriving QFT formulas for the energy and momentum operators for both massive and massless Majorana spinors, by means of which we have proven that energy and momentum operators of Majorana spinors are identically equal to zero.

Thus, we have obtained several independent proofs that Majorana spinors cannot be physical particles. The results obtained do not imply the impossibility of constructing QFT theory of a truly neutral fermion or the impossibility of the seesaw mechanism. They mean that the question of constructing a consistent theory of charge-self-conjugate fermions and the see-saw mechanism based on it remains open.

## Список литературы/References

1. Majorana E. Teoria simmetrica dell'elettrone e del positrone. *Il Nuovo Cimento*, 1937, no. 14, pp. 171–184.
2. Workman R. L. et al. (Particle Data Group) Neutrino masses, mixing and oscillations. *Prog. Theor. Exp. Phys.*, 2022, 083C01.
3. Mannheim P. D. Introduction to Majorana masses. *Int. J. of Theor. Phys.*, 1984, 23, pp. 643–674.
4. Monakhov V. Majorana Mass Term of Majorana Spinors. *Physical Sciences Forum*, 2023, 7, no. 1, 10.3390/ECU2023-14016.
5. Pal P. B. Dirac, Majorana, and Weyl fermions. *American J. of Physics*, 2011, 79, pp. 485—498.
6. Bjorken J. D., Drell S. D. *Relativistic quantum fields.* N.Y., Mcgraw-Hill College, 1965, 396 p.
7. Lounesto P. *Clifford Algebras and Spinors, 2nd ed.* Cambridge, Cambridge University Press, 2001, 346 p.
8. Kramers H. A. The use of charge-conjugated wave-functions in the hole-theory of the electron. *Proc. Kon. Neer. Akad. Wet.*, 1937, 40, pp. 814—823.
9. Weinberg S. *The Quantum Theory of Fields – Foundations (Vol. 1)* Cambridge, Cambridge University Press, 1995, 609 p.
10. Schwinger J. Quantum electrodynamics. I. A covariant formulation. *Phys. Rev.*, 1948, 74, no. 10, pp. 1439-–1461.

### Авторы

**Монахов Вадим Валериевич**, к.ф.-м.н., доцент, Санкт-Петербургский государственный университет, ул. Ульяновская, д. 1, г. Санкт-Петербург, 198504, Россия.
E-mail: v.v.monahov@spbu.ru

### Просьба ссылаться на эту статью следующим образом:

Монахов В. В. Невозможность существования майорановских спиноров как физических частиц. *Пространство, время и фундаментальные взаимодействия.* 2023. № 3-4. С. 211–217.

### Authors

**Monakhov Vadim Valerievich**, Ph.D., Associate Professor, Saint Petersburg State University, Ulyanovskaya st., 1, Saint Petersburg, 198504, Russia.
E-mail: v.v.monahov@spbu.ru

### Please cite this article in English as:

Monakhov V. V. The Impossibility Of The Existence Of Majorana Spinors As Physical Particles. *Space, Time and Fundamental Interactions*, 2023, no. 3-4, pp. 211–217.

УДК 530.122, 524.74



# ОРБИТЫ МАССИВНЫХ ЧАСТИЦ В СФЕРИЧЕСКИ СИММЕТРИЧНОМ ГРАВИТАЦИОННОМ ПОЛЕ С УЧЕТОМ КОСМОЛОГИЧЕСКОЙ ПОСТОЯННОЙ*

Накибов Р. С.[a,1], Урсулов А. В.[a,2]

[a] Уральский федеральный университет, г. Екатеринбург, 620002, Россия.

В данной работе представлены результаты теоретического исследования траекторий массивных тел в метрике Коттлера с учетом космологической постоянной $\Lambda$. В работе предложена классификация траекторий в одночастичном случае для метрики с положительной и отрицательной космологической постоянной, перебор вариантов основан на различных решениях уравнения траектории, полученных разложением соответствующей алгебраической кривой в ряд Пюизе. В работе также освещены некоторые представляющие интерес типы траекторий, связанные с различными значениями космологической постоянной. Для случая отрицательной космологической постоянной получена ее верхняя оценка на основании анализа кривых вращения галактик.

*Ключевые слова*: Общая теория относительности, космологическая постоянная, орбиты.

# ORBITS OF MASSIVE PARTICLES IN A SPHERICALLY SYMMETRIC GRAVITATIONAL FIELD IN VIEW OF COSMOLOGICAL CONSTANT

Nakibov R. S.[a,1], Ursulov A. V.[a,2]

[a] Ural Federal University, Yekaterinburg, 620002, Russia.

In this paper we present the results of a theoretical study of the trajectories of massive particles in the Köttler metric in view of the cosmological constant $\Lambda$. For both negative and positive signs of $\Lambda$ a classification of trajectories is proposed, with entries based on different solutions of the trajectory equation, obtained by the expansion of the corresponding algebraic curve in Puiseux series. We also provide some specific types of trajectories which correspond to different values of the cosmological constant. In the case of negative values of the cosmological constant its upper limit is estimated from the galaxy rotation curves.

*Keywords*: General Relativity, cosmological constant, orbits.

PACS: 95.10.Eg, 98.80.Es

DOI: 10.17238/issn2226-8812.2023.3-4.218-228

## Introduction

It was firstly pointed in 1916 by Einstein that the $\Lambda$-term (cosmological constant) should be included in gravitational field equations within the static Universe model[1]. Later in 1918 Köttler considered $\Lambda$-term in a centrally-symmetric gravitational field [2]. Subsequently, the study of the cosmological constant faded into the background, since, as it was believed, there were not enough physical grounds to take it into account[3]. Nowadays there is a renewed interest in exploring the contribution of the Lambda-term in the Einstein-Hilbert field equations. On the one hand, in the framework of $\Lambda$CDM model the presence of the $\Lambda$–term explains the observed accelerating expansion of the Universe[4]. On the other hand, diverting the value of cosmological constant from established in $\Lambda$CDM leads to explanation of some other observed astrophysical phenomena (e.g. rotational curves of some galaxies[5, 6]). Besides,

*Работа поддержана Министерством науки и высшего образования Российской Федерации (проект FEUZ20230017).

[1]E-mail: nakibov.ruslan@urfu.ru

[2]E-mail: AV.Ursulov@urfu.ru

the presence of cosmological constant has an effect on properties of black holes and event horizon[7, 8], on deflection of light and gravitational lensing[9, 13], and on orbits of massive particles in centrally-symmetric gravitational field[14, 15]. The study of gravitational fields with negative $\Lambda$ [5, 16] that induce the anti-de Sitter spacetimes[17] is particularly interesting.

## 1. General statements

Consider a metric tensor of centrally-symmetric gravitational field in coordinates $x^i = \{ct, r, \theta, \varphi\}$ of a remote observer:

$$g_{ik} = \begin{pmatrix} \alpha^2 & 0 & 0 & 0 \\ 0 & -\beta^2 & 0 & 0 \\ 0 & 0 & -\gamma^2 & 0 \\ 0 & 0 & 0 & -\gamma^2 \sin^2\theta \end{pmatrix}, \tag{1.1}$$

where $\alpha, \beta, \gamma$ are continuous functions with variable $r$, $\theta$ is an angle[3]. Without loss of generality consider a motion in an equatorial plane $\theta = \pi/2$. The Hamilton-Jacobi equations of a particle of mass $m$ are given by:

$$g^{ik}\frac{\partial S}{\partial x^i}\frac{\partial S}{\partial x^k} - m^2c^2 = 0 \tag{1.2}$$

where $S$ is action, $E$ is energy, $l$ is an angular momentum of a massive particle and $c$ is the speed of light.

Substituting

$$S = -Et + l\varphi + S_r(r) \tag{1.3}$$

we obtain the equation of trajectory by

$$\frac{\partial S}{\partial l} = \varphi_0 = const \tag{1.4}$$

$$\varphi - \varphi_0 = j\int \frac{dr}{\sqrt{-\frac{\gamma^2}{\beta^2}\left(\gamma^2 + j^2\right) + k^2\frac{\gamma^4}{\alpha^2\beta^2}}} \tag{1.5}$$

where $k = E/mc^2$, $j = l/mc^2$ is a reduced angular momentum. For a centrally-symmetric space $k$ and $j$ are constant in time. The latter can also be interpreted as a characteristic radius dependant on mass and angular momentum since it is measured in meters.

We obtain the potential energy $U(u)$ from the Binet equation[22],

$$\frac{d^2u}{d\varphi^2} + u = -\frac{1}{mc^2j^2}\frac{dU(u)}{du}, \tag{1.6}$$

$$U(r) = -\frac{1}{2}mc^2\left(j^2u^2 + u^4F(r)\right). \tag{1.7}$$

where $u = 1/r$. Effective potential of a two body problem is given as

$$U_{eff}(r) = -\frac{mc^2}{2}\frac{F(r)}{r^4} \tag{1.8}$$

Here $F(r)$ is a radicand from (1.5):

$$F(r) = -\frac{\gamma^2}{\beta^2}\left(\gamma^2 + j^2\right) + k^2\frac{\gamma^4}{\alpha^2\beta^2} \tag{1.9}$$

For the Köttler metric with a nonzero cosmological constant $\Lambda$ and a central body of Schwarzschild radius $r_g$

$$\alpha^2 = 1 - \frac{r_g}{r} - \frac{\Lambda r^2}{3}, \quad \beta^2 = \frac{1}{\alpha^2}, \quad \gamma^2 = r^2, \tag{1.10}$$

the function $F(r)$ takes the following form

$$F(r) = \frac{\Lambda}{3}r^6 + Kr^4 + r_gr^3 - j^2r^2 + j^2r_gr, \tag{1.11}$$

where $K = -(1-k^2) - \frac{1}{3}\Lambda j^2$.

In the following calculations we assume $r > r_g$, where $r_g$ is an event horizon defined by the equation

$$1 - \frac{r_g}{r} - \Lambda r^2 = 0. \tag{1.12}$$

## 2. Rotatonal curves

Consider $\Lambda < 0$. In this case, it becomes possible to explain the problem of galaxy rotational curves[5]. In the classical limit the linear velocity of a circular motion is given by

$$v = \sqrt{\frac{1}{m} r \frac{dU}{dr}} \tag{2.1}$$

Assuming $j = rv(r)/c$ we obtain a following rotational curve

$$\frac{v}{c} = \sqrt{\frac{\frac{1}{3}|\Lambda| r^2 + \frac{1}{2}\frac{r_g}{r}}{2 - \frac{3}{2}\frac{r_g}{r}}}. \tag{2.2}$$

Over large distances the rotational curve given by (2.2) expresses a slow linear growth $\sim \sqrt{|\Lambda|}r$. The linear speed has a minimum value if the inequality $r_g^2 < |\Lambda|^{-1}$ holds, which is the case for a motion outside the event horizon. The radius $r_{min}$ at which the minimum speed is reached and the corresponding speed value $v_{min}$ are given by

$$r_{min} = \sqrt[3]{\frac{3}{4}\frac{r_g}{|\Lambda|}} + \frac{3}{8} r_g \tag{2.3}$$

$$v_{min} = \frac{c}{2} \sqrt[6]{\frac{9}{2}|\Lambda| r_g^2}. \tag{2.4}$$

Since the linear speed exceeds its minimum $v \geqslant v_{min}$ a constraint can be placed on the value of $\Lambda$ observed in galaxies.

$$|\Lambda| \leqslant \frac{2}{9}\left(2\frac{v_{min}}{c}\right)^6 \frac{1}{r_g^2} = 8\left(\frac{2}{3}\right)^2 \frac{1}{G^2 c^4}\frac{v_{min}^6}{M^2} \approx 10^{-13}\frac{v_{min}^6}{M^2} \tag{2.5}$$

where $G$ is a gravitational constant, $M$ is a central body mass and $\Lambda < 0$. For a supermassive black hole of mass $M = 10^5 M_\odot$ and $v_{min} \approx 200$ km/s one gets $|\Lambda| < 10^{-52}$ m$^{-2}$, which is consistent with estimations given in [5].

## 3. Circular motion

In the classical limit stable circular orbits correspond to minima of effective potential energy (1.8), unstable orbits to maxima. Assuming (1.11) and $\Lambda < 0$ we get the effective potential

$$U_{eff}(r) = -\frac{mc^2}{2}\frac{1}{r^4}\left(-\frac{1}{3}|\Lambda| r^6 + K r^4 + r_g r^3 - j^2 r^2 + r_g j^2 r\right) \tag{3.1}$$

Finding the extrema of effective potential leads to an equation

$$\frac{1}{3}|\Lambda| r^5 + \frac{1}{2} r_g r^2 - j^2 r + \frac{3}{2} r_g j^2 = 0, \tag{3.2}$$

which was solved by the Puiseux method (p. 225), the roots of the equation are presented in the Table 1.

Concluding, for particles with angular momentum high enough or mass low enough so that the value of a parameter $J$ exceeds the critical value and the sign changes in the inequality $J < J_c$, where

$$J_c = \sqrt[6]{3/(|\Lambda| r_g^2)}, \tag{3.3}$$

the stable Schwarzschild root changes to a new value that is expressed explicitly through the cosmological constant. For such particles the gravitational pull is mostly provided by the negative cosmological constant. Fig. 1 depicts the stability diagram for the orbits.

**Таблица 1.** The radii of circular roots in the case of negative cosmological constant. The first case recreates Schwarzschild circular orbits, the second case is a novelty and arises if inequality $J > J_c$ holds, where $J = j/r_g$.

| No. | Conditions | Unstable root | Stable root | In dimensionless $\rho = r_g/r$ |
|---|---|---|---|---|
| 1 | $j < r_g^{2/3}/\vert\Lambda\vert^{1/6}, j > r_g, r_g^2 > \vert\Lambda\vert j^2$ | $r_1 \approx 3r_g/2$ | $r_2 \approx 2j^2/r_g$ | $\rho_1 = 3/2, \rho_2 = 2J^2$ |
| 2 | $j > r_g^{2/3}/\vert\Lambda\vert^{1/6}, j > r_g, j^2 > \vert\Lambda\vert r_g^4$ | $r_1 \approx 3r_g/2$ | $r_2 \approx \sqrt[4]{3j^2/\vert\Lambda\vert}$ | $\rho_1 = 3/2, \rho_2 = \sqrt{J} J_c^{3/2}$ |

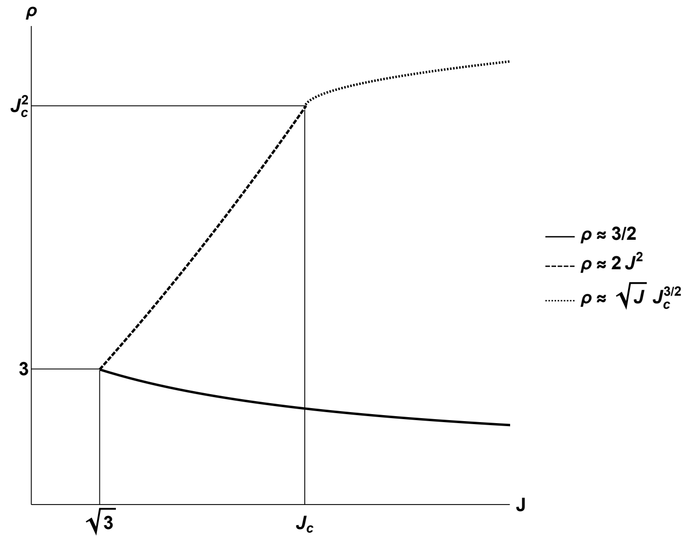


**Рис. 1.** Stability diagram for circular orbits in dimensionless coordinates. The upper branch corresponds to stable roots, the lower branch to unstable.

## 4. Non-circular motion. Classification and example orbits

All possible trajectories of non-circular orbits are determined by the equation (1.4) where $F(r)$ is provided by (1.11). Trajectories depend on the number and value of positive roots of the $p(r) = F(r)/r$, ($r \neq 0$).

$$p(r) = -\frac{1}{3}|\Lambda| r^5 + Kr^3 + r_g r^2 - j^2 r + j^2 r_g = 0 \tag{4.1}$$

It is possible to get some information by applying the Descartes' rule of signs[18]. For $\Lambda < 0$ there exist three roots or a singular root, for $\Lambda > 0$ there are four, two or zero positive roots.

The equation was solved and the roots are present in the Table 2. The roots are divided in eight configurations, and configurations $A$, $B$, and $C$ represent cases where finite motion is possible. Since the motion is possible if $p(r) > 0$, then in configurations with a single root ($r < r_1$) the particle may fall inside the central body or the system is located within event horizon, in double root configurations unbound trajectories are found outside the larger radius ($r > r_2$). In a three or five root configurations there exists a region of finite motion ($r_2 < r < r_3$).

Note that in the configuration $C$ with $K < 0$ the lambda-term can be neglected, thus reproducing the Schwarzschild solution. In other cases, the larger root depends on the cosmological constant, only these cases will be considered further.

Let us list some of the orbits. Unbound trajectories outside $r_{max} = \sqrt{3|K|/\Lambda}$ in case of $\Lambda > 0$ are either modified hyperbolic spirals if $K > 0$, or modified hyperbolas if $K < 0$:

$$r = \frac{1}{\sqrt{\frac{\Lambda}{3K} - \frac{K\varphi^2}{j^2}}} \tag{4.2}$$

The formula covers both cases. Corresponding trajectories are displayed in Fig. 2 and Fig. 3

**Таблица 2.** List of configurations and conditions that lead to such configurations. The order of roots can always be determined via conditions; $\sqrt[n]{1}$ is evaluated in a complex plane; only the first term of roots is present.

| No. | Conditions | Roots | | | |
|---|---|---|---|---|---|
| | | $\Lambda>0,\ K>0$ | $\Lambda>0,\ K<0$ | $\Lambda<0,\ K<0$ | $\Lambda<0,\ K>0$ |
| 1 | $\lvert\Lambda\rvert^3 r_g^2 j^4 > \lvert K\rvert^5$, $j^3\lvert\Lambda\rvert > r_g$, $\lvert\Lambda\rvert r_g^4 > j^2$ | $\sqrt[5]{-1}\sqrt[5]{\frac{3j^2 r_g}{\Lambda}}$ | $\sqrt[5]{-1}\sqrt[5]{\frac{3j^2 r_g}{\Lambda}}$ | $\sqrt[5]{1}\sqrt[5]{\frac{3j^2 r_g}{\lvert\Lambda\rvert}}$ | $\sqrt[5]{1}\sqrt[5]{\frac{3j^2 r_g}{\lvert\Lambda\rvert}}$ |
| 2 | $\lvert K\rvert^3 > \lvert\Lambda\rvert r_g^2$, $\lvert K\rvert^2 > \lvert\Lambda\rvert j^2$, $\lvert K\rvert^5 > \lvert\Lambda\rvert^3 j^4 r_g^2$, $\lvert K\rvert j > r_g$, $\sqrt{\lvert K\rvert} r_g > j$, | $\pm i\sqrt{\frac{K}{\Lambda}}$, $\sqrt[3]{-1}\sqrt[3]{\frac{j^2 r_g}{K}}$ | $\pm 1\sqrt{\frac{\lvert K\rvert}{\Lambda}}$, $\sqrt[3]{1}\sqrt[3]{\frac{j^2 r_g}{\lvert K\rvert}}$ | $\pm 1\sqrt{\frac{K}{\lvert\Lambda\rvert}}$, $\sqrt[3]{-1}\sqrt[3]{\frac{j^2 r_g}{K}}$ | $\pm i\sqrt{\frac{\lvert K\rvert}{\lvert\Lambda\rvert}}$, $\sqrt[3]{1}\sqrt[3]{\frac{j^2 r_g}{\lvert K\rvert}}$ |
| 3 | $\lvert\Lambda\rvert r_g^2 > \lvert K\rvert^3$, $r_g^4 > \lvert\Lambda\rvert j^6$, $r_g > \lvert\Lambda\rvert j^3$, $r_g > j$, | $\sqrt[3]{-1}\sqrt[3]{\frac{r_g}{\Lambda}}, \pm ij$ | $\sqrt[3]{-1}\sqrt[3]{\frac{r_g}{\Lambda}}, \pm ij$ | $\sqrt[3]{1}\sqrt[3]{\frac{r_g}{\lvert\Lambda\rvert}}, \pm ij$ | $\sqrt[3]{1}\sqrt[3]{\frac{r_g}{\lvert\Lambda\rvert}}, \pm ij$ |
| 4 | $\lvert\Lambda\rvert j^2 > K^2$, $j^6\lvert\Lambda\rvert > r_g^4$, $j^2 > \lvert\Lambda\rvert r_g^4$, | $\sqrt[4]{1}\sqrt[4]{\frac{j^2}{\Lambda}}, r_g$ | $\sqrt[4]{1}\sqrt[4]{\frac{j^2}{\Lambda}}, r_g$ | $\sqrt[4]{-1}\sqrt[4]{\frac{j^2}{\lvert\Lambda\rvert}}, r_g$ | $\sqrt[4]{-1}\sqrt[4]{\frac{j^2}{\lvert\Lambda\rvert}}, r_g$ |
| 5 | $\lvert K\rvert^3 > \lvert\Lambda\rvert r_g^2$, $\lvert K\rvert^2 > \lvert\Lambda\rvert j^2$, $\lvert K\rvert^5 > \lvert\Lambda\rvert^3 j^4 r_g^2$, $r_g^2 > j^2\lvert K\rvert$, $r_g > j\lvert K\rvert$, $r_g > j$, | $\pm i\sqrt{\frac{K}{\Lambda}}$, $-\frac{r_g}{K}, \pm ij$ | $\pm 1\sqrt{\frac{\lvert K\rvert}{\Lambda}}$, $\frac{r_g}{\lvert K\rvert}, \pm ij$ | $\pm 1\sqrt{\frac{K}{\lvert\Lambda\rvert}}$, $-\frac{r_g}{K}, \pm ij$ | $\pm i\sqrt{\frac{\lvert K\rvert}{\lvert\Lambda\rvert}}$, $\frac{r_g}{\lvert K\rvert}, \pm ij$ |
| A(6) | $\lvert\Lambda\rvert r_g^2 > \lvert K\rvert^3$, $r_g^4 > \lvert\Lambda\rvert j^6$, $r_g > \lvert\Lambda\rvert j^3$, $j > r_g$ | $\sqrt[3]{-1}\sqrt[3]{\frac{r_g}{\Lambda}}$, $\frac{j^2}{r_g}, r_g$ | $\sqrt[3]{-1}\sqrt[3]{\frac{r_g}{\Lambda}}$, $\frac{j^2}{r_g}, r_g$ | $\sqrt[3]{1}\sqrt[3]{\frac{r_g}{\lvert\Lambda\rvert}}$, $\frac{j^2}{r_g}, r_g$ | $\sqrt[3]{1}\sqrt[3]{\frac{r_g}{\lvert\Lambda\rvert}}$, $\frac{j^2}{r_g}, r_g$ |
| B(7) | $K^3 > \lvert\Lambda\rvert r_g^2$, $K^2 > \lvert\Lambda\rvert j^2$, $K^5 > \lvert\Lambda\rvert^3 j^4 r_g^2$, $j^2 K > r_g$, $j^2 > K r_g$, | $\pm i\sqrt{\frac{K}{\Lambda}}$, $\pm 1\frac{j}{\sqrt{K}}, r_g$ | $\pm 1\sqrt{\frac{\lvert K\rvert}{\Lambda}}$, $\pm i\frac{j}{\sqrt{K}}, r_g$ | $\pm 1\sqrt{\frac{K}{\lvert\Lambda\rvert}}$, $\pm 1\frac{j}{\sqrt{K}}, r_g$ | $\pm i\sqrt{\frac{\lvert K\rvert}{\lvert\Lambda\rvert}}$, $\pm i\frac{j}{\sqrt{K}}, r_g$ |
| C(8) | $K^3 > \lvert\Lambda\rvert r_g^2$, $K^2 > \lvert\Lambda\rvert j^2$, $\lvert K\rvert^5 > \lvert\Lambda\rvert^3 j^4 r_g^2$, $r_g^2 > j^2\lvert K\rvert$, $r_g > j\lvert K\rvert$, $j > r_g$ | $\pm i\sqrt{\frac{K}{\Lambda}}$, $-\frac{r_g}{K}, \frac{j^2}{r_g}, r_g$ | $\pm 1\sqrt{\frac{\lvert K\rvert}{\Lambda}}$, $\frac{r_g}{\lvert K\rvert}, \frac{j^2}{r_g}, r_g$ | $\pm 1\sqrt{\frac{K}{\lvert\Lambda\rvert}}$, $-\frac{r_g}{K}, \frac{j^2}{r_g}, r_g$ | $\pm i\sqrt{\frac{\lvert K\rvert}{\lvert\Lambda\rvert}}$, $\frac{r_g}{\lvert K\rvert}, \frac{j^2}{r_g}, r_g$ |

Consider a case of three roots and $\Lambda < 0$. Let us factorize the radical expression of (1.4):

$$\varphi = \int \frac{j dr}{\sqrt{-\frac{1}{3}|\Lambda| r(r-r_1)(r-r_2)(r-r_3)(r-r_4)(r-r_5)}} \tag{4.3}$$

In each of configurations $A, B, C$ (see Table 2) there is a total of five roots, some of which may be negative or complex. The root $r = r_g$ is present only once in each of those configurations and it's the smallest positive root. Assuming that the orbits take place in $r_{max} > r > r_{min} \gg r_g$, we can expand

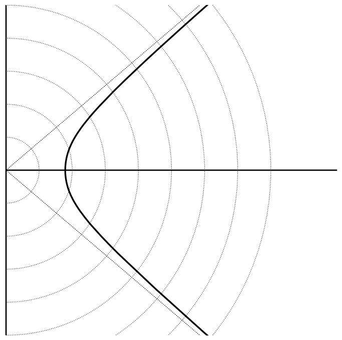

**Рис. 2.** Unbound orbit with $\Lambda > 0$, $K > 0$

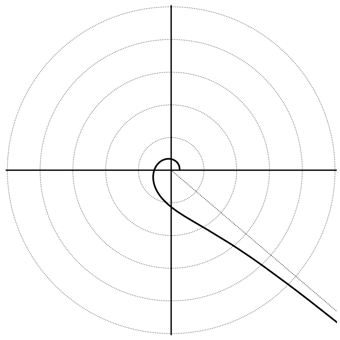

**Рис. 3.** Unbound orbit with $\Lambda > 0$, $K < 0$

the factor $(r - r_g)^{-1/2}$ as

$$\frac{1}{\sqrt{r - r_g}} \approx \frac{1}{\sqrt{r}} + \frac{1}{2}\frac{r_g}{r\sqrt{r}} + \dots \tag{4.4}$$

in which case trajectories can be expressed in a form of a linear combination of incomplete elliptic integrals and elementary functions.

$$\varphi = \sqrt{\frac{3j^2}{|\Lambda|}}\left[\int \frac{dr}{r\sqrt{(r_1 - r)(r - r_2)(r - r_3)(r - r_4)}} + \frac{r_g}{2}\int \frac{dr}{r^2\sqrt{(r_1 - r)(r - r_2)(r - r_3)(r - r_4)}}\right] \tag{4.5}$$

The corresponding formulas for the case of four real roots (conf. $B$, $C$) and two real and two complex roots (conf. $A$) are taken from[19]. Here $F(\vartheta|m)$, $E(\vartheta|m)$, $\Pi(\alpha^2;\vartheta|m)$ are incomplete elliptic integrals of first, second and third kind. Let us introduce the notation

$$\begin{gathered}
A^2 = (a - \mathrm{Re}(c))^2 + \mathrm{Im}(c)^2, \quad B^2 = (b - \mathrm{Re}(c))^2 + \mathrm{Im}(c)^2, \quad g = 1/\sqrt{AB} \\
\alpha = \frac{bA - aB}{aB + bA}, \quad \alpha_1 = \frac{A - B}{A + B}, \quad X_1 = 1, \quad X_2 = \frac{r_g}{2} \\
m = \frac{(a-b)^2 - (A-B)^2}{4AB}, \quad \theta = \arccos\frac{(a-r)B - (r-b)A}{(a-r)B + (r-b)A}, \quad \cos\theta = \mathrm{cn}u \\
R_{-2} = \frac{1}{m}((m - \alpha^2(1-m))F(\theta|m) + \alpha^2 E(\theta|m) + 2\alpha\sqrt{m}\arccos(\mathrm{dn}u)) \\
R_{-1} = F(\theta|m) + \frac{\alpha}{\sqrt{m}}\arccos(\mathrm{dn}u), \quad R_0 = F(\theta|m) \\
R_1 = \frac{1}{1-\alpha^2}\left(\Pi(\frac{\alpha^2}{\alpha^2 - 1};\theta|m) - \alpha\sqrt{\frac{1-\alpha^2}{m + (1-m)\alpha^2}}\arctan\left(\sqrt{\frac{m + (1-m)\alpha^2}{1-\alpha^2}}\mathrm{sd}u\right)\right) \\
R_2 = \frac{1}{(\alpha^2 - 1)(m + \alpha^2(1-m))}\left((\alpha^2(2m-1) - 2m)R_1 + 2mR_{-1} - mR_{-2} + \frac{\alpha^3 \mathrm{sn}u\,\mathrm{dn}u}{1 + \alpha\,\mathrm{cn}u}\right),
\end{gathered}$$

where $a > b, c, \bar{c}$ are the roots of the radicand. Then for configuration $A$ trajectories are given by the formula:

$$\varphi(r) = \sqrt{\frac{3j^2}{|\Lambda|}}\sum_{s=1}^{2}\frac{(A+B)^s g X_s}{(Ab - Ba)^s}\sum_{n=0}^{s}\frac{\alpha_1^{s-n}(\alpha - \alpha_1)^n s!}{(s-n)!n!}R_n \tag{4.6}$$

Introducing the notation

$$g = \frac{2}{\sqrt{(a-c)(b-d)}}, \quad \alpha = \frac{c}{b}\frac{a-b}{a-c}, \quad \alpha_1 = \frac{b}{c}\alpha, \quad X_1 = 1, \quad X_2 = \frac{r_g}{2}$$

$$m = \frac{(a-b)(c-d)}{(a-c)(b-d)}, \quad \theta = \arcsin\sqrt{\frac{(a-c)(r-b)}{(a-b)(r-c)}}$$

$$V_0 = F(\theta|m), \quad V_1 = \Pi(\alpha^2, \theta|m), \quad \sin\theta = \mathrm{sn}u$$

$$V_2 = \frac{1}{2(\alpha^2-1)(m-\alpha^2)}(\alpha^2 E(\theta|m) + (m-\alpha^2)F(\theta|m) + \\ + (2\alpha^2 m + 2\alpha^2 - \alpha^4 - 3m)\Pi(\alpha^2,\theta|m) - \frac{\alpha^4 \mathrm{sn}u\,\mathrm{cn}u\,\mathrm{dn}u}{1-\alpha^2\mathrm{sn}^2 u}\Bigg),$$

where $a > b > c > d$ are roots of the radicand we get trajectories formula for configurations $B$ and $C$:

$$\varphi(r) = \sqrt{\frac{3j^2}{|\Lambda|}}\sum_{s=1}^{2}\frac{gX_s}{b^s}\frac{\alpha_1^{2s}}{\alpha^{2s}}\sum_{n=0}^{s}\frac{(\alpha^2-\alpha_1^2)^n s!}{\alpha_1^{2n} n!(s-n)!}V_n \tag{4.7}$$

For any set of parameters $\{\Lambda, r_g, K, j\}$ this process allows to find the set of roots and a suitable formula of trajectory inside the region $r_{max} > r > r_{min}$. These formulas describe the motion from $r_{min}$ to $r_{max}$, then the particle returns along a similar trajectory.

Note two important cases. The first case arises if $\log_{10}(r_{max}/r_{min}) > 2..3$. The trajectory then is a modified hyperbolic spiral ($\Lambda < 0, K > 0$):

$$r = \frac{1}{\sqrt{\frac{K\varphi^2}{j^2} + \frac{|\Lambda|}{3K}}} \tag{4.8}$$

The second case describes a closed bound orbit in case of $r_g = 0$ and $\Lambda < 0$. Integrating the simplified expression

$$\varphi = \int \frac{j dr}{r\sqrt{\frac{1}{3}\Lambda r^4 + K r^2 - j^2}}. \tag{4.9}$$

we obtain the general formula for such orbits

$$r = \sqrt{\frac{2j^2/K}{1 - \sqrt{1 + \frac{4}{3}\frac{\Lambda j^2}{K^2}}\sin(2\zeta\varphi + \Delta\varphi)}}, \tag{4.10}$$

where $\Delta\varphi = 0$, $\zeta = 1$ in case of $r_g = 0$.

Equation (4.10) allows for several trajectories. For $\Lambda > 0$, regardless of the sign of $K$, hyperbolic orbits follow from the formula, however, if the attraction to the center is provided only by the cosmological constant $\Lambda < 0$, (and $K > 0$), then the formula implies a closed bound orbit. Accounting for the non-zero gravitational radius leads to deviations in the formula and perihelion precession:

$$\zeta = r_{min} r_{max}\sqrt{\frac{|\Lambda|}{3j^2}}, \tag{4.11}$$

$$\Delta\varphi = -\frac{r_g}{r_{min}} E\left(\arcsin\sqrt{\frac{r_{max}^2(r^2 - r_{min}^2)}{r^2(r_{max}^2 - r_{min}^2)}}\,\middle|\,1 - \frac{r_{min}^2}{r_{max}^2}\right) \tag{4.12}$$

where $E(\theta|m)$ is an incomplete elliptic integral of the second kind. These variations are displayed in Fig. 4–6. Expressions (4.10)–(4.12) can be used for configuration $B$ if $r_{min} \gg r_g$ due to both $r_{min}$, $r_{max}$ being independent on $r_g$ in the first term. In other configurations radii depend on gravitational radius and formulas (4.6) and (4.7) should be used.

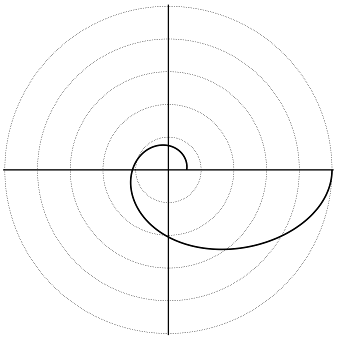

**Рис. 4.** Modified hyperbolic spiral $\Lambda < 0$, $K > 0$

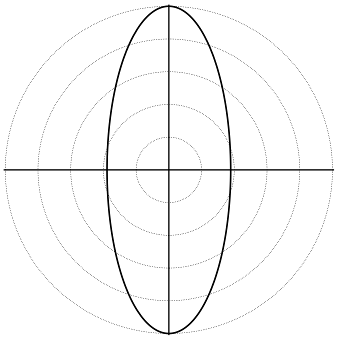

**Рис. 5.** Closed orbit with $\Lambda < 0$, $K > 0$ and $r_g = 0$.

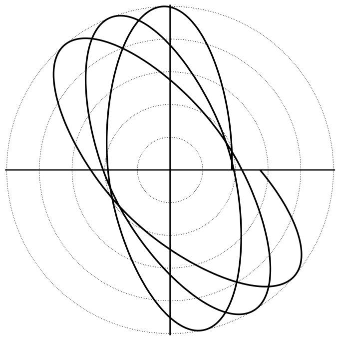

**Рис. 6.** Bound orbit with perihelion precession with $\Lambda < 0$, $K > 0$ due to accounting for $r_g$.

## 5. A study of trajectories

Let us fix $r_g$ and $\Lambda$ and vary parameters $j$ and $K$. Then for each pair $\{j, K\}$ one can calculate the value of any quantity $P$, thus obtaining the dependence $P = P(j, K)$ as a dataset. The function $P = P(j, K)$ then can be represented as a heatmap (e.g. Fig. 7). Finally, comparing the diagrams for different $r_g$ and $\Lambda$, one can study the influence of all four parameters on the particle trajectories. The script for such procedure is written and can be shared via e-mail.

In general, bound and spiral orbits are mathematically possible with a variety of combinations of parameters, but not all of them could have been observed in physical systems. It is worth noting some interesting properties of orbits in the case of $\Lambda < 0$.

Trajectories that belong to narrow regions of motion are located at characteristic radii from 100 pc to 100 kpc, which corresponds to the size of galaxies, and if the system is fairly remote the particles cannot escape. In particular, the orbits are limited by $r_{max} = \sqrt[3]{3r_g/|\Lambda|}$ in configuration $A$ (see Table 2), which corresponds to low-energy particles. This radius shows weak grows with $r_g$ and also weakly depends on the particle properties ($J$, $K$).

Trajectories in wider regions of motion form spiral trajectories despite of a bounded region. In this case the maximal radius can approach the size of an observable Universe ($\sqrt{3/\Lambda}$). There is merit in assuming that a particle at such distance would be captured by another gravitating system. However, not all particles can leave the system in a physically reasonable time. For «slow» particles, the escape along the spiral trajectory will take a significantly longer time and the particle for the observer will effectively remain on the spiral trajectory.

## Conclusion

In the present paper we consider the trajectories of massive particles in the Köttler metric for various values of the cosmological constant. A classification of these trajectories is proposed, which is based on the Puiseux method for polynomials. Some specific or notable types of trajectories are outlined. It should be noted that not all obtained trajectories can be found in a real system. However, in our opinion, in addition to academic interest, understanding the nature of trajectories may be useful in planning experiments to determine the sign and magnitude of the cosmological constant.

## Appendix. Puiseux method

In the present paper we use a proposed Puiseux method to analyse the main equation for trajectories. This section outlines some key theoretical points concerning the underlying theory and a proposed application of it as a root-finding method for poynomial equations.

The Newton-Puiseux theorem was originally devised for the study of algebraic curves. An algebraic

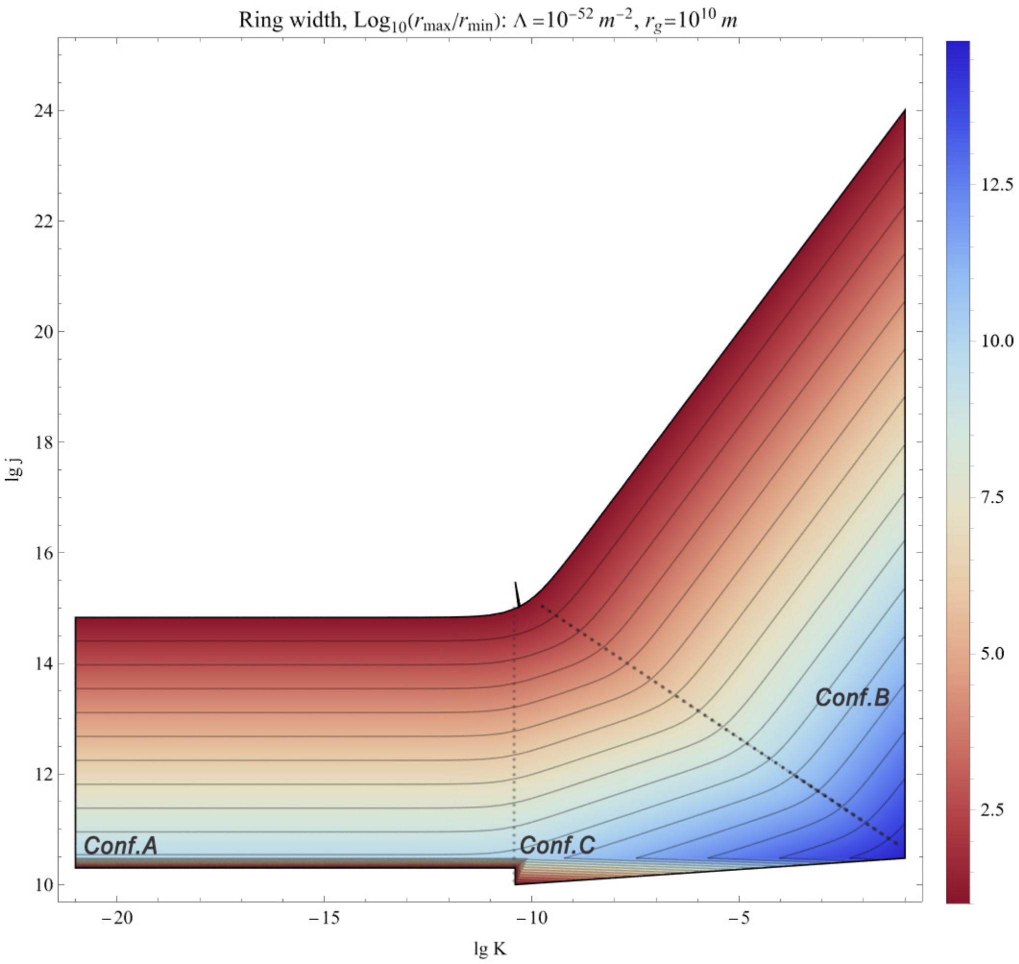


**Рис. 7.** An example of a heatmap: for any $j, K$ with fixed $\Lambda, r_g$ a logarithm of the ratio of outer and inner radii is calculated. Larger values correspond to the spiral trajectories, smaller values to bound orbits with precession.

curve $F(x, y) = 0$ is a polynomial function of each of its variables over the field of complex numbers. The theorem provides a method for finding formulas for all of the branches in the form of generalized power series which allows for negatives and fractions, the Puiseux series[21]. Given that the highest order of $y$ in $F(x, y) = 0$ is $n$, the theorem proves that it is possible to obtain exactly $n$ different expansions $y(x)$ for the branches. For technical details on algorithm see[20].

It is possible to use the Pusieux expansion for the study of polynomials and employ it as a tedious root finding algorithm for polynomials of higher orders. Consider an equation of the form

$$a_n y^n + a_{n-1} y^{n-1} + \ldots a_1 y + a_0 = 0, \tag{5.1}$$

where $a_n$ are parameters (e.g. (4.1)). It is possible to pick a number $x$ and a set of exponents $b_i$ so the following substitution holds

$$a_i = \mathrm{sign}(a_i) x^{b_i}. \tag{5.2}$$

In such form the algebraic equation becomes an algebraic curve and can be expanded in a Puiseux series. The next key point is the usage of Newton polygons. Originally the roots are determined from the slopes of a convex hull of points that represent the terms of a polynomial. Note that different sets of parameters may form the same convex hull, hence yielding same expansions and also note that for given polynomial there is a finite amount of Newton polygons. Consider then a set of all possible Newton polygons. Those are defined by relations of lines and dots which are easy to obtain in the form of sets of inequalities. After inverse substitution these sets become so-called conditions which mark the parameter space of an equation and Puiseux expansions become approximate formulas suitable for those conditions which effectively solves the equation.

Concluding, we find the main use of the proposed root-finding method not in obtaining precise formulas for equations of higher orders but in extracting valuable information about all possible sets of roots and conditions that induce these roots.

**Список литературы/References**


1. Einstein A. Kosmologische Betrachtungen zur allgemeinen Relativitätstheorie. *Sitzungsberichte der Königlich Preussischen Akademie der Wissenschaften*, 1917, pp. 142–152.
2. Köttler F. Über die physikalischen Grundlagen der Einsteinschen Gravitationstheorie. *Annalen der Physik*, 1918, vol. 361, pp. 401-462
3. Landau L. D., Lifschits E. M. *The Classical Theory of Fields*, Course of Theoretical Physics, Vol.2. Oxford, Pergamon Press, 1975.
4. Planck Collaboration. Planck 2015 results - XIII. Cosmological parameters *A&A*, 2016, vol. 594, p. A13. doi: 10.1051/0004-6361/201525830
5. Aryal B., Pandey R., Baral N., Khanal U., Saurer W. Estimation of mass and cosmological constant of nearby spiral galaxies using galaxy rotation curve. 2013, *arXiv:1307.1824 [astro-ph.CO]*
6. Farnes J. S. A Unifying Theory of Dark Energy and Dark Matter: Negative Masses and Matter Creation within a Modified ΛCDM Framework. *A&A*, 2016, vol. 620, p. A92. doi: 10.1051/0004-6361/201832898
7. Zakharov A. F. Are signatures of anti-de-Sitter black hole at the Galactic Center? *arXiv e-prints*, 2014, arXiv:1407.2591. doi: 10.48550/arXiv.1407.2591
8. Cruz N., Olivarez M., Villanueva J. R. The golden ratio in Schwarzschild–Kottler black holes. *The European Physical Journal C*, 2017, vol. 77, no. 2. doi: 10.1140/epjc/s10052-017-4670-7
9. Simpson F., Peacock J., Heavens A. On lensing by a cosmological constant. *Monthly Notices of the Royal Astronomical Society*, 2010, vol. 402, no. 3, pp. 2009–2016. doi: 10.1111/j.1365-2966.2009.16032.x
10. Ishak M., Rindler W., Dossett J. More on lensing by a cosmological constant. *Monthly Notices of the Royal Astronomical Society*, 2010, vol. 403, no. 4, pp. 2152-2156. doi: 10.1111/j.1365-2966.2010.16261.x
11. Ishak M., Rindler W. The relevance of the cosmological constant for lensing. *General Relativity and Gravitation*, 2010, vol. 42, no. 9, pp. 2247–2268. doi: 10.1007/s10714-010-0973-9
12. Arakida H., Kasai M. Effect of the cosmological constant on the bending of light and the cosmological lens equation. *Physical Review D*, 2012, vol. 85, no. 2. doi: 10.1103/physrevd.85.023006
13. Lake K. Bending of light and the cosmological constant. *Physical Review D*, 2002, vol. 65, no. 8 doi: 10.1103/physrevd.65.087301
14. Ono T., Suzuki T., Fushimi N., Yamada K., Asada H. Application of Sturm's theorem to marginal stable circular orbits of a test body in spherically symmetric and static spacetimes. 2015, *arXiv:1508.00101 [gr-qc]*
15. Solanki R. Kottler spacetime in isotropic static coordinates. *Classical and Quantum Gravity*, 2021, vol. 39, no. 1, p. 015015. doi: 10.1088/1361-6382/ac3aa0
16. Chruściel P., Simon W. Towards the classification of static vacuum spacetimes with negative cosmological constant. *Journal of Mathematical Physics*, 2001, vol. 42, no. 4, pp. 1779–1817. doi: 10.1063/1.1340869
17. Gibbons G. W. Anti-de-Sitter spacetime and its uses. 2011, *arXiv:1110.1206 [hep-th]*
18. Xiaoshen W. A Simple Proof of Descartes's Rule of Signs. *The American Mathematical Monthly*,

2004, vol. 111, no. 6, pp. 525-526. doi: 10.1080/00029890.2004.11920108

19. Byrd P.F., Friedman M.D. *Handbook of Elliptic Integrals for Engineers and Scientists*. Springler Berlin Heidelberg, 2012.
20. Willis N., Didier A., Sonnanburg K. How to compute Puiseux expansion. 2008, *arXiv:0807.4674 [math.AG]*
21. Wall C. T. C. *Singular Points of Plane Curves*, London Mathematical Society Student Texts. Cambridge University Press, 2004. doi: 10.1017/CBO9780511617560
22. Goldstein H. *Classical Mechanics*. Addison-Wesley Publishing Company, 1980.

**Авторы**

**Накибов Руслан Субхиддинович**, магистр физики, ассистент департамента фундаментальной и прикладной физики, ФГАОУ ВО Уральский федеральный университет, ул. Мира, д. 19, г. Екатеринбург, 620149, Россия.
E-mail: nakibov.ruslan@urfu.ru

**Урсулов Андрей Владимирович**, к.ф.-м.н., доцент департамента фундаментальной и прикладной физики, Уральский федеральный университет, ул. Мира, д. 19, г. Екатеринбург, 620002, Россия.
E-mail: AV.Ursulov@urfu.ru

**Просьба ссылаться на эту статью следующим образом:**

Накибов Р. С., Урсулов А. В. Орбиты массивных частиц в сферически симметричном гравитационном поле с учетом космологической постоянной. *Пространство, время и фундаментальные взаимодействия.* 2023. № 3-4. С. 218–228.

**Authors**

**Nakibov Ruslan Subkhiddinovich**, M.Phys., assistant at the department of fundamental and applied physics, Ural Federal University, Mira st., 19, Yekaterinburg, 620149, Russia.
E-mail: nakibov.ruslan@urfu.ru

**Ursulov Andrey Vladimirovich**, Ph.D., Associate Professor at the department of fundamental and applied physics, Ural Federal University, Mira st., 19, Yekaterinburg, 620002, Russia.
E-mail: AV.Ursulov@urfu.ru

**Please cite this article in English as:**

Nakibov R. S., Ursulov A. V. Orbits of massive particles in a spherically symmetric gravitational field in view of cosmological constant. *Space, Time and Fundamental Interactions*, 2023, no. 3-4, pp. 218–228.

УДК 530.12, 681.7



# СНИЖЕНИЕ ТЕПЛОВОГО ШУМА ЗЕРКАЛ В ДЕТЕКТОРЕ ГРАВИТАЦИОННЫХ ВОЛН. КРАТКИЙ ОБЗОР И НЕКОТОРЫЕ НОВЫЕ РЕЗУЛЬТАТЫ*

Пинто И. М.[a,b,c,1]

[a] Итальянский национальный институт ядерной физики (INFN).
[b] ЛВК Научное сотрудничество.
[c] Университет имени Федерико II, Неаполь 80138, Италия (Профессор пенсионер).

Оптические покрытия играют решающую роль в интерферометрических детекторах гравитационных волн. Представлен краткий, актуальный обзор соответствующих областей и результатов исследований, включая новые методы и результаты от исследовательской группы Автора.

*Ключевые слова*: Детекторы гравитационных волн, многослойные оптические покрыти, тепловой шум.

# REDUCING THERMAL NOISE IN THE MIRRORS OF GRAVITATIONAL WAVE DETECTORS. A SHORT REVIEW AND SOME NEW RESULTS

Pinto I. M.[a,b,c,1]

[a] Istituto Nazionale di Fisica Nucleare (INFN), Italy.
[b] LVK Scientific Collaboration.
[c] University Federico II, Napoli 80138, Italy (retired professor).

Optical coatings play a crucial role in interferometric detectors of gravitational waves. A short up-to-date review of related research lines and results is proposed, including new methods and results from the Author's resarch group.

*Keywords*: Gravitational Wave Detectors, Optical Coatings, Thermal Noise.
PACS: 04.80.Nn, 42.79.Wc, 05.40.Ca
DOI: 10.17238/issn2226-8812.2023.3-4.229-246

## 1. Introduction

The spectral coverage of Earth-bound interferometric detectors of gravitational waves (GW), including LIGO [1], Virgo [2] and KAGRA [3] is set by seismic noise and laser shot noise, at low ($\lesssim$ 20Hz) and high ($\gtrsim$ 200Hz) frequencies, respectively. The noise level in the core ($20 - 200\mathrm{H}z$) observation-band is presently dominated by thermal noise in the highly reflecting (HR) coatings of the test masses terminating the optical cavities that make the interferometer arms. A typical 2nd-generation GW detector noise budget is shown in 1.

Coating thermal noise must be suitably reduced, to extend the detectors' range, and is needed to take advantage of already well developed quantum-noise reduction strategies [4].

Efforts to reduce coating thermal noise are ongoing, following different directions. This paper aims to provide a short, yet up-to-date summary of the relevant research lines and achievements, including key references to the topical Literature.

The needed modeling tools are summarized in Appendix-A and -B, where the relevant notation is introduced.

*Работа частично поддерживается «Национальным институтом ядерной физики» (INFN), Италия (проект Virgo). Work funded by "Istituto Nazionale di Fisica Nucleare"(INFN) of Italy (Virgo project).

[1]E-mail: pinto@sa.infn.it

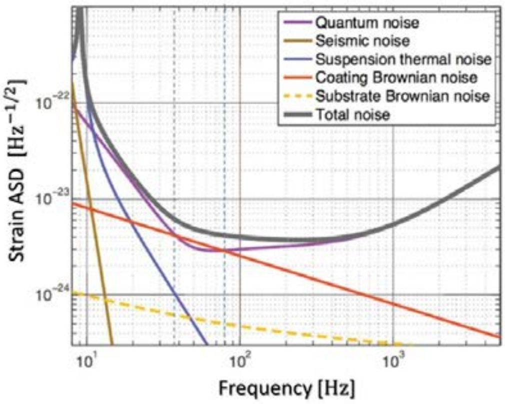


**Рис. 1.** Left: projected noise budget of 2nd generation GW detector (LIGO doc. P0900115). The strain amplitude spectral density and the observation bandwidth determine the detector sensitivity and its visibility range. Right: the aLIGO mirrors coated at CNRS-LMA (Lyon, FR); the coatings are deposited on 35cm⊘, 20cm thick fused silica substrates.

## 2. Materials and Methods

HR coatings consist of $N_T$ homogeneous plane dielectric layers laid on a homogeneous half-space (substrate), as sketched in Figure A1, placed in high-vacuum.
Candidate coating materials, and coating design optimization methods are discussed below.
More *radical* routes to coating thermal noise (CTN) reduction include coating-free mirrors [5], compound mirrors [6] , and grating/diffractive reflectors [7]. These would require substantial modifications to existing detectors.

### 2.1. Coating Materials

The simplest reflective coating design consists of stacked identical pairs of high (H) and low (L) refractive index layers, each pair (doublet) having a total phase thickness of $\psi_H + \psi_L = \pi$ (Bragg condition) [8]. Using Appendix-A it is easily shown that the minimum number $N_D$ of doublets for which the coating transmittance at a reference wavelength does not exceed a prescribed value is a non-increasing piecewise-constant function of the dielectric contrast $n_H/n_L$, which is minimum for $\psi_H = \psi_L = \pi/2$, i.e., for quarter-wavelength (QWL) layers.
On the other hand, as seen from eq. (B.1) of Appendix-B, coating thermal noise increases monotonically with the total metric thickness of the (L) and (H) layers, and the material noise-coefficients (B.2).
It is thus seen that “good” coating material pairs should feature a large optical contrast, and small noise-coefficients (B.2).

#### 2.1.1 Material Downselection

Early material downselection surveys [9], [10] found that $SiO_2$ and $Ta_2O_5$ were the best available option for the L and H materials, featuring also low optical absorption (required to limit thermal deformation of the mirrors [11]) and diffusion. The introduction of $Ti$-doped (co-sputtered) $Ta_2O_5$ was an important step forward [12], yielding a substantial (roughly $-30\%$) reduction of CTN power spectral density (PSD). Other material mixtures were tried, but failed to meet all needed requirements in terms of mechanical losses (thermal noise), optical absorption and scattering [13], with the notable exception of $SiO_2 : TiO_2$ [14]. A 2010 review of candidate coating materials, for use at ambient or cryogenic temperatures, can be found in [15].

### 2.1.2 Exploratory Material Searches

The range of optical coating materials for HR coatings is wide, and includes many oxides, halides, chalcogenides, nitrides, carbides, and a few amorphous metalloids. An exhaustive characterization of such materials and mixtures would require decades, and be fairly expensive.
Only a few beyond those already mentioned have been investigated so far, including, e.g., $MgF_2$ [16], $AlF_3$ [17], $SiC$ [18] and $GaN$ [19].
Also, a number of co-sputtered mixtures, besides $Ti:Ta_2O_5$, have been characterized, including, e.g., $SiO_2:HfO_2$ [20], $Sc_2O_3:Ta_2O_5$ [21], $TiO_2:Nb_2O_5$ [22], $ZrO_2:Ta_2O5$ [23], and $ZrO_2:TiO_2:Ta_2O_5$ [24]. See [25], [26] for comprehensive reviews of viable options. As of today, $Ti:Ta_2O_5$ and $SiO_2$ are still used in all working detectors.
In the last couple of years, much hope and effort has been put into the development of $TiO_2:GeO_2$ mixtures [27],[28]. Coating prototypes using $TiO_2:GeO_2/SiO_2$ doublets recently achieved remarkably low noise levels, a factor $\approx 0.5$ lower in terms of PSD compared to the current $Ti:Ta_2O_5/SiO_2$ based aLIGO design [29]. This is not far from the 0.25 design goal of aLIGO+, but optical absorption is still too high (by a factor $\approx 2$), and defects (bubbles, cracks, delamination) and aging phenomena have been observed [30], whose origin and remediation are not yet fully understood.
Titania-Silica ($TiO_2:SiO_2$) mixtures could be another option, perhaps less-critical, and are also under active development [31].

### 2.1.3 Nanolayered Mixtures

Nanolayered metamaterials are an alternative to co-sputtered mixtures. Modeling their relevant optical and viscoelastic properties is straightforward [32], and their technology faces almost no challenge. Nanolayering $SiO_2:TiO_2$ was shown in [33] to hinder crystallization of $TiO_2$ during post-deposition annealing, thus preventing the ensuing blow-up of optical (and mechanical) losses [1].
It was further found that in nanolayered $SiO_2:TiO_2$ films the mechanical loss-peak observed in Silica films at cryogenic temperatures is almost suppressed [35], [36]. Nanolayered mixtures with high and low refractive index have been discussed [37], [38].
Nanolayered films have been deposited by several Groups. The key role of glass-forming (Silica) nanolayers in preventing interdiffusion has been noted [39]. It has been confirmed that, for some materials, nanolayered mixtures may exhibit lower mechanical losses than their (isorefractive) cosputtered counterparts [40].
In a solid-state perspective, nano-layering can be seen as a wavefunction-confinement strategy, providing a simple *band-gap engineering* tool, whereby both the refractive index and the extinction coefficient of the composite can be tuned almost indendently over relatively wide ranges [41].

### 2.1.4 Mixture Modeling and Process Engineering Tools

Effective medium theories (EMT) [42] provide a simple yet accurate modeling tool to predict the optical properties of mixtures [43]. A formal extension of EMT to visco-elastic properties was formulated in [44], and used in [45] to model $Ti:Ta_2O_5$.
At a more fundamental level, our working knowledge of optical and viscoelastic properties and their interplay [46], [47] is improving, thanks to progress in molecular modeling [48], [49] that sheds light into the link between microscopi structure/morphology and macroscopic properties, [50]-[52], and in perspective, may suggest criteria for *engineering* the materials [53].
Molecular/atomistic modeling has been recently used to simulate film deposition processes [54]-[56]. This may help understanding the non obvious observed dependence of coating properties on deposition

[1]Early coating prototypes based on $TiO_2/SiO_2$ Bragg doublets were spoiled by almost complete crystallization after annealing [34].

technology, assisting gases, substrate heating, etc., and allow for considerable time saving in process optimization.

### 2.1.5 Material Metrology

Research on optical coating materials for interferometric GW detectors triggered important advances in the related Metrology.
The development of techniques [57], [58] for measuring extremely low optical absorption (photon common path interferometry, PCPI) and scattering [59], the invention of new strategies for measuring the thermoelastic and thermorefractive coefficients in thin films and multilayers [60], [61], the introduction of improved setups for multi-mode mechanical ringdown measurement in thin films [62] and the extraction of bulk and shear elastic moduli thereof [63], and of reliable instruments for the *direct* measurement of the thermal noise power spectral density in HR optical coatings and optical thin films [64]-[68] are noteworthy examples.

### 2.1.6 Crystalline Coatings

High-stakes research work has been focused on crystalline materials, offering a potential large reduction of thermal (Brownian) noise [69] in HR coatings. Two possible material options have been explored so far : $GaP/AlGaP$ doublet-stacks grown on (lattice-matched) $c$-Silicon substrate - see [70]-[72], and $GaAs/AlGaAs$ doublet-stacks grown on $GaAs$ and substrate-transferred [73] - see [74] for a recent status report, and a review of relevant technological challenges.
It has been long assumed that thermal noise in crystalline coatings would be dominated by thermo-optic (TO) and photo-thermal (PT) fluctuations. The thermoelastic and thermorefractive components of TO and PT noise [75] may cancel out in part, insofar as they add coherently [76], and cancellation can be maximized by suitably optimizing the layer thicknesses [77]. However, recent measurements in $GaAs/AlGaAs$ coatings found additional birefringence-related extra noise [78], and highly spatially-correlated excess-noise [79], that need to be addressed [2].

### 2.1.7 Silicon Nitrides

Silicon Nitride films have been proposed as candidate materials for both the H and L layers in binary coatings [80]. Plasma-enhanced chemical vapor deposition (PECVD - a technology that has almost no substrate-size limitations) can be used to produce non-stoichiometric $SiN_x$ films with flexible composition, yielding a wide range of refractive indexes, with fairly low mechanical loss angles ($\phi \lesssim 10^{-4}$).
A recently introduced $NH_3$-free PECVD process has further improved the material parameters. Films with $n \approx 2.68$ and $\kappa \approx 1.2 \cdot 10^{-5}$ @1550nm, with $\phi \lesssim 10^{-4}$ down to cryogenic temperatures have been produced [81].
Silicon Nitrides deposited via IBS [25] and IBD [82] are being developed too, and look promising.

### 2.1.8 Amorphous Silicon

Amorphous silicon has been indicated as an excellent candidate for multimaterial coatings [83]-[87], featuring a large refractive index ($n = 3.5$@1550nm), and low mechanical losses, both at ambient ($\phi \approx 10^{-4}$ at 290K) and cryogenic temperatures ($\phi \approx 2 \cdot 10^{-5}$ @ 20K).
Current efforts are focused on reducing its optical absorption [88], and increasing its maximum annealing temperature [89]. As noted in Section 3, $aSi$ could be an effective ingredient for ternary coatings even assuming its optical extinction to remain relatively large (e.g., $\kappa \approx 10^{-3}$); however, increasing its maximum annealing temperature is mandatory, in order to bring the mechanical losses of the other

[2] Spatial fluctuations correlation across the coating face would make the use *wide* beams ineffective to reduce noise.

materials in the coating to comparably (low) values.
As a conclusion, several options exist, with different degrees of reliability and knowledge, for future coating materials, both at ambient and cryogenc temperatures. As of today, Silica and Ti-doped Tantala remain the best known and reliable candidates low- and high-index materials. However, new materials may provide better performances, once stable and reliable deposition protocols are found, especially if used in the advanced optimized designs discussed in the next sub-Section.

### 2.2. Coating Design Optimization

An early insightful analysis of HR binary coatings consisting of identical cascaded doublets of lossy dielectrics, aimed at determining the doublet structure and the number of doublets yielding the largest reflectance at a given wavelength was introduced by Zel'dovich and Vinogradov [90].
The more general case of $m$-ary coatings consisting of stacked $m$-tuplets of $m > 2$ lossy dielectrics was later studied by Larruquert in a series of papers [91]-[93]. He notably pointed out that in order to achieve the largest reflectance, the materials in each $m$-tuplet should be orderd so as to turn *clockwise* in the complex refractive-index plane when moving toward the substrate from one layer to the next in each $m$-tuplet.
In the present context the optimization goal is minimizing coating thermal noise at some assigned transmittance, while also keeping coating absorbance below some prescribed level, and the previous results are not directly applicable.
Robust (genetic) optimization shew that even in this case, the optimal (binary) coating design consists of almost identical stacked quasi-Bragg doublets, where the thickness of the noisier material ($Ti\!:\!Ta_2O_5$, at the time of the study) is trimmed to the advantage of the other one ($SiO_2$). Only a few layers near the coating top and bottom may deviate (slightly) from the above regularity in the optimized design, and can be adjusted sequentially [94]. This suggested a simple iterative coating design procedure [8] that was experimentally validated [95], and eventually adopted to build the aLIGO mirrors [96] used in the first GW observations [97]. A more refined analysis, including subtler effects in [98], led to equivalent results.
Some general bounds to the noise reduction (compared to the simplest QWL design) achievable by the above optimization were obtined in [99].

## 3. Ternary Coatings: Rationale and Early Results

Using three different materials in HR oatings for GW detectors was first suggested in [100], [101], in connection with the development of $aSi$, and demonstrated in [103].
Denote as $L$, $H$ and $H'$ three different materials, and assume that

$$n_{H'}/n_L > n_H/n_L,\ b_L < b_{H'} < b_H,\ \kappa_{H'} \gg \kappa_H \sim \kappa_L. \tag{3.1}$$

where $n - \imath\kappa$ is the complex refractive index, and $b$ the noise coefficient (B.2). In view of (3.1) a coating using $[L|H']$ doublets would exhibit lower mechanical losses (hence noise) but larger absorbance compared to a coating using $[L|H]$ doublets feauring the same transmittance.
The basic idea proposed in [100], [101] is using $H'$ only in the doublets close to the substrate, where the field intensity is sufficiently low to make the larger extinction coefficient of $H'$ harmless [3]. The resulting coating will thus consists of a stack of $N_t$ doublets $[L|H]$ laid on top of a stack of $N_b$ doublets $[L|H']$.
In the simplest case, all layers can be QWL (i.e., with phase thickness $\pi/2$), and the design optimization problem has only two degrees of freedom, $(N_t, N_b)$.
By analogy with the binary case, a better coating design may be obtained by assuming the phase thicknesses

$$\psi_{L,H} = \pi/2(1 \pm \xi),\ \psi_{L,H'} = \pi/2(1 \pm \xi'), \text{with } \xi, \xi' \in (0, 1( \tag{3.2}$$

[3]It was also suggested to put a crystalline layer (or a few high-contrast, low-noise doublets) on top of the coating stack, to further reduce the field transmitted beyond the first layers [102].

whereby all doublets fulfill the Bragg condition. In this case the design/optimization problem has four degrees of freedom $(N_t, N_b, \xi, \xi')$.
The performance of doublet-based ternary designs has been discussed in [104], where also the more general cases of *quasi*-Bragg doublets, and end-layer tweaked stacks have been considered, and shown to provide only marginally better results. The main results of the analysis in [104] are illustrated in Figure 2, that refers to optimized ternary coatings with QWL layers, using $SiO_2$ $(L)$, $Ti\!:\!Ta_2O_5$ $(H)$, $aSi$ $(H')$ on $cSi$ substrate operating at 1550 nm. The figure shows the calculated coating thermal noise reduction factor (w.r.t. the current aLIGO design), for different values of the $H'$ extinction coefficient, under the constraints $\tau_C \leq$ 6ppm and $\alpha_C \leq$ 1ppm.. Each design is identified by the couple of integers $(N_t, N_b)$ representing the number of QWL doublets in the top and bottom stack.
The noise reduction achievable by the triplet-based optimal design discussed in the next Section is also shown for comparison. Note that noise reduction is quite effective even for relatively large values of the the extinction coefficient $\kappa_{H'}$ .
Prototypes of optimized $SiO_2/Ti\!:\!Ta_2O_5/SiNx$ QWL coatings have been deposited and characterized

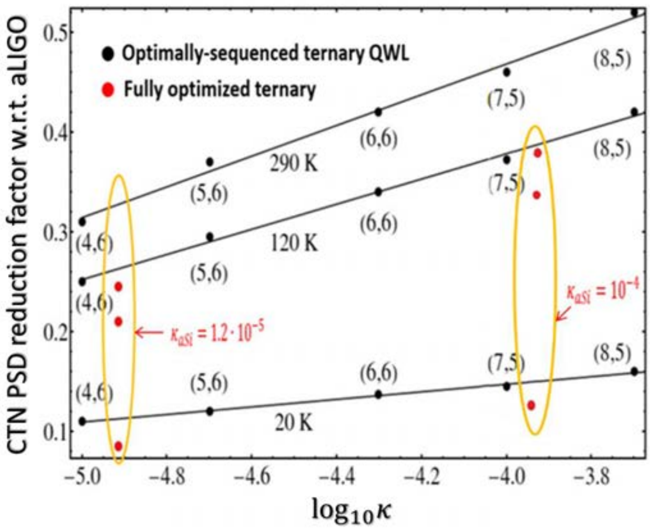


**Рис. 2.** Coating thermal noise PSD reduction factor (w.r.t. the current aLIGO design) for Silica/Ti-doped Tantala/$a$Silicon based ternary coatings with QWL layers, vs log of extinction coefficient of $aSi$. Three different operating temperatures (290, 120, and 20 K) are considered. The red markers refer to the optimized triplet-based design discussed in Section 3.2.

at LMA-CNRS, and their thermal noise has been measured using the MIT-CTN facility, with promising results [105].

### 3.1. Multiobjective M-ary Coating Optimization

Optimizing the design of $M$-ary coatings with $M > 2$ without any prior assumption on the coating structure requires a more general approach.
A coating design is fully specified by the set

$$\mathcal{D} = \{(m_k, \delta_k)|k = 1, 2, \ldots, N_T\} \tag{3.3}$$

where $m_k \in \mathbf{N}$ identifies the material making the $k-$th layer, out of a finite list of candidates, and $\delta_k \in (0, 1/2)$ is the optical thickness of the $k-$th layer. As already stated, the sought optimal design should minimize coating thermal noise (i.e., the coating loss angle $\phi_C$) subject to the constraints[4]

$$\tau_C \leq \tau_0,\ \alpha_C \leq \alpha_0 \tag{3.4}$$

with typical (LIGO) values $\tau_C = 6$ppm and $\tau_C = 1$ppm.

This a constrained/multi-objective optimization problem with *conflicting* requirements. Such problems are most conveniently managed by constructing their Pareto (or tradeoff) manifold P [106]. In our case, P is a 2D-surface in the 3D-space $(\tau_C, \alpha_C, \phi_C)$ (objective-space). Each point of P corresponds to a coating design (a point in the design space) for which (3.4) are met; different points represent different tradeoffs among the conflicting requirements. The manifold P is the set of all *non-dominated designs*, i.e., those designs that are *better* than any other in terms of *at least one* objective, and *not worse* in terms of *all* other objectives.

Constructing the Pareto manifold is nontrivial: exhaustive sampling of the design space is unaffordable due to the combinatorial blow-up of the computational burden with the number of layers, and candidate materials. To attack the problem, meta-heuristics are used [107]- a branch of experimental (i.e., computer aided) Mathematics, that uses an arsenal of robust algorithmic tools like, e.g., evolutionary [108] and co-operative-agent [109] engines, to sample the manifold P as densely/uniformly as possible/needed, capitalizing on the accumulating knowledge about its structure.

To obtain the ternary optimized designs illustrated in the next Subsection we used a state-of-the-art meta-heuristics based tool [110], freely available to non-commercial users [111], that allows to set the desired resolution along each direction in the $(\tau_C, \alpha_C, \phi_C)$ space.

A typical Pareto manifold is shown in Figure 3, for the special case of a ternary coating using $SiO_2$, $Ti:Ta_2O_5$ and $aSi$ with $cSi$ substrate working at $\lambda = 1550nm$ and $T = 20K$. The manifold sections with $\tau_C = 6$ppm and $\alpha_C = 1$ppm are also shown, illustrating the corresponding tradeoff curves.

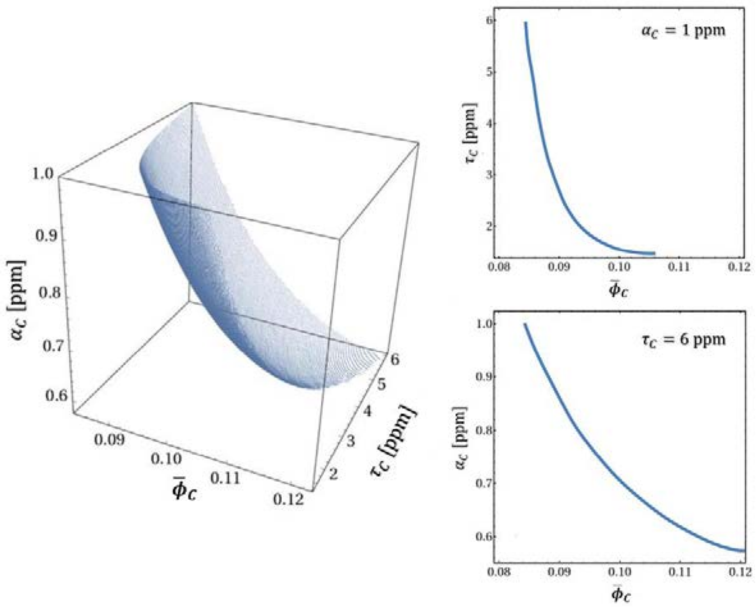


**Рис. 3.** Ternary coating using $SiO_2$, $Ti:Ta_2O_5$ and $aSi$ with $cSi$ substrate working at $\lambda = 1550nm$ and $T = 20K$. Left: computed Pareto manifold in the objective space ($\bar{\phi}_C$ is the coating loss angle scaled to the current aLIGO one). Right: its sections $\tau_C = 6$ppm and $\alpha_C = 1$ppm.

[4]Further constraints, e.g., requiring moderate reflectance at a second wavelength (for alignment purposes) and/or a reflection coefficients phase close to $\pi$ at the working wavelength (so as to minimize the electric field on the coating face, and reduce contamination) may be also enforced.

### 3.2. Some New Results and Discussion

A systematic study of optimized ternary coatings using $SiO_2$ as the low-index (L) material, $aSi$ or $SiNx$ for the large-extinction high-index material (H'), and different ($Ti{:}Ta_2O_5,\ Ti:SiO_2,\ Ti:GeO_2$) for the high-index low extinction material (H) is ongoing, in the above described framework, based on the above framework and tools. A preliminary account can be found in [112].
The typical structure of an optimized ternary coating is illustrated in Figure 4. It consists of triplets $[L|H|H']$ satisfying Larruquert criterion. Close to the coating top and the substrate, the triplets degenerate into $[L|H]$ and $[L|H']$doublets, respectively. In between, there is a group of *bridging* triplets where as we move toward the substrate, the $H$ layers get thinner, while the $H'$ ones become thicker.

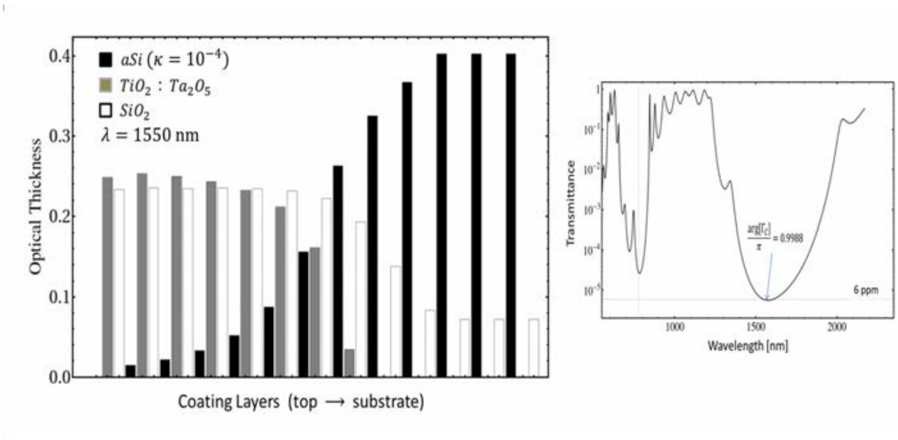


**Рис. 4.** Left: Typical structure of optimized ternary coating. The simulation assumes a $cSi$ substrate and $T = 20K$. The calculated coating thermal noise PSD reduction factor w.r.t. the current aLIGO design is $\approx 0.126$. Right: transmittance vs wavelength. Additional requirements on a second reflectance window, and on the phase of $\Gamma_C$ at the working wavelength are satisfied.

The calculated CTN PSD reduction factor of a number of ternary coatings (both doublet and triplet based) using $SiO_2$, $Ti:SiO_2$ and $aSi$ are collected in the following Table. As anticipated, the CTN

**Таблица 1.** Table I - CTN PSD reduction factor of some optimized ternary coatings fulfilling (3.4) w.r.t. the current aLIGO design.

| *L, H, H'* | Substrate | *λ* [nm] | *T*[*K*] | $\kappa_{H'}$ | CTN PSD reduction factor | | |
|---|---|---|---|---|---|---|---|
| | | | | | Doublet based | | Triplet based |
| | | | | | QWL | Bragg | |
| $SiO_2$, $Ti{:}Ta_2O_5$ | $SiO_2$ | 1064 | 290 | - | 1 | - | - |
| $SiO_2$, $Ti{:}SiO_2$ | $SiO_2$ | 1064 | 290 | - | 0.67 | - | - |
| | | | | | | | |
| $SiO_2$, $Ti{:}SiO_2$, *a*Si | $SiO_2$ | 1550 | 290 | $1.\cdot 10^{-4}$ | 0.284 | 0.251 | 0.234 |
| $SiO_2$, $Ti{:}SiO_2$, *a*Si | $SiO_2$ | 1550 | 290 | $1.\cdot 10^{-3}$ | 0.373 | 0.337 | 0.324 |
| | | | | | | | |
| $SiO_2$, $Ti{:}SiO_2$, *a*Si | cSi | 1550 | 120 | $1.\cdot 10^{-4}$ | 0.126 | 0.119 | 0.097 |
| $SiO_2$, $Ti{:}SiO_2$, *a*Si | cSi | 1550 | 120 | $1.\cdot 10^{-3}$ | 0.163 | 0.151 | 0.141 |
| | | | | | | | |
| $SiO_2$, $Ti{:}SiO_2$, *a*Si | cSi | 1550 | 20 | $1.\cdot 10^{-4}$ | 0.084 | 0.070 | 0.044 |
| $SiO_2$, $Ti{:}SiO_2$, *a*Si | cSi | 1550 | 20 | $1.\cdot 10^{-3}$ | 0.108 | 0.088 | 0.068 |

reduction is quite good (and reaches the aLIGO+ goals) even for relatively large values of the $aSi$ optical extinction.
As a conclusion, we stress that optimized multimaterial coatings may achieve superior performances in terms of CTN, under the given transmittance and absorbance requirements, compared to binary

coatings, using new materials at their present stage of development.

## 4. Conclusion and Recommendations

The science of HR coatings with extremely faible thermal noise has been developing in the last few years, driven by the GW detectors' Community. Its application potential is however not limited to GW detectors, but impacts several fields, including optical frequency standards, ultra-stable clocks, and estreme Metrology at large.

Substantial efforts have been made during the last two decades, and important results have been achieved. Many research directions and tools remain to be explored, though. Studying the properties of more glass-forming materials, e.g., $TeO_2$, and using powerful material modeling tools like, e.g., Kramers-Konig and universal-relaxation relationships may offer new insight into the physics of low-noise optical coatings, and open new directions.

## Acknowledgments

I'm indebted with many Colleagues for fruitful cooperation, and in particular with S. Chao (NTHU), R. DeSalvo, V. Pierro and M. Principe (Sannio U), who co-authored with me most of the papers on coating optimization and nanolayered materials. The results in Sect. 3 are largely based on V. Pierro's extensive coding and simulation work. Valuable discussions with M. Granata, Ch. Michel, L. Mereni, L. Pinard and B. Sassolas all from LMA, from N. Demos (MIT), A. Gretarsson (ERAU), G. Harry (AU), I. Martin, G. McGhee and S. Tait (U Glasgow), E.D. Black and G. Vajente (Caltech), J. Steinlechner (Maastricht U), L. Bellon (ENS Lyon), G. Cagnoli (UCB Lyon), and all fellow members of the USannio/UniSA LVK groups are acknowledged.

Special thanks are due to the PIRT-23 Organizers for their kind invitation, and the highly professional BMSTU Staff for continued support. Большое спасибо !

This work has been funded in part by Italy's National Institute for Nuclear Physics (INFN).

## Список литературы/References

1. J. Aasi et al., Advanced LIGO, *Class. Quantum Grav.* 32 (2015) 074001
2. F. Acernese et al., Advanced Virgo: a 2nd Generation GW Detector, *Class. Quantum Grav.* 32 (2015) 024001
3. T. Akutsu et al., Overview of KAGRA: Detector Design and Construction History, *Progr. Th. Experim. Phys.* 2021 (2021) 05A101
4. LSC, Instrument Science White Paper, *LIGO Document T2200384* (2022) `https://dcc.ligo.org/LIGO-T2200384`
5. S. Gossler et al., Coating-Free Mirrors for High Precision Interferometric Experiments, *Phys. Rev.* A76 (2007) 053810
6. A.G. Gurkovsky et al., Reducing Thermal Noise in Future Gravitational Wave Detectors by Employing Khalili Etalons, *Phys. Lett. A.* 375 (2011) 4147
7. D. Heinert et al., Calculation of Thermal Noise in Grating Reflectors, *Phys. Rev. D.* 88 (2013) 042001
8. I.M. Pinto, M. Principe, R. DeSalvo, Reflectivity and Thickness Optimization, Ch. 12 in *Optical Coatings and Thermal Noise in Precision Measurements,* G. Harry et al., Eds., Cambridge Univ. Press, Cambridge (UK), 2012, ISBN 978-1-107-00338-5.
9. D.R.M. Crookes et al., Experimental Measurements of Mechanical Dissipation Associated with Dielectric Coatings Formed Using $SiO_2$ , $Ta_2O_5$ and $Al_2O_3$, *Class. Quantum Grav.* 23 (2006) 4953
10. G M. Harry, Material Downselect Rationale and Directions, *LIGO Document G-G050088-00-R* `https://dcc.ligo.org/DocDB/0035/G050088/000/G050088-00.pdf`

11. A.F. Brooks et al., Direct Measurement of Absorption-Induced Wavefront Distortion in High Optical Power Systems, *Appl. Opt.* 48 (2009) 355
12. G.M. Harry et al., Titania-Doped Tantala/Silica Coatings for Gravitational-Wave Detection, *Class. Quantum Grav.* 24 (2007) 405
13. R. Flaminio et al., A Study of Coating Mechanical and Optical Losses in View of Reducing Mirror Thermal Noise in Gravitational Wave Detectors, *Class Quantum Grav.* 27 (2010) 084030
14. R.M. Netterfeld, M. Gross, Investigation of Ion-Beam-Sputtered Silica-Titania Mixtures for Use in Gravitational Wave Interferometer Optics, *Proc. OSA-OIC-2007*, paper ThD2
15. J. Franc et al., Mirror Thermal Noise in Laser Interferometer Gravitational Wave Detectors Operating at Room and Cryogenic Temperature, Einstein Telescope Note ET-021-09, *arXiv:0912.0107*
16. M. Granata et al., Optical and Mechanical Properties of Ion-Beam-Sputtered $MgF_2$ Thin Films for Gravitational-Wave Interferometers, *Phys. Rev. Appl.* 17 (2022) 034058
17. M. Bischi et al., Characterization of Ion-Beam-Sputtered $AlF_3$ Thin Films for Gravitational-Wave Interferometers, *Phys. Rev. Applied* 18 (2022) 054074
18. G. Favaro et al., Measurement and Simulation of Mechanical and Optical Properties of Sputtered Amorphous $SiC$ Coatings, *Phys. Rev. Appl.* 18 (2022) 044030
19. M. Segreti et al., Mechanical and Optical Characterization of Sputtered Amorphous GaN Thin Film for High-Reflectvity and Low-Loss Coatings, GWADW 2023 (poster) , `https://agenda.infn.it/event/32907/contributions/200157/attachments/106040/149266/Poster_versione6-2.pdf`
20. K. Craig et al., Mirror Coating Solution for the Cryogenic Einstein Telescope, *Phys. Rev. Lett.* 122 (2019) 231102 1
21. M. Fazio et al., Growth and Characterization of $Sc_2O_3$ Doped $Ta_2O_5$ Thin Films, *Appl. Opt.* 5 (2020) A106
22. A. Amato et al., Optical and Mechanical Properties of Ion-Beam-Sputtered $Nb_2O_5$ and $TiO_2 - Nb_2O_5$ Thin Films for Gravitational-Wave Interferometers and an Improved Measurement of Coating Thermal Noise in Advanced LIGO, *Phys. Rev. D.* 103 (2021) 072001
23. M. Abernathy et al., Exploration of Co-sputtered $Ta_2O_5 - ZrO_2$ Thin Films for Gravitational Wave Detectors, *Class. Quantum Grav.* 38 (2021) 195021
24. E. Lalande et al., Zirconia-Titania-Doped Tantala Optical Coatings for Low Mechanical Loss Bragg Mirrors, *J. Vac. Sci. Technol. A.* 39 (2021) 1
25. M. Granata et al., Progress in the Measurement and Reduction of Thermal Noise in Optical Coatings for Gravitational-Wave Detectors , *Appl. Opt.* 59 (2020) A229
26. M. Fazio et al., Comprehensive Study of Amorphous Metal Oxide and $Ta_2O_5$-based Mixed Oxide Coatings for Gravitational-Wave Detectors, *Phys. Rev. D* 105 (2022) 102008,
27. G. Vajente et al., Low Mechanical Loss TiO2:GeO2 Coatings for Reduced Thermal Noise in Gravitational Wave Interferometers, *Phys. Rev. Lett.* 127 (2021) 071101
28. S. Khadka et al.,Cryogenic Mechanical Loss of Amorphous Germania and Titania-Doped Germania Thin Films, *Class. Quantum Grav.* 40 (2023) 205002
29. A. Davenport, Investigation of $TiO_2 : GeO_2$ for High Reflector Stacks, *LIGO document G2302140*, `https://dcc.ligo.org/LIGO-G2302140`
30. E. Lalande et al, $Ar$ Transport and Blister Growth Kinetics in Titania-doped Germania-based Optical Coatings, *LIGO Document P2300328*, `https://dcc.ligo.org/LIGO-P2300328`
31. G.I. McGhee et al., Titania Mixed with Silica: A Low Thermal-Noise Coating Material for Gravitational-Wave Detectors, *Phys. Rev. Lett.* 131 (2023) 171401

32. I.M. Pinto et al., nm-Layered Amorphous Glassy Oxide Composites for 3rd Generation Interferometric Gravitational Wave Detectors, *LIGO Document-G1401358* (2014), `https://dcc.ligo.org/DocDB/0116/G1401358/001/G1401358.pdf`
33. H.-W. Pan et al., Thickness-Dependent Crystallization on Thermal Anneal for Titania/Silica nm-Layer Composites Deposited by Ion-Beam Sputter Method, *Opt. Express* 22 (2014) 29847
34. P. Amico et al., Investigation on Mechanical Losses in $TiO_2/SiO_2$ Dielectric Coatings, *J. Phys. Conf. Ser.* 32 (2006) 413
35. L.-C. Kuo et al., Low Cryogenic Mechanical Loss Composite Silica Thin Film for Low Thermal Noise Dielectric Mirror Coatings, *Optics Lett.* 44 (2019) 247
36. L.-C. Kuo et al., Annealing Effect on the Nano-meter Scale Titania/Silica Multi-layers for Mirror Coatings of the Laser Interferometer Gravitational Waves Detector, *Proc. of the 2019 PhotonIcs & Electromagnetics Research Symposium (PIERS),* p. 2347
37. I. Pinto, Which Nanolayers are Worth a Try,, LIG*O Document G2000413* (2020) `https://dcc.ligo.org/LIGO-G2000413`
38. I. Pinto, Nanolayered Silica/Alumina Composites, *LIGO Document G2001499* (2020) `https://dcc.ligo.org/LIGO-G2001499`
39. B. Larsen et al., Crystallization in Zirconia Film Nano-Layered with Silica, *Nanomaterials* 11 (2021) 344
40. Le Yang et al., Structural Evolution that Affects the Room-Temperature Internal Friction of Binary Oxide Nanolaminates: Implications for Ultrastable Optical Cavities, ACS Appl. *Nano Mater.* 3 (2020) 12308
41. M. Steinecke et al., Quantizing Nanolaminates as Versatile Materials for Optical Interference Coatings, *Appl. Optics* 59 (2020) A236
42. D.E. Aspnes, Local Field Effects and Effectve-Medium Theory: a Microscopic Perspective, *Am. J. Phys.* 50 (1981) 704
43. O. Stenzel et al., Mixed Oxide Coatings for Optics, *Appl. Opt.* 50 (2011) C69
44. S. Barta, Effective Young's Modulus and Poisson's Ratio for the Particulate Composite, *J. Appl. Phys.* 75 (1994) 3258
45. M. Principe et al., Material Loss Angles from Direct Measurements of Broadband Thermal Noise, *Phys. Rev. D.* 91 (2015) 022005
46. K.S. Gilroy, W.A. Phillips, An Asymmetric Double-Well Potential Model for Structural Relaxation Processes in Amorphous Materials, *Phil. Mag. B.* 43 (1981) 735
47. A. Amato et al., Observation of a Correlation Between Internal Friction and Urbach Energy in Amorphous Oxides Thin Films, *Sci. Rep.* 10 (2020) 1670
48. R. Bassiri et al., Correlations Between the Mechanical Loss and Atomic Structure of Amorphous $TiO_2$-doped $Ta_2O_5$ Coatings, *Acta Mater.* 61 (2013) 1070
49. J.P. Trinastic et al., Molecular Dynamics Modeling of Mechanical Loss in Amorphous Tantala and Titania-Doped Tantala, *Phys. Rev. B.* 93 (2016) 014105
50. T. Damart, D. Rodney, Atomistic Study of Two-level Systems in Amorphous Silica, *Phys. Rev. B.* 97 (2018) 014201
51. K. Prasai et al., Annealing-Induced Changes in the Atomic Structure of Amorphous Silica, Germania, and Tantala Using Accelerated Molecular Dynamic, *Phys. Stat. Sol. B.* 258 (2021) 2000519
52. J. Jiang et al., Amorphous Zirconia-doped Tantala Modeling and Simulations using Explicit Multi-Element Spectral Neighbor Analysis Machine Learning Potentials (EME-SNAP), *Phys. Rev. Mater.* 7 (2023) 045602

53. M. Kim et al., Atomic Structure Characterization of Titania-doped Germania, *LIGO Document G2301799*, https://dcc.ligo.org/LIGO-G2301799
54. M. Turowski, et al., Practice-Oriented Optical Thin Film Growth Simulation via Multiple Scale Approach, *Thin Solid Films* 592 (2015) 240
55. F.V. Grigoriev, V.B. Sulimov, A.V.Tikhonravov, Application of a Large-Scale molecular dynamics approach to modelling the Deposition of $TiO_2$ Thin Films, *Computat. Mater. Sci.* 188 (2021) 110202
56. F.V. Grigoriev, V.B. Sulimov,Atomistic Simulation of Physical Vapor Deposition of Optical Thin Films, *Nanomaterials*, 13 (2023) 1717
57. A. Alexandrovski et al., Photothermal Common-Path Interferometry (PCI): New Developments, *SPIE Proceedings* 7193 (2009) 71930D
58. K.V. Vlasova et al., High-sensitive Absorption Measurement in Transparent Isotropic Dielectrics with Time-resolved Photothermal Common-Path Interferometry, *Appl. Opt.*, 57 (2018) 6318
59. J.R. Smith et al., Apparatus to Measure Optical Scatter of Coatings Versus Annealing Temperature, *Proc. OSA-OIC* 2019, FA.2
60. G.H. Ogin et al., Measuring the Thermo-Optic Response of Dielectric Stack Mirrors, *Proc. OSA-OIC* 2016, MB.7
61. E.M. Gretarsson, A.M. Gretarsson, Three Methods for Characterizing Thermo-Optic Noise in Optical Cavities, *Phys. Rev. D.* 98 (2018) 122004
62. E. Cesarini et al., A 'Gentle' Nodal Suspension for Measurements of the Acoustic Attenuation in Materials, *Rev. Sci. Instrum.* 80 (2009) 053904
63. G. Vajente et al., Method for the Experimental Measurement of Bulk and Shear Loss Angles in Amorphous Thin Films, *Phys. Rev. D.* 101 (2020) 042004
64. K. Numata et al., Wide-Band Direct Measurement of Thermal Fluctuations in an Interferometer, *Phys. Rev. Lett.* 91 (2003) 260602
65. E.D. Black et al., Direct Observation of Broadband Coating Thermal Noise in a Suspended Interferometer, *Phys. Lett. A.* 328 (2004) 1
66. T. Chalermsongsak et al., Broadband Measurement of Coating Thermal Noise in Rigid Fabry–Perot Cavities, *Metrologia* 52 (2015) 17
67. S. Gras, M. Evans, Direct Measurement of Coating Thermal Noise in Optical Resonators, *Phys. Rev. D* 98 (2018) 122001
68. R. Pedurand, Instrumentation for Thermal Noise Spectroscopy, PhD Thesis (2019), Univ. Lyon (FR), 2019, https://theses.hal.science/tel-02612035
69. G.D. Cole et al., Tenfold Reduction of Brownian Noise in High-Reflectivity Optical Coatings, *Nature Photonics* 7 (2013) 644
70. A.C. Lin et al., Epitaxial Growth of GaP/AlGaP Mirrors on Si for Low Thermal Noise Optical Coatings, Opt. *Mater. Express* 8 (2015) 1890
71. A.V. Cumming et al., Measurement of the Mechanical Loss of Prototype GaP/AlGaP Crystalline Coatings for Future Gravitational Wave Detectors, *Class. Quantum Grav.* 32 (2015) 035002
72. P.G. Murray et al., Cryogenic Mechanical Loss of a Single-Crystalline GaP Coating Layer for Precision Measurement Applications, *Phys. Rev. D.* 95 (2017) 042004
73. G.D. Cole et al., High-Performance Near- and Mid-Infrared Crystalline Coatings, *Optica* 3 (2016) 647
74. G.D. Cole et al., Substrate-Transferred GaAs/AlGaAs Crystalline Coatings for Gravitational-Wave Detectors, *Appl. Phys. Lett.* 122 (2023) 110502
75. M.L. Gorodetsky, Thermal Noises and Noise Compensation in High-Reflection Multilayer Coating, *Phys. Lett. A.* 372 (2008) 6813

76. M. Evans et al., Thermo-Optic Noise in Coated Mirrors for High-Precision optical Measurements, *Phys. Rev. D.* 78 (2008) 102003
77. T. Chalermsongsak et al., Coherent Cancellation of Photothermal Noise in $GaAs/Al_{0.92}Ga_{0.08}As$ Bragg Mirrors, *Metrologia* 53 2016 860
78. S. Kryhin, E.D. Hall, V. Sudhir, Thermorefringent Noise in Crystalline Optical Materials, *Phys. Rev. D.* 107 (2023) 022001
79. J. Yu et al., Excess Noise and Photoinduced Effects in Highly Reflective Crystalline Mirror Coatings, *Phys. Rev. X.* 13 (2023) 041002
80. H.-W. Pan et al., Silicon Nitride Films Fabricated by a Plasma-Enhanced Chemical Vapor Deposition Method for Coatings of the Laser Interferometer Gravitational Wave Detector, *Phys. Rev. D.* 87 (2018) 022004
81. D.-S. Tsai et al., Amorphous Silicon Nitride Deposited by an $NH_3$-free Plasma Enhanced Chemical Vapor Deposition Method for the Coatings of the Next Generation Laser Interferometer Gravitational Waves Detector, *Class. Quantum Grav.* 39 (2022) 15LT01
82. G.S. Wallace et al., Non-stoichiometric Silicon Nitride for Future Gravitational Wave Detectors, *LIGO Document P-2300539* (2023), `https://dcc.ligo.org/LIGO-P2300359`
83. P. G. Murray et al., Ion-beam Sputtered Amorphous Silicon Films for Cryogenic Precision Measurement Systems, *Phys. Rev. D* 92 (2015) 062001
84. J. Steinlechner et al., Optical Absorption of Ion-Beam Sputtered Amorphous Silicon Coatings, *Phys. Rev. D* 93 (2016) 062005
85. J. Steinlechner et al., Silicon-Based Optical Mirror Coatings for Ultrahigh Precision Metrology and Sensing, *Phys. Rev. Lett.* 120 (2018) 3602
86. R. Birney et al., Amorphous Silicon with Extremely Low Absorption: Beating Thermal Noise in Gravitational Astronomy, *Phys. Rev. Lett.* 121 (2018) 191101
87. L. Terkowsky et al., Influence of Deposition Parameters on the Optical Absorption of Amorphous Silicon Thin Films, *Phys. Rev. Res.* 2 (2020) 033308
88. M. Molina-Ruiz, Hydrogen-Induced Ultralow Optical Absorption and Mechanical Loss in Amorphous Silicon for Gravitational-Wave Detectors, *Phys. Rev. Lett.* 131 (2023) 256902
89. M. Kinley-Hanlon et al., Update on Nanolayer $aSi/SiO_2$ Coatings and Ion Implantation (SIMOX) Layers for Mechanical Loss,*LIGO Document G2300684* (2023) `https://dcc.ligo.org/LIGO-G2300684`
90. A. V. Vinogradov and Ya. B. Zel'dovich, X-ray and Far UV Multilayer Mirrors: Principles and Possibilities, *Appl. Opt.*, 16 (1977) pp. 89-93
91. J.I. Larruquert, Reflectance Enhancement in the Extreme Ultraviolet and Soft X Rays by Means of Multilayers with More than Two Materials, *J. Opt. Soc. Am.* 19 (2002) pp. 391-397
92. J.I. Larruquert. Inreflectance: a New Function for the Optimization of Multilayers with Absorbing Materials, *J. Opt. Soc. Am.* A22 (2005) 1607.
93. J.I. Larruquert et al., Constructing Multilayers with Absorbing Materials, *Chinese Opt. Lett.* 8 (2010) 159
94. J. Agresti et al., Optimized Multilayer Dielectric Mirror Coatings for Gravitational Wave Interferometers, *Proc. of SPIE*, 6286 (2006) 628608,
95. A.E. Villar et al., Measurement of Thermal Noise in Multilayer Coatings with Optimized Layer Thickness, *Phys. Rev. D* 81 (2010) 122001
96. L.Pinard et al., Mirrors Used in the LIGO Interferometers for First Detection of Gravitational Waves, *Appl. Optics* 56 (2017) C11
97. D.V. Martynov et al., Sensitivity of the Advanced LIGO Detectors at the Beginning of Gravitational

Wave Astronomy, *Phys. Rev. D.* 93 (2016) 112004,

98. N.M. Kondratiev, A.G. Gurkovsky, M.L. Gorodetsky, Thermal Noise and Coating Optimization in Multilayer Dielectric Mirrors, *Phys. Rev. D.* 84 (2011), 022001
99. V. Pierro et al., On the Performance Limits of Coatings for Gravitational Wave Detectors Made of Alternating Layers of Two Materials, *Optical Mater.* 96 (2019) 109269
100. J. Steinlechner et al., Thermal Noise Reduction and Absorption Optimization via Multimaterial Coatings, *Phys. Rev. D* 91 (2015) 042001
101. W. Yam, S. Gras, M. Evans, Multimaterial Coatings with Reduced Thermal Noise, *Phys. Rev. D* 91 (2015) 042002
102. J. Steinlechner, I.W. Martin, High Index Top Layer for Multimaterial Coatings, *Phys. Rev. D.* 93 (2016) 102001
103. S. Tait et al., 'Demonstration of the Multimaterial Coating Concept to Reduce Thermal Noise in Gravitational-Wave Detectors, *Phys. Rev. Lett.* 125 (2020) 011102
104. V. Pierro et al., Ternary Quarter Wavelength Coatings for Gravitational Wave Detector Mirrors: Design Optimization via Exhaustive Search, *Phys. Rev. Res.* 3 (2021) 023172
105. M. Granata et al., Present Results and Future Perspectives of SiNx-based Multi-Material Mirror Coatings, *LIGO Document G2300642* https://dcc.ligo.org/LIGO-G2300642
106. C.A. Coello-Coello et al., Evolutionary Multiobjective Optimization: Open Research Areas and Some Challenges Lying Ahead , *Complex & Intelligent Sys.* 6 (2020) 221
107. C. Blum, A. Roli, Metaheuristics in Combinatorial Optimization: Overview and Conceptual Comparison, ACM *Comput. Surv.* 35 (2003) 268
108. A. Konak, D.W. Coit, A.E. Smith, Multi-Objective Optimization Using Genetic Algorithms: A Tutorial, *J. RESS* 91 (2006) 992
109. M. Dorigo et al., Ant Colony Optimization: Artificial Ants as a Computational Intelligence Technique, *IEEE Computat. Intell. Mag.*, 1 (2006) 28
110. D. Hadka , P.M. Reed , BORG: An Auto-Adaptive Many-Objective Evolutionary Computing Framework, *Evolutionary Computation* 21 (2013) 231
111. http://borgmoea.org/
112. I.M. Pinto et al., Optimized Ternary Coatings : Options and Performance, *LIGO Document G2201509* https://dcc.ligo.org/LIGO-G2201509
113. R. Schnabel et al., Building Blocks for Future Detectors: Silicon Test Masses and 1550 nm Laser Light, *J. Phys. Conf. Ser.* 228 (1010) 012029.
114. R.X. Adikhari et al.,A Cryogenic Silicon Interferometer for Gravitational-wave Detection, *Class. Quantum Grav.* 37 (2020) 165003
115. P.R. Saulson, *Fundamentals of Interferometric Gravitational Wave Detectors,* World Scientific, Singapore, 2017, ISBN 978-9813143074
116. Yu. Levin, Internal Thermal Noise in the LIGO Test Masses: a Direct Approach, *Phys. Rev D.* 57 (1998) 659
117. M.L. Gorodetsky, Thermal Noises and Noise Compensation in High-Reflection Multilayer Coating, *Phys. Lett. A.* 372 (2008) 6813
118. V.B. Braginsky, M.L. Gorodetsky, S.P. Vyatchanin, Compendium of Thermal Noises in Optical Mirrors, Ch. 3 in *Optical Coatings and Thermal Noise in Precision Measurements,* G. Harry et al. (Eds.), Cambridge Univ. Press, Cambridge (UK), 2012, ISBN 978-1-107-00338-5.
119. G.M. Harry et al., Optical Coatings for Gravitational Wave Detection, *Proc. SPIE* 5527 (2004) 33
120. A.G. Gurkovsky and S.P. Vyatchanin, The Thermal Noise in Multilayer Coatings, *Phys. Lett. A.* 374 (2010) 3267

121. M. Fejer, Effective Medium Description of Multilayer Coatings , *LIGO Document T-T2100186*, https://dcc.ligo.org/LIGO-T2100186
122. K. Somiya, K. Yamamoto, Coating thermal Noise of a Finite-Size Cylindrical Mirror, *Phys. Rev. D.* 79 (2009) 102004
123. T. Hong et al., Brownian Thermal Noise in Multilayer Coated Mirrors, *Phys. Rev. D.* 87 (2013) 082001
124. V. Pierro et al., Perspectives on Beam-Shaping Optimization for Thermal-Noise Reduction in Advanced Gravitational-Wave Interferometric Detectors: Bounds, Profiles, and Critical Parameters, *Phys. Rev. D.* 76 (2007) 122003
125. https://cosmicexplorer.org/
126. https://apps.et-gw.eu/tds/?call_file=ET-0028A-20_EinsteinTelescopeScienceCaseDe.pdf
127. I.W. Martin et al., Low Temperature Mechanical Dissipation of an Ion-Beam Sputtered Silica Film, *Class. Quantum Grav.* 31 (2014) 035019
128. I.W. Martin et al., Comparison of the Temperature Dependence of the Mechanical Dissipation in Thin Films of $Ta_2O_5$ and $Ta_2O_5$ doped with $TiO_2$, *Class. Quantum Grav.* 26 (2009) 155012
129. M. Granata et al., Cryogenic Measurements of Mechanical Loss of High-Reflectivity Coating and Estimation of Thermal Noise, *Optics Lett.* 38 (2013) 5268
130. E. Hirose et al., Mechanical Loss of a Multilayer Tantala/Silica Coating on a Sapphire Disk at Cryogenic Temperatures: Toward the KAGRA Gravitational Wave Detector, *Phys. Rev. D.* 90 (2014) 102004

## Appendix A - Coating Reflection and Absorption

Let the coating operate in vacuum, and consist of $N_T$ homogeneous plane layers laid on a homogeneous half-space, as sketched in Figure A1.

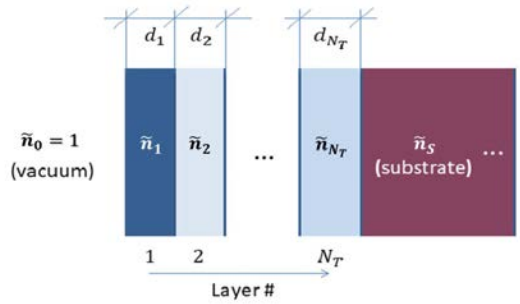


**Рис. A1.** Coating structure and notation

For a monochromatic, locally plane-wave with normal incidence, the transmission matrix of the $m$-th layer is [8]

$$\mathbf{T}_m = \begin{bmatrix} \cos(\psi_m) & (\imath/\tilde{n}_m)\sin(\psi_m) \\ \imath\tilde{n}_m \sin(\psi_m) & \cos(\psi_m) \end{bmatrix}, \tag{A.1}$$

where

$$\psi_m = \frac{2\pi}{\lambda_0}\tilde{n}_m d_m, \tag{A.2}$$

is the layer (complex) phase-thickness, $d_m$ being its metric thickness,

$$\tilde{n}_m = n_m - \imath\kappa_m, \tag{A.3}$$

its complex refractive index, and $\lambda_0$ the free-space wavelength [5]. An $\exp(\imath\omega_0 t)$ time dependence is understood. The transmission matrix (A.1) connects the electromagnetic fields at the input (left, in Figure A1) and output (right) face of the $m$-layer as follows:

$$\begin{bmatrix} E^{(m)} \\ Z_0 E^{(m)} \end{bmatrix} = \mathbf{T}_m \begin{bmatrix} E^{(m+1)} \\ Z_0 H^{(m+1)} \end{bmatrix}, \tag{A.4}$$

$Z_0$ being the free-space characteristic impedance.
The coating optical response is fully described by its transmission matrix $\mathbf{T}$,

$$\mathbf{T} = \mathbf{T}_1 \cdot \mathbf{T}_2 \cdot \cdots \cdot \mathbf{T}_{N_T}. \tag{A.5}$$

The equivalent (complex) refractive index of the whole substrate-terminated coating is,

$$\tilde{n}_C = \frac{T_{21} + \tilde{n}_S T_{22}}{T_{11} + \tilde{n}_S T_{12}}, \tag{A.6}$$

whence the coating reflection coefficient and power transmittance can be written:

$$\Gamma_C = \frac{1 - \tilde{n}_C}{1 + \tilde{n}_C}, \ \tau_C = \frac{\mathcal{P}_{\text{in}}}{\mathcal{P}^+} = 1 - |\Gamma_c|^2, \tag{A.7}$$

$\mathcal{P}_{\text{in}}$ being the power density (power per unit area) flowing into the coating face, and $\mathcal{P}^+$ the power density of the incident wave,

$$\mathcal{P}^+ = \frac{1}{2Z_0}|E_{\text{inc}}|^2. \tag{A.8}$$

The power density dissipated in the coating is

$$\mathcal{P}_{in} - \mathcal{P}_{out}, \tag{A.9}$$

where

$$\mathcal{P}_{\text{out}} = \frac{1}{2}\text{Re}[E^{(S)} H^{(S)*}] \tag{A.10}$$

is the power density flowing into the substrate, $E^{(S)}$ and $H^{(S)}$ being the electric and magnetic fields at the coating/substrate interface,

$$\begin{bmatrix} E^{(S)} \\ Z_0 H^{(S)} \end{bmatrix} = \mathbf{T}^{-1} \begin{bmatrix} E^{(0)} \\ Z_0 H^{(0)} \end{bmatrix} = \mathbf{T}^{-1} \begin{bmatrix} E_{\text{inc}}(1 + \Gamma_C) \\ E_{\text{inc}}(1 - \Gamma_C) \end{bmatrix}. \tag{A.11}$$

The coating absorbance is therefore

$$\alpha_C = \frac{(\mathcal{P}_{\text{in}} - \mathcal{P}_{\text{out}})}{\mathcal{P}^+}. \tag{A.12}$$

Typical design values for the HR coatings of interferometric detectors of gravitational waves are $\tau_C \approx 5ppm$ and $\alpha_C \approx 1ppm$. Transmittance affects the light-storage time (and bandwidth) and the effective optical path-length (and minimum detectable GW geodetic deviation) of the detector; absorbance originates thermal-lensing mirror distortion, that should be actively compensated to avoid alignment loss [115].

### Appendix B - Coating Thermal Noise

The power spectral density (PSD) of coating thermal noise can be derived from the fluctuation-dissipation theorem [116].
Coating thermal noise has multiple origins [117], [118]. We restrict here to Brownian noise, which turns out to be dominant for amorphous metal-oxides based coatings, and assume the same coating structure

[5] Running GW detectors use a 1064nm laser sources; future interferometers may use 1550nm [113] or 2000nm sources [114].

as in Figure A1.
The frequency dependent power spectral density $S_{\text{coat}}^{(B)}(f)$ of coating thermal noise can be written :

$$S_{\text{coat}}^{(B)}(f) = \frac{2k_B T}{\pi^2 w^2 f} \sum_{k=1}^{N_T} b_k d_k, \tag{B.1}$$

where $k_B$ is Boltzmann constant, $T$ the (absolute) temperature, $w$ the (assumed Gaussian) laser-beam waist, $f$ the frequency, $d_k$ the metric thicknesses of the $k$-th coating layer, and

$$b_k = \frac{\phi_k}{Y_S} \left[ \frac{Y_S}{Y_k} \frac{(1+\nu_k)(1-2\nu_k)}{1-\nu_k} + \frac{Y_k}{Y_S} \frac{(1+\nu_S^2)(1-2\nu_S^2)}{(1-\nu_k^2)} \right], \tag{B.2}$$

$\phi$, $Y$ and $\nu$ being the mechanical loss angle and the elastic Young and Poisson moduli, and the suffixes $k$ and $S$ referring to the $k$-th layer and the substrate, respectively.
Equation (B.1) is often rewritten in terms of a whole-coating loss angle $\phi_C$ as

$$S_{\text{coat}}^{(B)}(f) = \frac{2k_B T}{\pi^{3/2} w f Y_S} \phi_C, \text{with } \phi_C = \frac{1}{\pi^{1/2}} \sum_{k=1}^{N_T} \phi_k \frac{d_k}{w} \left[ \frac{Y_S}{Y_k} \frac{(1+\nu_k)(1-2\nu_k)}{1-\nu_k} + \frac{Y_k}{Y_S} \frac{(1+\nu_S^2)(1-2\nu_S^2)}{(1-\nu_k^2)} \right]. \tag{B.3}$$

Equation (B.2) was independently derived in [119] in terms of the elastic moduli for parallel and perpendicular stresses, and in [120], from first principles. More recently, it has been re-obtained in [121], using an effective-medium approach[6]. Equation (B.2) neglects correlation between intra-layer (1st term) and layer-substrate (2nd term) fluctuations, and other subtler effects discussed in [117] - [123].
It is seen from (B.1) that CTN could be reduced by increasing $w$, i.e., the illuminated area (see [124] for a broad discussion), and/or reducing temperature $T$ - a choice made, e.g., for KAGRA and the planned Cosmic Explorer [125]and ET [126] detectors. It should be noted that mechanical loss-peaks at cryo temperatures are observed (with a few notable exceptions, including $TiO_2$) in most coating materials, including $SiO_2$ [127] and $Ta_2O_5$ [128] films [7].
The following remarks are in order:

- material noisyness should *not* be gauged on the basis of the mechanical loss angle $\phi_k$ alone (a frequent/persistent mistake in the technical Literature), since the $b_k$ coefficients (B.2) are strongly dependent on the Young modulus ratio $Y_k/Y_S$ as well (the Poisson moduli have a lesser impact, as seen from Figure B1, being $\nu \approx 0.25$ for all materials of interest);

- computation of the $b_k$ via eq. (B.2) requires accurate knowledge of the elastic moduli and loss angles of the coating materials - which isn't available for many materials of potential interest (the situation is even worse for more complicated noise models, like, e.g., in [123], that depend on additional material parameters);

- loss angle measurements based on mechanical ringdown experiments on single- vs. multi-layer coatings lead to inconsistent results (see the discussion in Sect. V of [45]), for reasons yet to be understood;

- equation (B.1) can be seen as an *operational definition* of the material-dependent coefficients $b_k$. These latter can be cheaply retrieved from direct thermal noise PSD measurements made on a suitable number of different coatings that use the same layer materials, with different total thicknesses. In this connection, several instruments for the direct measurement of coating thermal noise PSD have been devised and built in recent years - see, e.g., [64] - [66], and some are currently in operation [67], [68].

[6]In ref [121] the coefficients B.2 are also written in terms of the bulk and shear elastic moduli.
[7]Cryogenic mechanical loss measurements on multilayer HR films laid on different substrates gave contradictory results [129], [130], for yet unclear reasons.

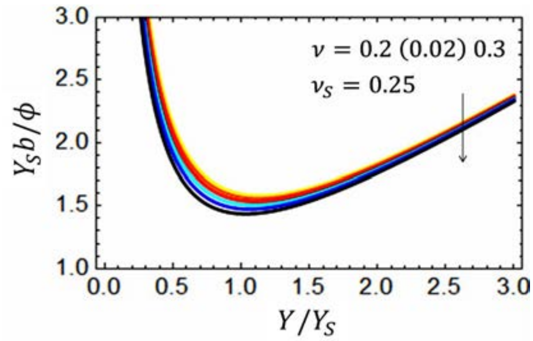


**Рис. B1.** Coating noise coefficient dependence on $Y/Y_S$ for various $\nu$ values and $\nu_S = 0.25$.

**Авторы**

**Пинто Иноченцо М.**, Итальянский национальный институт ядерной физики (INFN); ЛВК Научное сотрудничество; Университет имени Федерико II, Неаполь 80138, Италия (Профессор пенсионер).
E-mail: pinto@sa.infn.it

**Просьба ссылаться на эту статью следующим образом:**
Пинто И. М. Снижение теплового шума зеркал в детекторе гравитационных волн. Краткий обзор и некоторые новые результаты. *Пространство, время и фундаментальные взаимодействия.* 2023. № 3-4. С. 229–246.

**Authors**

**Pinto Innocenzo M.**, Istituto Nazionale di Fisica Nucleare (INFN); LVK Scientific Collaboration; University Federico II, Naples 80138, Italy (retired professor).
E-mail: pinto@sa.infn.it

**Please cite this article in English as:**
Pinto I. M. Reducing Thermal Noise in the Mirrors of Gravitational Wave Detectors. A Short Review and Some New Results. *Space, Time and Fundamental Interactions*, 2023, no. 3-4, pp. 229–246.

УДК 530.12, 539.125.523.32



## ВОЗВРАЩЕНИЕ ПОЛЯ ПРОКА*

Ромеро К.[a,1], Дуарте М. П.[a,2]

[a] Федеральный университет Параибы, г. Жуан-Песота, 58059-970, Бразилия.

Новая версия старой единой теории поля Вейля, основанная на строгом применении принципа калибровочной инвариантности, приводит к появлению массивного векторного поля, которое имеет полностью геометрическую природу и может быть интерпретировано, при некоторых условиях, как поле Прока. Мы исследуем некоторые возможные последствия присутствия этого поля в современном астрофизическом сценарии.

*Ключевые слова*: Единые теории поля, Поле Прока, Темная материя.

## THE COMING BACK OF THE PROCA FIELD

Romero C.[a,1], Duarte M. P.[a,2]

[a] Departamento de Fisica, Universidade Federal da Paraiba, Caixa Postal 5008, Joao Pessoa, PB, Brazil

A new version of the old Weyl's unified field theory based on a strict application of the principle of gauge invariance leads to the appearance of a massive vector field, which has an entirely geometric nature and can be interpreted, under some conditions, as the Proca field. We investigate some possible consequences of the presence of this field in the modern astrophysical scenario.

*Keywords*: Unified field theories, Proca field, Dark matter.

PACS: 04.20.Jb, 11.10.kk, 98.80.Cq

DOI: 10.17238/issn2226-8812.2023.3-4.247-250

### Introduction

Proca's theory appeared in 1936 in the context of the classical and quantum electrodynamics of a massive photon. It was proposed as a model to describe the weak interaction and the motion of spin-1 mesons [1]. Despite its interesting and original ideas, the model did not survive too long and soon gave away to other proposals, being subsequently almost forgotten. However, the quanta of the Proca field would reappear as the massive gauge bosons $Z$ , $W^+$ and $W_-$in the standard model of particle physics [2]. Recently, there has appeared new motivation to reconsider the role that Proca's field can play in other areas of physics. Mention to the Proca field mainly appears coming from two distinct contexts. Firstly, the idea of the presence of a massive vector field in the universe is motivated by current research in astrophysics and cosmology, namely, the dark matter problem [3]. Indeed, it has been argued that the massive vector field considered earlier by nuclear physicists can play a role in modelling what is called dark matter. The second motivation comes from the folowing fact: In standard gravitation theory, i.e., general relativity, the Proca field does not appear in a natural way, and has to be put in by hand as a matter field in much the same way as we do in the case of other physical (i.e, non-geometrical) fields. However, a recent proposed theory of gravity, deeply inspired in the original Weyl's unified field theory, seems to suggest the appearance of a massive vector field, which has an entirely geometrical nature.

*C. Romero and M. P. Duarte would like to thank, respectively, CNPq and FAPESQ-PB for funding this research.

[1]E-mail: cromero@fisica.ufpb.br

[2]E-mail: mauro.parnaiba@estudantes.ufpb.br

### A. Weyl's theory

Let us recall that, in his attempt to unify gravity with electromagnetism, H. Weyl developed a new geometry, which constitutes one of the simplest generalizations of Riemannian geometry [4]. Recently Weyl's unified field theory was significantly reframed into a modified theory of gravity in order to allow matter to couple with the geometry in a gauge-invariant way [5]. This is done by strictly following a prescription of "minimum coupling which complies with the principle of gauge invariance postulated by Weyl. An interesting outcome of this procedure comes as an unexpected appearance of a vector field in the gravitation sector of the action. As it happens, for some choices of both the values of the cosmological constant $\Lambda$ and $\omega$ ( a free parameter of the theory) this vector field may be formally interpreted as a massive vector field satisfying an equation that is identical to Proca equation. Moreover, unlike the fact that the original Proca field, defined in Minkowski spacetime is not gauge-invariant, a fact that is characteristics of massive fields, here we should emphasize that the gauge invariance of the geometrical vector field is granted by first principles. Finally, let us remark that the investigation of massive vector fields within the framework of general relativity has been done by several authors [6]. A particularly interesting development of this line of research has recently shown the possibility of cosmic inflation being driven by a vector field [7].

### B. The field equations

Let us start by recalling that the field equations in the Weyl's invariant theory are given by [5]

$$\frac{1}{\sqrt{-g}}\partial_\nu\left(\sqrt{-g}F^{\mu\nu}\right)=\frac{3\Lambda}{2\omega}\sigma^\mu, \tag{B.1}$$

$$\widetilde{R}_{\mu\nu}-\frac{1}{2}\widetilde{R}g_{\mu\nu}+\frac{\Lambda}{4}g_{\mu\nu}+\frac{3}{2}(\sigma_\mu\sigma_\nu-\frac{1}{2}g_{\mu\nu}\sigma^\alpha\sigma_\alpha)=\frac{\omega}{\Lambda}T_{\mu\nu}-\kappa T^{(m)}_{\mu\nu}, \tag{B.2}$$

where $\widetilde{R}_{\mu\nu}$ and $\widetilde{R}$ denote, respectively, the Ricci tensor and the scalar curvature defined with respect to the Riemannian connection, $\sigma$ is a 1-form field, $T_{\mu\nu}=F_{\mu\alpha}F^{\alpha}_{\ \nu}+\frac{1}{4}g_{\mu\nu}F_{\alpha\beta}F^{\alpha\beta}$ and $T^{(m)}_{\mu\nu}$ represents the energy-momentum tensor of matter, $\kappa$ being a coupling constant. Let us make a short comment on the role of $\sigma$. In Weyl's original approach, $\sigma$ led naturally to a new notion of curvature, a sort of "length curvature"represented by the 2-form $F=d\sigma$ (*Streckenkrummung*) in addition to the "direction curvature"(*Richtungkrummung*), the latter given by the Riemann tensor [4]. To his amazement, Weyl found that the length curvature $F=d\sigma$ presents striking similarities with the electromagnetic tensor, and it was this discovery, together with the invariance of his modified compatibiliy condition (between the metric and the affine connection), that led him to the attempt to geometrize the electromagnetic field. It is worth of mention here that the discovery of this new symmetry, which Weyl called *gauge symmetry,* is now celebrated as one of the most significant facts in the history of modern physics: it represents the birth of modern gauge theories [8].

Let us remark that the above equations may be obtained from varying the action given by

$$S=\int d^4x\sqrt{-g}[\widetilde{R}+\frac{\omega}{2\Lambda}F_{\mu\nu}F^{\mu\nu}+6\sigma_\mu\sigma^\mu-\frac{\Lambda}{2}+\kappa L_m],$$

which is identical to the action of the Proca's neutral spin-1 field in curved space-time with the cosmological constant coupled to gravity.

It is not difficult to verify that the equation B.2 can be rewritten as

$$\tilde{R}_{\mu\nu}-\frac{1}{2}\tilde{R}g_{\mu\nu}+\frac{\Lambda}{4}g_{\mu\nu}=\frac{\omega}{\Lambda}T^{(P)}_{\mu\nu}-\kappa T^{(m)}_{\mu\nu}, \tag{B.3}$$

where $L_m$ denotes the Lagrangian density of matter, and

$$T^{(P)}_{\mu\nu}=F_{\mu\alpha}F^{\alpha}_{\ \nu}+\frac{1}{4}g_{\mu\nu}F_{\alpha\beta}F^{\alpha\beta}\ -\frac{3\Lambda}{2\,\omega}\left(\sigma_\mu\sigma_\nu-\frac{1}{2}g_{\mu\nu}\sigma_\alpha\sigma^\alpha\right). \tag{B.4}$$

### C. The original Proca's theory

Let us start by writing the Lagrangian assumed by Proca in his theory. As is well known, the 4-potential $A^{\alpha}$ may be thought as a massive vector boson field that governs the weak interaction and the motion of spin-1 mesons. Proca's equation describe this kind of fields and is frequently used in quantum field theory [1]. The mentioned Lagrangian has the form

$$L = -\frac{1}{16\pi c} F_{\alpha\beta} F^{\alpha\beta} + \frac{m^2}{8\pi c} A^{\alpha} A_{\alpha}, \tag{C.1}$$

where $m$ is the mass of the field and $c$ is the speed of light. The energy-momentum tensor of the Proca field obtained from the above Lagrangian will be given by

$$T_{\mu\nu} = F_{\mu\alpha} F^{\alpha}_{\ \nu} + \frac{1}{4} g_{\mu\nu} F_{\alpha\beta} F^{\alpha\beta} + m^2 \left( A_{\mu} A_{\nu} - \frac{1}{2} g_{\mu\nu} A_{\alpha} A^{\alpha} \right). \tag{C.2}$$

By comparing (C.2) with (B.4), we see that $T^{(P)}_{\mu\nu}$ may be formally considered as the energy-momentum tensor of the Proca field provided that we define $m = \sqrt{-\frac{3\Lambda}{2\,\omega}}$ as its mass. (If $\Lambda > 0$ is interpreted as the cosmological constant, then we must set $\omega < 0$). In virtue of the analogy with Proca theory, it seems plausible to reinterpret the former Weyl field $\sigma$ not as the electromagnetic field, as Weyl did, but as a sort of massive vector field, which enters the theory through a purely geometrical reasoning.

### Possible applications of the Proca geometrical field in modern astrophysics

One of the main open questions in modern astrophysics, still unsolved, is to know what is the nature of the so-called *dark matter* [3]. As is well known, it is a component of the universe whose presence is inferred from its gravitation attraction rather than its luminosity. Dark matter does not interact with ordinary matter and is believed to be composed of not yet discovered subatomic particles. In the Lambda-CDM model it is thought to be responsible for approximately 26,8% of the total energy of the cosmos. Some proposed candidates for explaining dark matter are *wimps*, *primordial black holes* and *axions*. Recently, however, there have appeared new proposals considering the possibility of the Proca field being a component of dark matter [9].

### Conclusion

The reinterpretation of Weyl's theory considered here allows us to build models to treat the origin of dark matter in a different way. Indeed, there is no longer need to explain why we cannot detect the nature of the supposed non-interacting particles and fields which constitute dark matter. This is because, in this approach, their nature is entirely geometric. We only need to consider a modified form of the theory of general relativity [10].

### Список литературы/References


1. A. Proca, J. Phys. Radium, **7**, 347 (1936). Veja, por exemplo, W. Greiner, e J. Reinhardt, *Field Quantization* (Springer, 1996).
2. D. J. Griffiths, *Introduction to Elementary Particles* (John Wiley & Sons, 1987).
3. Sean Carroll, Dark Matter, Dark Energy: *The dark side of the universe*. (The Teaching Company. Guidebook(2007)
4. Weyl, H. (1918). Gravitation und Elektrizität, *Sitzungesber Deutsch. Akad. Wiss. Berlin, 465*. Adler, A., Bazin, M. and Schiffer, M. (1975). *Introduction to General Relativity*, Ch. 15 (McGraw-Hill).
5. T. A. T. Sanomiya, I. P. Lobo, J. B. Formiga, F. Dahia, and C. Romero, *Phys. Rev. D* **102**, 124031 (2020).

6. G. E. Tauber, J. Math. Phys. **10**, 633 (1968). S. Changsheng, Z. Liu, Int. *J. Theor. Phys,* **44**, 303 (2005).
7. L. Ford, *Phys. Rev. D* **40**, 967 (1989).
8. L. O'Raiefeartaigh, *The Dawning of Gauge Theory* (Princeton University Press, 1997).
9. R. W. Tucker and C. Wang, *Nucl. Phys. B* **57**, 259 (1997). L. Gabriel Gómez, Yeinzon Rodríguez, *Phys. Dark Univ.* **31**, 100759. In connection with this, see also A. Loeb and N. Weiner, *Phys. Rev. Lett.* **106**, 171302 (2011).
10. For other geometrical proposal of modelling dark matter, see P. Burikan et al, *Phys. Rev. D* **107**, 064008 (2023).


**Авторы**


**Карлос Августо Ромеро Фильо**, д.ф.-м.н., доцент кафедры "Физика", Федеральный Университеть Параибы, Жуан-Песоса, 58059-970, Бразилия.
E-mail: cromero@fisica.ufpb.br

**Мауро Парнаиба Дуарте**, к.ф.-м.н., кафедра "Физика", Федеральный Университеть Параибы, Жуан-Песоса, 58059-970, Бразилия.
E-mail: mauro.parnaiba@estudantes.ufpb.br


**Просьба ссылаться на эту статью следующим образом:**


Ромеро К., Дуарте М. П. Возвращение поля Прока. *Пространство, время и фундаментальные взаимодействия.* 2023. № 3-4. С. 247–250.


**Authors**


**Carlos Augusto Romero Filho**, Ph.D., Associate Professor, Departamento de Fisica, Universidade Federal da Paraiba, Caixa Postal 5008, 58059-970 Joao Pessoa, PB, Brazil
E-mail: cromero@fisica.ufpb.br

**Mauro Parnaiba Duarte**, PhD Student, Departamento de Fisica, Universidade Federal da Paraiba, Caixa Postal 5008, 58059-970 Joao Pessoa, PB, Brazil
E-mail: mauro.parnaiba@estudantes.ufpb.br


**Please cite this article in English as:**


Romero C., Duarte M. P. The Coming Back of the Proca Field. *Space, Time and Fundamental Interactions*, 2023, no. 3-4, pp. 247–250.

УДК 530.12



# СТАНДАРТНО-МЕРНЫЕ СИСТЕМЫ ПРЕОБРАЗОВАНИЙ ДЛЯ СПЕЦИАЛЬНОЙ ТЕОРИИ ОТНОСИТЕЛЬНОСТИ

Салума С.[a,1], Тауфик А. Н.[b,2]

[a] Университет Сохага, г. Сохаг, 82524, Египет.

[b] Университет будущего в Египте, г. Новый, 11835, Египет.

Мы представляем комплексную систему, включающую стандартные и размерные системы отсчета. Мы предлагаем теорию, состоящую из трех взаимосвязанных систем преобразований. Стандартно-мерная система преобразований сочетается с размерно-мерной системой преобразований, соответствующей типичному преобразованию Лоренца-Эйнштейна и стандартно-мерной системой. Скорость, с которой движется размерная рамка, играет решающую роль для того, чтобы уравнение сферических волн Максвелла оставалось инвариантным, а переход волновой природы света в природу частиц подчинялся системе преобразований.

Согласованность предложенных стандартно-мерных систем преобразований можно также проверить в следствиях. Мы привели уравнения массы и энергии свободной частицы и обнаружили, что скорость частицы и скорость движущейся рамки являются существенными. Мы также пришли к выводу, что уравнение Шредингера остается инвариантным при предложенных преобразованиях. Дальнейшие следствия для явлений, бросающих вызов специальной относительности, могут быть получены в другом месте.

*Ключевые слова*: Специальная относительность, системы отсчета, стандартные и размерные величины, основы квантовой механики.

# STANDARD-DIMENSIONAL TRANSFORMATION SYSTEMS FOR SPECIAL RELATIVITY

Salouma S.[a,1], Tawfik A. N.[b,2]

[a] Sohag University, Sohag, 82524, Egypt.

[b] Future University in Egypt, Новый Каир, 11835, Egypt.

We introduce a comprehensive framework comprising standard and dimensional reference frames. We suggest a theory composed of three interconnected transformation systems. The standard-dimensional transformation system is combined with a dimensional-dimensional transformation system corresponding to the typical Lorentz–Einstein transformation and the standard-standard system. The velocity at which the dimensional frame moves plays a crucial role so that the Maxwell spherical wave equation remains invariant and the transition of the wave-nature to particle-nature of light becomes subject to the transformation system.

The consistency of the proposed standard-dimensional transformation systems can also be examined in implications. We drove the mass and energy equations of a free particle and found that the particle's velocity and that of the moving frame are essential. We also conclude that the Schrodinger equation remains invariant under the proposed transformation. Further implications to the phenomena challenging special relativity could be carried out elsewhere.

*Keywords*: Special Relativity; Reference Frames; Standard and Dimensional Values; Foundations of Quantum Mechanics.

PACS: 04.20.-q

DOI: 10.17238/issn2226-8812.2023.3-4.251-270

[1]E-mail: email@mail.ru

[2]E-mail: email2@inbox.ru

### A. Introduction

The recently observed violations of some principles of the special theory of relativity urged theoretical interpretation and experimental confirmation to be proposed [1, 2, 3]. The Lorentz invariance violation [4, 5, 6, 7, 8, 9] and deformed special relativity (DSR) [10, 11] including doubly special relativity [12, 13] and modified dispersion relations [14, 15, 16] are a few examples to be recalled. The present script suggests an alternative i) to preserve the special theory of relativity but instead ii) to take into consideration Einstein's original ideas about *"time"* and *"space"* including the distinction between *"position"* and *"place"* [17, 18] and iii) to account for the situations where the observer would be incapable of tracking the trajectory of the motion [18, 19]. To resolve the observed violations of some special relativity principles, the restriction to the standard-standard transformation system is relaxed and a standard-dimensional transformation system shall be proposed.

The trio of event, reference frame, and observer can be categorized according to the observer's capability of monitoring the movement trajectory:

- Observer cannot monitor the movement trajectory: a set of values for time and space is perceived. These are the standard values.
- Observer can monitor the movement trajectory: a set of values for time and space known as dimensional values are then perceived. These are the dimensional values.

Let us assume that the stationary frame has i) the standard values $(x', y', z', t')$ and ii) dimensional values $(x, y, z, t)$. Accordingly, i) the standard values $(\xi', \eta', \zeta', T')$ and ii) dimensional values $(\xi, \eta, \zeta, T)$ can be assigned to the moving frame. From the definition of the inertial reference frame in special relativity [20], the spacetime transformation of an event from an inertial reference frame with velocity $\upsilon$ to an observer in a stationary inertial reference encompasses four types of spacetime transformations.

1. From the standard values of a stationary frame (rest) to the standard values of a moving frame (standard-standard system),
2. From standard values of a stationary frame (rest) to dimensional values of a moving frame (standard-dimensional system),
3. From the dimensional values of a stationary frame (rest) to the standard values of a moving frame (dimensional-standard system), and
4. From the dimensional values of a stationary frame (rest) to the dimensional values of a moving frame (dimensional-dimensional system).

With standard-dimensional, we mean that the frame of standard values is at rest while the frame of dimensional values is moving. Equivalently, with dimensional-standard, we refer to the frame of dimensional values which is at rest, while the frame of standard values moves. For the sake of simplicity, we suggest to combine both transformations into one category, standard-dimensional transformation system. Thus, the transformations in special relativity can be categorized into standard-standard, standard-dimensional, and dimensional-dimensional transformation systems.

In this regard, we emphasize that the standard values within a frame are unaffected by the frame's motion. But upon leaving the frame, the standard values become impacted. Therefore, the relationship between the standard values in a stationary frame and the ones in a moving frame relies on an unknown function $\delta(\upsilon)$.

The standard-dimensional transformation system entails transformation between the standard values conceived by an observer in a stationary frame and the corresponding dimensional values in a moving frame with velocity $\upsilon$. Moreover, this system also represents the transformation between the dimensional values observed by an observer in a stationary frame and the corresponding standard values in a moving frame with velocity $\upsilon$.

It should be noticed that the conclusions drawn from the three spacetime transformation systems are based on the following assumptions:

1. All laws of physics are subject to the standard-standard transformation system.

2. The physical laws which are subject to the dimensional-dimensional transformation system is also subject to the standard-dimensional transformation system with an assertion that the transition of the wave-nature to particle-nature of light under the standard-dimensional transformation system [20]. The physical laws which are not subject to the dimensional-dimensional transformation system will be subject to the standard-dimensional transformational system without any additional ingredients.

3. Under a standard-dimensional transformation, the speed of light in free space, $c$, remains constant across all inertial reference frames regardless their relative motion to the source or each another, and

4. The standard-dimensional transformation occurs in a homogeneous and isotropic spacetime [21].

When referring to subjecting laws to a specific transformation system, it implies that the laws remain consistent across all inertial reference frames within that transformation system.

This paper is structured as follows. The formalism is outlined in section B. The transformations under standard-dimensional system are introduced in section B.1. The velocity transformation and Maxwell spherical wave equation under standard-dimensional transformation system are derived in sections B.1.3 and B.1.4, respectively. The spacetime transformation under dimensional-dimensional system is given in section B.2. The results are discussed in section C. As examples, we first discuss the mass and energy under the standard-dimensional transformation system in section C.1. Then, in section C.2, the Schrödinger equation shall be derived under the standard-dimensional transformation system. Section D is devoted to the conclusions.

## B. Formalism

We assume that the reference frame describing an event is denoted by $k$ and has the dimensional values $(\xi, \eta, \zeta, T)$ and the standard values $(\xi', \eta', \zeta', T')$ of the spacetime. Also, let us assume that the reference frame describing an observer is denoted by $\mathbf{K}$ whose dimensional and standard values are $(x, y, z, t)$ and $(x', y', z', t')$, respectively. In this regards, we emphasize that under the standard-dimensional transformation system, the reference frame $k$ moves with velocity $\upsilon$ in the direction of increasing $\mathbf{x}$-axis relative to the observer's frame $\mathbf{K}$.

### B.1. Standard-Dimensional Transformation Systems

In this section, we introduce comprehensive details about the proposed standard-dimensional transformation system. As introduced, such a transformation comprises two kinds. The first one is the translation from the observer's standard values in a stationary frame to the dimensional values in a frame which moves at velocity $\upsilon$ (standard-dimensional). The second one is the translation of the observer's dimensional values in a stationary frame to the standard values in a frame which moves at velocity $\upsilon$ (dimensional-standard).

#### B.1.1 Spacetime under Standard-Dimensional Transformation System

How the standard values observed by an observer in a stationary frame are to be transformed to the corresponding dimensional values in a moving frame with velocity $\upsilon$? By using the specification of the standard-standard transformation system as a guide, we can suggest an answer to this question.

First, we express the spacetime transformations under standard-standard system

$$\begin{aligned}
&(i)\;\; x' = \delta(\upsilon)\xi', \\
&(ii)\; y' = \delta(\upsilon)\eta', \\
&(iii) z' = \delta(\upsilon)\zeta', \\
&(iv)\; t' = \delta(\upsilon)T'.
\end{aligned} \tag{B.1}$$

This transformation system is valid regardless whether the frame moves in the direction of increasing $x$-axis or in the opposite direction. The set of transformations, Eq. (B.1), shall be utilized in deriving the standard-dimensional transformation system.

For an event in $k$, we assume that the origin points of $k$ and $\mathbf{K}$ were identical, at a dimensional time $T_0$ and a corresponding standard time in $t'$ in $\mathbf{K}$. We then suggest that a ray of light is emitted from the origin point at the time $T_o$ along the $\xi$-axis and propagates in the direction of increasing $\xi$-axis. We also assume that the ray of light has to cover a standard distance $\xi'$ over the time $T_1$ before it reflects back to its origin point in $k$. The ray of light returns in time $T_2$. Based on the assumptions outlined in section A, we can now express the relationships in $k$ as

$$T_2 - T_1 = T_1 - T_0, \qquad \frac{1}{2}\left(T_o + T_2\right) = T_1. \tag{B.2}$$

From the definition of the dimensional values, we then conclude that

$$T = T\left(\xi', \eta', \zeta', T'\right), \quad T_0 = T\left(0,0,0,T_0'\right), \quad T_1 = T\left(\xi', 0, 0, T_1'\right), \quad T_2 = T\left(0,0,0,T_2'\right). \tag{B.3}$$

Also, when a ray of light is emitted along the $\xi$-axis, the concept of forward and backward directions is then applicable to the standard values of *"place"* in the $\xi'$ dimension. However, this concept does not apply to $(\eta', \zeta')$ dimensions. Then, we obtain

$$T_0' = \frac{t'}{\delta(\upsilon)}, \qquad T_1' = T_0' + \frac{\xi'}{c} = \frac{t'}{\delta(\upsilon)} + \frac{\xi'}{c}, \qquad T_2{}' = T_0' + \frac{\xi'}{c} - \frac{\xi'}{c} = \frac{t'}{\delta(\upsilon)}. \tag{B.4}$$

When substituting these quantities into Eq. (B.2), we get

$$\frac{1}{2}\left[T\left(0,0,0,\frac{t'}{\delta(\upsilon)}\right) + T\left(0,0,0,\frac{t'}{\delta(\upsilon)}\right)\right] = T\left(\xi', 0, 0, \frac{t'}{\delta(\upsilon)} + \frac{\xi'}{c}\right). \tag{B.5}$$

By differentiating Eq. (B.5) with respect to $t'$ and applying $t'/\delta(\upsilon) + \xi'/c = \rho$, we obtain

$$\frac{1}{2}\left[\frac{2}{\delta(\upsilon)}\frac{\partial T}{\partial t'}\right] = \frac{1}{\delta(\upsilon)}\frac{\partial T}{\partial \rho}, \qquad \frac{\partial T}{\partial \rho} = \frac{\partial T}{\partial t'}. \tag{B.6}$$

Now, by differentiating Eq. (B.5) with respect to $\xi'$ and applying $\partial\rho/\partial\xi' = 1/c$, we find

$$\frac{\partial T}{\partial \xi'} + \left(\frac{1}{c}\frac{\partial T}{\partial \rho}\right) = 0, \tag{B.7}$$

in which Eq. (B.6) can be substituted,

$$\frac{\partial T}{\partial \xi'} + \frac{1}{c}\frac{\partial T}{\partial t'} = 0. \tag{B.8}$$

With this regard we emphasize that the origin point of a coordinate system would be any other point of the ray's starting position. As a result, Eq. (B.8) holds true for all possible values of $(\xi', \eta', \zeta')$. The same conclusion could be drawn for $\eta'$- and $\zeta'$-axes. It is important to realize that when observed from the stationary frame, the ray of light consistently travels along these axes, at the speed of light $c$, and therefore, the variation in both term of Eq. (B.8) vanish,

$$\frac{\partial T}{\partial \eta'} = 0, \qquad \frac{\partial T}{\partial \zeta'} = 0. \tag{B.9}$$

Now we recall expression (iv) in Eq. (B.1), that of the standard-standard transformation system, as well as (B.3), and (B.9). This allows to draw the conclusion that $T$ represents a function, $T = T(t', \xi')$,

$$T = a \cdot t' + b \cdot \xi', \tag{B.10}$$

where $a$ and $b$ are constants. Here, the partial differentials of Eq. (B.10) with respect to $t', \xi'$, separately, lead to

$$\frac{\partial T}{\partial t'} = a, \qquad \frac{\partial T}{\partial \xi'} = b. \tag{B.11}$$

From Eqs. (B.8) and (B.11), $b$ can be related to $a$,

$$b \;\; = \;\; -\frac{1}{c}a. \tag{B.12}$$

whose substitution into Eq. (B.10) leads to

$$T \;\; = \;\; a\left(t' - \frac{1}{c}\xi'\right). \tag{B.13}$$

By substituting $t' = x'/c$ and $\xi' = x'/\delta(\upsilon)$, whose relationship reads $t' = \delta(\upsilon)\xi'/c$, into Eq. (B.13) and applying $\xi = cT$, we get

$$\xi = a\left[\delta(\upsilon) - 1\right]\xi'. \tag{B.14}$$

When taking into account that $\xi' = x' - \upsilon t'/\delta(\upsilon)$, which expresses the motion of the reference frame $k$, we conclude that

$$x' = \frac{\xi\delta(\upsilon)}{a\left[\delta(\upsilon) - 1\right]} + \upsilon t'. \tag{B.15}$$

Now, we consider that a ray of light is emitted along the $\eta$-axis in the direction of its increment and covers the standard distance $\eta'$. This leads to

$$T = a\left(t' - \frac{\eta'}{c}\right). \tag{B.16}$$

Given that $t' = y'/c$ and $\eta' = y'/\delta(\upsilon)$, Eq. (B.16) can be reexpressed as

$$T = \frac{a}{c}\left(1 - \frac{1}{\delta(\upsilon)}\right)y'. \tag{B.17}$$

By using $\eta = cT$, we can derive that

$$y' = \frac{\delta^2(\upsilon)}{a\left[\delta(\upsilon) - 1\right]}\frac{\eta}{\delta(\upsilon)}. \tag{B.18}$$

Similarly, for a ray of light which is emitted along $\zeta$-axis in the direction of its increment and intersects the axis at the standard distance $\zeta'$, then

$$T = a\left(t' - \frac{\zeta'}{c}\right). \tag{B.19}$$

Given that $t' = z'/c$ and $\zeta' = z'/\delta(\upsilon)$ and by using $\zeta = cT$, we obtain

$$z' = \frac{\delta^2(\upsilon)}{a\left[\delta(\upsilon) - 1\right]}\frac{\zeta}{\delta(\upsilon)}. \tag{B.20}$$

We are now able to determine $t'$. Since $\xi' = x'/\delta(\upsilon)$ and $\xi' = cT'$, we find that

$$T' = \frac{x'}{c\delta(\upsilon)}. \tag{B.21}$$

Then from Eq. (B.15) and Eq. (B.21), we conclude that

$$T' = \frac{1}{\delta(\upsilon)}\left(\frac{\xi}{c}\frac{\delta(\upsilon)}{a\left[\delta(\upsilon)-1\right]} + \frac{\upsilon t'}{c}\right). \tag{B.22}$$

By substituting $\xi/c = T$ and $t'/\delta(\upsilon) = T'$ into Eq. (B.22), we obtain

$$\frac{T\delta(\upsilon)}{a\left[\delta(\upsilon)-1\right]} = t'\left(1-\frac{\upsilon}{c}\right), \tag{B.23}$$

$$t' = \frac{\delta^2(\upsilon)}{a\left[\delta(\upsilon)-1\right]}\frac{T}{(1-\frac{\upsilon}{c})\delta(\upsilon)}. \tag{B.24}$$

Let $\varphi(\upsilon) = \delta^2(\upsilon)/a(\delta(\upsilon)-1)$. Then, we get

$$t' = \frac{\varphi(\upsilon)}{(1-\frac{\upsilon}{c})\delta(\upsilon)}T. \tag{B.25}$$

Now, we are ready to derive the spacetime transformations under standard-dimensional system. This comprises various cases as follows.

(i) When the frame $k$ moves with velocity $\upsilon$ in the direction of increasing $x$-axis

$$\begin{aligned}
&(i)\;\; x' = \varphi(\upsilon)\left[\frac{\xi}{\delta(\upsilon)} + \frac{\upsilon}{\left(1-\frac{\upsilon}{c}\right)\delta(\upsilon)}T\right],\\
&(ii)\; y' = \varphi(\upsilon)\frac{\eta}{\delta(\upsilon)},\\
&(iii) z' = \varphi(\upsilon)\frac{\zeta}{\delta(\upsilon)},\\
&(iv)\; t' = \frac{\varphi(\upsilon)}{(1-\frac{\upsilon}{c})\delta(\upsilon)}T.
\end{aligned} \tag{B.26}$$

Alternatively, when substituting Eq. (B.25) into Eqs. (B.15), (B.18), and (B.20), we obtain the same transformations as in Eq. (B.26).

(ii) When the frame $k$ moves at velocity $\upsilon$ in the direction of increasing $x$-axis (inverse transformation), we find that

$$\begin{aligned}
&(i)\;\; \xi = \frac{\delta(\upsilon)}{\varphi(\upsilon)}\left[x' - (\upsilon t')\right],\\
&(ii)\; \eta = \frac{\delta(\upsilon)}{\varphi(\upsilon)}y',\\
&(iii) \zeta = \frac{\delta(\upsilon)}{\varphi(\upsilon)}z',\\
&(iv)\; T = \frac{\delta(\upsilon)(1-\frac{\upsilon}{c})}{\varphi(\upsilon)}t'.
\end{aligned} \tag{B.27}$$

(iii) In a specific scenario that the frame $\bar{k}$ moves at velocity $\upsilon$ in the opposite direction of increasing $x$-axis, an observation can be made but within the frame $\bar{\mathbf{K}}$. When assuming that the standard values of the frame $\bar{\mathbf{K}}$ read $(\bar{x}', \bar{y}', \bar{z}', \bar{t}')$ and the dimensional values of the frame $\bar{k}$ read $(\bar{\xi}, \bar{\eta}, \bar{\zeta}, \bar{T})$, then, we get

$$\begin{aligned}
&(i)\;\; \bar{x}' = \varphi(-\upsilon)\left[\frac{\bar{\xi}}{\delta(-\upsilon)} - \frac{\upsilon}{\left(1+\frac{\upsilon}{c}\right)\delta(-\upsilon)}\bar{T}\right],\\
&(ii)\; \bar{y}' = \varphi(-\upsilon)\frac{\bar{\eta}}{\delta(-\upsilon)},\\
&(iii) \bar{z}' = \varphi(-\upsilon)\frac{\bar{\zeta}}{\delta(-\upsilon)},\\
&(iv)\; \bar{t}' = \varphi(-\upsilon)\frac{\bar{T}}{(1+\frac{\upsilon}{c})\delta(-\upsilon)},
\end{aligned} \tag{B.28}$$

where $\varphi(-\upsilon) = \delta^2(-\upsilon)/\{\bar{a}\,[\delta(-\upsilon) - 1]\}$.

(iv) The fourth case deals with the inverse transformation of the previous case. When the frame $\bar{k}$ moves at velocity $\upsilon$ in the opposite direction of increasing $x$-axis, we then find that

$$
\begin{aligned}
&(i)\ \ \bar{\xi} = \frac{\delta(-\upsilon)}{\varphi(-\upsilon)}\left[\bar{x'} + \left(\upsilon\bar{t'}\right)\right],\\
&(ii)\ \bar{\eta} = \frac{\delta(-\upsilon)}{\varphi(-\upsilon)}\bar{y'},\\
&(iii)\bar{\zeta} = \frac{\delta(-\upsilon)}{\varphi(-\upsilon)}\bar{z'},\\
&(iv)\ \bar{T} = \frac{\delta(-\upsilon)}{\varphi(-\upsilon)}\left(1 + \frac{\upsilon}{c}\right)\bar{t'}.
\end{aligned}
\tag{B.29}
$$

Now, we are capable of describing different scenarios and even the wave front of the light pulse.

1. From the four sets of standard-dimensional transformation systems, Eqs. (B.26) - (B.29), we can define two scenarios as follows.

   (a) First scenario: if the dimensional values of the frame $k$ are equivalent to the dimensional values of the frame $\bar{k}$, i.e., $(\xi, \eta, \zeta, T) = (\bar{\xi}, \bar{\eta}, \bar{\zeta}, \bar{T})$, then from Eqs. (B.27) and (B.29), the inverse transformations, we obtain that

   $$\frac{\delta(\upsilon)}{\varphi(\upsilon)}\left[x' - (\upsilon t')\right] = \frac{\delta(-\upsilon)}{\varphi(-\upsilon)}\left[\bar{x'} + \left(\upsilon\bar{t'}\right)\right]. \tag{B.30}$$

   Since $(\xi, \eta, \zeta, T = (\bar{\xi}, \bar{\eta}, \bar{\zeta}, \bar{T}))$, it follows that $(x', y', z', t') = (\bar{x}', \bar{y}', \bar{z}', \bar{t}')$. Because the only possible condition which invalidates forward and backward directions should be $\upsilon = 0$. Then, the concept of direction along and opposite the frame of reference disappears, i.e., $(x', y', z', t')_{\upsilon=0} = (\bar{x}', \bar{y}', \bar{z}', \bar{t}')_{\upsilon=0}$, and we obtain

   $$\frac{\delta(\upsilon)}{\varphi(\upsilon)}x' = \frac{\delta(-\upsilon)}{\varphi(-\upsilon)}x'. \tag{B.31}$$

   From $\delta(\upsilon)_{\upsilon=0} = \delta(-\upsilon)_{\upsilon=0} = 1$, it is obvious to conclude that,

   $$\varphi(\upsilon) = \varphi(-\upsilon), \tag{B.32}$$

   i.e., equivalent forward and backward motion.

   (b) Second scenario: if the standard values of the frame **K** are equivalent to the dimensional values of the frame $\bar{k}$. Then from Eqs. (B.26) and (B.29), we obtain

   $$\frac{\delta(-\upsilon)}{\varphi(-\upsilon)}\left(\bar{x'} + \left(\upsilon\bar{t'}\right)\right) = \varphi(\upsilon)\left[\frac{\xi}{\delta(\upsilon)} + \frac{\upsilon}{\left(1 - \frac{\upsilon}{c}\right)\delta(\upsilon)}T\right]. \tag{B.33}$$

   The condition $\left(\bar{x'}, \bar{y'}, \bar{z'}, \bar{t'}\right)_{\upsilon=0} = (\xi, \eta, \zeta, T)_{\upsilon=0}$ allows to rewrite Eqs. (B.33) as

   $$\frac{\delta(-\upsilon)}{\varphi(-\upsilon)}\bar{x'} = \frac{\varphi(\upsilon)}{\delta(\upsilon)}\bar{x'}, \tag{B.34}$$

   which in turn leads to

   $$\varphi(\upsilon)\varphi(-\upsilon) = \delta(\upsilon)\delta(-\upsilon). \tag{B.35}$$

   From $\delta(\upsilon)_{\upsilon=0} = \delta(-\upsilon)_{\upsilon=0} = 1$, Eq. (B.35) can be rewritten as

   $$\varphi(\upsilon)\varphi(-\upsilon) = 1. \tag{B.36}$$

   Then, with Eq. (B.32), we obtain

   $$\varphi(\upsilon) = \varphi(-\upsilon) = 1, \tag{B.37}$$

   i.e., a normalization condition.

2. To describe the wave front of the light pulse, an alternative set of the spacetime transformations must be formulated. Based on the information provided so far and the conditions outlined in section A, the wave front of the light pulse is then described as

$$\begin{aligned} \xi &= cT, && \text{(B.38)} \\ x' &= ct'. && \text{(B.39)} \end{aligned}$$

By substituting (iv) of Eqs. (B.1) into Eq. (B.39), we get

$$x' = c\delta(v)T'. \tag{B.40}$$

Also, by substituting Eq. (B.38) and Eq. (B.40) into (i) of Eq. (B.26),

$$\delta^2(v)T' = T + \frac{\frac{v}{c}}{1-\frac{v}{c}}T. \tag{B.41}$$

From the assumption 3 which was introduced in section A and the propagation of ray of light in a straight line, we notice that $T = T'$. Therefore, with simple mathematical operations, we get

$$\delta(v) = \frac{1}{\sqrt{1-\frac{v}{c}}}. \tag{B.42}$$

Similarly, it is easy to find that

$$\delta(-v) = \frac{1}{\sqrt{1+\frac{v}{c}}}. \tag{B.43}$$

Now, we can apply this to the set of spacetime transformations under the standard-dimensional system of special relativity, Eq. (B.26),

$$\begin{matrix} (i)\ x' = \dfrac{\xi}{\delta(v)} + v\delta(v)T, \\ (ii)\ y' = \dfrac{\eta}{\delta(v)}, \\ (iii)\ z' = \dfrac{\zeta}{\delta(v)}, \\ (iv)\ t' = \delta(v)T \end{matrix}. \tag{B.44}$$

### B.1.2 Spacetime under Dimensional-Standard Transformation System

The second case derives a set of equations for the transformation of spacetime under dimensional-standard system. This translates the dimensional values observed by an observer in a stationary frame to the corresponding standard values in a moving frame with velocity $v$. According to Eq. (B.44), when the moving frame $k$ is stationary within the standard-dimensional transformation system, the dimensional values $(\xi, \eta, \zeta, T)$ become equivalent to the standard values $(x', y', z', t')$. Consequently, when the moving frame $k$ is at rest, the dimensional values $(x, y, z, t)$ become equivalent to the standard values $(\xi', \eta', \zeta', T')$. Therefore, we consider the process of establishing a stationary state for the moving frame $k$ by aligning it with respect to $(x, y, z, t)$ and $(\xi', \eta', \zeta', T')$. To this end, another frame is utilized, This is a frame moving at velocity $v$ in the opposite direction of increasing $x$-axis within the standard-dimensional system. The motion of this frame impacts both $\mathbf{K}$ and $k$. Consequently, to establish the values $(\xi', \eta', \zeta', T')$ and $(x, y, z, t)$ at the rest of the standard-dimensional transformation system without impacting both frames, $k$ and $\mathbf{K}$, we suggest to follow a procedure as follows.

- The values $(\xi', \eta', \zeta', T')$ when transformed to the corresponding ones in the frame $\mathbf{K}$ become $(x', y', z', t')$. The latter values within the frame $\mathbf{K}$ have motion in the direction of increasing $x-$axes.

- Since the frame **K** is at rest, we can apply a frame with velocity $\upsilon$ in the opposite direction of increasing $x$-axes whose values are $(x', y', z', t')$. By transformation, this now frame get the values $(x, y, z, t)$.

  In this regard, we draw two conclusions.

- The concept of opposite direction of velocity does appear in $x$ and $t$ dimensions only, because the movements of $y$ and $z$ are not influenced by the concept of opposite direction of increasing $x$-axis. Hence, the standard values $x'$ and $t'$ are affected by the value of $\delta(-\upsilon)$, while the standard values $y'$ and $z'$ are affected by the value of $\delta(\upsilon)$. In addition, the values of $x'$ and $t'$ represent the observed values outside the frame, while the standard values $y'$ and $z'$ represent the observed values within the frame.

- Based on the foregoing information and the spacetime transformations in a generalized form under the standard-standard system, it is possible to deduce that the standard values observed outside the frame are equal to the standard values observed inside the frame multiplied by the velocity function, $\upsilon$-function.

  Accordingly, the dimensional values $x$ and $t$ can be expressed as

$$\begin{aligned} x &= \frac{x'}{\delta(-\upsilon)}, \\ t &= \frac{t'}{\delta(-\upsilon)}, \end{aligned} \tag{B.45}$$

while the values $y$ and $z$ read

$$\begin{aligned} y &= \delta(\upsilon)y', \\ z &= \delta(\upsilon)z'. \end{aligned} \tag{B.46}$$

From the standard-standard transformation system, Eqs. (B.45) and (B.46), we can summarize both kinds of spacetime transformation under standard-dimensional system,

1. the set of equations describing the spacetime transformation under standard-dimensional system when the frame $k$ moves with velocity $\upsilon$ in the direction of increasing $x$-axis is given as

$$\begin{aligned} &(i)\ \ x = \frac{\delta(\upsilon)}{\delta(-\upsilon)}\xi', \\ &(ii)\ y = \delta^2(\upsilon)\eta', \\ &(iii) z = \delta^2(\upsilon)\zeta', \\ &(iv)\ t = \frac{\delta(\upsilon)}{\delta(-\upsilon)}T', \end{aligned} \tag{B.47}$$

2. we can now derive the spacetime transformations under standard-dimensional system by repeating the same steps when the frame $k$ moves with velocity $\upsilon$ in the opposite direction of increasing $x$-axis

$$\begin{aligned} &(i)\ \ \bar{x} = \frac{\delta(-\upsilon)}{\delta(\upsilon)}\bar{\xi}', \\ &(ii)\ \bar{y} = \delta^2(-\upsilon)\bar{\eta}', \\ &(iii) \bar{z} = \delta^2(-\upsilon)\bar{\zeta}', \\ &(iv)\ \bar{t} = \frac{\delta(-\upsilon)}{\delta(\upsilon)}\bar{T}'. \end{aligned} \tag{B.48}$$

Obviously, we find that the velocity plays a crucial role in the proposed theory of the standard-dimensional transformation system. In the section that follows, we derive the velocity transformations under the same system.

### B.1.3 Velocity under Standard-Dimensional Transformation System

To derive the velocity under standard-dimensional transformation system in frame $k$ which moves with velocity $\upsilon$ in the direction of increasing $x$-axis, we have two scenarios.

1. **The first scenario** deals with the transformation between the observer's standard values in a stationary frame and the corresponding dimensional values in a moving frame. By differentiating the expression (i) of Eqs. (B.44) with respect to $t'$, we get

$$\frac{dx'}{dt'} = \frac{1}{\delta(\upsilon)}\left(\frac{d\xi}{dT}\frac{dT}{dt'}\right) + \delta(\upsilon)\upsilon\frac{dT}{dt'}, \tag{B.49}$$

and by differentiating the expression (iv) of Eqs. (B.44) with respect to $t'$, we obtain

$$1 = \delta(\upsilon)\frac{dT}{dt'} \Rightarrow \frac{dT}{dt'} = \frac{1}{\delta(\upsilon)}. \tag{B.50}$$

The substitution of Eq. (B.50) into Eq. (B.49) leads to

$$\frac{dx'}{dt'} = \frac{1}{\delta^2(\upsilon)}\frac{d\xi}{dT} + \upsilon. \tag{B.51}$$

Hence, the velocity in the $x$-axis reads

$$u_{x'} = \frac{u_\xi}{\delta^2(\upsilon)} + \upsilon, \tag{B.52}$$

where $u_{x'} = dx'/dt'$. Likewise, the velocity transformations in $y$- and $z$-axis can be expressed, respectively, as

$$\begin{aligned} u_{y'} &= \frac{u_\eta}{\delta^2(\upsilon)}, \\ u_{z'} &= \frac{u_\zeta}{\delta^2(\upsilon)}. \end{aligned} \tag{B.53}$$

2. **Second scenario** elaborates the transformation between the observer's dimensional values in a stationary frame and the corresponding standard values in a moving frame.

By differentiating the expression (i) of Eqs. (B.47) with respect to $t$, we find that

$$\frac{dx}{dt} = \frac{\delta(\upsilon)}{\delta(-\upsilon)}\left(\frac{d\xi'}{dT'}\frac{dT'}{dt}\right). \tag{B.54}$$

Also, by differentiating the expression (iv) of Eqs. (B.47) with respect to $t$, we obtain

$$1 = \frac{\delta(\upsilon)}{\delta(-\upsilon)}\frac{dT'}{dt} \to \frac{dT'}{dt} = \frac{\delta(-\upsilon)}{\delta(\upsilon)}. \tag{B.55}$$

Then, the substitution of Eq. (B.55) into Eq. (B.54) leads to

$$\frac{dx}{dt} = \frac{d\xi'}{dT'}. \tag{B.56}$$

Hence, the velocity transformation in the $x$-axis reads

$$u_x = \frac{dx}{dt} = u_{\xi'}. \tag{B.57}$$

Likewise, the velocity transformations in $y$- and $z$-axis can be respectively expressed as

$$u_y = \frac{dy}{dt} = \delta(\upsilon)\delta(-\upsilon)u_{\eta'}, \tag{B.58}$$

$$u_z = \frac{dy}{dt} = \delta(\upsilon)\delta(-\upsilon)u_{\zeta'}. \tag{B.59}$$

Now, we conclude this section by studying the Maxwell spherical wave equation in spacetime transformations under standard-dimensional system, section B.1.4.

### B.1.4 Maxwell Spherical Wave Equation under Standard-Dimensional Transformation System

To study the Maxwell spherical wave equation under standard-dimensional transformation system [22, 23], we assume that the frame $k$ moves at velocity $\upsilon$ in a specific direction relative to an observer in the frame $\mathbf{K}$. Furthermore, we suggest that at time $t = T = 0$, the origins and axes of both frames, $k$ and $\mathbf{K}$, coincide. Also, we assume that a light pulse, which was emitted at time $t = T = 0$ in the frame $\mathbf{K}$ has a spherical wave front which is characterized by

$$x^2 + y^2 + z^2 = c^2 t^2, \qquad (x')^2 + (y')^2 + (z')^2 = c^2 (t')^2. \tag{B.60}$$

Based on the assumptions outlined in section A, the wave front of light pulse when observed from the perspective of the frame $k$ has two scenarios.

First scenario considers the difference between the observer's standard values in a stationary frame and the corresponding dimensional values in a moving frame at velocity $\upsilon$ along the direction of increasing $x$-axis. In view of Eqs. (B.44) and the second part of Eq. (B.60), we obtain

$$\left[\frac{\xi}{\delta(\upsilon)} + (\delta(\upsilon)\upsilon T)\right]^2 + \left[\frac{\eta}{\delta(\upsilon)}\right]^2 + \left[\frac{\zeta}{\delta(\upsilon)}\right]^2 = c^2 \left[\delta(\upsilon)T\right]^2. \tag{B.61}$$

Therefore,

$$\xi^2 + \eta^2 + \zeta^2 + \upsilon^2\delta^4(\upsilon)T^2 + 2\delta^2(\upsilon)\xi\upsilon T - c^2\delta^4(\upsilon)T^2 = 0. \tag{B.62}$$

Let us assume $\xi^2 + \eta^2 + \zeta^2 = c^2 T^2$. Then, we find that

$$\left[\frac{c^2}{\delta^4(\upsilon)} + \upsilon^2 - c^2\right]\delta^2(\upsilon)T = -2\xi\upsilon. \tag{B.63}$$

With some substitutions, we reach at the wave front

$$\xi \quad = \quad cT. \tag{B.64}$$

Second scenario considers the difference between the observer's dimensional values in a stationary frame and the corresponding standard values in a moving frame at velocity $\upsilon$ along the direction of increasing $x$-axis. In view of Eqs. (B.47) and the first part of Eq. (B.60), we obtain

$$\left[\frac{\delta(\upsilon)}{\delta(-\upsilon)}\right]^2 (\xi')^2 + \delta^4(\upsilon)\,(\eta')^2 + \delta^4(\upsilon)\,(\zeta')^2 = \left[\frac{\delta(\upsilon)}{\delta(-\upsilon)}\right]^2 c^2\,(T')^2. \tag{B.65}$$

Therefore,

$$\frac{\left(1+\frac{\upsilon}{c}\right)^2 (\xi')^2}{\left(1+\frac{\upsilon}{c}\right)\left(1-\frac{\upsilon}{c}\right)} + \frac{(\eta')^2}{\left(1+\frac{\upsilon}{c}\right)\left(1-\frac{\upsilon}{c}\right)} + \frac{(\zeta')^2}{\left(1+\frac{\upsilon}{c}\right)\left(1-\frac{\upsilon}{c}\right)} \quad = \quad \frac{\left(1+\frac{\upsilon}{c}\right)^2 c^2\,(T')^2}{\left(1+\frac{\upsilon}{c}\right)\left(1-\frac{\upsilon}{c}\right)}. \tag{B.66}$$

This implies that

$$(\xi')^2 + \frac{\upsilon^2}{c^2}(\xi')^2 + 2\frac{\upsilon}{c}(\xi')^2 + (\eta')^2 + (\zeta')^2 = c^2\,(T')^2 + \upsilon^2\,(T')^2 + 2\upsilon c\,(T')^2. \tag{B.67}$$

With the assumption that $(\xi')^2 + (\eta')^2 + (\zeta')^2 = c^2(T')^2$, the wave front becomes

$$\xi' = cT'. \tag{B.68}$$

To summarize the findings of this section, we recall the analytical observation that the Maxwell spherical wave equation which was determined under spacetime transformations of the standard-dimensional-type is found invariant, i.e., the Maxwell spherical wave equation remains unchanged although this type of spacetime transformations. Furthermore, this constancy can be interpreted as being conditioned to the motion within the frame $k$ which follows a straight line parallel to the $x$-axis with velocity equal to the speed of light, $c$. Also, according to principles of optics, which assert that the phenomena resulting from the propagation of light in straight lines support the hypothesis that light has particle-nature, this type of motion seems to be consistent with the particle's behavior. As a result of these observations and by consulting refs. [24, 25], we conclude that the spacetime transformations under standard-dimensional system adheres to the second assumption outlined in section A.

### B.2. Spacetime under Dimensional-Dimensional Transformation System

In this section, we delve into the dimensional-dimensional transformation system. As the dimensional values are in the moving frame, we divide the moving observer's frame into two possible directions. The first case considers that the frame $k$ moves at velocity $\upsilon$ *in the same direction* of increasing $x$-axis. The second case counts for frame $k$ which moves at velocity $\upsilon$ *in the opposite direction* of increasing $x$-axis.

Case 1: Spacetime transformations under dimensional-dimensional system in the frame $k$ which moves at velocity $\upsilon$ in the same direction of increasing $x$-axis. In view of Eqs. (B.44), Eqs. (B.45) and Eqs. (B.46), we obtain,

$$\begin{aligned} &(i)\ \ x = \frac{\xi}{\delta(\upsilon)\delta(-\upsilon)} + \frac{\delta(\upsilon)}{\delta(-\upsilon)}\upsilon T,\\ &(ii)\ y = \eta,\\ &(iii) z = \zeta,\\ &(iv)\ t = \frac{\delta(\upsilon)}{\delta(-\upsilon)}T. \end{aligned} \tag{B.69}$$

From the identities $\delta(\upsilon) = 1/\sqrt{1-\frac{\upsilon}{c}}$ and $\delta(-\upsilon) = 1/\sqrt{1+\frac{\upsilon}{c}}$, the corresponding set of dimensional-dimensional transformation equations becomes

$$\begin{aligned} &(i)\ x = \frac{\xi}{\sqrt{1-\frac{\upsilon^2}{c^2}}} + \frac{\delta(\upsilon)}{\delta(-\upsilon)}\upsilon T,\\ &(ii)\ y = \eta,\\ &(iii)\ z = \zeta,\\ &(iv)\ t = \frac{T}{\left(1-\frac{\upsilon}{c}\right)/\sqrt{1-\frac{\upsilon^2}{c^2}}}. \end{aligned} \tag{B.70}$$

From the third assumption introduced in section A, we notice that the wave front of the light pulse can be described by

$$\xi = cT, \qquad\qquad t = \frac{x}{c}. \tag{B.71}$$

Let $\gamma = 1/\sqrt{1-\frac{\upsilon^2}{c^2}}$, then we get

$$T = \gamma\left[t - t\frac{\upsilon}{c}\right]. \tag{B.72}$$

From $t = \frac{x}{c}$ for the light pulse [22], we find that

$$T = \gamma\left[t - \frac{\upsilon x}{c^2}\right]. \tag{B.73}$$

Then, in view of expression (i) in Eq. (B.70), we obtain

$$x = \frac{\xi}{\gamma} + \frac{\delta(\upsilon)}{\delta(-\upsilon)}\upsilon T. \tag{B.74}$$

By substituting Eq. (B.73) into (**??**), we get

$$x - \frac{xv^2}{c^2} = \frac{1}{\gamma}(\xi + vT). \tag{B.75}$$

Therefore, we suggest that

$$x = \gamma(\xi + vT). \tag{B.76}$$

Also, by substituting Eq. (**??**) into (B.73), we arrive at

$$t = \frac{T}{\gamma} + \frac{xv}{c^2}. \tag{B.77}$$

Hence, we derive $t$

$$\begin{aligned} t &= \frac{T}{\gamma} + \frac{v}{c^2}\left(\frac{\xi}{\gamma} + vt\right), \\ t - \frac{tv^2}{c^2} &= \frac{T}{\gamma} + \frac{v}{c^2}\frac{\xi}{\gamma}, \\ t &= \gamma\left(T + \frac{v\xi}{c^2}\right). \end{aligned} \tag{B.78}$$

This allows to summarize the dimensional-dimensional transformation system as

$$\begin{aligned} &(i) \;\; x = \gamma(\xi + vT), \\ &(ii) \; y = \eta, \\ &(iii) z = \zeta, \\ &(iv) \; t = \gamma\left(T + \frac{v\xi}{c^2}\right). \end{aligned} \tag{B.79}$$

It is obvious that Eq. (B.79) represents the inverse Lorentz–Einstein spacetime transformations in special relativity [18, 22].

Case 2: The spacetime transformations under dimensional-dimensional system in the case that the frame $k$ moves at velocity $v$ in the opposite direction to increasing $x$-axis. Based in Eq. (B.79), we obtain

$$\begin{aligned} &(i) \;\; \bar{x} = \gamma\left(\bar{\xi} - v\bar{T}\right), \\ &(ii) \; \bar{y} = \bar{\eta}, \\ &(iii) \bar{z} = \bar{\zeta}, \\ &(iv) \; \bar{t} = \gamma\left(\bar{T} - \frac{v\bar{\xi}}{c^2}\right). \end{aligned} \tag{B.80}$$

Again, these transformations are the Lorentz–Einstein spacetime transformations in special relativity [18, 22].

We then conclude that in both directions of the moving frame $k$, the resulting spacetime transformations under dimensional-dimensional system are the Lorentz–Einstein spacetime transformations in special relativity.

## C. Consistency Results

### C.1. Mass and Energy Equations under Standard-Dimensional Transformation System

In this section, we refer to the standard-dimensional transformation system as the equations which govern the transformation of mass and energy in the spacetime. This relates the observed standard values measured by an observer in the rest frame to the corresponding dimensional values in the moving frame at velocity $v$.

Case I: Moving frame $k$ at velocity $\upsilon$ in the direction of increasing $x$-axis. Assuming a particle has a mass $m_g$ in the frame $\mathbf{K}$. According to Newton's second law motion in the frame $\mathbf{K}$, this particle is affected by a force $f$ [26, 27]

$$f = m_g \frac{d^2 x'}{d(t')^2}. \tag{C.1}$$

By differentiating Eq. (B.52) with respect to $t'$, we get

$$\frac{d^2 x'}{d(t')^2} = \frac{d}{dt'}\left(\frac{\frac{d\xi}{dT}}{\delta^2(\upsilon)} + \upsilon\right) = \frac{dT}{dt'}\frac{d}{dT}\left(\frac{\frac{d\xi}{dT}}{\delta^2(\upsilon)} + \upsilon\right). \tag{C.2}$$

By using $t' = \delta(\upsilon)\,T$, we then obtain

$$\frac{d^2 x'}{d(t')^2} = \frac{1}{\delta(\upsilon)}\frac{d}{dT}\left(\frac{\frac{d\xi}{dT}}{\delta^2(\upsilon)} + \upsilon\right) = \frac{1}{\delta^3(\upsilon)}\frac{d^2\xi}{dT^2}. \tag{C.3}$$

Accordingly, we obtain that

$$\frac{d^2 x'}{d(t')^2} = \left[1 - \left(\frac{\upsilon}{c}\right)\right]^{\frac{3}{2}} \frac{d^2\xi}{dT^2}. \tag{C.4}$$

If we assume that the particle was designated through that moment as being momentarily at rest from an observer's point of view in frame $\mathbf{K}$ and by using Eq. (B.52), then, the particle's velocity in relation to frame $k$ at that time becomes

$$\upsilon = \frac{\frac{d\xi}{dT}}{\frac{d\xi}{dT}\frac{1}{c} - 1}. \tag{C.5}$$

By substituting Eq. (C.5) into Eq. (C.4), we obtain

$$\frac{d^2 x'}{dt'^2} = \left[1 - \left(\frac{d\xi}{dT}\frac{1}{c}\right)\right]^{\frac{-3}{2}} \frac{d^2\xi}{dT^2} \tag{C.6}$$

Also by substituting Eq. (C.6) into Eq. (**??**), the equation of motion in the frame $k$ reads

$$f = m_g \left[1 - \left(\frac{d\xi}{dT}\frac{1}{c}\right)\right]^{-\frac{3}{2}} \frac{du_\xi}{dT}. \tag{C.7}$$

The velocity of the particle in the frame $k$, is given as $d\xi/dT = u_\xi$. Then, Eq. (C.7) can be rewritten as

$$f = m_g \left(1 - \frac{u_\xi}{c}\right)^{-\frac{3}{2}} \frac{du_\xi}{dT}. \tag{C.8}$$

In the special case that $u_\xi = \upsilon$, we arrive as

$$f = m_g \left(1 - \frac{\upsilon}{c}\right)^{\frac{-3}{2}} \frac{du_\xi}{dT}. \tag{C.9}$$

Back to the general situation, we suggest that

$$\frac{d}{dT}\frac{2m_g c}{\left(1 - \frac{u_\xi}{c}\right)^{\frac{1}{2}}} = \frac{m_g}{\left(1 - \frac{u_\xi}{c}\right)^{\frac{3}{2}}}\frac{du_\xi}{dT}. \tag{C.10}$$

From Eqs. (C.8) and (C.10), we can reformulate the force $f$ under standard-dimensional transformation system as

$$f = \frac{d}{dT}\left(2m_g \frac{\left(\frac{c}{u_\xi}\right) u_\xi}{\sqrt{1 - \frac{u_\xi}{c}}}\right). \tag{C.11}$$

Consequently, we can derive the rate of the change in the momentum, i.e., the force. Now, the mass of a particle in the frame $k$ can be determined,

$$M_k = \left(\frac{c}{u_\xi}\right)\frac{2m_g}{\sqrt{1 - \frac{u_\xi}{c}}}. \tag{C.12}$$

Case II: the frame $k$ moves at velocity $\upsilon$ in the opposite direction to the direction of increasing $x$-axis. Similarly, by using the same method as in the previous case, but with transformations in the opposite direction of the increasing $x$-axis, we determine the mass of a particle in the frame $\bar{k}$, whose velocity becomes $u_{\bar{\xi}}$,

$$M_{\bar{k}} = \left(\frac{c}{u_{\bar{\xi}}}\right)\frac{2m_g}{\sqrt{1-\frac{u_{\bar{\xi}}}{c}}}. \tag{C.13}$$

Consequently, the generalization of the mass transformation can be suggested as

$$M_{gd} = \left(\frac{c}{u}\right)\frac{2m_{gd}}{\sqrt{1-\frac{u}{c}}}, \tag{C.14}$$

where $u$ is the particle's velocity, $m_{gd}$ is the mass of the particle in the rest frame, while $M_{gd}$ is the mass of the particle in the moving frame. This specific transformation of mass should not be mixed with the relativistic mass as dictated by special relativity.

Now, we can derive a relationship between mass and energy.

$$\frac{d}{dx'}\left(2m_{gd}\frac{\left(2c^2-cu\right)}{\sqrt{1-\frac{u}{c}}}\right) = m_{gd}\frac{\frac{du}{dt}}{\left(1-\frac{u}{c}\right)^{\frac{3}{2}}}. \tag{C.15}$$

Since $f = (m_{gd}\cdot du/dt)/\left(1-\frac{u}{c}\right)^{\frac{3}{2}}$, hence

$$d\left(2m_{gd}\frac{\left(2c^2-cu\right)}{\sqrt{1-\frac{u}{c}}}\right) = f dx'. \tag{C.16}$$

By integrating both sides, we derive the work

$$2m_{gd}\frac{\left(2c^2-cu\right)}{\sqrt{1-\frac{u}{c}}} = \int f dx' \equiv \texttt{Work}. \tag{C.17}$$

From the work-energy theorem [27], the energy can be obtained

$$\texttt{Energy} = \frac{2m_{gd}\left(\frac{c}{u}\right)\left(2cu-u^2\right)}{\sqrt{1-\frac{u}{c}}}. \tag{C.18}$$

Since $M_{gd} = 2m_{gd}\left(\frac{c}{u}\right)/\sqrt{1-\frac{u}{c}}$, the energy can be expressed as

$$\texttt{Energy} = M_{gd}\left(2cu-u^2\right). \tag{C.19}$$

We conclude that the energy in the moving frame is proportional to $u$. Its positiveness is conditioned to $2c > u$, which is obviously fulfilled in special relativity.

### C.2. Schrödinger Equation under Standard-Dimensional Transformation System

The Schrödinger equation [28, 29, 30] can be expressed in the scenario where the spacetime transformation relates the observer's standard values in the stationary frame **K** to the corresponding dimensional values in the frame $k$ which moves at velocity $\upsilon$ in the direction of increasing $x$-axis. We assume that the potential $V$ can be solely determined by the *"position"*.

$$i\hbar\frac{\partial}{\partial t'}\psi\left(x',t'\right) = \frac{-\hbar^2}{2m}\frac{\partial^2}{\partial\left(x'\right)^2}\psi\left(x',t'\right) + V\left(x'\right)\psi\left(x',t'\right). \tag{C.20}$$

The solutions $\psi\left(x',t'\right) = A\exp[i(\kappa\cdot x' - \omega\cdot t')]$ satisfy Schrödinger equation, where $A$ is a constant, $\kappa = \omega/c$ is wave number and $\omega$ is angular frequency. Then, Eqs. (B.44) leads to

$$\psi\left(x',t'\right) = \psi\left(\frac{\xi}{\delta(\upsilon)} + \delta(\upsilon)\upsilon T, \delta(\upsilon)T\right) = A\exp\left\{i\left[\left(\frac{\kappa}{\delta(\upsilon)}\right)\xi - \left[\omega\delta(\upsilon) - \kappa\delta(\upsilon)\upsilon\right]T\right]\right\}. \tag{C.21}$$

When assuming $a = \kappa/\delta(\upsilon)$ and $b = \omega\delta(\upsilon) - \kappa\delta(\upsilon)\upsilon$, we obtain

$$\psi(x', t') = A \exp\left[i\left(a\xi - bT\right)\right]. \tag{C.22}$$

Now $b$ can be reexpressed as

$$\begin{aligned} b &= \omega\delta(\upsilon) - \kappa\delta(\upsilon)\upsilon = \kappa\delta(\upsilon)(c-\upsilon) = \frac{\kappa}{\delta(\upsilon)}\delta(\upsilon)(c-\upsilon)\delta(\upsilon) \\ &= ac\left(1-\frac{\upsilon}{c}\right)\frac{1}{1-\frac{\upsilon}{c}}. \end{aligned}$$

Hence, we find that $b$ is scaled by the speed of light, $c$,

$$b = c\,a. \tag{C.23}$$

From Eq. (C.23), we realize that $A\exp[i(a\xi - bT)]$ solves the Schrödinger equation in $\xi$ and $T$,

$$A \cdot \exp\left[i\left(a\xi - b \cdot T\right)\right] = \psi(\xi, T), \tag{C.24}$$

i.e., the solution represents an optical wave function of $\xi$ and $T$. From Eq. (C.22) and Eq. (C.24).

$$\psi(x', t') = \psi(\xi, T). \tag{C.25}$$

By substituting Eq. (C.25) and (iv) in Eq. (B.44), we obtain

$$i\hbar\frac{\partial}{\partial t'}\psi(x', t') = \frac{1}{\delta(\upsilon)} i\hbar\frac{\partial}{\partial T}\psi(\xi, T). \tag{C.26}$$

By differentiating (i) in Eq. (B.44) with respect to $\xi$, we find that

$$\frac{\partial x\prime}{\partial \xi} = \frac{1}{\delta(\upsilon)}. \tag{C.27}$$

Hence,

$$\frac{\partial \omega}{\partial \xi} = \frac{1}{\delta(\upsilon)}\frac{\partial \omega}{\partial x'}, \tag{C.28}$$

$$\frac{\partial^2 \omega}{\partial \xi^2} = \frac{1}{\delta^2(\upsilon)}\frac{\partial^2 \omega}{\partial (x')^2}. \tag{C.29}$$

According to the transformations introduced in section C.1, we conclude that the Newton's second law, $f = m_g[d^2x'/d(t')^2]$, in the frame $\mathbf{K}$ becomes

$$f = m_g\left[1 - \left(\frac{d\xi}{dT}\frac{1}{c}\right)\right]^{-\frac{3}{2}}\frac{du_\xi}{dT}. \tag{C.30}$$

Consequently, we express the transformation of the mass $m$ from the frame $\mathbf{K}$ to the frame $k$, i.e.,

$$m|_{\texttt{frame}\,\mathbf{K}} \rightarrow m\left(1-\frac{\upsilon}{c}\right)^{-\frac{3}{2}}\Bigg|_{\texttt{frame}\,k}. \tag{C.31}$$

From Eqs. (C.26), (**??**), and (C.31), we get

$$\frac{-\hbar^2}{2m}\frac{\partial^2}{\partial\left(x'\right)^2}\psi(x', t') = \frac{-\hbar^2}{2m}\delta(\upsilon)^{-3}\frac{\partial^2}{\partial\xi^2}\psi(\xi, T)\,\delta^2(\upsilon). \tag{C.32}$$

According to the relation $x' = \xi/\delta(\upsilon) + \delta(\upsilon)\upsilon T$, we note that $x'$ can be represented as a summation of two parts. The first part is $\xi/\delta(\upsilon)$, which is the value assigned to $x'$ in the frame $k$. The second part is

$\delta(v)vT$, which is the value that results from the movement of frame $k$. Therefore, the potential energy $V(x')$ in the frame **K** can be related to the potential energy $V(\xi/\delta(v))$ in the frame $k$,

$$V\left(x'\right)=\frac{1}{\delta(v)}V(\xi). \tag{C.33}$$

From Eqs. (C.26), (C.32), and (C.33), we get

$$i\hbar\frac{\partial}{\partial T}\psi(\xi,T)=\frac{-\hbar^2}{2m}\frac{\partial^2}{\partial\xi^2}\psi(\xi,T)+V(\xi)\psi(\xi,T). \tag{C.34}$$

We conclude that the Schrödinger equation under standard-dimensional transformation system is invariant. Also, this finding obviously demonstrates that the second assumption in section A is upheld by the Schrödinger equation.

**D. Conclusions and Outlook**

The recently observed violations of some principles of special relativity such as Lorentz invariance violation and modified dispersion relations urged theoretical interpretations. We suggest alternative transformation systems preserving the current version of special theory but taking into consideration that Einstein's original ideas about *"time"* and *"space"* and also his distinction between *"position"* and *"place"*. The proposed theory extends the standard-standard transformation system. The standard-dimensional transformation system suggested combines the dimensional-dimensional transformation system which corresponds to the typical Lorentz–Einstein transformation and the standard-standard transformation system.

The key ingredient is whether the observer able to monitor the movement trajectory (standard values time and space are perceived) or not (dimensional values time and space are then perceived). Accordingly, standard-standard transformation system from the standard values of a stationary frame to the standard values of a moving frame, standard-dimensional transformation system from standard values of a stationary frame to dimensional values of a moving frame or vice verse, i.e., dimensional-standard transformation system and finally dimensional-dimensional transformation system from the dimensional values of a stationary frame to the dimensional values of a moving frame can be defined. We conclude that the standard-dimensional transformation system combines both dimensional-dimensional system, which is typical to the Lorentz–Einstein transformation and the standard-standard transformation system. In this regard, we find that the relationship between the standard values in a stationary frame and the ones in a moving frame seems to rely on a velocity function $\delta(v)$. This means that the velocity at which the dimensional frame moves plays a crucial role. Therefore, even the velocity transformations of this velocity under the standard-dimensional transformation system are found $\delta(v)$-dependent.

Under standard-dimensional transformation system, we conclude that the Maxwell spherical wave equation remains unchanged although this type of spacetime transformations. This observed invariance is conditioned to the motion within the moving frame in the rays are parallel to the $x$-axis and moving at speed of light. We conclude that straight rays manifest the particle-nature of light. We found that the dimensional-dimensional transformation system is identical to the typical Lorentz–Einstein spacetime transformation. Also, we conclude that the spacetime transformations under standard-dimensional system adheres the assumption that the physical laws are straightforwardly subject to the standard-dimensional transformational system.

For the mass and energy equations of a free particle under the standard-dimensional transformation system, we conclude that both quantities in both standard and dimensional frames depend on the velocity of the free particle and that of the moving frame. Another implication, we discussed, is the Schrödinger equation under standard-dimensional transformation system. We conclude that the Schrödinger equation remains invariant, which means that assumption of speed of light is upheld by the Schrödinger equation. Further implications, especially where special relativity is challenged, shall be carried out elsewhere

**Acknowledgment**

AT acknowledges the generous support by the Egyptian Center for Theoretical Physics (ECTP) and World Laboratory for Cosmology And Particle Physics (WLCAPP) at the Future University in Egypt (FUE)!

**Conflicts of Interest**

The authors declare that there are no conflicts of interest regarding the publication of this published article!

**Dataset Availability**

All data generated or analyzed during this study are included in this published article. The data used to support the findings of this study are included within the published article and properly cited! All of the material is owned by the authors.

**Funding**

The authors declare that this research received no specific grants from any funding agency in the public, commercial, or not-for-profit sectors.

**Competing interests**

The authors declare that they have no known competing financial interests or personal relationships that could have appeared to influence the work reported in this paper.

**Список литературы/References**

1. A. K. A. Maciel and J. Tiomno. On Experiments To Detect Possible Weak Violations of Special Relativity. *Phys. Rev. Lett.*, 55:143, 1985. 10.17238/issn2226-8812.2023.3-4.251-27010.1103/PhysRevLett.55.143. [Erratum: Phys.Rev.Lett. 57, 1382 (1986)].
2. Gian Luigi Fogli, E. Lisi, A. Marrone, and G. Scioscia. Testing violations of special and general relativity through the energy dependence of muon-neutrino <—> tau-neutrino oscillations in the Super-Kamiokande atmospheric neutrino experiment. *Phys. Rev. D*, 60:053006, 1999. 10.17238/issn2226-8812.2023.3-4.251-27010.1103/PhysRevD.60.053006.
3. T. Jacobson, Stefano Liberati, and D. Mattingly. A Strong astrophysical constraint on the violation of special relativity by quantum gravity. *Nature*, 424:1019–1021, 2003. 10.17238/issn2226-8812.2023.3-4.251-27010.1038/nature01882.
4. S. L. Dubovsky and P. G. Tinyakov. Violation of Lorentz invariance and neutral component of UHECR. *Astropart. Phys.*, 18:89–96, 2002. 10.17238/issn2226-8812.2023.3-4.251-27010.1016/S0927-6505(02)00114-7.
5. O. W. Greenberg. CPT violation implies violation of Lorentz invariance. *Phys. Rev. Lett.*, 89: 231602, 2002. 10.17238/issn2226-8812.2023.3-4.251-27010.1103/PhysRevLett.89.231602.
6. G. Amelino-Camelia, John R. Ellis, N. E. Mavromatos, and Dimitri V. Nanopoulos. Distance measurement and wave dispersion in a Liouville string approach to quantum gravity. *Int. J. Mod. Phys. A*, 12:607–624, 1997. 10.17238/issn2226-8812.2023.3-4.251-27010.1142/S0217751X97000566.
7. Giovanni Amelino-Camelia. Testable scenario for relativity with minimum length. *Phys. Lett. B*, 510:255–263, 2001. 10.17238/issn2226-8812.2023.3-4.251-27010.1016/S0370-2693(01)00506-8.
8. P. Adamson et al. A Search for Lorentz Invariance and CPT Violation with the MINOS

Far Detector. *Phys. Rev. Lett.*, 105:151601, 2010. 10.17238/issn2226-8812.2023.3-4.251-27010.1103/PhysRevLett.105.151601.

9. A. Tawfik, H. Magdy, and A. Farag Ali. Lorentz Invariance Violation and Generalized Uncertainty Principle. *Phys. Part. Nucl. Lett.*, 13:59–68, 2016. 10.17238/issn2226-8812.2023.3-4.251-27010.1134/S1547477116010179.
10. Florian Girelli, Tomasz Konopka, Jerzy Kowalski-Glikman, and Etera R. Livine. The Free particle in deformed special relativity. *Phys. Rev. D*, 73:045009, 2006. 10.17238/issn2226-8812.2023.3-4.251-27010.1103/PhysRevD.73.045009.
11. Sergio Doplicher, Klaus Fredenhagen, and John E. Roberts. Spacetime quantization induced by classical gravity. *Physics Letters B*, 331(1):39–44, 1994. 10.17238/issn2226-8812.2023.3-4.251-270https://doi.org/10.1016/0370-2693(94)90940-7. URL `https://www.sciencedirect.com/science/article/pii/0370269394909407`.
12. J. Kowalski-Glikman and S. Nowak. Doubly special relativity theories as different bases of kappa Poincare algebra. *Phys. Lett. B*, 539:126–132, 2002. 10.17238/issn2226-8812.2023.3-4.251-27010.1016/S0370-2693(02)02063-4.
13. Giovanni Amelino-Camelia. Doubly special relativity. *Nature*, 418:34–35, 2002. 10.17238/issn2226-8812.2023.3-4.251-27010.1038/418034a.
14. A. Tawfik. Impacts of Generalized Uncertainty Principle on Black Hole Thermodynamics and Salecker-Wigner Inequalities. *JCAP*, 07:040, 2013. 10.17238/issn2226-8812.2023.3-4.251-27010.1088/1475-7516/2013/07/040.
15. Abdel Nasser Tawfik and Eiman Abou El Dahab. Corrections to entropy and thermodynamics of charged black hole using generalized uncertainty principle. *Int. J. Mod. Phys. A*, 30(09):1550030, 2015. 10.17238/issn2226-8812.2023.3-4.251-27010.1142/S0217751X1550030X.
16. Abdel Nasser Tawfik and Abdel Magied Diab. Black Hole Corrections due to Minimal Length and Modified Dispersion Relation. *Int. J. Mod. Phys. A*, 30(12):1550059, 2015. 10.17238/issn2226-8812.2023.3-4.251-27010.1142/S0217751X15500591.
17. J.B. Marion. *Classical Dynamics of Particles and Systems*. Academic Press International Edition. Academic Press, 1965. URL `https://books.google.com.eg/books?id=-FjvAAAAMAAJ`.
18. A. Einstein. *The Special and General Theory: The Special and General Theory by Albert Einstein: The Special and General Theory - Einstein's Groundbreaking Work*. Prabhat Prakashan, 1948. ISBN 9788184302288. URL `https://books.google.com.eg/books?id=CbwwBQAAQBAJ`.
19. Rachel E Scherr, Peter S Shaffer, and Stamatis Vokos. Student understanding of time in special relativity: Simultaneity and reference frames. *American Journal of Physics*, 69(S1):S24–S35, 2001.
20. Youshan Dai and Liang Dai. New derivation of space-time linear transformation between inertial frames based on the principle of relativity. *Results in Physics*, 19:103552, 2020. ISSN 2211-3797. 10.17238/issn2226-8812.2023.3-4.251-270https://doi.org/10.1016/j.rinp.2020.103552. URL `https://www.sciencedirect.com/science/article/pii/S2211379720319975`.
21. Frank Verheest. On the linearity of the generalized Lorentz transformation. *American Journal of Physics*, 90(6):425–429, 06 2022. ISSN 0002-9505. 10.17238/issn2226-8812.2023.3-4.251-27010.1119/10.0010234. URL `https://doi.org/10.1119/10.0010234`.
22. S.T. Thornton and A. Rex. *Modern Physics for Scientists and Engineers*. Cengage Learning, 2012. ISBN 9781133712237. URL `https://books.google.com.eg/books?id=pWAKAAAAQBAJ`.
23. R.H. Dicke and J.P. Wittke. *Introduction to Quantum Mechanics, by Robert H. Dicke and James P. Wittke*. Addison-Wesley Publishing Company, 1961. URL `https://books.google.com.eg/books?id=tbHCswEACAAJ`.
24. E. Huggins. *Physics 2000*. Moose Mountain Digital Press, 1999. ISBN 9780970783639. URL `https://books.google.com.eg/books?id=03HvwQEACAAJ`.

25. M. Katz. *Introduction to Geometrical Optics.* G - Reference,Information and Interdisciplinary Subjects Series. World Scientific, 2002. ISBN 9789812382245. URL https://books.google.com.eg/books?id=agsOmxYsyCIC.
26. I. Newton, A. Motte, and N.W. Chittenden. *Newton's Principia: The Mathematical Principles of Natural Philosophy.* Nineteenth Century Collections Online (NCCO): Science, Technology, and Medicine: 1780-1925. Geo. P. Putnam, 1850. URL https://books.google.com.eg/books?id=N-hHAQAAMAAJ.
27. H. Goldstein, C.P. Poole, and J.L. Safko. *Classical Mechanics.* Addison-Wesley series in physics. Addison Wesley, 2002. ISBN 9780321188977. URL https://books.google.com.eg/books?id=EE-wQgAACAAJ.
28. D. McMahon. *Quantum Mechanics Demystified.* Demystified series. McGraw-Hill Education, 2005. ISBN 9780071486705. URL https://books.google.com.eg/books?id=VAq1Z4GClUoC.
29. D.J. Griffiths and D.F. Schroeter. *Introduction to Quantum Mechanics.* Cambridge University Press, 2018. ISBN 9781107189638. URL https://books.google.com.eg/books?id=82FjDwAAQBAJ.
30. N. Ashby and S.C. Miller. *Principles of Modern Physics.* Holden-Day series in physics. Holden-Day, 1970. URL https://books.google.com.eg/books?id=my4bAQAAIAAJ.

**Авторы**

**Салем Салума**,Математическое отделение, факультет естественных наук, Университет Сохаг, Сохаг 82524, Египет
E-mail: email@mail.ru

**Абдель Насер Тауфик**, Университет будущего в Египте (FUE), Пятое поселение, 11835 Новый Каир, Египет
E-mail: email2@inbox.ru

**Просьба ссылаться на эту статью следующим образом:**

Салума С., Тауфик А. Н. Стандартно-мерные системы преобразований для специальной теории относительности. *Пространство, время и фундаментальные взаимодействия.* 2023. № 3-4. С. 251–270.

**Authors**

**Salem Salouma**,Mathematics Department, Faculty of Science, Sohag University, Sohag 82524, Egypt
E-mail: email@mail.ru

**Tawfik Abdel Nasser**, Future University in Egypt (FUE), Fifth Settlement, 11835 New Cairo, Egypt.
E-mail: email2@inbox.ru

**Please cite this article in English as:**

Salouma S., Tawfik A. N. Standard-Dimensional Transformation Systems for Special Relativity. *Space, Time and Fundamental Interactions*, 2023, no. 3-4, pp. 251–270.

УДК 530.12, 531.551



# РАЗЛИЧНЫЕ ИНФЛЯЦИОННЫЕ КОСМОЛОГИЧЕСКОЙ МОДЕЛИ С ВРАЩЕНИЕМ

Сандакова О. В.[a,1], Панов В. Ф.[a,2], Кувшинова Е. В.[a,3]

[a] Пермский государственный национальный исследовательский университет, г. Перьм, 614068, Россия.

Рассматривается первая инфляционная стадия развития Вселенной для метрики типа IX по Бьянки для случая гибридной инфляции с двумя скалярными полями с вращением. В качестве источников гравитации на этапе инфляции используется анизотропная жидкость и два скалярных поля. Сделана попытка сравнения различных видов инфляции - хаотической инфляции, "новой инфляции"и гибридной инфляции - для вращающихся моделей.

*Ключевые слова*: Гибридная инфляция, «новая инфляция», хаотическая инфляция,темная энергия, космологическая модель.

# VARIOUS INFLATIONARY COSMOLOGICAL MODELS WITH ROTATION

Sandakova O. V.[a,1], Panov V. F.[a,2], Kuvshinova E. V.[a,3]

[a] Perm State University, Perm, 614068, Russia.

The first inflationary stage of the development of the Universe is considered for the Bianchi type IX metric for the case of hybrid inflation with two scalar fields with rotation. An anisotropic fluid and two scalar fields are used as sources of gravity at the inflation stage. An attempt has been made to compare different types of inflation - chaotic inflation, "new"inflation and hybrid inflation - for rotating models.

*Keywords*: Hybrid inflation, “new inflation”, chaotic inflation, dark energy, cosmological model.

PACS: 04.20.-q, 98.80.-k, 98.80.Cq

DOI: 10.17238/issn2226-8812.2023.3-4.271-276

## A. Введение

В данной работе мы рассматриваем первую инфляционную стадию эволюции Вселенной для метрики типа IX по Бьянки для случая гибридной инфляции с двумя скалярными полями и вращением. В качестве источников гравитации на этапе инфляции используется анизотропная жидкость и два скалярных поля. Приведены ранее полученные решения [1] и [2] для моделей с хаотической и "новой"инфляцией, которые заполнены скалярным полем и анизотропной жидкостью. Сделана попытка понять, как выбор характера инфляции - хаотической инфляции, "новой инфляции"или гибридной инфляции - влияет на возможное вращение Вселенной в раннюю и современную эпоху.

## B. Описание первой стадии инфляции в модели с гибридной инфляцией

В рамках общей теории относительности построен инфляционный сценарий с анизотропной космологической моделью с расширением и вращением с метрикой типа IX по Бьянки вида

$$ds^2 = \eta_{\alpha\beta}\theta^\alpha\theta^\beta. \tag{B.1}$$

[1]E-mail: o_sandakova@list.ru
[2]E-mail: panov@psu.ru
[3]E-mail: kuvlenka@narod.ru

Здесь $\eta_{\alpha\beta}$ матричный элемент Лоренца, $\alpha$, $\beta = \{0, 1, 2, 3\}$, $\theta^\alpha$ - ортонормированные 1-формы, которые связаны с масштабным фактором $R$ через следующие соотношения:

$$\theta^0 = dt - R\nu_1 e^1, \quad \theta^1 = RK_1 e^1, \theta^2 = RK_2 e^2, \theta^3 = RK_3 e^3, \tag{B.2}$$

где имеются константы $\nu_1 > 0$, $K_1 > 0$, $K_2 = K_3 = \sqrt{K_1^2 - \nu_1^2} > 0$.

Базовые 1-формы $e^A$ задаются в виде:

$$e^1 = \cosh(y)\cos(z)dx - \sin(z)dy, \; e^2 = \cosh(y)\sin(z)dx + \cos(z)dy,$$

$$e^3 = \sinh(y)dx + dz.$$

Источниками гравитации на этапе инфляции являются анизотропная жидкость и два скалярных поля.

Тензор энергии – импульса сопутствующей анизотропной жидкости в тетрадном представлении записывается в виде:

$$T_{ab} = (\pi + \rho)\, u_a u_b + (\sigma - \pi)\psi_a\psi_b - \pi\eta_{ab}, \tag{B.3}$$

где $\pi$, $\sigma$ это компоненты давления анизотропной жидкости, $\rho$ это плотность энергии анизотропной жидкости, $\psi_a = \{0, 1, 0, 0\}$ это проекция анизотропного 4-вектора на тетраду, $u_a = \delta_0^a$ это вектор 4-скорости сопутствующей анизотропной жидкости, спроектированный на тетраду.

Тензор энергии – импульса скалярных полей в координатном представлении имеет вид:

$$T_{ab} = \phi_{,a}\phi_{,b} + \chi_{,a}\chi_{,b} - \left\{\frac{1}{2}\left(\phi_{,k}\phi_{,l} + \chi_{,k}\chi_{,l}\right) g^{kl} - V(\phi,\chi)\right\} g_{ab}, \tag{B.4}$$

а уравнения двух скалярных полей имеют вид

$$\frac{1}{\sqrt{-g}}\partial_i\left(\sqrt{-g}g^{ik}\phi_{,k}\right) + \frac{dV}{d\phi} = 0, \tag{B.5}$$

$$\frac{1}{\sqrt{-g}}\partial_i\left(\sqrt{-g}g^{ik}\chi_{,k}\right) + \frac{dV}{d\chi} = 0, \tag{B.6}$$

с потенциалом вида

$$V(\phi,\chi) = \frac{1}{2}\left(g^2\phi^2 - \mu^2\right)\chi^2 + \frac{h_1}{4}\chi^4 - \frac{h_2}{4}\phi^4 + \frac{1}{2}m^2\phi^2 + V_0, \tag{B.7}$$

Для решения уравнений Клейна-Гордона-Фока найдем частные производные $\frac{dV}{d\phi}$ и $\frac{dV}{d\chi}$, и исследуем функцию $V(\phi,\chi)$ методами дифференциального исчисления на экстемальные точки.

Решая систему уравнений $\frac{dV}{d\phi} = 0$, $\frac{dV}{d\chi} = 0$, мы найдем три критические точки.

Точка максимума $M_1(\phi = \frac{m}{\sqrt{h_2}}, \chi = 0)$, $V(M_1) = V_0 + \frac{m^4}{4h_2}$.

Точка минимума $M_2(\phi = 0, \chi = \frac{\mu}{\sqrt{h_1}})$, $V(M_2) = V_0 - \frac{\mu^4}{4h_1}$.

Седловая точка $M_3(\phi = 0, \chi = 0)$, $V(M_3) = V_0$.

Идея гибридной инфляции состоит в том, что во время инфляционной стадии поле $\phi$ велико, и система медленно скатывается вдоль долины $\chi = 0$. После того как долина $\chi = 0$ превращается в седло, происходит скатывание в перпендикулярном направлении, инфляция заканчивается, а осцилляции вблизи минимума $M_2(\phi = 0, \chi = \frac{\mu}{\sqrt{h_1}})$, приводят к разогреву Вселенной.

Таким образом, мы считаем, что происходит медленное скатывание от точки максимума $M_1$ до седловой точки $M_3$ , а затем от седловой точки до точки минимума $M_2$ , где инфляция заканчивается. При этом потенциал поля $V(\phi,\chi)$ равен нулю в точке $M_2$, следовательно $V_0 = \frac{\mu^4}{4h_1}$.

Тогда в рассматриваемой метрике система уравнений Эйнштейна имеет вид:

$$-\left(2\frac{\ddot{R}}{R} + \frac{\dot{R}^2}{R^2}\right)\frac{\nu_1^2}{K_1^2} + 3\frac{\dot{R}^2}{R^2} + \frac{2K_1^2 + K_2^2}{4K_2^4R^2} = \rho + V + \frac{\dot{\phi}^2 + \dot{\chi}^2}{2}\left(1 + \frac{\nu_1^2}{K_1^2}\right), \tag{B.8}$$

$$-\left(2\frac{\ddot{R}}{R}+\frac{\dot{R}^2}{R^2}\right)+3\frac{\dot{R}^2}{R^2}\frac{\nu_1^2}{K_1^2}+\frac{2K_1^2-3K_2^2}{4K_2^4R^2}=\sigma-V+\frac{\dot{\phi^2}+\dot{\chi^2}}{2}\left(1+\frac{\nu_1^2}{K_1^2}\right), \tag{B.9}$$

$$\left(2\frac{\ddot{R}}{R}+\frac{\dot{R}^2}{R^2}\right)\left(\frac{\nu_1^2}{K_1^2}-1\right)-\frac{1}{4K_2^2R^2}=\pi-V+\frac{\dot{\phi^2}+\dot{\chi^2}}{2}\left(1-\frac{\nu_1^2}{K_1^2}\right), \tag{B.10}$$

$$2\left(-\frac{\ddot{R}}{R}+\frac{\dot{R}^2}{R^2}\right)\frac{\nu_1}{K_1}+\frac{\nu_1K_1}{2K_2^4R^2}=\frac{\nu_1\left(\dot{\phi^2}+\dot{\chi^2}\right)}{K_1}. \tag{B.11}$$

Таким образом, для нахождения неизвестных функций $R=R(t)$, $\phi=\phi(t)$, $\chi=\chi(t)$ получим систему трех дифференциальных уравнений (с учетом (5), (6), (11)):

$$3\frac{\dot{R}}{R}\dot{\phi}+\ddot{\phi}+\frac{K_1^2}{K_2^2}\phi\left(g^2\chi^2-h_2\phi^2+m^2\right)=0. \tag{B.12}$$

$$3\frac{\dot{R}}{R}\dot{\chi}+\ddot{\chi}+\frac{K_1^2}{K_2^2}\chi\left(g^2\phi^2+h_1\chi^2-\mu^2\right)=0. \tag{B.13}$$

$$-\frac{\ddot{R}}{R}+\frac{\dot{R}^2}{R^2}+\frac{K_1^2}{4K_2^4R^2}=\frac{\left(\dot{\phi^2}+\dot{\chi^2}\right)}{2}. \tag{B.14}$$

Пусть $R=R_0e^{Ht}$, тогда $-\frac{\ddot{R}}{R}+\frac{\dot{R}^2}{R^2}=0$, $\left(\dot{\phi^2}+\dot{\chi^2}\right)=\frac{K_1^2}{2K_2^4R_0^2e^{2Ht}}$.

Выберем $\chi=C\phi$, где $C$ - некая константа. Тогда получим:

$$\phi=\frac{K_1}{\sqrt{2+2C^2}K_2^2R_0e^{Ht}} \tag{B.15}$$

$$\chi=\frac{CK_1}{\sqrt{2+2C^2}K_2^2R_0e^{Ht}} \tag{B.16}$$

Рассматриваем первый этап, когда система медленно скатывается вдоль долины $\chi=0$ от точки максимума $M_1(\phi=\frac{m}{\sqrt{h_2}},\chi=0)$, $V(M_1)=V_0+\frac{m^4}{4h_2}$ до седловой точки $M_3(\phi=0,\chi=0)$, $V(M_3)=V_0$.

Условие медленного скатывания выполняется при

$$\left|\frac{\ddot{\phi}}{3\frac{\dot{R}}{R}\dot{\phi}}\right|\ll 1. \tag{B.17}$$

Тогда мы можем пренебречь второй производной $\ddot{\phi}$ и уравнение Клейна - Гордона - Фока (12) приобретает вид

$$3\frac{\dot{R}}{R}\dot{\phi}+\frac{K_1^2}{K_2^2}\phi\left(g^2\chi^2-h_2\phi^2+m^2\right)=0. \tag{B.18}$$

Решая уравнение (18) с учетом (15), мы получим:

$$-3H^2\frac{K_1}{\sqrt{2+2C^2}K_2^2R_0e^{Ht}}+\frac{K_1^2}{K_2^2}\frac{K_1}{\sqrt{2+2C^2}K_2^2R_0e^{Ht}}\left(\left(g^2C^2-h_2\right)\frac{K_1^2}{\left(2+2C^2\right)K_2^4R_0^2e^{2Ht}}+m^2\right)=0. \tag{B.19}$$

Тогда из уравнения (19) получаем следующее соотношение между константами:

$$m^2=3H^2\frac{K_2^2}{K_1^2}, h_2=\frac{C^2}{g^2}. \tag{B.20}$$

Скатывание на втором этапе может быть как медленным, так и быстрым. Мы предполагаем, что происходит быстрое скатывание вдоль долины $\phi=0$ от седловой точки $M_3(\phi=0,\chi=0)$, $V(M_3)=V_0$ до точки минимума $M_2(\phi=0,\chi=\frac{\mu}{\sqrt{h_1}})$, $V(M_2)=0$.

Решаем уравнение Клейна - Гордона - Фока (13) с учетом (16), и получаем в результате:

$$-2H^2\frac{CK_1}{\sqrt{2+2C^2}K_2^2R_0e^{Ht}}+\frac{K_1^2}{K_2^2}\frac{CK_1}{\sqrt{2+2C^2}K_2^2R_0e^{Ht}}\left(\left(g^2+h_1C^2\right)\frac{K_1^2}{\left(2+2C^2\right)K_2^4R_0^2e^{2Ht}}-\mu^2\right)=0. \tag{B.21}$$

Тогда данное уравнение выполняется при

$$\mu^2=-2H^2\frac{K_2^2}{K_1^2}, h_1=-\frac{g^2}{C^2}. \tag{B.22}$$

Мы можем сделать вывод, что скалярное поле $\chi$ будет носить фантомный характер с мнимой массой $\mu=i\sqrt{\frac{2}{3}}m$.

Окончательно получим:

$$\phi=\frac{K_1g}{\sqrt{2g^2+2h_2}K_2^2R_0e^{Ht}} \tag{B.23}$$

$$\chi=\frac{K_1\sqrt{h_2}}{\sqrt{2g^2+2h_2}K_2^2R_0e^{Ht}} \tag{B.24}$$

Тогда из системы уравнений Эйнштейна мы находим плотность энергии

$$\rho=\frac{3H^2K_2^2}{K_1^2}-V, \tag{B.25}$$

а также компоненты давления анизотропной жидкости

$$\pi=-\frac{3H^2K_2^2}{K_1^2}+V+\frac{2K_1^2-K_2^2}{2K_2^4R_0^2e^{2Ht}}, \tag{B.26}$$

$$\sigma=-\frac{3H^2K_2^2}{K_1^2}+V+\frac{K_1^2}{2K_2^4R_0^2e^{2Ht}}. \tag{B.27}$$

Таким образом, была построена модель первой инфляционной стадии Вселенной с двумя скалярными полями и анизотропной жидкостью. Можно считать, что имеется одно комплексное скалярное поле, в духе работы [7].

После окончания первой инфляции энергия скалярного поля переходит в энергию рожденных частиц, а анизотропная инфлатонная жидкость переходит в темную энергию, которая наблюдается на современной стадии эволюции Вселенной.

## C. Описание первой стадии инфляции в моделях с хаотической и "новой"инфляцией

В духе работы [4], ранее нами были построены различные модели для метрики IX типа по Бьянки с разными видами инфляции. Приведем здесь решения для тех моделей, в которых в качестве источников гравитации мы взяли скалярное поле и анизотропную жидкость того же типа, что и в данной работе.

Модель хаотической инфляции была построена нами в работе [1].

Был найден масштабный фактор $R=R(t)$:

$$R=\frac{K_1}{2HK_2^2}ch(Ht). \tag{C.1}$$

Решение системы дается выражениями:

$$\pi=\sigma=\frac{3H^2\nu_1^2}{K_1^2}-3H^2+V, \tag{C.2}$$

$$\rho=-\frac{3H^2\nu_1^2}{K_1^2}+3H^2-V. \tag{C.3}$$

Потенциал скалярного поля в данной модели имеет вид:

$$V = \frac{m^2\phi^2}{2}, \tag{C.4}$$

а скалярное поле мы находим в следующем виде:

$$\phi = \phi_0 \left(sh(Ht)\right)^{-\frac{K_1^2 m^2}{3K_2^2 H^2}}. \tag{C.5}$$

Модель "новой"инфляции была построена нами в работе [2].

Одно из решений, представленных в работе [2], представляет собой космологическую модель для метрики типа IX по Бьянки, заполненную анизотропной жидкостью и скалярным полем. Найденный масштабный фактор для модели с "новой"инфляцией [2] полностью совпадает с масштабным фактором (28), ранее найденным для модели хаотической инфляции [1]. Решение системы уравнений Эйнштейна для модели "новой"инфляции [2], а именно, компоненты давления анизотропной жидкости $\pi$, $\sigma$, а также плотность энергии $\rho$, также совпадают с формулами (29), (30) для модели [1].

В отличие от модели хаотической инфляции, в модели "новой"инфляции мы предполагаем, что

$$\phi = \phi_0 e^{kt}, \tag{C.6}$$

а из уравнения скалярного поля мы находим потенциал $V = V(\phi)$ при $k \ll H$:

$$V = V_0 + \varepsilon\phi^2 - \varepsilon k\phi_0^2 (\frac{\phi}{\phi_0})^{\frac{2H}{k}}, \tag{C.7}$$

где $\varepsilon = \frac{3H^2K_1^2}{2K_2^2}$.

На первой стадии инфляции для обеих моделей мы считаем, что условия медленного скатывания выполняются.

### D. Заключение

Нами были вычислены кинематические параметры моделей, описанных в этой работе. Сдвиг отсутствует. Параметры расширения, ускорения и вращения анизотропной жидкости (темной энергии) для моделей с "новой"инфляцией, хаотической инфляцией и гибридной инфляцией имеют одинаковый вид:

$$\theta = \frac{3\dot{R}}{R}, a = \frac{\dot{R}}{R}\frac{\nu_1}{K_1}, \omega = \frac{\nu_1}{2K_2^2 R}. \tag{D.1}$$

В духе работы [5] во всех перечисленных выше моделях мы считаем, что первая инфляция заканчивается при $10^{-35}$ с, а сразу после первой инфляции начинается радиационная стадия эволюции Вселенной. Поэтому можно состыковать составляющие анизотропной жидкости в конце первой инфляции и в начале ультрарелятивистской стадии. Эта работа была проделана в нашей статье [1] для хаотической инфляции.

Для моделей хаотической инфляции стадия расширения Вселенной длится $\sim 10^{-35}$ с и за это время Вселенная успевает увеличить свой размер минимум в $\sim 10^{100000}$ раз. Это приводит к тому, что в современную эпоху анизотропную жидкость можно считать практически не вращающейся.

Аналогично, в модели с "новой"инфляцией происходит увеличение характерного размера пузырька (Вселенной) с размера в момент его образования порядка $\sim 10^{-20}$ см до размера порядка $\sim 10^{800}$ см после расширения, что намного больше размеров наблюдаемой части Вселенной $l \sim 10^{28}$ см [3, 6]. То есть и для случая "новой"инфляции анизотропная жидкость, которой мы моделировали темную энергию в работе [2], в настоящее время не вращается.

В модели же с гибридной инфляцией с двумя скалярными полями и анизотропной жидкостью, построенной в данной работе, сохраняется возможность того, что если скорость вращения анизотропной жидкости в планковскую эпоху составляла $\sim 10^{43}$ $c^{-1}$, то в современную эпоху эта скорость может быть достаточно велика для будущих возможных наблюдений.

**Список литературы/References**


1. Sandakova O.V., Panov V.F., Kuvshinova E.V. Inflationary cosmology with rotation and chaotic inflation *Russian Phys. J.* 2022. Vol. 65. № 6. P. 944–953.
2. Panov V.F., Sandakova O.V., Kuvshinova E.V. “New Inflation” for a Bianchi Type IX Cosmological Model with Rotation and Dark Energy *Gravitation and Cosmology.* 2023. Vol. 29. № 4. P. 362–366.
3. Линде А.Д. Физика элементарных частиц и инфляционная космология. М.: Наука, 1990. 279 с.
4. Горбунов Д.С., Рубаков В.А. *Введение в теорию ранней Вселенной: космологические возмущения. Инфляционная теория.* М.: КРАСАНД, 2010. 568 с.
5. Фильченков М.Л., Лаптев Ю.П. *Квантовая гравитация. От микромира к мегамиру.* М.: Ленанд, 2016. 304 с.
6. Розенталь И.Л., Архангельская И.В. *Геометрия, динамика, Вселенная.* М.: КРАСАНД, 2016. 200 с.
7. Боголюбов Н.Н., Ширков Д.В. *Введение в теорию квантованных полей.*-4-е изд., испр. М.: Наука Главной редакции физико-математической литературы, 1984. 600 с.


**Авторы**


**Сандакова Ольга Васильевна**, к.ф.-м.н., доцент, кафедра высшей математики, Пермский государственный национальный исследовательский университет, 614068, Россия, г. Пермь, ул. Букирева, 15.
E-mail: o_sandakova@list.ru

**Панов Вячеслав Федорович**, д. ф.-м. н., профессор, кафедра высшей математики, Пермский государственный национальный исследовательский университет, 614068, Россия, г. Пермь, ул. Букирева, 15.
E-mail: panov@psu.ru

**Кувшинова Елена Владимировна**, к. ф.-м. н., доцент, кафедра высшей математики, Пермский государственный национальный исследовательский университет, 614068, Россия, г. Пермь, ул. Букирева, 15.
E-mail: kuvlenka@narod.ru


**Просьба ссылаться на эту статью следующим образом:**


Сандакова О. В., Панов В. Ф., Кувшинова Е. В. Различные инфляционные космологической модели с вращением. *Пространство, время и фундаментальные взаимодействия.* 2023. № 3-4. С. 271–276.


**Authors**


**Sandakova Olga Vasil’evna**, Candidate of Physics and Mathematics, Assistant Professor, Perm State University, Bukireva st., 15, Perm, 614068, Russia.
E-mail: o_sandakova@list.ru

**Panov Vyacheslav Fedorovich**, Doctor of Physics and Mathematics, Professor, Perm State University, Bukireva st., 15, Perm, 614068, Russia.
E-mail: panov@psu.ru

**Kuvshinova Elena Vladimirovna**, Candidate of Physics and Mathematics, Assistant Professor, Perm State University, Bukireva st., 15, Perm, 614068, Russia.
E-mail: kuvlenka@narod.ru


**Please cite this article in English as:**


Sandakova O. V., Panov V. F., Kuvshinova E. V. Various inflationary cosmological models with rotation. *Space, Time and Fundamental Interactions*, 2023, no. 3-4, pp. 271–276.

УДК 530.122, 524.83



## О ТЕОРИИ ГРАВИТАЦИИ ВЕЙЛЯ-ДИРАКА И ЕЕ РАЗВИТИИ

Седов С. Ю.[a,b,1]

[a] Российский федеральный ядерный центр – Всероссийский научно-исследовательский институт экспериментальной физики, пр. Мира, д. 37, г. Саров, 607188, Россия.
[b] Саровский Государственный Физико-технический Институт, Филиал Национального Исследовательского Ядерного Университета МИФИ, г. Саров, 607186, Россия.

В статье обсуждаются модели конформной гравитации с лагранжианами, линейными по скалярной кривизне и неминимальной связью со скалярным полем. Предложен новый вариант конформного лагранжиана с двумя скалярными полями, в котором вектор Вейля заменен на вектор, преобразующийся как и вектор Вейля, но не входящий в вейлевскую связность. Пространством такой модели является интегрируемое пространство Вейля . В рамках теории гравитации Вейля с неминимальной связью вещественного скалярного поля рассмотрена задача описания конформной стадии эволюции Вселенной на основе метрики Фридмана. Приведены конформно-инвариантные решения для масштабного фактора и показано, что квантовые поправки к следу тензора энергии-импульса частично компенсируются калибровкой функции Дирака, приводящей к лагранжиану общей теории относительности.

*Ключевые слова*: конформная гравитация, гравитация Вейля-Дирака, конформные лагранжианы, вектор Вейля, космология.

## ON WEYL-DIRAC GRAVITATION THEORY AND ITS DEVELOPMENT

Sedov S. Yu.[a,b,1]

[a] Russian Federal Nuclear Center-All-Russia Research Institute of Experimental Physics, Mira Ave., 37, Sarov, 607188, Russia
[b] Sarov Physics and Technology Institute of the National Research Nuclear University MEPhI (SarPhTI MEPhI), Sarov, 607186, Russia.

Models of conformal gravitation that contain Lagrangians, which are linear on scalar curvature and with nonminimal connection with the scalar field, are discussed in this report. Theory of Weyl-Dirac gravitation has been reported in detail. A new version of conformal Lagrangian with two scalar fields is proposed, in which the Weyl vector is replaced with the vector which is transformed as a Weyl vector, but is not contained in Weyl connection. Weyl integrable space is the space of such model. The problem of describing a conformal stage in the evolution of the Universe on the basis of Friedmann metrics is considered within Weyl-Dirac gravitation theory with nonminimum connection with the real scalar field. Conformal invariant solutions for the scale factor are presented. It is demonstrated that quantum corrections to the trace of energy-momentum tensor are partially compensated by gauging the Dirac function, which results in the Lagrangian of the General Relativity theory.

*Keywords*: conformal gravitation, Weyl-Dirac gravitation, conformal lagrangians, Weyl vector, cosmology.
PACS: 04.50.Kd, 98.80.-k
DOI: 10.17238/issn2226-8812.2023.3-4.277-289

### Introduction

More than a century ago, in 1918, G. Weyl proposed a theory of gravitation based on local symmetry with respect to the gauging of measurements [1]. The original idea of G. Weyl was the geometric

[1]E-mail: SerWhites@yandex.ru, SYuSedov@vniief.ru

unification of gravity and electromagnetism. In 1918, G. Weyl generalized Riemannian geometry. This generalization was called Weyl geometry. The action had the form:

$$S_W = \int d^4x \sqrt{|\det g|} \cdot L_W, L_W = \breve{R}^2 - \omega^2 F_{\mu\nu} F^{\mu\nu}, \qquad (.1)$$

where $\breve{R}$ is a Weyl curvature of a space-time (different from Riemann curvature), $F_{\mu\nu}$ is a strength of the electromagnetic field, $\omega$ is a parameter of the theory. In case of local changes of a scale, the value of the Lagrangian density $\sqrt{-g} \cdot L_W$ stays invariant. The vector of the electromagnetic field $A^\mu$ was subjected to a gauge transformation taking into account a change in the scale, leaving unchanged the value of $\sqrt{-g} \cdot F_{\mu\nu} F^{\mu\nu}$. Let us note that this value is invariant for dimension 4 of space-time only.

In its original form, integration of gravitation and electromagnetism appeared to be incompatible with observations and enlarged the collection of inviable theories of gravitation. The basic objections against Weyl theory are given in the famous review on gravitation by V.Pauli [2]. Since the original Weyl theory did not satisfy astronomical observations and contradicted quantum theory, it was abandoned.

Now it is recognized that Weyl vector $A^\lambda$ as a part of both strength $F_{\mu\nu}$ and geometric connection $\breve{\Gamma}^\lambda_{\mu\nu}$ cannot be of electromagnetic origin. Nevertheless, the ideas of using a quadratic term of curvature in gravitational Lagrangian, as well as a compensating vector field in geometric connection in order to preserve the local scale invariance of the action, are still of interest today.

According to E.Sholtz [3], let us briefly describe further research. In the middle of the 20th century, the interest to Weyl's ideas renewed as it was understood that local scale transformation can play an important role in physics. Different groups of physics brought their attention back to Weyl's ideas 40 years later: Omote, Utiyama, Dirac, Kanuto, Pirani et al. [4] - [8].

In the beginning of 1960s, Carl Brans and Robert Dicke proposed a modified relativistic gravitation theory with non-minimal connection with scalar field [9]. This theory allowed consistent introduction of a variable parameter of the intensity of gravity. Brans and Dicke developed a theory of gravitation, which, with a certain choice of parameter, corresponds to a special case of the theory of gravitation with Weyl geometry of integrable type. Then many authors, in the spirit of Weyl's ideas, introduced a scalar field connecting gravity and particle physics into their models.

The fundamental paper by Dirac [6] develops a new approach to the Weyl gravity. Dirac used Weyl geometry that had been forgotten by physics by 1970s. Dirac followed Eddington's notation and terminology of geometric covariants and invariants for scale-covariant fields.

Dirac introduced a very important concept of the scale-covariant derivative for large-scale covariant fields into the arsenal of Weyl geometry. Besides, the same as Brans and Dikke, Dirac introduced a fundamental scalar field into the theory and marked it with $\beta$. Dirac connected this $\beta$ field with gravitation in a non-minimal way.

In the 1980s, the interest in local scale transformations in gravitational physics began to intersect with the study of the mechanisms of mass generation in elementary particle physics [10], [11]. In addition, alternative theories of gravity based on Weyl geometry began to be used to solve the problem of the origin of dark matter and dark energy [12].

The problems of cosmology caused some interest to conformal versions of gravitation with a scalar field. As a result, Weyl's approach to the description of the gravity in the 21 $^{st}$ century has gained the second wind. Here, we can mention the papers by Nathan Rosen and Mark Izraelit [13], and detailed reviews by Erhard Scholz [3], [14].

Russian author also contributed to the research on scale invariant gravitation theories. Here we can mention the works by K.P.Stanyukevich, V.N.Melnikov et al [15].The publications by M.V. Gorbatenko, A.V.Pushkin and Yu.A. Romanov [15] - [18] describe an approach close to the works of Kanuto [7].The work by A.T.Filippov offers the models of affine gravitation on the basis of Weyl ideas [19].In the publications by O.V.Baburova and V.N.Frolov the space-time is attributed with a geometric structure of Kartan–Weyl space with the curvature, torsion and nonmetric properties of the Weyl type with the scalar Deser-Dirac field [20]. In the works of V.A. Berezin, V.I. Dokuchaev, Y.N. Eroshenko, cosmological models based on Weyl geometry are developed [20], [21].

During the last five years different alternatives to apply Weyl (local) conformal symmetry towards gravitation are considered from the point of view of modification of the general theory of relativity (GR) for describing dark matter, dark energy, evolution of early Universe. Modifications of the GR on the basis of the local conformal invariance has been studied for a long period of time as the attempts to solve different problems. In particular they search for the ways to do renormalization in quantum gravitation, consider consequences of renormalization of the energy-momentum tensor, and study the dynamics of the inflation in the early Universe and origin of mass for elementary particles.

Currently, there are many researchers dealing with different versions of gravitation based on Weyl geometry. The number of publications is currently increasing. As some examples we shall mention such authors as Philip Mannheim [23], [24], Ichiro Oda [25], [26], Israel Quiros [27], Beltran Jimenez [28], Carlos Romero [29], Dimitru Ghilencea [30], Tiberiu Harko [31].

Here, we shall focus only on Weyl-Dirac gravitation theory.

### A. Weyl geometry

The subject of Weyl geometry is a differential manifold $M$ with a set bi-linear non-degenerate differential 2-form (metric function) $g$ and differential 1-form $A$. This geometric object is called Weyl space, it can be marked as $(M, g, A)$. We shall specify a particular signature of metric $g$. A new thing as compared to Riemann geometry is introduction of additional 1-form $A$. This 1-form is closed if $dA = 0$, and is exact if there is such 2-form $\sigma$, that $A = d\sigma$. Here, $d$ is the operator of exterior differentiation.To put it short, an exact form $A$ corresponds to the case when vector $A_\alpha$ can be represented as a gradient of some scalar $A_\alpha = \frac{\partial\varphi(x)}{\partial x^\alpha}$. A closed form corresponds to the case when $F_{\alpha\beta} = \frac{\partial A_\beta}{\partial x^\alpha} - \frac{\partial A_\alpha}{\partial x^\beta} \equiv 0$. In a general case of Weyl geometry $A$ is not a closed form.

Weyl (local scale) transformation is set with ratios:

$$g \to \tilde{g} = \Omega^2 \cdot g \quad , \quad A \to \tilde{A} = A - d\log\Omega \quad , \tag{A.1}$$

where $\Omega$ is a strictly positive differential real function. In the coordinate form, it looks as follows:

$$g_{\mu\nu}(x) \to \tilde{g}_{\mu\nu}(x) = \Omega^2(x) \cdot g_{\mu\nu}(x) \quad , \quad \Omega(x) = \exp(\sigma(x)), \tag{A.2}$$

$$A_\mu \to \tilde{A}_\mu = A_\mu - \frac{\partial\sigma}{\partial x^\mu} = A_\mu - \nabla_\mu\sigma, \quad \sigma = \ln\Omega\,(x) \quad . \tag{A.3}$$

Here, the transformed quantities are marked with a wavy line above. Coefficients of Weyl connection $\breve{\Gamma}$ is found with metric $g_{\alpha\beta}(x)$ and Weyl vector $A_\nu(x)$. In the coordinate form, they look as follows:

$$\breve{\Gamma}^\lambda_{\mu\nu} = \frac{1}{2} g^{\lambda\alpha}\left(\breve{\partial}_\mu g_{\alpha\nu} + \breve{\partial}_\nu g_{\alpha\mu} - \breve{\partial}_\alpha g_{\mu\nu}\right) = \Gamma^\lambda_{\mu\nu} + \delta^\lambda_\mu A_\nu + \delta^\lambda_\nu A_\mu - g_{\mu\nu}A^\lambda \quad , \tag{A.4}$$

where

$$\breve{\partial}_\mu g_{\alpha\beta} = (\partial_\mu + 2A_\mu)\, g_{\alpha\beta} \quad , \tag{A.5}$$

$$\Gamma^\lambda_{\mu\nu} = \frac{1}{2} g^{\lambda\alpha}\left(\partial_\mu g_{\alpha\nu} + \partial_\nu g_{\alpha\mu} - \partial_\alpha g_{\mu\nu}\right) \tag{A.6}$$

Here gamma's are regular Christoffel symbols of connection of Levi-Civita. A convex line above shows Weyl analogues of the quantities of Riemann geometry.

A condition of non-metric property for the metric tensor in the case of Weyl geometry is:

$$\breve{\nabla}_\lambda g_{\alpha\beta} = -2A_\lambda g_{\alpha\beta} \quad . \tag{A.7}$$

$\breve{\nabla}_\lambda$ is defined similarly in a general case with replacement of Levi-Civita connection with the Weyl one: $\Gamma$ for $\breve{\Gamma}$. Let's remember that metric conditions are valid for Riemann space

$$\nabla_\lambda g_{\alpha\beta} = 0. \tag{A.8}$$

Number $k = W(H)$ is called Weyl weight of the geometric quantity $H$;it is the degree in the Weyl transformation:

$$H \to \tilde{H} = \Omega^k H. \tag{A.9}$$

Weyl covariant derivatives are determined as follows in the general form for scalar $h$, vector $h_\alpha$ and tensor $h_{\alpha\beta}$:

$$\breve{D}_\mu h(x) = \left[\breve{\nabla}_\mu + W(h)A_\mu\right] h(x) = \breve{\partial}_\mu h(x), \tag{A.10}$$

$$\breve{D}_\mu h_\alpha \equiv \left[\breve{\nabla}_\mu + W(h_\alpha)A_\mu\right] h_\alpha, \tag{A.11}$$

$$\breve{D}_\mu h_{\alpha\beta} \equiv \left[\breve{\nabla}_\mu + W(h_{\alpha\beta})A_\mu\right] h_{\alpha\beta}. \tag{A.12}$$

Geometric quantities that get transformed with Weyl weight $W$are called Weyl covariants, and if $W(H) = 0$, then they are Weyl invariants. The action for the Weyl gravitation $S$ should be Weyl invariant: $\tilde{S} = S$. Lagrangian of gravitation $L$ respectively should be Weyl covariant with weight $W(L) = -4$, since $W\left(\sqrt{|\det g|}\right) = 4$, and

$$S_g = \int d^4x\sqrt{|\det g|} \cdot L_g. \tag{A.13}$$

Let us note that spaces $(M, g, A)$ and $(M, \tilde{g}, \tilde{A})$ coincide up to isomorphism a Weyl transformation, i.e. a local scale transformation does not change Weyl space. All examples of $(M, \tilde{g}, \tilde{A})$ are equivalent. They are joined in the class of equivalency with regard to gauge $\Omega$. Real physical space-time $(M, g_1, A_1)$ is unique with regard to the choice of gauge, i.e. among the set of all Weyl equivalent examples from the class of $(M, g, A)$ one example is separated at a fixed gauge function $\Omega = \Omega_1$. In this case, we shall say that Weyl invariance is violated. Such violation is related to the fact that in physical gravitation the scales of time, distance and mass are well-defined. Let's point out that in the case when $A$ is the exact 1-form in the object $(M, g, A)$, we can select gauge $\Omega$ in such a way that $\tilde{A}_\mu$ will turn to zero on the all space $M$:

$$A_\mu \to \tilde{A}_\mu = A_\mu - \frac{\partial\sigma}{\partial x^\mu} = 0. \tag{A.14}$$

Such Weyl space is called an integrable Weyl space. For integrable Weyl geometry $A = d\sigma$. Object $(M, g, d\sigma)$ is called in the references as IWG (Integrable Weyl Geometry) or WIST (Weyl Integrable Space Time).

### B. Weyl-Dirac Theory

The action of Weyl-Dirac gravitation is written as follows:

$$S_\beta = -\frac{M_P^2}{2}\int L_\beta\sqrt{|g|}d^4x = -\frac{1}{16\pi}\int L_\beta\sqrt{|g|}d^4x, \tag{B.1}$$

where Lagrangian $L_\beta$ is written as:

$$L_\beta = \beta^2 R - 6\beta^2 A_\lambda A^\lambda + 12\beta\beta_\lambda A^\lambda + \alpha\left(\beta_\mu - A_\mu\cdot\beta\right)\cdot\left(\beta^\mu - A^\mu\cdot\beta\right) + 2\lambda\beta^4 + \omega^2 F^{\mu\nu}F_{\mu\nu}, \tag{B.2}$$

or

$$L_\beta = \beta^2 R + 6\beta_\lambda\beta^\lambda + (\alpha - 6)\left(\beta_\mu - A_\mu\cdot\beta\right)\cdot\left(\beta^\mu - A^\mu\cdot\beta\right) + 2\lambda\beta^4 + \omega^2 F^{\mu\nu}F_{\mu\nu}, \tag{B.3}$$

And the strength of vector $A^\lambda$ :

$$F_{\mu\nu} = \partial_\mu A_\nu - \partial_\nu A_\mu. \tag{B.4}$$

Let us introduce an ordinary matter. Its presence can both preserve Weyl symmetry (electromagnetic, radiation) and violate it (baryon matter). Equations of motion are obtained by varying the action by metric $\delta g_{\mu\nu}$, by field $\delta\beta$ and by vector $\delta A^\nu$:

$$R^{\mu\nu} - \frac{1}{2}g^{\mu\nu}R \equiv G^{\mu\nu} = T^{\mu\nu} = T^{(\beta)\mu\nu} + T^{(A)\mu\nu} + T^{(F)\mu\nu} + \frac{8\pi T^{(m)\mu\nu}}{\beta^2} - g^{\mu\nu}\lambda\cdot\beta^2(x) \quad , \tag{B.5}$$

where
$$T^{(\beta)\mu\nu} = \frac{1}{\beta^2}\left(-2 + \frac{\alpha}{2}\right) g^{\mu\nu}\beta_\alpha\beta^\alpha + \frac{1}{\beta^2}(2-\alpha)\beta^{\mu\nu} - \frac{2}{\beta^2} g^{\mu\nu}\beta\cdot\beta^{\alpha}_{;\alpha} + \frac{2}{\beta^2}\beta\beta^{\mu;\nu}, \tag{B.6}$$

$$T^{(A)\mu\nu} = (\alpha-6)\left(-A^\mu A^\nu + \tfrac{g^{\mu\nu}}{2}A^\lambda A_\lambda\right) + \tfrac{(\alpha-6)}{\beta}\left(\beta^\mu A^\nu + \beta^\nu A^\mu - g^{\mu\nu}\beta_\lambda A^\lambda\right) \quad , \tag{B.7}$$

$$T^{(F)\mu\nu} = \omega^2\frac{8\pi}{\beta^2}\left[\frac{1}{16\pi}g^{\mu\nu}F^{\lambda\rho}F_{\lambda\rho} - \frac{1}{4\pi}F^\mu_\lambda F^{\nu\lambda}\right] = \frac{\omega^2}{\beta^2}\left[\frac{1}{2}g^{\mu\nu}F^{\lambda\rho}F_{\lambda\rho} - 2F^\mu_\lambda F^{\nu\lambda}\right], \tag{B.8}$$

$T^{(m)\mu\nu}$ is the tensor of energy-momentum of regular matter. Quantities $T^{(m)\mu\nu}$,$\psi$ and $J^\mu$ are parts of the expression for variation of Lagrangian $L_{matter}$ of the regular matter:

$$S_m = \int d^4x \cdot L_{matter}\sqrt{-g} \quad , \tag{B.9}$$

$$\delta\left(L_{matter}\sqrt{-g}\right) = 8\pi T^{(m)\mu\nu}\delta g_{\mu\nu}\sqrt{-g} + 16\pi J^\lambda\delta A_\lambda\sqrt{-g} + \Psi\delta\beta\sqrt{-g}. \tag{B.10}$$

This density of the Weyl charge of the regular matter and the density of the Weyl current of the usual matter. Variations by field $\delta\beta$ give the following equation:

$$R = \alpha\frac{\beta^{\lambda}_{;\lambda}}{\beta} - 4\beta^2\lambda - (\alpha-6)\left(A^\lambda A_\lambda + A^\lambda_{;\lambda}\right) - \frac{\psi}{2\beta} \quad . \tag{B.11}$$

Variation by vector $\delta A^\nu$ gives the equation:

$$4\omega^2 F^{\mu\nu}_{;\nu} = 16\pi J^\mu - 2(\alpha-6)\beta\left(\beta^\mu - \beta A^\mu\right) \quad . \tag{B.12}$$

Let us say some words about different gauges.

As it follows from the equation for function $\beta$ (B.11) when parameters $\lambda > 0$, $\alpha = 0$, $\Psi = 0$, the following ratio is valid

$$\beta^2 = -\frac{1}{4\lambda}\breve{R}. \tag{B.13}$$

With replacements of this value in the Weyl-Dirac operation, we get:

$$S_\beta = \frac{1}{16\pi}\int\left(\frac{\breve{R}^2}{8\lambda} - \omega^2 F^{\mu\nu}F_{\mu\nu}\right)\sqrt{|g|}d^4x, \tag{B.14}$$

That is we get Weyl gravitation action.

If we put $A^\lambda \equiv \beta^\lambda$, then we get integrable Weyl geometry, and $F_{\mu\nu} = 0$.

If we put $\beta = 1$, then conformal symmetry gets violated, and Weyl-Dirac operation complies with GR operation; but there is a small detail – when $F_{\mu\nu} \neq 0$, the geometry of space-time will not be the Riemann one and there will be the "second clock effect".

### C. Problems of Weyl-Dirac theory

1. Weyl vector $A^\lambda$ as a part of Weyl connection can't be associated with electromagnetic potential $B^\lambda$. Let us emphasize that unlike electromagnetic potential Weyl vector $A^\mu$ acts on the particle not only due to the Weyl charge available and non-zero strength, but also as it is via Weyl connection.

   In fact, if Weyl vector $A^\lambda$ is a vector of electromagnetic potential $B^\lambda$, it will be a part of electromagnetic connection and then you have to differentiate two metrics $ds^2_E$ and $ds^2_A$. Metric $ds^2_E$ is connected with gravitation and electromagnetism equations, and metric $ds^2_A$ is connected with the distances measured in atomic physics and elementary particle physics. It is not natural, as Albert Einstein noted [2]. Besides, the development of quantum mechanics has shown that electromagnetic potential $B^\lambda$ is connected with a compact group of transformations of the field phase and so it is a part of "long derivative" as $ieB^\lambda$, that is with a multiplier in the form of an imaginary unit. Vector $A^\lambda$ is connected with a noncompact group of length scale transformations.

2. As Albert Einstein noted, existence of sharp spectral lines in the radiation from stars is impossible in space-time described with non-integrable Weyl geometry due to the fact that the velocity of travel speed of the atomic clock depends on its past history or, in other words, two clocks that have travelled in the Universe in different ways and come back to the initial point will have different rate speed (the "second clock effect").

   Weyl geometry results to two types of geodesic lines – invariant and covariant. Covariant geodesic lines can be interpreted as extremals of action for the point particle with a variable mass. Equations of free motion, respectively, for a point particle in Weyl geometry contain an additional term that can be called a specific Weyl force.This term changes the scale of the mass until violation of conformal invariance, but after the local conformal invariance is violated, it results into real changes in the mass of a physical particle.

   A violation of the conformal invariance implies the choice of a particular example of Weyl space from the class of equivalence with regard to Weyl transformations.

   Change of the 4-momentum of $p^\mu$ classical Weyl particle is defined with equation

$$\frac{dp^\lambda}{ds}+\frac{1}{m}\Gamma^\lambda_{\mu\nu}p^\mu p^\nu=m\cdot A^\lambda+q_W\cdot F^\lambda_\mu\frac{dx^\mu}{ds}, \tag{C.1}$$

   where

$$p^\lambda=mu^\lambda \quad , \quad u^\alpha=\frac{dx^\alpha}{ds}, \quad ds=\sqrt{|g_{\alpha\beta}dx^\alpha dx^\beta|}, \quad |u_\alpha u^\alpha|=1 \quad , \quad W(u)=-1, \tag{C.2}$$

   $q_W$ is Weyl charge.

   In a non-relativistic case the change of the momentum is $\Delta\vec{p}=\Delta\left(m\vec{v}\right)=m\cdot\Delta\vec{v}+\Delta m\cdot\vec{v}.$

   In a non-integrable case in the loop at $F^\nu_\mu\neq 0$ the change of mass $\Delta m$ takes take place for the mass point mass point. This is also a manifestation of the so-called "second-clock effect". Our interpretation of the mass change is based on parameterization set with expression (C.2), which is most close to the parameterization of geodesic lines in the general theory of relativity.

   We note that manifestation of the "second-clock effect" can be interesting as the way to change the mass of the particle when going through microscopic areas of nonzero strength $F^\lambda_\mu$ of Weyl vector $A_\mu$. But such change of the mass surely must be a discrete one; that is the field of the Weyl vector and its strength must be quantum. Besides, such a possibility should not contradict experimental facts and general concepts of particle physics.

   Some authors use the gradient of scalar function $\beta$ instead of the Weyl vector in geodesic lines despite the fact that there is a nonzero strength $F_{\alpha\beta}$ of Weyl vector $A^\lambda$ in the Lagrangian. In our opinion, it is inconsistent option. Of course, it allows getting rid of the"second-clock effect", but it does not correspond to the spirit of the Weyl geometry.

### D. Solving the problems of Weyl-Dirac gravitation theory

In a non-integrable case of the Weyl vector,we offer two ways out. In particular, these methods are as follows:

1. a non-integrable Weyl vector has small norm at the macroscopic scales, and changes chaotically, so averaging by vector field results in some stochastization of the motion of the particle;

2. a non-zero value of the Weyl vector is only in the area of Plank scales, in analogues of vortons–vortex rings. And here the change in the mass of other particles at interaction with Weyl analogues of vortons happens in a discrete way.

- *Method 1. Stochastic Weyl vector.* Let the influence of random Weyl vector field $A^\lambda$ on the motion of the particle be rather small, the field of vector $A^\lambda$ itself does not have preferential directions and is isotropic. Let us consider the equation of particle motion in compliance with covariant Weyl geodesic line

$$du^\mu + \Gamma^\mu_{\alpha\beta} u^\alpha u^\beta \cdot ds = -\left[ \left(A^\alpha u_\alpha\right) u^\lambda - A^\lambda \right] \cdot ds \tag{D.1}$$

Let us consider value

$$\xi^2 = -\left(A^\lambda - \left(A^\alpha u_\alpha\right) u^\lambda\right)\left(A_\lambda - \left(A^\alpha u_\alpha\right) u_\lambda\right) = \left(A^\alpha u_\alpha\right)^2 - A^\lambda A_\lambda. \tag{D.2}$$

This value is invariant. So, we can introduce density distribution of the normal type for random value

$$\xi = \sqrt{-g_{\alpha\beta}(x) A^\alpha_\perp(x) A^\beta_\perp(x)}, \tag{D.3}$$

where $A^\lambda_\perp = A_\lambda - \left(A^\alpha u_\alpha\right) \cdot u^\lambda$.

Let's introduce Lagrangian equation with the proper time of the particle $d\tau = ds$,

$$du^\mu + \Gamma^\mu_{\alpha\beta} u^\alpha u^\beta \cdot d\tau = \sigma A^\mu_\perp \cdot d\tau, \quad \left\langle A^\lambda_\perp(\tau)\right\rangle = 0 \quad , \quad \left\langle A^\lambda_\perp(\tau_1) \cdot A_\perp \mu(\tau_2)\right\rangle = -\sigma^2 \cdot \delta^\lambda_\mu \cdot \delta\left(\tau_1 - \tau_2\right). \tag{D.4}$$

We get an equation that describes Brownian process. In fact, there is fluctuation around classical GR trajectory.

- *Method 2. Tubes of weylons.* Let us assume that the field of Weyl vector at quantization results to very massive particles - weylons [13]. Weylons interact with usual particles at very small distances. Let us consider non-relativistic motion of very heavy weylons. If weylons form structures as closed, chaotically directed tubes, then we see analogue with superfluid vortex lines in helium. It would have been more realistic to consider a model of vortex threads in the form of vortons analogues.

With the chaotic orientation of these vortons, the average contribution to the change in the mass of particles when passing through a region of vortons is zero. If the mass of the weylon is close to the Planck mass, then the processes of particle scattering on the vortons are significant only at small (Planck) distances. In that case, the "second-clock effect" at macroscopic distances is not observed, and at small (Plank) distances the particles should be described with quantum theory and can change the mass in discrete way interacting withweylon. So, these vortons that are analogues to rotons. These processes could take place at the early stage of the Universe existence at very high energies.

- *Method 3.Integrable Weyl Geometry (IWG).* Let Weyl vector $A$ in defining Weyl space $(M, g, A)$be equal to the gradient of scalar function:

$$A_\nu = \frac{\partial_\nu \beta(x)}{\beta}, \tag{D.5}$$

where $\beta(x)$ is Dirac function. Let us introduce another vector, $C_\mu(x)$, that changes the same way as Weyl vector $A_\mu$ in Weyl transformation:

$$C_\mu \to \tilde{C}_\mu = C_\mu - \frac{\partial \ln \Omega(x)}{\partial x^\mu}. \tag{D.6}$$

Then modified Weyl-Dirac Lagrangian takes the form:

$$L_{\text{mod}} = \beta^2 R + 6\beta_\lambda \beta^\lambda + \alpha\left(\beta_\mu - C_\mu \cdot \beta\right) \cdot \left(\beta^\mu - C^\mu \cdot \beta\right) + 2\lambda\beta^4 + \omega^2 E^{\mu\nu} E_{\mu\nu}, \tag{D.7}$$

There is the strength of vector $C^\lambda$ in the Lagrangian:

$$E_{\mu\nu} = \partial_\mu C_\nu - \partial_\nu C_\mu \quad , \tag{D.8}$$

and Weyl vector $A^\lambda$ is not a part of the Lagrangian any more, and number 6 is not subtracted from $\alpha$. Let us emphasize again that $A_\mu$ and $C_\mu$ are completely different vectors. Exactly vector $A_\mu$ is used in defining Weyl connection:

$$\breve{\Gamma}^\lambda_{\mu\nu} = \Gamma^\lambda_{\mu\nu} + \delta^\lambda_\mu A_\nu + \delta^\lambda_\nu A_\mu - g\mu\nu A^\lambda. \tag{D.9}$$

- *Accounting for the electromagnetic field.* Let us introduce a complex field $\varphi$. And let us introduce a complex gauge Weyl vector $w$ that combines real vector $C$ (related to the changes in the norm of field $\varphi$) and real electromagnetic potential $B$ (related to the changes in the phase of field $\varphi$):

  $$w = C + iB. \tag{D.10}$$

  An electric charge is included in the electromagnetic potential vector $B$. Let us introduce the expression for the complex scalar field:

  $$\varphi(x) = \sigma(x) \cdot \exp\left(i \cdot \eta(x)\right). \tag{D.11}$$

  Then we can define the complex invariant Weyl derivative:

  $$\mathring{\hat{\partial}}_\mu \varphi = \partial_\mu \varphi - w_\mu \cdot \varphi = \left(\frac{\sigma_\mu}{\sigma} - C_\mu\right)\chi + i\left(\eta_\mu - B_\mu\right)\chi. \tag{D.12}$$

## E. Modification of the Weyl-Dirac theory of gravitation

Taking into account all the comments made, we formulate a modified model of gravitation close in spirit to the Weyl-Dirac gravitation.

*Modified model.* In our model there is a real dilaton field $\beta(x)$, a complex scalar field $\varphi(x)$, a real vector $C_\mu(x)$, electromagnetic potential $B_\mu(x)$. Let us introduce dimensionless parameters $\alpha$, $\mu$,$\lambda$, $\rho$, $\xi$, $\omega^2$, $\delta^2$. Action

$$S_{\beta\varphi} = -\frac{M_P^2}{2}\int d^4x\sqrt{-g}\cdot L_{\beta\varphi} \quad . \tag{E.1}$$

The Lagrangian of the model gets written as:

$$\begin{gathered} L_{\beta\varphi} = \beta^2 R + 6\beta_\lambda\beta^\lambda + \alpha g^{\mu\nu}\left(\beta_\mu - C_\mu\cdot\beta\right)\cdot\left(\beta_\mu - C_\mu\cdot\beta\right) + \mu\left(\varphi\varphi^* - \rho\cdot\beta^2\right)^2 \\ +2\lambda\beta^4 + \xi g^{\mu\nu}\left(\partial_\mu\varphi - \left(C_\mu + iB_\mu\right)\cdot\varphi\right)^*\cdot\left(\partial_\nu\varphi - \left(C_\nu + iB_\nu\right)\cdot\varphi\right) \\ +\delta^{2\mu\nu}H_{\mu\nu} + \omega^2 E^{\mu\nu}E_{\mu\nu} \end{gathered} \quad . \tag{E.2}$$

Affine connection is written within the framework of the integrable Weyl geometry (IWG),that is Weyl vector is gradient:

$$A_\nu \equiv \frac{\partial\beta_\nu}{\beta}. \tag{E.3}$$

Before the violation of conformal symmetry, the mass of the particles depends on the dilaton field: $m = m_0\cdot\beta\,(x)$. The strengths of vector fields $C$ and $B$, generally speaking, are nonzero:

$$E_{\mu\nu} = \partial_\mu C_\nu - \partial_\nu C_\mu, \quad H_{\mu\nu} = \partial_\mu B_\nu - \partial_\nu B_\mu. \tag{E.4}$$

In this model, the vector $C$ also transformed by local conformal transformations as the Weyl vector $A$:

$$g_{\mu\nu} \to \tilde{g}_{\mu\nu} = \Omega^2(x)\cdot g_{\mu\nu} \quad , \quad A_\mu \to \tilde{A}_\mu = A_\mu - \frac{\partial\ln\Omega(x)}{\partial x^\mu} \quad , \quad C_\mu \to \tilde{C}_\mu = C_\mu - \frac{\partial\ln\Omega(x)}{\partial x^\mu}, \tag{E.5}$$

but does not coincide with it. This property allows getting rid of the ”second clock effect”.

In model (E.2) you can replace scalar $\varphi$ with a doublet of the Higgs field: $\varphi(x) \to H(x)$, as well as add interaction with fermions. You can also enter gauge fields.

Let us note that vector $C^\lambda$ after fixing the gauge of $\beta = 1$ satisfies Proca equations [13], and can be studied as a component of the dark matter. Constant $\Lambda$ in Einstein equations comes from the term $2\lambda\beta^4$ in the Lagrangian (E.2), and can be a source of dark energy.

### F. Violation of conformal symmetry in Weyl-Dirac gravitation

In the real Universe, the symmetry of the gravity equations with regard to local scale transformations of the metric is violated; the mass scale is fixed at the atomic level and the level of elementary particles. So, here comes the question: What is the "right" way to break this symmetry?

1. It can be broken "manually", by putting $\beta(x) = 1 + \varepsilon(x)$, $|\varepsilon(x)| << 1$. Many researchers did that, including Dirac, Rosen, and Israelit.
2. You can try to come up with a mechanism for spontaneous breaking of this symmetry, combining it with the Higgs mechanism of mass generation in particle physics.
3. Note that its "natural" violation occurs due to quantum corrections. We will consider this mechanism further in more detail using an example.

As an example, we shall further consider conformal invariant operation with Dirac field $\beta$ and real scalar massless field $\varphi$:

$$\begin{array}{l} S_{\beta\varphi} = -\frac{1}{16\pi}\int d^4x\sqrt{-g}\{R\cdot\beta^2 + 6g^{\mu\nu}\beta_\mu\beta_\nu \\ +2\lambda\cdot\beta^4 + 2\lambda_\varphi\varphi^4 + \xi g^{\mu\nu}\left(\partial_\mu\varphi - \frac{\beta_\mu}{\beta}\cdot\varphi\right)\cdot\left(\partial_\nu\varphi - \frac{\beta_\nu}{\beta}\cdot\varphi\right)\} \end{array} \tag{F.1}$$

- *The first type of quantum corrections.* This kind of quantum corrections is related to the fact that the term $2\lambda_\varphi\cdot\varphi^4$ changes taking into account quantum fluctuations. We will interpret field $\varphi$ in a quantum way by introducing classical parts of the field $\varphi_{quant} = \varphi + \Delta\varphi$, where $\Delta\varphi$ are quantum fluctuations. If the classical part of the field is nonzero, then a replacement should be made [32]:

$$2\lambda_\varphi\varphi^4 \to 2\lambda_\varphi\varphi^4\cdot\frac{1}{1-\frac{9\lambda_\varphi}{\pi^2}\ln\left(\frac{\varphi}{M}\right)} + R\varphi^2\left[1 + (\varsigma - 1)\cdot\frac{1}{\left(1-\frac{9\lambda_\varphi}{\pi^2}\ln\left\{\frac{\varphi}{M}\right\}\right)^{\frac{1}{3}}}\right] \quad . \tag{F.2}$$

  This type of corrections does not violate Weyl invariance if we introduce an additional conformal –invariant field for cutting mass $M(x) \sim \beta(x)$.

  If we turn to splitting the potential

$$2\lambda_\varphi\varphi^4 \to 2\lambda_\varphi\left\langle\varphi^2\right\rangle\varphi^2,$$

  then we can put $\left\langle\varphi^2\right\rangle \sim \beta^2(x)$. So, there is a way to avoid the violation of the local scale symmetry for the first type of quantum corrections.

- *The second type of quantum corrections.* Vacuum polarization takes place in a strong gravitation field, and the trace of the energy-momentum tensor of the quantized field $\varphi$ receives quantum additives. Let us note that value $\psi(x) = \frac{\varphi(x)}{\beta(x)}$ is Weyl invariant. Let $\psi = 0$. Nevertheless, there are additives due to quantum fluctuations in field $\psi$. The vacuum state $|0>$ should be taken for the field $\varphi = \beta\psi$, and consider the renormalized energy-momentum tensor $\left\langle 0\left|T_\mu^{(\varphi)}\nu\right|0\right\rangle_{ren} = \left\langle 0\left|\beta^2 T_\mu^{(\psi)}\nu\right|0\right\rangle_{ren}$, taking $\beta$ as a classical quantity. Let us note that $\beta$ function should not be quantized as it is a part of geometric connection (D.3), (40). Besides, the function is strictly positive $\beta(x) > 0$ , and vacuum state with $\beta = 0$ is not determined for it. We presume field $\beta(x)$ as non-physical dilaton field.

  Let us provide an expression for anomalous trace of the energy-momentum tensor (see [33]):

$$\frac{\left\langle T_\lambda^{(0)}\lambda\right\rangle_{ren}}{8\pi} = \frac{1}{2880\pi^2}\left(e\cdot C_{\alpha\beta\gamma\delta}C^{\alpha\beta\gamma\delta} + b\left(R_{\alpha\beta}R^{\alpha\beta} - \frac{1}{3}R^2\right) + cR + d\cdot R^2\right) \quad , \tag{F.3}$$

  where $C_{\alpha\beta\gamma\delta}$ is Weyl tensor, $b, c, d, e$ are numerical coefficients.

Unsteady-state isotropic metrics of FLRW with conformal time $\eta$ :

$$ds^2 = a^2(\eta)\left[d\eta^2 - dr^2 - h^2(r)\left(d\vartheta^2 + \sin^2\vartheta d\varphi^2\right)\right] \quad , \quad h(r) = \left\{ \begin{array}{l} sh(r), k=-1 \\ \sin(r), k=+1 \\ r, k=0 \end{array} \right\} \quad , \tag{F.4}$$

result into the equation for $f$ as follows (see [15], [34]):

$$\ddot{f} + k \cdot f - sign(\lambda) \cdot f^3 = 0 \tag{F.5}$$

Here, $f(\eta)$ is determined with the expression with random $\beta(x) > 0$:

$$\beta(\eta) \cdot a(\eta) = \sqrt{\frac{3}{2|\lambda|}} f(\eta). \tag{F.6}$$

Accounting for quantum corrections of the second type, we get:

$$\ddot{f} + k \cdot f - sign(\lambda) \cdot f^3 = \sqrt{\frac{3}{2}|\lambda|} \cdot \frac{a^3}{\beta} \frac{\xi}{2160\pi}\left(b\left(R_{\alpha\beta}R^{\alpha\beta} - \frac{1}{3}R^2\right) + cR + d \cdot R^2\right). \tag{F.7}$$

Anomalous quantum additives have appeared that violate scale invariance of the initial equation.

- *Example.* Let's consider a flat case, $k=0$. Then, having taken the values of parameters $b=-1$, $c=6$, $d=-\frac{5}{2}$ from [33], we get here $\beta^{(n)} \equiv \frac{d^n\beta(\eta)}{d\eta^n}$) :

$$b\left(R_{\alpha\beta}R^{\alpha\beta} - \tfrac{1}{3}R^2\right) + c \cdot \Box R + d \cdot R^2 \sim -\tfrac{2\lambda^2}{3} \cdot 58\beta^4 - \tfrac{2\lambda^2}{3}\left(44\beta^3\beta^{(1)}\eta + 104\beta^2\beta^{(2)}\eta^2 + 44\beta\beta^{(3)}\eta^3\right.$$
$$+58\beta^{(4)}\eta^4 - \left(94\beta^{(2)}\eta^2 - 16\beta\beta^{(1)}\eta + 22\beta^2\right)\beta^2\beta^{(2)}\eta^2$$
$$\left.+33\beta^2\beta^{(2)}\beta^{(2)}\eta^4 + 24\beta^2\beta^{(3)}\beta^{(1)}\eta^4 - 6\beta^3\beta^{(4)}\eta^4\right).$$

At $\beta = 1$

$$b\left(R_{\alpha\beta}R^{\alpha\beta} - \frac{1}{3}R^2\right) + cR + d \cdot R^2 \sim -\frac{2\lambda^2}{3} \cdot 58\beta^4.$$

So, the equation for scale factor $a(\eta)$ takes the form:

$$\ddot{f} + k \cdot f - sign(\lambda_{ren}) \cdot f^3 = 0 \quad , \tag{F.8}$$

where

$$\lambda_{ren} = \lambda + \frac{\xi}{1080\pi}(b - 12d)\lambda^2, \quad f(\eta) = a(\eta)\sqrt{\frac{2|\lambda|}{3}}.$$

So, anomalous trace of the energy-momentum tensor (F.7) leads to appearance of derivatives of the function $\beta$ by conformal time $\eta$ in Einstein equation.These derivatives explicitly have violated conformity of equations of gravitation with Lagrangian (F.1). However, we have nullified quantum additives containing derivatives of function $\beta$ over conformal time $\eta$. To do this, we put $\beta(\eta) = const$ and in such a way fix gauge $\beta$. For agreement with GR we put $\beta = 1$. We have got rid of quantum corrections in Einstein equations that depend on derivatives: $\left\langle 0 \left| T_{\mu}^{(\varphi)}\nu \right| 0 \right\rangle_{ren} = 0$, but cosmological parameter $\lambda$ happened to be renormalized: $\lambda_{ren} = \lambda + \frac{\xi}{1080\pi}(b-12d)\lambda^2$.

So, in our opinion, a natural way to violate Weyl invariance is accounting for quantum vacuum corrections for the energy-momentum tensor of different physical fields in the Lagrangian.

## G. On Mannheim-Kazanas solution

Within Einstein's standard equations of general relativity, the flat rotation curves of galaxies cannot be explained without the hypothesis of dark matter, the particles of which have not yet been identified. The vacuum centrally symmetric solution of the equations of conformal gravity is the well-known

Mannheim-Kazanas metric (see [23]), on the basis of which these curves have got a purely geometric explanation [24]. In 2017, we showed (see [35]), that the Mannheim-Kazanas metric is a solution not only to the Bach equations obtained from the Weyl conformal invariant Lagrangian, but also the solution of the equations of a simplified version of the Weyl-Dirac theory with a nonzero Weyl vector [16], [17]:

$$R_{\alpha\beta} - \frac{1}{2} g_{\alpha\beta} R = -2A_\alpha A_\beta - g_{\alpha\beta} A^2 - 2 g_{\alpha\beta} A^\nu_{;\nu} + A_{\alpha;\beta} + A_{\beta;\alpha} + \lambda(x) g_{\alpha\beta}$$

The solution looks as follows:

$$ds'^{*}2 = -F\left(R\right) dt^2 + \frac{dR^2}{F\left(R\right)} + R^2 \left[d\theta^2 + \sin^2\theta d\varphi^2\right],$$

$$A'^{*} = \frac{1}{\left(R_0 - R\right)}, \quad \lambda'^{*} = \frac{\lambda_0 R_0^2}{\left(R_0 - R\right)^2},$$

$$F(R) = \left(1 - \frac{R}{R_0}\right)^2 \left(1 + \frac{r_0}{R_0} - \frac{r_0}{R}\right) + \frac{\lambda_0 R^2}{3} \quad .$$

This solution can lead to the Mannheim-Kazanas solution

$$ds^2 = -\left(e^\gamma\right)_{MK} dt^2 + \left(e^{-\gamma}\right)_{MK} dR^2 + R^2 \left[d\theta^2 + \sin^2\theta d\varphi^2\right],$$

where

$$\left(e^\gamma\right)_{MK} = \left(1 - 3\beta\gamma\right) - \frac{\beta\left(2 - 3\beta\gamma\right)}{R} + \gamma R - \kappa R^2.$$

To do this, you need to turn parameters $\beta,\ \gamma,\ \kappa$ into parameters $r_0,\ R_0$ as follows:

$$\left.\beta = \frac{r_0}{R_0\left(2 + 3\frac{r_0}{R_0}\right)}, \qquad \gamma = -\frac{\left(2 + 3\frac{r_0}{R_0}\right)}{R_0}, \quad \kappa = -\frac{1}{R_0^2}\left(1 + \frac{r_0}{R_0}\right) + \frac{\lambda_0}{3},\right\}$$

Piyabut Burikham, Tiberiu Harko, Kulapant Pimsamaru and Shahab Shabidi [31] showed that the Mannheim-Kazanas metric is the solution of Weyl-Dirac gravitation equations in the integrable case. Their solution is as follows:

$$\exp(-\lambda) = \exp\left(\nu\right) = 2\beta + \frac{1 + 2\beta}{C_2} r - \frac{C_2(1 - 2\beta)}{3}\frac{1}{r} + C_3 r^2$$

It is evident that it gets down to Mannheim-Kazanas solution.

So, Weyl-Dirac gravitation can be used as an alternative theory to explain the dark matter phenomenon. We should note that the required deviation of Dirac function $\beta(x)$ from unit is small (when measured in Planck units of mass).

**Conclusion**

The paper discusses the models of conformal gravitation with Lagrangians linear in scalar curvature and minimal coupling with the scalar field. A variant of the conformal Lagrangian with two scalar fields is proposed, in which the Weyl vector is replaced by a vector that gets transformed like the Weyl vector, but is not a part of the Weyl connection. The space of such a model is the integrable Weyl space.

Within the Weyl's theory of gravitation with a non-minimal coupling of a real scalar field, the problem of describing the conformal stage of the evolution of the Universe, based on the Friedmann metric, is considered. Conformal-invariant solutions for the scale factor are presented and it is shown that quantum corrections to the trace of the energy-momentum tensor violate conformity, partially they are compensated by the gauging of the Dirac function that leads to the Lagrangian of the general theory of relativity.

**Список литературы/References**


1. Weyl H. *Space-Time-Matter.* Translated from the 4th German edition by H. Brose. London: Methuen. Reprint New York: Dover, 1952.
2. Pauli W. *Theory of relativity.* Pergamon Press, 1958.
3. Scholz E. Weyl's scale gauge geometry in late 20th century physics. Preprint submitted to: *"Beyond Einstein: Perspectives on Geometry, Gravitation, and Cosmology"*, ed. David Rowe. Einstein Studies Basel: Birkhäuser, 2011. ArXiv:1111.3220 [gr-qc].
4. Omote M. Scale transformations of the second kind and the Weyl space-time. *Lett. Nuovo Cim.*, 1971, no.2, pp. 58–60.
5. Utiyama R. On Weyl's gauge field. *Progress of Theoretical Physics*, 1973, no. 50, pp. 2028–2090.
6. Dirac P.A.M. Long range forces and broken symmetries. *Proceedings of Royal Society London A*, 1973, no. 333, pp. 403–418.
7. Canuto V., Hsieh S.H. and Adams P.J. Scale-Covariant Theory of Gravitation and Astrophysical Applications. *Phys. Rev. Lett.*, 1977, no. 39, pp. 429-432.
8. Ehlers J., Pirani F., Schild A. The geometry of free fall and light propagation. In General Relativity, Papers in Honour of J.L. Synge, ed. L. O'Raifertaigh. Oxford: Clarendon Press, 1972, pp. 63–84
9. Brans C., Dicke, Robert H. Mach's principle and a relativistic theory of gravitation. *Phys. Rev.*, 1961, no. 124, pp. 925–935.
10. Smolin L. Towards a theory of spacetime structure at very short distances. *Nucl. Phys. B*, 1979, no. 160, pp. 253–268.
11. Cheng H. Possible existence of Weyl's vector meson. *Phys. Rev. Lett.*, 1988, no. 61, pp. 2182–2184.
12. Rosen N. Weyl's geometry and physics. *Foundations of Physics,* 1982, no. 12, pp. 213-248.
13. Israelit M., Rosen N. Weyl-Dirac geometry and dark matter. *Foundations of Physics,* 1992, no. 22, pp. 555–568.
14. Scholz E. Paving the way for transitions - a case for Weyl geometry. ArXiv:1206.1559v6 [gr-qc].
15. Staniukovich K.P. and Melnikov V.N. *Gidrodinamika, polya I konstanty v teorii gravitacii [Hydrodynamics, Fields and Constants in the Theory of Gravitation]*. Moscow: Energoatomizdat, 1983 (in Russian). See an updated English translation of the first 5 chapters in: Melnikov V.N. *Fields and Constants in the Theory of Gravitation*, CBPF MO-02/02, Rio de Janeiro, 2002.
16. Gorbatenko M. V., Pushkin A. V. and Schmidt H.-J. On a Relation between the Bach Equation and theEquation of Geometrodynamics. *Gen. Relat. Grav.,* 2002, no. 34, pp. 9-22.
17. Gorbatenko M.V., Pushkin A.V. Conformally Invariant Generalization of Einstein Equation and the Causality Principle. *Gen. Relat. Grav.,* 2002, no. 34, pp. 175; no. 34, pp. 1131.
18. Romanov Yu.A. *Dinamika prostranstva affinnoi svyaznosti [Space dynamics of affine connectivity]. Voprosy atomnoi nauki i tekhniki [Problems of atomic science and technology. Series: Theoretical and Applied Physics]*, 1996, Issue 3. pp. 55-57. (in Russian).
19. Filippov A.T. On Einstein–Weyl unified model of dark energy and dark matter. ArXiv:0812.2616.
20. Babourova O.V., Frolov B.N. *Matematicheskie osnovy sovremennoi teorii gravitacii [Mathematical foundations of the modern theory of Gravitation]*. 2012, MPGU, Moscow, pp. 128 (in Russian).
21. Berezin V. A., Dokuchaev V. I. Weyl geometry and cosmological particle creation. *Space, Time and Fundamental Interactions,* 2022, no. 40, pp. 13–29.
22. Berezin V.A., Dokuchaev V.I. and Eroshenko Yu.N. Particle creation phenomenology, Dirac sea and the induced Weyl and Einstein–dilaton gravity. arXiv:1604.07753v2 [gr-qc].
23. Mannheim Ph.D. and Kazanas D. Exact vacuum solution to conformal Weyl gravity and galactic rotation curves. *The Astrophysical Journal,* 1989, no. 342, pp. 635-638.

24. O'Brien J.G. , Mannheim P.D. Fitting dwarf galaxy rotation curves with conformal gravity. *Monthly Notices of the Royal Astronomical Society,* 2012, no. 421, pp. 1273–1282.
25. Oda I. Planck and Electroweak Scales Emerging from Conformal Gravity. *School and Workshops on Elementary Particle Physics and Gravity (CORFU2019).* 31 August - 25 September 2019.
26. Oda I. Planck Scale from Broken Local Conformal Invariance in Weyl Geometry. ArXiv, 2019. arXiv:1909.09889v1 [hep-th].
27. Quiros I. Scale invariant theory of gravity and the standard model of particles. arXiv:1401.2643v4 [gr-qc].
28. Jimenez J.B. and Koivisto T.S. Extended Gauss-Bonnet gravities in Weyl geometry. ArXiv:1402.1846v1 [gr-qc].
29. Adriano Barrosand Carlos Romero. Homogeneous Cosmological Models in Weyl's Geometrical Scalar–Tensor Theory. *Universe,* 2023,no. 9, pp. 283.
30. Ghilencea D. M. and Lee H.M. Weyl gauge symmetry and its spontaneous breaking in Standard Model and inflation. ArXiv:1809.09174v3 [hep-th].
31. Burikham P., Harko T., Pimsamarn K. and Shahidi S. Dark matter as a Weyl geometric effect. ArXiv:2302.08289v1 [gr-qc].
32. Elizalde E. and Odintsov S.D. Renormalization group improved effective potential for gauge theories in curved space-time. *Phys. Lett. B*, 1993, no. 303, pp. 240-248.
33. Birrell N. D. and Davies P. C. W. *Quantum Fields in Curved Space*, Cambridge: Cambridge University Press, 1982.
34. Grib, A. A., Mamayev, S. G., and Mostepanenko, V. M. *Vakuumnie effekty v silnyh polyah [Vacuum effects in strong fields].* St. Petersburg: Friedmann Laboratory Publishing, 1994 (in Russian).
35. Gorbatenko M.V., Sedov S.Yu. The Mannheim-Kazanas Solution, the conformal Geometrodynamics and the Dark Matter.ArXiv:1711.06189 [gr-qc].

**Авторы**

**Седов Сергей Юрьевич**, старший научный сотрудник, Российский федеральный ядерный центр – Всероссийский научно-исследовательский институт экспериментальной физики, пр. Мира, д. 37, г. Саров, 607188, Россия
E-mail: SerWhites@yandex.ru, SYuSedov@vniief.ru

**Просьба ссылаться на эту статью следующим образом:**

Седов С. Ю. О теории гравитации Вейля-Дирака и ее развитии. *Пространство, время и фундаментальные взаимодействия.* 2023. № 3-4. С. 277–289.

**Authors**

**Sedov Sergey Yurievich**, senior staff scientist, Russian Federal Nuclear Center-All-Russia Research Institute of Experimental Physics, Mira Ave., 37, Sarov, 607188, Russia
E-mail: SerWhites@yandex.ru, SYuSedov@vniief.ru

**Please cite this article in English as:**

Sedov S. Yu. On Weyl-Dirac gravitation theory and its development. *Space, Time and Fundamental Interactions*, 2023, no. 3-4, pp. 277–289.

УДК 514.822, 530.145.65



# РАССЕЯНИЕ ЭЛЕКТРОНОВ НА ЧЕРВОТОЧИНЕ В БОРНОВСКОМ ПРИБЛИЖЕНИИ

Тимофеев В. Н.[a,1]

[a] Санкт-Петербургский государственный университет гражданской авиации имени Главного маршала авиации А.А. Новикова, г. Санкт-Петербург, 196210, Россия.

Одним из интригующих гипотетических объектов в физике гравитационного взаимодействия являются червоточины, которые соединяют либо две удаленные области одной и той же Вселенной, либо две разные вселенные. Для того, чтобы червоточины были проходимыми, т.е. позволяли путешественнику безопасно их пересекать, червоточины в общей теории относительности должны быть заполнены экзотической материей. В данной работе показано, что при определенных условиях количество упруго рассеянных на червоточине Эллиса-Бронникова электронов превосходит количество электронов падающего потока. Дополнительные электроны появляются в результате их перехода через червоточину с противоположной стороны катеноида. Иными словами, с помощью потока электронов, направленных на червоточину, в ней создается отрицательное давление. Это позволяет сделать вывод о том, что таким способом можно стабилизировать червоточину без экзотической материи.

*Ключевые слова*: Рассеяние электронов, функция Грина уравнения Дирака, червоточина, экзотическая материя.

# ELECTRON SCATTERING ON A WORMHOLE IN THE BORN APPROXIMATION

Timofeev V. N.[a,1]

[a] Saint Petersburg State University of Civil Aviation named after Air Chief Marshal A.A. Novikov, Saint Petersburg, 196210, Russia.

The wormholes which connect either two distant regions of the same Universe or two universes are one of the intriguing hypothetical objects in the physics of gravitational interaction. For wormholes to be traversable, i.e., to allow a traveler to cross them safely, the wormholes must be filled with exotic matter within the framework of general relativity. In this paper it is shown that under certain conditions the number of electrons elastically scattered on an Ellis-Bronnikov wormhole exceeds the number of electrons of the incident flux. The additional electrons appear as a result of their transition through the wormhole from the opposite side of the catenoid. In other words, a negative pressure is created in the wormhole by means of the flux of electrons directed to the wormhole. This allows us to conclude that the wormhole can be stabilized without exotic matter in this way.

*Keywords*: Electron scattering, Green's function of the Dirac equation, wormhole, exotic matter.

PACS: 04.20.-q, 11.80.-m

DOI: 10.17238/issn2226-8812.2023.3-4.290-298

## Introduction

Since John Wheeler introduced the concept "wormhole" in 1957, wormholes have caused a huge interest among relativistic researchers, and till now this interest does not decrease. In particular, it is worth noting the message [1], which states that as of January 19, 2023 the word "wormhole" for all time occurs in the titles of 1614 articles on the resource ArXiv.org, and for the last 12 months 175 articles have this term in their titles. Over the past decades, scientists have done a lot of work to study the nature of wormholes, but there are still many unsolved problems. Nevertheless, scientists remain optimistic and, moreover, researchers are making various efforts to search for astrophysical wormholes

[1]E-mail: WTimoff@yandex.ru

in the Universe [2]. The main method of wormhole detection is currently gravitational lensing [3,4]. After the Event Horizon Telescope project obtained an image of the shadow of a black hole in the center of the galaxy M87 [5], the method of wormhole detection by its shadow became relevant [6-8]. Researchers are most interested in traversable wormholes. Such wormholes would allow to travel long distances without violating the velocity limit. In GR, for wormholes to be traversable, the presence of exotic matter is required [9-14]. Traversable wormholes that are not filled with an exotic type of matter are possible only in alternative theories of gravity [15-25]. However, unfortunately, one cannot be sure in the absolute correctness of any theory of gravitation for our Universe. Therefore, it is impossible to state definitively that the existence of traversable wormholes requires the presence or absence of exotic matter. Nevertheless, it is concluded in this work within the framework of GR that by means of a particle stream directed to the wormhole it is possible to create such a condition under which the wormhole could remain open without exotic matter. Thus, the following task is set: to find out within the framework of the Born approximation, what are the properties of the flux of electrons which are scattered on the Ellis-Bronnikov wormhole.

To solve the task, let us:

1. determine the Green's function for the Dirac equation in the gravitational field;
2. convert the Dirac equation to the integral form;
3. find the scattering amplitude in the Born approximation;
4. calculate the total cross sections for elastic and inelastic scattering;
5. describe the properties inherent in the character of electron scattering on a wormhole.

### A. Green's function

It is known that the Green's function $G_o\left(x-x^{'}\right)$ of the Dirac equation for a free particle

$$i\gamma^{(a)}\partial_a\psi - m\psi = 0$$

satisfies the equation

$$i\gamma^{(a)}\partial_a G_o\left(x-x^{'}\right) - mG_o\left(x-x^{'}\right) = \delta\left(x-x^{'}\right)$$

and has the form

$$G_o\left(x-x^{'}\right) = \frac{1}{(2\pi)^4}\int \frac{\widehat{p}+m}{\widehat{p}^2-m^2} e^{-ip\left(x-x^{'}\right)} d^4p, \tag{1}$$

where $\widehat{p} = \gamma^{(a)}p_a$.

Similarly, we can define the Green's function $G\left(x-x^{'}\right)$ for the Dirac equation in an external gravitational field

$$i\gamma^{\mu}\nabla_{\mu}\psi - m\psi = 0$$

as a solution of the equation

$$i\gamma^{\mu}\nabla_{\mu}G\left(x-x^{'}\right) - mG\left(x-x^{'}\right) = \delta\left(x-x^{'}\right), \tag{2}$$

where $\gamma^{\mu} = \gamma^{(a)}e^{\mu}_{(a)}$, $e^{\mu}_{(a)}$ is an orthonormal tetrad.

To characterize the gravitational field let us define the operator $\widehat{\Gamma}$ by the equality

$$\widehat{\Gamma} = \gamma^{(a)}\left(e^{\mu}_{(a)}\nabla_{\mu} - e_{o}{}^{\mu}_{(a)}\nabla_{o\mu}\right),$$

where $\nabla_{\mu} = \partial_{\mu} + \Gamma_{\mu}$ is a covariant derivative in a gravitational field; $\Gamma_{\mu} = \frac{1}{4}\gamma^{\lambda}\gamma_{\lambda;\mu}$ is a spinor connection in a gravitational field; $\nabla_{o\mu} = \partial_{\mu} + \Gamma_{o\mu}$; $e_{o}{}^{\mu}_{(a)}$ and $\Gamma_{o\mu}$ are orthonormal tetrad and spinor connection in curvilinear coordinates in the absence of external gravitational field. In a Cartesian coordinate system $e_{o}{}^{\mu}_{(a)} = \delta^{\mu}_{a}$ and $\Gamma_{o\mu} = 0$.

Then equation (2) can be rewritten as

$$i\gamma^{(\mu)}\nabla_{o\mu}G\left(x-x^{'}\right)+i\widehat{\Gamma}G\left(x-x^{'}\right)-mG\left(x-x^{'}\right)=\delta\left(x-x^{'}\right).$$

This equation can be represented in the integral form

$$G\left(x-x^{'}\right)=G_o\left(x-x^{'}\right)+i\int G\left(x-x^{''}\right)\widehat{\Gamma}\left(x^{''}\right)G_o\left(x^{''}-x^{'}\right)\sqrt{-g\left(x^{''}\right)}d^4x^{''}, \tag{3}$$

where $g(x)$ is a determinant of the matrix $(g_{\mu\nu})$. It is possible to verify the validity of (3) by acting on the left and right parts of the equality (3) with the operator

$$i\gamma^{(\mu)}\nabla_{o\mu}+i\widehat{\Gamma}(x)-m.$$

In the case when the gravitational disturbance is small, it is possible to solve the equation (3) by applying the method of successive approximations and find the Green's function in the form of a series:

$$\begin{aligned}G\left(x-x^{'}\right)=G_o\left(x-x^{'}\right)+i\int G_o\left(x-x^{''}\right)\widehat{\Gamma}\left(x^{''}\right)G_o\left(x^{''}-x^{'}\right)\sqrt{-g\left(x^{''}\right)}d^4x^{''}+\\+i^2\int G_o\left(x-x^{'''}\right)\widehat{\Gamma}\left(x^{'''}\right)G_o\left(x^{'''}-x^{''}\right)\widehat{\Gamma}\left(x^{''}\right)G_o\left(x^{''}-x^{'}\right)\sqrt{-g\left(x^{'''}\right)}\sqrt{-g\left(x^{''}\right)}d^4x^{'''}d^4x^{''}+\ldots.\end{aligned} \tag{4}$$

**B. Dirac Integral Equation**

The following **theorem** is valid: Let a gravitational field be given in which the Green's function $G\left(x^{'}-x\right)$ can be expressed as a uniformly convergent series (4). Then at an arbitrary point $x^{'}$ of the space-time region bounded by the closed hypersurface $\Sigma$ the bispinor describing the motion of an electron in this field can be represented as

$$\psi\left(x^{'}\right)=i\oint G\left(x^{'}-x\right)\gamma^{\mu}(x)\psi(x)\sqrt{-g(x)}dS_{\mu}, \tag{5}$$

where $\oint\ldots\sqrt{-g(x)}dS_{\mu}$ is the integral over the closed three-dimensional hypersurface $\Sigma$.

To prove the theorem let us first prove two auxiliary lemmas:

**Lemma 1.** The equality is valid:

$$\gamma^{\mu}_{;\mu}-\frac{1}{4}\gamma_{\lambda;\mu}\gamma^{\lambda}\gamma^{\mu}-\frac{1}{4}\gamma^{\mu}\gamma^{\lambda}\gamma_{\lambda;\mu}=0,$$

where $\gamma_{\lambda;\mu}=\nabla_{\mu}\gamma_{\lambda}$ is the covariant derivative of $\gamma_{\lambda}$.

**Proof.** It is known that

$$\gamma_{\lambda}\gamma^{\mu}\gamma^{\lambda}=-2\gamma^{\mu}.$$

Let us take the covariant derivative of both sides of this equality

$$\gamma_{\lambda;\mu}\gamma^{\mu}\gamma^{\lambda}+\gamma_{\lambda}\gamma^{\mu}_{;\mu}\gamma^{\lambda}+\gamma_{\lambda}\gamma^{\mu}\gamma^{\lambda}_{;\mu}=-2\gamma^{\mu}_{;\mu}. \tag{6}$$

Considering the equality

$$\gamma^{\mu}\gamma^{\lambda}+\gamma^{\lambda}\gamma^{\mu}=2g^{\mu\lambda}$$

let us rewrite (6) in the form

$$\gamma_{\lambda;\mu}\left(2g^{\mu\lambda}-\gamma^{\lambda}\gamma^{\mu}\right)+\gamma_{\lambda}\gamma^{\mu}_{;\mu}\gamma^{\lambda}+\left(2\delta^{\mu}_{\lambda}-\gamma^{\mu}\gamma_{\lambda}\right)\gamma^{\lambda}_{;\mu}=-2\gamma^{\mu}_{;\mu}.$$

From where

$$6\gamma^{\mu}_{;\mu}-\gamma_{\lambda;\mu}\gamma^{\lambda}\gamma^{\mu}-\gamma^{\mu}\gamma^{\lambda}\gamma_{\lambda;\mu}+\gamma_{\lambda}\gamma^{\mu}_{;\mu}\gamma^{\lambda}=0.$$

Since
$$\gamma_\lambda \gamma^\mu_{;\mu} \gamma^\lambda = \gamma_\lambda \left( e^\mu_{(a);\mu} \gamma^{(a)} \right) \gamma^\lambda = -2 e^\mu_{(a);\mu} \gamma^{(a)} = -2 \gamma^\mu_{;\mu},$$
we get
$$4\gamma^\mu_{;\mu} - \gamma_{\lambda;\mu} \gamma^\lambda \gamma^\mu - \gamma^\mu \gamma^\lambda \gamma_{\lambda;\mu} = 0.$$

Q.E.D.

**Lemma 2.** For the Green's function $G\left(x' - x\right)$ the following equality is valid:
$$\gamma^{(0)} G^+ \left(x - x'\right) \gamma^{(0)} = G\left(x' - x\right).$$

**Proof.** From the equality
$$\gamma^{(0)} \gamma^{(\mu)+} \gamma^{(0)} = \gamma^{(\mu)},$$
for the operators of the form $\widehat{A} = \gamma^{(\mu)} A_\mu$ follows
$$\gamma^{(0)} \widehat{A}^+ \gamma^{(0)} = \widehat{A}, \tag{7}$$
and for the multiplication of operators follows
$$\gamma^{(0)} \left(\widehat{A}\widehat{B}\widehat{C}\right)^+ \gamma^{(0)} = \gamma^{(0)} \widehat{C}^+ \gamma^{(0)} \gamma^{(0)} \widehat{B}^+ \gamma^{(0)} \gamma^{(0)} \widehat{A}^+ \gamma^{(0)} = \widehat{C}\widehat{B}\widehat{A}. \tag{8}$$

Let us substitute the series (4) into the expression $\gamma^{(0)} G^+ \left(x - x'\right) \gamma^{(0)}$. Given the uniform convergence of series (4) and using (7) and (8) we obtain
$$\gamma^{(0)} G^+ \left(x - x'\right) \gamma^{(0)} = G\left(x' - x\right). \tag{9}$$

Here the sign of the argument changes because the sign of the exponent changes at the complex conjugation (1).

Q.E.D.

**Proof of the theorem.** Consider 4-vector
$$F^\mu = \overline{G}\left(x - x'\right) \gamma^\mu(x) \psi(x). \tag{10}$$

Let us calculate the covariant derivative of this 4-vector
$$\nabla_\mu F^\mu = \partial_\mu F^\mu + \Gamma^\mu_{\mu\nu} F^\nu = \frac{\partial \overline{G}\left(x - x'\right)}{\partial x^\mu} \gamma^\mu(x)\psi(x) + \overline{G}\left(x - x'\right) \frac{\partial \gamma^\mu(x)}{\partial x^\mu} \psi(x) +$$
$$+ \overline{G}\left(x - x'\right) \gamma^\mu(x) \frac{\partial \psi(x)}{\partial x^\mu} + \overline{G}\left(x - x'\right) \Gamma^\mu_{\mu\nu} \gamma^\nu(x) \psi(x) =$$
$$= -i\left(i\nabla_\mu \overline{G} \cdot \gamma^\mu \psi + \overline{G} \cdot i\gamma^\mu \nabla_\mu \psi\right) + \overline{G}\left(\nabla_\mu \gamma^\mu - \overline{\Gamma}_\mu \gamma^\mu - \gamma^\mu \Gamma_\mu\right) \psi.$$

Here spinor connections have the form
$$\Gamma_\mu = \frac{1}{4} \gamma^\lambda \gamma_{\lambda;\mu}, \quad \overline{\Gamma}_\mu = \frac{1}{4} \gamma_{\lambda;\mu} \gamma^\lambda.$$

Then given lemma 1 we obtain
$$\nabla_\mu F^\mu(x) = i\gamma^{(0)} \delta\left(x - x'\right) \psi(x). \tag{11}$$

Substituting (10) and (11) into Gauss' formula
$$\int \nabla_\mu F^\mu \sqrt{-g} d^4x = \oint F^\mu \sqrt{-g} dS_\mu$$

we obtain

$$\psi\left(x'\right) = -i\oint \gamma^{(0)}\overline{G}\left(x' - x\right)\gamma^{\mu}(x)\psi(x)\sqrt{-g(x)}dS_{\mu}. \tag{12}$$

By using lemma 2 it is possible to transform the equation (12) into the following form:

$$\psi\left(x'\right) = -i\oint G\left(x' - x\right)\gamma^{\mu}(x)\psi(x)\sqrt{-g(x)}dS_{\mu}.$$

Q.E.D.

The closed 3-surface over which integration is performed (5) consists of infinitely distant timelike 3-surfaces and spacelike 3-surfaces $t = t_1$ and $t = t_1'$ $\left(t_1 < t_1'\right)$. The Green's function in spacelike directions decreases to zero at infinity. Therefore, the integrals on timelike 3-surfaces will be equal to zero. Then given that

$$\gamma^{\mu}\sqrt{-g}dS_{\mu} = \gamma^{\mu}\sqrt{-g}n_{\mu}dS = \pm\gamma^{\mu}\sqrt{-g}e_{\mu}^{(a)}dS = \pm\gamma^{(a)}\sqrt{-g}dS,$$

we represent the equation (5) in the form

$$\psi\left(x_2\right) = i\int_{t_1} G\left(x_2 - x_1\right)\gamma^{(0)}\psi\left(x_1\right)\sqrt{-g\left(x_1\right)}d^3x_1 - i\int_{t_1'} G\left(x_2 - x_1'\right)\gamma^{(0)}\psi\left(x_1'\right)\sqrt{-g\left(x_1'\right)}d^3x_1'. \tag{13}$$

The first summand corresponds to electrons with positive energy, and the second summand corresponds to electrons with negative energy. In this form the equation has a more universal character. It can be used not only for the Born approximation, but also in solving the particle scattering problem by the method of Feynman diagrams. In addition, the equation allows a visual interpretation. The Green's function determines the amplitude of the transition of the electron from the initial state with the wave function $\psi\left(x_1\right)$ to the state with the wave function $\psi\left(x_2\right)$ under the influence of the gravitational field.

### C. Born Approximation

Let the gravitational field be central and stationary. Then we have

$$\psi(x) = \psi\left(\boldsymbol{r}\right)e^{-i\varepsilon t},$$

where $\varepsilon$ is the energy of an electron. In this paper the case of interest is that the function $\psi\left(\boldsymbol{r}\right)$ at $r \to \infty$ has the form of a superposition of plane and spherical divergent waves

$$\psi\left(\boldsymbol{r}\right) \sim ue^{i\boldsymbol{p}_0\boldsymbol{r}} + A\left(\boldsymbol{n}\right)\frac{e^{ipr}}{r},$$

where $\boldsymbol{p}_0$ and $\boldsymbol{p}$ are electron momenta before and after scattering at infinity; $u$ is a bispinor describing the state of an electron with momentum $\boldsymbol{p}_0$; $\boldsymbol{n} = \frac{\boldsymbol{r}}{r}$. Let the initial state of the electron be described by a plane wave

$$\psi\left(x_1\right) = ue^{-i(\varepsilon t - \boldsymbol{p}_0\boldsymbol{r})}.$$

Let us substitute (4) into the first summand of equation (13). Let us restrict ourselves to the first approximation. Then after the transformations known from quantum mechanics [26, 27], we obtain the bispinor $A\left(\boldsymbol{n}\right)$ in the form

$$A\left(\boldsymbol{n}\right) = i\frac{1}{4\pi}\left(-\boldsymbol{\gamma}\cdot\boldsymbol{p} + \gamma^{(0)}\varepsilon + m\right)\int\Gamma\left(\boldsymbol{r}'\right)ue^{i\boldsymbol{K}\boldsymbol{r}'}d^3\boldsymbol{r}', \tag{14}$$

where $\boldsymbol{K} = \boldsymbol{p}_0 - \boldsymbol{p}$. Here the function $\Gamma\left(\boldsymbol{r}\right)$ is defined from the equality

$$\widehat{\Gamma}ue^{-i(\varepsilon t - \boldsymbol{p}_0\boldsymbol{r})} = \Gamma\left(\boldsymbol{r}\right)ue^{-i(\varepsilon t - \boldsymbol{p}_0\boldsymbol{r})}.$$

Choosing the normalization in the form $\overline{u}u = 2m$, $\overline{u}\gamma^{\mu}u = 2p^{\mu}$ [28], we find the scattering amplitude and differential cross section for scattering of electrons which possess polarization $s$ in the final state in the form

$$f_s\left(\boldsymbol{n}\right) = \frac{1}{2m}\overline{u}_sA\left(\boldsymbol{n}\right), \tag{15}$$

$$d\sigma_s = |f_s(\boldsymbol{n})|^2 \, d\Omega, \tag{16}$$

where $u_s$ is a bispinor describing the state of elastically scattered electrons on a wormhole with momentum $\boldsymbol{p} = p_0\boldsymbol{n}$ and polarization $s$, $d\Omega$ is the solid angle element having direction $\boldsymbol{n}$.

Given that $\overline{u}_s\left(-\boldsymbol{\gamma}\cdot\boldsymbol{p} + \gamma^{(0)}\varepsilon - m\right) = 0$,, from (14) and (15) we obtain

$$f_s(\boldsymbol{n}) = \frac{i}{4\pi}\overline{u}_s \int \Gamma\left(\boldsymbol{r}'\right) u e^{i\boldsymbol{K}\boldsymbol{r}'} d^3\boldsymbol{r}'.$$

By substituting this expression into the (16) and averaging the differential scattering cross section over the polarization states, we obtain it in the form

$$d\sigma = \overline{B}(\boldsymbol{n})\,\overline{u_s\overline{u}_s}B(\boldsymbol{n})\,d\Omega,$$

where $B(\boldsymbol{n}) = \frac{i}{4\pi}\int \Gamma\left(\boldsymbol{r}'\right) u e^{i\boldsymbol{K}\boldsymbol{r}'} d^3\boldsymbol{r}'$; the line above $\overline{u_s\overline{u}_s}$ means averaging along the direction of vector $\boldsymbol{n}$. It can be shown that the density matrix of electrons which are scattered by the solid angle element $d\Omega$,

$$\rho(\boldsymbol{n}) = \overline{u_s(\boldsymbol{n})\,\overline{u}_s(\boldsymbol{n})}$$

and the density matrix of electrons for the incident flux

$$\rho_0 = u\overline{u}$$

are equal. This means that the fraction of electrons of a certain polarization which are scattered in the direction of the vector $\boldsymbol{n}$ is equal to the fraction of electrons of the same polarization in the incident flux. Then for the differential cross section for scattering we have

$$d\sigma = \overline{B}(\boldsymbol{n})\,u\overline{u}B(\boldsymbol{n})\,d\Omega.$$

From where we find that the scattering amplitude of the electron is equal to

$$f(\boldsymbol{n}) = \overline{u}B(\boldsymbol{n}) = \frac{i}{4\pi}\overline{u}\int \Gamma\left(\boldsymbol{r}'\right) u e^{i\boldsymbol{K}\boldsymbol{r}'} d^3\boldsymbol{r}'. \tag{17}$$

### D. Electron Scattering on an Ellis-Bronnikov Wormhole

As a scattering center we choose the Ellis-Bronnikov wormhole, the metric of which has the following form

$$ds^2 = dt^2 - \frac{dr^2}{1 - \frac{R^2}{r^2}} - r^2\left(d\theta^2 + \sin^2\theta\ d\varphi^2\right) \tag{18}$$

where $R$ is the radius of the throat. In spite of the fact that in spacetime with metric (18) there is no gravitation, the scattering on such a wormhole can be described by the above formulas. To find the operator $\widehat{\Gamma}$ let us write out the nonzero components of the Christoffel symbols for the metric (17):

$$\Gamma^1_{11} = -\frac{R^2}{r^3 - rR^2},\ \ \Gamma^1_{22} = -r\left(1 - \frac{R^2}{r^2}\right),\ \ \Gamma^1_{33} = -r\sin^2\theta\left(1 - \frac{R^2}{r^2}\right),$$
$$\Gamma^2_{12} = \frac{1}{r},\ \ \Gamma^2_{33} = -sin\theta\ cos\theta,\ \ \Gamma^3_{13} = \frac{1}{r},\ \ \Gamma^3_{23} = ctg\theta, \tag{19}$$

and also choose the orthonormal tetrad in the form

$$e^{\mu}_{(a)} = diag\left(\ 1; \sqrt{1 - \frac{R^2}{r^2}}; \frac{1}{r}; \frac{1}{rsin\theta}\right). \tag{20}$$

Substituting (19) and (20) into the expression for spinor connection

$$\Gamma_\mu = \frac{1}{4} e^\lambda_{(b)} e_{(c)\lambda;\mu} \gamma^{(b)} \gamma^{(c)},$$

we find that all its components are equal to zero. Then assuming $R$ is small, for the operator $\widehat{\Gamma}$ we get

$$\widehat{\Gamma} = -\frac{1}{2} \gamma^{(1)} \frac{R^2}{r^2} \frac{\partial}{\partial r}.$$

Then from (17) we obtain the scattering amplitude in the form

$$f(\boldsymbol{n}) = \frac{1}{4} \pi R^2 p_0^2 \int \frac{\cos\alpha}{r'^2} e^{i\boldsymbol{K}\boldsymbol{r}'} d^3\boldsymbol{r}',$$

where $\alpha = \left(\widehat{\boldsymbol{r}', \boldsymbol{p}_0}\right)$, $\boldsymbol{r}'$ is the radius-vector of an arbitrary point. The integration is performed over such points. The angle $\alpha$ is equal to

$$\alpha = \frac{\pi}{2} - \frac{\theta}{2} - \theta', \text{where } \theta' = \left(\widehat{\boldsymbol{r}', \boldsymbol{K}}\right).$$

Writing down the result of the integration as a series and leaving only the terms that give the summands containing the sixth degree $R^6$ and below for the total cross section for elastic scattering, we obtain

$$f(\boldsymbol{n}) = -\frac{\pi}{4} R^3 p_0^2 \cos\frac{\theta}{2} + \frac{i}{2} R^2 p_0 \left(1 - \frac{2}{3} R^2 p_0^2 \sin^2\frac{\theta}{2}\right).$$

As a result, we obtain the total cross section for elastic scattering in the form

$$\sigma_{\text{el}} = \pi R^4 p_0^2 + 2\pi \left(\frac{\pi^2}{16} - \frac{1}{3}\right) R^6 p_0^4.$$

From the optical theorem

$$\sigma_{\text{tot}} = \frac{4\pi}{p_0} \cdot Imf(0).$$

we find that the total cross section for scattering is equal to

$$\sigma_{\text{tot}} = 2\pi R^2.$$

Then the total cross section for inelastic scattering has the form

$$\sigma_{\text{inel}} = 2\pi R^2 - \pi R^4 p_0^2 - 2\pi \left(\frac{\pi^2}{16} - \frac{1}{3}\right) R^6 p_0^4,$$

and the fraction of inelastically scattered electrons is equal to

$$\frac{\sigma_{\text{inel}}}{\sigma_{\text{tot}}} = 1 - \frac{1}{2} R^2 p_0^2 - \left(\frac{\pi^2}{16} - \frac{1}{3}\right) R^4 p_0^4.$$

It follows that at $Rp_0 \approx 1,0923$ electron scattering will be completely elastic, and when the condition $Rp_0 > 1,0923$ is satisfied, the total cross section for inelastic scattering becomes negative.

## Conclusion

Within the framework of the approximations used, the following statements can be made:

1. There is no total absorption of electrons by the wormhole. The existence of inelastic reaction channels necessarily entails the existence of elastic scattering.
2. There is a condition on the size of the throat $R$ and on the value of the initial electron momentum $p_0$, at which the flux of electrons will be completely scattered elastically.

3. There is a condition on the size of the throat $R$ and on the value of the initial electron momentum $p_0$, at which the total cross section for inelastic scattering becomes negative. The Born approximation used in this study restricts the inelastic scattering channels. The electron creation processes in this problem can be excluded. Therefore, there remains only one possibility to increase the number of elastically scattered electrons which exceeds the number of electrons in the initial flux. Additional electrons can appear only as a result of transition of electrons through the wormhole from the region of space located on the opposite side of the wormhole. Thus, it is possible to create such a flow directed to the wormhole which will create a "negative pressure" in the region containing the wormhole. Perhaps wormholes can be stabilized without exotic matter in this way.

**Список литературы/References**

1. Bronnikov K.A., Sushkov S.V. Current Problems and Recent Advances in Wormhole Physics, *Universe*, 2023, 9, 81. https://doi.org/10.3390/universe9020081
2. Bambi C., Stojkovic D. Astrophysical Wormholes, arXiv:2105.00881v2 [gr-qc]
3. Kim S.W., Cho Y.M. Wormhole Gravitational Lens. *Proceedings of the 37th Yamada Conference: Evolution of the Universe and its Observational Quest. Tokyo, Japan, 8-12 June 1993*, ed. K. Sato, Universal Academy Press, Tokyo, 1994, pp. 353–354.
4. Cramer J.G., Forward R.L., Morris M.S., Visser M., Benford G. and Landis G.A. Natural wormholes as gravitational lenses, *Phys. Rev*, 1995, D 51, pp. 3117–3120. doi:10.1103/PhysRevD.51.3117 [arXiv:astro-ph/9409051 [astro-ph]].
5. Akiyama K., et al. First M87 Event Horizon Telescope Results. I. The Shadow of the Supermassive Black Hole, *Astrophys. J. Lett.*, 2019, 875, 1. https://doi.org/10.3847/2041-8213/ab0ec7
6. Shaikh R., Banerjee P., Paul S., Sarkar T. A novel gravitational lensing feature by wormholes, *Phys. Lett*, 2019, B 789, pp. 270–275 https://doi.org/10.1016/j.physletb.2018.12.030
7. Repin S.V., Bugaev M.A., Novikov I.D., Novikov I.D. jr. Silhouettes of wormholes traversed for radiation, arXiv:2205.10168v1 [gr-qc]
8. Ishkaeva V.A., Sushkov S.V. The Shadow of the Ellis-Bronnikov Wormhole and Its Throat Silhouette, *Space, Time and Fundamental Interactions*, 2023, 1, pp. 79–84.
9. Morris M.S. and Thorne K.S.. Wormholes in Space-Time and Their Use for Interstellar Travel: A Tool for Teaching General Relativity. *Am. J. Phys*, 1988, 56, pp. 395–412. doi:10.1119/1.15620
10. Morris M.S., Thorne K.S. and Yurtsever U. Wormholes, Time Machines, and the Weak Energy Condition. *Phys. Rev. Lett*, 1988, 61, pp. 1446–1449. doi:10.1103/PhysRevLett.61.1446
11. Visser M. Traversable Wormholes: Some Simple Examples. *Phys. Rev*, 1989, D 39, pp. 3182–3184. doi:10.1103/PhysRevD.39.3182 [arXiv:0809.0907 [gr-qc]].
12. Fewster C.J., Roman T.A. On Wormholes with Arbitrarily Small Quantities of Exotic Matter. *Phys. Rev*, 2005, D 72, 044023. DOI: 10.1103/PhysRevD.72.044023
13. Kuhfittig P.K.F. More on Wormholes Supported by Small Amounts of Exotic Matter. *Phys. Rev* 2006, D 73, 084014. DOI: 10.1103/PhysRevD.73.084014
14. Sukhanova L.A., Khlestkov Yu.A. Geometrical Properties Of Exotic Matter In The Solution Of The Einstein–Maxwell Equations Of Wormhole Type. *Russ. Phys. J*, November, 2017, 60, 7. (Russian Original No. 7, July, 2017)
15. Gravanis E. and Willison S. Mass without mass'from thin shells in Gauss-Bonnet gravity. *Phys. Rev* 2007, D 75, 084025. doi:10.1103/PhysRevD.75.084025 [arXiv:gr-qc/0701152 [gr-qc]].
16. Richarte M.G. and Simeone C. Thin-Shell Wormholes Supported by Ordinary Matter in Einstein-Gauss-Bonnet Gravity. *Phys. Rev*, 2007, D 76, 087502 [erratum: *Phys. Rev*, 2008, D 77, 089903 ] doi:10.1103/PhysRevD.77.089903 [arXiv:0710.2041 [gr-qc]].

17. Eiroa E.F., Richarte M.G. and Simeone C. Thin-Shell Wormholes in Brans-Dicke Gravity, *Phys. Lett*, 2008, A 373, 1–4 [erratum: *Phys. Lett*, 2009 373, 2399–2400] doi:10.1016/j.physleta.2008.10.065 [arXiv:0809.1623 [gr-qc]].
18. Harko T., Lobo F.S.N., Mak M.K., Sushkov S.V. Modified-Gravity Wormholes Without Exotic Matter, arXiv:1301.6878v3 [gr-qc] 21 Mar 2013
19. Bronnikova K.A., and Galiakhmetov A.M. Wormholes Without Exotic Matter in Einstein-Cartan Theory, arXiv:1508.01114v1 [gr-qc] 5 Aug 2015
20. Kar S., Lahiri S., SenGupta S. Can Extra Dimensional Effects Allow Wormholes Without Exotic Matter? *Phys. Lett*, 2015, B 750, pp. 319–324.
21. Mironova S., Rubakov V, Volkova V. In Hot Pursuit of A Stable Wormhole In Beyond Horndeski Theory arXiv:2212.05969v1 [gr-qc] 12 Dec 2022
22. Lu J., Yang S., Han X., Wang J., Xu M. Validation of Energy Conditions in Traversable Wormhole For GBD Modified Theory, *Int. J. Mod. Phys*, 2022, D 31, 16, 2250117 (14 pages)
23. Agrawal A.S., Mishra B., Moraes P. H. R. S., Unimodular Gravity Traversable Wormholes arXiv:2201.08392v4 [gr-qc] 28 Mar 2023
24. Tayde M., Santos J.R.L, Araujo J.N., and Sahoo P.K. Wormhole Solutions in f (Q, T) Gravity with a Radial Dependent B Parameter arXiv:2212.07943v2 [gr-qc] 8 May 2023
25. Godani N. Stable traversable wormholes in f(Q) gravity, *Int. J. Geom. Methods Mod. Phys*, 2023, 20, 8, 2350128 (11 pages)
26. Levich V.G., Vdovin YU.A., Myamlin V.A. *Theoretical Physics Course Vol. 2* [Kurs teoreticheskoy fiziki. Vol. II]. 1971, Nauka, Moscow, (in Russ.)
27. Ahiezer A.I., Berestetskii V.B. *Quantum Electrodynamics* [Kvantovaya elektrodinamika], Moscow, Nauka Publ., 1981. (in Russ.)
28. Berestetskii V.B., Lifshitz E.M., and Pitaevskii L.P. Quantum Electrodynamics, Oxford, Pergamon, 1982. https://doi.org/10.1016/B978-0-08-050346-2.50020-9

**Авторы**

**Тимофеев Владимир Николаевич**, к.ф.-м.н., Санкт-Петербургский государственный университет гражданской авиации имени Главного маршала авиации А.А. Новикова, ул. Пилотов, д. 38, г. Санкт-Петербург, 196210, Россия.
E-mail: WTimoff@yandex.ru

**Просьба ссылаться на эту статью следующим образом:**

Тимофеев В. Н. Рассеяние электронов на червоточине в борновском приближении. *Пространство, время и фундаментальные взаимодействия.* 2023. № 3-4. С. 290–298.

**Authors**

**Timofeev Vladimir Nikolaevich**, Ph.D., Saint Petersburg State University of Civil Aviation named after Air Chief Marshal A.A. Novikov, Pilotov st., 38, Saint Petersburg, 196210, Russia.
E-mail: WTimoff@yandex.ru

**Please cite this article in English as:**

Timofeev V. N. Electron Scattering on a Wormhole in the Born Approximation. *Space, Time and Fundamental Interactions*, 2023, no. 3-4, pp. 290–298.

УДК 514



## АУФБАУ ДИФФЕРЕНЦИАЛЬНОЙ ГЕОМЕТРИИ ЛИ АТОМОВ И МОЛЕКУЛ

Трелл Э.[a,1]

[a] Линчёпингский университет, 581 83, Швеция.

На предыдущих конференциях PIRT я докладывал о дифференциально-геометрическом структурном построении стандартной модели элементарных частиц и периодической системы атомов в соответствии с докторской диссертацией Мариуса Софуса Ли “Over en Classe Geometriske Transformationer” в Кристианском (ныне Ословском) университете в 1871 году. Этот тезис, по сути, описывает природу на бесконечно малом уровне, которая предстает как "переход от точки к прямой линии как элементу"как математически, так и материально целостной дифференциальной конституции. В условиях нуклеосинтеза ее частичная производная квадратных волновых шагов “длины равной нулю” переходит в заполняющую пространство модульную "криво-сетчатую"формацию. В первом поколении, начиная с $10^{-15}$-метрового размера радиуса нуклона, это двухслойное волновое пакетное накопление палиндромной боровской конфигурации Aufbau, многократное применение которой, как в восточной плитке или ковре, впервые очерчивает ее рисунок в периодической таблице на более чем в 10 000 раз большей площади поперечного сечения атома. Когда целостный поверхностный слой покрыт полным экскурсом узла, возвращающегося к истоку, поезд продолжает движение вверх по нуклонному стволу к новой грани кристалла, которая сохраняет форму своего бесконечно малого модуля и поэтому может самособираться в полимерный наноструктурный кластер из себя или молекулярных комбинаций с другими атомами точно и полно, как указано в установленных химических формулах. Примером тому служат некоторые основные и более сложные органические соединения, включая протеиногенные аминокислоты и ДНК.

*Ключевые слова*: Атомы, принцип Ауфбау, дифференциальная геометрия, алгебра Ли, молекулы, периодические системы.

## LIE DIFFERENTIAL GEOMETRY AUFBAU OF THE ATOMS AND MOLECULES

Trell E.[a,1]

[a] Linköping University, Linköping, 581 83, Sweden.

In previous PIRT conferences I have reported on a differential geometry structural make-up of the standard model of the elementary particles and the periodic system of the atoms following Marius Sophus Lie’s Ph.D. dissertation Over en Classe Geometriske Transformationer at Christiana (now Oslo) University in 1871. This thesis essentially describes Nature at the infinitesimal level it appears as by “a transition from a point to a straight line as element” both mathematically and materially of a coherent differential constitution. Under nucleosynthetic conditions its partial derivative square wave steps “of length equal to zero” goes into a space-filling modular “curve-net” formation. In the first generation, from the $10^{-15}$ meter size of the Nucleon radius, this is a bi-layer wave-packet accumulation of palindromic Bohr Aufbau configuration, whose repeated application like in an oriental tiling or carpet first outlines its pattern in the periodic table over the more than 10,000 times larger extension of the atom cross-section area. When an integral surface layer is covered by a full excursion of the knot returning to the origin, the train continues by moving upward the Nucleon shaft to a new facet of the crystal which retains the shape of its infinitesimal module and so can self-assemble into a polymeric nanostructure cluster of itself or molecular combinations with other atoms exactly and extensively as specified in established chemical formulas. This is here exemplified by some basic and more advanced organic compounds including the proteinogenic amino acids and DNA.

*Keywords*: Atoms, Aufbau, Differential Geometry, Lie algebra, Molecules, Periodic System.

PACS: 02.40.-k

DOI: 10.17238/issn2226-8812.2023.3-4.299-313

[1]E-mail: erik.trell@gmail.com

## Introduction

In his Norwegian Ph. D. thesis Over en Classe Geometriske Transformationer at Christiania (now Oslo) university in 1871 [1],[2], Marius Sophus Lie's quite profound subject was the "nature of Cartesian geometry". On par with the leading geometers of the time [3] his revolutionary advance was the discovery of the "fundamental relation between the Plücker line geometry and a spatial geometry whose element is the sphere" [1],[2] and the "study of the space relative to the given line complex" of this "according to the general theory for reciprocal curves", which "transform the spaces r's straight lines into the space R's spheres". As shown in Figure 1

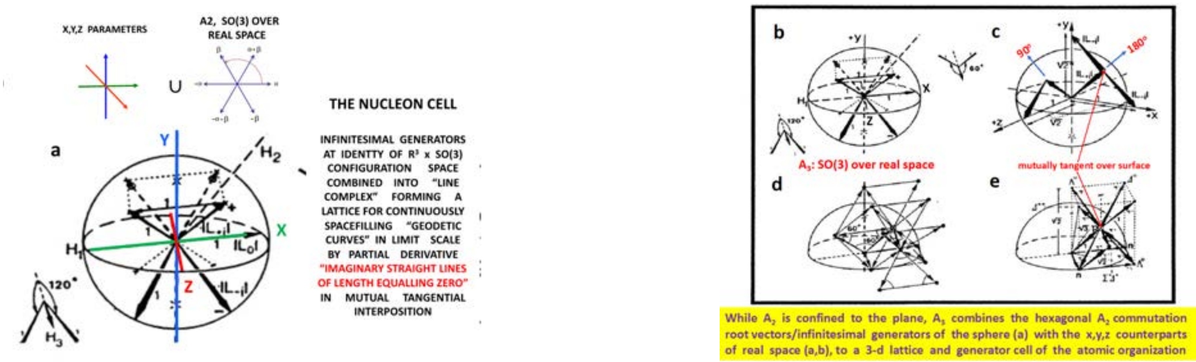


**Рис. 1.** a,b) Nucleon projective line complex of $R^3SO(3)$ configuration space. c) Orthogonal root vector sequences. d) Hexagonal root vector lattice. e) Hexagonal SO(3) root vector bundle in orthogonal R3 cell. *These and following figures, many from earlier PIRT meetings, with permission from IMBIC*

it is a digital "line congruence" [Ib.] system "fundamental... in classical differential geometry" [4] and formed as a union between the parameters of Euclidean space and the "sphere's rectilinear generatrices" [1],[2], and has the characteristics of the Nucleon as can be illustrated in Figure 1 a,b, while Figure 1 c-e shows the "complex of curves that are enveloped by the line-complexe's lines" whose "curve-net... we in the following designate the line-complexe's main tangential curves". [Ib.]

## A. Methods

In this way a commutating root vector lattice is spanned in which the surface and internal symmetries, transformations and interactions and other Standard Model events of the elementary particles – which were not known at Lie's time – can be directly reproduced [5]-[14]. But also the external; periodic table, atomic and molecular panorama can be displayed in the Lie line congruence system [10]-[14]. Its identity line-complex (Figure 1 a,b) combines the orthogonal and spherical infinitesimal generators to a common origin of the two reciprocal "characteristic curves... which are determined by the curve complexe's c and C" parts, and "the two spaces are thus mapped into each other" by both's "image-curve enveloped by the other complexe's lines" [1],[2]. Figure 2 outlines this mutual realization of the ground Euclidean and spherical "geodetic curves" [Ib.].

In order not to clog up from start, this realization has to be bisected in two complementary longitudinal strands (Figure 3 a) simultaneously emitted in sequences of various length of their combined or separate R3 and SO(3) strings and thus incomplete but still maintaining a "general reciprocity between the figures in the two spaces" [1],[2]. So in the early universe there would be an isotropic distribution of such literal half measures occupying the volumes and figures of the full elements and thus appearing as ready e.g. Neutrons and Electrons/Positrons plus straight $\nu$ and zig-zag $\gamma$ rays of their respective lattice edges, but except for occasional encounters unable to fill out their saturated "material bodies". [Ib.]

However, there are bound to be some fluctuations and irregularities in the primordial vapor [12], and they will build up and aggregate over time to reach after billions of years the present astrophysical conditions, which changes the situation (Figure 3b). The stellar clashes and

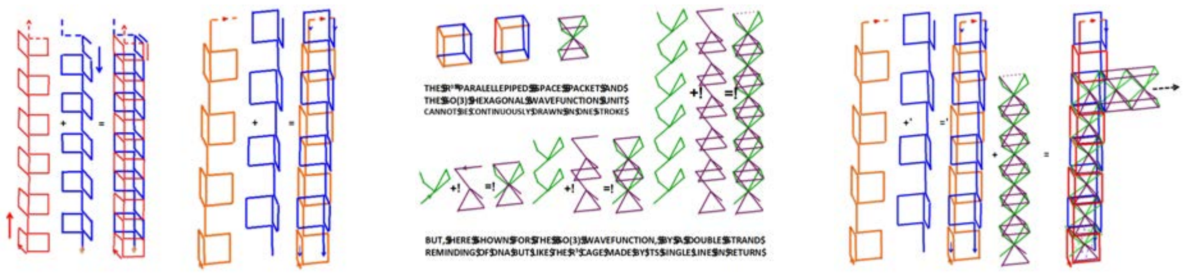

a b c

**Рис. 2.** a) Non-overcrossing concatenation of Euclidean frame space infinitesimal generators to outgoing $R^3$ characteristic curve varieties (red) complemented to full cages by returning flank (blue). b) same in SO(3) and c) integrated $R^3$SO(3) line congruence

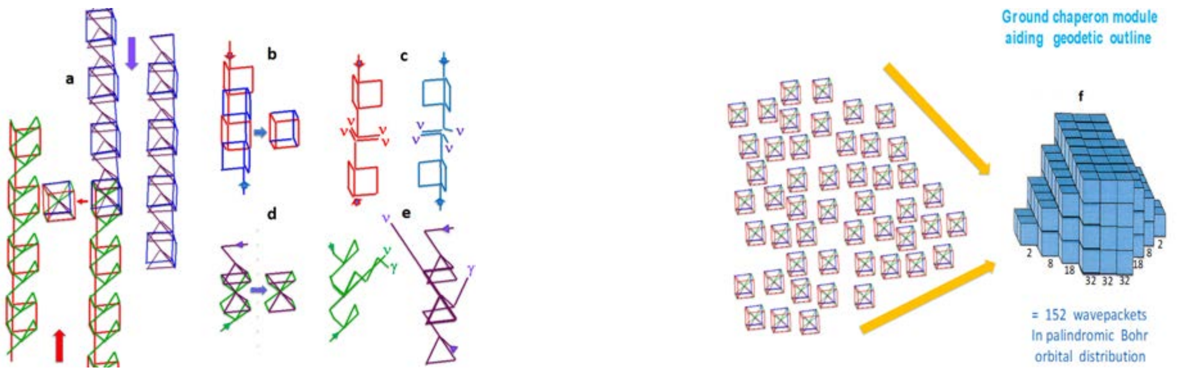


**Рис. 3.** a) Reciprocal spherical transformation complex-curves in complementary flanks with wave-packet generation in contralateral meetings while ipsilateral confrontation gives annihilation (not shown). b-c) Same in 'cage space' and d,e) 'wave space' curves. f) The nucleosynthesis products, here wave-packets, find further space-filling via Bohr Aufbau piling

implosions converge the diverse rudimentary "curve-lines" from all directions together so that they will "touch" [1],[2] in the interior to produce a variety of outcomes, from annihilation with $\nu$ and $\gamma$ discharge when ipsilateral contours confront, to entanglement superposition when contralateral couples meet to generate frame or wave or wave-packet boxes/bricks, all of equal parallelepiped perimeter (Figure 3 a-e). Squeezed together in the nucleogenetic crossfire and coming out in its exhaust they must find an optimal packing order to continue their space-filling without instantly jamming, and the solution for the mixture while shown here only by the wave-packets is a common hierarchical Bohr *Aufbau* (Figure 3 f) [15].

## B. Results

As reported in earlier papers [10]-[14] the construction starts with a consecutive piling of a flat-bottomed fundament complemented by a flat-roofed cap and after further tangential modifications reaching the triangular form described in Figure 4 a. Each brick contains 12, in the $R^3$SO(3) wavepackets $2 \times 12$, line steps and the modules in each plane are tessellated in palindromic Bohr Aufbau order by 153 bricks, giving a peripheral versus central inertial moment $= 153 \times 12 = 1836$ which is the same as the Proton/Electron mass ratio. The composition of the modules provides continuity/connectivity of their lines in all directions and the flat bottom/roof perpetuity of their crystal ascent. Figures 4 e and f further exemplify that they work at their infinitesimal level precisely as the intrastellar nucleogenetic processes where they fuse, also in here not shown burning sequences [10]-[14] , to the successive atoms and their spectrum up to Iron and then by marginal Neutron capture over the rest of the periodic table - and beyond [14]. This far-reaching structural identity and theoretical Lie geometry of space heritage and down-to-Earth Bohr *Aufbau* architecture plan cannot but verify the truth and reality of the system.

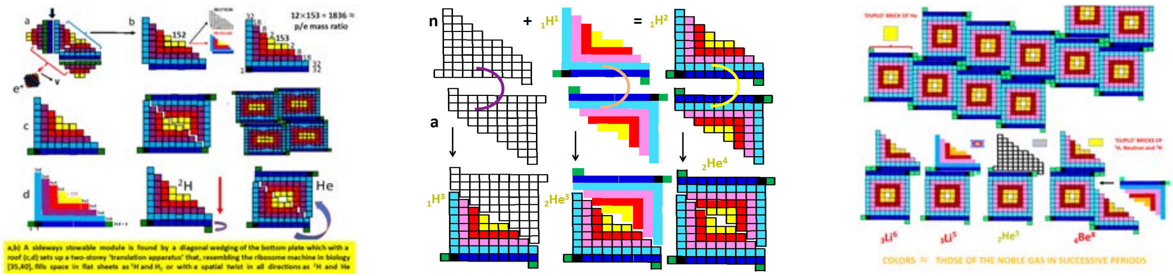

**Рис. 4.** a-d) Diagonal root vector module in triangular outline which can link laterally to inert H2 gas or be twisted to Deuterium and further to Helium module. e) Consecutive first. period isotopes. f) Serial fusion *Aufbau* of first states of the second period

Next the stable(st) atoms of the second period are displayed in larger scale (Figure 5) because including the basic building blocks of organic chemistry, namely, beside Hydrogen in period 1, Carbon, Nitrogen and Oxygen. They are of mid-symmetric shape and provide a distinct set of jigsaw tesselation pieces filling space from the centre rather than from the periphery as is the mode in inorganich chemistry, albeit some atoms, e,g, Phosphorus and Sulfur may rearrange to take part in certain amino acids and DNA and ATP, respectively.

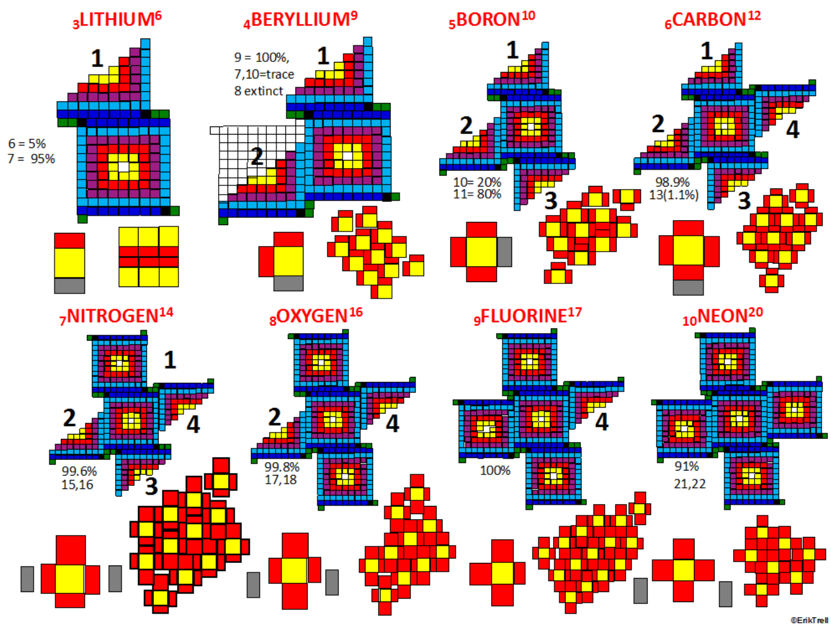


**Рис. 5.** Second period atoms in space-filling fine-grained Lego and simplified 'Duplo' [16] graphics, the latter of which is the actual form in magnification to atomic size. *The numbers are oxidation sites. In all figures, the colors are those of the noble gas in respective periods*

To visualize this and also to enable expansion from infinitesmal size in the order of $10^{-15}$ to $10^{-14}$ meter to the up to 10,000 times wider atomic size a simplified 'duplo' representation [16] is applied and repeated like the knot in an oriental rug or tiling, first over the cross-section "integral surface" area and when a layer is covered there it moves up to the next and so on till of height for a gaseous, liquid or solid state. The size has grown to the ?ngstr?m range and the apparent propagation velocity due to the volume increase diminished from the speed of light in the infinitesimal modules to the order of micrometer/second in the atomic blocks.

Next follow, in Duplo representation alone, the third period states (Figurer 6 a). Numbers in bold are oxidation states, in italics frequencies. In all figures, the colors are those of the noble gases in successive periods. One notes the tendency to quadratic/parallelepiped outline in the module formation even to the extent of uniqueness by Neutron marginal filling, e.g. in the only isotopes of Sodium and Phosphorus (Figure 6 b).

This remains the 'game of Lie' [14] algorithm in all following periods. Up to Iron the formation is mainly in fusion processes (except in Scandium where it is rapid Neutron capture). From Iron where the square contour is firmly established, the chief mechanism is marginal accretion by initially slow and in heavier states rapid Neutron capture, and in the heaviest by synthesis. All observed isotopes and channels occur in the realization as in reality, establishing with astronomic probability the actual identity between them.

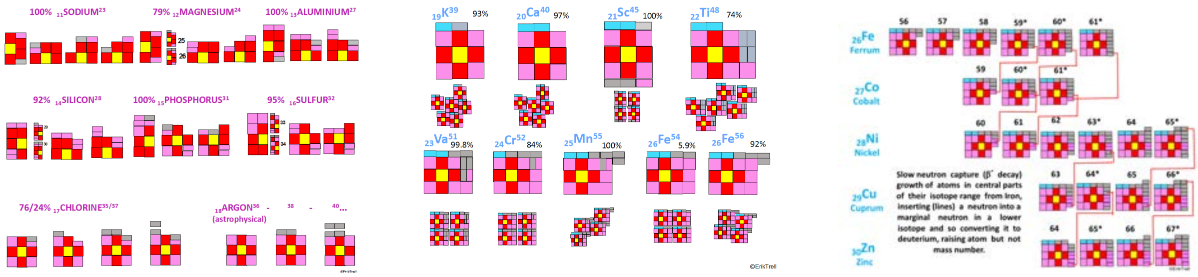

a b c

**Рис. 6.** a) Third period atoms in 'Duplo' graphics, which is the actual form in magnification to atomic size. b,c). Fourth period from Potassium to Zinc

Then follow the rest of the fourth period atoms (Figure 7).

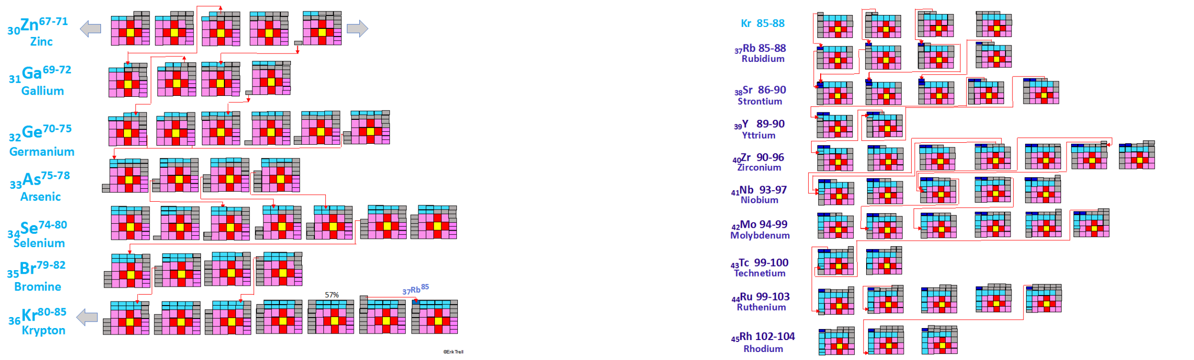

a a

**Рис. 7.** a) Remaining fourth period atoms and their central isotopes. Like in all other atoms they are plane-filling by aggregation which does not mean they are stable. Slow Neutron capture beta channels are shown like in other figures. Note complete alpha filling in Krypton. b) Initial states in the fifth period, including Technetium which has no stable isotopes

Fifth period is fulfilled in Figure 8a and sixth period is started in Figure 8b

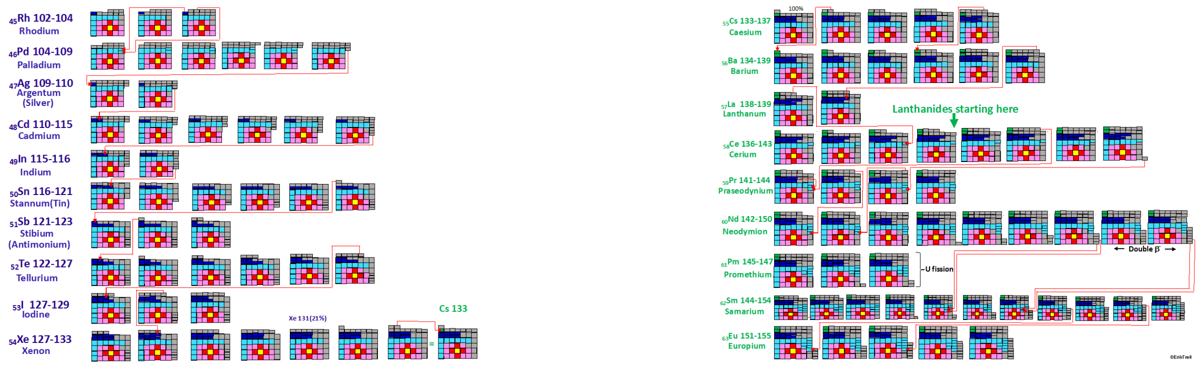


a b

**Рис. 8.** a Fifth period concludes it layer with full alpha blocks in Xenon. b) Start of sixth period

Sixth period continues in Figure 9.


a b

**Рис. 9.** Continuation of sixth period till gold

And concludes in Figure 10 a. Seventh period starts in Figure 10 b.

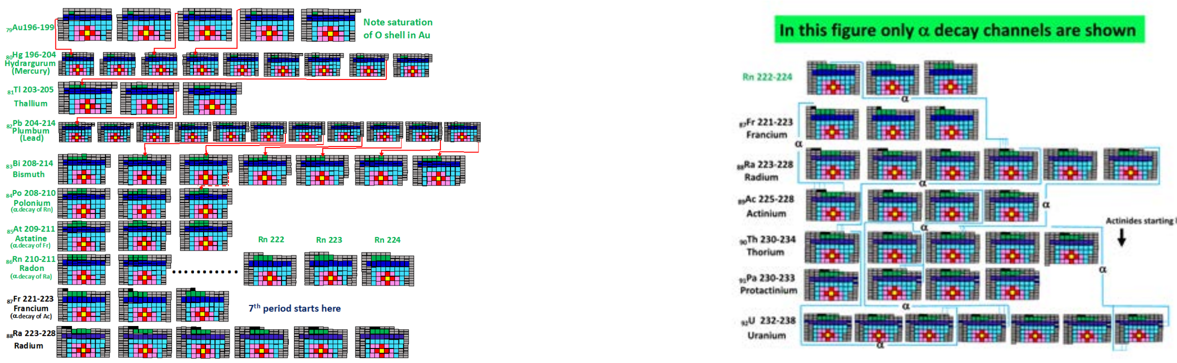


a b

**Рис. 10.** a) completion of sixth period. b) Start of seventh period. Alpha channels are shown. In the seventh period most states are synthetic and extremely short-lived. But their outlines can all be step-by-step reproduced exactly as they appear in observations and experiments, next in Uranium to Hassium (Figure 11)

Now approaching the end of the cavalcade it must be emphasized that it contains a lot of information not further commented upon in the text but marked out in the figures; the Lanthanides, the Actinides, the covering of subshells etc. in the same order as in Reality and bringing so strong evidence that it is indeed the true "Nature of Cartesian Geometry" which is literally surfacing that it is beyond any denial.


a b

**Рис. 11.** Uranium to Hassium

A larger jubilee portrait of this finale is therefore granted (Figure 12):

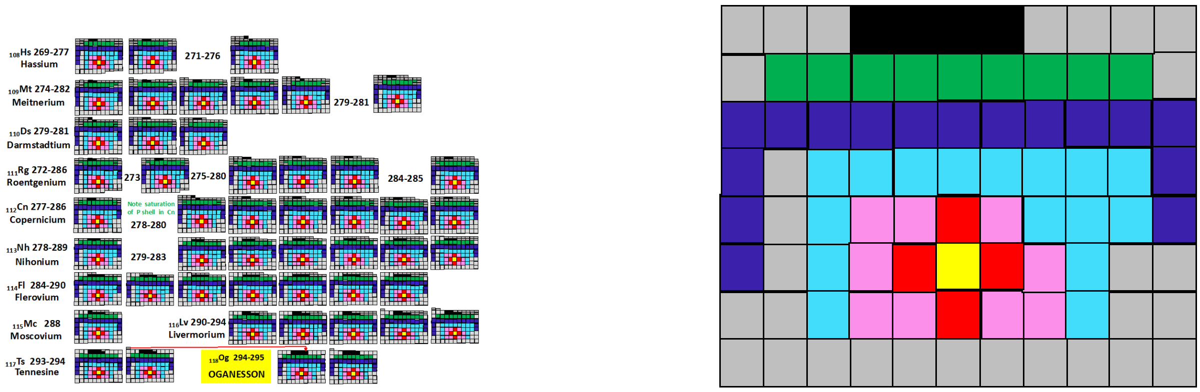


**Рис. 12.** Finale of period seven,. concluding the stepwise meandering over the periodic table to exactly reach and replicate Oganesson - and the first step of period eight.

In its successive completion Oganesson is therefore both Integral and Icon of the presently known Periodic Table; canvas as well as palette of all the patterns within its perfectly rectangular frame; all the shells with $1+4+9+16+16+9+4$ saturated alpha bricks, that is, completing the seventh round of a full theoretically possible eight-period Bohr Aufbau cycle [14], plus $2 \times 29 = 58$ excess Neutron contour fillers in right K L M N O P Q positions, and everything tiled by just two brick varieties; a quadratic and its latitudinal half, and laid in alternating, Fermionic and Bosonic order and hence exhausting all forms under them so that they can be applied in all scales and media It is a new hierarchical level of realization where the enormously size-increased, sharply shape-preserved atomic modules can gather with likes to flat-roofed/floored solid crystals of recognized atom outlook or be directly applied as building bricks in a polymeric nanostructure self-assembly of themselves and molecular combinations with other atoms.

This will here be performed in the organic chemistry atoms and compounds by as many pictures with as little text as possible, letting the results talk [17]. Figure 13 a shows the basic construction set as jig-saw pieces of the cross-section figure and mosaic blocks of the whole body including isomeric forms of Hydrogen, Carbon, Nitrogen and Oxygen while figure 13 b compares some self-assemblies of Carbon atoms to orthogonal and diagonal aggregates with a graphical reconstruction of Graphene as balls and sticks and empty space and a photo of the actual surface.

Next the basic hydrocarbons and the single building block hydrides of Nitrogen and Oxygen are surveyed (Figure 14 a) and then a larger image of water in two forms, one of which is proportionately intermingled in different types of ice (Figure 14 b).

In Figure 15 some further basic molecular combinations of the first and second period atoms with

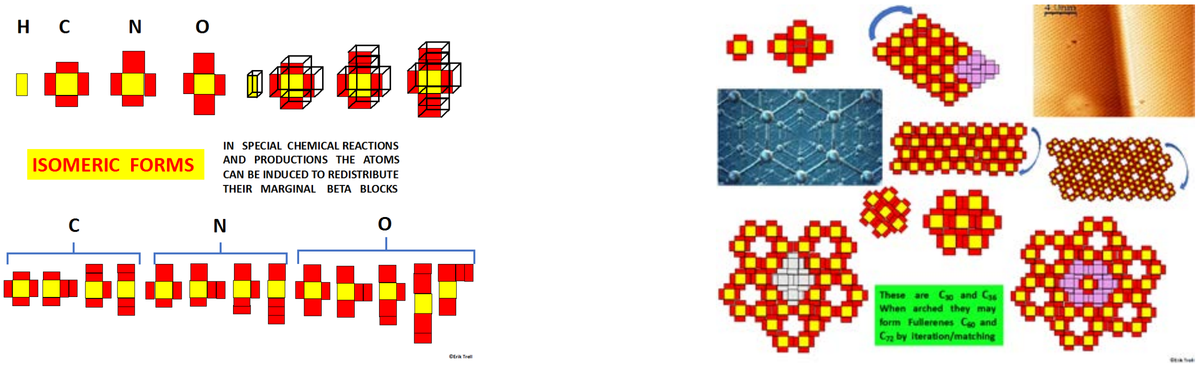


**Рис. 13.** a) Basic construction set of organic Carbon chemistry. b) Some self-assemblies of Carbon atoms. The orthogonal and hexagonal sheets can be very long and when of few layers folded to nanotubes and arched into domes and Fullerenes, e.g. the smallest C60

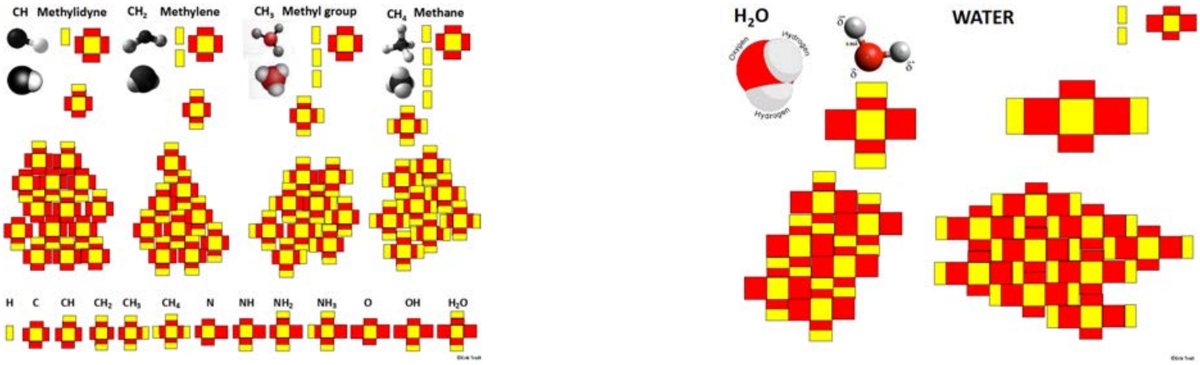


**Рис. 14.** a) Single building block hydrides of Carbon, Nitrogen and Oxygen. b) Water. *Ball and stick and space-filling globular images for comparison taken from open Google/Wikipedia picture galleries*

each other are surveyed.

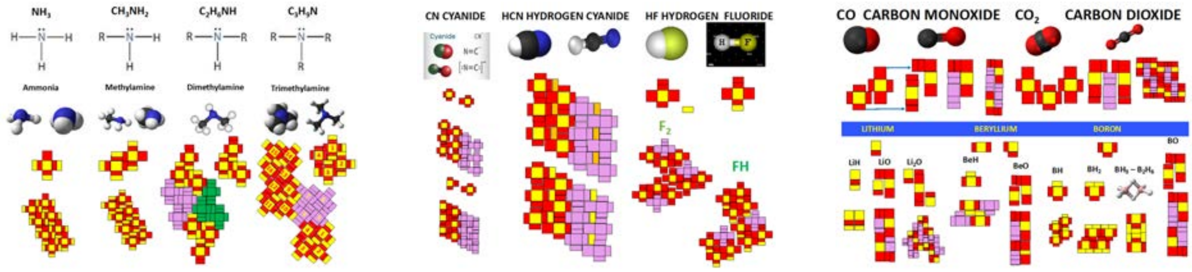


a b c

**Рис. 15.** a) Single building block hydrides of Carbon and Nitrogen. b) Cyanides, Fluorine, and Hydrogen Fluoride. c) Carbon monoxide and dioxide and, lower part, basic hydrides and oxides of Lithium, Beryllium and Boron. Note isomers needed in the compounds

Going to larger molecules Figure 16 demonstrates the build-up of the isomers ethenone and ethynol by a single CH turn and of ethanol by a larger amount of Hydrogen.

In the same tentative way (and with a certain amount of artistic freedom) the three main varieties of sugar and their compounds are reproduced by assorted combinations of six Carbon, six Oxygen and twelve Hydrogen atoms with D- and L-forms in Fructose and also other features as observed (Figure 17). It is reasonable that the different structural arrangements can alter e.g taste and other properties in ways that would be possible to examine and clarify in further studies.

The hydrocarbons form a large polymer class consisting entirely of Carbon and Hydrogen arranged

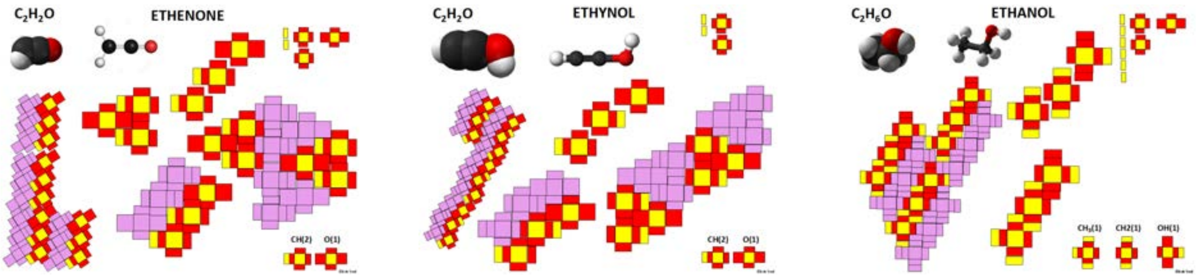


**Рис. 16.** Ethenone, ethynol and ethanol

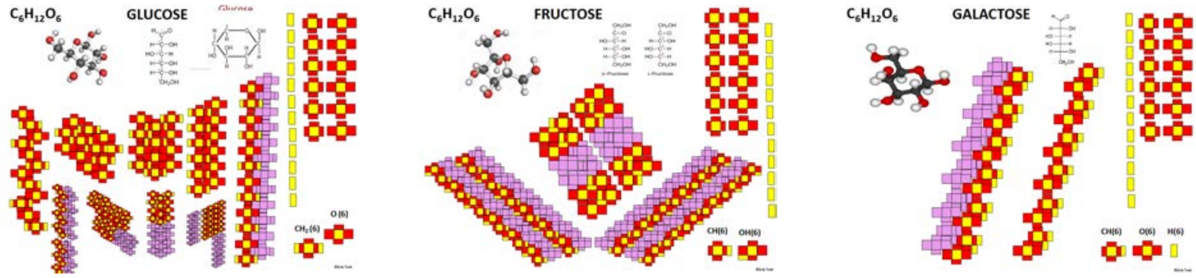


**Рис. 17.** The three main varieties of sugar

in chains and cycles in a great number of variations and isomers and couplings to plastics etc. Here only lightest of them beyond methane, viz ethane, propane, butane and pentane are presented in their simplest execution (Figure 18 a) but it is possible to reproduce the whole family by their isomers and enantiomers by matching recombinations of their atoms and their branches and bindings. The same applies to the lipids of which here only cholesterol and its layering are displayed in comparison with present ball and stick and space-filling models (Figure 18 b). There is a good agreement, e.g. of the sole Oxygen, but the analog varieties fail in the global packing, which the digital version achieves by both definition and structure.

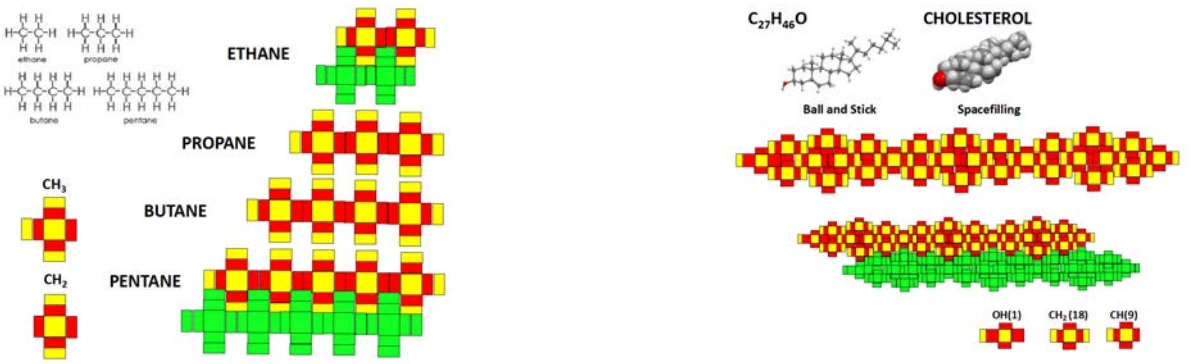


a b

**Рис. 18.** a) Basic hydrocarbons and their spacefilling. b) Cholesterol. It is not spacefilling but like in the blood vessels longitudinally layerable with hooks for tissue integration.

So, after these examples, the outstanding, each enormous organic polymer fields are those of the amino acids and proteins and DNA/RNA. Starting with the former, the proteinogenic amino acids will be surveyed in alphabetic rather than systematic order, but it is hoped that many matters of construction and function will be illuminated in the series.

They include alpha helices, beta sheets, parallel/tube formation, rings, nests and others, and presumes a concrete building plan and elements with precise interlacing and interlinking, suggesting a common caliber and inclination. This is first illustrated in alanine (Figure 19), which is a non-essential amino acid but essential in the protein system, holding nearly nine per cent of its contents.

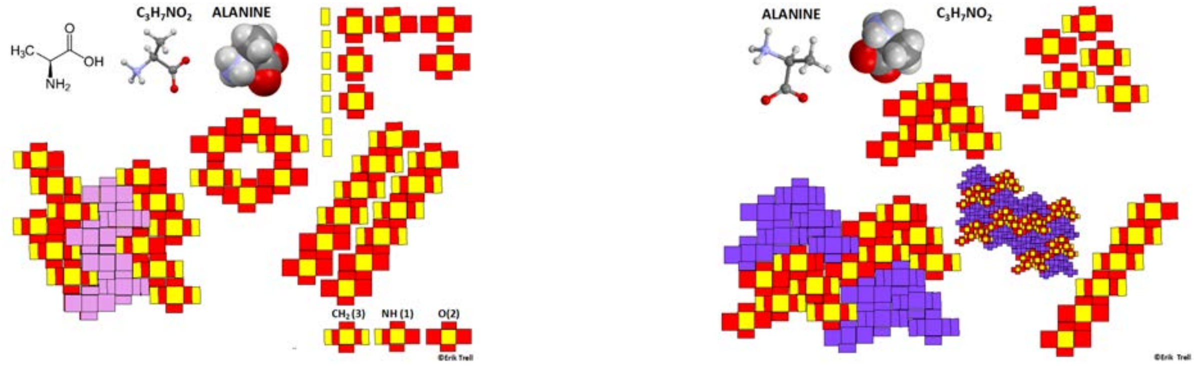


**Рис. 19.** a) Basic hydrocarbons and their spacefilling. b) Cholesterol. It is not spacefilling but like in the blood vessels longitudinally layerable with hooks for tissue integration.

Then follow arginine to lysine. Their linear sequences are shown as much as possible following the ball and stick diagrams. and can from e.g. element placing order and interatomic forces have a wide variation of courses, just hinted at in the drawings (Figure 20). L forms are represented since used in the amino acids but in leucine a D form is shown for comparison.

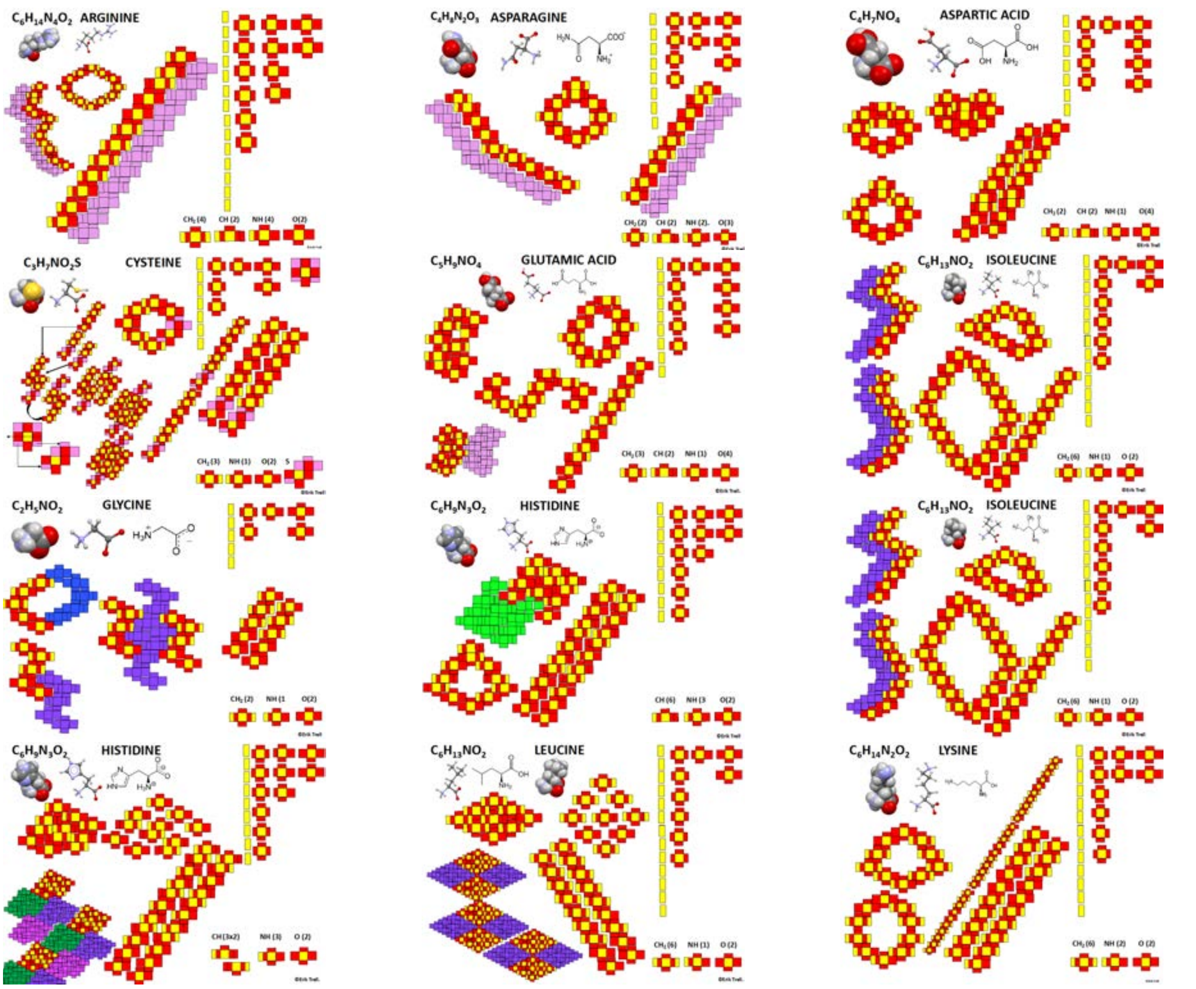


**Рис. 20.** Horizontal plane diagrams of arginine to lysine. As in Figure 13. Note parallel tracks (some color marked) enabling tube and other protein organelle formation. Note also end-to-end and side-congruity enabling inter- and intra-linking. A D-form in shown in Leucine for comparison

Now reflecting a bit on the case at this preliminary stage, one might begin with a floral parable where the ribosomes dispense the amino acids as seeds in sideway order to spread by a curved path over the smooth endoplasmic reticulum flower bed till they root and then grow up along their own coordinates in stem and twigs in a hydrous environments like crystal trees to form with others their fabrics and scaffolds and cages and pores with exact machine precision. . . One can only say that the diagrams may give a vague but still useful impression of this Terra Incognito. One day it will be possible to chart prospectively in detail so the sketching will go on, from methionine to valine (Figure 21).


**Рис. 21.** Methionine to valine plus pyrimidine which is not an amino acid but included as a precursor of DNA nucleobases

Pyrimidine (Figure 21), of which the DNA nucleobases cytosine (C) , thymine (T) and guanine (G) are derivatives, hands over a defined slope, even width and collinear side contour to these and adenine (A) so that they can run parallel as space-filling covalent links between the DNA backbone strands. Shown here first in cytosine (Figure 22) they are composed in tight interlocking of monomer Hydrogen, Carbon, Nitrogen and Oxygen atoms alone and thus extremely strong


**Рис. 22.** Starting with cytosine, the DNA nucleobases will be shown in rising mass and length order, without and with marginal Hydrogen (marked in green for visibility).

lightweight alloys, in which most of the Hydrogen atoms are placed marginally to provide exact frontal boundary [18] while on the rear end there is a square click-in zipper lock profile. Next shown are thymine, adenine and guanine (Figure 23). They have different length, which is key to the C - G and T - A linking of the genetic code transmission and mRNA transcription of it.

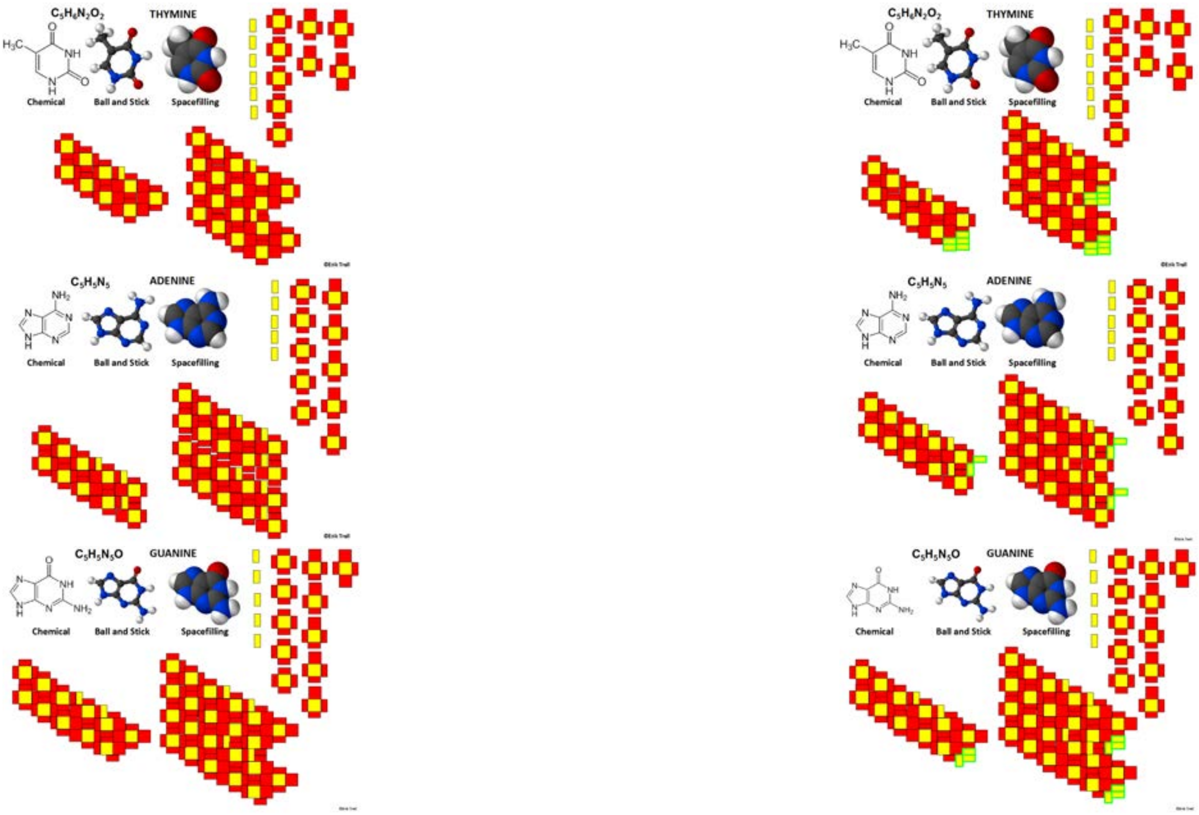


**Рис. 23.** The Thymine, Adenine and Guanine DNA nucleobases

The nucleobases are attached to a backbone which provides the two-component layout of the DNA molecule. Figure 24 a,b shows the self-assembly of the constituent atoms by the space-filling packing of five Carbon, eight Oxygen (one in ionic state), ten Hydrogen plus a phosphate and to

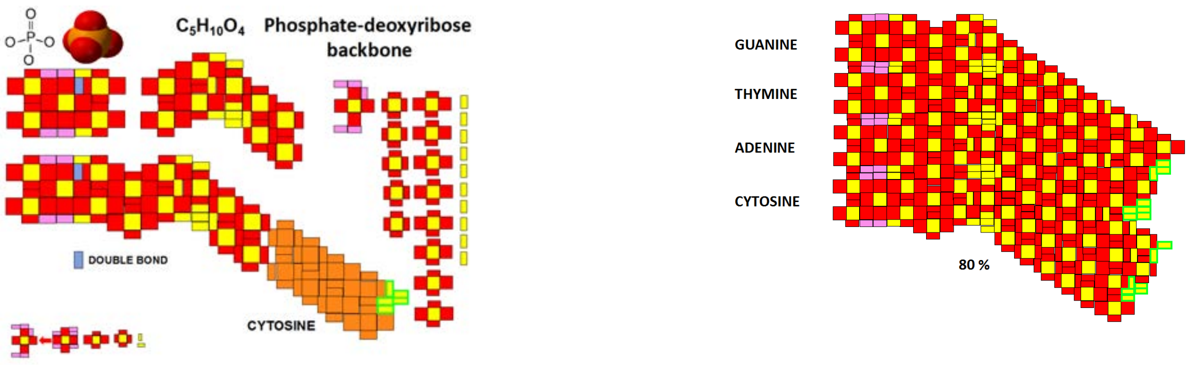


b b

**Рис. 24.** Starting with cytosine, the DNA nucleobases will be shown in rising mass and length order, without and with marginal Hydrogen (marked in green for visibility)

which the nucleobases are connected to the corresponding nucleotides which as demonstrated in Figure 24 b are of different length but laterally jigsaw layerable (and vertically by flat floor/roof). Frontally there is a specific profile which, as in RNA, suffices for transcription by a single strand. But DNA has a double helix for which there are many evolutionary reasons such as stability, repair and replication. The transcription is mediated by the same process as the DNA duplication which can be described as folding the “coding” nucleotide back to the start by a complementary “template” nucleotide returning to zip in with the backbone rear end from which a new round starts. By various support structures in a hydrous milieu the process assumes a tube form but is here visualized by the two sides folded out (Figure 25 a,b). One will note the key role of the marginal Hydrogen modules, as was first clarified both structurally and mathematically in the pioneering work of Rowlands and Hill 2007 [18]: “Hydrogen bonding…is precisely this which keeps the bases together in the two strands of DNA…appear to behave in a way pre-determined by the mathematical structure required for nilpotency”.

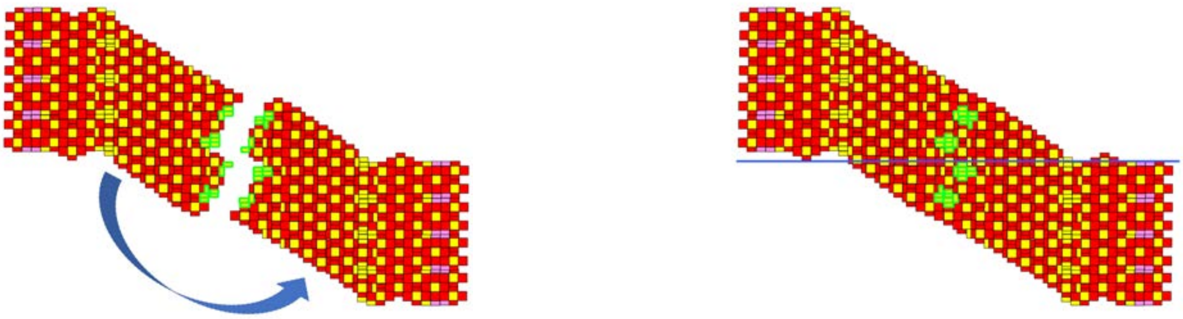

**Рис. 25.** a) Nucleotides in coding strand sheet are mirrored in returning template strand sheet. b) Brought together reciprocal nucleotides fuse and, as indicated by the horizontal line, in tube formation will zip in with the backbone rear contour forming one of the DNA contralateral grooves. b) when the template strand nucleoside(s) are complementary to those of the coding strand, closure will occur, forming the other DNA groove

As illustrated in Figure 25, when the first coding nucleotide is a guanine complex, a cytosine is recruited to fill the seam by its complementary marginal Hydrogen modules, and when next thymine an adenine and so on. The recruitment is from the adjacent RNA polymerase pool and causes gaps in this which can immediately be translated to mRNA transcription. It can be mathematically characterized as a net zero balance over the folding groove [Ib.] and mechanically imposes a crucial dynamic and brick-laying role of Hydrogen in the chemical reaction. This also explains the anti-parallel course of the ‘returning’ template strand and how transcription as well as non-coding sequences proceed simultaneously with the coding strand.

Most of the above applies to RNA and ATP and other systems, too. The only mystery, also discussed in [18], is why thymine is replaced by uracil in RNA, but that can have to do with the up to hairpin bending of the RNA backbone since uracil is shorter than thymine but has equal e.g. binding potential. However, this is highly speculative and the present report stops short of RNA.

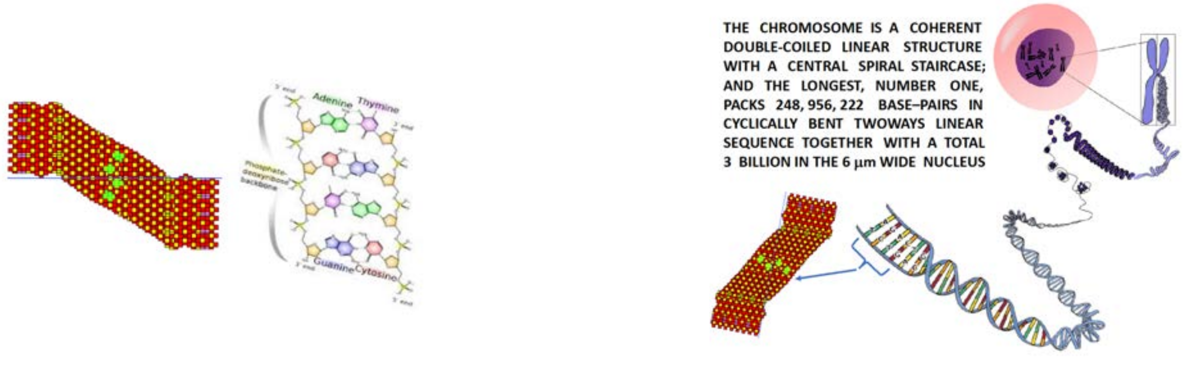


**Рис. 26.** a) Present and prevailing structure diagrams of a DNA segment in b) relation to whole molecule

Of course, there are a legion of outstanding aspects of DNA as well. In this report only a superficial glimpse of a few albeit fundamental aspects is offered – rather convincingly, however. For the first time, and more realistic than current structure models (Figure 26 a), it is possible to come close and examine and test out both composition and mechanisms in detail. The approach, here covering just four base-pairs of the gigantic DNA molecule (Figure 26 b), can be extended over this and its surroundings in an explorative way.

## Conclusion

This article is intended as a descriptive case report as much as possible displayed by a representative, hopefully largely self-explaining picture series. Much of pertaining discussion and comments and figures is found in previous PIRT publications [10]-[14], and therefore only a few brief notes will be made of the, still quite disruptive, back to the future findings. They rest upon classical sources and are in no conflict with Quantum Mechanics (QM), where on the contrary it has long been known that the Aufbau principle as "compiled by Bohr and others" is instrumental in the "quantum mechanical explanation of the periodic system". [19] And QM is in sole command when it comes to the atomic collision and decay processes with their plethora of Electron (and Positron) and Neutron lattice fragments and straight Neutrino and zig-zag Photon edge trajectories, all in entanglement [20]. One further notes the analogy with the Clifford algebra three-vector units formed as a mixture of a parallelepiped and a rotation tensor with similar operative conduct [13],[14]. The space frame lattice engineering system is another parallel [12], especially useful in the reproduction of inorganic chemistry which is likewise feasible by application of the periodic system modules directly taken as both templates, elements and computer pixels of the material *Aufbau* and structure of the atoms and molecules and compounds. These studies are under way.

## Список литературы/References


1. Lie, M.S. *Over en Classe geometriske Transformationer.* Ph.D. Thesis, Kristiania (now Oslo,) University, 12 06 1871.
2. Trell, E. *English translation of Marius Sophus Lie's doctoral thesis Over en Classe geometriske Transformationer. Algebras, Groups and Geometries* 1998, 15, 396-445 and hadronicpress.com/lie.pdf, internet open accessible.
3. Pluecker, J. *Neue Geometrie des Raumes gegr?ndet auf die Betrachtung der geraden Linie als Raum Element*; Druck und Verlag von B. G. Teubner, Leipzig, 1868.
4. Bobenko, A.I., Schief, W.K. Discrete line complexes and integrable evolution of minors. arXiv 2015, 1410.5794v2, 1-30.
5. Trell, E. Representation of particle masses in hadronic SU(3) transformation diagram. *Acta Phys. Austriaca* 1983, 55, 97-110.
6. Trell, E. On rotational symmetry and real geometrical representations of the elementary particles with special reference to the N and D series. *Phys. Essays* 1991, 4, 272-283.
7. Trell, E. Real forms of the elementary particles with a report of the S resonances. *Phys. Essays* 1992, 5, 362-373.
8. Trell, E. Elementary particle spectroscopy in regular solid rewrite. *AIP Conference Proceedings* 2008, 1051, 127-141.
9. Trell, E. Digital outline of the elementary particles via a root space diagram approach, *J. Comput. Meth. Sci. Eng.* 2013, 13, 245-270.
10. Trell, E. Lie, Santilli, and nanotechnology. *AIP Conference Proceedings* 2014, 1637, 1100-1109.
11. Trell, E.; Akpojotor, G.; Edeagu, S.; Animalu, A. Structural wave-packet tessellation of the periodic table and atomic constitution in real R3 x SO(3) configuration space. *J. Phys.: Conf. Ser.* 2019,

1251 012047, 1-15.

12. Trell, E. A space-frame periodic table representation system testing relativity in nucleosynthesis of the elements. *J. Phys.: Conf. Ser.* 2020, 1557 012006, 1-10.
13. Trell, E. From Photon to Oganesson. Lie algebra realization of the Standard Model extending over the Periodic Table. *J. Phys.: Conf. Ser.* 2021, 2081 012034, 1-12.
14. Trell, E. A bottom-up 'Game of Lie' cellular automaton evolution in SO(3) root space both nucleating, crystallizing and space-filling the complete atomic realm. *J. Phys.: Conf. Ser.* 2022, 2197 012025, 1-15.
15. Bohr, N. Der Bau der Atome und die physikalischen und chemischen Eigenschaften der Elemente. *Zeitschr.Phys.* 1922, 9, 1-67.
16. Portegeis Zwart, S. Computational astrophysics for the future. *Science* 2018, 36, 979-980.
17. Trell, E. Self-assembled nanostructures of atoms and molecules with examples of various organic compounds including the proteinogenic amino acids and DNA. *Proceedings of IMBIC* 2022, 11, 1-9.
18. Rowlands, P. Zero to Infinity. The foundations of Physics; New Jersey, London, Singapore, Beijing, Shanghai, Hong Kong, Taipei, Chennai, *World Scientific*, 2007.
19. Scerri, E.R. How Good is the Quantum Mechanical Explanation of the Periodic System? *J. Chem. Ed.* 1998, 75, 1384-1385.
20. Aspect, A. Bell's inequality test: more ideal than ever. *Nature* 1999, 398, 189-190.

**Авторы**

**Трелл Эрик**, Линчёпингский университет, г. Линчёпинг, Швеция.
E-mail: erik.trell@gmail.com

**Просьба ссылаться на эту статью следующим образом:**

Трелл Э. Ауфбау дифференциальной геометрии Ли атомов и молекул. *Пространство, время и фундаментальные взаимодействия.* 2023. № 3-4. С. 299–313.

**Authors**

**Trell Erik**, Linköping University, Linköping, Sweden.
E-mail: erik.trell@gmail.com

**Please cite this article in English as:**

Trell E. Lie differential geometry aufbau of the atoms and molecules. *Space, Time and Fundamental Interactions*, 2023, no. 3-4, pp. 299–313.

УДК 524.8, 524.82



# ПАРАДИГМА МАСШТАБНО-ИНВАРИАНТНОГО ВАКУУМА: ОСНОВНЫЕ РЕЗУЛЬТАТЫ И ТЕКУЩИЙ ПРОГРЕСС ПЛЮС BBNS РЕЗУЛЬТАТЫ

Георгиев В. Г.[a,b,1], Маедер А.[c,2]

[a] Институт Съвременни Физических Исследований, София, Болгария

[b] Институт Ронина, Монклер, Нью-Джерси, США.

[c] Женевская Обсерватория, Женевский Университет, Женева, Швейцария

Обзор основные результаты в рамках парадигмы масштабно-инвариантного вакуума (SIV), что касается интегрируемой геометрии Вейля как расширение Общей теории относительности Эйнштейна. После краткого очерка математической основы, основные результаты до 2023 года [1] выделяются по отношению к: инфляция внутри SIV [2], рост флуктуаций плотности [3], применение SIV к масштабно-инвариантной динамике галактик, MOND, темная материя и карликовые сфероиды [4], и самые последние результаты по содержанию легких элементов BBNS в SIV [5].

*Ключевые слова*: космология: теория, темная материя и энергия, инфляция, BBNS; галактики: образование, вращение.

# THE SCALE INVARIANT VACUUM PARADIGM: MAIN RESULTS PLUS THE CURRENT BBNS PROGRESS

Gueorguiev V. G.[a,b,1], Maeder A.[c,2]

[a] Institute for Advanced Physical Studies, Sofia, Bulgaria.

[b] Ronin Institute for Independent Scholarship, Montclair, NJ, USA

[c] Geneva Observatory, University of Geneva, Geneva, Switzerland.

We summarize the main results within the Scale Invariant Vacuum (SIV) paradigm as related to the Weyl Integrable Geometry (WIG) as an extension to the standard Einstein General Relativity (EGR). After a short sketch of the mathematical framework, the main results until 2023 [1] are highlighted in relation to: the inflation within the SIV [2], the growth of the density fluctuations [3], the application of the SIV to scale-invariant dynamics of galaxies, MOND, dark matter, and the dwarf spheroidals [4], and the most recent results on the BBNS light-elements' abundances within the SIV [5].

*Keywords*: cosmology: theory, dark matter and energy, inflation, BBNS; galaxies: formation, rotation.

PACS: 98.80.-k, 98.80.Cq, 26.35.+c

DOI: 10.17238/issn2226-8812.2023.3-4.314-326

## A. Motivation

The paper is a summary of the current main results within the Scale Invariant Vacuum (SIV) paradigm as related to the Weyl Integrable Geometry (WIG) as an extension to the standard Einstein General Relativity (EGR) as of Summer 2023. As such, it is a reflection of the corresponding online conference presentation during the XXIII International Meeting Physical Interpretations of Relativity Theory at the Bauman Moscow State Technical University, Moscow, 2023 (PIRT'23).

Our main goal is to present a condensed overview of the key results of the theory so far, along with the latest progress in applying the SIV paradigm to variety of physics phenomenon, and in doing

[1]E-mail: Vesselin at MailAPS.org

[2]E-mail: Andre.Maeder at UniGe.ch

so to help the intellectually curious reader gain some understanding as to where the paradigm has been tested and what is the success level of the inquiry. As such, the paper follows closely our previous 2022 paper [6] that was based on a talk presented at the conference Alternative Gravities and Fundamental Cosmology, at the University of Szczecin, Poland in September 2021. Our initial presentation and its conference contribution were covering, back then, only four main results: comparing the scale factor $a(t)$ within ΛCDM and SIV [13], the growth of the density fluctuations within the SIV [3], the application to scale-invariant dynamics of galaxies [4], and inflation of the early-universe within the SIV theory [2]. Back then, our article layout was aiming for focusing on each of these four main results via highlighting its most relevant figure or equation. As a result each topic was covered via one to two pages text preceded by short and concise description of the mathematical framework.

Here, we add one more sections related to the recent developments in the application of SIV paradigm since our previous summary paper in 2022 [6], it is our latest study of the Big-Bang Nucleosynthesis (BBNS) within the SIV Paradigm [5] that has been reported for a first time during PRIT'23 conference [7].

After a general introduction on the problem of scale invariance and physical reality, along with the similarities and differences of Einstein General Relativity and Weyl Integrable Geometry, we only highlight the mathematical framework as pertained to Weyl Integrable Geometry, Dirac Co-Calculus, and reparametrization invariance|. Rather than re-deriving the weak-field SIV results for the equations of motion, we have decided to use the idea of reparametrization invariance [8] to illustrate the corresponding equations of motion. The relevant discussion on reparametrization invariance is in the section on the Consequences of Going beyond Einstein's General Relativity. This section precedes the brief review of the necessary results about the Scale Invariant Cosmology idea needed in the section on Comparisons and Applications, where we highlight the main results related to inflation within the SIV [2], the growth of the density fluctuations [3], and the application of the SIV to scale-invariant dynamics of galaxies, MOND, dark matter, and the dwarf spheroidals [4]. The results section of the paper concludes with the most recent results on the BBNS light-elements' abundances within the SIV [5]. We end the paper with a section containing the Conclusions and Outlook for future research directions.

### A.1. Scale Invariance and Physical Reality

The presence of a scale is related to the existence of physical connection and causality. The corresponding relationships are formulated as physical laws dressed in mathematical expressions. The laws of physics (numerical factors in the formulae) change upon change of scale, but maintain a form-invariance. As a result, using consistent units is paramount in physics and leads to powerful dimensional estimates of the order of magnitude of physical quantities based on a simple dimensional analysis. The underlined scale is closely related to the presence of material content, which reflects the energy scale involved.

However, in the absence of matter, a scale is not easy to define. Therefore, an empty universe would be expected to be scale invariant! Absence of scale is confirmed by the scale invariance of the Maxwell equations in vacuum (no charges and no currents—the sources of the electromagnetic fields). The field equations of general relativity are scale invariant for empty space with zero cosmological constant. What amount of matter is sufficient to kill scale invariance is still an open question. Such a question is particularly relevant to cosmology and the evolution of the universe.

### A.2. Einstein General Relativity (EGR) and Weyl Integrable Geometry (WIG)

Einstein's General Relativity (EGR) is based on the premise of a torsion-free covariant connection that is metric-compatible and guarantees the preservation of the length of vectors along geodesics ($\delta \|\overrightarrow{v}\| = 0$). The theory has been successfully tested at various scales, starting from local Earth laboratories, the Solar system, on galactic scales via light-bending effects, and even on an extragalactic level via the observation of gravitational waves. The EGR is also the foundation for modern cosmology and astrophysics. However, at galactic and cosmic scales, some new and mysterious phenomena have appeared. The explanations for these phenomena are often attributed to unknown matter particles or fields that are yet to be detected in our laboratories—dark matter and dark energy.

As no new particles or fields have been detected in the Earth labs for more than twenty years, it seems reasonable to revisit some old ideas that have been proposed as a modification of the EGR. In 1918, Weyl proposed and extension by adding local gauge (scale) invariance [9]. Other approaches were more radical by adding extra dimensions, such as Kaluza?Klein unification theory. Then, via Jordan conformal equivalence, one comes back to the usual 4D spacetime as projective relativity theory, but with at least one additional scalar field. Such theories are also known as Jordan?Brans?Dicke scalar-tensor gravitation theories [10, 11]. In most such theories, there is a major drawback—a varying Newton constant $G$. As no such variations have been observed, we prefer to view Newton's gravitational constant $G$ as constant despite the experimental issues on its measurements [12].

In the light of the above discussion one may naturally ask: could the mysterious (dark) phenomena be artifacts of non-zero $\delta\,\|\overrightarrow{v}\|$, but often negligible; thus, almost zero value ($\delta\,\|\overrightarrow{v}\| \approx 0$), which could accumulate over cosmic distances and fool us that the observed phenomena may be due to dark matter and/or dark energy? An idea of extension of EGR was proposed by Weyl as soon as the General Relativity (GR) was proposed by Einstein. Weyl proposed an extension to GR by adding local gauge (scale) invariance that has the consequence that lengths may not be preserved upon parallel transport. However, it was quickly argued that such a model will result in a path dependent phenomenon and, thus, contradicting observations. A remedy was later found to this objection by introducing Weyl Integrable Geometry (WIG), where the lengths of vectors are conserved only along closed paths ($\oint \delta\,\|\overrightarrow{v}\| = 0$). Such formulation of the Weyl's original idea defeats the Einstein objection! Furthermore, given that all we observe about the distant universe are waves that reach us, the condition for Weyl Integrable Geometry is basically saying that the information that arrives to us via different paths is interfering constructively to build a consistent picture of the source.

One way to build a WIG model is to consider conformal transformation of the metric field $g'_{\mu\nu} = \lambda^2 g_{\mu\nu}$ and to apply it to various observational phenomena. As shown previously [1], the demand for homogeneous and isotropic space restricts the field $\lambda$ to depend only on the cosmic time and not on the space coordinates. The weak field limit of such a WIG model results in an extra acceleration in the equation of motion that is proportional to the velocity. This behavior is somewhat similar to the Jordan?Brans?Dicke scalar-tensor gravitation; however, the conformal factor $\lambda$ does not seems to be a typical scalar field as in the Jordan?Brans?Dicke theory [10, 11]. The Scale Invariant Vacuum (SIV) idea provides a way of finding out the specific functional form of $\lambda(t)$ as applicable to LFRW cosmology and its WIG extension [1, 13].

We also find it important to point out that extra acceleration in the equations of motion, which is proportional to the velocity of a particle, could also be justified by requiring re-parametrization symmetry. Not implementing re-parametrization invariance in a model could lead to un-proper time parametrization [8] that seems to induce "fictitious forces" in the equations of motion similar to the forces derived in the weak field SIV regime. It is a puzzling observation that may help us understand nature better.

### B. Mathematical Framework

The framework for the Scale Invariant Vacuum paradigm is based on the Weyl Integrable Geometry and Dirac co-calculus as mathematical tools for description of nature [9, 14].

The original Weyl Geometry uses a metric tensor field $g_{\mu\nu}$, along with a "connexion" vector field $\kappa_\mu$, and a scalar field $\lambda$. In the Weyl Integrable Geometry, the "connexion" vector field $\kappa_\mu$ is not an independent, but it is derivable from the scalar field $\lambda$ via the defining expression: $\kappa_\mu = -\partial_\mu \ln(\lambda)$. This form of the "connexion" vector field $\kappa_\mu$ guarantees its irrelevance, in the covariant derivatives, upon integration over closed paths. That is, $\oint \kappa_\mu dx^\mu = 0$. In other words, $\kappa_\mu dx^\mu$ represents a closed 1-form; furthermore, it is an exact form since its definition implies $\kappa_\mu dx^\mu = -d \ln \lambda$. Thus, the scalar function $\lambda$ plays a key role in the Weyl Integrable Geometry. Its physical meaning is related to the freedom of a local scale gauge, which provides a description upon scale change via local re-scaling $l' \to \lambda(x)l$.

The covariant derivatives use the rules of the Dirac co-calculus [14] where tensors also have co-tensor powers based on the way they transform upon change of scale. For the metric tensor $g_{\mu\nu}$ this power is $n = 2$. This follows from the way the length of a line segment $ds$ with coordinates $dx^\mu$ is defined via the usual expression $ds^2 = g_{\mu\nu}dx^\mu dx^\nu$. That is, one has: $l' \to \lambda(x)l \Leftrightarrow ds' = \lambda ds \Rightarrow g'_{\mu\nu} = \lambda^2 g_{\mu\nu}$. This leads to $g^{\mu\nu}$ having the co-tensor power of $n = -2$ in order to have the Kronecker $\delta$ as scale invariant object $(g_{\mu\nu}g^{\nu\rho} = \delta^\rho_\mu)$. That is, a co-tensor is of power $n$ when, upon local scale change, it satisfies: $l' \to \lambda(x)l :\ Y'_{\mu\nu} \to \lambda^n Y_{\mu\nu}$, That is a scale-invariant EGR quantity denoted by primed quantity can be obtained from a WIG co-tensor of power $n$ upon its multiplication by the $\lambda^n$ factor.

In the Dirac co-calculus, this results in the appearance of the "connexion" vector field $\kappa_\mu$ in the covariant derivatives of scalars, vectors, and tensors (see Table 1); where the usual Christoffel symbol $\Gamma^\nu_{\mu\alpha}$ is replaced by

$$^*\Gamma^\nu_{\mu\alpha} = \Gamma^\nu_{\mu\alpha} + g_{\mu\alpha}k^\nu - g^\nu_\mu \kappa_\alpha - g^\nu_\alpha \kappa_\mu. \tag{B.1}$$

The corresponding equation of the geodesics within the WIG was first introduced in 1973 by [14] and in the weak-field limit of Weyl gauge change redivided in 1979 by [15] ($u^\mu = dx^\mu/ds$ is the four-velocity):

$$u^\mu_{*\nu} = 0 \Rightarrow \frac{du^\mu}{ds} +^* \mathit{\Gamma}^\mu_{\nu\rho}u^\nu u^\rho + \kappa_\nu u^\nu u^\mu = 0\,. \tag{B.2}$$

This geodesic equation has also been derived from reparametrization-invariant action in 1978 by [16] given by $\delta\mathcal{A} = \int_{P_0}^{P_1} \delta\left(d\widetilde{s}\right) = \int \delta\left(\beta ds\right) = \int \delta\left(\beta \frac{ds}{d\tau}\right) d\tau = 0$.

**Таблица 1.** Derivatives for co-tensors of power $n$ defined via $Y'_{\mu\nu} \to \lambda^n Y_{\mu\nu}$ when $l' \to \lambda(x)l$.

| **Co-Tensor Type** | **Mathematical Expression** |
|---|---|
| co-scalar | $S_{*\mu} = \partial_\mu S - n\kappa_\mu S,$ |
| co-vector | $A_{\nu*\mu} = \partial_\mu A_\nu -\ ^*\Gamma^\alpha_{\nu\mu}A_\alpha - n\kappa_\nu A_\mu,$ |
| co-covector | $A^\nu_{*\mu} = \partial_\mu A^\nu +\ ^*\Gamma^\nu_{\mu\alpha}A^\alpha - nk^\nu A_\mu.$ |

### B.1. Consequences of Going beyond the EGR

Before we go into a specific examples, such as FLRW cosmology and weak-field limit, we would like to make few remarks. By using (B.1) in (B.2), one can see that the usual EGR equations of motion receive extra terms proportional to the four-velocity and its normalization:

$$\frac{du^\mu}{ds} + \mathit{\Gamma}^\mu_{\nu\rho}u^\nu u^\rho = (\kappa \cdot u)u^\mu - (u \cdot u)\kappa^\mu \tag{B.3}$$

In the weak-field approximation within the SIV, one assumes an isotropic and homogeneous space for the derivation of the terms beyond the usual Newtonian equations [16]. As seen from (B.3), the result is a velocity dependent extra term $\kappa_0 \vec{v}$ with $\kappa_0 = -\dot{\lambda}/\lambda$ and $\vec{\kappa} = 0$ due to the assumption of isotropic and homogeneous space. At this point, it is important to stress that the usual normalization for the four-velocity, $u \cdot u = \pm 1$ with sign related to the signature of the metric tensor $g_{\mu\nu}$, is a special choice of $s$-parametrization—the proper-time parametrization $\tau$.

Recently, similar $\kappa_0 \vec{v}$ term was derived as a consequence of non-reparametrization invariant mathematical modeling but without the need for a weak-field approximation. The effect is due to unproper time parametrization manifested as velocity dependent fictitious acceleration [8]. In this respect, the term $\kappa_0 \vec{v}$ is necessary for the restoration of the broken symmetry - the re-parametrization invariance of a process under study. To demonstrate this, one can apply an arbitrary time re-parametrization $\lambda = dt/d\tau$; then, the first term on the LHS of (B.3) becomes:

$$\lambda \frac{d}{dt}\left(\lambda \frac{d\vec{r}}{dt}\right) = \lambda^2 \frac{d^2\vec{r}}{dt^2} + \lambda\dot{\lambda}\frac{d\vec{r}}{dt}. \tag{B.4}$$

By moving the term linear in the velocity to the RHS, dividing by $\lambda^2$, and by using $\kappa(t) = -\dot{\lambda}/\lambda$, one obtains a $\kappa_0\vec{v}$-like term on the RHS. If we were to do such manipulation in the absence of $\kappa_0\vec{v}$ on the RHS of (B.3), then the term will be generated, while if $\tilde{\kappa}$ was present then it will be transformed $\tilde{\kappa} \to \kappa + \tilde{\kappa}$.

Furthermore, unlike in SIV, where one can justify $\lambda(t) = t_0/t$ [13], for re-parametrization symmetry the time dependence of $\lambda(t)$ could be arbitrary. Finally, as discussed in [8], the extra term $\kappa_0\vec{v}$ is not expected to be present when the time parametrization of the process is the proper time of the system. Thus, a term of the form $\kappa\vec{v}$ can be viewed as restoration of the re-parametrization symmetry and an indication of un-proper time parametrization of a process under consideration.

### B.2. Scale Invariant Cosmology

The scale invariant cosmology equations were first introduced in 1973 by [14] and then re-derived in 1977 by [17]. The equations are based on the corresponding expressions of the Ricci tensor and the relevant extension of the Einstein equations. The conformal transformation ($g'_{\mu\nu} = \lambda^2 g_{\mu\nu}$) of the metric tensor $g_{\mu\nu}$ in the more general Weyl's framework into Einstein's framework, where the metric tensor is $g'_{\mu\nu}$, induces a simple relation between the Ricci tensor and scalar in the Weyl's Integrable Geometry and the Einstein GR framework (using prime to denote Einstein GR framework objects):

$$R_{\mu\nu} = R'_{\mu\nu} - \kappa_{\mu;\nu} - \kappa_{\nu;\mu} - 2\kappa_\mu\kappa_\nu + 2g_{\mu\nu}\kappa^\alpha\kappa_\alpha - g_{\mu\nu}\kappa^\alpha_{;\alpha} \qquad \text{and} \qquad R = R' + 6\kappa^\alpha\kappa_\alpha - 6\kappa^\alpha_{;\alpha}\,.$$

By considering the Einstein equation $R_{\mu\nu} - \frac{1}{2}\, g_{\mu\nu}R = -8\pi G T_{\mu\nu} - \Lambda\, g_{\mu\nu}$ along with the above expressions, one gets:

$$R'_{\mu\nu} - \frac{1}{2}\, g_{\mu\nu}R' - \kappa_{\mu;\nu} - \kappa_{\nu;\mu} - 2\kappa_\mu\kappa_\nu + 2g_{\mu\nu}\kappa^\alpha_{;\alpha} - g_{\mu\nu}\kappa^\alpha\kappa_\alpha = -8\pi G T_{\mu\nu} - \Lambda\, g_{\mu\nu}\,. \tag{B.5}$$

The relationship $\Lambda = \lambda^2\Lambda_{\mathrm{E}}$ of $\Lambda$ in WIG to the Einstein cosmological constant $\Lambda_{\mathrm{E}}$ in the EGR was present in the original form of the equations to provide explicit scale invariance. This relationship makes explicit the appearance of $\Lambda_{\mathrm{E}}$ as invariant scalar (in-scalar), as then one has $\Lambda\, g_{\mu\nu} = \lambda^2\Lambda_{\mathrm{E}}\, g_{\mu\nu} = \Lambda_{\mathrm{E}}\, g'_{\mu\nu}$.

The above equation (B.5) ia a generalization of the original Einstein GR equation. Thus, they have an even larger class of local gauge symmetries that need to be fixed by a gauge choice. In Dirac's work, the gauge choice was based on the large numbers hypothesis. Here, we will discuss a different gauge choice - the SIV gauge.

The corresponding scale-invariant FLRW based cosmology equations within the WIG framework were first introduced in 1977 by [17]:

$$\frac{8\pi G\varrho}{3} = \frac{k}{a^2} + \frac{\dot{a}^2}{a^2} + 2\frac{\dot{\lambda}\,\dot{a}}{\lambda\, a} + \frac{\dot{\lambda}^2}{\lambda^2} - \frac{\Lambda_{\mathrm{E}}\lambda^2}{3}\,, \quad \text{and} \quad -8\pi G p = \frac{k}{a^2} + 2\frac{\ddot{a}}{a} + 2\frac{\ddot{\lambda}}{\lambda} + \frac{\dot{a}^2}{a^2} + 4\frac{\dot{a}\,\dot{\lambda}}{a\,\lambda} - \frac{\dot{\lambda}^2}{\lambda^2} - \Lambda_{\mathrm{E}}\,\lambda^2\,. \tag{B.6}$$

These equations clearly reproduce the standard FLRW equations in the limit $\lambda = const = 1$. The scaling of $\Lambda$ was recently used to revisit the Cosmological Constant Problem within quantum cosmology [18]. The conclusion of [18] is that our universe is unusually large, given that the expected mean size of all universes, where Einstein GR holds, is expected to be of a Plank scale. In the study, $\lambda = const$ was a key assumption as the universes were expected to obey the Einstein GR equations. What the expected mean size of all universes would be if the condition $\lambda = const$ is relaxed, as for a WIG-universes ensemble, remains an open question.

### B.3. The Scale Invariant Vacuum Gauge ($T = 0$ and $R' = 0$)

The idea of the Scale Invariant Vacuum was introduced first in 2017 by [13]. It is based on the fact that, for Ricci flat ($R'_{\mu\nu} = 0$) Einstein GR vacuum ($T_{\mu\nu} = 0$), one obtains from (B.5) the following equation for the vacuum:

$$\kappa_{\mu;\nu} + \kappa_{\nu;\mu} + 2\kappa_\mu\kappa_\nu - 2g_{\mu\nu}\kappa^\alpha_{;\alpha} + g_{\mu\nu}\kappa^\alpha\kappa_\alpha = \Lambda\, g_{\mu\nu}. \tag{B.7}$$

For homogeneous and isotropic WIG-space $\partial_i\lambda = 0$; therefore, only $\kappa_0 = -\dot{\lambda}/\lambda$ and its time derivative $\dot{\kappa}_0 = -\kappa_0^2$ can be non-zero. As a corollary of (B.7), one can derive the following set of equations [13]:

$$3\,\frac{\dot{\lambda}^2}{\lambda^2} = \Lambda\,,\ \text{and}\quad 2\frac{\ddot{\lambda}}{\lambda} - \frac{\dot{\lambda}^2}{\lambda^2} = \Lambda\,,\quad \text{or}\quad \frac{\ddot{\lambda}}{\lambda} = 2\,\frac{\dot{\lambda}^2}{\lambda^2}\,,\ \text{and}\quad \frac{\ddot{\lambda}}{\lambda} - \frac{\dot{\lambda}^2}{\lambda^2} = \frac{\Lambda}{3}\,. \tag{B.8}$$

One could derive these equations by using the time and space components of the equations (B.7) or by looking at the relevant trace invariant along with the relationship $\dot{\kappa}_0 = -\kappa_0^2$. Any pair of these equations is sufficient to prove the other pair of equations.

**Theorem 1.** *Using any one pair of two SIV Equations* (B.8) *along with* $\Lambda = \lambda^2\Lambda_E$ *one has:*

$$\Lambda_E = 3\frac{\dot{\lambda}^2}{\lambda^4}, \quad \text{with} \quad \frac{d\Lambda_E}{dt} = 0. \tag{B.9}$$

**Corollary.** *The solution of the SIV equations is:* $\lambda = t_0/t$, *with* $t_0 = \sqrt{3/\Lambda_E}$ *and* $c = 1$ *for the speed of light.*

Upon the use of the SIV gauge, first in 2017 by [13], one observes that *the cosmological constant disappears* from Equations (B.6):

$$\frac{8\,\pi G\varrho}{3} = \frac{k}{a^2} + \frac{\dot{a}^2}{a^2} + 2\,\frac{\dot{a}\dot{\lambda}}{a\lambda}\,, \quad \text{and} \quad -\,8\,\pi G p = \frac{k}{a^2} + 2\frac{\ddot{a}}{a} + \frac{\dot{a}^2}{a^2} + 4\frac{\dot{a}\dot{\lambda}}{a\lambda}\,. \tag{B.10}$$

## C. Comparisons and Applications

The predictions and outcomes of the SIV paradigm were confronted with observations in a series of papers by the current authors. Highlighting the main results and outcomes is the subject of current section.

### C.1. Comparing the Scale Factor $a(t)$ within ΛCDM and SIV

Upon arriving at the SIV cosmology Equations (B.10), along with the gauge fixing (B.9), which implies $\lambda = t_0/t$ with $t_0$ indicating the current age of the universe since the Big-Bang ($a = 0$ at $t_{\text{in}} < t_0$), the implications for cosmology were first discussed by [13] and later reviewed by [19]. The most important point in comparing ΛCDM and SIV cosmology models is the existence of SIV cosmology with slightly different parameters but almost the same curve for the standard scale parameter $a(t)$ when the time scale is set so that $t_0 = 1$ now [13, 19]. As seen in Figure 1, the difference between the ΛCDM and SIV models declines for increasing matter densities. Furthermore, for any ΛCDM curve at some $\Omega'_m$ there is a matching SIV curve at some $\Omega_m < \Omega'_m$. Thus, SIV needs less total matter to produce the same scale-factor evolution.

### C.2. Application to Scale-Invariant Dynamics of Galaxies

The next important application of the scale-invariance at cosmic scales is the derivation of a universal expression for the Radial Acceleration Relation (RAR) of $g_{\text{obs}}$ and $g_{\text{bar}}$. That is, the relation

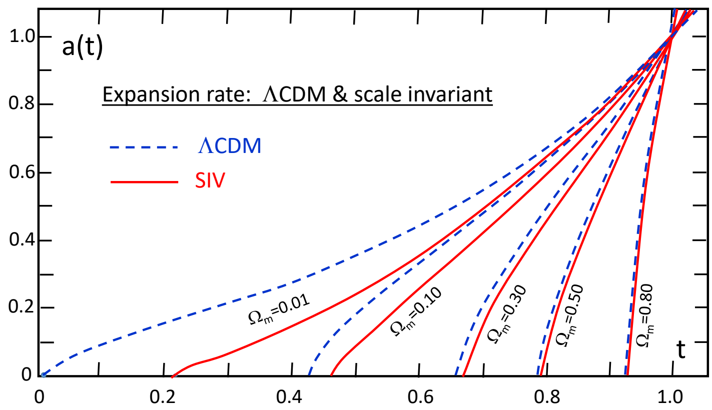


**Рис. 1.** Expansion rates $a(t)$ as a function of time $t$ in the flat ($k = 0$) ΛCDM and SIV models in the matter dominated era. The curves are labeled by the values of $\Omega_{\mathrm{m}}$.

between the observed gravitational acceleration $g_{\mathrm{obs}} = v^2/r$ and the baryonic matter acceleration due to the standard Newtonian gravity $g_{\mathrm{N}}$ by [4]:

$$g = g_{\mathrm{N}} + \frac{k^2}{2} + \frac{1}{2}\sqrt{4 g_{\mathrm{N}} k^2 + k^4}\,, \tag{C.1}$$

where $g = g_{\mathrm{obs}}$, $g_N = g_{\mathrm{bar}}$. For $g_{\mathrm{N}} \gg k^2 : g \to g_{\mathrm{N}}$ but for $g_{\mathrm{N}} \to 0 \Rightarrow g \to k^2$ is a constant.

As seen in Figure 2, MOND deviates significantly for the data on the Dwarf Spheroidals. This is well-known problem in MOND due to the need of two different interpolating functions, one in galaxies and one at cosmic scales. The SIV expression (C.1) resolves this issue via one universal parameter $k^2$ related to the gravity at large distances [4]. Even more, one can actually show that MOND is a peculiar case of the SIV theory [20].

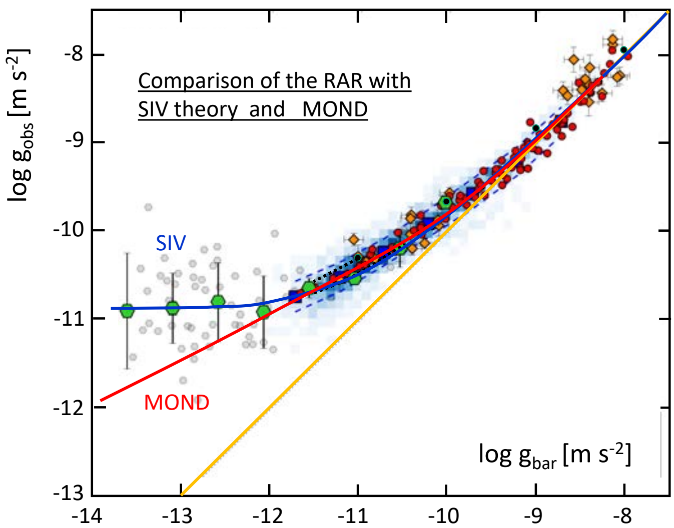


**Рис. 2.** Radial Acceleration Relation (RAR) for the galaxies studied by Lelli et al. (2017). Dwarf Spheroidals as binned data (big green hexagons), along with MOND (red curve), and SIV (blue curve) model predictions. The orange curve shows the 1:1-line for $g_{\mathrm{obs}}$ and $g_{\mathrm{bar}}$. Due to to the smallness of $g_{\mathrm{obs}}$ and $g_{\mathrm{bar}}$ the application of the log function results in negative numbers; thus, the corresponding axes' values are all negative.

The expression (C.1) follows from the Weak Field Approximation (WFA) of the SIV upon utilization of the Dirac co-calculus in the derivation of the geodesic equation within the relevant WIG (B.2) (see

[4] for more details, as well as the original derivation in [15]):

$$g_{ii} = -1,\ g_{00} = 1 + 2\Phi/c^2 \Rightarrow \Gamma^i_{00} = \frac{1}{2}\frac{\partial g_{00}}{\partial x^i} = \frac{1}{c^2}\frac{\partial \Phi}{\partial x^i} \Rightarrow \frac{d^2\overrightarrow{r}}{dt^2} = -\frac{GM}{r^2}\frac{\overrightarrow{r}}{r} + \kappa_0(t)\frac{d\overrightarrow{r}}{dt}. \qquad \text{(C.2)}$$

where $i \in 1,2,3$, while the potential $\Phi = GM/r$ is scale invariant.

By considering the scale-invariant ratio of the correction term $\kappa_0(t)\,\vec{v}$ to the usual Newtonian term in (C.2), one has: $x = \frac{\kappa_0 v r^2}{GM} = \frac{H_0}{\xi}\frac{v\,r^2}{GM} = \frac{H_0}{\xi}\frac{(r\,g_{\rm obs})^{1/2}}{g_{\rm bar}} \sim \frac{g_{\rm obs}-g_{\rm bar}}{g_{\rm bar}}$. Then, by utilizing an explicit scale invariance for canceling the proportionality factor: $\left(\frac{g_{\rm obs}-g_{\rm bar}}{g_{\rm bar}}\right)_2 \div \left(\frac{g_{\rm obs}-g_{\rm bar}}{g_{\rm bar}}\right)_1 = \left(\frac{g_{\rm obs,2}}{g_{\rm obs,1}}\right)^{1/2}\left(\frac{g_{\rm bar,1}}{g_{\rm bar,2}}\right)$, by setting $g = g_{\rm obs,2}$, $g_N = g_{\rm bar,2}$, and by collecting all the system-1 terms in $k = k_{(1)}$, then one arrives at (C.1) by solving for $g$ in $\frac{g}{g_{\rm N}} - 1 = k_{(1)}\frac{g^{1/2}}{g_{\rm N}}$ and keeping the bigger root (the positive sign in $\pm\sqrt{\ldots}$ factor).

## C.3. Growth of the Density Fluctuations within the SIV

Another interesting result was the possibility of a fast growth of the density fluctuations within the SIV [3]. This study accordingly modifies the relevant equations such as the continuity equation, Poisson equation, and Euler equation within the SIV framework. Here, we outline the main equations and the relevant results.

By using the notation $\kappa = \kappa_0 = -\dot{\lambda}/\lambda = 1/t$, the corresponding Continuity, Poisson, and Euler equations are:

$$\frac{\partial \rho}{\partial t} + \vec{\nabla}\cdot(\rho\vec{v}) = \kappa\left[\rho + \vec{r}\cdot\vec{\nabla}\rho\right],\ \vec{\nabla}^2\Phi = \triangle\Phi = 4\pi G\varrho,\ \frac{d\vec{v}}{dt} = \frac{\partial\vec{v}}{\partial t} + \left(\vec{v}\cdot\vec{\nabla}\right)\vec{v} = -\vec{\nabla}\Phi - \frac{1}{\rho}\vec{\nabla}p + \kappa\vec{v}\,.$$

For a density perturbation $\varrho(\vec{x},t) = \varrho_b(t)(1+\delta(\vec{x},t))$ the above equations result in:

$$\dot{\delta} + \vec{\nabla}\cdot\dot{\vec{x}} = \kappa\vec{x}\cdot\vec{\nabla}\delta = n\kappa(t)\delta, \qquad \vec{\nabla}^2\Psi = 4\pi G a^2\varrho_b\delta, \qquad \ddot{\vec{x}} + 2H\dot{\vec{x}} + (\dot{\vec{x}}\cdot\vec{\nabla})\dot{\vec{x}} = -\frac{\vec{\nabla}\Psi}{a^2} + \kappa(t)\dot{\vec{x}}. \text{(C.3)}$$

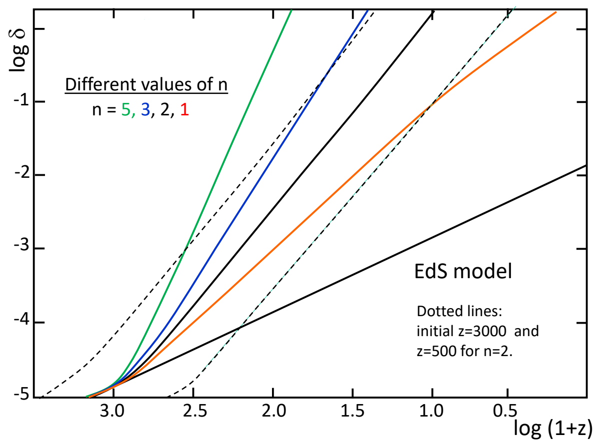


**Рис. 3.** The growth of density fluctuations for different values of parameter $n$ (the gradient of the density distribution in the nascent cluster), for an initial value $\delta = 10^{-5}$ at $z = 1376$ and $\Omega_{\rm m} = 0.10$. The initial slopes are those of the EdS models. The two light broken curves show models with initial $(z+1) = 3000$ and 500, with same $\Omega_{\rm m} = 0.10$ and $n = 2$. These dashed lines are to be compared to the black continuous line of the $n = 2$ model. All the three lines for $n = 2$ are very similar and nearly parallel. Due to to the smallness of $\delta$ the application of the log function results in negative numbers; resulting in negative vertical axis.

The final result $\ddot{\delta} + (2H - (1+n)\kappa)\dot{\delta} = 4\pi G\varrho_b\delta + 2n\kappa(H-\kappa)\delta$ recovers the standard equation in the limit of $\kappa \to 0$. The simplifying assumption $\vec{x}\cdot\vec{\nabla}\delta(x) = n\delta(x)$ in (C.3) introduces the parameter $n$ that measures the perturbation type (shape). For example, a spherically symmetric perturbation would have

$n = 2$. As seen in Figure 3, perturbations for various values of $n$ are resulting in faster growth of the density fluctuations within the SIV than in the Einstein–de Sitter model, even at relatively law matter densities. Furthermore, the overall slope is independent of the choice of recombination epoch $z_{\text{rec}}$. The behavior for different $\Omega_m$ is also very interesting, and is shown and discussed in detail by [3].

### C.4. Big-Bang Nucleosynthesis within the Scale Invariant Vacuum Paradigm

The SIV paradigm has been recently applied to the Big-Bang Nucleosynthesis using the known analytic expressions for the expansion factor $a$ and the plasma temperature $T$ as functions of the SIV time $\tau$ since the Big-Bang when $a(\tau = 0) = 0$ [5]. The results have been compared to the standard BBNS as calculated via the PRIMAT code [21]. Potential SIV-guided deviations from the local statistical equilibrium were also explored in ref. [5]. Overall, it was found that smaller than usual baryon and non-zero dark matter content, by a factor of three to five times reduction, result in compatible to the standard light elements abundances (Table 2).

The SIV analytic expressions for $a(T)$ and $\tau(T)$ were utilized to study the BBNS within the SIV paradigm [5, 22]. The functional behavior is very similar to the standard model within PRIMAT except during the very early universe where electron-positron annihilation and neutrino processes affect the $a(T)$ function (see Table I and Fig. 2 in ref. [5]). The distortion due to these effects encoded in the function $S(T)$ could be incorporated by considering the SIV paradigm as a background state of the universe where these processes could take place. It has been demonstrated that incorporation of the $S(T)$ within the SIV paradigm results in a compatible outcome with the standard BBNS see the last two columns of Table 2; furthermore, if one is to fit the observational data the result is $\lambda \approx 1$ for the SIV parameter $\lambda$ (see last column of Table 2 with $\lambda = \text{FRF} \approx 1$). However, a pure SIV treatment (the middle three columns) results in $\Omega_b \approx 1\%$ and less total matter, either around $\Omega_m \approx 23\%$ when all the $\lambda$-scaling connections are utilized (see Table 2 column 6), or around $\Omega_m \approx 6\%$ without any $\lambda$-scaling factors (see column 5 of Table 2). The need to have $\lambda$ close to 1 is not an indicator of dark matter content but indicates the goodness of the standard PRIMAT results that allows only for $\lambda$ close to 1 as an augmentation, as such this leads to a light but important improvement in D/H as seen when comparing columns three with eight and nine.

The SIV paradigm suggests specific modifications to the reaction rates, as well as the functional temperature dependences of these rates, that need to be implemented to have consistence between the Einstein GR frame and the WIG (SIV) frame. In particular, the non-in-scalar factor $T^\beta$ in the reverse reactions rates may be affected the most due to the SIV effects. As shown in [5], the specific dependences studied, within the assumptions made within the SIV model, resulted in three times less baryon matter, usually around $\Omega_b \approx 1.6\%$ and less total matter - around $\Omega_m \approx 6\%$. The lower baryon matter content leads to also a lower photon to baryon ratio $\eta_{10} \approx 2$ within the SIV, which is three tines less that the standard value of $\eta_{10} = 6.09$. The overall results indicated insensitivity to the specific $\lambda$-scaling dependence of the m$\check{\text{T}}$-factor in the reverse reaction expressions within $T^\beta$ terms. Thus, one may have to explore further the SIV-guided $\lambda$-scaling relations as done for the last column in Table 2, however, this would require the utilization of the numerical methods used by PRIMAT and as such will take us away from the SIV-analytic expressions explored that provided a simple model for understanding the BBNS within the SIV paradigm. Furthermore, it will take us further away from the accepted local statistical equilibrium and may require the application of the reparametrization paradigm that seems to result in SIV like equations but does not impose a specific form for $\lambda$ [8].

### C.5. SIV and the Inflation of the Early Universe

The latest published result within the SIV paradigm is the presence of inflation stage at the very early universe $t \approx 0$ with a natural exit from inflation in a later time $t_{\text{exit}}$ with value related to the parameters of the inflationary potential [2]. The main steps towards these results are outlined below.

| Element | Obs. | PRMT | $a_{SIV}$ | fit | fit* | $\bar{a}/\lambda$ | fit* | fit |
|---|---|---|---|---|---|---|---|---|
| H | 0.755 | 0.753 | 0.805 | 0.755 | 0.849 | 0.75 | 0.753 | 0.755 |
| $Y_P = 4Y_{\mathrm{He}}$ | 0.245 | 0.247 | 0.195 | 0.245 | 0.151 | 0.25 | 0.247 | 0.245 |
| $\mathrm{D/H} \times 10^5$ | 2.53 | 2.43 | 0.743 | 2.52 | 2.52 | 1.49 | 2.52 | 2.53 |
| $^3\mathrm{He/H} \times 10^5$ | 1.1 | 1.04 | 0.745 | 1.05 | 0.825 | 0.884 | 1.05 | 1.04 |
| $^7\mathrm{Li/H} \times 10^{10}$ | 1.58 | 5.56 | 11.9 | 5.24 | 6.97 | 9.65 | 5.31 | 5.42 |
| $N_{\mathrm{eff}}$ | 3.01 | 3.01 | 3.01 | 3.01 | 3.01 | 3.01 | 3.01 | 3.01 |
| $\eta_{10}$ | 6.09 | 6.14 | 6.14 | 1.99 | 0.77 | 1.99 | 5.57 | 5.56 |
| FRF | 1 | 1 | 1 | 1 | 1.63 | 1 | 1 | 1.02 |
| $\mathrm{m\check{T}}$ | 1 | 1 | 1 | 1 | 0.78 | 1 | 1 | 0.99 |
| $\mathrm{Q/\check{T}}$ | 1 | 1 | 1 | 1 | 1.28 | 1 | 1 | 1.01 |
| $\Omega_b$ [%] | 4.9 | 4.9 | 4.9 | 1.6 | 0.6 | 1.6 | 4.4 | 4.4 |
| $\Omega_m$ [%] | 31 | 31 | 31 | 5.9 | 23 | 5.9 | 86 | 95 |
| $\sqrt{\chi^2_\epsilon}$ | N/A | 6.84 | 34.9 | 6.11 | 14.8 | 21.9 | 6.2 | 6.4 |

**Таблица 2.** The observational uncertainties are 1.6% for $Y_P$, 1.2% for D/H, 18% for T/H, and 19% for Li/H. FRF is the forwards rescale factor for all reactions, while $\mathrm{m\check{T}}$ and $\mathrm{Q/\check{T}}$ are the corresponding rescale factors in the revers reaction formula based on the local thermodynamical equilibrium. The SIV $\lambda$-dependences are used when these factors are different from 1; that is, in the sixth and ninth columns where FRF$=\lambda$, $\mathrm{m\check{T}}= \lambda^{-1/2}$, and $\mathrm{Q/\check{T}}= \lambda^{+1/2}$. The columns denoted by fit contain the results for perfect fit on $\Omega_b$ and $\Omega_m$ to $^4$He and D/H, while fit* is the best possible fit on $\Omega_b$ and $\Omega_m$ to the $^4$He and D/H observations for the model considered as indicated in the columns four and seven. The last three columns are usual PRIMAT runs with modified $a(T)$ such that $\bar{a}/\lambda = a_{SIV}/S^{1/3}$, where $\bar{a}$ is the PRIMAT's $a(T)$ for the decoupled neutrinos case. Column seven is actually $a_{SIV}/S^{1/3}$, but it is denoted by $\bar{a}/\lambda$ to remind us about the relationship $a' = a\lambda$; the run is based on $\Omega_b$ and $\Omega_m$ from column five. The smaller values of $\eta_{10}$ are due to smaller $h^2\Omega_b$, as seen by noticing that $\eta_{10}/\Omega_b$ is always $\approx 1.25$.

If we go back to the first of the general scale-invariant cosmology Equations (B.6), we can identify a vacuum energy density expression that relates the Einstein cosmological constant with the energy density as expressed in terms of $\kappa = -\dot{\lambda}/\lambda$ by using the SIV result (B.9). The corresponding vacuum energy density $\rho$, with $C = 3/(4\pi G)$, is then:

$$\rho = \frac{\Lambda}{8\pi G} = \lambda^2 \rho' = \lambda^2 \frac{\Lambda_E}{8\pi G} = \frac{3}{8\pi G}\frac{\dot{\lambda}^2}{\lambda^2} = \frac{C}{2}\dot{\psi}^2 \,.$$

This provides a natural connection to inflation within the SIV via $\dot{\psi} = -\dot{\lambda}/\lambda$ or $\psi \propto \ln(t)$. The equations for the energy density, pressure, and Weinberg's condition for inflation within the standard inflation [23, 24, 25, 26] are:

$$\left.\begin{array}{c}\rho\\ p\end{array}\right\} = \frac{1}{2}\dot{\varphi}^2 \pm V(\varphi),\ \mid \dot{H}_{\mathrm{infl}} \mid \ll H^2_{\mathrm{infl}} \,. \tag{C.4}$$

If we make the identification between the standard inflation above with the fields within the SIV (using $C = 3/(4\pi G)$):

$$\dot{\psi} = -\dot{\lambda}/\lambda, \quad \varphi \leftrightarrow \sqrt{C}\,\psi, \quad V \leftrightarrow CU(\psi), \quad U(\psi) \,=\, g\,e^{\mu\,\psi} \,. \tag{C.5}$$

Here, $U(\psi)$ is the inflation potential with strength $g$ and field "coupling" $\mu$. One can evaluate the Weinberg's condition for inflation (C.4) within the SIV framework [2], and the result is:

$$\frac{\mid \dot{H}_{\mathrm{infl}} \mid}{H^2_{\mathrm{infl}}} \;=\; \frac{3\,(\mu+1)}{g\,(\mu+2)}\,t^{-\mu-2} \ll 1\, for\ \mu < -2,\ and\ t \ll t_0 = 1. \tag{C.6}$$

From this expression, one can see that there is a graceful exit from inflation at the later time:

$$t_{\mathrm{exit}} \approx \sqrt[n]{\frac{n\ g}{3(n+1)}} \qquad \text{with} \qquad n = -\mu - 2 > 0, \tag{C.7}$$

when the Weinberg's condition for inflation (C.4) is not satisfied anymore. For more details, we refer the reader to the derivation of the equation (C.6) presented in our previous papers [1, 2].

## D. Conclusions and Outlook

From the highlighted results in the previous section on various comparisons and potential applications, we see that the *SIV cosmology is a viable alternative to* $\Lambda$*CDM.* In particular, within the SIV gauge (B.10) *the cosmological constant disappears.* There are diminishing differences in the values of the scale factor $a(t)$ within $\Lambda$CDM and SIV at higher densities as emphasized in the discussion of (Figire 1) [13, 19]. Furthermore, the SIV also shows consistency for $H_0$ and the age of the universe, and the m-z diagram is well satisfied—see [19] for details.

Furthermore, *the SIV provides the correct RAR for dwarf spheroidals* (Figure 2) while MOND is failing, and dark matter cannot account for the phenomenon [4]. Therefore, it seems that *within the SIV, dark matter is not needed to seed the growth of structure* in the universe, as there is a fast enough growth of the density fluctuations as seen in (Figure 3) and discussed in more detail by [3].

As to the BBNS within the SIV, our main conclusion is that the SIV paradigm provides a concurrent model of the BBNS that is compatible to the description of $^4$He, D/H, T/H, and $^7$Li/H achieved in the standard BBNS. It suffers of the same $^7$Li problem as in the standard BBNS but also suggests a possible SIV-guided departure from local statistical equilibrium which could be a fruitful direction to be explored towards the resolution of the $^7$Li problem.

In our study on the inflation within the SIV cosmology [2], we have identified a connection of the scale factor $\lambda$, and its rate of change, with the inflation field $\psi \to \varphi\,,\ \dot{\psi} = -\dot{\lambda}/\lambda$ (C.5). As seen from (C.6), *inflation of the very-very early universe (*$t \approx 0$*) is natural, and SIV predicts a graceful exit from inflation* (see (C.7))!

Some of the obvious future research directions are related to the primordial nucleosynthesis, where preliminary results show a satisfactory comparison between SIV and observations [5, 22]. The recent success of the R-MOND in the description of the CMB [27], after the initial hope and concerns [28], is very stimulating and demands testing SIV cosmology against the MOND and $\Lambda$CDM successes in the description of the CMB, the Baryonic Acoustic Oscillations, etc.

Another important direction is the need to understand the physical meaning and interpretation of the conformal factor $\lambda$. As we pointed out in the Motivation Section, a general conformal factor $\lambda(x)$ seems to be linked to Jordan?Brans?Dicke scalar-tensor theory that leads to a varying Newton's constant G, which has not been found in nature. Furthermore, a spacial dependence of $\lambda(x)$ opens the door to local field excitations that should manifest as some type of fundamental scalar particles. The Higgs boson is such a particle, but a connection to Jordan?Brans?Dicke theory seems a far fetched idea. On the other hand, the assumption of isotropy and homogeneity of space forces $\lambda(t)$ to depend only on time, which is not in any sense similar to the usual fundamental fields we are familiar with.

In this respect, other less obvious research directions are related to the exploration of SIV within the solar system due to the high-accuracy data available, or exploring further and in more detail the possible connection of SIV with the re-parametrization invariance. For example, it is already known by [8] that un-proper time parametrization can lead to a SIV-like equation of motion (B.3) and the relevant weak-field version (C.2).

## Acknowledgments

A.M. expresses his gratitude to his wife for her patience and support. V.G. is extremely grateful to his wife and daughters for their understanding and family support during the various stages of the research presented. This research did not receive any specific grant from funding agencies in the public, commercial, or not-for-profit sectors. V.G. is grateful to the organizers of the PRIT'23 conference for their kind accommodations needed for V.G. to be able to present online this research results.

**Список литературы/References**


1. Gueorguiev, V. G., Maeder, A., The Scale Invariant Vacuum Paradigm: Main Results and Current Progress. *Universe* 2022, **8** (4) 213;
2. Maeder, A.; Gueorguiev, V.G. Scale invariance, horizons, and inflation. *MNRAS* **2021**, *504*, 4005.
3. Maeder, A.; Gueorguiev, V.G. The growth of the density fluctuations in the scale-invariant vacuum theory. *Phys. Dark Univ.* **2019**, *25*, 100315.
4. Maeder, A.; Gueorguiev, V.G. Scale-invariant dynamics of galaxies, MOND, dark matter, and the dwarf spheroidals. *MNRAS* **2019**, *492*, 2698.
5. Gueorguiev, V.G. and Maeder, A. "Big-Bang Nucleosynthesis within the Scale Invariant Vacuum Paradigm" under peer review (April 2023); arXiv e-Print: 2307.04269 [nucl-th].
6. Gueorguiev, V. G., and Maeder, A. The Scale Invariant Vacuum Paradigm: Main Results and Current Progress. *Universe* **2022**, *8*, 213 DOI: 10.3390/universe8040213; e-Print: 2202.08412 [gr-qc].
7. Gueorguiev, V. G., Maeder, A. (2023) The Scale Invariant Vacuum Paradigm: Main Results plus the Current BBNS Progress. arXiv e-prints. doi:10.48550/arXiv.2308.07483; e-Print: 2308.07483 [gr-qc].
8. Gueorguiev, V.G.; Maeder, A. Geometric Justification of the Fundamental Interaction Fields for the Classical Long-Range Forces. *Symmetry* **2021**, *13*, 379.
9. Weyl, H. *Raum, Zeit, Materie*; Vorlesungen über Allgemeine Relativitätstheorie; Springer-Verlag: Berlin/Heidelberg, Germany, 1993.
10. Carl, H. Brans Jordan-Brans-Dicke Theory. *Scholarpedia* **2014**, *9*, 31358.
11. Faraoni, V.; Gunzig, E.; Nardone, P. Conformal transformations in classical gravitational theories and in cosmology. *Fundam. Cosm. Phys.* **1999**, *20*, 121–175.
12. Xue, C.; Liu, J.P.; Li, Q.; Wu, J.F.; Yang, S.Q.; Liu, Q.; Shao, C., Tu, L., Hu, Z., Luo, J. Precision measurement of the Newtonian gravitational constant. *Natl. Sci. Rev.* **2020**, *7*, 1803.
13. Maeder, A. An Alternative to the LambdaCDM Model: the case of scale invariance. *Astrophys. J.* **2017**, *834*, 194.
14. Dirac, P.A.M. Long Range Forces and Broken Symmetries. *Proc. R. Soc. Lond. A* **1973**, *333*, 403.
15. Maeder, A.; Bouvier, P. Scale invariance, metrical connection and the motions of astronomical bodies. *Astron. Astrophys.* **1979**, *73*, 82–89.
16. Bouvier, P.; Maeder, A. Consistency of Weyl's Geometry as a Framework for Gravitation. *Astrophys. Space Sci.* **1978**, *54*, 497.
17. Canuto, V. et al. Scale-covariant theory of gravitation and astrophysical applications. *Phys. Rev. D* **1977**, *16*, 1643.
18. Gueorguiev, V.; Maeder, A. Revisiting the Cosmological Constant Problem within Quantum Cosmology. *Universe* **2020**, *5*, 108.
19. Maeder, A.; Gueorguiev, V.G. The Scale-Invariant Vacuum Theory: A Possible Origin of Dark Matter and Dark Energy. *Universe* **2020**, *6*, 46.
20. Andre Maeder, "MOND as a peculiar case of the SIV theory", *MNRAS* **2023**, *520*, 1447.
21. Pitrou, C., Coc, A., Uzan, J.-P., Vangioni, E. "Precision big bang nucleosynthesis with improved Helium-4 predictions." Physics Reports 754, 1?66 (2018). ArXiV: 1801.08023
22. Maeder, A., "Evolution of the early Universe in the scale invariant theory." *arXiv* **2019**, arXiv:1902.10115.
23. Guth, A. Inflationary universe: A possible solution to the horizon and flatness problems. *Phys. Rev. D* **1981**, *23*, 347.
24. Linde, A. D. Lectures on Inflationary Cosmology in Particle Physics and Cosmology. In Proceedings

of the Ninth Lake Louise Winter Institute, 20-26 February 1994. Lake Louise, Alberta, Canada. *Lect. Notes Phys.* **1995***,* 455*, pp363-372.*

25. Linde, A. Particle Physics and Inflationary Universe. *Contemp. Concepts Phys.* **2005**, *5*, pp1-362;
26. Weinberg, S. *Cosmology*; Oxford Univ. Press: Oxford, UK, 2008; p. 593.
27. Skordis, C.; Zlosnik, T. New Relativistic Theory for Modified Newtonian Dynamics. *Phys. Rev. Lett.* **2021** *127*, 1302, doi:10.1103/PhysRevLett.127.161302.
28. Skordis, C.; Mota, D.F.; Ferreira, P.G.; Boehm, C. Large Scale Structure in Bekenstein?s Theory of Relativistic Modified Newtonian Dynamics. *Phys. Rev. Lett.* **2006**, *96*, 11301.

**Authors**

**Vesselin Gueorguiev Gueorguiev**, Ph.D., Institute for Advanced Physical Studies, Sofia, Bulgaria and Ronin Institute, Montclair, NJ, USA.
E-mail: Vesselin at MailAPS.org

**Andre Maeder**, Ph.D., Professor, Geneva Observatory, University of Geneva, Geneva, Switzerland.
E-mail: Andre.Maeder at UniGe.ch

**Просьба ссылаться на эту статью следующим образом:**

Георгиев В. Г., Маедер А. Парадигма масштабно-инвариантного вакуума: основные результаты и текущий прогресс плюс BBNS результаты. *Пространство, время и фундаментальные взаимодействия.* 2023. № 3-4. С. 314–326.

**Авторы**

**Веселин Георгиев Георгиев**, Доктор философии, Институт Съвременни Физических Исследований, София, Болгария, и Институт Ронина, Монклер, Нью-Джерси, США.
E-mail: Vesselin at MailAPS.org

**Андре Маедер**, Доктор философии, профессор, Женевская Обсерватория, Женевский Университет, Женева, Швейцария.
E-mail: Andre.Maeder at UniGe.ch

**Просьба ссылаться на эту статью следующим образом:**

Георгиев В. Г., Маедер А. Парадигма масштабно-инвариантного вакуума: основные результаты и текущий прогресс плюс BBNS результаты. *Пространство, время и фундаментальные взаимодействия.* 2023. № 3-4. С. 314–326.

**Authors**

**Vesselin Gueorguiev Gueorguiev**, Ph.D., Institute for Advanced Physical Studies, Sofia, Bulgaria and Ronin Institute, Montclair, NJ, USA.
E-mail: Vesselin at MailAPS.org

**Andre Maeder**, Ph.D., Professor, Geneva Observatory, University of Geneva, Geneva, Switzerland.
E-mail: Andre.Maeder at UniGe.ch

**Please cite this article in English as:**

Gueorguiev V. G., Maeder A. The Scale Invariant Vacuum Paradigm: Main Results plus the Current BBNS Progress. *Space, Time and Fundamental Interactions*, 2023, no. 3-4, pp. 314–326.

УДК 53.01, 52.732, 530.12



## ВНЕГАЛАКТИЧЕСКИЕ ТЭВ-НЫЕ ФОТОНЫ И ПРЕДЕЛ СПЕКТРА НУЛЕВЫХ КОЛЕБАНИЙ

Жогин И. Л.[a,1]

[a] ИХТТМ, г. Новосибирск, 630090, Россия.

Вселенная не совсем прозрачна для фотонов очень высокой энергии, превышающей 100 ГэВ, из-за их поглощения межгалактическим фоновым ИК-излучением, с образованием электрон-позитронных пар. Ряд наблюдений таких фотонов от источников, находящихся за пределами нашей Галактики, указывают на возможную аномалию – неожиданно низкое поглощение ТэВ-ных фотонов. Высказывались предположения, что аномалия может быть связана с эффектами “новой физики”, например, аксионоподобными частицами, либо с возможным нарушением Лоренц-инвариантности.

Здесь предлагается иное объяснение, что аномалия есть проявление границы спектра нулевых колебаний. Предположено, что эта граница $U_{\rm ZV}$ изотропна в системе отсчета, где изотропно реликтовое излучение, и получена оценка: $U_{\rm ZV} \approx 7.4\,$ТэВ. Отмечено, что наличие $ZV$-границы приводит также к увеличенному времени бета-распада ускоренных частиц с Лоренц-фактором $\gamma > 50$ (в дополнение к обычному $\gamma\tau^{(\beta)}$).

Распространено мнение, что спектр нулевых колебаний продолжается вплоть до планковской энергии (в естественных единицах, гравитационная постоянная связана с квадратом планковской длины). Существует, однако, 5D-вариант теории Абсолютного Параллелизма (АП), свободный от сингулярностей решений, где появляется большая характерная длина $L$, определяющая толщину расширяющейся сферической $S^3$-оболочки (космологическое решение как продольная волна, бегущая по радиусу) в сопутствующей системе. Ньютоновский закон $\sim 1/r^2$ сменяется на $1/r$ на расстояниях, превышающих $L$, а планковская длина (составная величина) “возникает” из $L$ при выборе традиционного масштаба энергии-импульса (в котором энергия фотона есть его угловая частота).

Отмечаются особенности данной теории – классификация 15-ти поляризаций (поляризационных мод), тензор энергии-импульса (в продолженных уравнениях 4-го порядка), топологические заряды и квази-заряды локализованных конфигураций поля.

*Ключевые слова*: нулевые колебания; внегалактические ТэВ-ные фотоны; планковская длина; Абсолютный Параллелизм.

## EXTRAGALACTIC TEV PHOTONS AND THE ZERO-POINT VIBRATION SPECTRUM LIMIT

Zhogin I. L.[a,1]

[a] ISSCM, Novosibirsk, 630090, Russia.

There are observations indicating a possible anomalous transparency of intergalactic space (filled with infrared background light) for extragalactic gamma-rays of very high energy ($>$ 100 GeV). The anomaly is usually associated with effects of some new physics.

However, another explanation is possible — as a manifestation relating to a cut-off of the zero-point vibration spectrum. It is assumed that this boundary $U_{\rm ZV}$ is isotropic in the reference frame, where the cosmic microwave background (CMB) radiation is isotropic, and an estimate is obtained: $U_{\rm ZV} \approx 7.4\,$TeV. It is noted that the presence of a $ZV$ boundary also leads to an increased beta decay time of accelerated particles with the Lorentz factor $\gamma > 50$ (in the CMB rest frame; in addition to the usual $\gamma\tau^{(\beta)}$).

It is widely believed that the ZV-spectrum continues up to the Planck energy (in natural units, the gravitational constant is related to the square of the Planck length). There is, however, a 5D variant of the Absolute Parallelism theory (AP), free from singularities of solutions, where a large characteristic length $L$ appears, which determines the thickness of expanding spherical $S^3$ shell (a cosmological solution as the

[1]E-mail: zhogin@mail.ru

longitudinal wave along the radius) in co-moving co-ordinates. Newton's Law $\sim 1/r^2$ is replaced by $1/r$ at distances exceeding $L$, and the Planck length (a composite parameter) "arises" from $L$ when switching to the conventional energy-momentum scale (where the energy of a photon is its angular frequency).

The theory features are briefly exposed – description of 15 polarizations (degrees of freedom), the energy-momentum tensor (in prolonged 4th order equations), topological charges and quasi-charges of localized field configurations.

*Keywords*: zero-point vibrations; extragalactic TeV photons; Plank length; Absolute Parallelism.

PACS: 95.85.Pw, 11.90.-t, 04.50.Kd

DOI: 10.17238/issn2226-8812.2023.3-4.327-332

## Introduction

Very-high-energy (VHE) gamma-rays, $E_\gamma > 100\,\mathrm{GeV}$, are recorded by ground-based observatory facilities, clusters of atmospheric Cherenkov telescopes, etc. Extragalactic sources of VHE photons are active galactic nuclei, such as blazars (Markarian 501 [1], quasar 3C 279 [2]), while within the Galaxy VHE photons are produced, for instance, by the Crab Nebular pulsar (2 kpc; $E_\gamma$ over 100 TeV). The LHAASO observatory reported photons with energies of 1 . . . 1.4 PeV; it is possible that some of these quanta came from outside the Galaxy [3].

The universe is not entirely transparent to such hard photons, as they are absorbed by the extragalactic background light (EBL, which includes also photons with energies $E_b = 0.01\ldots 4\,\mathrm{eV}$ in addition to the cosmic microwave background radiation, CMB) through the electron-positron pair production. The threshold depends on the electron mass $m_e$, $E_\gamma\, E_b > m_e^2$, and the cross-section (absorption) peaks [3] if

$$E_\gamma\, E_b \approx 1\ldots 5\times 10^{12}\,\mathrm{eV}^2. \tag{.1}$$

Both brightness of VEH-sources and their limiting energies $E_\gamma$ can increase dramatically during ***flares***.

Let us consider a few sources of VHE photons, with their redshift $z$, distance $L$, and energy limit $E_\gamma$. The distance is estimated via the expression (we assume the linear expansion model $a(t) \propto t$)

$$L = c\,t_0\, z/(1+z), \quad L[\mathrm{Mpc}] = 4283\, z/(1+z)\,;$$

that is, we use $H_0 = {t_0}^{-1} = 70\ \mathrm{km\,s^{-1}Mpc^{-1}}$.

Here are just three such sources:

$\circledast^a$ the Mkn 501 blazar [1] (HEGRA), $z = 0.0336$, $L = 140\,\mathrm{Mpc}$, $E_\gamma = 20\,\mathrm{TeV}$;

$\circledast^b$ the 3C 279 radio-quasar [2] (MAGIC), $z = 0.536$, $L = 1.495\,\mathrm{Gpc}$, $E_\gamma = 0.3\ldots 0.5\,\mathrm{TeV}$;

$\circledast^c$ GRB 221009A [4, 5] (LHAASO / Carpet-2), $z = 0.1505$, $L = 560\,\mathrm{Mpc}$, $E_\gamma = 18\,\mathrm{TeV}\,/\,251\,\mathrm{TeV}$.

## A. TeV gamma-ray crisis?

The gamma-ray burst (GRB) of October 9th, 2022, had a record-breaking brightness [4, 5]; details on the Carpet-2 facility recording a 251 TeV photon were reported at the workshops of Theoretical Physics Department of the Institute for Nuclear Research [4] (S. Troitskiy, V. Romanenko; there are some problems with this photon: the proximity of Galactic disk and the presence of 2–3 marginal muons).

The plots on Figure 1 illustrate the mean free path of VHE photons along with the spectra of EBL and the Mkn 501 blazar (taken from [1]).

New measurements are being made, the spectra of background light (EBL) and TeV sources are being discussed; however, many authors believe that the extragalactic background light (EBL) is anomalously transparent for TeV photons, cf. Figure (the corrected Mkn 501 spectrum), and that the

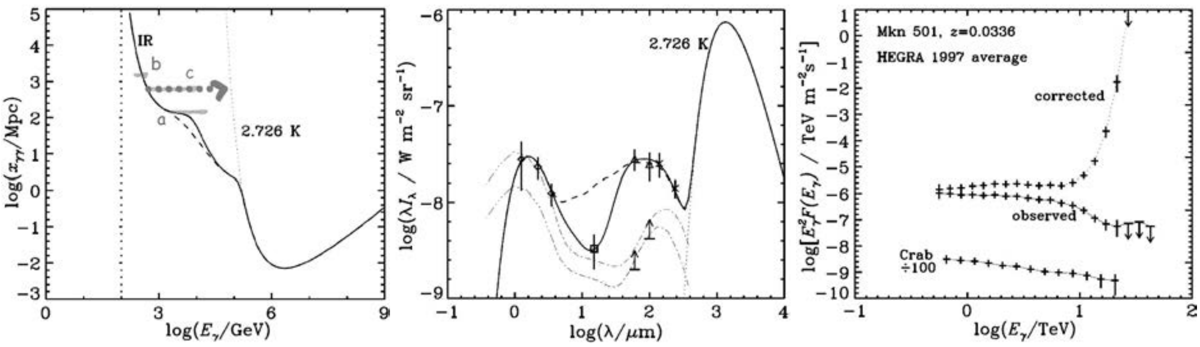


**Рис. 1.** The mean free path of VHE photons, the EBL intensity, and the Mkn 501 spectrum correction [1].

anomaly explanation requires a certain new physics [1, 2, 3, 4, 5, 6] (such as axion-like particles [3] or models violating the Lorentz invariance [6]).

It is simpler, however, to connect this anomaly to a manifestation of the zero-point vibration spectrum limit, $U_{\mathrm{ZV}}$. (It is hardly possible to stretch such a good thing as zero vibrations to infinity.)

One can assume that the ZV-ensemble is isotropic in the coordinate system, where the CMB radiation is almost isotropic (say, with an accuracy of about $\sim 10^{-5}$, or $v \sim \pm\, 3$ km/s).

### B. The limit of zero-point vibration (ZV) spectrum

An unstable particle (with a lifetime $\tau_0$), whose decay is associated with ZVs of the energy scale $U_0$, when moving relative to the ZV + CMB "ether" with the Lorentz factor $\gamma_e$ will sense this ZV spectrum boundary (i. e., the ZVs weakening in the backward direction) and will live some longer than mere $\gamma_e \tau_0$, if

$$U_0 \geqslant U_{\mathrm{ZV}}/(2\gamma_e), \text{ or } U_{\mathrm{ZV}} \leqslant 2\gamma_e\, U_0. \tag{B.1}$$

The photons with $E_\gamma = 16\,\mathrm{TeV}$ and $E_b = 0.3\,\mathrm{eV}$ form $e^+e^-$ pairs in a zero-momentum frame with the Lorentz factor (see Eq. (.1); this simple estimate is for the case of a head-on collision)

$$\gamma_e^{(\mathrm{p})} \approx 0.5\sqrt{E_\gamma/E_b} \approx 3.7{\cdot}10^6,$$

and the ZV energy required for pair production is about $U_0^{(\mathrm{p})} \approx 10^6$ eV (it is the $e^+e^-$ pair mass). If we assume that the ZV anomaly is already coming in effect, then the next estimate follows from Eq. (B.1):

$$U_{\mathrm{ZV}} \approx 2\gamma_e^{(\mathrm{p})} U_0^{(\mathrm{p})} \approx 7.4\,\mathrm{TeV}. \tag{B.2}$$

The shortest (or the "heaviest") ZVs are seemingly involved in the weak interactions. Therefore it would be very interesting to measure the anomalous increase in lifetime (compared to $\gamma\tau_0$) for particles featuring $\beta$-decay. Given that $U_0^{(\beta)} \approx 80\,\mathrm{GeV}$ (the $\mathrm{W}^\pm$ boson mass) and using Eq. (B.2), it is possible to estimate the Lorentz factor (relative to the ZV "ether") of the anomaly onset:

$$\gamma_e^{(\beta)} = U_{\mathrm{ZV}}/(2U_0^{(\beta)}) \approx 46. \tag{B.3}$$

Most likely, as is typical for the weak interactions, this lifetime anomaly ($\tau^{(\beta)}$-anomaly) should differ for particles of different helicity.

In addition to muons [the idea of $\mu^\pm$-collider (Budker, Skrinsky, *etc.*) is advancing somewhat, see MICE.iit.edu], $\beta^\pm$-decaying nuclides such as $^3$H ($\tau_{\beta^-} = 12.3\,\mathrm{y}$) and $^7$Be ($\tau_{\beta^+} = 53\,\mathrm{d}$) are of special interest. One should note that $(u,d)$-quarks already have Lorentz factors $\gamma_{\mathrm{q}}$ about 35…70 in their nucleons, and it is very significant – cf. Eq. (B.3).

(For the bottle-beam neutron anomaly [7], the velocity of thermal neutrons $v_{\mathrm{beam}}$ is too low; but bottle-neutrons often come in contact with the wall nucleons (protons), while their $d$-quark velocities ('relativism') can decrease — as can the lifetime.)

It is generally accepted that the ZV spectrum should be extended till the Planck energy. There exists, however, a 5D theory [8, 9, 10] in which the Planck length $\lambda_{\rm Pl}$ is a composite parameter that does not correspond to any characteristic scale, and where gravity does not have to be quantized.

### C. Periodic (annual and diurnal) changes in beta decay rates

Several experiments yielded evidence for the variability of beta decay rates (a number of nuclides were involed) [11]; the amplitude of annual oscillations is of the order $10^{-3}$, or 0.1%. The situation is still rather controversial because environmental influences could be in effect (along with other issues [12]).

Some experiments reported about diurnal variations in beta decays [13].

The Earth orbital velocity is about 30 km/s, and it adds to or subtracts from the Sun velocity relative to the CMB rest frame (sure one should account the ecliptic slope), $v_\odot \approx 369.8$ km/s; it corresponds to annual disturbances of the quark Lorentz factor $\gamma_{\rm q}\,(1.0012 \pm 10^{-4})$ – quite a small variation.

The direction of $\vec{v}_\odot$ (to Leo/Crater) has the next coordinates in the second equatorial system [14]:

- ⊙ the right ascension $\alpha = 167^\circ\!.942 \pm 0^\circ\!.007$
- ⊙ and declination $\delta = -6^\circ\!.944 \pm 0^\circ\!.007$ (J2000);
- ⊙ the galactic coordinates are $(l,\, b)$[deg] $= (264.02,\, 48.25)$.

An experimental setup can carry a peculiar vector, $\vec{v}_p$, e.g, directed from the source to detector, and the rate of beta decays could slightly depend on the angle between these two vectors. So, variations of this angle due to the Earth rotation can cause diurnal variations of beta decays in that experiment.

The 'directionality hypothesis' is also considered [12, 13]; usually the Sun direction is regarded as special.

### Conclusion

Perhaps in order to achieve 0.1 scale $\tau$-anomaly, there would be enough to accelerate tritons, the lightest beta decaying nuclides, to moderate speeds $v/c \sim 0.1$ (i.e., the triton momentum is about 0.3 GeV). This kind of experiment, where particles will collide not with other particles, but with the 'ZV-ether', will allow us to ask Nature new questions.

Special relativity (SR) united space and time but did not explain existence of any field or particle. General relativity (GR) relates gravity to space-time curvature; the other fields/particles form the energy-momentum tensor, EMT, and remain unexplained.

Einstein wasn't content with GR (the complete and true theory should explain more); he compared the GR-equation sides with a marble palace (the LHS, Einstein's tensor $G_{\mu\nu} = R_{\mu\nu} - g_{\mu\nu}R/2,\ G_{\mu\nu;\nu} \equiv 0$) and an old shed (the RHS with EMT, $T_{\mu\nu}$).

Later Einstein explored the co-frame field $h^a{}_\mu(x^\nu)$, with the metric $g_{\mu\nu} = \eta_{ab}h^a{}_\mu h^b{}_\nu$ where $\eta_{ab}$ is Minkowski's metric, and second order equations which symmetry unites symmetries of both SR (Latin indexes) and GR (Greek ones) – the third (or united) relativity, known as Absolute Parallelism (AP).

The list of compatible $2^d$-order AP equations (found by A. Einstein and W. Mayer in [15]; they used D=4) includes the two-parameter class of Lagrangian equations and three more classes. And there exists the exceptional equation (EE), non-Lagrangian, which solutions don't allow co-singularities (the principal terms do not remain regular for degenerate co-frame matrices), and, if D=5, contra-singularities (related to degenerate contra-frame densities of some weight) [9].

The additional spatial dimension manifests itself both in the cosmological expansion (there are spherically symmetric non-stationary solutions as a longitudinal wave running along the radius and forming a cosmological shallow waveguide, a region with non-zero Ricci tensor), and also in the nonlocal behavior of elementary particles (large size along the extra dimension; localized configurations of the frame field can carry discrete information – topological charges and, if configurations have some symmetry, topological quasi-charges).

It seems the frame field is only twice as large in number of components: ($D^2$–D) compared to vacuum GR. However, the increase in the number of polarizations (polarization modes or degrees of freedom, PDF) is more pronounced: D(D–2)=15 compared to D(D–3)/2 =5, the number of GW-polarizations in D=5 (two usual tensor plus additional three vector GW polarizations).

A simple (maybe the simplest) compatible AP equation (2d order; non-Lagrangian) looks as follow:

$$\Lambda^a{}_{\mu\nu;\lambda} g^{\nu\lambda} = 0, \text{ where } \Lambda^a{}_{\mu\nu} = h^a{}_{\mu,\nu} - h^b{}_{\nu,\mu} = 2h^a{}_{[\mu;\nu]}\,;$$

together with the identity $\Lambda^a{}_{\mu\nu;\lambda} \equiv 0$ ($\Lambda$-identity) it looks after linearization as a D-fold Maxwell equation, so the number of polarizations is D(D–2)=15; D=5 is the must for the EE which has the same number of polarizations as the simple equation.

These 15 polarizations can be separated [10] on four classes according to their very different amplitudes (and functions; a higher class means many orders smaller amplitudes) as they relate to various irreducible parts of tensor $\Lambda$ (and it's derivative $\Lambda'$) such as:

⊙ $\Phi_\mu = h_a^{\ \nu} \Lambda^a{}_{\nu\mu}$ (3+1 polarizations, $2^d$- and $1^{st}$-class; no gradient symmetry);
⊙ $S_{\mu\nu\lambda} = 3\Lambda_{[\mu\nu\lambda]}$ (3 polarizations, $1^{st}$-class);
⊙ and the Riemannian curvature tensor (or the Weyl tensor; 5 polarizations, $3^d$-class);
⊙ three unstable pol-ns ($0^{th}$-class) grow linearly under action of three stable polarizations relating to $f_{\mu\nu} = 2\Phi_{[\mu;\nu]}$ ($2^d$-class), while $h'^2$-terms are tiny (the divergence of $\Lambda$-identity):

$$\Lambda_{\lambda\mu\nu;\tau;\tau} = -\frac{2}{3} f_{\mu\nu;\lambda} + (\Lambda\Lambda', \Lambda^3) \ (\Box S \approx \Box\Phi \approx 0 \approx \Box f \approx \Box Riem - \text{stable polarizations}).$$

Only very small $2^d$-class polarizations take part in the energy-momentum tensor which apear in the prolonged 4th order equation (symmetrical part; 4th order gravity); it follows also from a Lagrangian quadratic in 2d order field equations (or the *weak* Lagrangian – in Ibragimov's sense).

Non-stationary $O_4$-symmetrical solutions exist which resemble a (single) longitudinal wave in Chaplygin gas [9] (the $1^{st}$-class pol-n relating to $\Phi_\mu$; others don't survive in this symmetry); the wave can serve as a cosmological shallow waveguide for tangential shorter waves, with ultrarelativistic expansion and different evolution of waves' amplitudes – according to the structures of quadratic terms (whether they include $0^{th}$-class parts or only lower class ones).

Non-linear localised $h$-field configurations can carry digital information – topological charges and (for symmetrical configurations) quasi-charges (when $0^{th}$-class waves become large enough), and a QM-like 4D-phenomenology emerges through averaging along the huge extra-dimension, along a length $L$, the width of large-scale $O_4$-wave in co-moving coordinates [8, 9]; note, two thin lines in a 4d-space have tiny chances to intersect in a single approach. The complete description is five-dimensional, not four!

Finally, it is useful to introduce auxiliary 4D-fields (quantised avatar-fields) for phenomenological description of topological (quasi)particles prone to interact (a kind of new actors!). So the overall picture turns out to be complex and interesting, and many features of the Standard Model becomes understandable including the lepton flavours and neutral (perhaps $CP$-symmetrical, like photons) neutrinos.

**Список литературы/References**


1. Protheroe R. J., Meyer H. An infrared background – TeV gamma-ray crisis? *Phys. Lett. B*, 2000, 493, pp. 1–6; arXiv: astro-ph/0005349 . See also YouTube: NASA | Blazar Bonanza .
2. The MAGIC Collaboration: Albert J., Aliu E., Anderhub H., Antonelli L.A., et al. Very-High-Energy Gamma Rays from a Distant Quasar: How Transparent Is the Universe? *Science*, 2008, 320, pp. 1752–1754; arXiv: 0807.2822 [astro-ph].
3. Zhang G., Ma B.-Q. Axion-Photon Conversion of LHAASO Multi-TeV and PeV Photons. *Chinese Phys. Lett.*, 2023, 40, pp. 011401–12400; arXiv: 2210.13120 [hep-ph].

4. Troitskiy S.V. Very-high-energy photons from the GRB 221009A gamma-ray burst. Workshops of the Theoretical Physics Department of the Institute for Nuclear Research, 2022. Available at: YouTube.com/@inrth (Romanenko V.S.).
5. Shtern B. The brightest gamma-ray burst ever: is new physics required? *Troitskiy variant – nauka* [Troitsk Variant Science], 2022, no. 23(367), pp. 1–2 (in Russ.); trv-science.ru/2022/12/.
6. Li H., Ma B.-Q. Lorentz invariance violation induced threshold anomaly versus VHE cosmic photon emission from GRB 221009A. *Astropart. Phys.*, 2023, 148, pp. 102831–102835; arXiv: 2210.06338 [astro-ph.HE].
7. Dubbers D., Saul H., Märkisch B., Soldner T., Abele H. Exotic decay channels are not the cause of the neutron lifetime anomaly. *Phys. Lett. B*, 2019, 791, pp. 6–10; arXiv: 1812.00626 [nucl-ex].
8. Zhogin I. Absolute Parallelism, modified gravity, and suppression of gravitational short waves. Proc. PIRT-2011. Moscow: BMSTU, 2012, pp. 337–346; arXiv: gr-qc/1109.1679
9. Zhogin I. *Old and new research on the Absolute Parallelism theory.* Lambert Academic Publishing: 2010. 104 p. ISBN 978-3-8383-8876-2; arXiv: gr-qc/0412130
10. Zhogin I. Large-scale virial relations in 5D Absolute Parallelism with $4^{\mathrm{th}}$-order gravity. *Physical Interpretations of Relativity Theory (PIRT-2023), XXIII International Scientific Conference*, Moscow, 2023, pp. 185–187; BMSTU.press PIRT-23 or pirt.bmstu.ru/en -> Abstracts.
11. Sturrock P.A., Parkhomov A.G., Fischbach E., Jenkins J.H. Power Spectrum Analysis of LMSU (Lomonosov Moscow State University) Nuclear Decay-Rate Data: Further Indication of r-Mode Oscillations in an Inner Solar Tachocline. *Astropart. Phys.*, 2012, 35, pp. 755–758; arXiv: 1203.3107 [astro-ph.SR].
12. Pommé S., Pelczar K. Neutrino-Induced Decay: A Critical Review of the Arguments. *Space Sci. Rev.*, 2022, 218, # 64; doi.org/10.1007/s11214-022-00932-0.
13. Baurov Yu.A., Sobolev Yu.G., Ryabov Yu.V., Kushniruk V.F. Experimental investigations of changes in the rate of beta decay of radioactive elements. *Phys. Atom. Nucl.*, 2007, 70, pp. 1825–1835. DOI: 10.1134/S1063778807110014
14. Planck Collaboration: Akrami Y., Arroja F., Ashdown M., Aumont J., Baccigalupi C., et al. Planck 2018 results. I. Overview and the cosmological legacy of *Planck*. *Astron. Astrophys.*, 2020, 641, A1, 56 p. arXiv: 1807.06205 [astro-ph.CO].
15. Einstein A., Mayer W. Systematische Untersuchung über kompatible Feldgleichungen, welche in einem Riemannschen Raume mit Fernparallelismus gesetzt werden können. *Sitzungsber. preuss. Akad. Wiss., phys.- math. Kl.*, 1931, pp. 257–265.


### Авторы

**Жогин Иван Львович**, к.ф.-м.н., ИХТТМ СО РАН, ул. Кутателадзе, д. 18, г. Новосибирск, 630090, Россия.
E-mail: zhogin@mail.ru

### Просьба ссылаться на эту статью следующим образом:

Жогин И. Л. Внегалактические ТэВ-ные фотоны и предел спектра нулевых колебаний. *Пространство, время и фундаментальные взаимодействия.* 2023. № 3-4. С. 327–332.

### Authors

**Zhogin Ivan L'vovich**, Ph.D., ISSCM SB RAS, Kutateladze st., 18, Novosibirsk, 630090, Russia.
E-mail: zhogin@mail.ru

### Please cite this article in English as:

Zhogin I. L. Extragalactic TeV Photons and the Zero-point Vibration Spectrum Limit. *Space, Time and Fundamental Interactions*, 2023, no. 3-4, pp. 327–332.

УДК 53.01+524+52-33+51-71



# НОВАЯ ТЕОРИЯ ТЯГОТЕНИЯ, ОСЦИЛЛЯЦИИ ЗВЕЗД И 11-ЛЕТНИЙ ЦИКЛ АКТИВНОСТИ СОЛНЦА

Журавлев В. М.[a,1]

[a] Ульяновский государственный педагогический университет, г. Ульяновск, 432071, Россия.

Излагается общая идеология использования нового способа описания ньютоновского поля тяготения к задачам осцилляции звезд , в частности, к задаче объяснения 11-летнего цикла солнечной активности. Дается краткое описание перехода от новой теории полей и частиц, представленной в предыдущих работах автора, к описаниюю поля тяготения Ньютона классической механики. Выведены уравнения динамического равновесия звезд и их атомодельной эволюции. Представлены применения данной модели к задаче описании 11-летнего цикла солненой активности.

*Ключевые слова*: Динамика самогравитирующего газа, новый способ описания теории гравитации Ньютона, осцилляции звезд.

# NEW THEORY OF GRAVITY, STELLAR OSCILLATIONS AND THE 11-YEAR CYCLE OF SOLAR ACTIVITY

Zhuravlev V. M.[a,1]

[a] Ulyanovsk State Pedagogical University, Ulyanovsk, 432071, Russia.

The general ideology of using a new method of describing the Newtonian gravitational field to problems of stellar oscillation, in particular, to the problem of explaining the 11-year cycle of solar activity, is outlined. A brief description is given of the transition from the new theory of fields and particles, presented in the author's previous works, to the description of Newton's gravitational field of classical mechanics. Equations for the dynamic equilibrium of stars and their automodel evolution are derived. Applications of this model to the problem of describing the 11-year cycle of solar activity are presented.

*Keywords*: Dynamics of self-gravitating gas, a new way to describe Newton's theory of gravity, oscillations of stars.

PACS: 04.40.-b, 04.20.Jb, 97.10.Cv, 95.30.Lz, 98.80.-k
DOI: 10.17238/issn2226-8812.2023.3-4.333-351

## A. Введение

В работах [1, 2, 3, 4, 5, 6] была предложена новая теория электромагнитных и гравитационных полей, основанная на принципе материальности физического трехмерного пространства в форме трехмерной гиперповерхности $V^3$ в объемлющем четырехмерном евклидовом пространстве $W^4$. Материальные объекты, такие как элементарные частицы, в этой теории связываются с геометрическими и топологическими структурами. В частности, электрический заряд связывается с экстремумами функции высоты гиперповерхности $V^3$, вложенной в $W^4$, а величина электрического заряда представляется целым числом, равным эйлеровой характеристике специальным образом выделенных на $V^3$ областей с границей. Частицы с барионным зарядом в этой теории представляются топологическими ручками типа ручек Уилера, а сам барионный заряд оказывается равным числу ручек Уилера, “вклеенных” в область пространства, соответствующую данной частице. Поля в данной теории ассоциируются с полями маркеров частиц гиперповерхности $V^3$ (лагранжевыми переменными), а исходные уравнения, которым они удовлетворяют, появляются в теории в виде тождеств, которым удовлетворяют некоторые комбинации маркерных полей и их производных.

[1]E-mail: zhvictorm@gmail.com

Необходимость в создании новой теории полей и частиц, которая бы включала в себя все основные теории современной физики в обновленном виде, такие, как теория тяготения, электромагнетизм и квантовая теория, обсуждалась в работах [3, 5, 6]. В кратком изложении основное требование к новой теории сводится к первому принципу материальности:

**Принцип 1. Любой объект физической теории, наделенный измеримыми физическими свойствами, должен являться материальным объектом.**

В противоположность этому пространство-время и Специальной (СТО) и Общей (ОТО) теорий относительности, являются нематериальными объектами, но при этом наделяются физическими свойствами, способными влиять на движение материальных тел в экспериментах. Например, в ОТО пространство-время наделяется свойством кривизны, которое, фактически, определяет свойства поля тяготения. В новой теории все поля и свойства частиц связываются с маркерными полями (лагранжевыми переменными), что гарантирует их материальность.

Применение данной новой теории в упрощенном виде для описания строения и динамики звезд ( в частности, звездных осцилляций) было изложено в работах [7, 8, 9, 10]. В этих работах на основе использования маркерных полей и их связи с полем тяготения была построена теория динамического равновесия звезд и других астрофизических объектов. В частности, была предложена модель автомодельных осцилляций звезд, в том числе модель осцилляций Солнца, объясняющая 11-летние колебания солнечной активности.

В данной работе обсуждается общая идеология использования новой теории тяготения в задачах описания динамического равновесия звезд и их автомодельных осцилляций. Приводятся уточняющие модель соотношения, касающиеся структуры зонального потока, а также теплового режима в звездах, которые сказываются на осцилляциях светимости звезд, а также диаграммы период-светимость.

## B. Маркерные тождества и поле тяготения в классической физике

Основным общим положением новой теории является постулат, что трехмерное физическое пространство является гладкой гиперповерхностью $V^3$ общего вида, вложенной в евклидово пространство четырех измерений $W^4$. Описание геометрии такой гиперповерхности в каждый момент времени $t$ строится с помощью одного уравнения:

$$u = \mathcal{F}(\mathbf{x}, t),$$

где $\mathcal{F}(\mathbf{x}, t)$ - функция высоты, $\mathbf{x} = (x^1, x^2, x^3)$ - декартовы координаты на выделенной в $W^4$ трехмерной гиперплоскости $P^3$, играющей роль системы отсчета, и $u$ - ортогональная декартова координата к $P^3$ в $W^4$ (см. рис. 1). Таким образом, нематериальное евклидово пространство $W^4$ вместе с вложенной в него гладкой гиперповерхностью $V^3$ представляет базовый уровень материальности. Следующий уровень материальности - это геометрические и топологические структуры $V^3$ как гиперповерхности.

Описание материальных объектов опирается на второй принцип материальности:

**Принцип 2. Любое физически измеримое свойство материальных объектов должно выражаться через свойства маркерных полей (лагранжевых переменных) $e^a(r, z, t)$, $a = 1, 2, 3$, связанных с материальными точками этого объекта, которые по определению удовлетворяют уравнению переноса:**

$$\frac{\partial e^a}{\partial t} + u\frac{\partial e^a}{\partial x} + v\frac{\partial e^a}{\partial y} + w\frac{\partial e^a}{\partial z} \equiv e^a_t + \Big(\mathbf{v}, \nabla\Big)e^a = 0, \quad a = 1, 2, 3. \qquad \text{(B.1)}$$

Здесь и далее везде будем использовать правило суммирования по повторяющемуся индексу.

Поскольку гиперповерхность $V^3$ является материальным объектом, то сама функция высоты $\mathcal{F}(\mathbf{x}, t)$ как величина, характеризующая физические свойства, также выражается через маркерные поля $e^a$. В каждой области $\mathcal{V}^3 \in V^3$, ограниченной изоповерхностью $\mathcal{F}(\mathbf{x}, t)$, должно выполняться соотношение:

$$\mathcal{F} = \mathcal{F}_0 + \frac{\varepsilon}{2}|\mathbf{e}|^2, \quad |\mathbf{e}|^2 = (e^1)^2 + (e^2)^2 + (e^3)^2,$$

где $\mathbf{e} = (e^1, e^2, e^3)$ - радиус-вектор в пространстве маркеров, $\varepsilon = +1$ в случае, если в точке с $|\mathbf{e}|^2 = 0$ $\mathcal{F}$ достигает максимума и $\varepsilon = -1$ - если минимума. $\mathcal{F}_0$ - значение $\mathcal{F}$ в точке $|\mathbf{e}|^2 = 0$ (см. [1, 2, 4, 6]).

### B.1. Плотность массы

Система (B.1) допускает дифференциальное тождество, которое можно записать в следующем виде:

$$\frac{\partial |J|}{\partial t} + \frac{\partial}{\partial x}\Big(u|J|\Big) + \frac{\partial}{\partial y}\Big(v|J|\Big) + \frac{\partial}{\partial z}\Big(w|J|\Big) \equiv |J|_t + \mathrm{div}(\mathbf{v}|J|) = 0, \tag{B.2}$$

где функция $|J|$ - якобиан преобразования от координат $z, r$ в координаты $e^1, e^2$ пространства значений маркеров:

$$|J| = |\det \hat{\mathbf{J}}|. \tag{B.3}$$

Здесь

$$\hat{\mathbf{J}} = \begin{vmatrix} e^1_x & e^1_y & e^1_z \\ e^2_x & e^2_y & e^2_z \\ e^3_x & e^3_y & e^3_z \end{vmatrix} \tag{B.4}$$

Уравнение (B.2) является стандартным уравнением теории маркеров в лагранжевом подходе в классической гидродинамике и представляет собой уравнение сохранения числа частиц. Как и в классической гидродинамике любая функция:

$$\rho = M_0 \mathcal{M}(e^1, e^2, e^3)|J|, \tag{B.5}$$

где $\mathcal{M}(e^1, e^2, e^3)$ - произвольная безразмерная дифференцируемая функция маркеров, может быть отождествлена с плотностью массы вещества, поскольку она автоматически удовлетворяет закону сохранения массы:

$$\rho_t + \mathrm{div}(\mathbf{u}\rho) = 0. \tag{B.6}$$

Здесь и далее масштабный коэффициент $M_0$ имеет размерность массы. В этом случае (B.2) эквивалентно уравнению неразрывности. Физический смысл безразмерной функции $\mathcal{M}(\mathbf{e})$ состоит в том, что она определяет относительную массивность каждой отдельной точки среды, связанной с маркерами $\mathbf{e} = (e^1, e^2, e^3)$. Величина $|J|$ представляет собой плотность маркеров, т.е. плотность числа точек гиперповерхности $V^3$ в окрестности точки с координатами $\mathbf{x}$.

В рассматриваемой теории $\rho$ - это плотность массы материи, из которой состоит сама гиперповерхность $V^3$. Вещество, которое является предметом описания классической физики и квантовой теории и которая фигурирует в качестве материи в СТО и ОТО, является геометрическими и топологическими элементами структуры $V^3$. Например, как уже упоминалось, частицы с барионным зарядом связываются с областями $V^3$, содержащими топологические ручки Уилера (см. [2, 4, 6]). Обоснование такой связи и общие принципы описания электрического заряда и строения частиц с помощью топологии $V^3$ содержатся в работах [2, 4, 6].

### B.2. Уравнение Пуассона и маркеры

Описание гравитационных и электромагнитных полей, параметры которых в силу второго принципа материальности должны выражаться через функции $e^a(\mathbf{x}, t)$, $a = 1, 2, 3$, строится на основе двух дифференциальных тождеств, первое из которых имеет вид дифференциального закона Кулона для точечного заряда в маркерных переменных:

$$\sum_{a=1}^{2} \frac{\partial}{\partial e^a}\left(\frac{e^a}{|\mathbf{e}|^3}\right) = 4\pi\delta(\mathbf{e}), \tag{B.7}$$

а второе имеет следующий вид:

$$\sum_{a=1}^{2}\frac{\partial e^a}{\partial e^a}=\frac{\partial e^1}{\partial e^1}+\frac{\partial e^2}{\partial e^2}+\frac{\partial e^3}{\partial e^3}=3. \tag{B.8}$$

Переходя в этих тождествах к физическим координатам $\mathbf{x}$, получаем форму этих тождеств, которую можно использовать для отождествления с электрическим полем и полем тяготения. В физических координатах тождеству (B.7) можно придать такой вид

$$\mathrm{div}\mathbf{D}=4\pi|J|\delta(\mathbf{e}), \tag{B.9}$$

где поле

$$\overset{\bullet}{\mathcal{D}}{}^{\gamma}=\frac{1}{|\mathbf{e}|^3}e^a\frac{\partial x^\gamma}{\partial e^a} \tag{B.10}$$

отождествляется с фундаментальным полем электрической индукции. Тождество же (B.8) представляется в форме:

$$\mathrm{div}\mathbf{g}=4\pi G\mathcal{D}(\mathbf{e})\rho, \tag{B.11}$$

где $G$ - постоянная тяготения Ньютона, а поле с компонентами:

$$\mathrm{g}^\gamma=\frac{4\pi}{3}G\mathcal{M}(\mathbf{e})|J|e^a\frac{\partial x^\gamma}{\partial e^a}+[\mathrm{rot}W]^\gamma \tag{B.12}$$

отождествляется с полем напряженности поля тяготения с точностью до некоторого поля, дивергенция от которого равна нулю. Функция $\mathcal{D}(\mathbf{e})$ имеет следующий вид:

$$\mathcal{D}=1+\frac{1}{-}e^a\frac{\partial\ln\mathcal{M}}{\partial e^a}. \tag{B.13}$$

Эта функция является атрибутом поля тяготения в случае, если массивность $\mathcal{M}(\mathbf{e})$ точек $\mathcal{V}^3$ меняется от точки к точке и может рассматриваться как параметр “скрытой” массы, поскольку в уравнение Пуассона (B.11) входит в виде множителя вместе с постоянной тяготения $G$. Поэтому $G_{eff}=G\mathcal{D}(\mathbf{e})$ можно рассматривать как эффективную “постоянную” тяготения. С другой стороны, оставляя постоянную тяготения неизменной, можно функцию $\rho_{eff}=\rho\mathcal{D}=\rho+\rho_D$ рассматривать как эффективную плотность материи, а величину $\rho_D$ как плотность скрытой массы или темной материи.

Далее в данной статье все внимание будет обращено на поле тяготения и не будем касаться вопросов, связанных с фундаментальным электромагнитным полем. Описание этого поля и его свойств можно найти в [1, 2, 4, 6]. Нас же будет интересовать поле $\mathbf{g}$ и его связь с динамикой астрофизических объектов в классическом приближении.

## C. Переход к непрерывной среде классической механики

Для описания процессов, протекающих на масштабах астрофизических объектов, таких, как звезды, не относящиеся сейчас к релятивистским объектам (нейтронные звезды, черные дыры и т.п.), достаточно использовать законы классической механики. Поэтому теория фундаментальных полей, кратко изложенная в предыдущем разделе, должна быть редуцирована, чтобы ее выводы привести в соответствие с основными положениями классической механики.

Процедура приведения общей схемы новой теории к классической сводится к двум шагам. Первый состоит в отождествлении трехмерной гиперплоскости $P^3\in W^4$ с плоским пространством классической механики. Второй шаг - это отождествление топологических структур, например, ручек Уилера, соответствующих барионам, с точками непрерывной среды, заполняющей пространство. Аналогичное отождествление возможно и для других частиц, например, электронов. Последнее можно сделать в силу малости размеров топологических структур типа ручек Уилера и других элементарных частиц по сравнению с расстояниями классической теории. Таким образом мы получаем мир классической механики. Переход к уравнениям Ньютона и уравнениям квантовой теории описан в работах [1, 2, 4, 6]. Наиболее существенным дополнением, которое остается в классической механике после такого перехода, - это описание поля тяготения с помощью маркерных полей, которое является универсальным как для новой теории, так и для классической.

Последним не “классическим” элементом редуцируемой теории является наличие в ней изменяющейся в пространстве функции $\mathcal{M}(\mathbf{e})$ массивности частиц среды. Эта функция не связана ни с представлением о неевклидовом пространстве в форме гиперповерхности $V^3 \in W^4$, ни с топологическими свойствами частиц. Вообще говоря, эта функция должна быть элементом классической теории тяготения для непрерывных самогравитирующих сред, которые представляют собой смесь частиц различной массы. Однако в классической механике эта функция не используется, хотя в большинстве астрофизических объектов присутствуют химические элементы с различным массовым числом. Эта же функция должна была бы появиться в теории строения и эволюции галактик и космологии, поскольку в моделях этих теорий в качестве элементов среды выступают сами звезды. Поскольку звезды существенно различаются по массам, то эффекты скрытой массы, связанные с изменениями $\mathcal{M}(\mathbf{e})$ в пространстве, должны иметь существенное значение, что, по всей видимости, обнаруживается в эксперименте в форме темной материи. В настоящей работе эти важные аспекты динамики различных астрофизических объектов не будут обсуждаться, поскольку в качестве примера того, как работает редуцированная теория тяготения, будет описана модель осцилляций звезд типа Солнца. Для звезд типа Солнца изменчивость $\mathcal{M}(\mathbf{e})$ в пространстве не играет существенной роли, поскольку такие звезды в основном состоят из водорода с относительно небольшой примесью гелия. Поэтому далее в данной работе мы будем полагать $\mathcal{M}(\mathbf{e}) = 1$, что соответствует $\mathcal{D} = 0$. Покажем как такой подход приводит к новым выводам в рамках классической механики, в том числе, позволяет описать 11-летний цикл солнечной активности.

### C.1. Уравнения динамики самогравитирующего газа

Рассмотрим движение самогравитирующего газа как непрерывной среды вблизи области с повышенной плотностью массы. Будем полагать, что система обладает цилиндрической симметрией, так, что все параметры среды не зависят от азимутального угла. В такой области имеется центр, в котором плотность достигает своего максимума и убывает некоторым образом при удалении от этого центра. В этот максимум поместим начало цилиндрической системы координат. Будем предполагать, что поток газа имеет зональную составляющую с осью вращения, совпадающей с осью $z$ цилиндрической системы координат. В этом случае уравнения движения газа и уравнения гравитационного поля можно записать в такой форме:

$$
\begin{aligned}
&u_t + uu_r + wu_z - \frac{v^2}{r} = -\frac{1}{\rho}p_r - \phi_r,\\
&w_t + uw_r + ww_z = -\frac{1}{\rho}p_z - \phi_z, \\
&v_t + uv_r + wv_z + \frac{uv}{r} = 0,
\end{aligned}
\tag{C.1}
$$

$$
\rho_t + \frac{1}{r}\frac{\partial}{\partial r}\Big(ru\rho\Big) + \frac{\partial}{\partial z}\Big(\rho w\Big) = 0, \tag{C.2}
$$

$$
\frac{1}{r}\frac{\partial}{\partial r}\Big(r\phi_r\Big) + \frac{\partial}{\partial z}\phi_z = 4\pi G\rho. \tag{C.3}
$$

К этой системе необходимо добавить уравнение состояния, которое близко к уравнению идеального газа:

$$
p = \frac{\mathring{A}}{\mu_g}\rho T. \tag{C.4}
$$

Здесь $\overset{\circ}{A}$ - универсальная газовая постоянная, $\mu_g$ - молярная масса газа, $T$ - абсолютная температура. Полагая, что процесс переноса плазмы в звездах является глобально адиабатическим, т.е. энтропия не меняется вдоль линий тока, приходим (см. Приложение 1 и [9]) к следующему общему уравнению состояния:

$$p = Ke^{s/c_v}\rho^{\gamma}, \tag{C.5}$$

где $s$ - энтропия, $c_v$ - молярная теплоемкость при постоянном объеме и $\gamma$ - показатель адиабаты. Параметр $K$ связан с состоянием газа при какой-то выделенной температуре.

### C.2. Динамика маркеров, плотность вещества и уравнение состояния

При наличии цилиндрической симметрии для описания полей достаточно двух маркерных полей $e^a(r,z,t),\ a=1,2$, которые теперь принимают следующий вид:

$$\frac{\partial e^a}{\partial t} + u\frac{\partial e^a}{\partial r} + w\frac{\partial e^a}{\partial z} = 0, \quad a = 1,2. \tag{C.6}$$

Уравнение сохранения числа частиц будет иметь такой вид:

$$\frac{\partial |J|}{\partial t} + \frac{\partial}{\partial r}\Big(u|J|\Big) + \frac{\partial}{\partial z}\Big(w|J|\Big) = 0, \tag{C.7}$$

где функция $|J|$ - якобиан преобразования от координат $z, r$ в координаты $e^1, e^2$ пространства значений маркеров, аналогичная (B.3), но с матрицей:

$$\hat{\mathbf{J}} = \begin{vmatrix} e^1_r & e^1_z \\ e^2_r & e^2_z \end{vmatrix} \tag{C.8}$$

Соответственно, плотность массы в общем случае будет выглядеть так :

$$\rho = M_0\mathcal{M}(\mathbf{e})|J|/r, \tag{C.9}$$

где $\mathcal{M}(\mathbf{e})$ - массивность частиц среды, которая теперь может быть связана с массовым числом ядер атомов среды в случае неоднородного химического состава газа, $M_0$ - масштабный коэффициент, имеющий размерность массы. В этом случае (C.7) эквивалентно уравнению неразрывности (C.2) в цилиндрической системе координат. Как было указано выше, в данной работе далее будем полагать $\mathcal{M}(\mathbf{e}) = 1$.

Полагая, что тепловые процессы в звезде являются квази-адиабатическими, для функции плотности энтропии $s$ имеем соотношение $s = S(\mathbf{e}) + s_0(t)$, где $S(\mathbf{e})$ - часть энтропии, переносимая без изменений вдоль линий тока, зависящая только от маркеров, а $s_0(t)$ - часть энтропии, изменяющаяся глобально со временем. В результате уравнение состояния можно записать в таком виде:

$$p = K\mathcal{S}(\mathbf{e})\sigma(t)\rho^{\gamma}, \tag{C.10}$$

где $\mathcal{S} = \exp(S(\mathbf{e})/c_v)$ и $\sigma(t) = \exp s_0(t)/c_v$. Теперь для абсолютной температуры имеем следующее выражение:

$$T = K_0\sigma(t)\mathcal{S}(\mathbf{e})\rho^{\gamma-1}. \tag{C.11}$$

### C.3. Уравнение Пуассона для самогравитирующего газа

Уравнение Пуассона в цилиндрической системе координат теперь появляется из формального тождества:

$$\sum_{a=1}^{2}\frac{\partial e^a}{\partial e^a} = \frac{\partial e^1}{\partial e^1} + \frac{\partial e^2}{\partial e^2} = 2, \tag{C.12}$$

которое приводит к такому уравнению для $|J|$:

$$\frac{\partial}{\partial x^\gamma}\left(|J|e^a\frac{\partial x^\gamma}{\partial e^a}\right) = 2|J|. \tag{C.13}$$

Введем векторное поле **K** с компонентами:

$$K^\gamma = \sum_{b=1}^{3} e^b \frac{\partial x^\gamma}{\partial e^b}, \quad \gamma = 1, 2, \tag{C.14}$$

Как и в [9], компоненты напряженности поля тяготения $g_a,\ a = 1, 2$ можно представить в виде:

$$\begin{aligned} -\phi_r \to g_1 &== -\frac{2\pi G M_0}{r}|J|K^1 - \frac{1}{r}\Psi_z, \\ -\phi_z \to g_2 &= -\frac{2\pi G M_0}{r}|J|K^2 + \frac{1}{r}\Psi_r, \end{aligned} \tag{C.15}$$

Отсюда находим, что компоненты напряженности гравитационного поля тождественно удовлетворяют уравнению Пуассона:

$$\frac{1}{r}\frac{\partial}{\partial r}(rg_1) + \frac{\partial}{\partial z}(g_2) = 4\pi G\rho. \tag{C.16}$$

### D. Параметры среды и потока в автомодельных переменных

Гидродинамический поток в моделях статического равновесия звезд отсутствует. В теории динамического равновесия поток существует и состоит из радиального потока с компонентами:

$$u = H(t)r = \dot{a}\xi, \quad w = F(t)z = \dot{b}\zeta, \tag{D.1}$$

и зонального со скоростью $v = v(r, z, t)$. В случае выбора радиального потока в форме (D.1), что аналогично закону Хаббла в космологии, маркерные функции $e^a = e^a(r, z, t)$ являются произвольными функциями двух **автомодельных переменных**:

$$\xi = r/a(t), \quad \zeta = z/b(t), \tag{D.2}$$

т.е.:

$$e^a = \mathcal{E}^a(\xi, \zeta)\ a = 1, 2.$$

Функции $a = a(t)$ и $b = b(t)$ называются масштабными факторами, а функции:

$$H = \frac{\dot{a}}{a}, \quad F = \frac{\dot{b}}{b} \tag{D.3}$$

- параметрами Хаббла. Из (D.1) следует:

$$\begin{aligned} \frac{du}{dt} &= \frac{\partial u}{\partial t} + u\frac{\partial u}{\partial r} + w\frac{\partial u}{\partial z} = \ddot{a}\xi, \\ \frac{dw}{dt} &= \frac{\partial w}{\partial t} + u\frac{\partial w}{\partial r} + w\frac{\partial w}{\partial z} = \ddot{b}\zeta. \end{aligned} \tag{D.4}$$

Плотность среды в автомодельные переменных будет иметь такой вид:

$$\rho = \frac{M_0}{a(t)^2 b(t)} \overset{\circ}{R}(\xi, \zeta), \tag{D.5}$$

где:

$$\overset{\circ}{R} = \frac{|\mathcal{J}(\xi, \zeta)|}{\xi}, \quad \mathcal{J} = \det\begin{vmatrix} \mathcal{E}^1_\xi & \mathcal{E}^1_\zeta \\ \mathcal{E}^2_\xi & \mathcal{E}^2_\zeta \end{vmatrix}. \tag{D.6}$$

Функцию $\overset{\circ}{R}(\xi,\zeta)$ в дальнейшем будем называть коэффициентом плотности. Из этого следует:

$$|J|K^1 = \frac{1}{b}\left(\mathcal{E}^1\frac{\partial \mathcal{E}^2}{\partial \zeta} - \mathcal{E}^2\frac{\partial \mathcal{E}^1}{\partial \zeta}\right) = \frac{1}{b}\mathcal{K}^1(\xi,\zeta), \tag{D.7}$$
$$|J|K^2 = -\frac{1}{a}\left(\mathcal{E}^1\frac{\partial \mathcal{E}^2}{\partial \xi} - \mathcal{E}^2\frac{\partial \mathcal{E}^1}{\partial \xi}\right) = \frac{1}{a}\mathcal{K}^2(\xi,\zeta).$$

Функции $\mathcal{K}_1$ и $\mathcal{K}_2$ удовлетворяют в силу (C.16) уравнению:

$$\frac{1}{\xi}\frac{\partial}{\partial \xi}(\xi\mathcal{K}_1) + \frac{\partial}{\partial \zeta}\mathcal{K}_2 = 2|\mathcal{J}|. \tag{D.8}$$

Используя теперь соотношения (C.10) и (C.11), получаем следующее представление для давления и абсолютной температуры:

$$p = M_0^\gamma K\mathcal{S}(\xi,\zeta)\sigma(t)a^{-2\gamma}b^{-\gamma}\overset{\circ}{R}{}^{\gamma}, \quad T = M_0^{\gamma-1}K_0\sigma(t)\mathcal{S}(\mathbf{e})a^{-2(\gamma-1)}b^{-\gamma+1}\overset{\circ}{R}{}^{\gamma-1} = \Pi(t)\mathcal{T}(\mathbf{e}), \tag{D.9}$$

где:

$$\mathcal{T}(\xi,\zeta) = \mathcal{S}(\xi,\zeta)\overset{\circ}{R}{}^{\gamma-1}(\xi,\zeta), \quad \Pi(t) = K_0\sigma(t)M_0^{\gamma-1}a^{-2(\gamma-1)}b^{-\gamma+1}.$$

Функцию $\mathcal{T} = \mathcal{T}(\xi,\zeta)$ будем называть коэффициентом температуры.

В терминах маркерных полей $e^a(r,z,t)$ выражается и зональная компонента скорости потока. Третье уравнение системы (C.1) в такой форме:

$$\left(\frac{\partial}{\partial t} + u\frac{\partial}{\partial r} + w\frac{\partial}{\partial z}\right)\mathcal{L} = 0,$$

где $\mathcal{L} = v(r,z,t)r$ - удельная плотность момента импульса среды. Отсюда следует, что функция $\mathcal{L}(r,z,t)$ является функцией маркеров $\mathcal{L} = \mathcal{L}(e^1,e^2)$ и следовательно :

$$v = \frac{\mathcal{L}(e^1,e^2)}{r}. \tag{D.10}$$

Это соотношение позволяет замкнуть описание динамики газа в терминах маркерных полей.

## E. Коэффициент энтропии

Одним из важных элементов модели, изложенной в [9], является появление в уравнениях модели пространственного распределения плотности и температуры коэффициента энтропии $\mathcal{S}(\xi,\zeta)$. Обычно при моделировании структуры и эволюции звезд для замыкания уравнений динамики их дополняют уравнением выделения энергии ядерным источником в центральной области звезд. Однако область выделения занимает относительно малый объем звезды, а во всех остальных ее слоях происходит перенос тепла и излучения с помощью различного рода механизмов. Дополнительное уравнение энерговыделения в силу сделанных предположений будет сводиться к уравнению для функции $\mathcal{S}(\xi,\zeta)$ для заданных коэффициентов непрозрачности вещества звезды и функции энерговыделения. Обе последние функции обычно выражаются через степенные функции температуры и плотности среды и носят, как правило, модельный характер, поскольку все коэффициенты этих функций установить с помощью лабораторных исследований невозможно. Поэтому в их записи остаются всегда не до конца точно известные параметры, которые устанавливаются с помощью подгонки под реальные наблюдательные данные. В силу этого в работе [9] был предложен другой подход для определения функции $\mathcal{S}(\xi,\zeta)$.

Вместо того, чтобы решать уравнение энерговыделения для отыскания функции $S(\mathbf{e})$, которое все равно требует определенной подгонки, в работе [9] было предложено сразу представить $S(\mathbf{e})$ как функцию плотности среды $\overset{\circ}{R}$ или температуры $\mathcal{T}$. В этой работе предлагалось представлять функцию $\mathcal{S}(\xi,\zeta)$ в следующем виде:

$$\mathcal{S} = H_0\overset{\circ}{R}{}^{\delta}, \tag{E.1}$$

где параметр $\delta$ подгонялся под определенные характеристики распределения температуры и плотности в пространстве. Такой подход подробно описан в [9].

Результатом такого подхода является то, что вследствие квази-адиабатичности процессов в условиях динамического равновесия и при учете потоков тепла в звезде, формулы для давления и температуры (D.9), принимают форму эффективных адиабат с показателем $\gamma_{eff} = \gamma + \delta$. Фактически это означает, что потоки тепла оставляют процесс адиабатическим и только меняют его показатель. Этот факт может играть очень важную роль в строении звезд, поскольку при определенных условиях может приводить к потере устойчивости звезды при нестандартных условиях. Как было показано в [9] подгонка параметра $\delta$ для Солнца приводит к такому наилучшему значению $\delta$, при котором $\gamma_{eff} \simeq 6/5$ при $\gamma = 5/3$. Следует отметить, что значение $\gamma = 6/5$ выделено в теории Лейна-Эмдена тем, что плотность и температура нигде не обращаются в ноль.

Таким образом, использование (E.1) или иной более общей модели такого типа приводит с одной стороны к упрощению процедур подгонки результатов моделирования, а с другой указывает на возможные существенные изменения во взглядах на условия устойчивости звезд, особенно вместе с общей идеей динамического, а не статического их равновесия.

### F. Уравнения в автомодельных переменных

Полученные соотношения, описывающие параметры среды и потока в автомодельных переменных, позволяют теперь записать уравнения динамики в этих же переменных. Следуя работе [9], будем полагать далее $b = a(t)$. Это упрощение необходимо для возможности разделить переменные в уравнениях динамики в автомодельных переменных. В этом случае уравнения динамики принимают такой вид:

$$\begin{aligned} &\ddot{a}\xi - \frac{\mathcal{L}^2(\xi,\zeta)}{a^3\xi^3} = -\frac{\Pi(t)}{a}\frac{1}{\overset{\circ}{R}}\frac{\partial}{\partial\xi}\Big(\mathcal{S}\ \overset{\circ}{R}{}^{\gamma}\Big) - \frac{2\pi G M_0}{a^2}\Big(\mathcal{K}_1 + \frac{1}{\xi}\Psi_\zeta\Big),\\ &\ddot{b}\zeta = -\frac{\Pi(t)}{a}\frac{1}{\overset{\circ}{R}}\frac{\partial}{\partial\zeta}\Big(\mathcal{S}\ \overset{\circ}{R}{}^{\gamma}\Big) - \frac{2\pi G M_0}{a^2}\Big(\mathcal{K}_2 - \frac{1}{\xi}\Psi_\xi\Big). \end{aligned} \tag{F.1}$$

Для разделения переменных теперь необходимо потребовать выполнения следующих условий:

$$\begin{aligned} &\mathcal{L}^2 = h(\xi,\zeta),\\ &\Psi = \Psi_0(\xi,\zeta) + a^{-1}(t)N(\xi,\zeta). \end{aligned} \tag{F.2}$$

где $h(\xi,\zeta)$, $\Psi_0(\xi,\zeta)$ и $N(\xi,\zeta)$ - некоторые вспомогательные функции, требующие уточнения. Для функции $\Pi(t)$, которая содержит одну произвольную пока функцию $\sigma(t)$, более общим требованием, чем в [9], для возможности разделения переменных является формальное представление:

$$\begin{aligned} &\sigma = \sigma_1(t) + \sigma_2(t)/a(t), \quad \Pi = \Pi_1(t) + \Pi_2(t),\\ &\Pi_1 = K_0\sigma_1(t)M_0^{\gamma-1}a^{-3(\gamma-1)},\\ &\Pi_2 = K_0\sigma_2(t)M_0^{\gamma-1}a^{-3(\gamma-1)-1}, \end{aligned} \tag{F.3}$$

где функции $\sigma_1(t)$ и $\sigma_2(t)$ определяются из условия разделения переменных. Потребуем выполнения следующих условий для функций $\Pi_1(t)$ и $\Pi_2(t)$:

$$\begin{aligned} &\frac{a\Pi_1(t)}{2\pi G M_0} = \frac{K_0 M_0^{\gamma-2}}{4\pi G}\sigma_1(t)a^{4-3\gamma} = Q_1 = \mathrm{const};\\ &\frac{a^2\Pi_2(t)}{2\pi G M_0} = \frac{K_0 M_0^{\gamma-2}}{4\pi G}\sigma_2(t)a^{3-3\gamma} = Q_2 = \mathrm{const};\\ &\Pi = \frac{2\pi G M_0}{a^2}\Big(Q_1 + Q_2 a^{-1}\Big) = \frac{2\pi G Q_1 M_0}{a^2}\Big(1 + \frac{a_T}{a}\Big). \end{aligned} \tag{F.4}$$

Из последнего соотношения следует, что отношение $a_T = Q_2/Q_1$ имеет размерность длины. В результате подстановки соотношений (F.2) и (F.4) в (F.1) приходим к уравнениям для пространственного распределения зонального потока:

$$\frac{h(\xi,\zeta)}{\xi^3} - 2\pi G M_0\left(\frac{1}{\xi}\frac{\partial N}{\partial \zeta} + \frac{Q_2}{\overset{\circ}{R}}\frac{\partial}{\partial \xi}\Big(\mathcal{S}\,\overset{\circ}{R}{}^{\gamma}\Big)\right) = \mu\xi,$$
$$2\pi G M_0\left(\frac{1}{\xi}\frac{\partial N}{\partial \xi} - \frac{Q_2}{\overset{\circ}{R}}\frac{\partial}{\partial \zeta}\Big(\mathcal{S}\,\overset{\circ}{R}{}^{\gamma}\Big)\right) = \mu\zeta. \tag{F.5}$$

и для распределения плотности среды вместе с компонентами вектора $\mathcal{K}_1$ и $\mathcal{K}_2$:

$$\Lambda\xi + \frac{Q_1}{\overset{\circ}{R}}\frac{\partial}{\partial \xi}\Big(\mathcal{S}\,\overset{\circ}{R}{}^{\gamma}\Big) + \mathcal{K}_1 - \frac{1}{\xi}\Psi_{0,\zeta} = 0, \tag{F.6}$$
$$\Lambda\zeta + \frac{Q_1}{\overset{\circ}{R}}\frac{\partial}{\partial \zeta}\Big(\mathcal{S}\,\overset{\circ}{R}{}^{\gamma}\Big) + \mathcal{K}_2 + \frac{1}{\xi}\Psi_{0,\xi} = 0.$$

Уравнение эволюции в этом случае будет иметь такой вид:

$$a^2\ddot{a} - \frac{\mu}{a} = 2\pi G M_0 \Lambda, \tag{F.7}$$

в точности совпадающее с аналогичным уравнением из работы [9]. Важным является то обстоятельство, что уравнение автомодельной эволюции со временем остается неизменным по отношению к работе [9]. Это означает, что все основные выводы, сделанные в [9], остаются в силе и после уточнений модели в данной работе.

## G. Пространственное распределение плотности и параметров зонального потока

Комбинируя уравнения (F.6) и (F.5), а затем исключая из уравнений для зонального потока перекрестным дифференцированием функцию $N$, получаем уравнение для функции $h$:

$$\frac{1}{\xi}\frac{\partial}{\partial \xi}\frac{h(\xi,\zeta)}{\xi^2} - q_2\left[\frac{1}{\xi}\frac{\partial}{\partial \xi}\left(\frac{\xi}{\overset{\circ}{R}}\frac{\partial}{\partial \xi}\Big(S\,\overset{\circ}{R}{}^{\gamma}\Big)\right) + \frac{\partial}{\partial \zeta}\left(\frac{1}{\overset{\circ}{R}}\frac{\partial}{\partial \zeta}\Big(S\,\overset{\circ}{R}{}^{\gamma}\Big)\right)\right] = 3\mu, \tag{G.1}$$

где $q_2 = 2\pi G M_0 Q_2$.

Аналогично, исключая из уравнений (F.6) функцию $\Psi_0$, приходим к модифицированному уравнению Лейна−Эмдена для функции $\overset{\circ}{R}$:

$$\lambda + \overset{\circ}{R} + \frac{Q_1}{2}\left[\frac{1}{\xi}\frac{\partial}{\partial \xi}\left(\frac{\xi}{\overset{\circ}{R}}\frac{\partial}{\partial \xi}\Big(S\,\overset{\circ}{R}{}^{\gamma}\Big)\right) + \frac{\partial}{\partial \zeta}\left(\frac{1}{\overset{\circ}{R}}\frac{\partial}{\partial \zeta}\Big(S\,\overset{\circ}{R}{}^{\gamma}\Big)\right)\right] = 0. \tag{G.2}$$

Параметр $\lambda = 3\Lambda/2$ называется (см. [9]) **параметром динамического равновесия**. Отличием этого уравнения от аналогичного уравнения в работе [9] является наличие множителя $\mathcal{D}$. Как уже отмечалось, эта функция фактически произвольна и определяется начальным распределением массивности частиц в пространстве в момент перехода звезды в режим автомодельных осцилляций. Кроме этого, при медленном изменении химического состава звезды за счет ядерных реакций эта функция также должна медленно меняться.

Комбинируя уравнения (G.1) и (G.2), в результате получаем уравнение для $h(\xi,\zeta)$:

$$\frac{1}{\xi}\frac{\partial}{\partial \xi}\left(\frac{h}{\xi^2}\right) = 3\mu - \gamma\Big(\lambda + \overset{\circ}{R}\Big), \tag{G.3}$$

где для сокращения записи введено обозначение:

$$\gamma = 4\pi G M_0 Q_2/Q_1 = 4\pi G M_0 a_T. \tag{G.4}$$

Уравнение (G.3) обобщает аналогичное соотношение в работе [9]. Интегрируя это уравнение (G.3), получаем следующее обобщенное выражение для $h(\xi,\zeta)$:

$$h = \left(\frac{3\mu}{2} - \lambda\gamma\right)\xi^4 - \gamma\xi^2 \int\limits_0^{\xi} \overset{\circ}{R}\, \xi d\xi + b_0(\zeta,t)\xi^2, \tag{G.5}$$

где $b_0(\zeta)$ - постоянная интегрирования по $\xi$, зависящая произвольным образом от $\zeta$. Последнее соотношение эквивалентно распределению зональной скорости следующего вида:

$$v = a^{-1}\frac{\sqrt{h}}{\xi} = a^{-1}\mathcal{V}(\xi,\zeta), \tag{G.6}$$

где

$$\mathcal{V} = \sqrt{\left(\frac{3\mu}{2} - \lambda\gamma\right)\xi^2 - \gamma \int\limits_0^{\xi} \overset{\circ}{R}\, \xi d\xi + b_0(\zeta,t)}. \tag{G.7}$$

Исходя из условия ограниченности $\overset{\circ}{R}$ на оси вращения и полагая $\lim\limits_{\chi\to 0} \overset{\circ}{R}=\overset{\circ}{R}_0(\zeta)$, где $\overset{\circ}{R}_0(\zeta)$ - некоторые ограниченные функции переменной $\zeta$, находим, что при $b_0(\zeta) \equiv 0$, локальная угловая скорость потока $\omega = va^{-1}/\xi$ на оси вращения будет иметь конечное значение:

$$\omega_0(\zeta) = \lim_{\xi\to 0}\omega = \lim_{\xi\to 0}\frac{\sqrt{h}}{a^2\xi^2} =$$
$$= a^{-2}\lim_{\xi\to 0}\sqrt{\left(\frac{3\mu}{2} - \lambda\gamma\right) - \gamma\xi^{-2}\int\limits_0^{\xi} \overset{\circ}{R}\, \xi d\xi} = a^{-2}(t)\sqrt{\left(\frac{3\mu}{2} - \lambda\gamma\right) - \gamma\, \overset{\circ}{R}_0(\zeta)}.$$

Введение функции $\overset{\circ}{R}_0(\zeta)$ обусловлено тем, что граничное условие $\overset{\circ}{R}(0) = 1$ в чистом виде имеет место только в сферическом приближении (см. [9]). В общем же случае плотность может меняться на оси вращения в зависимости от $\zeta$, оставаясь ограниченной величиной. Из последнего соотношения следует, что в данной работе решается проблема бесконечной угловой скорости вращения на оси $z$ в обновленном варианте разделения переменных, которая имелась в работе [9]. Вместе с тем, в плоскости экватора при $\zeta = 0$ соотношение (G.5) переходит в точности в соотношение для $h$ из работы [9]:

$$h = \frac{3\mu}{2}\xi_0^4 + h_0. \tag{G.8}$$

Из (G.7) получаем следующее выражение:

$$h_0 = h(\xi_0, 0) = \left(\frac{3\mu}{2} - \lambda\gamma\right)\xi_0^4 - \gamma\xi_0^2 \int\limits_0^{\xi_0} \overset{\circ}{R}\, \xi d\xi \Bigg|_{\zeta=0}. \tag{G.9}$$

Параметр $h_0$, согласно [9], является важным параметром для оценок периода осцилляций Солнца. Поскольку соотношение (G.8) не изменяется по сравнению с работой [9], то все дальнейшие выкладки и оценки из этой работ остаются в силе. Также неизменным по сравнению с аналогичным уравнением в [9] остается уравнение (G.2). Поэтому анализ пространственного распределения плотности, приведенный в [9], не требует дополнительного анализа здесь.

Отметим лишь некоторые, наиболее важные элементы этой новой модели строения звезд, которые изменяют некоторые установившиеся в этой теории представления.

### H. Параметр динамического равновесия

Уравнение (G.2) можно рассматривать как обобщенное уравнение Лейна-Эмдена (LEm), хорошо известное в астрофизике, как уравнение звездных политроп [11, 12]. Существенным отличием

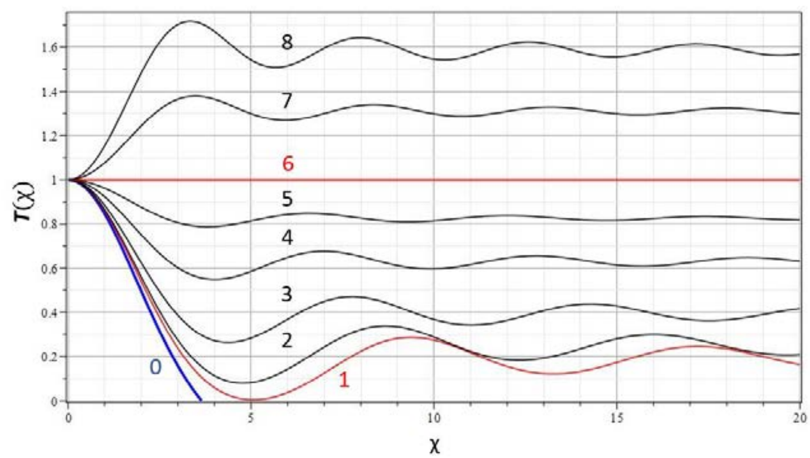


**Рис. 1.** Зависимости $\mathcal{T} = \mathcal{T}(\chi)$: 0 -$\lambda = 0$, 1 - $\lambda = -0.0851$, 2- $\lambda = -0.125$, 3 - $\lambda = -0.25$, 4 - $\lambda = -0.5$, 5 - $\lambda = -0.75$, 6 - $\lambda = -1$, , 7- $\lambda = -1.5$, 7- $\lambda = -2.0$

(G.2) от уравнения LEm является наличие ненулевого параметра $\lambda$, который в [9] был назван параметром динамического равновесия. Роль этого параметра в рассматриваемой теории строения звезд крайне важна, поскольку решает проблему отрицательных или мнимых значений плотности массы в теории звездных политроп. Эту проблему иллюстрируют графики на рис. 1. На этих графиках приведены кривые распределения температуры в звездах с показателем политропы $n = 3/2$ (одноатомный газ $\gamma = 5/3$) и однородным показателем энтропии $\mathcal{S}(\xi, \zeta) = 1$ для различных значений параметра динамического равновесия $\lambda$. График температуры представлен в приближении радиальной симметрии относительно радиальной координаты $\chi = \sqrt{\xi^2 + \zeta^2}$. Из представленного графика видно, что кривая с $\lambda = 0$ (синяя кривая с номером 0), что соответствует классическому уравнению LEm [11, 12], пересекает ось абсцисс в некоторой точке $\chi_0$, после которой решение становится комплексным. Это означает, что такая модель становится совершенно нефизичной при $\chi > \chi_0$. Обычно значение $\chi_0$ отождествляется с радиусом звезды, область не физических значений просто игнорируется. Поэтому считается, что обращение в ноль плотности на некотром расстоянии от центра звезды плотности, является хорошим граничным условием, хотя и не совсем точным. В большинстве простых моделей, но более общих, чем модель Лейна-Эмдена, заранее считается, что плотность должна обращаться в ноль на некотором расстоянии от центра звезды. Это расстояние признается радиусом звезды. За пределами этого радиуса строится другая модель, описывающая, по возможности, фотосферу и корону звезд.

В отличие от этого, остальные кривые на рис. (1) с $\lambda < 0$ демонстрируют другое поведение. Как было показано в [9], начиная с некоторого критического значения параметра динамического равновесия $\lambda$, равного для $n = 3/2$ значению $\lambda \simeq -0.851$ (красная кривая под номером 1), кривые вообще не пересекают ось абсцисс так, что температура и плотность всюду остаются положительными и ограниченными функциями. Последнее указывает на то, что такие модели имеют физический смысл на всем расстоянии от центра звезды. Более того, появление максимума температуры (и плотности), следующего за ее первым минимумом, который надо рассматривать как реальный радиус звезды (минимум температуры в фотосфере), указывает на естественное объяснение известного максимума температуры в короне Солнца.

Следует отметить, что при втором критическом значении $\lambda = -1.0$ решение с граничным условием $\mathcal{T}(0) = 1$ при всех показателях политропы $n$ при $\mathcal{S} = 1$ одно и то же $\mathcal{T} = 1$. Это напоминает космологические решения, для которых плотность остается всюду постоянной. При этом поведение масштабного фактора будет описываться уравнением, близким к уравнению для масштабного фактора в космологии Фридмана [13]. Уравнение для масштабного фактора в модели Фридмана не содержит слагаемого, связанного с зональным потоком или,другими словами, вращения структуры вокруг оси $z$.

Кривые со значениями $\lambda \leq -1$ (кривые с номерами 7 и 8) имеют минимум в центре структуры. По сути такие структуры можно рассматривать как модели войдов [14]. Такие структуры могут появляться и быть достаточно устойчивыми за счет радиального потока Хаббла из их центра и наличия зонального потока. Такие структуры могут появляться после взрыва массивных звезд или других объектов.

Из этого анализа следует, что введение параметра динамического равновесия в теорию звездных политроп решает целый ряд проблем и делает эти модели гораздо более жизнеспособными, чем считалось ранее.

## I. Модель 11-летних осцилляций Солнца

Работоспособность предложенной модели была доказана в работе [9], где было показано, что звезды с параметрами Солнца из стандартной модели последнего, вытекает период осцилляций близкий к наблюдаемому 11-летнему циклу солнечной активности. Этот результат является прямым следствием того, что рассматриваемые модели строятся на основе представления компонент поля тяготения с помощью поля маркеров (B.12) и общей идеи динамического равновесия звезд, а не строго статического. Именно эти идеи и приводят к уравнению для масштабного фактора (F.7), которое имеет при определенных условиях замкнутые фазовые траектории, которые и описывают осцилляции звезд. Сами соотношения (B.12) и (C.15) являются следствием связи между материальной структурой пространства, как гиперповерхности $V^3 \in W^4$, но могут интерпретироваться в рамках классической механики как формальные соотношения, позволяющие специальным образом представить компоненты поля тяготения.

Чтобы дать общее представление о модели осцилляций звезд в динамическом равновесии, кратко опишем основную схему исследований, в результате которых в [9] было дано объяснение 11-летнему циклу солнечных осцилляций. Анализ осцилляций звезд сводится к анализу уравнения (F.7) для заданных параметров звезды. Как и в работе [9] уравнение (F.7) приведем к виду динамической системы в безразмерной форме:

$$\frac{dy}{d\tau} = x^{-3} + \mathrm{sign}(\nu)x^{-2}, \quad \frac{dx}{d\tau} = y, \tag{I.1}$$

Здесь:

$$x = a/a_0, \quad y = t_0 c/a_0, \quad \tau = t/t_0,$$

Постоянные $a_0$ и $t_0$ определяются следующим образом: где

$$\nu = \frac{4\pi G M_0}{3}\lambda, \quad a_0 = \mu/|\nu|, \quad t_0 = \frac{\mu^{3/2}}{|\nu|^2}. \tag{I.2}$$

Динамическая система (I.1) имеет интеграл движения:

$$\frac{y^2}{2} + \mathrm{sign}(\nu)\frac{1}{x} + \frac{1}{2x^2} = E, \tag{I.3}$$

который аналогичен интегралу энергии частицы, совершающей одномерное движение в потенциальном поле сил.

Для моделей с $\nu < 0$ ($\lambda < 0$) все траектории динамической системы (I.1) для $-0.5 < E < 0$ являются замкнутыми, а траектории с $E > 0$ асимптотически стремятся к точкам ($x = \infty$, $y = \pm\sqrt{2E}$) при $t \to \pm\infty$ (см. Рис.1 c). Из (I.3) следует, что фазовые траектории для $-0.5 < E < 0$ пересекают ось абсцисс при значениях безразмерной координаты, равной:

$$x_{\pm} = \frac{1}{1 \pm \sqrt{2E+1}}. \tag{I.4}$$

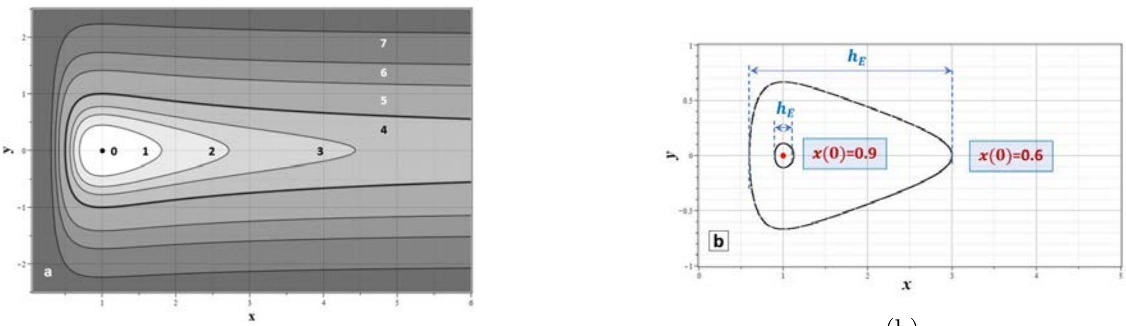


(a) (b)

**Рис. 2.** Фазовые траектории динамической системы (I.1) (a) для 0 - $E = -0.5$, 1 - $E = -0.4$, 2 - $E = -0.3$, 3 - $E = -0.2$, 4 - $E = 0.0$, 5 - $E = 0.5$, 6 - $E = 1.0$, 7 - $E = 2.0$; (b) для начальных значений $(x(0) = 0.9, y(0) = 0)$ и $(x(0) = 0.6, y(0) = 0)$

| Параметр | Значение |
|---|---|
| Радиус $R_\odot$ | $7 \cdot 10^8$[см] |
| Экваториальная скорость $v_\odot$ | $2 \cdot 10^5$[см/с] |
| Показатель адиабаты $\gamma$ | 5/3 (Одноатомный газ) |
| Плотность в центре $\rho_\odot$ | 150 [г/см$^3$] |
| Температура в центре $T_\odot$ | $\simeq 15 \cdot 10^6$ [К] |

**Таблица 1.** Основные параметры Солнца.

Точка $x_+$ соответствует максимальному сжатию структуры, а точка $x_-$ - максимальному расширению. Размах колебаний $h_E = |x_- - x_+|$ в случае осцилляций определяется следующим образом:

$$h_E = |x_- - x_+| = \frac{\sqrt{1 - 2|E|}}{|E|}. \tag{I.5}$$

Для $E = 0$ $x_- = \infty$, а при $E > 0$ эта точка лежит в отрицательной области значений $x_- < 0$, но траектории в полуплоскости $x < 0$ не имеют физического смысла.

Период колебаний $P_E$ газодинамического объекта, соответствующий определенному значению параметра $E$, вычисляется в соответствии со следующей формулой:

$$P_E = 2 \int\limits_{x_+}^{x_-} \frac{x dx}{\sqrt{2Ex^2 + 2x - 1}} = \frac{\pi\sqrt{2}}{2|E|^{3/2}}. \tag{I.6}$$

Как следует из этого соотношения при $E \to 0$ период колебаний стремится к бесконечности.

Типичные фазовые траектории системы (I.1) представлены на рис. (2).

В работе [9] приведена методика определения параметров модели, исходя из набора основных параметров звезды. В качестве таких параметров взяты следующие параметры: радиус звезды $R_*$, плотность в центре звезды $\rho_* = \rho(0)$, температура в центре звезды $T_*$, скорость зонального потока на экваторе звезды $v_*$ и показатель политропы $\gamma$. Для Солнца эти параметры приведены в Таб. 1.

Дополнительным подгоночным параметром модели, кроме параметра $\delta$ в (E.1), был параметр $h_0$, а точнее параметр $\varepsilon$:

$$\varepsilon = 1 - h_0\chi_0^2/(v_\odot R_\odot)^2.$$

Эти параметры связаны со скоростью зонального потока. Параметры в этом соотношении определены в Таб. 1 и Таб. 2. На графиках на рис. 3(a,b) приведены зависимости периода осцилляций и

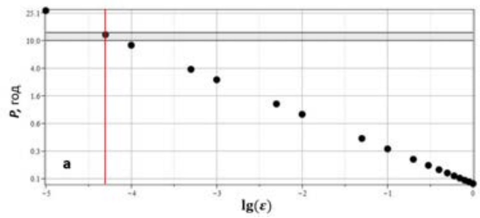


(a)

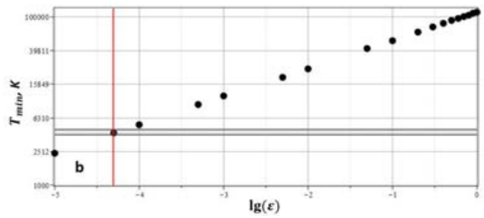


(b)

**Рис. 3.** Зависимость периода осцилляций $P(E)$ (a) и $T_{\min}$ (b) от $\varepsilon$

температуры в фотосфере от параметра $\varepsilon$. Фактически, подгонка по параметру $\varepsilon$ не является по сути подгонкой, поскольку, определяет сразу два параметра модели. Следовательно выбор одного из них автоматически должен приводить к выбору второго. Из графиков (3) следует, что период осцилляций примерно 11 лет соответствует наблюдаемой реально в фотосфере Солнца температуре примерно $4500K^o$. Что указывает на реальную работоспособность данной модели.

Как показано в работе [9] наилучшей моделью для Солнца является модель со следующими значениями параметров модели, которые были получены с помощью численных расчетов:

| Параметр | Значение |
|---|---|
| Показатель энтропии $\delta$ | $\simeq -7/15$ |
| Эффективный показатель адиабаты $\gamma'$<br>(с учетом потока тепла) | $\simeq 6/5$ |
| $P(E_*)$ | $\simeq 11.03$ [год] |
| $\lambda_*$ | $\simeq -7.788 \cdot 10^{-12}$ |
| $\chi_0$ | $\simeq 13537$ |
| $\chi_1$ | $\simeq 132000$ |
| $\mathcal{T}_{min}$ | $\simeq 6 \cdot 10^{-3}$ |
| $T_{min} = \mathcal{T}_{min} T_\odot$ | $\simeq 4500\ [K]$ |
| $\mathcal{T}_{max}$ | $\simeq 0.00717$ |
| $T_{max} = \mathcal{T}_{max} T_\odot$ | $\simeq 101000\ [K]$ |
| $\varepsilon$ | $\simeq 6 \cdot 10^{-5}$ |

Таб. 2. Параметры наилучшей модели для Солнца

Распределение коэффициентов температуры $\mathcal{T}$, плотности $\overset{\circ}{R}$ и энтропии $\mathcal{S}$, соответствующие наилучшей модели, представлены на рис. 4(a,b,c).

Таким образом, модель, основанная на приведении новой теории тяготения к условиям классической физики тяготения дает хорошее согласие с экспериментальными данными в отношении осцилляции звезд типа Солнца. Можно предполагать, что она пригодна для описния и звезд других классов, например, цефеид, хотя для подтверждения такого вывода необходимы дополнительные исследования.

### J. Диаграмма период-светимость

Одним из способов доказательства того, что данная модель пригодна для описания переменных звезд, в том числе и цефеид, может являться сравнение вычисляемой в рамках модели аналитической диаграммы период-светимость с реальными данными. В работе [9] было показано, что диаграмма период-светимость, соответствующая соотношению (I.6) и (D.9) при условии $Q_2 = 0$

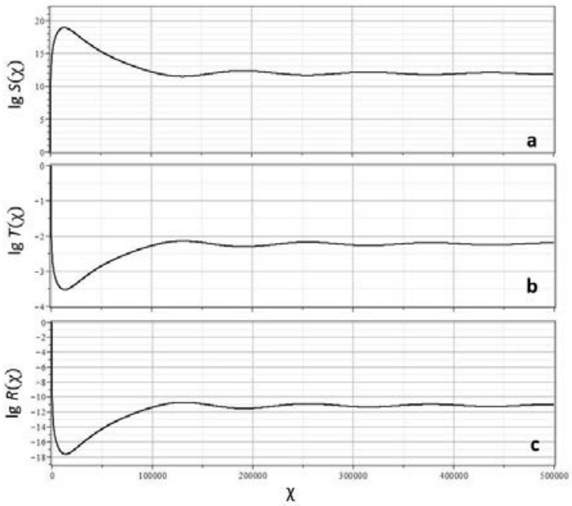


**Рис. 4.** Распределение параметров среды для наилучшей модели. (A) Коэффициенты энтропии $\lg(\mathcal{S})$ (a), температуры $\lg(\mathcal{T})$ (b) и плотности $\lg(\mathring{R})$ (c)

имеет вид:

$$\frac{L_{max}}{\mathcal{L}_0} = \left(1 + \sqrt{1 - \left(\frac{P_E}{2\pi}\right)^{-2/3}}\right)^2,$$
$$\frac{L_{min}}{\mathcal{L}_0} = \left(1 - \sqrt{1 - \left(\frac{P_E}{2\pi}\right)^{-2/3}}\right)^2. \tag{J.1}$$

Здесь $L_{max}$ - светимость в максимуме, $L_{min}$ - светимость в минимуме и

$$\mathcal{L}_0 = 4\pi\sigma_0 \left(\frac{4\pi G M_0(\gamma-1)}{\gamma}\right)^4 a_0^{-2}\mathcal{T}^4(\chi 0). \tag{J.2}$$

Постоянная $\mathcal{L}_0$ является масштабным множителем, содержащим неизвестный изначально параметр $\sigma_0$, который можно определить из реальных наблюдений $L_{max}$ и $L_{min}$. Следует отметить, что предложенная модель осцилляций не опирается на классический подход, который был предложен в работах [15, 16, 17], и который связывал осцилляции звезд с ионизацией верхних слоев звезды, содержащих гелий. Исходя из основных идей подхода, основанного на новой теории тяготения, осцилляции, аналогичные солнечным с той или иной амплитудой, но при других параметрах должны возникать в звездах любых типов, в том числе и массивных звездах на поздних стадиях эволюции.

В данной работе по аналогии с [9] можно показать, что в случае $Q_2 \neq 0$ формула для диаграммы период-светимость имеет более общую форму:

$$\frac{L_{max}}{\mathcal{L}_0} = \left(1 + \sqrt{1 - \left(\frac{P_E}{2\pi}\right)^{-2/3}}\right)^2 \mathcal{F}_+(P_E, \theta_0),$$
$$\frac{L_{min}}{\mathcal{L}_0} = \left(1 - \sqrt{1 - \left(\frac{P_E}{2\pi}\right)^{-2/3}}\right)^2 \mathcal{F}_-(P_E, \theta_0), \tag{J.3}$$

в которую входит дополнительный параметр $\theta = Q_2/(a_0 Q_1)$ и множитель:

$$\mathcal{F}_\pm(P_E, \theta_0) = \left(1 + \theta_0 \pm \theta_0 \sqrt{1 - \left(\frac{P_E}{2\pi}\right)^{-2/3}}\right)^4.$$

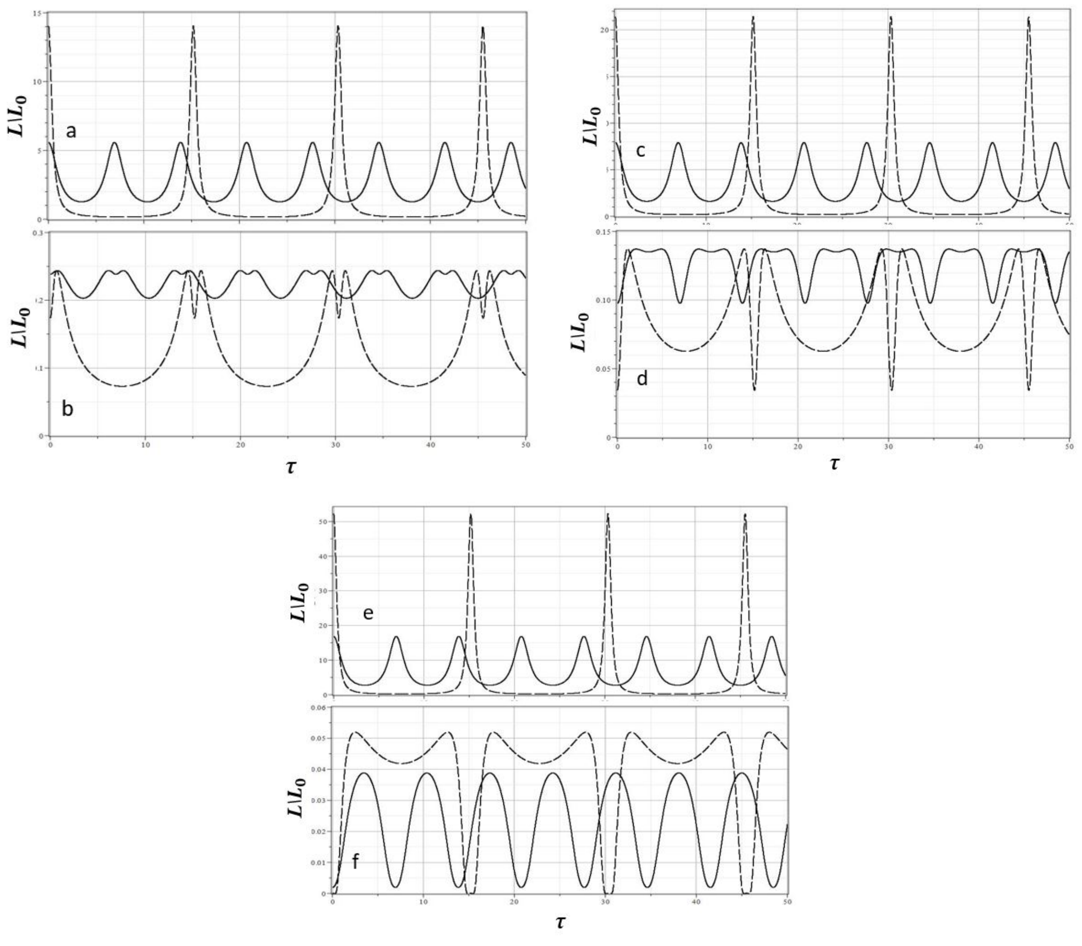


**Рис. 5.** Изменения относительной светимости для фазовых траекторий на рис. 2b: (a) $\theta_0 = 0.3$, (b) $\theta_0 = -0.3$, (c) $\theta_0 = 0.4$, (d) $\theta_0 = -0.4$, (e) $\theta_0 = 0.65$, (f) $\theta_0 = -0.65$

При этом характер осцилляций светимости переменных звезд, находящихся в динамическом равновесии, усложняется. На рис. 5(a,b,c,d) представлены графики осцилляций относительной светимости (J.2), соответствующие фазовым кривым на рис. 2c (с теми же обозначениями кривых, соответствующих разным начальным условиям) для четырех значений параметра $\theta_0$, как положительных (5(a,c)), так и отрицательных (5(b,d)).

Как видно из графиков на рис. 5, при отрицательных значениях параметра $\theta_0$ кривые блеска усложняются. Для некоторых типов цефеид в реальности имеются нестандартные детали кривой блеска. Некоторые типичные кривые блеска на примере конкретных цефеид приведены на рис. 6.

Сравнение кривых на рис. 5 и 6 показывает, что для определенного класса цефеид (типа FF-Орла) предлагаемая модель вполне способна описывать кривую блеска, а значит, и диаграмму период-светимость. Для цефеид второго типа ($\delta$-Цефея) модель должна быть подстроена под несимметричный характер кривой блеска. Вид кривой блеска на 6b близок к изменениям не радиуса звезды (переменная $x(t)$), с изменениями которого связана оценка светимости (J.3), а с изменениями переменной $y(t)$, которая описывает скорость изменения радиуса звезды. Т.е. в формулу для светимости необходимо включить некоторые эффекты изменения скорости радиуса (кривая лучевых скоростей) на саму светимость. Это требует дополнительных исследований.

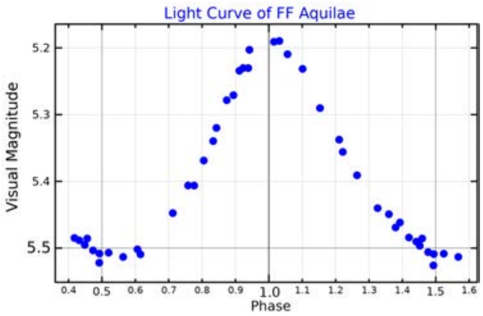


a

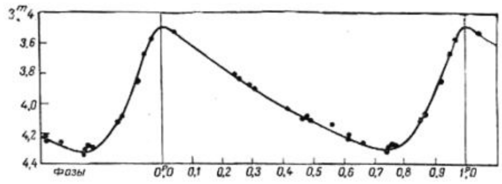


b

**Рис. 6.** Кривые блеска FF-Орла (a) [18] и $\delta$-Цефея (b) [19]

## K. Заключение

Как было показано в данной работе [9], новая теория тяготения при ее редукции к классической для условий структуры звезд дает новые результаты, вполне согласующиеся с реальными данными. В первую очередь это относится к возможности физически адекватно описать плотность и температуру как внутри звезд, так и за их пределами. Это достигается появлением в теории понятия динамического равновесия звезд и других астрофизических объектов. В условиях динамического равновесия звезды могут эволюционировать, но так, что в специальных автомодельных переменных их структура остается неизменной. В уравнениях пространственного строения звезд и их эволюции в рамках данной модели появляется важный параметр - параметр динамического равновесия. Именно наличие этого параметра приводит к новым элементам теории структуры и эволюции звезд, которые согласуются с наблюдениями. Для пространственного распределения этот параметр позволяет строить модели, в которых всюду плотность и температура являются неотрицательными величинами и возникают пространственные дополнительные максимумы и минимумы температуры и плотности, сопоставимые с изменениями этих параметров в короне. В модели эволюции звезд этот параметр является ключевым, поскольку обеспечивает появление фазовых замкнутых траекторий, т.е. нелинейных осцилляций большой амплитуды, в противовес стандартному подходу анализа малых колебаний.

Дополнительные нововведения в работе [9], с одной стороны, позволили упростить анализ модели (например, соотношение (E.1)), а с другой, позволили получить новые элементы описания звезд (например, аналитические соотношения для кривых блеска (J.3) и аналитических диаграмм период-светимость). Все это указывает не только на работоспособность модели осцилляций звезд, но и может служить подтверждением исходных положений новой теории тяготения или, в более общем понимании, теории топологической теории фундаментальных полей [1, 2, 3, 4, 5, 6].

## Список литературы/References

1. Zhuravlev V.M. A topological interpretation of quantum theory and elementary particle structure. *Gravitation and Cosmology*, 2011, Vol. 17, No. 3,pp. 201–217.

2. Журавлев В.М. Геометрия, топология и физические поля. *Пространство, время и фундаментальные взаимодействия*,
2014, вып. 4. С. 6-24.; *Масса и гравитация*, вып. 4. С. 25-39;
2015.;Уравнение индукции фундаментальных полей, N3-С. 44-60.; *Топологическая структура элементраных частиц,* N4-С. 104-118.

3. В.М. Журавлев. Материя и геометрия. ОТО и далее.... *Пространство, время и фундаментальные взаимодействия*, 2016.-N2-С. 5-26.

4. V. M. Zhuravlev. Induction Equations for Fundamental Fields and Dark Matter. *Gravitation and*

*Cosmology*, 2017, Vol. 23, No. 2, pp. 95–104

5. V. M. Zhuravlev. The principle of materiality of space and the theory of fundamental fields 2021 *J. Phys.: Conf. Ser.* 2081 012038
6. V.M. Zhuravlev. Matter and Space. New Theory of Fields and Particles. *Gravitation and Cosmology*, 2022, Vol. 28, No. 4, pp. 319–341
7. Модели динамики пылевидной материи в собственном гравитационном поле. Метод гидродинамических подстановок. *ЖЭТФ*, 2017, т. 152, вып. 3(9), с. 495-510
8. Журавлев В.М. Модели динамики самогравитирующего политропного газа. *Пространство, время и фундаментальные взаимодействия*, 2020, N4, с.10-22, (2020)
9. Журавлев В.М. Модели динамического равновесия астрофизических объектов. *ЖЭТФ*, 2022, Т. 162, N 6, стр. 850-877
10. Журавлев В.М. Магнитное поле звезд, находящихся в динамическом равновесии. *Пространство, время и фундаментальные взаимодействия.* 2022. N 4. С. 13-30
11. J. H. Lane, *American Journal of Science and Arts, Second Series*, 50, 57 (1870)
12. R. Emden, Gaskugeln. B.G. Teubner, Leipzig (1907)
13. Ландау Л. Д., Лифшиц Е. М. Теория поля. М.: Физматлит, 2012, 536 с.
14. Элыив А. А., Караченцев И. Д., Караченцева В. Е., Мельник О. В., Макаров Д. И. Структуры низкой плотности в Местной вселенной. II. Близкие космические пустоты. *Астрофизический бюллетень.* — Специальная астрофизическая обсерватория Российской академии наук, 2013. — Т. 68, N 1. — С. 1.; arXiv:1302.2369
15. С. А. Жевакин, *Астрон. журн.*, **30**, 161-179 (1953)
16. С. А. Жевакин, *Астрон. журн.* **31**, 141-153 (1954)
17. S. A. Zhevakin S.A., *Annual Review of Astron. and Astrophys.* **1**, 367-400. (1963)
18. https://commons.wikimedia.org/w/ index.php?curid=111182923
19. http://heritage.sai.msu.ru/ucheb/Samus/2_2.html

**Авторы**

**Журавлев Виктор Михайлович**, д.ф.-м.н., профессор, Ульяновский государственный педагогический университет, пл. Ленина, д. 4/5, г. Ульяновск, 432071 , Россия.
E-mail: zhvictorm@gmail.com

**Просьба ссылаться на эту статью следующим образом:**
Журавлев В. М. Новая теория тяготения, осцилляции звезд и 11-летний цикл активности Солнца. *Пространство, время и фундаментальные взаимодействия.* 2023. № 3-4. С. 333–351.

**Authors**

**Zhuravlev Viktor Mikhailovich**, Ph.D., Professor, Ulyanovsk State Pedagogical University, pl. Lenina., 4/5, Ulyanovsk, 432071, Russia.
E-mail: zhvictorm@gmail.com

**Please cite this article in English as:**
Zhuravlev V. M. New theory of gravity, stellar oscillations and the 11-year cycle of solar activity. *Space, Time and Fundamental Interactions*, 2023, no. 3-4, pp. 333–351.